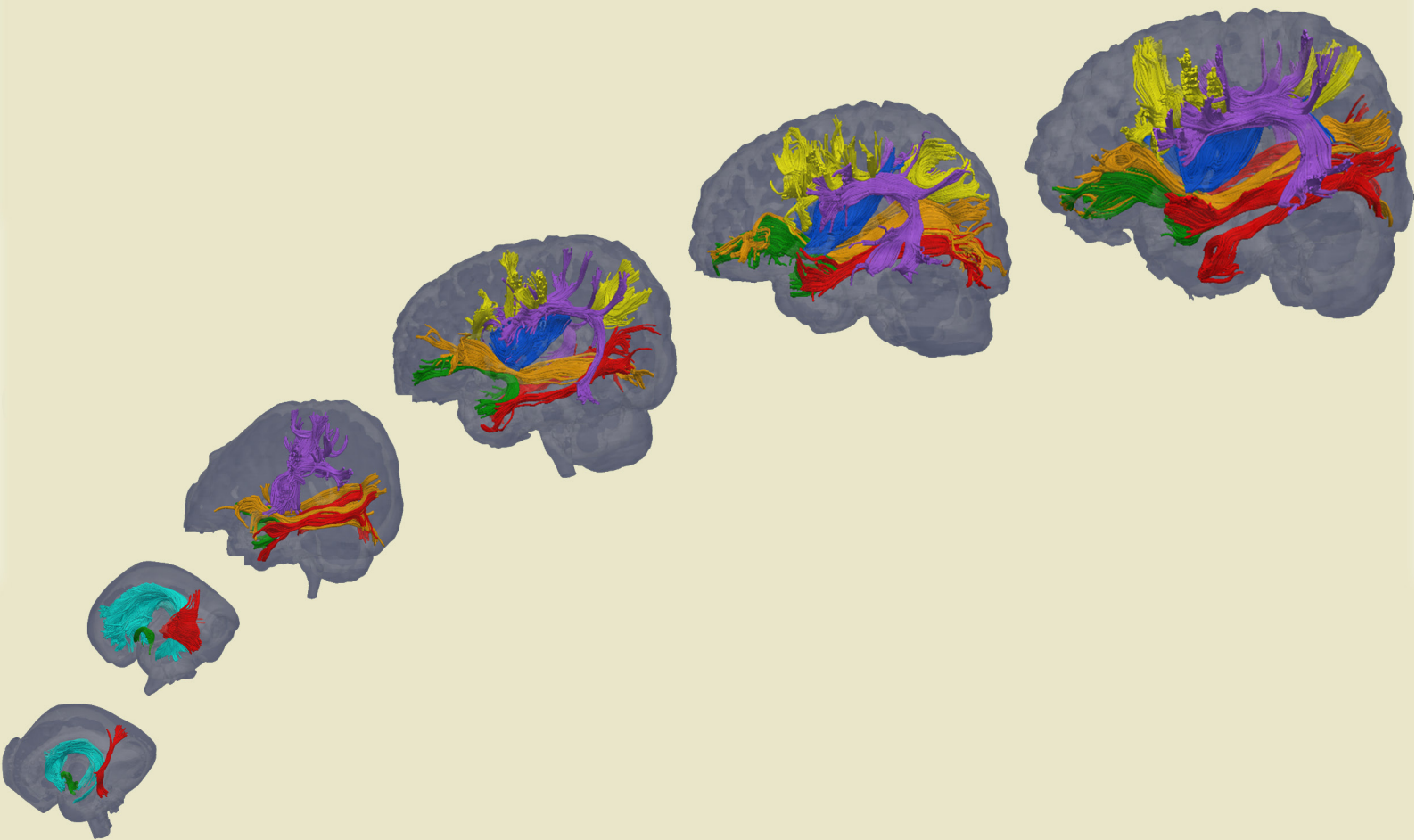


NEUROANATOMY OF HUMAN BRAIN DEVELOPMENT

EDITED BY : Hao Huang, Julia P. Owen and Pratik Mukherjee
PUBLISHED IN : Frontiers in Neuroanatomy





frontiers

Frontiers Copyright Statement

© Copyright 2007-2017 Frontiers Media SA. All rights reserved.

All content included on this site, such as text, graphics, logos, button icons, images, video/audio clips, downloads, data compilations and software, is the property of or is licensed to Frontiers Media SA ("Frontiers") or its licensees and/or subcontractors. The copyright in the text of individual articles is the property of their respective authors, subject to a license granted to Frontiers.

The compilation of articles constituting this e-book, wherever published, as well as the compilation of all other content on this site, is the exclusive property of Frontiers. For the conditions for downloading and copying of e-books from Frontiers' website, please see the Terms for Website Use. If purchasing Frontiers e-books from other websites or sources, the conditions of the website concerned apply.

Images and graphics not forming part of user-contributed materials may not be downloaded or copied without permission.

Individual articles may be downloaded and reproduced in accordance with the principles of the CC-BY licence subject to any copyright or other notices. They may not be re-sold as an e-book.

As author or other contributor you grant a CC-BY licence to others to reproduce your articles, including any graphics and third-party materials supplied by you, in accordance with the Conditions for Website Use and subject to any copyright notices which you include in connection with your articles and materials.

All copyright, and all rights therein, are protected by national and international copyright laws.

The above represents a summary only. For the full conditions see the Conditions for Authors and the Conditions for Website Use.

ISSN 1664-8714

ISBN 978-2-88945-120-3

DOI 10.3389/978-2-88945-120-3

About Frontiers

Frontiers is more than just an open-access publisher of scholarly articles: it is a pioneering approach to the world of academia, radically improving the way scholarly research is managed. The grand vision of Frontiers is a world where all people have an equal opportunity to seek, share and generate knowledge. Frontiers provides immediate and permanent online open access to all its publications, but this alone is not enough to realize our grand goals.

Frontiers Journal Series

The Frontiers Journal Series is a multi-tier and interdisciplinary set of open-access, online journals, promising a paradigm shift from the current review, selection and dissemination processes in academic publishing. All Frontiers journals are driven by researchers for researchers; therefore, they constitute a service to the scholarly community. At the same time, the Frontiers Journal Series operates on a revolutionary invention, the tiered publishing system, initially addressing specific communities of scholars, and gradually climbing up to broader public understanding, thus serving the interests of the lay society, too.

Dedication to Quality

Each Frontiers article is a landmark of the highest quality, thanks to genuinely collaborative interactions between authors and review editors, who include some of the world's best academicians. Research must be certified by peers before entering a stream of knowledge that may eventually reach the public - and shape society; therefore, Frontiers only applies the most rigorous and unbiased reviews.

Frontiers revolutionizes research publishing by freely delivering the most outstanding research, evaluated with no bias from both the academic and social point of view.

By applying the most advanced information technologies, Frontiers is catapulting scholarly publishing into a new generation.

What are Frontiers Research Topics?

Frontiers Research Topics are very popular trademarks of the Frontiers Journals Series: they are collections of at least ten articles, all centered on a particular subject. With their unique mix of varied contributions from Original Research to Review Articles, Frontiers Research Topics unify the most influential researchers, the latest key findings and historical advances in a hot research area! Find out more on how to host your own Frontiers Research Topic or contribute to one as an author by contacting the Frontiers Editorial Office: researchtopics@frontiersin.org

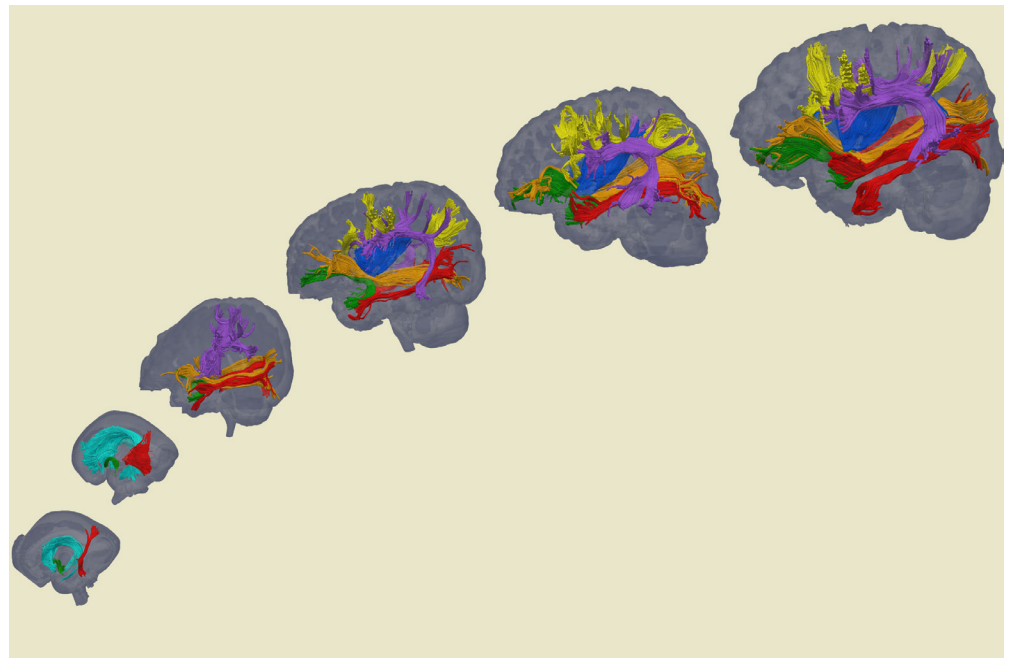
NEUROANATOMY OF HUMAN BRAIN DEVELOPMENT

Topic Editors:

Hao Huang, University of Pennsylvania, USA

Julia P. Owen, University of California, San Francisco, USA

Pratik Mukherjee, University of California, San Francisco, USA



Development of human brain white matter tracts reconstructed with diffusion magnetic resonance imaging from fetal and neonatal stage to adulthood. The colors of the white matter tracts are as follows: blue: external capsule; cyan: ganglionic eminence; red: inferior longitudinal fasciculus; brown: inferior occipitofrontal fasciculus; yellow: short association fibers. Courtesy of Dr Hao Huang, University of Pennsylvania.

The human brain is extraordinary complex and yet its origin is a simple tubular structure. Rapid and dramatic structural growth takes place during the fetal and perinatal period. By the time of birth, a repertoire of major cortical, subcortical and white matter structures resembling the adult pattern has emerged, however there are continued maturational changes of the gray matter and white matter throughout childhood and adolescence and into adulthood. The maturation of neuronal structures provides the neuroanatomical basis for the acquisition and refinement of cognitive functions during postnatal development. Histological imaging has been

traditionally dominant in understanding neuroanatomy of early brain development and still plays an unparalleled role in this field. Modern magnetic resonance imaging (MRI) techniques including diffusion MRI, as noninvasive tools readily applied to in vivo brains, have become an important complementary approach in revealing the detailed brain anatomy, including the structural connectivity between brain regions. In this research topic, we presented the most recent investigations on understanding the neuroanatomy and connectivity of human brain development using both histology and MRI. Modern advances in mapping normal developmental brain anatomy and connectivity should elucidate many neurodevelopmental disorders, ranging from rare congenital malformations to common disorders such as autism and attention deficit hyperactivity disorder (ADHD), which is a prerequisite for better diagnosis and treatment of these currently poorly understood diseases.

Citation: Huang, H., Owen, J. P., Mukherjee, P., eds. (2017). Neuroanatomy of Human Brain Development. Lausanne: Frontiers Media. doi: 10.3389/978-2-88945-120-3

Table of Contents

- 06** ***Altered Amygdala Development and Fear Processing in Prematurely Born Infants***
Anca Liliana Cismaru, Laura Gui, Lana Vasung, Fleur Lejeune, Koviljka Barisnikov, Anita Truttmann, Cristina Borradori Tolsa and Petra S. Hüppi
- 16** ***Toward Developmental Connectomics of the Human Brain***
Miao Cao, Hao Huang, Yun Peng, Qi Dong and Yong He
- 33** ***Multimodal Diffusion-MRI and MEG Assessment of Auditory and Language System Development in Autism Spectrum Disorder***
Jeffrey I. Berman, James C. Edgar, Lisa Blaskey, Emily S. Kushner, Susan E. Levy, Matthew Ku, John Dell and Timothy P. L. Roberts
- 42** ***Recent Progress in Magnetic Resonance Imaging of the Embryonic and Neonatal Mouse Brain***
Dan Wu and Jiangyang Zhang
- 50** ***Quantitative and Qualitative Analysis of Transient Fetal Compartments during Prenatal Human Brain Development***
Lana Vasung, Claude LePage, Milan Radoš, Mihovil Pletikos, Jennifer S. Goldman, Jonas Richiardi, Marina Raguž, Elda Fischi-Gómez, Sherif Karama, Petra S. Hüppi, Alan C. Evans and Ivica Kostovic
- 67** ***Maturation Along White Matter Tracts in Human Brain Using a Diffusion Tensor Surface Model Tract-Specific Analysis***
Zhang Chen, Hui Zhang, Paul A. Yushkevich, Min Liu and Christian Beaulieu
- 85** ***White Matter Microstructure is Associated with Auditory and Tactile Processing in Children with and without Sensory Processing Disorder***
Yi-Shin Chang, Mathilde Gratiot, Julia P. Owen, Anne Brandes-Aitken, Shivani S. Desai, Susanna S. Hill, Anne B. Arnett, Julia Harris, Elysa J. Marco and Pratik Mukherjee
- 99** ***Asymmetry of Radial and Symmetry of Tangential Neuronal Migration Pathways in Developing Human Fetal Brains***
Yuta Miyazaki, Jae W. Song and Emi Takahashi
- 109** ***Multivariate Analyses Applied to Healthy Neurodevelopment in Fetal, Neonatal, and Pediatric MRI***
Jacob Levman and Emi Takahashi
- 124** ***Validation of In utero Tractography of Human Fetal Commissural and Internal Capsule Fibers with Histological Structure Tensor Analysis***
Christian Mitter, András Jakab, Peter C. Brugger, Gerda Ricken, Gerlinde M. Gruber, Dieter Bettelheim, Anke Scharrer, Georg Langs, Johannes A. Hainfellner, Daniela Prayer and Gregor Kasprian

- 139 Synchronous Changes of Cortical Thickness and Corresponding White Matter Microstructure During Brain Development Accessed by Diffusion MRI Tractography from Parcellated Cortex**
Tina Jeon, Virendra Mishra, Minhui Ouyang, Min Chen and Hao Huang
- 152 High Resolution MRI Reveals Detailed Layer Structures in Early Human Fetal Stages: In Vitro Study with Histologic Correlation**
Rongpin Wang, Guangping Dai and Emi Takahashi
- 161 Characterization of Laminar Zones in the Mid-Gestation Primate Brain with Magnetic Resonance Imaging and Histological Methods**
Xiaojie Wang, David R. Pettersson, Colin Studholme and Christopher D. Kroenke
- 174 Construction and application of human neonatal DTI atlases**
Rajiv Deshpande, Linda Chang and Kenichi Oishi
- 184 The maturation of auditory responses in infants and young children: a cross-sectional study from 6 to 59 months**
J. Christopher Edgar, Rebecca Murray, Emily S. Kushner, Kevin Pratt, Douglas N. Paulson, John Dell, Rachel Golembski, Peter Lam, Luke Bloy, William Gaetz and Timothy P. L. Roberts
- 192 Abnormal surface morphology of the central sulcus in children with attention-deficit/hyperactivity disorder**
Shuyu Li, Shaoyi Wang, Xinwei Li, Qionglin Li and Xiaobo Li
- 203 The autistic brain in the context of normal neurodevelopment**
Mark N. Ziats, Catherine Edmonson and Owen M. Rennert
- 210 One hand clapping: lateralization of motor control**
Quentin Welniarz, Isabelle Dusart, Cécile Gallea and Emmanuel Roze



Altered Amygdala Development and Fear Processing in Prematurely Born Infants

Anca Liliana Cismaru^{1†}, Laura Gui^{1†}, Lana Vasung^{1*†}, Fleur Lejeune²,
Koviljka Barisnikov², Anita Truttmann³, Cristina Borradori Tolsa^{1‡}
and Petra S. Hüppi^{1*†}

¹ Division of Development and Growth, Department of Pediatrics, Hospital of Geneva, Geneva, Switzerland, ² Child Clinical Neuropsychology Unit, University of Geneva, Geneva, Switzerland, ³ Division of Neonatology, University Hospital of Lausanne, Lausanne, Switzerland

OPEN ACCESS

Edited by:

Pratik Mukherjee,
University of California, San
Francisco, USA

Reviewed by:

Christoph Schmitz,
Ludwig-Maximilians-University
of Munich, Germany
Steven Miller,
The Hospital for Sick Children,
Canada

*Correspondence:

Lana Vasung
lana.vasung@gmail.com;
Petra S. Hüppi
petra.huppi@hcuge.ch

[†]First co-authors.

[‡]Last co-authors.

Received: 09 November 2015

Accepted: 02 May 2016

Published: 18 May 2016

Citation:

Cismaru AL, Gui L, Vasung L,
Lejeune F, Barisnikov K, Truttmann A,
Borradori Tolsa C and Hüppi PS
(2016) Altered Amygdala
Development and Fear Processing in
Prematurely Born Infants.
Front. Neuroanat. 10:55.
doi: 10.3389/fnana.2016.00055

Context: Prematurely born children have a high risk of developmental and behavioral disabilities. Cerebral abnormalities at term age have been clearly linked with later behavior alterations, but existing studies did not focus on the amygdala. Moreover, studies of early amygdala development after premature birth in humans are scarce.

Objective: To compare amygdala volumes in very preterm infants at term equivalent age (TEA) and term born infants, and to relate premature infants' amygdala volumes with their performance on the Laboratory Temperament Assessment Battery (Lab-TAB) fear episode at 12 months.

Participants: Eighty one infants born between 2008 and 2014 at the University Hospitals of Geneva and Lausanne, taking part in longitudinal and functional imaging studies, who had undergone a magnetic resonance imaging (MRI) scan at TEA enabling manual amygdala delineation.

Outcomes: Amygdala volumes assessed by manual segmentation of MRI scans; volumes of cortical and subcortical gray matter, white matter and cerebrospinal fluid (CSF) automatically segmented in 66 infants; scores for the Lab-TAB fear episode for 42 premature infants at 12 months.

Results: Amygdala volumes were smaller in preterm infants at TEA than term infants (mean difference 138.03 mm³, $p < 0.001$), and overall right amygdala volumes were larger than left amygdala volumes (mean difference 36.88 mm³, $p < 0.001$). White matter volumes were significantly smaller ($p < 0.001$) and CSF volumes significantly larger ($p < 0.001$) in preterm than in term born infants, while cortical and subcortical gray matter volumes were not significantly different between groups. Amygdala volumes showed significant correlation with the intensity of the escape response to a fearsome toy ($r_s = 0.38$, $p = 0.013$), and were larger in infants showing an escape response compared to the infants showing no escape response (mean difference 120.97 mm³, $p = 0.005$). Amygdala volumes were not significantly correlated with the intensity of facial fear, distress vocalizations, bodily fear and positive motor activity in the fear episode.

Conclusion: Our results indicate that premature birth is associated with a reduction in amygdala volumes and white matter volumes at TEA, suggesting that altered amygdala development might be linked to alterations in white matter connectivity reported in premature infants. Moreover, our data suggests that such alterations might affect infants' fear-processing capabilities.

Keywords: amygdala, premature birth, fear, lab-TAB, amygdala development

INTRODUCTION

Children born prematurely have a high risk of developmental and behavioral disabilities (Larroque et al., 2004; Delobel-Ayoub et al., 2006). These include learning disabilities, behavioral problems and socio-emotional problems (Bhutta et al., 2002; Johnson and Marlow, 2011; Treyvaud et al., 2012) and are associated with an altered development of various brain regions (Ment et al., 2009; Kwon et al., 2014). The amygdala is a key part of the neural circuitry implicated in emotion processing and social development during early life (Bauman and Amaral, 2008). It is a bilateral structure located deep in the medial temporal lobes, whose strategic position, close to the temporal horn of lateral ventricles, enables the integration of limbic and neocortical information, but also makes it particularly vulnerable to injuries associated with premature birth (Rutherford, 2002).

The amygdala has been shown to play an important role in a wide range of behavioral and psychosocial processes. A patient who suffered a bilateral amygdala lesion during adolescence had deficits primarily related to fear processing, while her social behavior was unaffected (Adolphs et al., 1995, 1998). Most reproducibly activated by social stimuli, such as facial expressions depicting fear (Morris et al., 1996), the amygdala is also activated during nonsocial testing paradigms, such as fear conditioning (Büchel et al., 1998; LaBar et al., 1998; Cheng et al., 2003) and viewing of threatening and fearsome nonsocial stimuli (Hariri et al., 2003). Therefore, Bauman et al. (2004) suggested that the amygdala does not play an essential role in development of social behavior, but has a modulatory role achieved through emotion regulation (e.g., fear responses) that might be particularly important early on in development (Bauman et al., 2004; Leppänen and Nelson, 2012).

Studies on prenatal development and connectivity of the amygdala in humans are scarce (Nikolić and Kostović, 1986; Ulfing et al., 1998; Müller and O'Rahilly, 2006; Vasung et al., 2010b; ten Donkelaar, 2015). The literature regarding early development of emotion and social behavior in preterm born children is also limited. A few studies have found evidence that the socio-emotional development is different in premature children (Hughes et al., 2002; Spittle et al., 2009). When compared with term born peers, preterm born infants had higher emotional dysregulation (anger, frustration) scores at 12 months corrected age (Langerock et al., 2013), with similar tendencies at 42 months of age (Witt et al., 2014). Although many studies demonstrated a clear relationship between early cerebral abnormalities and

behavior at term age (Clark et al., 1988; Anderson and Doyle, 2003; Aust et al., 2014), few explored the role of the amygdala in this interplay.

The present study aimed to compare volumetric measures of the amygdala in very preterm and term born children at term equivalent age (TEA), and to assess the relationship between amygdala volumes and performance on a fear processing task in prematurely born children at 12 months of age.

MATERIALS AND METHODS

Participants

Among the infants born between 2008 and 2014 at the University Hospitals of Geneva (HUG) and Lausanne (CHUV), who participated in longitudinal and functional imaging studies, the 81 infants in our study were chosen as the ones who had undergone an magnetic resonance imaging (MRI) at TEA, and whose T2 images were of sufficient quality to enable the manual delineation of the amygdala. After receiving approval from the Research and Ethics Committees of the HUG and CHUV, informed parental consent was obtained for each infant included in the study. Infants were assigned to two groups based on their gestational age (GA) at birth (World Health Organization, 2012): 52 were born very prematurely (<29 gestational weeks) and 29 were born at term (>37 gestational weeks). An overall description of both groups is shown in **Table 1**. Birth weight z-scores were calculated for each child using German standard data (Voigt et al., 2006).

Methods

MRI Acquisition

Neonates underwent MRI scans at TEA at the Radiology Departments of the HUG and CHUV without sedation. Scans were performed on a 3.0-T Siemens Tim Trio scanner to obtain T2-weighted contiguous slices with 1.2 mm thickness (echo time (TE) = 150 ms, repetition time (TR) = 4600 ms, voxel dimensions = $0.8 \times 0.8 \times 1.2$ mm³). Four prematurely born infants had evidence of brain injury at TEA. Two had periventricular leukomalacia (PVL grade II/III) and the other two had intraventricular hemorrhage (IVH).

Image Segmentation and Volume Measurements

The amygdala was segmented manually by a senior scientist with experience in the delineation of amygdala during human brain development (Vasung et al., 2008), who was blind to infants' prematurity status. The segmentation was performed

TABLE 1 | Group characteristics.

	Preterm born infants (<i>n</i> = 52)	Term born infants (<i>n</i> = 29)	<i>p</i> -value ^a
Male, <i>N</i> (%)	26 (50)	16 (55.2)	0.66
GA at birth, mean (SD), weeks	27.16 (1.09)	39.72 (1.02)	<0.001
GA at MRI time, mean (SD), weeks	40.05 (0.91)	40.28 (1.29)	0.38
Birth weight, mean (SD), g	930.5 (204.3)	3289.3 (343.9)	<0.001
Birth weight z-score, mean (SD) ^b	−0.09 (0.72)	−0.37 (0.77)	0.11
IVH, <i>N</i> (%)	2 (3.8)	1 (3.4)	1.00
PVL, <i>N</i> (%)	2 (3.8)	0 (0)	0.54
BPD, <i>N</i> (%)	23 (44.2)	0 (0)	<0.001
PDA, <i>N</i> (%)	25 (48.1)	0 (0)	<0.001
NEC, <i>N</i> (%)	2 (3.8)	0 (0)	0.41
Antenatal steroids, <i>N</i> (%)	36 (69.2)	0 (0)	<0.001

Abbreviations: IVH, intraventricular hemorrhage; PVL, periventricular leukomalacia assessed by MRI at TEA; BPD, broncho-pulmonary disease; PDA, patent ductus arteriosus; NEC, necrotizing enterocolitis; SD, standard deviation. ^aGroup characteristics were compared using independent sample *t*-tests for continuous variables, and Chi-square or Fisher's exact test for categorical variables, as appropriate. ^bComputed as (weight−*M*)/SD, where the mean weight *M* and standard deviation SD were obtained according to the infant's sex and gestational age (Voigt et al., 2006).

on T2-weighted MR cerebral images (**Figure 1**), using the manual contour editing function of a three dimensional (3D) visualization software (Amira). It was based on anatomical guidelines for the localization of the amygdala (Paxinos and Mai, 2004). Histological atlases were used for the validation and correction of anatomical landmarks (Bayer and Altman, 2003), the Allen Institute for Brain Science: <http://www.brain-map.org/>.

The amygdala is situated in the anteromedial temporal lobe, separated from the lentiform nuclei by a substantia innominata, and from the basal forebrain by a massive fiber system. It is a heterogeneous structure encompassing three parts: a specialized ventromedial expansion of the striatum, the caudal olfactory cortex, and a ventromedial extension of the claustrum (Swanson and Petrovich, 1998).

To delineate the amygdala, first the rostral pole of amygdala, easily recognizable by the appearance of the basolateral nuclei in Nissl stained sections (Schumann and Amaral, 2006), was defined as the most rostral part of the amygdala in sagittal MRI slices. Next, the amygdala was outlined on coronal slices using the following anatomical landmarks: the external capsule, anterior commissure, and temporal stem (dorsolateral border of amygdala), putamen and pallidum (superior border of amygdala), substantia innominata and nucleus basalis of Meynert (dorsomedial border of amygdala), semiannular sulcus (ventromedial border of amygdala), separating entorhinal cortex from the amygdala), temporal horn of the lateral ventricle and the hippocampus (caudal border of the amygdala), and white matter of temporal lobe (ventral border of the amygdala). After delineation of the amygdala on coronal slices, its borders were corrected in axial and sagittal slices. Once the outline was complete, the amygdala

volume was calculated automatically and expressed in cubic millimeters.

Next, whole brain segmentation of the infants' T2 MR scans was performed using a novel automatic method for newborn brain segmentation, based on knowledge of newborn brain morphology (tissue location, connectivity and structure; Gui et al., 2012). First the intracranial cavity (ICC) was segmented, and then, after masking out the cerebellum and brainstem, the following tissues were segmented: cortical and subcortical gray matter, white matter and cerebrospinal fluid (CSF). In some cases whole brain segmentation was not possible due to low image quality (movement artifacts), leaving a total of 66 (39 prematurely born and 27 term born) infants with available whole brain segmentations.

Fear-Processing Abilities Evaluated at 12 Months

The Lab-TAB test (Goldsmith and Rothbart, 1996) was designed to evaluate children's temperament through a set of emotion-inducing behavioral episodes. Prematurely born infants who participated in longitudinal studies at the HUG and CHUV hospitals routinely undergo the Lab-TAB test. In our study of the amygdala, we were interested in the infants' reaction to the fear episode of the Lab-TAB using the Unpredictable Mechanical Toy task, in which a mechanical robot dog walks towards the child. Once in front of the child, the dog stops and barks and howls before he moves back to the starting position. This procedure is designed to elicit fear and is split in three time intervals: (1) the dog approaching; (2) the first 5 s in front of the child; and (3) the next 5 s in front of the child. Each time interval is coded in accordance with the Lab-TAB manual for the following variables: intensity of facial fear, intensity of distress vocalizations, intensity of bodily fear, intensity of escape and startle response. Moreover, the variable "positive motor activity" was coded to account for all behaviors of pointing towards, reaching for or grabbing the mechanical toy. All variables were rated on 4-point Likert scales according to the intensity of a specific behavior (for example for the intensity of escape and startle: 0 = no escape; 1 = mild or fleeting escape; 2 = moderate escape, resulting in significant, but not extreme attempts to get away or resist; 3 = vigorous escape behavior).

All children were evaluated in a quiet room with at least one reference person present. Children were seated in front of a table, in a baby chair or on the reference person's lap. All the evaluations were videotaped with parental consent for subsequent analysis.

Some infants did not want to perform or finish the cognitive testing, while others were excluded due to technical problems, weariness, stress or lack of interest, leaving a total of 42 prematurely born infants with Lab-TAB fear assessment at 12 months of age.

Statistical Analysis

Infants' characteristics are reported according to the preterm/term group as mean ± standard deviation (SD) for continuous outcomes, and as frequency and percentages for categorical data. Characteristics' differences between the

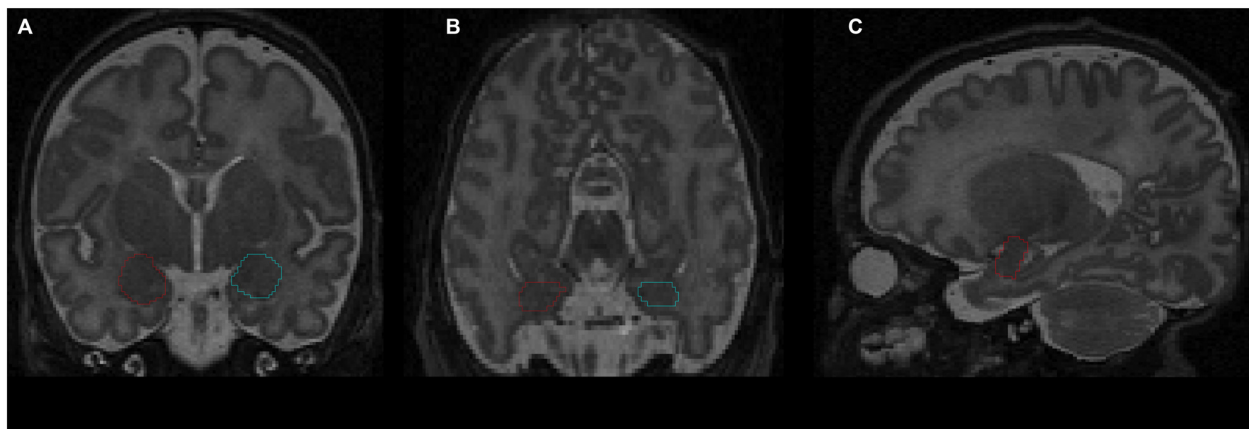


FIGURE 1 | Delineation of amygdala on T2-weighted magnetic resonance imaging (MRI) using the Amira software: (A) coronal view; (B) axial view; (C) sagittal view. Red contour—right amygdala, blue contour—left amygdala.

two groups were assessed using a Student *t*-test for continuous variables, and using a chi-square test or Fisher exact test, as appropriate, for categorical variables.

Differences in amygdala volumes between preterm and term born groups, and between left and right hemispheres were assessed using a generalized linear model, with prematurity, gender and GA at the time of the MRI as between-subjects effects, and hemisphere side as within-subjects effect. Differences in brain tissue volumes between preterm and term born groups were assessed using general linear models, with prematurity, gender, GA at the time of the MRI and volume of ICC as between-subjects effects. For the sub-cohort for which the volumes of the ICC were available, differences in amygdala volumes between preterm and term born groups, and between left and right hemispheres were assessed using a generalized linear model, with prematurity, gender, ICC volume and GA at the time of the MRI as between-subjects effects, and hemisphere side as within-subjects effect.

The relationship between total amygdala volumes and infants' response to the fear episode of the Lab-TAB at 12 months was assessed using Spearman correlations. Composite scores were binarized into equal to zero (no reaction to mechanical dog episode) and greater than zero (any reaction to mechanical dog episode), and amygdala volumes were compared between the reaction/no reaction infant groups with Student *t*-tests.

Statistical analysis was performed using SPSS Statistics Software. A two-tailed *p*-value ≤ 0.05 was considered significant for all analyses.

RESULTS

Group Characteristics

Gender distribution, GA at the time of the MRI scan, birth weight *z*-scores and brain pathology distribution (IVH, PVL) were not significantly different between the preterm and the term born groups (Table 1). Morbidities associated with prematurity

(broncho-pulmonary disease [BPD], patent ductus arteriosus [PDA] and necrotizing enterocolitis [NEC]) were not found in the term born group.

Amygdala Volumes

Amygdala volumes (Tables 2, 3) were significantly smaller in preterm born infants at TEA than in term born infants, (mean difference 138.03 mm³, 95% confidence interval [CI], 108.62–167.45, $p < 0.001$), adjusting for gender and GA at MRI time. Moreover, volumes of right amygdala were significantly larger than volumes of left amygdala (mean difference 36.88 mm³, 95% CI, 23.63–50.12, $p < 0.001$), adjusting for gender and GA at MRI time. No significant relationship was found between amygdala volumes and gender or GA at MRI time. Amygdala volumes were not significantly different between the 5 infants presenting brain pathologies (IVH or PVL) and the other 76 infants of the cohort (Supplementary Table 1). Among the premature infants, amygdala volumes were not significantly different between infants presenting prematurity-associated morbidities (BPD, PDA, NEC) or having received antenatal steroids and the other premature infants of the cohort (Supplementary Table 1).

Whole Brain Segmentation Volumes

White matter volumes (Table 4, column of B values) were significantly smaller in preterm born infants at TEA compared to term born infants (mean difference 17.27 cm³, $p < 0.001$),

TABLE 2 | Amygdala volumes.

	Preterm born infants (<i>n</i> = 52)	Term born infants (<i>n</i> = 29)
Left amygdala volume at TEA, mean (SD), mm ³	592.78 (73.15)	723.54 (75.04)
Right amygdala volume at TEA, mean (SD), mm ³	624.29 (73.46)	770.07 (71.95)

TABLE 3 | Parameter estimates for generalized linear model of amygdala volumes.

	B	95% CI		p-value ^a
Preterm born	−138.03	−108.62	−167.45	<0.001
Right hemisphere	36.88	23.63	50.12	<0.001
Male	12.41	−16.09	40.91	0.39
GA at MRI	−1.83	−11.97	8.31	0.72

^aGeneralized linear model with prematurity, gender and GA at the time of the MRI as between-subjects effects, and hemisphere side as within-subjects effect.

when adjusted for gender, GA at the time of the MRI and volume of ICC. CSF volumes were significantly larger in preterm born infants at TEA compared to term born infants (mean difference 17.04 cm³, $p < 0.001$), when adjusted for gender, GA at the time of the MRI and volume of ICC. We did not find any significant differences in cortical gray matter and subcortical gray matter volumes between preterm and term born infants, when adjusted for gender, GA at the time of the MRI and volume of ICC (Table 4).

Amygdala volumes (Table 5) were significantly smaller in preterm born infants at TEA than in term born infants (mean difference 165.64 mm³, 95% CI, 134.33–196.94, $p < 0.001$), adjusting for gender, ICC volume, and GA at MRI time. Moreover, volumes of right amygdala were significantly larger than volumes of left amygdala (mean difference 42.89 mm³, 95% CI, 28.48–57.30, $p < 0.001$) adjusting for gender, ICC volume, and GA at MRI time. No significant relationship was found between amygdala volumes and gender or GA at MRI time. Amygdala volumes were not significantly different between the 66 infants for whom whole brain segmentations were available and the other 15 infants of the cohort (Supplementary Table 1).

Relationship Between Amygdala Volumes and Lab-TAB Fear Episode Scores

Composite scores for the five variables describing the infants' reaction to the Unpredictable Mechanical Toy episode were computed by averaging over the three time intervals of the procedure (Larroque et al., 2004; Gagne et al., 2011; Table 6).

The analysis of composite fear scores in the 42 prematurely born infants subjected to the fear episode of the Lab-TAB test showed significant positive correlation between the intensity of the escape response and total amygdala volumes ($r_s = 0.38$, $p = 0.013$). No significant correlation was found between

total amygdala volumes and Lab-TAB scores measuring the intensity of facial fear, distress vocalizations, bodily fear and positive motor activity. Amygdala volumes were not significantly different between the infants who completed ($n = 42$) and those who did not complete ($n = 10$) the fear episode of the LabTAB test (Supplementary Table 1).

Amygdala volumes were significantly larger in infants showing an escape response compared to the infants showing no escape response (mean difference 120.97 mm³, Table 7, Figure 2). There were no significant differences in amygdala volumes between infants showing any reaction and infants showing no reaction of facial fear, bodily fear, distress vocalizations or positive motor action (Table 7, Figure 2).

DISCUSSION

Amygdala Development and Preterm Birth

To our knowledge, this is the first quantitative MRI study of amygdala volumes (right, left and bilateral) in preterm infants at TEA and term-born infants. The study also explored the association between amygdala volumes at TEA and the response to a fear-eliciting situation in preterm infants at 12 months of age. Amygdala volumes in very preterm infants at TEA were significantly smaller than in term born controls, while a rightward hemispheric asymmetry was present in the whole cohort. Moreover, the evaluation of the fear response of preterm infants at 12 months of age revealed that the intensity of the escape response when faced with fear-eliciting stimuli was significantly correlated with amygdala volumes at TEA.

Our results can be interpreted in the light of the developmental path of the human amygdala. First discernable around 5 post conceptional weeks (Müller and O'Rahilly, 2006), the amygdala becomes an inhomogeneous structure around 12 post conceptional weeks (Nikolić and Kostović, 1986). From this point onward, it displays transient architectonic features, being composed of continuous cell columns separated by cell-sparse septa, which are linked to continuous neuronal migration and the presence of radial glial cells (Nikolić and Kostović, 1986; Ulfig et al., 2003). Most of amygdala's neuronal cells come from the medial ganglionic eminence, with its medial nucleus developing slightly before the laterobasal one (Müller and O'Rahilly, 2006). While its basic cytoarchitecture is already defined at term (Humphrey, 1968; Ulfig et al., 1998), the amygdala still undergoes important structural and functional remodeling

TABLE 4 | Whole brain segmentation volumes.

Volume (cm ³)	Preterm born infants ($n = 39$)	Term born infants ($n = 27$)	p-value ^a	B	95% CI	
CGM, mean (SD)	165.35 (18.13)	153.52 (17.58)	0.87	−0.46	5.88	4.95
SGM, mean (SD)	21.09 (1.68)	19.68 (2.05)	0.53	0.20	0.43	0.83
WM, mean (SD)	143.26 (14.48)	149.97 (16.64)	<0.001	−17.27	22.28	−12.25
CSF, mean (SD)	98.68 (23.00)	69.44 (19.98)	<0.001	17.04	−8.10	25.97

CGM, cortical gray matter volume; SGM, subcortical gray matter volume; WM, white matter volume; CSF, cerebrospinal fluid volume. ^ageneral linear models with prematurity, gender, GA at the time of the MRI and volume of ICC as between-subjects effects.

TABLE 5 | Parameter estimates for generalized linear model of amygdala volumes adjusting for ICC volume.

	B	95% CI		p-value ^a
Preterm born	−165.64	−196.94	−134.33	<0.001
Right hemisphere	42.89	28.48	57.30	<0.001
Male	6.35	−24.42	37.13	0.69
GA at MRI	−9.33	−25.28	6.61	0.25
ICC volume	0.001	0	0.001	<0.001

^aGeneralized linear model with prematurity, gender, ICC volume and GA at the time of the MRI as between-subjects effects, and hemisphere side as within-subjects effect.

throughout its development from infancy to adolescence (Guo et al., 2007; Østby et al., 2009; Tottenham et al., 2009; Tottenham and Sheridan, 2010; Uematsu et al., 2012; Greimel et al., 2013). Many studies reported that the amygdala volumes tend to increase until early adolescence (Østby et al., 2009; Greimel et al., 2013), but the most rapid growth was shown to occur around birth (Vasung et al., 2008; Tottenham et al., 2009). Thus, our results showing lower amygdala volumes in preterm vs. term born infants at TEA reflect the vulnerability of the amygdala to premature birth and life ex-utero before term age, which seemingly cause disruptions of major developmental events taking place in the brain during the third trimester.

There are few quantitative MRI studies of regional brain volumes in preterm infants. Inder et al. (2005) reported lower cortical and subcortical gray matter volumes in preterm vs. term born infants at TEA, with major predictors of the altered volumes being GA at birth and the presence of white matter injury. Contrarily, Boardman et al. (2007) argued that brain tissue volumes of prematurely born infants at TEA are not reduced compared to term born infants, which is corroborated by our findings (Table 4). Rogers et al. (2014) did not find significant differences in the volumes of left or right amygdala between late preterm children (born between 34 and 36 gestational weeks) and term born peers at school age. In contrast to our study, these volumetric results were obtained at school age rather than

TABLE 6 | Lab-TAB fear composite scores (obtained by averaging scores for the three time intervals) in 42 prematurely born infants at 12 month of age.

Variable	Composite scores			
	score = 0	0 < score ≤ 1	1 < score ≤ 2	2 < score ≤ 3
Facial fear, N (%)	15 (35.7)	18 (42.9)	7 (16.7)	2 (4.8)
Distress vocalizations, N (%)	37 (88.1)	4 (9.5)	1 (2.4)	0 (0)
Bodily fear, N (%)	11 (26.2)	21 (50)	9 (21.4)	1 (2.4)
Escape response, N (%)	30 (71.4)	9 (21.4)	3 (7.1)	0 (0)
Positive motor activity, N (%)	16 (38.1)	12 (28.6)	11 (26.2)	3 (7.1)

TABLE 7 | Student t-test results comparing amygdala volumes between infants showing no reaction and infants showing any reaction to the mechanical dog episode (according to the corresponding composite score).

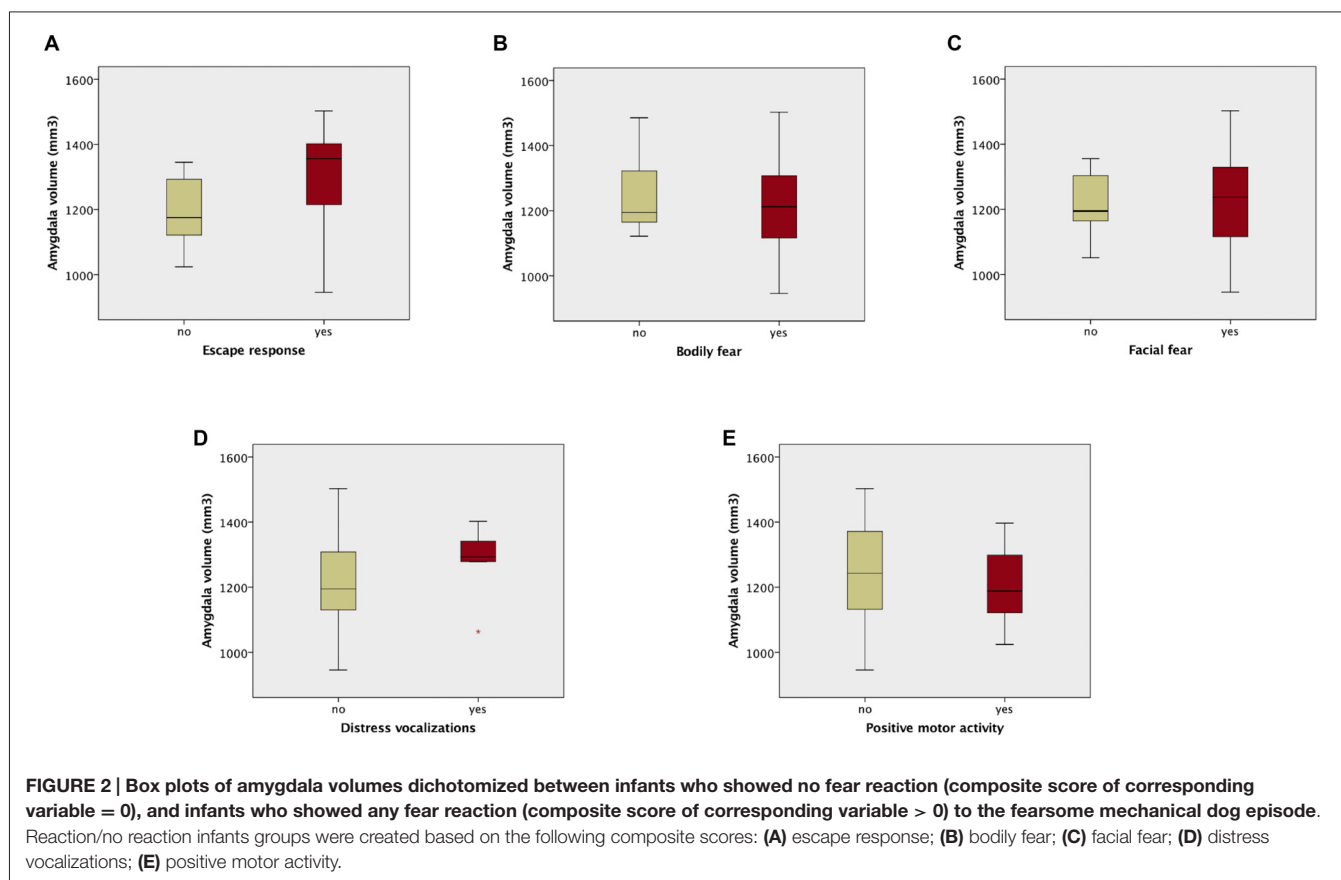
	Mean amygdala volume difference, mm ³ (95% CI)	t	df	p-value
Facial fear	−1.87 (−87.75–84.01)	−0.044	40	0.965
Distress vocalizations	58.12 (−67.59–183.84)	0.934	40	0.356
Bodily fear	−36.30 (−129.18–56.58)	−0.790	40	0.434
Escape response	120.97 (38.48–203.45)	2.964	40	0.005
Positive motor activity	−43.55 (−127.14–40.05)	−1.053	40	0.299

term age, and only included late preterm children (compared to very preterm infants in our study), therefore the premature birth occurred in a period when brain development is more advanced, and thus less susceptible to being perturbed. In a study of preterm children from a wider range of GAs, Peterson et al. (2000) reported significantly smaller amygdala volumes in preterm children compared to term controls at 8 years corrected age. These results are in agreement with our study, suggesting that perturbations in amygdala development engendered by premature birth are apparent at TEA and may persist well into childhood.

Moreover, the fact that the volumetric differences between the groups in our study were still present when correcting for total intracranial volumes indicates that the reduction in amygdala volumes cannot simply be explained by head size differences between term and preterm infants. Peterson et al. (2000) came to similar conclusions in their study of 8 year old preterm infants.

While the current *in vivo* MRI-based study does not allow us to specify precisely what caused the volume reductions of the amygdala in the preterm infants, possible explanations could be found by looking at brain microstructure. Studies focusing on white matter fiber organization have found a reduction in brain microstructural maturity and connectivity in preterm children (Hüppi et al., 1998; Fischi-Gómez et al., 2014). Such findings indicate alterations of white matter development associated with prematurity, confirmed by our volumetric results (Table 4). Currently, it is not clear to which extent axonal fibers (composing white matter) contribute to the volume growth of amygdala during early development. However, taking into account that the peak of neuronal migration into amygdala occurs before premature birth, and our results indicate reduced white matter volumes in prematurely born infants (Table 4), we postulate that the smaller volumes of amygdala in prematurely born infants might reflect a decreased number of axonal connections of the amygdala, as well as alterations of the neurogenic processes influenced by axonal ingrowth (e.g., dendritic differentiation, cell growth; Vasung et al., 2008).

Further evidence supporting our hypothesis can be found by looking at amygdala connectivity findings. The first fibers of the amygdala are visible as early as 11 post conceptional weeks, while its abundant connectivity pattern can be seen by 17 post conceptional weeks (Vasung et al., 2010a). One of amygdala's important connections involved in emotional significance processing and generation of emotional expressions



(Schmahmann and Pandya, 2009) is the uncinate fascicle. The uncinate fascicle connects the anterior temporal lobe with the medial and orbital prefrontal cortex, and, as it passes through the temporal stem, it contributes some projections to the latero-basal amygdala. Prematurely born children were shown to have significantly lower fractional anisotropy (a measure of fiber tract organization) values of the uncinate fascicle at 12 years (Constable et al., 2008). This finding corroborates our hypothesis that such alterations in connectivity, also reflected by reduced white matter volumes in premature infants of our cohort, might affect the growth of the amygdala in preterm infants.

Our results also uncovered the presence of a rightward hemispheric asymmetry in amygdala volumes at TEA, demonstrating the early appearance of this asymmetry that was reported in adults by Uematsu et al. (2012). This is an important finding given the well-known functional hemispheric asymmetry present in adults, where direct electric stimulation of the right amygdala induces negative emotions, while the stimulation of the left amygdala induces both pleasant and unpleasant emotions (Lanteaume et al., 2007).

Amygdala Development and the Regulation of Fear Responses

Research on prenatal development of the amygdala and the early development of socio-emotional competences is scarce. Studies on primates reported that subjects with neonatal amygdala lesions presented heightened fear responses when

faced with social stimuli, and diminished fear responses when faced with (potentially threatening) non social objects (Prather et al., 2001; Bauman et al., 2004). However, when amygdala lesions were induced in adult primates, they showed no indication of social fear (Emery et al., 2001), but demonstrated similar diminished fear responses when faced with threatening objects (Kalin et al., 2001). Bauman et al. (2004) concluded that while the amygdala may not play an essential role in social behavior, it has a key contribution in the identification of potential dangers and the production of appropriate responses, thus indirectly modulating social behavior. These findings are in agreement with our results showing that premature infants with smaller amygdala volumes at TEA had a blunted reaction to a fearsome mechanical dog (non-social stimulus) at 12 months of age. These different fear-processing capabilities, seen as impaired identification of potential danger, might therefore be linked to the altered development of amygdala in prematurely born children. Moreover, our results are consistent with the conclusions of a behavioral study indicating that 12-month-old preterm infants displayed less fear reactivity than term born infants when confronted to the fearsome mechanical dog of the LabTAB test (Langerock et al., 2013). However, a limitation of our study was that fear processing capabilities could not be assessed in normally-developing term-born infants, since their parents considered extensive neuropsychological testing to be too time-consuming.

Literature concerning human adults with bilateral amygdala damage showed that such subjects were impaired in judging negative emotion in facial expressions and making accurate judgments of trustworthiness (Adolphs et al., 1995, 1998). Nevertheless, such findings cannot be extrapolated to the premature infant population, since socio-emotional competences undergo significant development during early childhood. Thus, the role of the amygdala in the development of socio-emotional difficulties in preterm infants needs to be evaluated in further studies focusing on amygdala connectivity and functional response.

CONCLUSION

The present study brings new insights for understanding the impact of prematurity on brain development. Our data showed that amygdala volumes and whole brain white matter volumes were significantly smaller in preterm infants at TEA than in term born infants. Such findings reflect the altered growth of the amygdala associated with prematurity, which might be explained by modifications in white matter connectivity affecting the amygdala. Moreover, we presented evidence that a rightwards-hemispheric asymmetry of the amygdala is already present at TEA. In addition, in an exploratory analysis, we found that prematurely born children showing blunted escape responses to a fear-eliciting object had smaller amygdala volumes, suggesting that altered amygdala development might be linked with an impaired identification of fearsome and potentially dangerous objects in infancy. Further longitudinal studies of premature cohorts, as well as animal models of premature birth are needed to investigate the precise causes of such alterations in amygdala development associated with prematurity, as well as their long term developmental consequences. However, our preliminary findings have important clinical implications, as the detection of these regional abnormalities can improve early-targeted interventions.

REFERENCES

- Adolphs, R., Tranel, D., and Damasio, A. R. (1998). The human amygdala in social judgment. *Nature* 393, 470–474.
- Adolphs, R., Tranel, D., Damasio, H., and Damasio, A. R. (1995). Fear and the human amygdala. *J. Neurosci.* 15, 5879–5891.
- Anderson, P., Doyle, L. W., and Victorian Infant Collaborative Study Group (2003). Neurobehavioral outcomes of school-age children born extremely low birth weight or very preterm in the 1990s. *JAMA* 289, 3264–3272. doi: 10.1001/jama.289.24.3264
- Aust, S., Stasch, J., Jentschke, S., Alkan Härtwig, E., Koelsch, S., Heuser, I., et al. (2014). Differential effects of early life stress on hippocampus and amygdala volume as a function of emotional abilities. *Hippocampus* 24, 1094–1101. doi: 10.1002/hipo.22293
- Bauman, M. D., and Amaral, D. G. (2008). “Neurodevelopment of social cognition,” in *Handbook of Developmental Cognitive Neuroscience*, 2nd Edn, eds C. A. Nelson and M. Luciana (Cambridge, MA: MIT Press), 161–185.
- Bauman, M. D., Lavenex, P., Mason, W., Capitanio, J., and Amaral, D. G. (2004). The development of social behavior following neonatal amygdala lesions in rhesus monkeys. *J. Cogn. Neurosci.* 16, 1388–1411. doi: 10.1162/0898929042304741

AUTHOR CONTRIBUTIONS

ALC analyzed the data and wrote the manuscript. LG segmented the MRI images, helped with statistical analysis and manuscript revision. LV interpreted data, delineated amygdala, helped with statistical analysis, and wrote the manuscript. FL and KB evaluated prematurely born infants on fear episode of the LAB-TAB using the Unpredictable Mechanical Toy task at 12 month of age. AT was responsible for the MRI acquisition of infants at TEA. CBT designed the study and helped with interpretation. PSH designed the study, was responsible for the MRI acquisition of infants at TEA and helped with interpretation of the results.

FUNDING

This work was supported by Swiss National Science Foundation, Project SPUM: from Cortex to Classroom: enhancing Brain Development for Premature Infants No. 140334, to PSH, and by the Swiss National Science Foundation grant 32473B_135817 “Development of emotion and cognition in preterm born cohorts: neurostructural and neurofunctional correlates from birth to early adolescence”.

ACKNOWLEDGMENTS

We would like to thank our colleague Antoine Poncet from the Geneva University Hospitals, who provided his expertise for the statistical analysis, and whose comments helped to greatly improve the quality of this manuscript.

SUPPLEMENTARY MATERIAL

The Supplementary Material for this article can be found online at: <http://journal.frontiersin.org/article/10.3389/fnana.2016.00055/abstract>

- Bayer, S. A., and Altman, J. (2003). *The Human Brain During The Third Trimester*. (Boca Raton, FL: CRC Press).
- Bhutta, A. T., Cleves, M. A., Casey, P. H., Cradock, M. M., and Anand, K. J. (2002). Cognitive and behavioral outcomes of school-aged children who were born preterm: a meta-analysis. *JAMA* 288, 728–737. doi: 10.1001/jama.288.6.728
- Boardman, J. P., Counsell, S. J., Rueckert, D., Hajnal, J. V., Bhatia, K. K., Srinivasan, L., et al. (2007). Early growth in brain volume is preserved in the majority of preterm infants. *Ann. Neurol.* 62, 185–192. doi: 10.1002/ana.21171
- Büchel, C., Morris, J., Dolan, R. J., and Friston, K. J. (1998). Brain systems mediating aversive conditioning: an event-related fMRI study. *Neuron* 20, 947–957. doi: 10.1016/s0896-6273(00)80476-6
- Cheng, D. T., Knight, D. C., Smith, C. N., Stein, E. A., and Helmstetter, F. J. (2003). Functional MRI of human amygdala activity during Pavlovian fear conditioning: stimulus processing versus response expression. *Behav. Neurosci.* 117: 3–10. doi: 10.1037/0735-7044.117.1.3
- Clark, A. S., Macluskus, N. J., and Goldman-Rakic, P. S. (1988). Androgen binding and metabolism in the cerebral cortex of the developing rhesus monkey. *Endocrinology* 123, 932–940. doi: 10.1210/endo-123-2-932
- Constable, R. T., Ment, L. R., Vohr, B. R., Kesler, S. R., Fulbright, R. K., Lacadie, C., et al. (2008). Prematurely born children demonstrate white matter microstructural differences at 12 years of age, relative to term control subjects:

- an investigation of group and gender effects. *Pediatrics* 121, 306–316. doi: 10.1542/peds.2007-0414
- Delobel-Ayoub, M., Kaminski, M., Marret, S., Burguet, A., Marchand, L., Sylvie, N., et al. (2006). Behavioral outcome at 3 years of age in very preterm infants: the EPIPAGE study. *Pediatrics* 117, 1996–2005. doi: 10.1542/peds.2005-2310
- Emery, N. J., Capitanio, J. P., Mason, W. A., Machado, C. J., Mendoza, S. P., and Amaral, D. G. (2001). The effects of bilateral lesions of the amygdala on dyadic social interactions in rhesus monkeys (*Macaca mulatta*). *Behav. Neurosci.* 115, 515–544. doi: 10.1037/0735-7044.115.3.515
- Fischi-Gómez, E., Vasung, L., Meskaldji, D. -E., Lazeyras, F., Borradori-Tolsa, C., Hagmann, P., et al. (2014). Structural brain connectivity in school-age preterm infants provides evidence for impaired networks relevant for higher order cognitive skills and social cognition. *Cereb. Cortex*, 25, 2793–2805. doi: 10.1093/cercor/bhu073
- Gagne, J. R., Van Hulle, C. A., Aksan, N., Essex, M. J., and Goldsmith, H. H. (2011). Deriving childhood temperament measures from emotion-eliciting behavioral episodes: scale construction and initial validation. *Psychol. Assess.* 23, 337–353. doi: 10.1037/a0021746
- Goldsmith, H. H., and Rothbart, M. K. (1996). Prelocomotor and locomotor Laboratory Temperament Assessment Battery (Lab-TAB; version 3.0, Technical Manual). *Madison: University of Wisconsin, Department of Psychology.*
- Greimel, E., Nehrkorn, B., Schulte-Rüther, M., Fink, G. R., Nickl-Jockschat, T., Herpertz-Dahlmann, B., et al. (2013). Changes in grey matter development in autism spectrum disorder. *Brain Struct. Funct.* 218, 929–942. doi: 10.1007/s00429-012-0439-9
- Gui, L., Lisowski, R., Faundez, T., Hüppi, P. S., Lazeyras, F., and Kocher, M. (2012). Morphology-driven automatic segmentation of MR images of the neonatal brain. *Med. Image Anal.* 16, 1565–1579. doi: 10.1016/j.media.2012.07.006
- Guo, X., Chen, C., Chen, K., Jin, Z., Peng, D., and Yao, L. (2007). Brain development in Chinese children and adolescents: a structural MRI study. *Neuroreport* 18, 875–880. doi: 10.1097/wnr.0b013e328152777e
- Hariri, A. R., Mattay, V. S., Tessitore, A., Fera, F., and Weinberger, D. R. (2003). Neocortical modulation of the amygdala response to fearful stimuli. *Biol. Psychiatry* 53, 494–501. doi: 10.1016/s0006-3223(02)01786-9
- Hughes, M. B., Shults, J., Mcgrath, J., and Medoff-Cooper, B. (2002). Temperament characteristics of premature infants in the first year of life. *J. Dev. Behav. Pediatr.* 23, 430–435. doi: 10.1097/00004703-200212000-00006
- Humphrey, T. (1968). The development of the human amygdala during early embryonic life. *J. Comp. Neurol.* 132, 135–165. doi: 10.1002/cne.901320108
- Hüppi, P. S., Maier, S. E., Peled, S., Zientara, G. P., Barnes, P. D., Jolesz, F. A., et al. (1998). Microstructural development of human newborn cerebral white matter assessed *in vivo* by diffusion tensor magnetic resonance imaging. *Pediatr. Res.* 44, 584–590. doi: 10.1203/00006450-199810000-00019
- Inder, T. E., Warfield, S. K., Wang, H., Hüppi, P. S., and Volpe, J. J. (2005). Abnormal cerebral structure is present at term in premature infants. *Pediatrics* 115, 286–294. doi: 10.1542/peds.2004-0326
- Johnson, S., and Marlow, N. (2011). Preterm birth and childhood psychiatric disorders. *Pediatr. Res.* 69, 11R–18R. doi: 10.1203/pdr.0b013e318212faa0
- Kalin, N. H., Shelton, S. E., Davidson, R. J., and Kelley, A. E. (2001). The primate amygdala mediates acute fear but not the behavioral and physiological components of anxious temperament. *J. Neurosci.* 21, 2067–2074.
- Kwon, S. H., Vasung, L., Ment, L. R., and Hüppi, P. S. (2014). The role of neuroimaging in predicting neurodevelopmental outcomes of preterm neonates. *Clin. Perinatol.* 41, 257–283. doi: 10.1016/j.clp.2013.10.003
- LaBar, K. S., Gatenby, J. C., Gore, J. C., Ledoux, J. E., and Phelps, E. A. (1998). Human amygdala activation during conditioned fear acquisition and extinction: a mixed-trial fMRI study. *Neuron* 20, 937–945. doi: 10.1016/s0896-6273(00)80475-4
- Langerod, N., Van Hanswijck De Jonge, L., Bickle Graz, M., Hüppi, P. S., Borradori-Tolsa, C., and Barisnikov, K. (2013). Emotional reactivity at 12 months in very preterm infants born at <29 weeks of gestation. *Infant Behav. Dev.* 36, 289–297. doi: 10.1016/j.infbeh.2013.02.006
- Lanteaume, L., Khalfa, S., Régis, J., Marquis, P., Chauvel, P., and Bartolomei, F. (2007). Emotion induction after direct intracerebral stimulations of human amygdala. *Cereb. Cortex* 17, 1307–1313. doi: 10.1093/cercor/bhl041
- Larroque, B., Breart, G., Kaminski, M., Dehan, M., Andre, M., Burguet, A., et al. (2004). Survival of very preterm infants: Epipage, a population based cohort study. *Arch. Dis. Child. Fetal. Neonatal. Ed.* 89, F139–F144. doi: 10.1136/adc.2002.020396
- Leppänen, J. M., and Nelson, C. A. (2012). Early development of fear processing. *Curr. Dir. Psychol. Sci.* 21, 200–204. doi: 10.1177/0963721411435841
- Ment, L. R., Hirtz, D., and Hüppi, P. S. (2009). Imaging biomarkers of outcome in the developing preterm brain. *Lancet Neurol.* 8, 1042–1055. doi: 10.1016/s1474-4422(09)70257-1
- Morris, J. S., Frith, C. D., Perrett, D. I., Rowland, D., Young, A. W., Calder, A. J., et al. (1996). A differential neural response in the human amygdala to fearful and happy facial expressions. *Nature* 383, 812–815.
- Müller, F., and O'Rahilly, R. (2006). The amygdaloid complex and the medial and lateral ventricular eminences in staged human embryos. *J. Anat.* 208, 547–564. doi: 10.1111/j.1469-7580.2006.00553.x
- Nikolić, I., and Kostović, I. (1986). Development of the lateral amygdaloid nucleus in the human fetus: transient presence of discrete cytoarchitectonic units. *Anat. Embryol.* 174, 355–360. doi: 10.1007/bf00698785
- Østby, Y., Tamnes, C. K., Fjell, A. M., Westlye, L. T., Due-Tønnessen, P., and Walhovd, K. B. (2009). Heterogeneity in subcortical brain development: a structural magnetic resonance imaging study of brain maturation from 8 to 30 years. *J. Neurosci.* 29, 11772–11782. doi: 10.1523/jneurosci.1242-09.2009
- Paxinos, G., and Mai, J. K. (2004). *The Human Nervous System.* (Cambridge: Academic Press).
- Peterson, B. S., Vohr, B., Staib, L. H., Cannistraci, C. J., Dolberg, A., Schneider, K. C., et al. (2000). Regional brain volume abnormalities and long-term cognitive outcome in preterm infants. *JAMA* 284, 1939–1947. doi: 10.1001/jama.284.15.1939
- Prather, M., Lavenex, P., Mauldin-Jourdain, M., Mason, W., Capitanio, J., Mendoza, S., et al. (2001). Increased social fear and decreased fear of objects in monkeys with neonatal amygdala lesions. *Neurosci.* 106, 653–658. doi: 10.1016/s0306-4522(01)00445-6
- Rogers, C. E., Barch, D. M., Sylvester, C. M., Pagliaccio, D., Harms, M. P., Botteron, K. N., et al. (2014). Altered gray matter volume and school age anxiety in children born late preterm. *J. Pediatr.* 165, 928–935. doi: 10.1016/j.jpeds.2014.06.063
- Rutherford, M. A. (2002). *MRI of the Neonatal Brain.* (Philadelphia, PA: WB Saunders Co.).
- Schmahmann, J. D., and Pandya, D. (2009). *Fiber Pathways of The Brain.* (New York, NY: Oxford University Press)
- Schumann, C. M., and Amaral, D. G. (2006). Stereological analysis of amygdala neuron number in autism. *J. Neurosci.* 26, 7674–7679. doi: 10.1523/jneurosci.1285-06.2006
- Spittle, A. J., Treyvaud, K., Doyle, L. W., Roberts, G., Lee, K. J., Inder, T. E., et al. (2009). Early emergence of behavior and social-emotional problems in very preterm infants. *J. Am. Acad. Child Adolesc. Psychiatry* 48, 909–918. doi: 10.1097/chi.0b013e3181af8235
- Swanson, L. W., and Petrovich, G. D. (1998). What is the amygdala?. *Trends Neurosci.* 21, 323–331.
- ten Donkelaar, H. J. (2015). Development of the basal ganglia and the basal forebrain introduction to anatomy and physiology. *Brain Mapp.* 2, 357–365. doi: 10.1016/B978-0-12-397025-1.00236-0
- Tottenham, N., and Sheridan, M. A. (2010). A review of adversity, the amygdala and the hippocampus: a consideration of developmental timing. *Front. Hum. Neurosci.* 3: 68. doi: 10.3389/fnhum.09.068.2009
- Tottenham, N., Hare, T. A., and Casey, B. (2009). *A Developmental Perspective on Human Amygdala Function.* (New York, NY: Guilford Press).
- Treyvaud, K., Doyle, L. W., Lee, K. J., Roberts, G., Lim, J., Inder, T. E., et al. (2012). Social-emotional difficulties in very preterm and term 2 year olds predict specific social-emotional problems at the age of 5 years. *J. Pediatr. Psychol.* 37, 779–785. doi: 10.1093/jpepsy/jss042
- Uematsu, A., Matsui, M., Tanaka, C., Takahashi, T., Noguchi, K., Suzuki, M., et al. (2012). Developmental trajectories of amygdala and hippocampus from infancy to early adulthood in healthy individuals. *PLoS One* 7:e46970. doi: 10.1371/journal.pone.0046970
- Ulfing, N., Setzer, M., and Bohl, J. (1998). Transient architectonic features in the basolateral amygdala of the human fetal brain. *Acta. Anat. Basel.* 163, 99–112. doi: 10.1159/000046489

- Ulfing, N., Setzer, M., and Bohl, J. (2003). Ontogeny of the human amygdala. *Ann. N. Y. Acad. Sci.* 985, 22–33. doi: 10.1111/j.1749-6632.2003.tb07068.x
- Vasung, L., Čuljat, M., Radoš, M., Pogledić, I., Radoš, M. and Kostović, I. (2008). “Development of human amygdala; correlation of *in vitro* MRI and histology,” in *6th FENS Forum of European Neuroscience*. (Geneva: Federation of European Neuroscience Societies).
- Vasung, L., Huang, H., Jovanov-Milošević, N., Pletikos, M., Mori, S., and Kostović, I. (2010a). Development of axonal pathways in the human fetal fronto-limbic brain: histochemical characterization and diffusion tensor imaging. *J. Anat.* 217, 400–417. doi: 10.1111/j.1469-7580.2010.01260.x
- Vasung, L., Huang, H., Jovanov-Milošević, N., Pletikos, M., Mori, S., and Kostović, I. (2010b). Development of axonal pathways in the human fetal fronto-limbic brain: histochemical characterization and diffusion tensor imaging. *J. Anat.* 217, 400–417. doi: 10.1111/j.1469-7580.2010.01260.x
- Voigt, M., Fusch, C., Olbertz, D., Hartmann, K., Rochow, N., Renken, C., et al. (2006). Analyse des Neugeborenenkollektivs der Bundesrepublik Deutschland 12. Mitteilung: Vorstellung engmaschiger Perzentilwerte (-kurven) für die Körpermaße Neugeborener. *Geburtshilfe Frauenheilkd.* 66, 956–970. doi: 10.1055/s-2006-924458
- Witt, A., Theurel, A., Tolsa, C. B., Lejeune, F., Fernandes, L., De Jonge, L. V. H., et al. (2014). Emotional and effortful control abilities in 42-month-old very preterm and full-term children. *Early Hum. Dev.* 90, 565–569. doi: 10.1016/j.earlhumdev.2014.07.008
- World Health Organization. (2012). “Born too soon: the global action report on preterm birth,” in *World Health Organization Report*. (Geneva: World Health Organization), 126.

Conflict of Interest Statement: The authors declare that the research was conducted in the absence of any commercial or financial relationships that could be construed as a potential conflict of interest.

Copyright © 2016 Cismaru, Gui, Vasung, Lejeune, Barisnikov, Truttmann, Borradori Tolsa and Hüppi. This is an open-access article distributed under the terms of the Creative Commons Attribution License (CC BY). The use, distribution and reproduction in other forums is permitted, provided the original author(s) or licensor are credited and that the original publication in this journal is cited, in accordance with accepted academic practice. No use, distribution or reproduction is permitted which does not comply with these terms.



Toward Developmental Connectomics of the Human Brain

Miao Cao¹, Hao Huang^{2,3}, Yun Peng⁴, Qi Dong¹ and Yong He^{1*}

¹ State Key Laboratory of Cognitive Neuroscience and Learning and International Data Group/McGovern Institute for Brain Research, Beijing Normal University, Beijing, China, ² Department of Radiology, Children's Hospital of Philadelphia, Philadelphia, PA, USA, ³ Department of Radiology, Perelman School of Medicine, University of Pennsylvania, Philadelphia, PA, USA, ⁴ Department of Radiology, Beijing Children's Hospital Affiliated to Capital Medical University, Beijing, China

Imaging connectomics based on graph theory has become an effective and unique methodological framework for studying structural and functional connectivity patterns of the developing brain. Normal brain development is characterized by continuous and significant network evolution throughout infancy, childhood, and adolescence, following specific maturational patterns. Disruption of these normal changes is associated with neuropsychiatric developmental disorders, such as autism spectrum disorders or attention-deficit hyperactivity disorder. In this review, we focused on the recent progresses regarding typical and atypical development of human brain networks from birth to early adulthood, using a connectomic approach. Specifically, by the time of birth, structural networks already exhibit adult-like organization, with global efficient small-world and modular structures, as well as hub regions and rich-clubs acting as communication backbones. During development, the structure networks are fine-tuned, with increased global integration and robustness and decreased local segregation, as well as the strengthening of the hubs. In parallel, functional networks undergo more dramatic changes during maturation, with both increased integration and segregation during development, as brain hubs shift from primary regions to high order functioning regions, and the organization of modules transitions from a local anatomical emphasis to a more distributed architecture. These findings suggest that structural networks develop earlier than functional networks; meanwhile functional networks demonstrate more dramatic maturational changes with the evolution of structural networks serving as the anatomical backbone. In this review, we also highlighted topologically disorganized characteristics in structural and functional brain networks in several major developmental neuropsychiatric disorders (e.g., autism spectrum disorders, attention-deficit hyperactivity disorder and developmental dyslexia). Collectively, we showed that delineation of the brain network from a connectomics perspective offers a unique and refreshing view of both normal development and neuropsychiatric disorders.

OPEN ACCESS

Edited by:

James A. Bourne,
Australian Regenerative Medicine
Institute, Australia

Reviewed by:

Lidia Alonso-Nanclares,
Universidad Politécnica de Madrid,
Spain

Zhengyi Yang,
The University of Queensland,
Australia

*Correspondence:

Yong He
yong.he@bnu.edu.cn

Received: 06 December 2015

Accepted: 29 February 2016

Published: 31 March 2016

Citation:

Cao M, Huang H, Peng Y, Dong Q and
He Y (2016) Toward Developmental
Connectomics of the Human Brain.
Front. Neuroanat. 10:25.
doi: 10.3389/fnana.2016.00025

Keywords: connectomics, network, hub, rich club, brain development, ADHD, autism, dyslexia

INTRODUCTION

Brain development is characterized by complicated microstructural and macrostructural processes that span from the appearance of the first neurons to the establishment of the fully functioning adult brain. Revealing these complicated processes is important to understanding the formation of neural circuits and brain functions. Previous developmental hypotheses were mostly summarized from

behavior or neuron perspectives, such as “Hebbian learning” (Hebb, 1949) or the “orthogenetic principle” (Werner, 1957; Sameroff, 2010), which are still in need of neurobiological evidence. With the recent advancement of non-invasive neuroimaging techniques and their applications to the pediatric population, comprehensive macroscopic brain structure and activity can be readily accessed in children *in vivo*. Studies employing advanced imaging techniques have revealed that regional structure and function develop according to specific principles, with a well-known example being that the regions responsible for higher-level cognition are the last to fully mature (Tau and Peterson, 2010; Dennis and Thompson, 2013a; Dehaene-Lambertz and Spelke, 2015).

Imaging connectomics, which evaluates the inter-regional structural and functional connectivity patterns among regions, has opened new avenues toward understanding the organization and function of the human brain (Sporns et al., 2005; Biswal et al., 2010; Sporns, 2011). The brain is believed to support global and local information communication through an integrative network (Bullmore and Sporns, 2009, 2012). With the establishment of the NIH Human Connectome Project, the importance of describing the network and its development trajectory was recently underscored (Van Essen et al., 2013). Using graph theory, recent studies on connectomics have demonstrated a number of nontrivial topological features in adult human brain networks, including their efficient small-world architecture, prominent modular structure, and highly connected and centralized network hubs (He and Evans, 2010; Stam, 2010; Bullmore and Bassett, 2011; van den Heuvel and Sporns, 2013; Berchicci et al., 2015). These brain network properties have been observed to be established as early as birth and exhibit continuous and dramatic maturational changes throughout infancy, childhood and even adolescence (Power et al., 2010; Collin and van den Heuvel, 2013; Dennis and Thompson, 2013b; Menon, 2013; Vertes and Bullmore, 2014).

With a collection of publications on the structural and functional network development, several questions emerge. Do the structural and functional brain networks develop with different maturation patterns? Are the developmental patterns different across age-ranges, such as during infancy and childhood? Do developmental brain disorders exhibit an abnormal developmental profile in brain networks compared with normal populations? In this review, we aimed to shed light on these important questions by collecting information regarding the recent progress in research on typical and atypical development of human brain networks from birth to early adulthood, focusing specifically on studies using advanced neuroimaging techniques and graph theoretical approaches. First, we introduce basic concepts about imaging connectomics, with a particular emphasis on graph-based network analysis approaches. Second, we discuss the recent findings on the healthy development of brain connectomes with different imaging modalities, concerning the developmental changes of topological properties. Third, we briefly mention abnormal network development in neuropsychiatric disorders [e.g., attention-deficit hyperactivity disorder (ADHD), autism spectrum disorder (ASD), and developmental dyslexia].

Finally, we discuss the limitations and future considerations of brain network development using imaging connectomics approaches.

BRAIN CONNECTOME AND GRAPH THEORY

Brain Connectome Construction

In graph theory, a network can mathematically be modeled as a graph with a set of discrete elements (nodes or vertices) and their mutual relationships (edges or links), which can be summarized in the form of a connection matrix. In the context of brain networks, nodes usually represent imaging voxels, regions of interest, or sensors, whereas links represent structural, morphological or functional connections, depending on the imaging modality considered (Bullmore and Sporns, 2009, 2012; He and Evans, 2010). In particular, structural connectivity can be obtained by reconstructing diffusion MRI (dMRI)-traced white matter projections (Mori and van Zijl, 2002; Hagmann et al., 2007; Gong et al., 2009) or through computing the covariance of brain morphological features among regions (e.g., gray matter volume or cortical thickness) derived from structural MRI (sMRI) data (Lerch et al., 2006; He et al., 2007). Functional connectivity can be measured by examining synchronous neural activity over the distributed brain areas with functional MRI (fMRI), electroencephalography/magnetoencephalography (EEG/MEG), or functional near-infrared spectroscopy (fNIRS; Friston, 1994; Micheloyannis et al., 2006; Niu and He, 2014). Once network nodes and connections are defined, a brain network can be obtained and further classified as directed or undirected, based on whether the edges have a sense of direction, and as unweighted (binary) or weighted, based on whether the edges in the graph have strength information. The present review focuses on the undirected binary or weighted brain networks. Notably, to avoid confusion, we used structural connectivity networks to refer to those constructed with white matter tracts and structural covariance networks for the morphological covariance based ones. Below, we briefly introduce several key graph theory metrics for network descriptions. For more details, see (Rubinov and Sporns, 2010; Stam, 2010; Bullmore and Bassett, 2011).

Segregated and Integrated Network Measures

Segregation and integration represent crucial information processing patterns of the brain, which ensure functional specialization and efficient global communication (Rubinov and Sporns, 2010; Sporns, 2013). Specifically, topological segregation (or local clustering) in the brain's information processing refers to the neuronal processing carried out among groups of regions or within modules (i.e., sets of nodes that are highly inter-connected but with relatively fewer connections to the others in different modules; **Figure 1A**). Clustering coefficients and modularity are two related metrics that quantify the features of topological segregation in brain networks. Mathematically, the clustering coefficient is defined by the fraction of the node's neighbors that

TABLE 1 | Overview of studies about structural network development.

	Study	Modality	Subject n: ages	Network type	Node numbers	Connectivity metrics
Infancy	Yap et al., 2011	DTI	39 sub (longitudinal): 2 wk, 1 y, 2 y	S B	78 (AAL template)	Deterministic tractography
	Tymofiyeva et al., 2012	DTI	17 sub: 6 mo	S B	40	Deterministic tractography
	Tymofiyeva et al., 2012	DTI	8 sub: 31.14–39.71 wk 8 sub: 1–14 d; 10 sub: 181–211 d; 7 sub: 24–31 y	S B	100	Deterministic tractography
	Ball et al., 2014	DTI	28 infants: 25–33 PMA 63 infants: 38–44 PMA	S B	100	Deterministic tractography
	van den Heuvel et al., 2015	DWI fMRI	27 infants: 27/1.6 PMA 27 infants: 30.8/0.7 PMA 42 adults: 29/8.0 y	S W	56	Deterministic tractography; Pearson's correlation
	Fan et al., 2011	sMRI	28 infants (longitudinal): 6.1 ± 2.8 wk, 59.3 ± 3.0 wk, 100.7 ± 6.8 wk; 27 adult controls: 24 ± 3 y	S B	90 (AAL template)	Pearson's correlation of the regional gray matter volume
Childhood and adolescence	Hagmann et al., 2010	DTI fMRI	30 sub for anatomical networks: 18 mo–18 y; 14 sub for functional networks: 2–18 y	S W S W	66 241	Deterministic tractography; Pearson's correlation
	Echtermeyer et al., 2011	DTI	9 sub: 12–14 y; 20 sub: 15–17 y; 16 sub: 18–20 y; 8 sub: 21–23 y	S W	414, 813, 1615	Deterministic tractography
	Dennis et al., 2013a	HARDI	47 sub: 12.3 ± 0.18 y; 55 sub: 16.2 ± 0.37 y; 336 sub: 23.6 ± 2.2 y	S B	68	Deterministic tractography
	Dennis et al., 2013b	HARDI	439 sub: 12–30 y	S W	70 (Desikan–Killiany atlas)	Deterministic tractography
	Chen et al., 2013	DTI	36 sub: 6.0–9.7 y 36 sub: 9.8–12.7 y; 36 sub: 12.9–17.5 y; 36 sub: 17.6–21.8 y; 36 sub: 21.9–29.6 y	S W	78 (AAL template)	Deterministic tractography
	Grayson et al., 2014	HARDI fMRI	15 sub: 7–11 y; 14 sub: 24–35 y	S W S W	219	Deterministic tractography; Pearson's correlation
	Lim et al., 2015	DTI	121 sub: 4–40 y	S W	82 (Freesurfer parcellation)	Deterministic tractography
	Huang et al., 2015	DTI	25 neonates: 37–43 wk; 13 toddlers: 1.79–3.12 y; 25 preadolescents: 10.7–13.5 y; 18 adults: 25–44 y	S W	80 (AAL template)	Probabilistic tractography
	Zhao et al., 2015	DTI	113 sub: 9–85 y	S W	1024	Deterministic tractography
	Baker et al., 2015	HARDI	31 sub (longitudinal): 15.58–17.94 y, 17.89–19.96 y	S W	80 (Freesurfer parcellation)	Probabilistic tractography;
	Koenis et al., 2015	DTI	183 sub (longitudinal): 9.9 ± 1.4 y; 12.9 ± 1.4 y	S W	90 (AAL template)	Deterministic tractography
	Wierenga et al., 2015	DTI	85 sub: 7.0–22.6 y; 38 sub: 7.4–22.9 y	S W	68 (Desikan–Killiany template)	Deterministic tractography

(Continued)

TABLE 1 | Continued

Study	Modality	Subject n: ages	Network type	Node numbers	Connectivity metrics
Khundrakpam et al., 2013	sMRI	51 sub: 8.5–11.3 y; 51 sub: 11.4–14.7 y; 51 sub: 14.8–18.3 y	S B	78 (AAL template)	Pearson's correlation of the regional cortical thickness
Alexander-Bloch et al., 2013	sMRI fMRI	108 sub for anatomical network: 11.1–20.0 y;	S W	360	Pearson's correlation of the regional cortical thickness and the change rate of regional cortical thickness; Wavelet correlation
		108 sub (longitudinal) for maturational network:	S W		
		9.0–22.8 y; 32 sub for functional network: 15.21–33.7 y	S W		
Nie et al., 2013	sMRI	445 sub (longitudinal):3–20 y	S B	78 (AAL template)	Pearson's correlation of the regional cortical thickness and cortical folding

Sub, subjects; d, days; wk, weeks; mo, months; y, years; PMA, postmenstrual age; S, symmetric; W, weighted; B, binary; AAL, automatic anatomical labeling.

are also neighbors of each other (Watts and Strogatz, 1998), while the modularity is determined by a single statistic of reflecting the modular structures of a network (Newman, 2006; Blondel et al., 2008). By contrast, integration refers to the efficiency of global information communication or the ability to integrate distributed information in the network, which is usually measured by the characteristic path length of a network, i.e., the average shortest path length between nodes (Figure 1B; Watts and Strogatz, 1998). Here, a path is a unique sequence of edges that connects two nodes with each other, and its length is given by the number of steps (in a binary graph) or the sum of the edge lengths (in a weighted graph), with the shortest one referred to as the shortest path length. Notably, in a complementary form, Latora and Marchiori (2001) also defined the local efficiency of each node, which is similar but not equivalent to its clustering coefficient or fault tolerance, and global efficiency that is inversely proportional to the characteristic path length of the network, thus allowing computation of a finite value for graphs with disconnected nodes.

Based on perspectives of information segregation and integration, networks can be divided into different types, including regular, small-world and random networks. Notably, a small-world structure characterizes an optimized balance between segregation and integration, which is essential for high synchronizability and fast information transmission in a complex network (Watts and Strogatz, 1998; Latora and Marchiori, 2001). A small-world network has both high global and local information transformation capacity, which is characterized as a shorter characteristic path length than a regular network and a greater clustering coefficient than a random network. Quantitatively, a small-world network is examined with the measurements of the normalized characteristic path length, defined as the ratio of the characteristic path length of the brain network to that of matched random networks, and the normalized clustering coefficient, defined as the ratio of the clustering coefficient of the network to that of matched random networks (Watts and Strogatz, 1998). Typically, for small-world networks, the ratio between the normalized characteristic path

length and the normalized clustering coefficient should be $\gg 1$ (Humphries and Prescott, 2005; Achard et al., 2006).

Hubs and Rich-Clubs

In brain networks, nodal regions that are positioned to make strong contributions to global network communication can be identified as network hubs using numerous different graph measures (van den Heuvel and Sporns, 2013). The simplest graph measure used for identifying hubs is degree centrality, which evaluates the number of connections attached to a given node (Figure 1C). Another measurement is betweenness centrality, defined as how many of the shortest paths between all other node pairs in the network pass through a given node, which reflects the ability of information transformation (Freedman, 1977). Nodal efficiency is also a frequently used measurement, which scales the average shortest path length between the given node and all the other nodes in the network (Achard and Bullmore, 2007). Importantly, these high-degree or high-central hubs strongly tend to be densely interconnected and form a rich-club structure in the brain organization (Figure 1C; van den Heuvel and Sporns, 2011). These hubs and rich-clubs are found to play important roles in global information transformation at the expense of relatively higher wiring, running costs, and vulnerability (Bullmore and Sporns, 2012; van den Heuvel et al., 2012; Liang et al., 2013; Tomasi et al., 2013).

TYPICAL DEVELOPMENT OF HEALTHY BRAIN CONNECTOMES

Here, we focused on the development of the human brain connectome during the first two decades of life, in which dramatic brain structure changes happen and complex cognitive functions emerge (Giedd and Rapoport, 2010; Tau and Peterson, 2010). By searching PubMed (<http://www.ncbi.nlm.nih.gov/pubmed>) using the keywords “graph theory,” “small world,” “connectome” and “development” or “maturation,” we selected

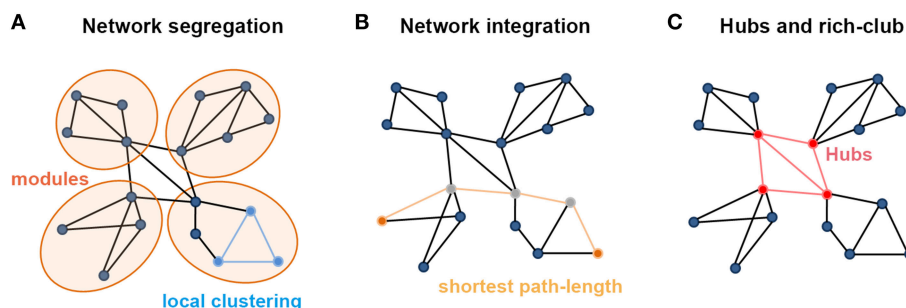


FIGURE 1 | Summary of the main measures with graph theoretical analysis. (A) Metrics regarding the segregation of a network. Local clustering describes the tendency of nodes to form local triangles, providing insight into the local organization of the network. There are four modules in the graph in which connections within modules are much denser than connections between them. (B) Metrics about the integration of a network. The shortest path length describes the minimum number of steps needed to travel between two nodes (dots in yellow) and provides insight into the capacity of the network to communicate between remote regions. (C) The existence of a small set of high-degree nodes with a central position in the network may suggest the existence of hub nodes. High-level connectivity (lines in red) between hub nodes (dots in red) may suggest the existence of a central so-called rich club within the overall network structure.

articles that used graph theory to analyze the brain networks based on MRI, fNIRS and EEG/MEG data. In total, we included 43 papers and discussed the development patterns of topological properties of brain connectomes (Tables 1, 2). According to the literature we reviewed, we found that the development of structural and functional brain connectomes followed distinct changing patterns from infancy to childhood and adolescence periods. Thus, we separately discussed the brain's structural and functional development, with each section proceeding chronologically from infancy (approximately 0–2 years old) to childhood and adolescence (approximately 2–10 years old).

Development of Structural Brain Connectomes

Structural Connectivity Networks

Recent advances in dMRI and tractography methods enable us to noninvasively study human brain structural networks. Specifically, through mapping the local diffusivity of water molecules in brain tissues, dMRI tractography allows us to map structural connectivity by traced white-matter fibers with deterministic or probabilistic tractography methods (Mori et al., 1999; Mori and van Zijl, 2002; Behrens et al., 2007). Whole-brain structural connectivity networks are then constructed by linking distinct regions with detected fiber tracts (Hagmann et al., 2007; Gong et al., 2009).

Infancy

Using dMRI data, many studies have demonstrated that the adult-like topological organization of structural brain networks, such as the small-world, modular, hub, and rich-club structures, is well established by the time of birth (Figures 2A,C; Yap et al., 2011; Tymofiyeva et al., 2012, 2013; Ball et al., 2014; Huang et al., 2015; van den Heuvel et al., 2015). During the first few years of development, the topological structure of the brain structural connectivity networks were reported to exhibit increased global integration with decreased characteristic path length in approximately 6-month-old infants compared with term neonates (Tymofiyeva et al., 2013), increased global

efficiency in 2-years-old toddlers compared with term neonates (Huang et al., 2015), as well as increased fiber length in 1-year-old infants compared with 2-week-old neonates (Yap et al., 2011). In contrast, decreased network segregation properties were reported, with a decreased clustering coefficient and modularity during the first half year (Tymofiyeva et al., 2013), as well as a decreased normalized clustering coefficient and modularity and increased number of modules and connectors in 2-year-old toddlers compared with term neonates (Huang et al., 2015). Moreover, although the degree distribution was found to follow a truncated power law across this period (Yap et al., 2011), which makes the network resilient to attacks, the network robustness to both random and targeted attack was reported to increase with age (Figure 2D; Huang et al., 2015), referring to the continuous refining of brain networks. Behavioral studies found that in half-year-old infants, the characteristic path length of brain structural networks inversely correlates with the neuromotor outcomes (Tymofiyeva et al., 2012).

Regionally, brain hubs were also found to be well-established by the time of birth (Figure 2C). Specifically, the hubs in neonates, calculated with both degree centrality and nodal efficiency, were found to be located in the medial superior parietal lobule and cuneus, which were adult-like, and in lateral regions including the rolandic operculum, Heschl's gyrus and sensorimotor regions, which were infant-specific (Gong et al., 2009; Yap et al., 2011; Huang et al., 2015; van den Heuvel et al., 2015). With development, the nodal efficiency of the medial hubs and fronto-medial regions was found to be significantly increased, whereas that of the regions located laterally decreased with age, until the hub locations in toddlers were highly similar to those in adults (Huang et al., 2015).

Gender differences in babies' brain networks were not detected until they were 2 years old, with females exhibiting higher global efficiency and lower local efficiency than males (Yap et al., 2011). Network asymmetry was already detected in neonates' brains, with an overall higher nodal betweenness in the right brain than the left brain, and this increased with age (Yap et al., 2011). Notably, this study reported increased

TABLE 2 | Overview of studies about functional network development.

	Study	Modality	Subject n: ages	Network type	Node numbers	Connectivity metrics
Infancy	Fransson et al., 2011	fMRI	18 infants: 39 wk and 2 days; 18 sub: 22–41 y	S B	Voxel-wise	Pearson's correlation
	Gao et al., 2011	fMRI	51 neonates: 23 ± 12 d; 50 sub: 13 ± 1 mo; 46 sub: 24 ± 1 mo	S B	90 (AAL template)	Pearson's correlation
	Gao et al., 2014	fMRI	178 sub: 1 mo; 132 sub: 12 mo; 100 sub: 24 mo	S W	Voxel-wise	Pearson's correlation
	Pruett et al., 2015	fMRI	64 sub: 6 mo; 64 sub: 12 mo	S W	230	Pearson's correlation
	Homae et al., 2010	fNIRS	15 sub: 2–11 d; 21 sub: 102–123 d; 16 sub: 180–206 d	S W	47	Pearson's correlation
Childhood and adolescence	Fair et al., 2007	fMRI	49 sub: 7–9 y; 43 sub: 10–15 y; 47 sub: 21–31 y	S W	39	Pearson's correlation
	Fair et al., 2009	fMRI	66 sub: 7–9 y; 53 sub: 10–15 y; 91 sub: 19–31 y	S WB	34	Pearson's correlation
	Supekar et al., 2009	fMRI	23 sub: 7–9 y; 22 sub: 19–22 y	S WB	90 (AAL template)	Wavelet correlation
	Dosenbach et al., 2010	fMRI	238 sub: 7–30 y	S W	160	Pearson's correlation
	Uddin et al., 2011	fMRI DTI	23 children: 7–9 y; 22 adults: 19–22 y	S W D W S W	9	Partial correlation; Granger causality analyses; Diffusion MRI deterministic tractography
	Zuo et al., 2012	fMRI	1003 sub: ~15–40 y	S W	Voxel-wise	Pearson's correlation
	Wang et al., 2012	fMRI	137 sub: 8–79 y	S W	116 (AAL template)	Pearson's correlation
	Hwang et al., 2013	fMRI	28 children: 10–12 y; 41 adolescents: 13–17 y; 30 adults: 18–20 y	S BW	Voxel-wise, 160 (Dosenbach)	Pearson's correlation
	Wu et al., 2013	fMRI	60 sub: 5.7–18.4 y	S B	90 (AAL template)	Pearson's correlation
	Cao et al., 2014b	fMRI	126 sub: 7–85 y	S W	1024, 106 (Dosenbach), 131 (Yeo)	Pearson's correlation
	Betzel et al., 2014	fMRI DTI	126 sub: 7–85 y	S W S W	114 (Yeo)	Pearson's correlation; Diffusion MRI deterministic tractography
	Sato et al., 2014	fMRI	447 sub: 7–15 y	S W	325 (AT325 atlas)	Pearson's correlation
	Sato et al., 2015	fMRI	447 sub: 7–15 y	S W	28	Pearson's correlation
	Qin et al., 2015	fMRI	183 sub: 7–30 y	S W	116 (AAL template)	Pearson's correlation
	Gu et al., 2015a	fMRI	780 sub: 8–22 y	S W	264 (Power)	Wavelet correlation
	Boersma et al., 2011	EEG	227 sub: 5–7 y	S W	14	Synchronization likelihood
	Miskovic et al., 2015	EEG	61 sub: 7 y; 53 sub: 8 y; 52 sub: 9 y; 56 sub: 10 y; 47 sub: 11 y	S W	33	Phase lag index

Sub: subjects; d: days; wk: weeks; mo: months; y: years; S: symmetric; D: directed; W: weighted; B: binary; AAL: automatic anatomical labeling.

local segregation and consistent global integration during early development, which was not consistent with the above-discussed papers (Tymofiyeva et al., 2013; Huang et al., 2015). Specifically, Yap et al. (2011) found that 2-week-old neonates' brain networks exhibit lower local efficiency but similar global efficiency compared with that of 1-year-olds and 2-year-olds, indicating the needs for further studies with larger sample sizes.

Childhood and adolescence

After the first few years, increased integration and decreased segregation were generally found to continue until adulthood (Hagmann et al., 2010; Chen et al., 2013; Dennis et al., 2013b; Huang et al., 2015). Specifically, from 2 years of age to adulthood, human brain structural networks experience the continued increases in global efficiency, nodal strength, number of modules and connectors and decreased local clustering and modularity (Hagmann et al., 2010; Uddin et al., 2011; Chen et al., 2013; Dennis et al., 2013b; Huang et al., 2015; Koenis et al., 2015; Wierenga et al., 2015; Zhao et al., 2015). The numbers of streamlines of fiber tracts, which were short, within modules and within hemispheres, were found to significantly decrease with development (Lim et al., 2015). Moreover, these types of topological changes were found to be highly heritable and significantly correlated with IQ (Koenis et al., 2015).

The location of hubs was found to be relatively consistent across this period, with subtle changes taking places (**Figure 2C**; Hagmann et al., 2010; Chen et al., 2013; Huang et al., 2015). Specifically, relatively strong developmental changes in the intra-lobe connections within the frontal and parietal lobes compared to changes in the temporal and occipital lobes and between subcortical structures were observed (Wierenga et al., 2015). Furthermore, the regions located within the default mode network were found to mature later than other regions (Chen et al., 2013; Zhao et al., 2015). The rich-club organization, which consisted of densely interconnected hubs and comprised the postero-medial core with extensions into the temporo-parietal junction and fronto-medial cortices, was also found to be established in the brains of children and remained stable with development (Hagmann et al., 2010; Chen et al., 2013; Dennis et al., 2013a; Grayson et al., 2014), with subtle connection changes, including decreased correlation within the subcortical hub and increased connections between the frontal and temporal as well the frontal and subcortical hubs (**Figure 2B**; Dennis et al., 2013b; Baker et al., 2015). Network motifs, a specific connectivity pattern, were found to change across ages, but they were significantly affected by template resolution (Echtermeyer et al., 2011). Meanwhile, anatomical measurement of fiber length was found to significantly increase during development (Zhao et al., 2015), with a robust distribution relative to the spatial resolution (Echtermeyer et al., 2011).

Gender differences during this period were reported, which included the earlier streamline losses (Lim et al., 2015) and significantly higher small-worldness and normalized local clustering in females than in males (Dennis et al., 2013b). Brain asymmetry was also found, including inverse development curves between the left and right hemispheres with respect to global efficiency, local clustering, and modularity (Dennis et al., 2013b).

Notably, there were also some inconsistent findings, which are mainly reflected in increased local efficiency during development (Chen et al., 2013; Koenis et al., 2015; Wierenga et al., 2015). Given that both decreased (Lim et al., 2015) and increased fiber streamline counts (Chen et al., 2013) and increased mean fractional anisotropy (Koenis et al., 2015), as well as decreased average apparent diffusion coefficients, diffusivity, and radial diffusivity, were found during development (Hagmann et al., 2010; Wierenga et al., 2015), we inferred that different weighting methods may explain these different results. In an analysis of dMRI data from the same group, Koenis et al. (2015) found that fractional anisotropy weighted networks showed increased local efficiency, whereas fiber number weighted networks showed decreased local efficiency with development.

Taken together, these findings indicate that structural connectivity networks already exhibit adult-like organization at the time of birth and then experience continued increased integration and robustness with development, indicating the refining of brain circuits. Throughout this period, hub locations were relatively consistent in the postero-medial core, with extensions into the temporo-parietal junction and fronto-medial cortices, with fine-tuning in the strengthening of the frontal and temporal hubs, as well as weakening of the subcortical hubs and lateral non-hub regions in the cortex. Notably, increased FA was found to be significantly correlated with the changes in network properties, indicating that the development of network structure is associated with microstructural modifications of white matter, such as synaptogenesis and synaptic and axonal pruning, as well as myelination (Tau and Peterson, 2010; Huang et al., 2015). However, discrepancies between different studies also exist, which may be due to differences in network construction approaches and limited sample sizes.

Structural Covariance Networks

Structural covariance networks are established based on coordinated variations in brain morphology (e.g., gray-matter volume and thickness), which are established by structural MRI, as measures of structural association between regions (Lerch et al., 2006; He et al., 2007).

Infancy

There is only one work conducted by Fan et al. (2011), exploring the structural covariance network development during infancy. They found that the economic small world and modular structure were also established in the structural covariance networks of 1-month-old infants. During early development, from 1 month to 3 years old, network integration consistently enhanced with increased global efficiency, whereas network segregation properties showed inverted U-shape curves, with the modularity and local efficiency of 2-year-olds being higher than those of the brain networks of younger and older participants.

Childhood and adolescence

Khundrakpam et al. (2013) explored the development of structural covariance networks from early childhood to adulthood. Complex topological structure changes were detected: from 4 years to 11 years, network integration

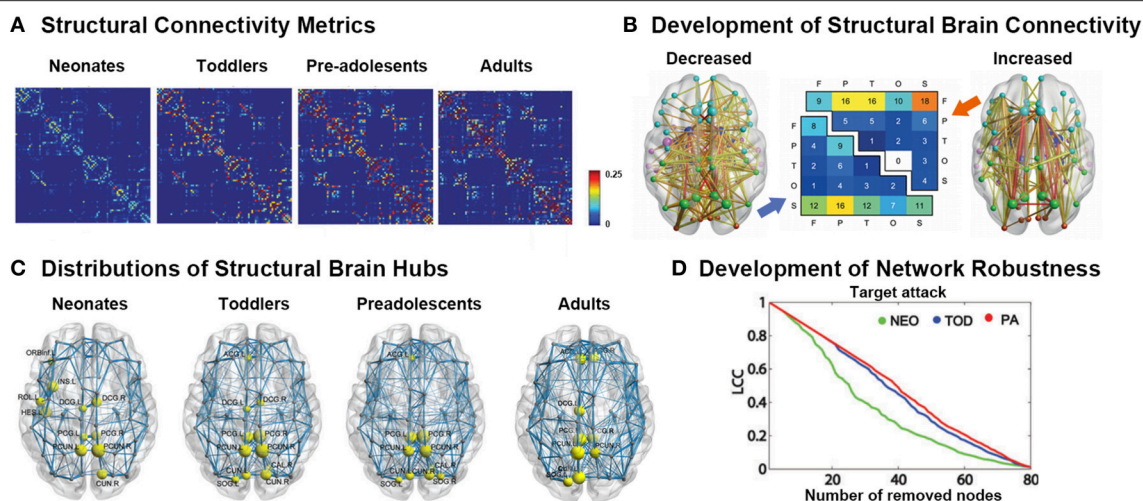


FIGURE 2 | Development of white-matter connectomes. (A) Structural connectivity matrices of the neonates, toddlers, pre-adolescents, and adults group-averaged connectome. Adapted from Huang et al. (2015). **(B)** Late adolescent developmental changes in structural connectivity, with the thickness of each connection weighted by its associated one-tailed *t*-test statistic (FWE corrected, $p < 0.05$). Edge color represents connection type: non-hub to non-hub (yellow), hub to non-hub (orange), and hub to hub (red), with larger nodes corresponding to hub regions. Node color represents the assignment of each region of interest to one of five broad anatomical divisions: frontal (cyan), parietal (lime), temporal (magenta), occipital (orange-red), or subcortical (blue). The center panel illustrates the anatomical distribution of developmental decreases (lower triangular matrix) and increases (upper triangular matrix) in connectivity based on the classification of edges according to the anatomical divisions they interconnected. The values in these matrices represent relative proportions, calculated as the ratio between the frequency of edges linking each pair of divisions and the total number of edges belonging to the two categories. Adapted from Baker et al. (2015). **(C)** Distributions of hub regions in different age groups based on nodal efficiency centrality. PCG, precentral gyrus; PCUN, precuneus; CUN, cuneus; DCG, dorsal cingulate gyrus; INS, insular; ACG, anterior cingulate gyrus; SOG, superior occipital gyrus; ORBinf, inferior frontal gyrus; ROL, rolandic operculum; HES, Heschl's gyrus. Adapted from Huang et al. (2015). **(D)** Topological robustness of the structural networks in each group. The graphs show the AUC of the largest connected component (LCC) as a function of the removed node number by targeted attacks. The brain networks in the preadolescents (red line) were approximately as robust as those in toddlers (blue line) in response to both target failures. However, the neonates (green line) displayed remarkably reduced stability against both targeted attack and random failure compared with the other two groups. Adapted from Huang et al. (2015).

continuously enhanced characterized by increased global efficiency and numbers of connectors, whereas segregation decreased, characterized by decreased local clustering; from 11 years to 15 years, contrasting development curves were found, including decreased global efficiency and numbers of connectors with increased local efficiency; thereafter, the networks became stable until adulthood. However, a longitudinal study of a large sample with 3- to 29-year-old subjects, which employed two correlation calculation methods, the correlation of cortical thickness and cortical curvedness, to construct the brain networks, reported inconsistent findings (Nie et al., 2013). Specifically, the global efficiencies of both types of networks were found to decrease from 3 years old to 7 years old and then increase until approximately 9 years old and then become stable. In contrast, the local efficiency increased from 3 to 7 years old and then decreased with age. The peak age for both developmental curves was ~7 years old, when brain cortical thickness reaches its highest value and cortical folding becomes stable.

Although the network reorganized during the developmental period, the location of hubs was relatively consistent comprising the medial posterior parietal and frontal core and some temporal regions with subtle changes from the language-related regions to the frontal lobes (Fan et al., 2011; Khundrakpam et al., 2013; Nie et al., 2013). Regional analysis also found that the primary regions matured earlier and were well developed by 5 years old, followed by the paralimbic and association regions, which

developed mainly during early to late childhood (~5–11 years old; Khundrakpam et al., 2013).

Recently, one work employed the similarity in maturational curves of cortical thickness between regions in participants ranging from 6 to 12 years old to construct brain structural networks (Alexander-Bloch et al., 2013). They found that the topological properties of these maturational networks exhibit similar topological properties to the structural covariance networks. Furthermore, both the maturational and structural covariance networks could predict the functional networks well. These findings indicate that maturational trajectories may underlie the properties of structural covariance networks, as well as functional networks.

In summary, during development the global topological properties of structural covariance networks undergo complicated changes, which still need further exploration. In contrast, the regional findings were relatively consistent in the hub locations, which were similar to the hubs in structural connectivity networks. The developmental order from primary to high functioning regions was also detected. Notably, the structural covariance connections were previously reported to partly reflect underlying fiber connections but contain exclusive information (Gong et al., 2012). Specifically, graph theoretic analysis reveals that the thickness correlation network has a more randomized overall topology than the structural connectivity network, whereas the regional characteristics in these two

networks are statistically correlated, which may be in agreement with the findings during development.

Development of Functional Brain Connectomes

The functional network in the human brain *in vivo* can be constructed from EEG/MEG, fNIRS, and fMRI data by calculating the temporal correlation between the fluctuations in measured electric, magnetic and blood oxygen level-dependent signal. Specifically, the resting-state functional imaging data measures the endogenous or spontaneous brain activity of subjects who are not performing any specific tasks, which is very suitable for the study of development (Biswal et al., 1995; Stam, 2010; Niu and He, 2013).

Infancy

Studies that employed resting-state fMRI (rsfMRI) have found that typical organizational principles, such as the existence of hubs and small-world structure, were already present by the time of birth (Fransson et al., 2011; Gao et al., 2011). In the first 2 years of life, both the functional network integration and segregation properties were found to significantly increase with age from birth to 1 year of age (Gao et al., 2011). Thereafter, the network efficiency became stable. The robustness of the networks linearly increased with age (Gao et al., 2011). Global and local efficiency in the specific functional network of the sensorimotor system significantly increased from 1 year of age to 2 years of age, which was also reported with MEG data (Berchicci et al., 2015).

Hub regions were also detected in newborn infants. Fransson et al. (2011) found that the functional hub regions in the brains of neonates born ~1 week before were located in primary regions, including sensorimotor cortex, caudate, supplementary motor area, superior temporal cortex, occipital cortex, and lateral and medial prefrontal cortex (**Figure 3A**). Gao et al. (2011) studied hub evolution during the early development. Specifically, they also detected that the regions located in the lateral frontal cortex, caudate, and occipital cortex acted as hubs in newborn neonates. With development, bilateral supplementary motor areas were noted among the hubs in 1-year-old infants. In 2-year-olds, the hub regions moved toward to areas involved in high order cognitive functions, such as the medial superior frontal gyrus (Gao et al., 2011). Notably, they found that the bilateral insula consistently performed as hubs for all three age groups. Moreover, during the first 2 years, the hub regions showed increases in their long-range connections to possess an increasingly more efficient strategy. Inter-subject variability was found to be relatively lower in primary functional areas but higher in association areas during the first 2 years (Gao et al., 2014). Although inter-subject variability in infants was similar to that in adults, specific patterns were still present in infants. Specifically, the medial prefrontal/anterior cingulate, auditory, subcortical and insula regions exhibited lower variability in infants than in adults, which may indicate “skill learning” development (Gao et al., 2014).

Consistent with increasingly efficient communication, connectional analysis found that during the first 6 months, the connections of the temporal, parietal and occipital cortex

significantly increased with age, with the clusters comprising homolog regions formed (Homae et al., 2010). Meanwhile, the homotopic connections of the frontal regions decreased with age, whereas the connections of the frontoposterior regions decreased until ~3 months of age but then increased (Homae et al., 2010). Another study found that the thalamus-sensorimotor and thalamus-salience connectivities were found already formed in neonates, whereas the thalamus-medial visual and thalamus-default mode network connectivity emerged at 1 year of age (Alcauter et al., 2014). Moreover, classification analysis revealed that the functional connectivity could provide critical information to accurately identify infants at high-risk for autism versus infants at low-risk, both in 6-month-old and 12-month-old infants (Pruett et al., 2015).

Childhood and adolescence

After early development, brain functional networks still showed increased segregation with increased local clustering or local efficiency, within-module connectivity, and network hierarchy after 5 years of age (Supekar et al., 2009; Dosenbach et al., 2010; Boersma et al., 2011; Wu et al., 2013; Betzel et al., 2014; Cao et al., 2014b). Notably, increased global efficiency (Miskovic et al., 2015) and long distance connections (Fair et al., 2007, 2009; Supekar et al., 2009; Dosenbach et al., 2010; Cao et al., 2014b), as well as the organization of modules, shifted from a local anatomical emphasis in children to a more distributed architecture in young adults (**Figure 3B**; Fair et al., 2009), indicating an increased global integration process. Taken together, these findings indicated that the functional specification and integration in the brain increased during development. One recent study conducted a modular analysis of the subjects from 8 to 22 years old and found that different systems with diverse roles in whole-brain networks showed different change trajectories with development (Gu et al., 2015a). Specifically, sensorimotor systems and higher order cognitive systems (cognitive control, salience, memory, and attention systems), tending to be cohesive provincial and incohesive connector systems, respectively, all became increasingly segregated from other systems during development. Subcortical and cerebellar systems, tending to be incohesive provincial systems, became increasingly differentiated during development. Uniquely, the default mode system, tending to be a cohesive connector system, was shown to be both increasingly cohesive and increasingly associated with other systems during development.

Hub distributions after 5 years old were found to be stable until adulthood located at the insula, superior visual cortex, postcentral gyrus, thalamus, caudate, and default mode network (DMN), comprising the precuneus/posterior cingulate cortex, angular cortex, superior frontal gyrus, parahippocampal, medial prefrontal cortex, and middle temporal gyrus (Zuo et al., 2012; Hwang et al., 2013; Wu et al., 2013; Cao et al., 2014b). Notably, these hubs intensely interconnected to form the rich-club organization. With development, the normalized rich-club coefficients, i.e., the connectivity between the hub regions, significantly increased (**Figure 3C**; Fair et al., 2008; Uddin et al., 2011; Cao et al., 2014b; Grayson et al., 2014), indicating enhanced communication between hubs. The regional properties of the

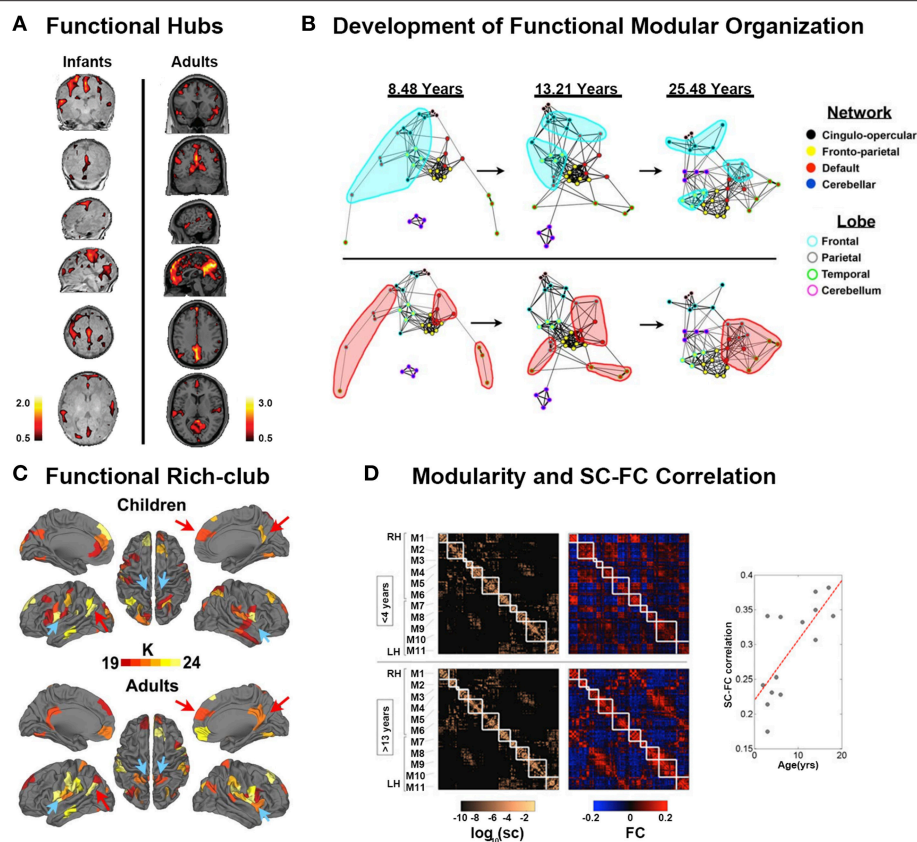


FIGURE 3 | Development of functional connectomes. (A) Distribution of hub regions in the functional networks of infants and adults based on degree centrality. In infants, the majority of cortical hubs were located in the homomodal cortex, mostly in the auditory, visual, and sensorimotor areas, and to a lesser extent in the PFC. Prominent locations for hubs in adults included the precuneus/posterior cingulate cortex, medial PFC, anterior cingulate cortex, bilateral parietal lobule, and bilateral insula. Adapted from Fransson et al. (2011). **(B)** The figure showed the dynamic development of the default network, and cerebellar network using spring embedding. The figure highlights the segregation of local, anatomically clustered regions, and the integration of functional networks over development. Nodes are color coded by their adult network profile (core of the nodes) and by their anatomical location (node outlines). Connections with $r > 0.1$ were considered connected. Adapted from Fair et al. (2009). **(C)** The functional rich-club organizations in children and adults. Although many regions overlap (red arrows, for example), there are bilateral regions that appear only in adults (blue arrows, for example). Adapted from Grayson et al. (2014). **(D)** Modularity and SC-FC correlation. Cortical SC and FC matrices averaged over the younger (<4 years) and older (>13 years) age group. Structural modules are delineated by the superimposed white grid. Eleven modules (M1–M6 in the right hemisphere, M7–M11 in the left hemisphere) were identified, and the two sets of SC and FC matrices are displayed such that modules correspondence across age is maximized. Although modules are highly conserved (normalized mutual information = 0.82), there is a notable increase in SC-FC correspondence from younger to older brains. There is an increasing statistically significant relationship between SC and FC across age ($R = 0.74$, $p < 0.005$). Adapted from Hagmann et al. (2010).

frontal brain regions, superior temporal gyrus, and angular gyrus were found to increase with age, whereas those of the regions related to motor, somatosensory, auditory, and visual functions, as well as the bilateral precuneus and subcortical regions decreased with age (Supekar et al., 2009; Dosenbach et al., 2010; Wang et al., 2012; Zuo et al., 2012; Hwang et al., 2013; Wu et al., 2013; Cao et al., 2014b; Sato et al., 2014, 2015). These findings suggested that the regions for high order cognitive functions matured late compared with the primary regions. Moreover, the functional connectivity information could be used to accurately predict brain maturity (Dosenbach et al., 2010; Wang et al., 2012). Interestingly, recent neuroscience studies suggested that resting-state FC may be dynamic and exhibit significant spontaneous fluctuation (Kang et al., 2011; Hutchison et al., 2013). The spontaneous fluctuations of resting-state functional

connectivity, which significantly increased with age, could be used to accurately predict brain age (Qin et al., 2015). Notably, the correlations between structural and functional connectivity showed an increasing trend with age (Figure 3D; Hagmann et al., 2010; van den Heuvel et al., 2015). In particular, the functional connectivity without direct structural connections was primarily strengthened with development (Betzel et al., 2014).

Gender effects explorations found that girls exhibited higher local clustering than boys (Boersma et al., 2011; Wu et al., 2013), whereas boys showed higher global efficiency than girls (Wu et al., 2013). Regional differences in gender were found in the DMN, language, sensorimotor, and the visual systems, which may indicate cognitive differences between females and males in visuospatial, language and emotion processing (Zuo et al., 2012; Wu et al., 2013). IQ was found to be significantly

correlated with regional properties in the frontal, parietal and temporal lobes (Wu et al., 2013; Santarnecchi et al., 2014), which was consistent with the parieto-frontal integration theory of the integrative roles of these regions. However, inconsistent findings were also reported, including stable (Wu et al., 2013) or decreased global efficiency (Boersma et al., 2011; Cao et al., 2014b) and decreased modularity (Cao et al., 2014b; Miskovic et al., 2015) during development. Notably, functional networks were relatively sensitive to the choice of template, ways of computing correlations and methods for determining the threshold of the network (Wang et al., 2009a; Liang et al., 2012). All of these factors may account for the inconsistent findings. Further studies are still urgently needed to elucidate this problem.

In summary, the functional networks experienced more dramatic reorganization during development than the structural ones. Both increased information integration and segregation continuously progressed since birth. The hub locations were moved from the primary regions to those involving high-order cognitive functions as the organization of modules shifted from a local anatomical emphasis to a more distributed architecture. Moreover, the physiological bases including blood supply and glucose metabolism of functional network properties in both infants and adults and modulation in response to task demands were also detected (Chugani, 1998; Liang et al., 2013; Tomasi et al., 2013). Therefore, we inferred that functional networks matured with both the underlying structural networks and environment-driving training to meet cognitive challenges at different stages of life.

ATYPICAL DEVELOPMENT OF BRAIN CONNECTOMES IN NEUROPSYCHIATRIC DISORDERS

In this part, we briefly introduce the findings regarding abnormal brain networks in neurodevelopment disorders (ADHD, ASD and dyslexia) using imaging connectomics.

ADHD is one of the most common neurodevelopment disorders in childhood, with core symptoms of inattention, hyperactivity and impulsivity (American Psychiatric Association. DSM-5 Task Force, 2013). Convergent evidence suggested that children with ADHD had abnormal small-world properties in both functional and structural brain networks characterized by higher local clustering and lower global integrity, indicating a disorder-related regular shift in organizational properties (**Figure 4A**; Wang et al., 2009b; Ahmadi et al., 2012a,b; Cao et al., 2013). Regional and connectional alterations were found to be mainly involved in the default-mode, attention, sensorimotor, and subcortical systems (**Figure 4A**; Fair et al., 2010, 2013; Colby et al., 2012; Tomasi and Volkow, 2012; Di Martino et al., 2013; Sripada C. et al., 2014a). Specifically, the two primary symptoms of ADHD were found to be correlated with different connectivity changing patterns. Decreased connectivity in prefrontal-dominant circuitry and increased connectivity in orbitofrontal-striatal circuitry correlated with behavioral scores of inattention and hyperactivity/impulsivity symptoms, respectively (**Figure 4A**; Tomasi and Volkow, 2012; Cao et al.,

2013; Fair et al., 2013). Notably, a developmental perspective has recently been increasingly noted in the research of psychiatric disorders (Di Martino et al., 2014). For ADHD, a delayed developmental model has been proposed (Fair et al., 2010; Cao et al., 2014a). Specific maturational lag in functional connections within the DMN and in DMN interconnections with the frontoparietal network and ventral attention network were detected (Sripada C. S. et al., 2014b). Further studies are still in needed to test the hypothesis from the connectomic perspective using both multimodality data and whole-brain topological analysis.

ASD manifests early in development and is characterized by deficits in social interaction and communication, as well as stereotyped and repetitive behaviors and restricted interests in domains of activities (American Psychiatric Association. DSM-5 Task Force, 2013). The findings about alterations in global topological architecture in ASD were inconsistent. Whereas the topological properties of functional networks were found to exhibit a randomized tendency of decreased segregation, both decreased and increased local clustering were found in the structural networks of ASD patients (Rudie et al., 2012; Jakab et al., 2013; Li et al., 2014; Valk et al., 2015). In contrast, the regional findings suggested the disruption of both functional and structural hubs in ASD (**Figure 4B**; Di Martino et al., 2013; Crossley et al., 2014; Eilam-Stock et al., 2014). Connectional analyses show hypoconnectivity in the so-called “social network” encompassing the default mode, attention and executive networks, and hyperconnectivity in limbic regions (**Figure 4B**; Anderson et al., 2011; Gotts et al., 2012; Rudie et al., 2012; Tyszka et al., 2014; Cheng et al., 2015). Specifically, a lack of long-range connections and an increase in short-range connections in ASD patients compared with healthy controls were reported (Khan et al., 2013; Bernhardt et al., 2014; Ameis and Catani, 2015; Kitzbichler et al., 2015). For ASD, an overgrowth developmental hypothesis has been raised (Courchesne et al., 2007; Uddin et al., 2013). Interestingly, a recent DTI study conducted on 2-year-old babies showed significantly disturbed local and global efficiency in high-risk infants diagnosed with ASD, compared with both low- and high-risk infants not diagnosed with ASD, indicating that the abnormality occurred at a very early stage (Lewis et al., 2014).

Developmental dyslexia, also known as reading disorder, is a neurobiological deficit characterized by persistent difficulty in learning to read in children and adults who otherwise possess normal intelligence (American Psychiatric Association. DSM-5 Task Force, 2013). Thus far, the connectomic studies in dyslexia are relatively few with divergent findings. Studies employing sMRI data to explore alterations in Chinese dyslexia found both decreased (Qi et al., 2016) and increased (Liu et al., 2015) local clustering with constant global efficiency in the structural networks compared with healthy participants. Moreover, structural networks of children with familial risk of reading difficulties showed no significant difference in global topological properties compared with healthy controls (Hosseini et al., 2013). Functional networks based on MEG data in dyslexia showed reduced global and local efficiency during both resting and task states compared with healthy controls (Vourkas

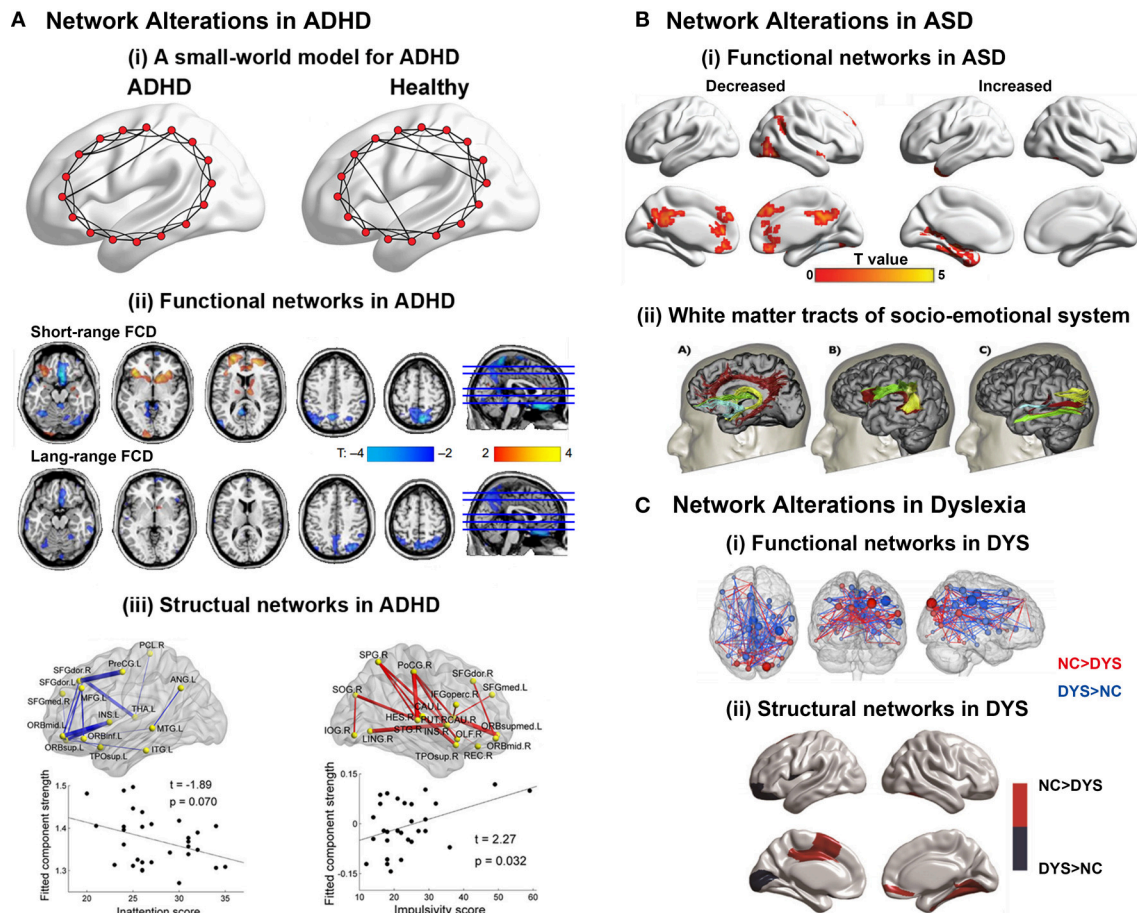
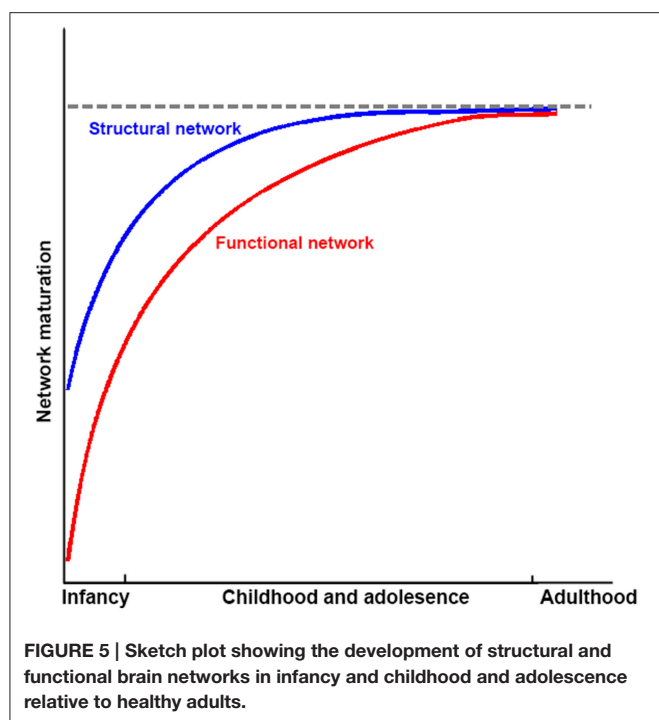


FIGURE 4 | (A) Brain network alterations in ADHD. (i) Small-world models for ADHD and healthy brain networks. The ADHD networks showed a regular tendency compared with healthy controls. Adapted from Cao et al. (2014a). (ii) Decreased or increased functional connectivity density (FCD) in ADHD patients compared with healthy controls. Adapted from Tomasi and Volkow (2012). (iii) Decreased or increased white matter connections in ADHD participants compared with healthy controls and their relationships with the clinical characteristics of the patients. Blue curve: the significantly decreased network-based statistic (NBS) component; red curve: the significantly increased NBS component. Adapted from Cao et al. (2013). **(B)** Brain regions displaying disrupted functional connectivity in autism. (i) Voxels displaying altered functional connectivity in autism. Voxels that displayed weaker functional connectivity in the autistic population than in the controls are shown in blue, and the voxels that displayed stronger functional connectivity in the autistic population are shown in red. The color bar represents the degree of connectivity according to the number of significantly affected edges relating to a given voxel. Adapted from Eilam-Stock et al. (2014). (ii) White matter tracts of the socio-emotional processing system. Left: white matter tracts of the limbic system; middle: white matter tracts linking the mirror neuron system; right: white matter tracts of the face processing system. Adapted from Ameis and Catani (2015). **(C)** Brain network alterations in dyslexia. (i) Whole-brain functional connectivity differences between groups. Three-dimensional representation of healthy controls readers (NC) > dyslexic readers (DYS) and DYS > NC edge components ($p < 0.01$ after NBS correction). Adapted from Finn et al. (2014). (ii) Between-group differences in regional nodal characteristics in cortical thickness networks. Group differences of and nodal degree in cortical thickness networks. Blue represents the brain areas with significantly lower nodal properties in DYS than in NC, whereas red represents the brain areas with significantly higher nodal properties in NC than in DYS. Adapted from Qi et al. (2016).

et al., 2011; Dimitriadis et al., 2013). Regional alterations in both structural and functional networks were reported in the visual cortex for visual information integration and prefrontal areas for attention modulation, as well as the supramarginal gyrus, precentral gyrus, Heschl's gyrus, posterior cingulate, and hippocampus (Figure 4C; Hosseini et al., 2013; Finn et al., 2014; Liu et al., 2015; Valk et al., 2015; Qi et al., 2016). Interestingly, the hub locations in the structural networks of Chinese dyslexia were found to be more bilateral and anterior than those of healthy controls (Qi et al., 2016), which was consistent with the findings

that in functional networks, non-impaired readers have stronger left lateralization for language than dyslexic readers, who rely on bilateral systems (Finn et al., 2014).

Together, many previous studies have shown topological disorganization of brain networks in these neurodevelopmental disorders. In the future, it will be important to compare commonalities and differences in developmental brain networks among these neuropsychiatric disorders. These imaging connectomics studies will be critical for deepening our understanding of developmental mechanisms and to discover



biomarkers for early diagnosis, treatment evaluation, and identification of intervention targets.

CONCLUSION AND FURTHER CONSIDERATIONS

Taken together, structural connectivity networks, structural covariance networks, and functional networks already exhibit an efficient small-world modular structure, with the appearance of hubs at the time of birth. The organizations of structural connectivity networks in infants were somewhat similar to those of adults, with the refining of enhanced network integration with development. In contrast, functional networks in infants showed dramatically different architecture from those in adults, although the critical topological structure was also established. With development, functional networks are reorganized, with both increased segregation and integration as hubs move from primary regions toward high order cognitive regions. These findings suggest that structural connectivity networks may mature earlier than the functional ones (Figure 5). Given that previous studies that employed empirical and simulated data have demonstrated that structural connectivity provides crucial structural substrates underlying the brain's functional connections in adults (Honey et al., 2009; van den Heuvel et al., 2009; Wang et al., 2015), this developmental pattern may reflect preparation for the potential structural constraints of further development of the brain's functional networks. Further studies are needed to verify this hypothesis. The brain networks constructed with structural covariance using sMRI data showed different maturational curves than those of either structural connectivity networks or functional networks.

Specifically, structural covariance networks with sMRI are more complex and seem heavily affected by cortical morphological changes with development. Finally, the literature reviewed here suggests abnormal network development in populations with developmental psychiatric disorders, such as ADHD and ASD.

Although these findings shed light on our understanding of human development at a macroscopic level, some issues and problems still need to be addressed. First, most of the connectome developmental changes were detected based on cross-sectional data; thus, they may be influenced by inter-subject variability and unbalanced cohort distributions. Thus far, only a few studies regarding the structural connectome development have employed longitudinal data, with relatively small sample sizes. Investigations of longitudinal network dynamics with large sample sizes should be undertaken in the future to reveal the nature of developmental changes. Second, it is now commonly accepted that development is conjointly driven by structural maturation of the brain as well as skill learning. However, more evidence is needed to understand when and how genes and the environment influence the human brain, especially the differences between brain systems. Moreover, the underlying physiological bases of behavior performances at different ages remain largely unclear. Further studies employing multimodal data should be conducted to ascertain the genetic/environment-brain-behavior model during development. Third, according to previous discussions, several inconsistencies existed in the findings of connectomes in different imaging modalities, and a significantly increased function-and-structure coherence was observed. Although we summarized this as the earlier maturation of structural networks compared with functional networks (Figure 5), further studies are still needed to explore whether these discrepancies reflect additional biological information or limitations of the analysis or imaging methods. Fourth, some new connectome analysis approaches have been raised recently, such as dynamic connectivity, which more comprehensively describes the brain's dynamic integration, coordination and responses to internal and external stimuli across multiple time scales (Hutchison et al., 2013), and network controllability, which reflects the underlying mechanism of brain transformation between cognitive states (Gu et al., 2015b). Further studies using these methods on brain connectome development would provide additional information. Fifth, novel imaging acquisition protocols emerged recently. For example, multiband fMRI (Feinberg et al., 2010; Moeller et al., 2010) with high sampling rates may provide temporally complementary information about functional integration among brain regions and simultaneously reduce the effects of high frequency physiological noise compared with traditional fMRI with low sampling rates (Liao et al., 2013). Further studies with these new protocols will dramatically increase our knowledge of network development.

AUTHOR CONTRIBUTIONS

MC and YH designed the study; MC, HH and YH wrote this manuscript; YP and QD provided interpretation and revisions of the manuscript.

ACKNOWLEDGMENTS

We thank Mark Graham for careful language editing on the manuscript. This work was supported by the National Key Basic Research Program of China (973 Project, Grant No. 2014CB846102), the Natural Science Foundation of China

(Grant No. 81225012 and 31221003), the 111 Project (Grant No. B07008), National Institute of Health of United States (Grant No: NIH MH092535 and U54HD086984), and the Open Research Fund of the State Key Laboratory of Cognitive Neuroscience and Learning (Grant No. CNLYB1407, YH and HH).

REFERENCES

- Achard, S., and Bullmore, E. (2007). Efficiency and cost of economical brain functional networks. *PLoS Comput. Biol.* 3:e17. doi: 10.1371/journal.pcbi.0030017
- Achard, S., Salvador, R., Whitcher, B., Suckling, J., and Bullmore, E. (2006). A resilient, low-frequency, small-world human brain functional network with highly connected association cortical hubs. *J. Neurosci.* 26, 63–72. doi: 10.1523/JNEUROSCI.3874-05.2006
- Ahmadlou, M., Adeli, H., and Adeli, A. (2012a). Graph theoretical analysis of Organization of functional brain networks in ADHD. *Clin. EEG Neurosci.* 43, 5–13. doi: 10.1177/1550059411428555
- Ahmadlou, M., Rostami, R., and Sadeghi, V. (2012b). Which attention-deficit/hyperactivity disorder children will be improved through neurofeedback therapy? A graph theoretical approach to neocortex neuronal network of ADHD. *Neurosci. Lett.* 516, 156–160. doi: 10.1016/j.neulet.2012.03.087
- Alcauter, S., Lin, W., Smith, J. K., Short, S. J., Goldman, B. D., Reznick, J. S., et al. (2014). Development of thalamocortical connectivity during infancy and its cognitive correlations. *J. Neurosci.* 34, 9067–9075. doi: 10.1523/JNEUROSCI.0796-14.2014
- Alexander-Bloch, A., Raznahan, A., Bullmore, E., and Giedd, J. (2013). The convergence of maturational change and structural covariance in human cortical networks. *J. Neurosci.* 33, 2889–2899. doi: 10.1523/JNEUROSCI.3554-12.2013
- Ameis, S. H., and Catani, M. (2015). Altered white matter connectivity as a neural substrate for social impairment in Autism Spectrum Disorder. *Cortex* 62, 158–181. doi: 10.1016/j.cortex.2014.10.014
- American Psychiatric Association. DSM-5 Task Force (2013). *Diagnostic and Statistical Manual of Mental Disorders DSM-5 in 5th Edn. Online Resource (xlv, 947.)*. (Arlington, VA: American Psychiatric Association).
- Anderson, J. S., Nielsen, J. A., Froehlich, A. L., DuBray, M. B., Druzgal, T. J., Cariello, A. N., et al. (2011). Functional connectivity magnetic resonance imaging classification of autism. *Brain* 134, 3742–3754. doi: 10.1093/brain/awr263
- Baker, S. T., Lubman, D. I., Yucel, M., Allen, N. B., Whittle, S., Fulcher, B. D., et al. (2015). Developmental changes in brain network hub connectivity in late adolescence. *J. Neurosci.* 35, 9078–9087. doi: 10.1523/JNEUROSCI.5043-14.2015
- Ball, G., Aljabar, P., Zebari, S., Tusor, N., Arichi, T., Merchant, N., et al. (2014). Rich-club organization of the newborn human brain. *Proc. Natl. Acad. Sci. U.S.A.* 111, 7456–7461. doi: 10.1073/pnas.1324118111
- Behrens, T. E., Berg, H. J., Jbabdi, S., Rushworth, M. F., and Woolrich, M. W. (2007). Probabilistic diffusion tractography with multiple fibre orientations: what can we gain? *Neuroimage* 34, 144–155. doi: 10.1016/j.neuroimage.2006.09.018
- Berchicci, M., Tamburro, G., and Comani, S. (2015). The intrahemispheric functional properties of the developing sensorimotor cortex are influenced by maturation. *Front. Hum. Neurosci.* 9:39. doi: 10.3389/fnhum.2015.00039
- Bernhardt, B. C., Valk, S. L., Silani, G., Bird, G., Frith, U., and Singer, T. (2014). Selective disruption of sociocognitive structural brain networks in autism and alexithymia. *Cereb. Cortex* 24, 3258–3267. doi: 10.1093/cercor/bht182
- Betz, R. F., Byrge, L., He, Y., Goni, J., Zuo, X. N., and Sporns, O. (2014). Changes in structural and functional connectivity among resting-state networks across the human lifespan. *Neuroimage* 102(Pt 2), 345–357. doi: 10.1016/j.neuroimage.2014.07.067
- Biswal, B., Yetkin, F. Z., Haughton, V. M., and Hyde, J. S. (1995). Functional connectivity in the motor cortex of resting human brain using echo-planar MRI. *Magn. Reson. Med.* 34, 537–541. doi: 10.1002/mrm.1910340409
- Biswal, B. B., Mennes, M., Zuo, X. N., Gohel, S., Kelly, C., Smith, S. M., et al. (2010). Toward discovery science of human brain function. *Proc. Natl. Acad. Sci. U.S.A.* 107, 4734–4739. doi: 10.1073/pnas.0911855107
- Blondel, V. D., Guillaume, J.-L., Lambiotte, R., and Lefebvre, E. (2008). Fast unfolding of communities in large networks. *J. Stat. Mech.* 2008:P10008. doi: 10.1088/1742-5468/2008/10/P10008
- Boersma, M., Smit, D. J., de Bie, H. M., Van Baal, G. C., Boomsma, D. I., de Geus, E. J., et al. (2011). Network analysis of resting state EEG in the developing young brain: structure comes with maturation. *Hum. Brain Mapp.* 32, 413–425. doi: 10.1002/hbm.21030
- Bullmore, E., and Sporns, O. (2009). Complex brain networks: graph theoretical analysis of structural and functional systems. *Nat. Rev. Neurosci.* 10, 186–198. doi: 10.1038/nrn2575
- Bullmore, E., and Sporns, O. (2012). The economy of brain network organization. *Nat. Rev. Neurosci.* 13, 336–349. doi: 10.1038/nrn3214
- Bullmore, E. T., and Bassett, D. S. (2011). Brain graphs: graphical models of the human brain connectome. *Annu. Rev. Clin. Psychol.* 7, 113–140. doi: 10.1146/annurev-clinpsy-040510-143934
- Cao, M., Shu, N., Cao, Q., Wang, Y., and He, Y. (2014a). Imaging functional and structural brain connectomics in attention-deficit/hyperactivity disorder. *Mol. Neurobiol.* 50, 1111–1123. doi: 10.1007/s12035-014-8685-x
- Cao, M., Wang, J. H., Dai, Z. J., Cao, X. Y., Jiang, L. L., Fan, F. M., et al. (2014b). Topological organization of the human brain functional connectome across the lifespan. *Dev. Cogn. Neurosci.* 7, 76–93. doi: 10.1016/j.dcn.2013.11.004
- Cao, Q., Shu, N., An, L., Wang, P., Sun, L., Xia, M. R., et al. (2013). Probabilistic diffusion tractography and graph theory analysis reveal abnormal white matter structural connectivity networks in drug-naïve boys with attention deficit/hyperactivity disorder. *J. Neurosci.* 33, 10676–10687. doi: 10.1523/JNEUROSCI.4793-12.2013
- Chen, Z., Liu, M., Gross, D. W., and Beaulieu, C. (2013). Graph theoretical analysis of developmental patterns of the white matter network. *Front. Hum. Neurosci.* 7:716. doi: 10.3389/fnhum.2013.00716
- Cheng, W., Rolls, E. T., Gu, H., Zhang, J., and Feng, J. (2015). Autism: reduced connectivity between cortical areas involved in face expression, theory of mind, and the sense of self. *Brain* 138, 1382–1393. doi: 10.1093/brain/aww051
- Chugani, H. T. (1998). A critical period of brain development: studies of cerebral glucose utilization with PET. *Prev. Med.* 27, 184–188. doi: 10.1006/pmed.1998.0274
- Colby, J. B., Rudie, J. D., Brown, J. A., Douglas, P. K., Cohen, M. S., and Shehzad, Z. (2012). Insights into multimodal imaging classification of ADHD. *Front. Syst. Neurosci.* 6:59. doi: 10.3389/fnsys.2012.00059
- Collin, G., and van den Heuvel, M. P. (2013). The ontogeny of the human connectome: development and dynamic changes of brain connectivity across the life span. *Neuroscientist* 19, 616–628. doi: 10.1177/1073858413503712
- Courchesne, E., Pierce, K., Schumann, C. M., Redcay, E., Buckwalter, J. A., Kennedy, D. P., et al. (2007). Mapping early brain development in autism. *Neuron* 56, 399–413. doi: 10.1016/j.neuron.2007.10.016
- Crossley, N. A., Mechelli, A., Scott, J., Carletti, F., Fox, P. T., McGuire, P., et al. (2014). The hubs of the human connectome are generally implicated in the anatomy of brain disorders. *Brain* 137, 2382–2395. doi: 10.1093/brain/awu132
- Dehaene-Lambertz, G., and Spelke, E. S. (2015). The infancy of the human brain. *Neuron* 88, 93–109. doi: 10.1016/j.neuron.2015.09.026
- Dennis, E. L., Jahanshad, N., McMahon, K. L., de Zubicaray, G. I., Martin, N. G., Hickie, I. B., et al. (2013b). Development of brain structural connectivity between ages 12 and 30: a 4-Tesla diffusion imaging study in 439 adolescents and adults. *Neuroimage* 64, 671–684. doi: 10.1016/j.neuroimage.2012.09.004
- Dennis, E. L., Jahanshad, N., Toga, A. W., McMahon, K. L., de Zubicaray, G. I., Hickie, I., et al. (2013a). Development of the “Rich Club” in brain connectivity

- networks from 438 adolescents & adults aged 12 to 30. *Proc. IEEE Int. Symp. Biomed. Imaging* 2013, 624–627. doi: 10.1109/ISBI.2013.6556552
- Dennis, E. L., and Thompson, P. M. (2013a). Typical and atypical brain development: a review of neuroimaging studies. *Dialogues Clin. Neurosci.* 15, 359–384.
- Dennis, E. L., and Thompson, P. M. (2013b). Mapping connectivity in the developing brain. *Int. J. Dev. Neurosci.* 31, 525–542. doi: 10.1016/j.ijdevneu.2013.05.007
- Di Martino, A., Fair, D. A., Kelly, C., Satterthwaite, T. D., Castellanos, F. X., Thomason, M. E., et al. (2014). Unraveling the miswired connectome: a developmental perspective. *Neuron* 83, 1335–1353. doi: 10.1016/j.neuron.2014.08.050
- Di Martino, A., Zuo, X. N., Kelly, C., Grzadzinski, R., Mennes, M., Schvarcz, A., et al. (2013). Shared and distinct intrinsic functional network centrality in autism and attention-deficit/hyperactivity disorder. *Biol. Psychiatry* 74, 623–632. doi: 10.1016/j.biopsych.2013.02.011
- Dimitriadis, S. I., Laskaris, N. A., Simos, P. G., Micheloyannis, S., Fletcher, J. M., Rezaie, R., et al. (2013). Altered temporal correlations in resting-state connectivity fluctuations in children with reading difficulties detected via MEG. *Neuroimage* 83, 307–317. doi: 10.1016/j.neuroimage.2013.06.036
- Dosenbach, N. U., Nardos, B., Cohen, A. L., Fair, D. A., Power, J. D., Church, J. A., et al. (2010). Prediction of individual brain maturity using fMRI. *Science* 329, 1358–1361. doi: 10.1126/science.1194144
- Echtermeyer, C., Han, C. E., Rotarska-Jagiela, A., Mohr, H., Uhlhaas, P. J., and Kaiser, M. (2011). Integrating temporal and spatial scales: human structural network motifs across age and region of interest size. *Front. Neuroinform.* 5:10. doi: 10.3389/fninf.2011.00010
- Eilam-Stock, T., Xu, P., Cao, M., Gu, X., Van Dam, N. T., Anagnostou, E., et al. (2014). Abnormal autonomic and associated brain activities during rest in autism spectrum disorder. *Brain* 137, 153–171. doi: 10.1093/brain/awt294
- Fair, D. A., Cohen, A. L., Dosenbach, N. U., Church, J. A., Miezin, F. M., Barch, D. M., et al. (2008). The maturing architecture of the brain's default network. *Proc. Natl. Acad. Sci. U.S.A.* 105, 4028–4032. doi: 10.1073/pnas.0800376105
- Fair, D. A., Cohen, A. L., Power, J. D., Dosenbach, N. U., Church, J. A., Miezin, F. M., et al. (2009). Functional brain networks develop from a “local to distributed” organization. *PLoS Comput. Biol.* 5:e1000381. doi: 10.1371/journal.pcbi.1000381
- Fair, D. A., Dosenbach, N. U., Church, J. A., Cohen, A. L., Brahmbhatt, S., Miezin, F. M., et al. (2007). Development of distinct control networks through segregation and integration. *Proc. Natl. Acad. Sci. U.S.A.* 104, 13507–13512. doi: 10.1073/pnas.0705843104
- Fair, D. A., Nigg, J. T., Iyer, S., Bathula, D., Mills, K. L., Dosenbach, N. U., et al. (2013). Distinct neural signatures detected for ADHD subtypes after controlling for micro-movements in resting state functional connectivity MRI data. *Front. Syst. Neurosci.* 6:80. doi: 10.3389/fnsys.2012.00080
- Fair, D. A., Posner, J., Nagel, B. J., Bathula, D., Dias, T. G., Mills, K. L., et al. (2010). Atypical default network connectivity in youth with attention-deficit/hyperactivity disorder. *Biol. Psychiatry* 68, 1084–1091. doi: 10.1016/j.biopsych.2010.07.003
- Fan, Y., Shi, F., Smith, J. K., Lin, W., Gilmore, J. H., and Shen, D. (2011). Brain anatomical networks in early human brain development. *Neuroimage* 54, 1862–1871. doi: 10.1016/j.neuroimage.2010.07.025
- Feinberg, D. A., Moeller, S., Smith, S. M., Auerbach, E., Ramanna, S., Gunther, M., et al. (2010). Multiplexed echo planar imaging for sub-second whole brain fMRI and fast diffusion imaging. *PLoS ONE* 5:e15710. doi: 10.1371/journal.pone.0015710
- Finn, E. S., Shen, X., Holahan, J. M., Scheinost, D., Lacadie, C., Papademetris, X., et al. (2014). Disruption of functional networks in dyslexia: a whole-brain, data-driven analysis of connectivity. *Biol. Psychiatry* 76, 397–404. doi: 10.1016/j.biopsych.2013.08.031
- Fransson, P., Aden, U., Blennow, M., and Lagercrantz, H. (2011). The functional architecture of the infant brain as revealed by resting-state fMRI. *Cereb. Cortex* 21, 145–154. doi: 10.1093/cercor/bhq071
- Freedman, L. (1977). A set of measures of centrality based on betweenness. *Sociometry* 40, 35–41. doi: 10.2307/3033543
- Friston, K. J. (1994). Functional and effective connectivity in neuroimaging: a synthesis human brain. *Mapping* 2, 56–78. doi: 10.1002/hbm.460020107
- Gao, W., Elton, A., Zhu, H., Alcauter, S., Smith, J. K., Gilmore, J. H., et al. (2014). Intersubject variability of and genetic effects on the brain's functional connectivity during infancy. *J. Neurosci.* 34, 11288–11296. doi: 10.1523/JNEUROSCI.5072-13.2014
- Gao, W., Gilmore, J. H., Giovanello, K. S., Smith, J. K., Shen, D., Zhu, H., et al. (2011). Temporal and spatial evolution of brain network topology during the first two years of life. *PLoS ONE* 6:e25278. doi: 10.1371/journal.pone.0025278
- Giedd, J. N., and Rapoport, J. L. (2010). Structural MRI of pediatric brain development: what have we learned and where are we going? *Neuron* 67, 728–734. doi: 10.1016/j.neuron.2010.08.040
- Gong, G., He, Y., Chen, Z. J., and Evans, A. C. (2012). Convergence and divergence of thickness correlations with diffusion connections across the human cerebral cortex. *Neuroimage* 59, 1239–1248. doi: 10.1016/j.neuroimage.2011.08.017
- Gong, G., He, Y., Concha, L., Lebel, C., Gross, D. W., Evans, A. C., et al. (2009). Mapping anatomical connectivity patterns of human cerebral cortex using *in vivo* diffusion tensor imaging tractography. *Cereb. Cortex* 19, 524–536. doi: 10.1093/cercor/bhn102
- Gotts, S. J., Simmons, W. K., Milbury, L. A., Wallace, G. L., Cox, R. W., and Martin, A. (2012). Fractionation of social brain circuits in autism spectrum disorders. *Brain* 135, 2711–2725. doi: 10.1093/brain/awt160
- Grayson, D. S., Ray, S., Carpenter, S., Iyer, S., Dias, T. G., Stevens, C., et al. (2014). Structural and functional rich club organization of the brain in children and adults. *PLoS ONE* 9:e88297. doi: 10.1371/journal.pone.0088297
- Gu, S., Pasqualetti, F., Cieslak, M., Telesford, Q. K., Yu, A. B., Kahn, A. E., et al. (2015b). Controllability of structural brain networks. *Nat. Commun.* 6, 8414. doi: 10.1038/ncomms9414
- Gu, S., Satterthwaite, T. D., Medaglia, J. D., Yang, M., Gur, R. E., Gur, R. C., et al. (2015a). Emergence of system roles in normative neurodevelopment. *Proc. Natl. Acad. Sci. U.S.A.* 112, 13681–13686. doi: 10.1073/pnas.1502829112
- Hagmann, P., Kurrant, M., Gigandet, X., Thiran, P., Wedeen, V. J., Meuli, R., et al. (2007). Mapping human whole-brain structural networks with diffusion MRI. *PLoS ONE* 2:e597. doi: 10.1371/journal.pone.0000597
- Hagmann, P., Sporns, O., Madan, N., Cammoun, L., Pienaar, R., Wedeen, V. J., et al. (2010). White matter maturation reshapes structural connectivity in the late developing human brain. *Proc. Natl. Acad. Sci. U.S.A.* 107, 19067–19072. doi: 10.1073/pnas.1009073107
- He, Y., Chen, Z. J., and Evans, A. C. (2007). Small-world anatomical networks in the human brain revealed by cortical thickness from MRI. *Cereb. Cortex* 17, 2407–2419. doi: 10.1093/cercor/bhl149
- He, Y., and Evans, A. (2010). Graph theoretical modeling of brain connectivity. *Curr. Opin. Neurol.* 23, 341–350. doi: 10.1097/wco.0b013e32833aa567
- Hebb, D. O. (1949). *Organization of Behavior: A Neuropsychological Theory*. New York, NY: Wiley & Sons.
- Homae, F., Watanabe, H., Otobe, T., Nakano, T., Go, T., Konishi, Y., et al. (2010). Development of global cortical networks in early infancy. *J. Neurosci.* 30, 4877–4882. doi: 10.1523/JNEUROSCI.5618-09.2010
- Honey, C. J., Sporns, O., Cammoun, L., Gigandet, X., Thiran, J. P., Meuli, R., et al. (2009). Predicting human resting-state functional connectivity from structural connectivity. *Proc. Natl. Acad. Sci. U.S.A.* 106, 2035–2040. doi: 10.1073/pnas.0811168106
- Hosseini, S. M., Black, J. M., Soriano, T., Bugescu, N., Martinez, R., Raman, M. M., et al. (2013). Topological properties of large-scale structural brain networks in children with familial risk for reading difficulties. *Neuroimage* 71, 260–274. doi: 10.1016/j.neuroimage.2013.01.013
- Huang, H., Shu, N., Mishra, V., Jeon, T., Chalak, L., Wang, Z. J., et al. (2015). Development of human brain structural networks through infancy and childhood. *Cereb. Cortex* 25, 1389–1404. doi: 10.1093/cercor/bht335
- Humphries, M. D. G. K., and Prescott, T. J. (2005). The brainstem reticular formation is a small world, not scale-free, network. *Proc. R. Soc. Lond. B Biol. Sci.* 273, 503–511. doi: 10.1098/rspb.2005.3354
- Hutchinson, R. M., Womelsdorf, T., Allen, E. A., Bandettini, P. A., Calhoun, V. D., Corbetta, M., et al. (2013). Dynamic functional connectivity: promise, issues, and interpretations. *Neuroimage* 80, 360–378. doi: 10.1016/j.neuroimage.2013.05.079
- Hwang, K., Hallquist, M. N., and Luna, B. (2013). The development of hub architecture in the human functional brain network. *Cereb. Cortex* 23, 2380–2393. doi: 10.1093/cercor/bhs227

- Jakab, A., Emri, M., Spisak, T., Szeman-Nagy, A., Beres, M., Kis, S. A., et al. (2013). Autistic traits in neurotypical adults: correlates of graph theoretical functional network topology and white matter anisotropy patterns. *PLoS ONE* 8:e60982. doi: 10.1371/journal.pone.0060982
- Kang, J., Wang, L., Yan, C., Wang, J., Liang, X., and He, Y. (2011). Characterizing dynamic functional connectivity in the resting brain using variable parameter regression and Kalman filtering approaches. *Neuroimage* 56, 1222–1234. doi: 10.1016/j.neuroimage.2011.03.033
- Khan, S., Gramfort, A., Shetty, N. R., Kitzbichler, M. G., Ganesan, S., Moran, J. M., et al. (2013). Local and long-range functional connectivity is reduced in concert in autism spectrum disorders. *Proc. Natl. Acad. Sci. U.S.A.* 110, 3107–3112. doi: 10.1073/pnas.1214533110
- Khundrakpam, B. S., Reid, A., Brauer, J., Carbonell, F., Lewis, J., Ameis, S., et al. (2013). Developmental changes in organization of structural brain networks. *Cereb. Cortex* 23, 2072–2085. doi: 10.1093/cercor/bhs187
- Kitzbichler, M. G., Khan, S., Ganesan, S., Vangel, M. G., Herbert, M. R., Hamalainen, M. S., et al. (2015). Altered development and multifaceted band-specific abnormalities of resting state networks in autism. *Biol. Psychiatry* 77, 794–804. doi: 10.1016/j.biopsych.2014.05.012
- Koenis, M. M., Brouwer, R. M., van den Heuvel, M. P., Mandl, R. C., van Soelen, I. L., Kahn, R. S., et al. (2015). Development of the brain's structural network efficiency in early adolescence: a longitudinal DTI twin study. *Hum. Brain Mapp.* 36, 4938–4953. doi: 10.1002/hbm.22988
- Latora, V., and Marchiori, M. (2001). Efficient behavior of small-world networks. *Phys. Rev. Lett.* 87:198701. doi: 10.1103/PhysRevLett.87.198701
- Lerch, J. P., Worsley, K., Shaw, W. P., Greenstein, D. K., Lenroot, R. K., Giedd, J., et al. (2006). Mapping anatomical correlations across cerebral cortex (MACACC) using cortical thickness from MRI. *Neuroimage* 31, 993–1003. doi: 10.1016/j.neuroimage.2006.01.042
- Lewis, J. D., Evans, A. C., Pruett, J. R., Botteron, K., Zwaigenbaum, L., Estes, A., et al. (2014). Network inefficiencies in autism spectrum disorder at 24 months. *Transl. Psychiatry* 4:e388. doi: 10.1038/tp.2014.24
- Li, H., Xue, Z., Ellmore, T. M., Frye, R. E., and Wong, S. T. (2014). Network-based analysis reveals stronger local diffusion-based connectivity and different correlations with oral language skills in brains of children with high functioning autism spectrum disorders. *Hum. Brain Mapp.* 35, 396–413. doi: 10.1002/hbm.22185
- Liang, X., Wang, J., Yan, C., Shu, N., Xu, K., Gong, G., et al. (2012). Effects of different correlation metrics and preprocessing factors on small-world brain functional networks: a resting-state functional MRI study. *PLoS ONE* 7:e32766. doi: 10.1371/journal.pone.0032766
- Liang, X., Zou, Q., He, Y., and Yang, Y. (2013). Coupling of functional connectivity and regional cerebral blood flow reveals a physiological basis for network hubs of the human brain. *Proc. Natl. Acad. Sci. U.S.A.* 110, 1929–1934. doi: 10.1073/pnas.1214900110
- Liao, X. H., Xia, M. R., Xu, T., Dai, Z. J., Cao, X. Y., Niu, H. J., et al. (2013). Functional brain hubs and their test-retest reliability: a multiband resting-state functional MRI study. *Neuroimage* 83, 969–982. doi: 10.1016/j.neuroimage.2013.07.058
- Lim, S., Han, C. E., Uhlhaas, P. J., and Kaiser, M. (2015). Preferential detachment during human brain development: age- and sex-specific structural connectivity in diffusion tensor imaging (DTI) data. *Cereb. Cortex* 25, 1477–1489. doi: 10.1093/cercor/bht333
- Liu, K., Shi, L., Chen, F., Waye, M. M., Lim, C. K., Cheng, P. W., et al. (2015). Altered topological organization of brain structural network in Chinese children with developmental dyslexia. *Neurosci. Lett.* 589, 169–175. doi: 10.1016/j.neulet.2015.01.037
- Menon, V. (2013). Developmental pathways to functional brain networks: emerging principles. *Trends Cogn. Sci.* 17, 627–640. doi: 10.1016/j.tics.2013.09.015
- Micheloyannis, S., Pachou, E., Stam, C. J., Vourkas, M., Erimaki, S., and Tsirka, V. (2006). Using graph theoretical analysis of multi channel EEG to evaluate the neural efficiency hypothesis. *Neurosci. Lett.* 402, 273–277. doi: 10.1016/j.neulet.2006.04.006
- Miskovic, V., Ma, X., Chou, C. A., Fan, M., Owens, M., Sayama, H., et al. (2015). Developmental changes in spontaneous electrocortical activity and network organization from early to late childhood. *Neuroimage* 118, 237–247. doi: 10.1016/j.neuroimage.2015.06.013
- Moeller, S., Yacoub, E., Olman, C. A., Auerbach, E., Strupp, J., Harel, N., et al. (2010). Multiband multislice GE-EPI at 7 tesla, with 16-fold acceleration using partial parallel imaging with application to high spatial and temporal whole-brain fMRI. *Magn. Reson. Med.* 63, 1144–1153. doi: 10.1002/mrm.22361
- Mori, S., Crain, B. J., Chacko, V. P., and van Zijl, P. C. (1999). Three-dimensional tracking of axonal projections in the brain by magnetic resonance imaging. *Ann. Neurol.* 45, 265–269.
- Mori, S., and van Zijl, P. C. (2002). Fiber tracking: principles and strategies - a technical review. *NMR Biomed.* 15, 468–480. doi: 10.1002/nbm.781
- Newman, M. E. (2006). Modularity and community structure in networks. *Proc. Natl. Acad. Sci. U.S.A.* 103, 8577–8582. doi: 10.1073/pnas.0601602103
- Nie, J., Li, G., and Shen, D. (2013). Development of cortical anatomical properties from early childhood to early adulthood. *Neuroimage* 76, 216–224. doi: 10.1016/j.neuroimage.2013.03.021
- Niu, H., and He, Y. (2013). Resting-state functional brain connectivity: lessons from functional near-infrared spectroscopy. *Neuroscientist* 20, 173–188. doi: 10.1177/1073858413502707
- Niu, H., and He, Y. (2014). Resting-state functional brain connectivity: lessons from functional near-infrared spectroscopy. *Neuroscientist* 20, 173–188. doi: 10.1177/1073858413502707
- Power, J. D., Fair, D. A., Schlaggar, B. L., and Petersen, S. E. (2010). The development of human functional brain networks. *Neuron* 67, 735–748. doi: 10.1016/j.neuron.2010.08.017
- Pruett, J. R. Jr., Kandala, S., Hoertel, S., Snyder, A. Z., Ellison, J. T., Nishino, T., et al. (2015). Accurate age classification of 6 and 12 month-old infants based on resting-state functional connectivity magnetic resonance imaging data. *Dev. Cogn. Neurosci.* 12, 123–133. doi: 10.1016/j.dcn.2015.01.003
- Qi, T., Gu, B., Ding, G., Gong, G., Lu, C., Peng, D., et al. (2016). More bilateral, more anterior: alterations of brain organization in the large-scale structural network in Chinese dyslexia. *Neuroimage* 124, 63–74. doi: 10.1016/j.neuroimage.2015.09.011
- Qin, J., Chen, S. G., Hu, D., Zeng, L. L., Fan, Y. M., Chen, X. P., et al. (2015). Predicting individual brain maturity using dynamic functional connectivity. *Front. Hum. Neurosci.* 9:418. doi: 10.3389/fnhum.2015.00418
- Rubinov, M., and Sporns, O. (2010). Complex network measures of brain connectivity: uses and interpretations. *Neuroimage* 52, 1059–1069. doi: 10.1016/j.neuroimage.2009.10.003
- Rudie, J. D., Brown, J. A., Beck-Pancer, D., Hernandez, L. M., Dennis, E. L., Thompson, P. M., et al. (2012). Altered functional and structural brain network organization in autism. *Neuroimage Clin.* 2, 79–94. doi: 10.1016/j.nicl.2012.11.006
- Sameroff, A. (2010). A unified theory of development: a dialectic integration of nature and nurture. *Child Dev.* 81, 6–22. doi: 10.1111/j.1467-8624.2009.01378.x
- Santarnecchi, E., Galli, G., Polizzotto, N. R., Rossi, A., and Rossi, S. (2014). Efficiency of weak brain connections support general cognitive functioning. *Hum. Brain Mapp.* 35, 4566–4582. doi: 10.1002/hbm.22495
- Sato, J. R., Salum, G. A., Gadelha, A., Picon, F. A., Pan, P. M., Vieira, G., et al. (2014). Age effects on the default mode and control networks in typically developing children. *J. Psychiatr. Res.* 58, 89–95. doi: 10.1016/j.jpsychires.2014.07.004
- Sato, J. R., Salum, G. A., Gadelha, A., Vieira, G., Zugman, A., Picon, F. A., et al. (2015). Decreased centrality of subcortical regions during the transition to adolescence: a functional connectivity study. *Neuroimage* 104, 44–51. doi: 10.1016/j.neuroimage.2014.09.063
- Sporns, O., Tononi, G., and Kotter, R. (2005). The human connectome: a structural description of the human brain. *PLoS Comput. Biol.* 1:e42. doi: 10.1371/journal.pcbi.0010042
- Sporns, O. (2011). The human connectome: a complex network. *Ann. N.Y. Acad. Sci.* 1224, 109–125. doi: 10.1111/j.1749-6632.2010.05888.x
- Sporns, O. (2013). Network attributes for segregation and integration in the human brain. *Curr. Opin. Neurobiol.* 23, 162–171. doi: 10.1016/j.conb.2012.11.015
- Sripada, C., Kessler, D., Fang, Y., Welsh, R. C., Prem Kumar, K., and Angstadt, M. (2014a). Disrupted network architecture of the resting brain in attention-deficit/hyperactivity disorder. *Hum. Brain Mapp.* 35, 4693–4705. doi: 10.1002/hbm.22504

- Sripada, C. S., Kessler, D., and Angstadt, M. (2014b). Lag in maturation of the brain's intrinsic functional architecture in attention-deficit/hyperactivity disorder. *Proc. Natl. Acad. Sci. U.S.A.* 111, 14259–14264. doi: 10.1073/pnas.1407787111
- Stam, C. J. (2010). Characterization of anatomical and functional connectivity in the brain: a complex networks perspective. *Int. J. Psychophysiol.* 77, 186–194. doi: 10.1016/j.ijpsycho.2010.06.024
- Supekar, K., Musen, M., and Menon, V. (2009). Development of large-scale functional brain networks in children. *PLoS Biol.* 7:e1000157. doi: 10.1371/journal.pbio.1000157
- Tau, G. Z., and Peterson, B. S. (2010). Normal development of brain circuits. *Neuropsychopharmacology* 35, 147–168. doi: 10.1038/npp.2009.115
- Tomasi, D., and Volkow, N. D. (2012). Abnormal functional connectivity in children with attention-deficit/hyperactivity disorder. *Biol. Psychiatry* 71, 443–450. doi: 10.1016/j.biopsych.2011.11.003
- Tomasi, D., Wang, G. J., and Volkow, N. D. (2013). Energetic cost of brain functional connectivity. *Proc. Natl. Acad. Sci. U.S.A.* 110, 13642–13647. doi: 10.1073/pnas.1303346110
- Tymofiyeva, O., Hess, C. P., Ziv, E., Lee, P. N., Glass, H. C., Ferriero, D. M., et al. (2013). A DTI-based template-free cortical connectome study of brain maturation. *PLoS ONE* 8:e63310. doi: 10.1371/journal.pone.0063310
- Tymofiyeva, O., Hess, C. P., Ziv, E., Tian, N., Bonifacio, S. L., McQuillen, P. S., et al. (2012). Towards the “baby connectome”: mapping the structural connectivity of the newborn brain. *PLoS ONE* 7:e31029. doi: 10.1371/journal.pone.0031029
- Tyszka, J. M., Kennedy, D. P., Paul, L. K., and Adolphs, R. (2014). Largely typical patterns of resting-state functional connectivity in high-functioning adults with autism. *Cereb. Cortex* 24, 1894–1905. doi: 10.1093/cercor/bht040
- Uddin, L. Q., Supekar, K., and Menon, V. (2013). Reconceptualizing functional brain connectivity in autism from a developmental perspective. *Front. Hum. Neurosci.* 7:458. doi: 10.3389/fnhum.2013.00458
- Uddin, L. Q., Supekar, K. S., Ryali, S., and Menon, V. (2011). Dynamic reconfiguration of structural and functional connectivity across core neurocognitive brain networks with development. *J. Neurosci.* 31, 18578–18589. doi: 10.1523/JNEUROSCI.4465-11.2011
- Valk, S. L., Di Martino, A., Milham, M. P., and Bernhardt, B. C. (2015). Multicenter mapping of structural network alterations in autism. *Hum. Brain Mapp.* 36, 2364–2373. doi: 10.1002/hbm.22776
- van den Heuvel, M. P., Kahn, R. S., Goni, J., and Sporns, O. (2012). High-cost, high-capacity backbone for global brain communication. *Proc. Natl. Acad. Sci. U.S.A.* 109, 11372–11377. doi: 10.1073/pnas.1203593109
- van den Heuvel, M. P., Kersbergen, K. J., de Reus, M. A., Keunen, K., Kahn, R. S., Groenendaal, F., et al. (2015). The neonatal connectome during preterm brain development. *Cereb. Cortex* 25, 3000–3013. doi: 10.1093/cercor/bhu095
- van den Heuvel, M. P., Mandl, R. C., Kahn, R. S., and Hulshoff Pol, H. E. (2009). Functionally linked resting-state networks reflect the underlying structural connectivity architecture of the human brain. *Hum. Brain Mapp.* 30, 3127–3141. doi: 10.1002/hbm.20737
- van den Heuvel, M. P., and Sporns, O. (2011). Rich-club organization of the human connectome. *J. Neurosci.* 31, 15775–15786. doi: 10.1523/JNEUROSCI.3539-11.2011
- van den Heuvel, M. P., and Sporns, O. (2013). Network hubs in the human brain. *Trends Cogn. Sci.* 17, 683–696. doi: 10.1016/j.tics.2013.09.012
- Van Essen, D. C., Smith, S. M., Barch, D. M., Behrens, T. E., Yacoub, E., Ugurbil, K., et al. (2013). The WU-Minn Human Connectome Project: an overview. *Neuroimage* 80, 62–79. doi: 10.1016/j.neuroimage.2013.05.041
- Vertes, P. E., and Bullmore, E. T. (2014). Annual research review: growth connectomics - the organization and reorganization of brain networks during normal and abnormal development. *J. Child Psychol. Psychiatry* 56, 299–320. doi: 10.1111/jcpp.12365
- Vourkas, M., Micheloyannis, S., Simos, P. G., Rezaie, R., Fletcher, J. M., Cirino, P. T., et al. (2011). Dynamic task-specific brain network connectivity in children with severe reading difficulties. *Neurosci. Lett.* 488, 123–128. doi: 10.1016/j.neulet.2010.11.013
- Wang, J., Wang, L., Zang, Y., Yang, H., Tang, H., Gong, Q., et al. (2009a). Parcellation-dependent small-world brain functional networks: a resting-state fMRI study. *Hum. Brain Mapp.* 30, 1511–1523. doi: 10.1002/hbm.20623
- Wang, L., Su, L., Shen, H., and Hu, D. (2012). Decoding lifespan changes of the human brain using resting-state functional connectivity MRI. *PLoS ONE* 7:e44530. doi: 10.1371/journal.pone.0044530
- Wang, L., Zhu, C., He, Y., Zang, Y., Cao, Q., Zhang, H., et al. (2009b). Altered small-world brain functional networks in children with attention-deficit/hyperactivity disorder. *Hum. Brain Mapp.* 30, 638–649. doi: 10.1002/hbm.20530
- Wang, Z., Dai, Z., Gong, G., Zhou, C., and He, Y. (2015). Understanding structural-functional relationships in the human brain: a large-scale network perspective. *Neuroscientist* 21, 290–305. doi: 10.1177/1073858414537560
- Watts, D. J., and Strogatz, S. H. (1998). Collective dynamics of ‘small-world’ networks. *Nature* 393, 440–442. doi: 10.1038/30918
- Werner, H. (1957). “The concept of development from a comparative and organismic point of view,” in *The Concept of Development*, ed D. B. Harris (Minneapolis, MN: University of Minnesota Press), 78–108.
- Wierenga, L. M., van den Heuvel, M. P., van Dijk, S., Rijks, Y., de Reus, M. A., and Durston, S. (2015). The development of brain network architecture. *Hum. Brain Mapp.* 37, 717–729. doi: 10.1002/hbm.23062
- Wu, K., Taki, Y., Sato, K., Hashizume, H., Sassa, Y., Takeuchi, H., et al. (2013). Topological organization of functional brain networks in healthy children: differences in relation to age, sex, and intelligence. *PLoS ONE* 8:e55347. doi: 10.1371/journal.pone.0055347
- Yap, P. T., Fan, Y., Chen, Y., Gilmore, J. H., Lin, W., and Shen, D. (2011). Development trends of white matter connectivity in the first years of life. *PLoS ONE* 6:e24678. doi: 10.1371/journal.pone.0024678
- Zhao, T., Cao, M., Niu, H., Zuo, X. N., Evans, A., He, Y., et al. (2015). Age-related changes in the topological organization of the white matter structural connectome across the human lifespan. *Hum. Brain Mapp.* 36, 3777–3792. doi: 10.1002/hbm.22877
- Zuo, X. N., Ehmke, R., Mennes, M., Imperati, D., Castellanos, F. X., Sporns, O., et al. (2012). Network centrality in the human functional connectome. *Cereb. Cortex* 22, 1862–1875. doi: 10.1093/cercor/bhr269

Conflict of Interest Statement: The authors declare that the research was conducted in the absence of any commercial or financial relationships that could be construed as a potential conflict of interest.

Copyright © 2016 Cao, Huang, Peng, Dong and He. This is an open-access article distributed under the terms of the Creative Commons Attribution License (CC BY). The use, distribution or reproduction in other forums is permitted, provided the original author(s) or licensor are credited and that the original publication in this journal is cited, in accordance with accepted academic practice. No use, distribution or reproduction is permitted which does not comply with these terms.



Multimodal Diffusion-MRI and MEG Assessment of Auditory and Language System Development in Autism Spectrum Disorder

Jeffrey I. Berman^{1,2*}, James C. Edgar^{1,2}, Lisa Blaskey¹, Emily S. Kushner¹, Susan E. Levy³, Matthew Ku¹, John Dell¹ and Timothy P. L. Roberts^{1,2}

¹ Department of Radiology, Children's Hospital of Philadelphia, Philadelphia, PA, USA, ² Department of Radiology, Perelman School of Medicine, University of Pennsylvania, Philadelphia, PA, USA, ³ Department of Pediatrics, Children's Hospital of Philadelphia, Philadelphia, PA, USA

Background: Auditory processing and language impairments are prominent in children with autism spectrum disorder (ASD). The present study integrated diffusion MR measures of white-matter microstructure and magnetoencephalography (MEG) measures of cortical dynamics to investigate associations between brain structure and function within auditory and language systems in ASD. Based on previous findings, abnormal structure-function relationships in auditory and language systems in ASD were hypothesized.

Methods: Evaluable neuroimaging data was obtained from 44 typically developing (TD) children (mean age 10.4 ± 2.4 years) and 95 children with ASD (mean age 10.2 ± 2.6 years). Diffusion MR tractography was used to delineate and quantitatively assess the auditory radiation and arcuate fasciculus segments of the auditory and language systems. MEG was used to measure (1) superior temporal gyrus auditory evoked M100 latency in response to pure-tone stimuli as an indicator of auditory system conduction velocity, and (2) auditory vowel-contrast mismatch field (MMF) latency as a passive probe of early linguistic processes.

Results: Atypical development of white matter and cortical function, along with atypical lateralization, were present in ASD. In both auditory and language systems, white matter integrity and cortical electrophysiology were found to be coupled in typically developing children, with white matter microstructural features contributing significantly to electrophysiological response latencies. However, in ASD, we observed uncoupled structure-function relationships in both auditory and language systems. Regression analyses in ASD indicated that factors other than white-matter microstructure additionally contribute to the latency of neural evoked responses and ultimately behavior. Results also indicated that whereas delayed M100 is a marker for ASD severity, MMF delay is more associated with language impairment.

Conclusion: Present findings suggest atypical development of primary auditory as well as auditory language systems in ASD. Findings demonstrate the need for additional multimodal studies to better characterize the different structural features (white matter,

OPEN ACCESS

Edited by:

Ricardo Insausti,
University of Castilla-la Mancha, Spain

Reviewed by:

Alino Martinez-Marcos,
University of Castilla-la Mancha, Spain
Guy Elston,
Centre for Cognitive Neuroscience,
Australia

*Correspondence:

Jeffrey I. Berman
BermanJ@email.chop.edu

Received: 01 December 2015

Accepted: 07 March 2016

Published: 23 March 2016

Citation:

Berman JI, Edgar JC, Blaskey L, Kushner ES, Levy SE, Ku M, Dell J and Roberts TPL (2016) Multimodal Diffusion-MRI and MEG Assessment of Auditory and Language System Development in Autism Spectrum Disorder. *Front. Neuroanat.* 10:30. doi: 10.3389/fnana.2016.00030

gray matter, neurochemical concentration) that contribute to brain activity, both in typical development and in ASD. Finally, the neural latency measures were found to be of clinical significance, with M100 associated with overall ASD severity, and with MMF latency associated with language performance.

Keywords: autism spectrum disorders (ASD), multimodal imaging, magnetoencephalography (MEG), diffusion MRI, auditory pathways, language

INTRODUCTION

The etiology or, indeed, etiologies of autism spectrum disorder (ASD) is currently unknown. It is hypothesized that alterations to brain structure and function contribute to the clinical symptoms common to ASD. Given the high rate of occurrence of communication and language impairments in ASD, research has focused on the brain regions associated with basic auditory processes and more complex language skills, with prior imaging studies showing alterations in temporal lobe structure, connectivity and function (Klin et al., 2002; Boddaert et al., 2004; Redcay and Courchesne, 2005; Lee et al., 2007; Lange et al., 2010; Schipul et al., 2011; Nickl-Jockschat et al., 2012; Roberts et al., 2013). Although, atypical development of temporal regions is believed to precede and possibly underlie language impairments in ASD (Wolff et al., 2012; Edgar et al., 2015a), the links between abnormal development of brain structure and function with the behavioral phenotype of ASD are poorly understood.

To investigate associations between structure and function within auditory and language systems in ASD, the present study integrated diffusion magnetic resonance imaging (dMRI) measures of white-matter microstructure with magnetoencephalography (MEG) measures of cortical neural dynamics. Diffusion MRI is sensitive to microstructural properties of white matter such as axon density and myelination and has been used in quantitative studies of the superior temporal gyrus and arcuate fasciculus in ASD (Lee et al., 2009; Nagae et al., 2012; Berman et al., 2013). MEG is a non-invasive neuroimaging modality that records neuronal currents with high temporal resolution and has been used in many studies to examine the neural dynamics of auditory encoding processes in ASD (Wilson et al., 2007; Roberts et al., 2010; Stroganova et al., 2013). In the present study, associations between the rate of encoding auditory information and the structural integrity of two white-matter tracks were examined. The white matter and cortical neural measures selected for this study followed the propagation of auditory input from basic auditory encoding processes (primary/secondary auditory cortex and auditory radiations) to higher-level auditory linguistic processes (vowel mismatch discrimination and arcuate fasciculus). To examine maturation of these measures, cross-sectional associations with age were also examined.

The first white-matter track examined was the auditory radiation, the pathway that relays acoustic information from the medial geniculate nucleus (MGN) of the thalamus to the primary/secondary auditory cortex of the superior temporal gyrus (STG). The second white matter pathway examined was the arcuate fasciculus (AF), a tract from the STG to higher-order

language areas. These circuits represent relatively early stages of connection relevant for auditory processing and then later stages relevant for language functioning. To this end, the first functional MEG measure examined was the 100 ms (M100) STG auditory response. Auditory evoked M100 latency has been shown to be due, in part, to thalamocortical conduction velocity along the auditory radiation (Roberts et al., 2009, 2013). The second functional measure examined was the auditory mismatch field (MMF) elicited in response to an odd-ball stimulus among a series of otherwise similar stimuli (e.g., the “/u/” in “/a//a//a//a//u//a/”). The MMF response is involved in passive sound processing and is a precursor to language processing (Näätänen et al., 2007). Thus, M100 latency is considered to reflect relatively basic auditory encoding processes and MMF latency an index of preparatory language function.

This study was motivated by prior studies that individually focused on auditory or language systems in ASD (Oram Cardy et al., 2005; Roberts et al., 2010, 2013). For example, the latency of the auditory M100 decreases between infancy and adulthood, with M100 latency delays, indicating slower conduction and processing of auditory stimuli, observed in ASD (Rojas et al., 1998; Wunderlich et al., 2006; Roberts et al., 2010). The latency of the MMF has also been examined and appears to be a marker of language impairment, with MMF latency delays observed in individuals with specific language impairment (SLI) and associated with language impairment in ASD (Roberts et al., 2011).

Recent studies combining MEG and diffusion MR have shown associations between M100 conduction velocity and Heschl's gyrus white-matter integrity in typically developing (TD) children, with these associations less evident in children with ASD (Roberts et al., 2013). The present study extended prior studies from our laboratory to support the hypothesis that abnormal structure–function relationships are pervasive across auditory and language systems. To this end, high angular resolution diffusion imaging (HARDI) tractography was employed to measure the microstructural integrity of the entire auditory radiation to assess associations between auditory radiation tract microstructure and M100 latency. Similarly, diffusion MR white-matter measures of the arcuate fasciculus were obtained and associations with vowel-contrast MMF latency examined.

MATERIALS AND METHODS

Participants

Children with a prior clinical ASD diagnosis were recruited from the Regional Autism Center of The Children's Hospital

of Philadelphia (CHOP) and from local parent support groups. During the research visit, clinical and diagnostic testing by licensed child psychologists were performed to confirm ASD diagnosis and to ensure that typically developing children met inclusion criteria. ASD diagnosis was confirmed with the *Autism Diagnostic Observation Schedule* (ADOS; Lord et al., 2000) and parent report on the *Social Communication Questionnaire* (SCQ; Rutter et al., 2003) and the *Social Responsiveness Scale* (SRS; Constantino et al., 2003). In the rare event that diagnosis could not be confirmed with the ADOS and parent questionnaires alone, the Autism Diagnostic Interview-Revised (ADI-R) was administered to resolve diagnostic discordances (Lord et al., 1994). To diagnose language impairment (LI), all subjects were evaluated with the *Clinical Evaluation of Language Fundamentals – 4th edition* (CELF-4; Semel et al., 2003). Language impairment (LI) was defined based on the CELF-4 core language index, using a threshold of at or below 1SD from the mean and the 16th percentile (i.e., $SS < 85$).

Inclusion criteria for the typically developing children included having no history of neurodevelopmental, psychiatric, or neurological disorders, scoring below cut-offs for ASD on the ADOS and on parent questionnaires, and performing above the 16th percentile on the CELF-4. All subjects scored at or above the second percentile ($SS > 70$) on either the Perceptual Reasoning Index (PRI) or the Verbal Comprehension Index (VCI) of the Wechsler Intelligence Scale for Children-IV (WISC-IV). Detailed inclusion and exclusion criteria of the ASD and TD groups have been described previously (Roberts et al., 2010). The study was approved by the CHOP Institutional Review Board and all participants' legal guardian(s) gave informed written consent. Where competent to do so, children over 7 years gave verbal assent.

The pool of participants with evaluable neuroimaging data for this multimodal study included 44 TD (mean age 10.4 ± 2.4 years) and 95 ASD (mean age 10.2 ± 2.6 years). MEG and DTI findings from a smaller subset of these participants have been previously reported (Roberts et al., 2010, 2011). Group differences in age were not significant [t -test, $t_{(127)} = 0.35$, $p = 0.70$]. Of the children with ASD with diagnostic language scores, 35 were classified as ASD with language impairment (ASD/+LI; mean age 9.3 ± 2.5 years) and 56 as ASD without language impairment (ASD/-LI; mean age 10.6 ± 2.5 years). Although, the difference in age between ASD/+LI and ASD/-LI was significant (t -test, $p = 0.04$), the age difference was small. Given the challenges of multimodal imaging, complete diffusion MR and MEG datasets were not available for all subjects. In particular, 28 participants had evaluable HARDI and DTI for measurement of the auditory radiation as well as evaluable M100 latency. Eighty-two participants had evaluable MMF latency and 78 participants had evaluable DTI for measurement of the arcuate fasciculus.

MEG

Data were acquired in a magnetically shielded room using a 275-channel whole-cortex CTF magnetometer (VSM MedTech Inc., Coquitlam, BC). The details of the M100 and MMF tasks and data processing have been previously described (Roberts et al., 2010, 2011). In brief, for the M100 task, tones of 200, 300, 500, and

1000 Hz (300 ms duration, 10 ms ramps) were passively presented at 45 dB sensation level and repeated 130 times. The inter-stimulus interval varied randomly between 900 and 1100 ms. The left and right STG M100 latency response was obtained using a left and right STG dipole source model that transformed MEG sensor signals into source space. For the MMF task, auditory stimuli consisted of the vowels /a/ and /u/ (300 ms in duration), with deviant stimuli occurring at random positions in the sequence with a 15% probability. Inter-stimulus interval was 700 ms. Two runs with the vowels alternating as standard/deviant allowed matched token subtraction (i.e., deviant /u/-standard /a/). MMF latency, again obtained using a left and right STG dipole source model, was defined at the maximal deflection in the difference waveform, occurring between 150 and 350 ms after stimulus onset, and after identifiable M50 and M100 components in the unsubtracted waveforms.

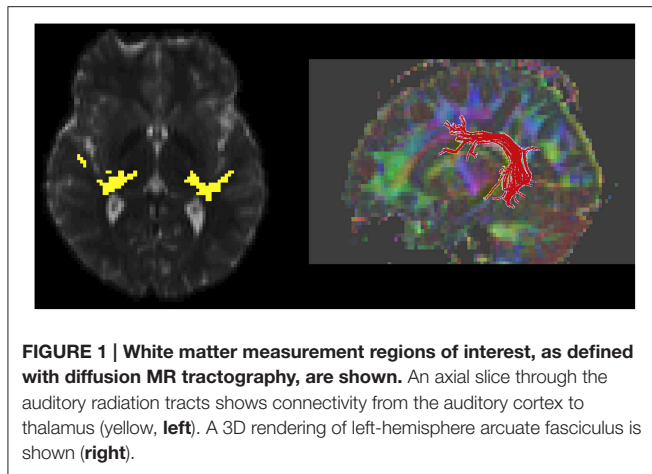
MR Imaging

MR imaging was performed with a 3T Siemens Verio™ and 32-channel head coil (Siemens Medical Solutions, Erlangen, Germany). HARDI and conventional DTI were performed. Whole-brain HARDI acquisition included 64 gradient directions at $b = 3000$ s/mm², $TR/TE = 14.8$ s/111 ms, voxel size = $2 \times 2 \times 2$ mm, and 128×128 matrix. DTI acquisition used 30 diffusion gradient directions at $b = 1000$ s/mm², one $b = 0$ s/mm² volume, $TR/TE = 11$ s/76 ms, voxel size $2 \times 2 \times 2$ mm, and 128×128 matrix. The HARDI acquisition was 18 min in duration and the DTI acquisition 6 min in duration. Anatomical T1-weighted MP-RAGE volumes were also acquired with $TR/TE/TI = 1900/2.87/1050$ ms, 1 mm isotropic voxels, and full head coverage.

Solid angle q-ball reconstruction of the HARDI data was used with a probabilistic fiber tracking algorithm to delineate the left and right auditory radiation (Figure 1; Berman et al., 2008, 2013). Although, difficult to obtain in children, HARDI tractography is necessary to traverse the crossing fibers of the auditory radiation (Berman et al., 2013). In contrast, DTI deterministic fiber tracking is sufficient to follow the core of the left and right arcuate fasciculus tracts (Figure 1; Mori et al., 1999). The arcuate fasciculus was selected based on previous reports and by a *priori* hypothesis to reduce statistical confounds associated with multiple comparisons in more comprehensive explorations (Nagae et al., 2012). DTI parameters (fractional anisotropy “FA,” mean diffusivity “MD,” radial diffusivity “RD,” and axial diffusivity “AD”) were determined from the eigenvalues of the diffusion tensor and evaluated voxelwise over the course of the left and right auditory radiations and arcuate fasciculus as determined with tractography.

Statistical Analysis

Statistical analyses included group comparisons, multivariate regression, and linear mixed models. Analyses were performed using JMP (Version 11, SAS). A single “effective” M100 latency for each participant's left and right STG was calculated with a linear mixed model to reduce the number of M100 latency analyses (Roberts et al., 2000). Given that M100 latency varies by stimulus tone frequency, the “effective” M100 latencies were



computed with a linear mixed-model. The M100 latency model contained fixed effects of hemisphere, stimulus frequency, group, age, and a random effect of subject. Fitted values from the model were used to predict M100 latency for participants with partially missing observations (e.g., absent response to a stimulus tone and/or in one hemisphere) to enable comparisons across participants with different distributions of missing data. Considering subject as a random effect (on the model intercept) allows retention of inter-individual differences when modeling and imputing missing data.

RESULTS

Auditory System: Auditory Radiation and M100

Each DTI parameter was linearly modeled with main effects of group, age, and hemisphere, along with each two-way interaction term. Auditory radiation MD and RD decreased with age and FA increased with age, indicating white matter maturation across both ASD and TD in the studied age range [MD: $F_{(1, 52)} = 9.1$, $p = 0.004$; RD: $F_{(1, 52)} = 11.8$, $p = 0.001$; FA: $F_{(1, 52)} = 6.63$, $p = 0.013$]. The main effect of group was not significant for any DTI parameter. Significant age by group interactions for FA and RD [FA: $F_{(1, 52)} = 4.66$, $p = 0.036$; RD: $F_{(1, 52)} = 4.85$, $p = 0.032$], indicated group differences in maturation. In particular, collapsing across hemisphere, FA increased by 0.013 per year (95th CI [0.003, 0.02]) in TD vs. 0.001 per year (95th CI [-0.005, 0.007]) in ASD, and RD decreased by 15.2×10^{-6} mm²/s/year (95th CI [-25, -46] $\times 10^{-6}$) in TD vs. 3.04×10^{-6} mm²/s/year (95th CI [-9, 2.5] $\times 10^{-6}$) in ASD.

Although, there was no significant group by hemisphere by age interaction, given overall group maturation rate differences and *a priori* hypotheses relating to the development of lateralized hemisphere functional specialization, left and right hemisphere DTI parameters were assessed separately. In the left hemisphere, significant group by age interaction terms indicated group differences in the maturation of left hemisphere FA [$F_{(1, 26)} = 7.9$, $p = 0.01$], RD [$F_{(1, 26)} = 6.2$, $p = 0.02$], and AD [$F_{(1, 26)} = 5.4$, $p = 0.03$]. As depicted in **Figure 2**, left hemisphere FA increased at a faster rate in the TD than ASD, driving the overall

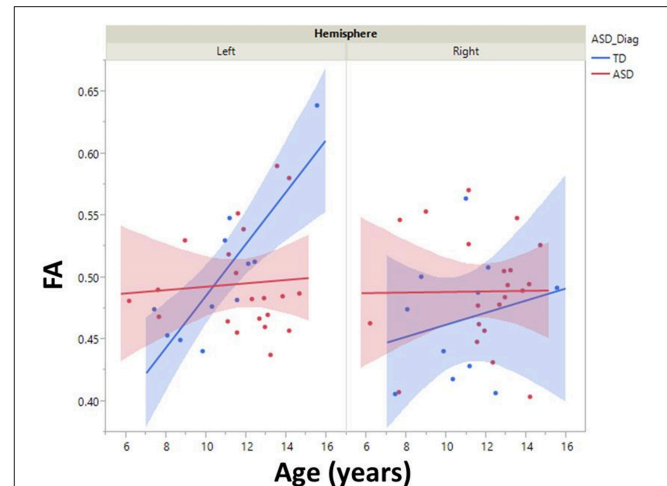


FIGURE 2 | Developmental trajectory of left and right auditory radiation microstructure are shown with 95% confidence intervals (shading). Left-hemisphere FA increased at a faster rate in the TD vs. ASD group ($p < 0.01$). No right-hemisphere group difference in maturation was observed.

group by age difference. The slower maturation of FA in ASD was likely due to a slower rate of RD decrease in ASD vs. TD. No differences in rate of maturation were detected in the right hemisphere.

M100 was similarly modeled with group, age and hemisphere as main effects, as well as each interaction term. A main effect of hemisphere, $F_{(1, 52)} = 8.0$, $p = 0.01$, indicated that M100 responses were 11 ms later in the left than right hemisphere, consistent with prior reports (Paetau et al., 1995; Howard and Poeppel, 2009). A main effect of age, $F_{(1, 52)} = 28.6$, $p < 0.0001$, showed that M100 decreased ~ 4.5 ms per year (**Figure 3**). No group difference in rate of maturation was detected. Again, despite the absence of a group by hemisphere interaction, *a priori* hypotheses called for the interrogation of M100 latency maturation in each hemisphere. **Figure 4** compares the left and right hemisphere maturation rates for FA and M100. Left-hemisphere M100 latency tended to decrease at a faster rate in TD than ASD. Although, the group difference in left hemisphere M100 maturation did not reach significance, this group difference pattern is conspicuously similar to the significant group differences in maturation of left hemisphere FA. Also of note, although in this sample groups did not differ in M100 latency, **Figure 3** suggests later right-hemisphere M100 responses in ASD vs. TD, a pattern consistent with prior reports (Roberts et al., 2010; Edgar et al., 2015b).

To examine the association between M100 and behavior, ASD symptom and language ability measures (SRS and CELF-4) were modeled with M100 latency, age, and hemisphere as factors. M100 was a significant predictor of SRS [$F_{(1, 57)} = 6.1$, $p = 0.02$]. M100 did not predict language ability (CELF-4). A mean adjusted leverage plot was used to isolate and visualize the relationship between SRS and M100 latency (**Figure 5**).

For the multimodal analysis, to account for additional variance in the M100 latency, a linear model of each participant's effective M100 latency with average DTI parameters and group

as effects was constructed. Age was not included given the above results indicating that both DTI and M100 measures show age dependence and may have interdependent maturational trajectories. A main effect of RD, $F_{(1, 27)} = 4.7$, $p = 0.04$, showed that increased RD was related to longer M100 latencies (slope = $15.7 \times 10^4 \text{ ms} \cdot \text{s/mm}^2$). A similar trend was observed between MD and M100 latency, $F_{(1, 27)} = 3.4$, $p = 0.08$. Analyzing groups separately showed this structure-function relationship was primarily driven by the TD group: RD was positively correlated with M100 in TD, $F_{(1, 8)} = 6.2$, $p = 0.04$ (slope = $20.2 \times 10^4 \text{ ms} \cdot \text{s/mm}^2$, 95th CI: $[1.4, 39] \times 10^4$), but not in ASD, $F_{(1, 18)} = 0.8$, $p = 0.4$ (slope = $10.4 \times 10^4 \text{ ms} \cdot \text{s/mm}^2$).

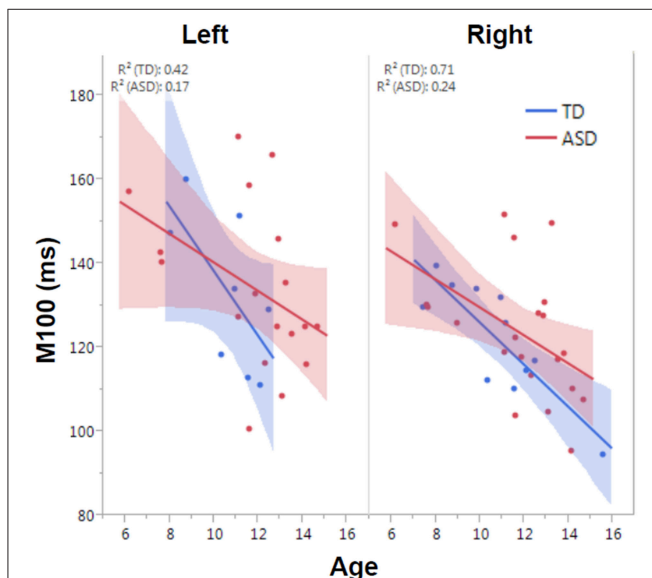


FIGURE 3 | Developmental trajectory of left and right auditory M100 latency. M100 latency shortened with age across the population ($p < 0.0001$). Although no group difference in rate of maturation was observed, the TD group trended toward faster maturation.

Language System: MMF Latency and Arcuate Fasciculus

Given the reported relationship between MMF latency and language ability, group comparisons of CELF-4 and MMF latency included three groups: ASD with and without language impairment (ASD/+LI, ASD/-LI) as well as TD. As expected, mean CELF-4 Core Language Index (CLI) scores were significantly different for all pairwise group comparisons (TD: 109 ± 11.9 ; ASD/-LI: 98.6 ± 10.2 ; ASD/+LI: 70.7 ± 14.6 ; p 's < 0.005 with Tukey-Kramer Adjustment for multiple comparisons). MMF latency was modeled with group, stimulus type (vowel /a/ or /u/), and

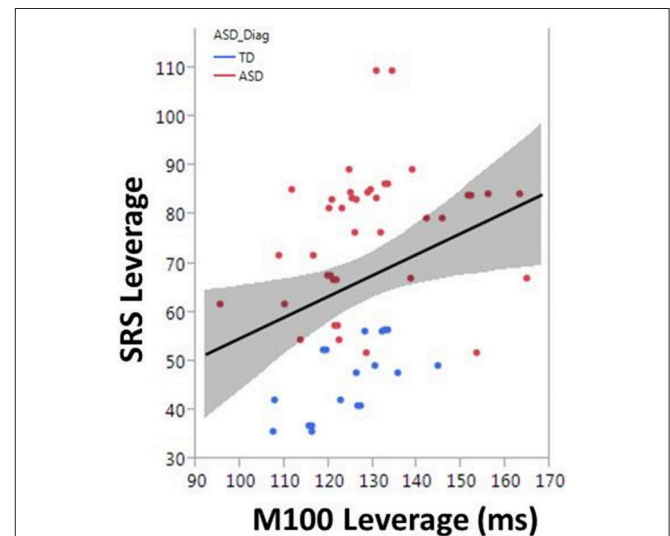


FIGURE 5 | The correlation between M100 and SRS is observed in the partial regression leverage plot. The ordinate (y-axis) of the leverage plot shows the residuals of the response variable (SRS) when regressed on all model parameters except M100. The abscissa (x-axis) of the leverage plot shows the residuals from regressing M100 against the other independent variables. M100 is a significant predictor of SRS ($p = 0.02$).

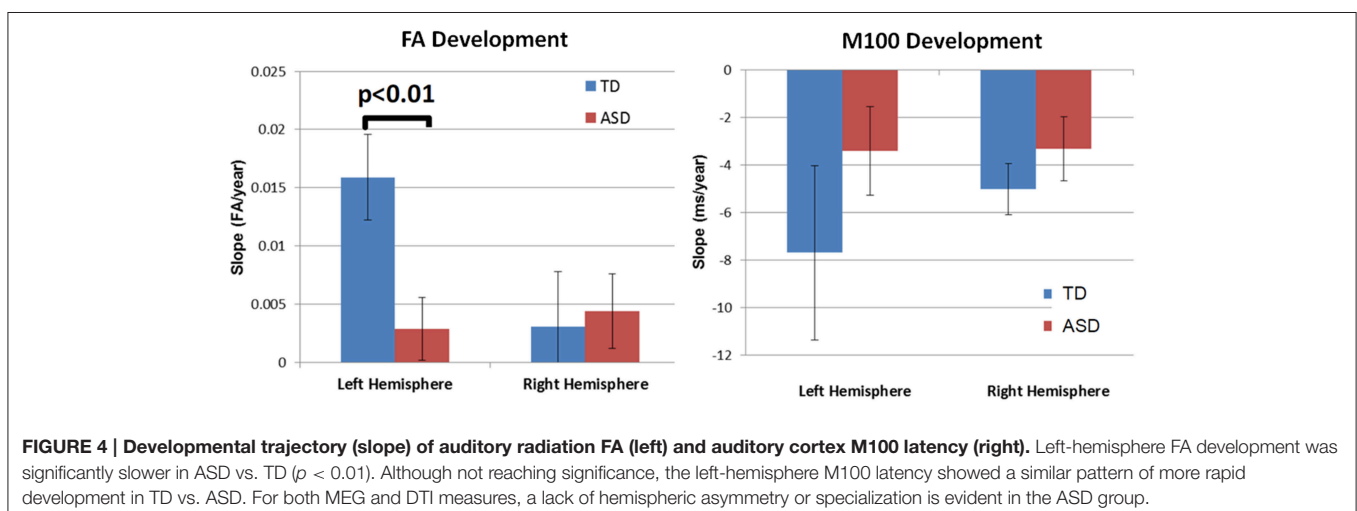


FIGURE 4 | Developmental trajectory (slope) of auditory radiation FA (left) and auditory cortex M100 latency (right). Left-hemisphere FA development was significantly slower in ASD vs. TD ($p < 0.01$). Although not reaching significance, the left-hemisphere M100 latency showed a similar pattern of more rapid development in TD vs. ASD. For both MEG and DTI measures, a lack of hemispheric asymmetry or specialization is evident in the ASD group.

hemisphere as fixed effects and subject as a random effect. Additionally, PRI was considered as a potential confounding covariate.

There was a main effect of group on MMF latency, $F_{(2, 72.4)} = 4.2$, $p = 0.02$ (mean TD: 229.9 ± 6.7 ms; ASD/-LI: 220.1 ± 5.9 ms; ASD/+LI: 248.3 ± 8.1 ms; Roberts et al., 2011). ASD/+LI exhibited MMF latencies ~ 25 ms later than ASD/-LI ($p < 0.02$, Tukey-Kramer Adjustment for multiple comparisons). MMF latency did not differ with respect to stimulus type or hemisphere and was not associated with PRI or age. Within the combined ASD group, MMF latency (latency collapsed across hemisphere) correlated with CELF-4 CLI, $F_{(1, 49.4)} = 8.4$, $p = 0.01$ (Figure 6). Separately examining the left and right hemisphere, in ASD, both left and right hemisphere MMF latency correlated with language ability, $F_{(1, 43.5)} = 7.5$, $p = 0.01$ in left; $F_{(1, 42.8)} = 6.1$, $p = 0.01$ in right. No significant association between MMF latency and language ability (CELF-4 CLI) was observed in TD. In contrast to M100 latency, no significant association between MMF latency and SRS was observed in ASD or TD.

To examine the role of white-matter microstructure on MMF latency as well as language ability, arcuate fasciculus DTI parameters were measured. Arcuate fasciculus FA increased with age in the ASD, $F_{(1, 85)} = 4.0$, $p = 0.05$ (slope = $0.0024/\text{year}$) and TD groups, $F_{(1, 55)} = 21.8$, $p < 0.0001$ (slope = $0.0052/\text{year}$). MD decreased with age in the ASD, $F_{(1, 85)} = 22.4$, $p < 0.0001$ (slope = $-0.052 \times 10^{-4} \text{ mm}^2/\text{s}/\text{year}$) and TD groups $F_{(1, 55)} = 28.6$, $p < 0.0001$ (slope = $-0.076 \times 10^{-4} \text{ mm}^2/\text{s}/\text{year}$). Group by age interactions were not significant, indicating no detectable group difference in FA or MD maturation slopes. DTI parameters (with age as a covariate) were not predictive of CELF-4 CLI in either ASD or TD.

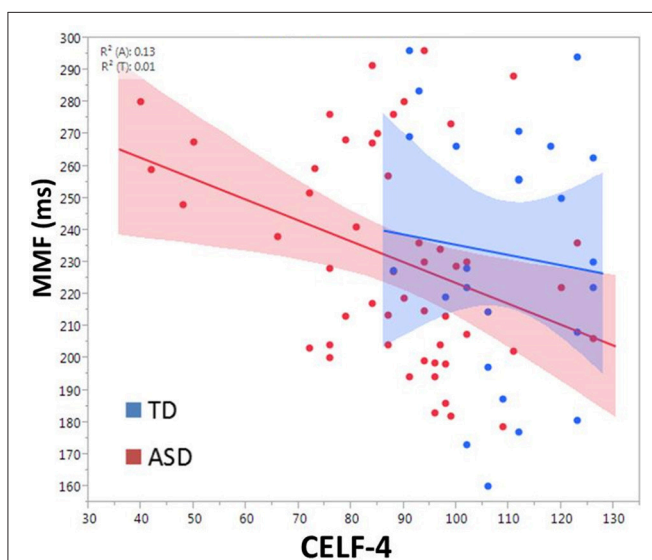


FIGURE 6 | Relationship between CELF-4 score and MMF latency is shown for ASD (red) and TD (blue). The correlation is significant for ASD ($p < 0.005$). Although not significant in TD, the slope suggests a negative correlation between MMF and language ability.

To explore contributions to MMF latency by arcuate fasciculus microstructure, linear mixed models with MMF latency as the dependent variable were constructed with DTI parameter, PRI, group (ASD and TD), age, stimulus type, and hemisphere as main effects and subject as the random effect. A main effect of FA, $F_{(1, 103)} = 4.2$, $p = 0.04$, indicated associations between FA and MMF latency. Explored in each group, FA predicted MMF in TD, $F_{(1, 45.8)} = 4.60$, $p = 0.04$ (Figure 7), and not in ASD ($p = 0.3$) or in the ASD/+LI ($p = 0.4$) or ASD/-LI ($p = 0.4$) subgroups. No associations with MMF latency were observed for the other DTI parameters (MD, RD, and AD; $p > 0.05$).

DISCUSSION

The present multimodal and multi-circuit study examined associations between brain structure and function in auditory and language areas. In both auditory and language systems, white-matter integrity, and cortical electrophysiology were found to be coupled in TD, with white-matter microstructural features contributing to M100 and MMF latency. However, in ASD, these structure–function relationships were less obvious or uncoupled. Results also suggested that the neural latency measures are of clinical significance, with a delayed M100 associated with increased ASD severity (as measured with SRS) and a delayed MMF delay associated with greater language impairment (CELF-4 CLI).

Accurate and rapid encoding of auditory information is critical for receptive language. A prior study of auditory processing observed abnormal brainstem and cortical electrophysiology in children with language learning problems (Wible et al., 2005). M100 latency provides information about the average auditory pathway conduction velocity to

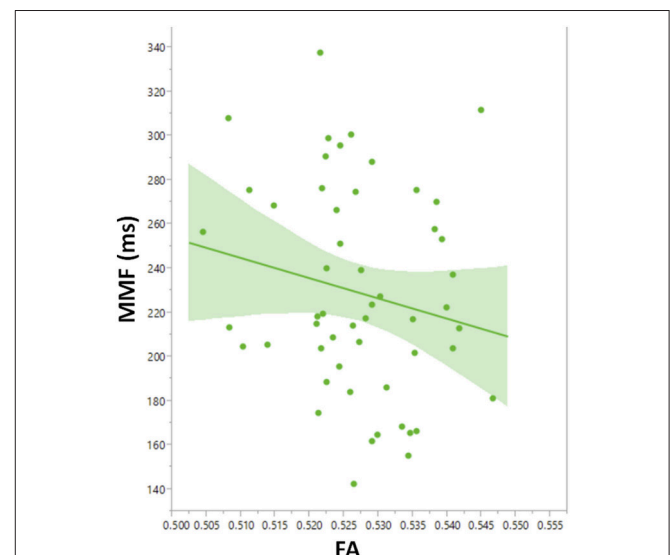


FIGURE 7 | Leverage plot of arcuate fasciculus FA vs. MMF latency in TD showing a significant correlation ($p < 0.01$). Left and right hemisphere measures are combined in the scatter plot.

primary/secondary auditory areas, with delayed auditory encoding reported in ASD (Roberts et al., 2010). In the present study, M100 latency was observed to shorten with age in both groups. Regarding brain structure, diffusion MR analyses also demonstrated maturation of the thalamocortical segment of the central auditory pathway in TD and ASD. As the midbrain white matter and vestibulocochlear nerve portions of the auditory system were not examined, it remains undetermined if the thalamocortical measurements are representative of the entire auditory pathway. Despite observing maturation of white-matter measures and M100 latency in ASD, analyses indicated slower maturation in ASD vs. TD, especially in the left hemisphere. Although, maturation of conduction efficiency occurs in ASD, there was some suggestion of a lateralized abnormality in ASD, with left-hemisphere maturation of FA slower in ASD vs. TD. Additionally, in the TD group, a hemisphere asymmetry in microstructural development trajectory was observed, consistent with the known structural and volumetric asymmetries of the auditory and language systems (Geschwind and Levitsky, 1968; Morillon et al., 2010). The children with ASD, however, did not exhibit this hemispheric asymmetry, consistent with prior reports of abnormal hemispheric asymmetry of STG and arcuate fasciculus white matter in ASD (Fletcher et al., 2010; Lange et al., 2010). Mirroring structural maturation, M100 latency results also indicated a lack of hemispheric asymmetry in ASD. In particular, although not reaching significance, the rate of left hemisphere M100 latency shortening appeared diminished in children with ASD vs. TD. Given that in ASD the FA and M100 analyses both suggested a loss of the hemispheric asymmetry observed in TD, present findings lend support to the hypothesis of a lack of hemispheric functional specialization in ASD. It should be noted that many studies with methods ranging from structural to functional support the atypical development of left and right hemispheres in ASD (Lange et al., 2010; Herbert et al., 2002, 2005; De Fossé et al., 2004; Flagge et al., 2005).

Coupling of structure and function in typically developing children was evidenced by associations between auditory radiation and arcuate fasciculus white-matter microstructure and M100 and MMF latency. In ASD, however, white-matter microstructure was not predictive of either M100 or MMF latency. A prior study observed a similar structure-function uncoupling in ASD when examining the latency of the earlier M50 auditory response and Heschl's Gyrus white-matter microstructure (Roberts et al., 2013). Of note, in the present study, the specificity of "auditory radiation to M100" and "arcuate fasciculus to MMF" coupling was established by considering cross-regional correlations of M100 to arcuate microstructure and MMF to auditory radiation microstructure, with each of these pairings found to be unrelated (although with findings limited by the number of subjects with complete data sets).

Appropriate white matter structural maturation appears necessary, but not sufficient for efficient auditory conduction and processing. Other factors that contribute to M100 and MMF latency likely include cortical architecture and synaptic transmission. Age-related changes in synaptic efficiency and cortical layers are associated with maturation of the auditory response (Steinschneider et al., 1994; Eggermont and Ponton, 2003). Pyramidal cells are the primary source of MEG activity

and maturation of these neurons can modulate MEG recording (Lewine and Orrison, 1995; Spruston, 2008; Elston et al., 2010; Lange et al., 2010; Elston and Fujita, 2014). As an example, studies have noted associations between gray matter cortical thickness and the strength of auditory responses (Edgar et al., 2012). Future studies examining the contributions of white matter, gray matter, and neurochemistry to M100 and MMF latencies in ASD are needed.

In the present study, M100 latency was associated with the severity of autism symptoms, as assessed by the SRS. M100 latency was not associated with language performance. In contrast, the observed difference in MMF latency between ASD subjects with and without language impairment, as well as the bilateral associations of MMF latency and CELF-4 performance (and the concomitant lack of MMF association with SRS or PRI), supported the hypothesis that MMF latency is an index of language impairment rather than ASD severity or intellectual ability (Roberts et al., 2011). An association of MMF latency with language ability only in ASD suggested that MMF latency tracks with language *impairment* and not the normal variation in CELF-4 CLI scores observed in the controls. MMF does not predict language *abilities* in excess of the CELF-4 median. Impaired auditory perception and auditory discrimination are expected to have upstream ramifications for language cognition (Bishop, 2007). The MMF latency and language ability associations in both hemispheres suggests that passive auditory change detection is neither a very basic sensory function nor a higher-level language process restricted to the presumed language-dominant left hemisphere. Basic auditory detection, as measured with the M100, has not been correlated with language ability in this or prior studies. DTI parameters were not directly related to CELF-4 scores in this study. However, as previously reported, when our dataset is not limited to those subjects with both evaluable DTI and MEG data, arcuate fasciculus diffusivity was observed to correlate with CELF-4 scores (Roberts et al., 2014).

A limitation of this and other multimodal studies included incomplete or even sparse datasets. As the number of independent measures or modalities increases, the number of participants expected to have complete data sets unfortunately decreases. It is also of note that although **Figure 3** suggested delayed right STG M100 latencies in ASD vs. TD, this group difference was not statistically significant. Failure to replicate previous studies showing right STG M100 latency group differences is likely due to a lack of power given much smaller samples in the present study vs. previous studies.

To conclude, multimodal examination of auditory and language systems in ASD indicated atypical development of white matter and cortical neural function, including abnormal hemispheric lateralization in children with ASD. Analyses also demonstrated a lack of coupling between structure and function in early auditory (M100) as well as later-stage auditory processing (MMF) in ASD. As white-matter microstructure did not explain all the variance in M100 and MMF latency, other aspects of brain structure clearly contribute to age-related changes in M100 and MMF latency. Future multimodal studies examining a broader array of brain structure measures (e.g., gray matter, brainstem white matter, MRS) are needed to more fully understand auditory encoding impairments in children with ASD. Finally, the neural

latency measures were found to be of clinical significance, with M100 associated with SRS (but not CELF-4 CLI) indicating that slow auditory processing is an indicator of overall ASD severity, and with MMF latency associated with language performance.

AUTHOR CONTRIBUTIONS

JB, TR, JE, SL, LB, and EK were involved in study conception and design. All authors were involved in acquisition of MRI,

MEG, or clinical scores. JB, TR, JE, LB, EK, JD, and MK were involved in the interpretation or analysis of data. JB, JE, and TR drafted the manuscript. All authors approved the final manuscript.

FUNDING

This work was supported by K01MH096091, R01DC008871-07, and the CHOP/UPenn IDDRC grant U54 HD086984.

REFERENCES

- Berman, J. I., Chung, S., Mukherjee, P., Hess, C. P., Han, E. T., and Henry, R. G. (2008). Probabilistic streamline Q-Ball tractography using the residual bootstrap. *Neuroimage* 39, 215–222. doi: 10.1016/j.neuroimage.2007.08.021
- Berman, J. I., Lanza, M. R., Blaskey, L., Edgar, J. C., Roberts, T. P. (2013). High angular resolution diffusion imaging probabilistic tractography of the auditory radiation. *Am. J. Neuroradiol.* 34, 1573–1578. doi: 10.3174/ajnr.A3471
- Bishop, D. V. (2007). Using mismatch negativity to study central auditory processing in developmental language and literacy impairments: where are we, and where should we be going? *Psychol. Bull.* 133, 651–672. doi: 10.1037/0033-2909.133.4.651
- Boddaert, N., Chabane, N., Gervais, H., Good, C. D., Bourgeois, M., Plumet, M. H., et al. (2004). Superior temporal sulcus anatomical abnormalities in childhood autism: a voxel-based morphometry MRI. *Neuroimage* 23, 364–369. doi: 10.1016/j.neuroimage.2004.06.016
- Constantino, J. N., Davis, S. A., Todd, R. D., Schindler, M. K., Gross, M. M., Brophy, S. L., et al. (2003). Validation of a brief quantitative measure of autistic traits: comparison of the social responsiveness scale with the autism diagnostic interview-revised. *J. Autism Dev. Disord.* 33, 427–433. doi: 10.1023/A:1025014929212
- De Fossé, L., Hodge, S. M., Makris, N., Kennedy, D. N., Caviness, V. S. Jr. McGrath, L., et al. (2004). Language-association cortex asymmetry in autism and specific language impairment. *Ann. Neurol.* 56, 757–766. doi: 10.1002/ana.20275
- Edgar, J. C., Fisk, C. L. IV, Berman, J. I., Chudnovskaya, D., Liu, S., Pandey, J., et al. (2015a). Auditory encoding abnormalities in children with autism spectrum disorder suggest delayed development of auditory cortex. *Mol. Autism* 6, 1.
- Edgar, J. C., Hunter, M. A., Huang, M., Smith, A. K., Chen, Y., Sadek, J., et al. (2012). Temporal and frontal cortical thickness associations with M100 auditory activity and attention in healthy controls and individuals with schizophrenia. *Schizophr. Res.* 140, 250–257. doi: 10.1016/j.schres.2012.06.009
- Edgar, J. C., Khan, S. Y., Blaskey, L., Chow, V. Y., Rey, M., Gaetz, W., et al. (2015b). Neuromagnetic oscillations predict evoked-response latency delays and core language deficits in autism spectrum disorders. *J. Autism Dev. Disord.* 45, 395–405. doi: 10.1007/s10803-013-1904-x
- Eggermont, J. J., and Ponton, C. W. (2003). Auditory-evoked potential studies of cortical maturation in normal hearing and implanted children: correlations with changes in structure and speech perception. *Acta Otolaryngol.* 123, 249–252. doi: 10.1080/0036554021000028098
- Elston, G. N., and Fujita, I. (2014). Pyramidal cell development: postnatal spinogenesis, dendritic growth, axon growth, and electrophysiology. *Front Neuroanat.* 8:78. doi: 10.3389/fnana.2014.00078
- Elston, G. N., Okamoto, T., Oga, T., Dornan, D., and Fujita, I. (2010). Spinogenesis and pruning in the primary auditory cortex of the macaque monkey (*Macaca fascicularis*): an intracellular injection study of layer III pyramidal cells. *Brain Res.* 1316, 35–42. doi: 10.1016/j.brainres.2009.12.056
- Flagg, E. J., Cardy, J. E. O., Roberts, W., and Roberts, T. P. (2005). Language lateralization development in children with autism: insights from the late field magnetoencephalogram. *Neurosci. Lett.* 386, 82–87. doi: 10.1016/j.neulet.2005.05.037
- Fletcher, P. T., Whitaker, R. T., Tao, R., DuBray, M. B., Froehlich, A., Ravichandran, C., et al. (2010). Microstructural connectivity of the arcuate fasciculus in adolescents with high-functioning autism. *Neuroimage* 51, 1117–1125. doi: 10.1016/j.neuroimage.2010.01.083
- Geschwind, N., and Levitsky, W. (1968). Human brain: left-right asymmetries in temporal speech region. *Science* 161, 186–187.
- Herbert, M. R., Harris, G. J., Adrien, K. T., Ziegler, D. A., Makris, N., Kennedy, D. N., et al. (2002). Abnormal asymmetry in language association cortex in autism. *Ann. Neurol.* 52, 588–596. doi: 10.1002/ana.10349
- Herbert, M. R., Ziegler, D. A., Deutsch, C. K., O'Brien, L. M., Kennedy, D. N., Filipek, P. A., et al. (2005). Brain asymmetries in autism and developmental language disorder: a nested whole-brain analysis. *Brain* 128, 213–226. doi: 10.1093/brain/awh330
- Howard, M. F., and Poeppel, D. (2009). Hemispheric asymmetry in mid and long latency neuromagnetic responses to single clicks. *Hear. Res.* 257, 41–52. doi: 10.1016/j.heares.2009.07.010
- Klin, A., Jones, W., Schultz, R., Volkmar, F., and Cohen, D. (2002). Visual fixation patterns during viewing of naturalistic social situations as predictors of social competence in individuals with autism. *Arch. Gen. Psychol.* 59, 809–816. doi: 10.1001/archpsyc.59.9.809
- Lange, N., Dubray, M. B., Lee, J. E., Froimowitz, M. P., Froehlich, A., Adluru, N., et al. (2010). Atypical diffusion tensor hemispheric asymmetry in autism. *Autism Res.* 3, 350–358. doi: 10.1002/aur.162
- Lee, J. E., Bigler, E. D., Alexander, A. L., Lazar, M., DuBray, M. B., Chung, M. K., et al. (2007). Diffusion tensor imaging of white matter in the superior temporal gyrus and temporal stem in autism. *Neurosci. Lett.* 424, 127–132. doi: 10.1016/j.neulet.2007.07.042
- Lee, K., Yoshida, T., Kubicki, M., Bouix, S., Westin, C. F., Kindlmann, G., et al. (2009). Increased diffusivity in superior temporal gyrus in patients with schizophrenia: a diffusion tensor imaging study. *Schizophrenia Res.* 108, 33–40. doi: 10.1016/j.schres.2008.11.024
- Lewine, J. D., Orrison, W. W. (1995). "Magnetencephalography and magnetic source imaging," in *Functional Brain Imaging*, eds W. W. Orrison, J. D. Lewin, J. A. Sanders, and M. F. Hartshorne (St. Louis, MI: Mosby), 369–417.
- Lord, C., Risi, S., Lambrecht, L., Cook, E. H. Jr, Leventhal, B. L., DiLavore, P. C., et al. (2000). The autism diagnostic observation schedule-generic: a standard measure of social and communication deficits associated with the spectrum of autism. *J. Autism Dev. Disord.* 30, 205–223. doi: 10.1023/A:1005592401947
- Lord, C., Rutter, M., and Le Couteur, A. (1994). Autism diagnostic interview-revised: a revised version of a diagnostic interview for caregivers of individuals with possible pervasive developmental disorders. *J. Autism Dev. Disord.* 24, 659–685.
- Mori, S., Crain, B. J., Chacko, V. P., and van Zijl, P. C. (1999). Three-dimensional tracking of axonal projections in the brain by magnetic resonance imaging. *Ann. Neurol.* 45, 265–269.
- Morillon, B., Lehongre, K., Frackowiak, R. S., Ducorps, A., Kleinschmidt, A., Poeppel, D., et al. (2010). Neurophysiological origin of human brain asymmetry for speech and language. *Proc. Natl. Acad. Sci. U.S.A.* 107, 18688–18693. doi: 10.1073/pnas.1007189107
- Näätänen, R., Paavilainen, P., Rinne, T., and Alho, K. (2007). The mismatch negativity (MMN) in basic research of central auditory processing: a review. *Clin. Neurophysiol.* 118, 2544–2590. doi: 10.1016/j.clinph.2007.04.026
- Nagae, L. M., Zarnow, D. M., Blaskey, L., Dell, J., Khan, S. Y., Qasmieh, S., et al. (2012). Elevated mean diffusivity in the left hemisphere superior longitudinal fasciculus in autism spectrum disorders increases with more profound language impairment. *Am. J. Neuroradiol.* 33, 1720–1725. doi: 10.3174/ajnr.A3037

- Nickl-Jockschat, T., Habel, U., Michel, T. M., Manning, J., Laird, A. R., Fox, P. T., et al. (2012). Brain structure anomalies in autism spectrum disorder—a meta-analysis of VBM studies using anatomic likelihood estimation. *Hum. Brain Mapp.* 33, 1470–1489. doi: 10.1002/hbm.21299
- Oram Cardy, J. E., Flagg, E. J., Roberts, W., and Roberts, T. P. (2005). Delayed mismatch field for speech and non-speech sounds in children with autism. *Neuroreport* 16, 521–525. doi: 10.1097/00001756-200504040-00021
- Paetau, R., Ahonen, A., Salonen, O., and Sams, M. (1995). Auditory evoked magnetic fields to tones and pseudowords in healthy children and adults. *J. Clin. Neurophysiol.* 12, 177–185.
- Redcay, E., and Courchesne, E. (2005). When is the brain enlarged in autism? A meta-analysis of all brain size reports. *Biol. Psychiatry* 58, 1–9. doi: 10.1016/j.biopsych.2005.03.026
- Roberts, T. P., Ferrari, P., Stufflebeam, S. M., and Poeppel, D. (2000). Latency of the auditory evoked neuromagnetic field components: stimulus dependence and insights toward perception. *J. Clin. Neurophysiol.* 17, 114–129.
- Roberts, T. P. L., Cannon, K. M., Tavabi, K., Blaskey, L., Khan, S. Y., Monroe, J. F., et al. (2011). Auditory magnetic mismatch field latency: a biomarker for language impairment in autism. *Biol. Psychiatry* 70, 263–269. doi: 10.1016/j.biopsych.2011.01.015
- Roberts, T. P. L., Heiken, K., Zarnow, D., Dell, J., Nagae, L., Blaskey, L., et al. (2014). Left hemisphere diffusivity of the arcuate fasciculus: influences of autism spectrum disorder and language impairment. *AJNR Am. J. Neuroradiol.* 35, 587–592. doi: 10.3174/ajnr.A3754
- Roberts, T. P. L., Khan, S. Y., Blaskey, L., Dell, J., Levy, S. E., Zarnow, D. M., et al. (2009). Developmental correlation of diffusion anisotropy with auditory-evoked response. *Neuroreport* 20, 1586–1591. doi: 10.1097/WNR.0b013e3283306854
- Roberts, T. P. L., Khan, S. Y., Rey, M., Monroe, J. F., Cannon, K., Blaskey, L., et al. (2010). MEG detection of delayed auditory evoked responses in autism spectrum disorders: towards an imaging biomarker for autism. *Autism Res.* 3, 8–18. doi: 10.1002/aur.111
- Roberts, T. P. L., Lanza, M. R., Dell, J., Qasmieh, S., Hines, K., Blaskey, L., et al. (2013). Maturation differences in thalamocortical white matter microstructure and auditory evoked response latencies in autism spectrum disorders. *Brain Res.* 1537, 79–85. doi: 10.1016/j.brainres.2013.09.011
- Rojas, D. C., Walker, J. R., Sheeder, J. L., Teale, P. D., and Reite, M. L. (1998). Developmental changes in refractoriness of the neuromagnetic M100 in children. *Neuroreport* 9, 1543–1547.
- Rutter, M., Bailey, A., and Lord, C. (2003). *Social Communication Questionnaire (SCQ)*. Los Angeles, CA: Western Psychological Services.
- Schipul, S. E., Keller, T. A., and Just, M. A. (2011). Inter-regional brain communication and its disturbance in autism. *Front Syst Neurosci.* 5:7. doi: 10.3389/fnsys.2011.00010
- Semel, E. M., Wiig, E. H., and Secord, W. (2003). *Clinical Evaluation of Language Fundamentals (CELF-4)*. San Antonio, TX: The Psychological Corporation.
- Spruston, N. (2008). Pyramidal neurons: dendritic structure and synaptic integration. *Nat. Rev. Neurosci.* 9, 206–221. doi: 10.1038/nrn2286
- Steinschneider, M., Schroeder, C. E., Arezzo, J. C., and Vaughan, H. G. (1994). Speech-evoked activity in primary auditory cortex: effects of voice onset time. *Electroencephalogr. Clin. Neurophysiol.* 92, 30–43.
- Stroganova, T. A., Kozunov, V. V., Posikera, I. N., Galuta, I. A., Gratchev, V. V., and Orekhova, E. V. (2013). Abnormal pre-attentive arousal in young children with autism spectrum disorder contributes to their atypical auditory behavior: an ERP study. *PLoS ONE* 8:e69100. doi: 10.1371/journal.pone.0069100
- Wible, B., Nicol, T., and Kraus, N. (2005). Correlation between brainstem and cortical auditory processes in normal and language-impaired children. *Brain* 128, 417–423. doi: 10.1093/brain/awh367
- Wilson, T. W., Rojas, D. C., Reite, M. L., Teale, P. D., and Rogers, S. J. (2007). Children and adolescents with autism exhibit reduced MEG steady-state gamma responses. *Biol. Psychiatry* 62, 192–197. doi: 10.1016/j.biopsych.2006.07.002
- Wolff, J. J., Gu, H., Gerig, G., Elison, J. T., Styner, M., Gouttard, S., et al. (2012). Network differences in white matter fiber tract development present from 6 to 24 months in infants with autism. *Am. J. Psychol.* 169, 589–600. doi: 10.1176/appi.ajp.2011.11091447
- Wunderlich, J. L., Cone-Wesson, B. K., and Shepherd, R. (2006). Maturation of the cortical auditory evoked potential in infants and young children. *Hear. Res.* 212, 185–202. doi: 10.1016/j.heares.2005.11.010

Conflict of Interest Statement: JB is a consultant for McGowan Associates. The other authors declare that the research was conducted in the absence of any commercial or financial relationships that could be construed as a potential conflict of interest.

The reviewer AM and the handling Editor declared their shared affiliation, and the handling Editor states that the process nevertheless met the standards of a fair and objective review.

Copyright © 2016 Berman, Edgar, Blaskey, Kushner, Levy, Ku, Dell and Roberts. This is an open-access article distributed under the terms of the Creative Commons Attribution License (CC BY). The use, distribution or reproduction in other forums is permitted, provided the original author(s) or licensor are credited and that the original publication in this journal is cited, in accordance with accepted academic practice. No use, distribution or reproduction is permitted which does not comply with these terms.



Recent Progress in Magnetic Resonance Imaging of the Embryonic and Neonatal Mouse Brain

Dan Wu¹ and Jiangyang Zhang^{1,2*}

¹ Department of Radiology, Johns Hopkins University School of Medicine, Baltimore, MD, USA, ² Bernard and Irene Schwartz Center for Biomedical Imaging, Department of Radiology, New York University School of Medicine, New York, NY, USA

The laboratory mouse has been widely used as a model system to investigate the genetic control mechanisms of mammalian brain development. Magnetic resonance imaging (MRI) is an important tool to characterize changes in brain anatomy in mutant mouse strains and injury progression in mouse models of fetal and neonatal brain injury. Progress in the last decade has enabled us to acquire MRI data with increasing anatomical details from the embryonic and neonatal mouse brain. High-resolution *ex vivo* MRI, especially with advanced diffusion MRI methods, can visualize complex microstructural organizations in the developing mouse brain. *In vivo* MRI of the embryonic mouse brain, which is critical for tracking anatomical changes longitudinally, has become available. Applications of these techniques may lead to further insights into the complex and dynamic processes of brain development.

Keywords: magnetic resonance imaging, microscopy, brain anatomy, brain development, embryonic mouse brain, high resolution

OPEN ACCESS

Edited by:

Hao Huang,
University of Pennsylvania, USA

Reviewed by:

David A. Leopold,
National Institutes of Health, USA
Nyoman Dana Kurniawan,
The University of Queensland,
Australia

*Correspondence:

Jiangyang Zhang
Jiangyang.zhang@nyumc.org

Received: 07 December 2015

Accepted: 15 February 2016

Published: 03 March 2016

Citation:

Wu D and Zhang J (2016) Recent Progress in Magnetic Resonance Imaging of the Embryonic and Neonatal Mouse Brain. *Front. Neuroanat.* 10:18. doi: 10.3389/fnana.2016.00018

INTRODUCTION

The mammalian brain undergoes rapid growth during the prenatal and neonatal periods. Structural changes, from the formation of basic functional units and neural circuitry to axonal pruning and myelination, are critical for normal brain functions at the adult stage. In order to investigate normal and pathological changes during these critical periods, advanced imaging tools have been developed to dissect the developing brain from macroscopic (Toga et al., 2012; Van Essen et al., 2013) to microscopic (Helmstaedter et al., 2013; Takemura et al., 2013) levels. Magnetic resonance imaging (MRI) has been increasingly used in the clinics to examine fetal brain development and injuries (Sevely and Manelfe, 2001; Limperopoulos and Clouchoux, 2009). Compared to other clinical imaging modalities that are commonly used to image the developing brain, primarily ultrasound, MRI provides high resolution and rich tissue contrasts for delineation of brain structures as well as several diagnostic markers for detecting fetal brain injuries (Rutherford, 2002). Once abnormalities in the brain are detected by ultrasound, MRI is the technique of choice in the clinic to establish the pattern of injuries (Sevely and Manelfe, 2001). Even though fetal brain MRI is increasingly adopted, there are still many questions remained to be answered. For example, what are the relationships between MRI signals and brain microstructures under normal and pathological conditions in the developing brain? To answer these questions, it is necessary to have model systems that allow direct comparisons between MRI signals and histopathology.

The laboratory mouse has been extensively used to study the genetic control mechanisms of brain development and insult-pathology correlation. Mouse brain development has also

been a major focus area of neuroscience research, and a tremendous amount of resources have been generated over the last decade, e.g., the Allen developing mouse brain atlas (<http://developingmouse.brain-map.org>). With the increasingly sophisticated gene technology (e.g., *in vivo* gene transfer Saito and Nakatsuji, 2001), there is an acute demand for high-throughput and sensitive techniques for screening anatomical phenotypes in genetically modified mouse brains during embryonic and neonatal development. In addition, several mouse models of fetal and neonatal brain disorders (e.g., Vannucci and Vannucci, 2005; Burd et al., 2009, 2010) have been established, and imaging tools that can sensitively detect disease progression in these and similar models will be beneficial for understanding the mechanisms of injury and the development of new treatments. While histology has been commonly used to characterize anatomical phenotypes, MRI has its unique advantages as described previously (Johnson et al., 2002; Turnbull and Mori, 2007). For example, the data are in 3D format and digitized, which is convenient for quantitatively analysis. Without the sectioning and staining processes, which are time consuming and may introduce tissue damages and deformation, MRI can provide whole brain coverage and does not require a prior knowledge of the location of anatomical changes, albeit at much lower resolution and specificity. Furthermore, MRI can potentially be used to acquire longitudinal data to capture the dynamic processes of brain development and to characterize disease progression.

During the last decade, tremendous progresses have been made in using MRI to study mouse brain development as described in several excellent articles. These articles cover early pioneering works on the use of MRI to study vertebrate animal development (Effmann et al., 1988; Smith et al., 1994; Jacobs et al., 1999); the development of high-resolution MRI (or MR microscopy) for virtual dissection of the adult mouse brain (Badea et al., 2009), as well as the developing mouse brain (Petiet et al., 2008); the development of advanced MRI contrasts for structural delineation in the developing mouse brain and comparisons with optical and ultrasound imaging (Turnbull and Mori, 2007), and quantitative characterization of brain development (Verma et al., 2005; Zhang et al., 2005; Baloch et al., 2009; Chuang et al., 2011; Ingallhalikar et al., 2015). For a general review on techniques commonly used for imaging the developing mouse brain, two recent review articles provide rather comprehensive lists with pros and cons (Nieman et al., 2011; Norris et al., 2013b). In this review, we mostly focus on the latest developments in using MRI to study the developing mouse brain.

EX VIVO HIGH-RESOLUTION MRI OF THE DEVELOPING MOUSE BRAIN

The average volume of an adult human brain is ~3000 times of that of an average adult mouse brain (Badea et al., 2009). In order to reliably delineate structures in the mouse brain, a spatial resolution of 0.1 mm or higher is often needed. As the size of individual voxel becomes smaller, the signals originated from each voxel decrease proportionally. This reduction in signals

can be partially compensated by using high field magnets (7 T or higher), high-sensitivity coils that closely match the brain in terms of size and geometry, the addition of signal enhancing contrast agents, and more signal averages at the cost of prolonged imaging time. Acquiring high-resolution images also demands gradient systems that can generate strong and fast-switching magnetic field gradients for efficient spatial-encoding. In general, it is necessary to have a gradient system capable of generating 400 mT/m or higher gradient strength and fast slew rates in order to reach a spatial resolution of 0.1 mm or higher (Johnson et al., 2002). These conditions can be more easily met in *ex vivo* imaging than *in vivo* imaging, as the brain can be dissected out to fit into the most sensitive coil and imaged for several hours on high field preclinical MR systems with high performance gradient systems. In this section, we reviewed several recent developments in *ex vivo* imaging of the embryonic and neonatal mouse brain.

Ex vivo T₁/T₂-Weighted MRI of the Developing Mouse Brain

T₁/T₂-weighted and diffusion MRI have been commonly used to study the developing mouse brain (Mori et al., 2001; Johnson et al., 2002; Mori and Zhang, 2006; Petiet et al., 2008; Zhang et al., 2012). One commonly used procedure to increase signal-to-noise ratio (SNR) in *ex vivo* high-resolution MRI is the application of Gadolinium (Gd)-based contrast agents, e.g., Gd-DTPA. It has been shown that several of these agents can penetrate post-mortem tissue specimens and significantly shorten the T₁ and T₂ relaxation times of mouse brain tissue to enhance signals and tissue contrasts (Sharief and Johnson, 2006). Petiet et al. studied the relationships between tissue T₁ and T₂ and the concentrations of ProHance, a Gd-based contrast agent, in the embryonic mouse brain, and showed that tissue T₁ and T₂ values change with both the concentration of ProHance as well as the immersion time (Petiet et al., 2007; Petiet and Johnson, 2010). Similar studies have been performed with Gd-DTPA in the mouse brain (Huang et al., 2009; Kim et al., 2009; Cleary et al., 2011), with the T₁ and T₂* of the embryonic mouse brain shortened from ~2000 and 40 ms without Gd-DTPA to 50 and 5 ms, respectively, after immersion in 8 mM of Gd-DTPA (Norris et al., 2013a). Interestingly, the same study also demonstrated that Gd-DTPA and a Manganese (Mn)-based contrasts agent (Mn-DPDP) enhanced different gray matter regions in the embryonic mouse brain (e.g., Figure 2 in Norris et al., 2013a). Even though the mechanisms of this selective enhancement are still not well understood, it is a promising approach to enhance tissue contrasts in the *ex vivo* embryonic and neonatal mouse brain MRI. With imaging protocols optimized for resolution and tissue contrasts, T₁/T₂-weighted images can now be acquired at spatial resolutions that approach the size of large cells in the brain. For example, Petiet et al. recently reported whole body MRI of embryonic and postnatal mice at a spatial resolution of 0.019 mm and used the technique to characterize anatomical phenotypes in a mutant mouse strain (Petiet et al., 2008; See **Table 1** for the imaging parameters).

TABLE 1 | Imaging parameters of selected reports on *ex vivo* MRI of the embryonic and neonatal mouse brain.

Study	Age	Instrument	Contrast agent (Concentration)	Resolution	Contrast and Sequence	Scan time
Petiet et al., 2008	E10.5–E19.5 P0–P32	9.4 T and 7 T	Prohance (20 mM)	0.0195 × 0.0195 × 0.0195 mm	T ₁ , 3D SE TE/TR = 5.2/75 ms	3–12 h
Aggarwal et al., 2015	E12.5–E18.5	11.7 T	Magnevist (3 mM)	0.052 × 0.052 × 0.052 mm	3D dw- GRASE, b = 1400 s/mm ² , 18 directions	21.5–32 h
Norris et al., 2015	E15.5	9.4 T	Magnevist (2 mM)	0.075 × 0.075 × 0.075 mm	3D dw- FSE/SE, b = 1498 s/mm ² , 42 directions	76 h for 3D SE 19 h for 3D FSE

dw, diffusion-weighted; FSE, fast spin echo; GRASE, gradient and spin echo; SE, spin echo; T, Tesla; TE, echo time; TR, repetition time.

Ex vivo Diffusion MRI of the Developing Mouse Brain

While conventional T₁/T₂-weighted MRI provides satisfactory contrasts for delineation of internal organs and major brain compartments, such as the ventricles and cerebellum, it often lacks good contrasts to further distinguish internal structures within major brain compartments (Zhang et al., 2005), e.g., early white matter tracts. As shown in Zhang et al. (2005), the T₂ contrasts between gray and white matter structures in the developing mouse brain change dramatically as the brain matures. For example, in embryonic and neonatal mouse brains, the corpus callosum has higher T₂ values than the surrounding gray matter structures, and this contrast is inverted in the adult mouse brain, which may reflect the changes in tissue water and myelin contents during development and maturation. The lack of consistent contrasts makes it difficult to reliably trace structural development using conventional T₁/T₂-weighted MRI. In comparison, diffusion MRI techniques, e.g., diffusion tensor imaging (DTI; Basser et al., 1994; Basser and Pierpaoli, 1996), provide superior contrasts for delineation of the premature gray and white matter structures. The image contrasts of DTI are sensitive to microscopic organization of tissue microstructures, and the contrast patterns remain relatively stable over the late embryonic and early postnatal periods (Zhang et al., 2005). This is one of the advantages that makes diffusion MRI the ideal tool to examine the development of early white matter tracts in the embryonic mouse brain as well as several gray matter structures, e.g., the embryonic cortex (Zhang et al., 2003).

In the recent years, high-resolution diffusion MRI of the developing mouse brain using sophisticated diffusion MRI techniques has been implemented to enhance our ability to resolve microstructural organizations of the developing mouse brain. Previously, it was common to acquire diffusion MRI data along a small set of 6–12 diffusion encoding directions with a moderate diffusion weighting (*b*-value = 1000–1500 s/mm²) and an isotropic spatial resolution of 0.1 mm (Mori et al., 2001; Zhang et al., 2003; Wang et al., 2006). Because DTI is inherently limited by the use of Gaussian model for water diffusion, it cannot resolve complex tissue microstructures, which demands more sophisticated diffusion MRI techniques, such as Q-ball (Tuch et al., 2003), high angular resolution diffusion imaging

(HARDI; Frank, 2001), and diffusion spectrum imaging (Wedeen et al., 2005). These techniques, however, all require diffusion MRI data acquired along more diffusion directions (also called high angular resolution) than the minimal set required by DTI and with relatively strong diffusion weighting (*b*-value > 2000 s/mm²), which will result in prolonged imaging time and reduced SNR. These challenges can be addressed by using Gd-DTPA and fast imaging sequences. It is necessary to note that, for diffusion MRI, Gd-based contrast agents should be added at lower concentration than conventional T₁/T₂-weighted MRI (~2 mM for Gd-DTPA vs. 20 mM for ProHance as in Petiet et al., 2008) due to the fact that high concentration of Gd-based contrast agent can shorten tissue T₂ values to the extent that signal attenuation due to spin-spin relaxation during the diffusion encoding time will cancel the gain from shortened T₁. Norris et al. reported an optimized for *ex vivo* diffusion MRI of the embryonic mouse brain (Norris et al., 2015). Fast imaging can be achieved using the modified diffusion weighted sequence, such as diffusion weighted fast spin echo or gradient-and-spin echo (GRASE) sequences (Aggarwal et al., 2010; Norris et al., 2013a). Using a GRASE sequence, Aggarwal et al. demonstrated diffusion MRI of the embryonic mouse brain at 0.05 mm isotropic resolution and 12 diffusion-encoding directions (Aggarwal et al., 2010; See Table 1 for the imaging parameters). Figure 1 shows diffusion MRI data acquired from embryonic mouse brains using a modified version of the GRASE sequence at 0.03 mm isotropic resolution and 30 diffusion encoding directions (Wu et al., 2014).

With high spatial and angular resolution diffusion MRI data, several techniques can be used to potentially reconstruct early axonal tracts and resolve complex tissue microstructures in the brain. For example, probabilistic tractography (Behrens et al., 2007) based on constrained spherical deconvolution (CSD; Tournier et al., 2007) allow more robust determination of axonal tracts that cross each other (Moldrich et al., 2010), and tract-density imaging (TDI; Calamante et al., 2010, 2012) facilitates more direct visualization of microstructural organization in the embryonic mouse brain based on high-resolution diffusion MRI data. Aggarwal et al. recently used high-resolution TDI to visualize the changing microstructural organizations in the embryonic mouse cortex (Aggarwal et al., 2015), which share comparable patterns to human fetal brain (Xu et al., 2014).

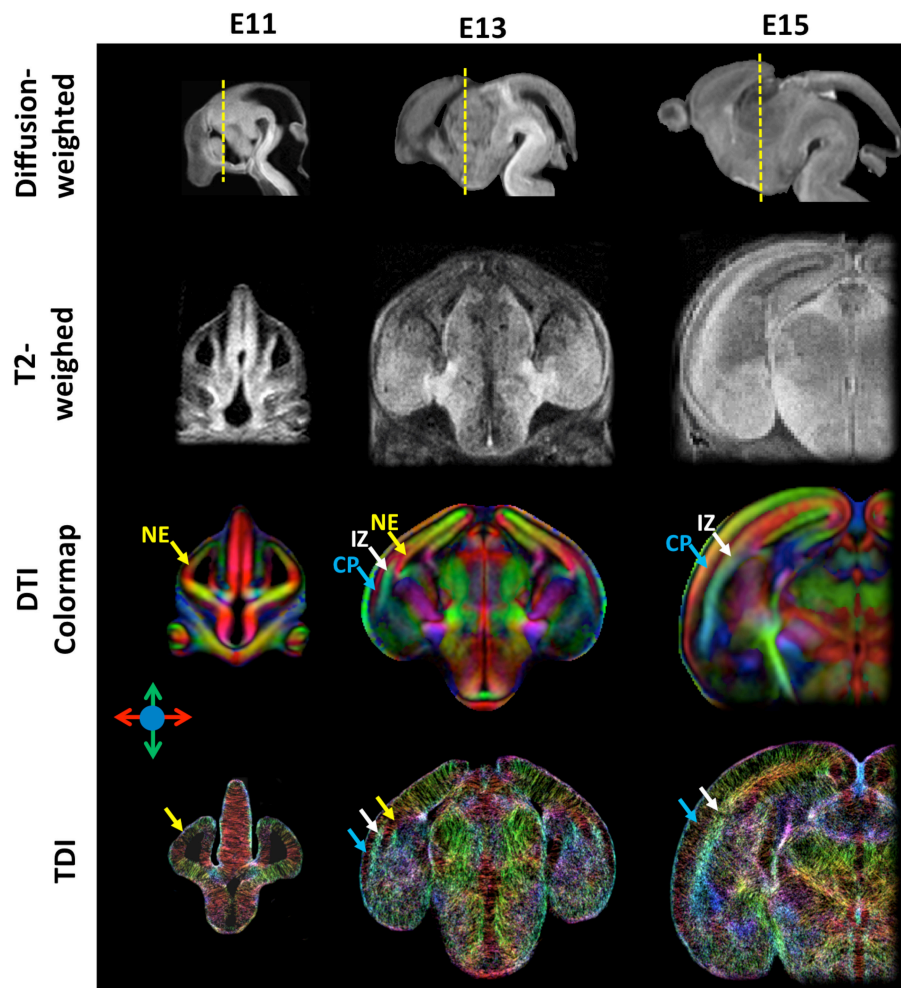


FIGURE 1 | High-resolution diffusion-weighted, T₂-weighted, diffusion tensor directionally encoded colormap (DTI colormap), and track density images of embryonic mouse brains at embryonic day 11, 13, and 15. The diffusion-weighted images show the mid-sagittal plane of the mouse brain, and the T₂-weighted, DTI colormap, and TDI data show a coronal plane as indicated by the yellow dash lines in the corresponding diffusion-weighted images. The MRI data were acquired at an isotropic spatial resolution of 0.03 mm, and the diffusion MRI data were acquired with 30 diffusion encoding directions and *b*-value of 1300–1500 s/mm². Early cortical structures can be appreciated in the DTI colormaps and TDI data. Structural abbreviations are: CP, cortical plate; IZ, intermediate zone; NE, neuroepithelium. The color scheme used in the DTI colormaps and TDI are: red: left-right; green: ventral-dorsal; blue: rostral-caudal, as indicated by the color arrows.

IN VIVO MRI OF THE DEVELOPING MOUSE BRAIN

Compared to *ex vivo* MRI, *in vivo* MRI of the developing mouse brain faces several challenges. The total imaging time is often limited to less than 2 h as long exposure of anesthesia has detrimental effects on the developing brain (Liang et al., 2010). In addition, the sensitivity of *in vivo* MRI coils is often lower than *ex vivo* MRI due to the increased coil size needed to accommodate the entire head, the air anesthesia setup, and animal monitoring system. Furthermore, it is often difficult to restrain motions in neonatal mice and mouse embryos in the uterus even with anesthesia. For example, the ear canal and teeth are not fully developed in neonatal mice, and conventional motion restriction setups based on ear pins and bite bars for adult mouse cannot be applied. Due to these challenges, *in vivo* MRI of the embryonic

and neonatal mouse brain has not been frequently reported. This has started to change in recent years, and in this section, we will highlight a few recent developments on *in vivo* MRI of the embryonic mouse brain.

In vivo MRI of the Embryonic Mouse Brain

In vivo MRI of the embryonic mouse brain is extremely challenging. There are usually 6–12 embryos in the uterus of a pregnant mouse, as shown in **Figure 2**, each within its own embryonic sac. Motions from both the embryos and maternal mice are cause severe motion artifacts, and the large variations in the locations and orientations of embryos make it difficult to apply high-sensitivity surface coils, which limits the SNR. In addition, high resolution in all three dimensions is often required to resolve structures within the miniature brains (< 6 mm in any dimensions). *In vivo* MRI of mouse embryos have

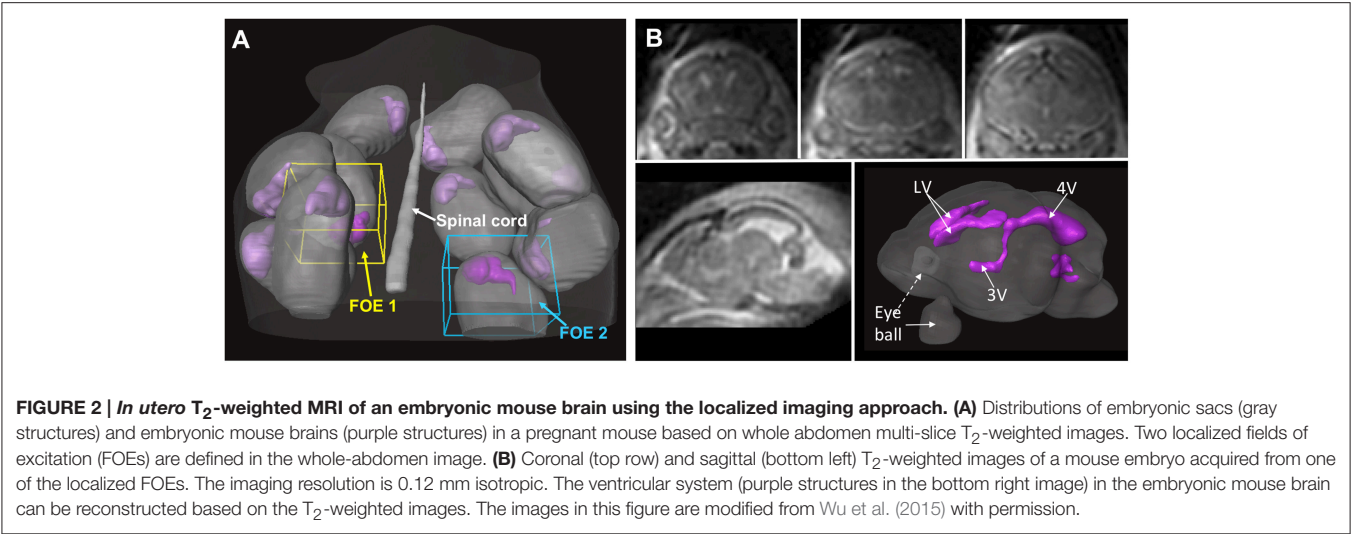


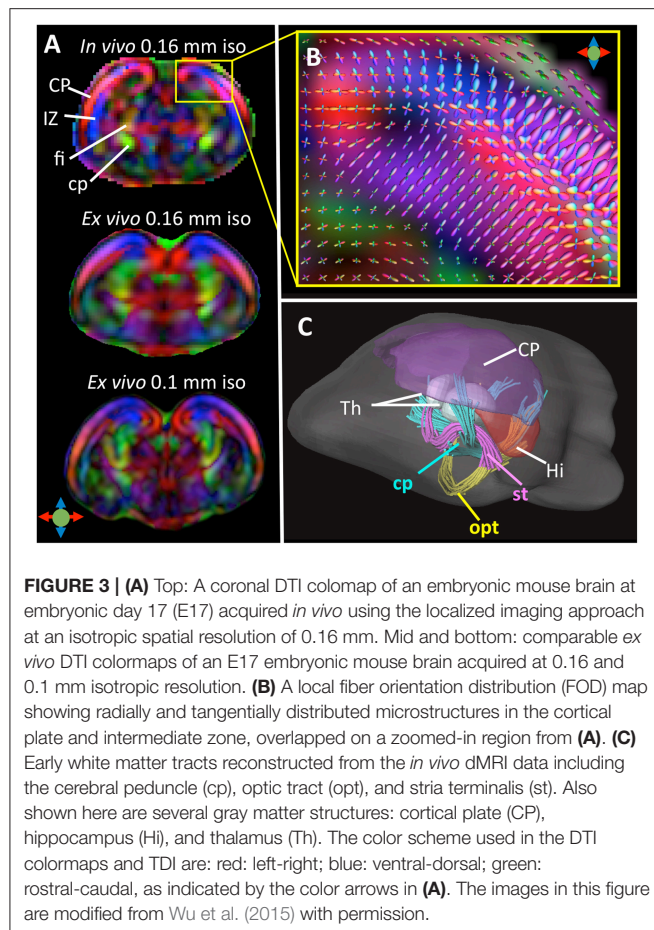
TABLE 2 | Imaging parameters of selected reports on *in vivo* MRI of the embryonic and neonatal mouse brain.

Study	Age	Instrument	Contrast agent (Concentration)	Resolution	Contrast and Sequence	Scan time
Szulc et al., 2015	P1–P11	7 T	MnCl ₂ (50 mg/kg maternal i.p. injection, 24 h prior MRI)	0.1 × 0.1 × 0.1 mm	T1, 3D GE TE/TR = 3.6/50 ms	~ 2 h
Deans et al., 2008	E12.5–E18.5	7 T	MnCl ₂ (up to 80 mg/kg maternal i.p. injection, 24 h prior MRI)	0.1 × 0.1 × 0.1 mm	T1, 3D GE TE/TR = 5/40 ms	70–90 min
Wu et al., 2015	E17	11.7 T	Magnevist (0.4 mMol/Kg, maternal i.p. injection, 2 h prior MRI)	0.16 × 0.16 × 0.16 mm	3D dw-GRASE, b = 1000 s/mm ² , 30 directions	~ 2 h

dw, diffusion-weighted; FSE, fast spin echo; GRASE, gradient and spin echo; SE, spin echo; T, Telsa; TE, echo time; TR, repetition time.

been demonstrated before (Hogers et al., 2000; Chapon et al., 2002, 2005) with 2D multi-slice imaging. Recently, Turnbull and colleagues demonstrated successful *in vivo* embryonic mouse brain T₁-weighted MRI using advanced motion correction techniques on a 7 Tesla MRI system (Nieman et al., 2009; Berrios-Otero et al., 2012; Parasoglou et al., 2013), and have successfully imaged vasculature of embryonic mouse brain and use it to study a mutant mouse strain (Berrios-Otero et al., 2009, 2012). Furthermore, they recently demonstrated that Mn-enhanced MRI (MEMRI) of the embryonic (Deans et al., 2008) and neonatal mouse brain (Szulc et al., 2015; See **Table 2** for the imaging parameters used in related studies). They showed that, at various stages, the spatial pattern of Mn enhancement gradually changes, corresponding to neuronal development in the brain. Deans et al. reported that mouse embryos as early as E11.5 can survive for at least 24 h after a single dose of MnCl₂ of 80 mg/Kg (Deans et al., 2008), suggesting the feasibility of using MEMRI to study embryonic mouse brain development. The neurotoxicity of Mn (Sánchez et al., 1993), however, is a potential limiting factor for longitudinal studies. For example, Szulc et al. reported reduced body weights in neonatal mice after Mn exposure (Szulc et al., 2015). Future studies are needed to define the effects Mn exposure on mouse brain development.

Compared to *in vivo* T₁/T₂-weighted MRI, *in vivo* diffusion MRI of the embryonic mouse brain is even more challenging because diffusion MRI is more susceptible to motion, requires length acquisition, and generally has lower SNR due to diffusion-related signal attenuation. In our recent study (Wu et al., 2015), we demonstrated the feasibility of *in-utero* diffusion MRI of the embryonic mouse brain using a localized imaging approach (Finsterbusch, 2010; Schneider et al., 2013) with spatially selective excitation pulses (Pauly et al., 1989; See **Table 2** for the imaging parameters). The localized imaging strategy is advantageous because localization can significantly reduce the field-of-view from the whole abdomen to selected embryos, and therefore, shortens the imaging time for 3D imaging and enables high spatial resolution at a given scan time. Combined with a 3D fast imaging sequence and motion correction techniques, we achieved *in-utero* diffusion MRI to study microstructural features in normal and injured embryonic mouse brains. The technique was used to acquire high-resolution T₂-weighted images (0.12 mm isotropic resolution in 12 mins; **Figure 2B**) and diffusion MRI data (up to 0.16 mm isotropic resolution, 30 directions in 2 h; **Figure 3A**). The basic organization of cortical microstructures (**Figure 3B**) and 3D trajectories of early axonal tracts (**Figure 3C**), albeit at lower resolution than *ex vivo* MRI results, can be visualized non-invasively for the first time.



comparison, *in vivo* MRI, especially, for embryonic mouse brains, still faces many challenges, but has the potential to contribute to better understanding of brain development. Further optimization may improve the resolution and speed of *in vivo* MRI of the embryonic and neonatal mouse brain. New imaging contrasts, e.g., perfusion and more sophisticated diffusion techniques, may be introduced to study the developing mouse brain.

With the increasingly availability of high-resolution MRI data of embryonic and neonatal mouse brains, it is imperative to develop quantitative tools to characterize anatomical phenotypes sensitively and efficiently. MRI-based atlases of the developing mouse brain are important assets (Chuang et al., 2011) to facilitate quantitative measurement of volume and other tissue properties in the brain. Several groups have demonstrated the use of advanced computational tools to characterize the developing mouse brain in terms of their volumetric changes (Verma et al., 2005; Zhang et al., 2005; Baloch et al., 2009) and connectivity (Ingallhalikar et al., 2015). In addition, techniques that can register MRI and histological data have been developed. For example, the Allen brain reference atlas was built on histological images normalized to a MRI dataset of the adult mouse brain (Lein et al., 2007). More sophisticated image registration technique can potentially correct distortions in histological images to a certain degree and form a 3D volume, which will enable systematic examination of the spatial patterns of MRI and histological data.

AUTHOR CONTRIBUTIONS

All authors listed, have made substantial, direct and intellectual contribution to the work, and approved it for publication.

FUNDING

The authors are supported by Howard Hughes Medical Institute (HHMI) International Student Research Fellowship (DW) and National Institute of Health (NIH) NIH R01 NS070909 (JZ) and NIH R01 HD074593 (JZ).

FUTURE DIRECTIONS

In the last decade, multiple technical developments have allowed us to acquire MRI data from the developing mouse brain with increasing resolution. *Ex vivo* MRI can now be routinely used to study anatomical phenotypes in mutant mouse strains. In

REFERENCES

- Aggarwal, M., Gobius, I., Richards, L. J., and Mori, S. (2015). Diffusion MR microscopy of cortical development in the mouse embryo. *Cereb. Cortex* 25, 1970–1980. doi: 10.1093/cercor/bhu006
- Aggarwal, M., Mori, S., Shimogori, T., Blackshaw, S., and Zhang, J. (2010). Three-dimensional diffusion tensor microimaging for anatomical characterization of the mouse brain. *Magn. Reson. Med.* 64, 249–261. doi: 10.1002/mrm.22426
- Badea, A., Johnson, G. A., and Williams, R. W. (2009). Genetic dissection of the mouse CNS using magnetic resonance microscopy. *Curr. Opin. Neurol.* 22, 379–386. doi: 10.1097/WCO.0b013e32832d9b86
- Baloch, S., Verma, R., Huang, H., Khurd, P., Clark, S., Yarowsky, P., et al. (2009). Quantification of brain maturation and growth patterns in C57BL/6J mice via computational neuroanatomy of diffusion tensor images. *Cereb. Cortex* 19, 675–687. doi: 10.1093/cercor/bhn112
- Basser, P. J., Mattiello, J., and LeBihan, D. (1994). MR diffusion tensor spectroscopy and imaging. *Biophys. J.* 66, 259–267. doi: 10.1016/S0006-3495(94)80775-1
- Basser, P. J., and Pierpaoli, C. (1996). Microstructural and physiological features of tissues elucidated by quantitative-diffusion-tensor MRI. *J. Magn. Reson. B* 111, 209–219. doi: 10.1006/jmrb.1996.0086
- Behrens, T. E., Berg, H. J., Jbabdi, S., Rushworth, M. F., and Woolrich, M. W. (2007). Probabilistic diffusion tractography with multiple fibre orientations: what can we gain? *Neuroimage* 34, 144–155. doi: 10.1016/j.neuroimage.2006.09.018
- Berrios-Otero, C. A., Nieman, B. J., Parasoglou, P., and Turnbull, D. H. (2012). *In utero* phenotyping of mouse embryonic vasculature with MRI. *Magn. Reson. Med.* 67, 251–257. doi: 10.1002/mrm.22991
- Berrios-Otero, C. A., Wadghiri, Y. Z., Nieman, B. J., Joyner, A. L., and Turnbull, D. H. (2009). Three-dimensional micro-MRI analysis of cerebral artery development in mouse embryos. *Magn. Reson. Med.* 62, 1431–1439. doi: 10.1002/mrm.22113
- Burd, I., Bentz, A. I., Gonzalez, J., Chai, J., Monnerie, H., Le Roux, P. D., et al. (2010). Inflammation-induced preterm birth alters neuronal morphology in the mouse fetal brain. *J. Neurosci. Res.* 88, 1872–1881. doi: 10.1002/jnr.22368

- Burd, I., Chai, J., Gonzalez, J., Ofori, E., Monnerie, H., Le Roux, P. D., et al. (2009). Beyond white matter damage: fetal neuronal injury in a mouse model of preterm birth. *Am. J. Obstet. Gynecol.* 201, 279.e1–279.e8. doi: 10.1016/j.ajog.2009.06.013
- Calamante, F., Tournier, J. D., Jackson, G. D., and Connelly, A. (2010). Track-density imaging (TDI): super-resolution white matter imaging using whole-brain track-density mapping. *Neuroimage* 53, 1233–1243. doi: 10.1016/j.neuroimage.2010.07.024
- Calamante, F., Tournier, J. D., Kurniawan, N. D., Yang, Z., Gyengesi, E., Galloway, G. J., et al. (2012). Super-resolution track-density imaging studies of mouse brain: comparison to histology. *Neuroimage* 59, 286–296. doi: 10.1016/j.neuroimage.2011.07.014
- Chapon, C., Franconi, F., Roux, J., Le Jeune, J. J., and Lemaire, L. (2005). Prenatal evaluation of kidney function in mice using dynamic contrast-enhanced magnetic resonance imaging. *Anat. Embryol. (Berl.)* 209, 263–267. doi: 10.1007/s00429-004-0451-9
- Chapon, C., Franconi, F., Roux, J., Marescaux, L., Le Jeune, J. J., and Lemaire, L. (2002). *In utero* time-course assessment of mouse embryo development using high resolution magnetic resonance imaging. *Anat. Embryol. (Berl.)* 206, 131–137. doi: 10.1007/s00429-002-0281-6
- Chuang, N., Mori, S., Yamamoto, A., Jiang, H., Ye, X., Xu, X., et al. (2011). An MRI-based atlas and database of the developing mouse brain. *NeuroImage* 54, 80–89. doi: 10.1016/j.neuroimage.2010.07.043
- Cleary, J. O., Wiseman, F. K., Norris, F. C., Price, A. N., Choy, M., Tybulewicz, V. L., et al. (2011). Structural correlates of active-staining following magnetic resonance microscopy in the mouse brain. *Neuroimage* 56, 974–983. doi: 10.1016/j.neuroimage.2011.01.082
- Deans, A. E., Wadghiri, Y. Z., Berrios-Otero, C. A., and Turnbull, D. H. (2008). Mn enhancement and respiratory gating for *in utero* MRI of the embryonic mouse central nervous system. *Magn. Reson. Med.* 59, 1320–1328. doi: 10.1002/mrm.21609
- Effmann, E. L., Johnson, G. A., Smith, B. R., Talbott, G. A., and Cofer, G. (1988). Magnetic resonance microscopy of chick embryos in ovo. *Teratology* 38, 59–65. doi: 10.1002/tera.1420380109
- Finsterbusch, J. (2010). Fast-spin-echo imaging of inner fields-of-view with 2D-selective RF excitations. *J. Magn. Reson. Imaging* 31, 1530–1537. doi: 10.1002/jmri.22196
- Frank, L. R. (2001). Anisotropy in high angular resolution diffusion-weighted MRI. *Magn. Reson. Med.* 45, 935–939. doi: 10.1002/mrm.1125
- Helmstaedter, M., Briggman, K. L., Turaga, S. C., Jain, V., Seung, H. S., and Denk, W. (2013). Connectomic reconstruction of the inner plexiform layer in the mouse retina. *Nature* 500, 168–174. doi: 10.1038/nature12346
- Hogers, B., Gross, D., Lehmann, V., Zick, K., De Groot, H. J., Gittenberger-De Groot, A. C., et al. (2000). Magnetic resonance microscopy of mouse embryos *in utero*. *Anat. Rec.* 260, 373–377. doi: 10.1002/1097-0185(20001201)260:4<373::AID-AR60>3.0.CO;2-Q
- Huang, S., Liu, C., Dai, G., Kim, Y. R., and Rosen, B. R. (2009). Manipulation of tissue contrast using contrast agents for enhanced MR microscopy in *ex vivo* mouse brain. *Neuroimage* 46, 589–599. doi: 10.1016/j.neuroimage.2009.02.027
- Ingalhalikar, M., Parker, D., Ghanbari, Y., Smith, A., Hua, K., Mori, S., et al. (2015). Connectome and maturation profiles of the developing mouse brain using diffusion tensor imaging. *Cereb. Cortex* 25, 2696–2706. doi: 10.1093/cercor/bhu068
- Jacobs, R. E., Ahrens, E. T., Meade, T. J., and Fraser, S. E. (1999). Looking deeper into vertebrate development. *Trends Cell Biol.* 9, 73–76. doi: 10.1016/S0962-8924(98)01435-4
- Johnson, G. A., Cofer, G. P., Fubara, B., Gewalt, S. L., Hedlund, L. W., and Maronpot, R. R. (2002). Magnetic resonance histology for morphologic phenotyping. *J. Magn. Reson. Imaging* 16, 423–429. doi: 10.1002/jmri.10175
- Kim, S., Pickup, S., Hsu, O., and Poptani, H. (2009). Enhanced delineation of white matter structures of the fixed mouse brain using Gd-DTPA in microscopic MRI. *NMR Biomed.* 22, 303–309. doi: 10.1002/nbm.1324
- Lein, E. S., Hawrylycz, M. J., Ao, N., Ayres, M., Bensinger, A., Bernard, A., et al. (2007). Genome-wide atlas of gene expression in the adult mouse brain. *Nature* 445, 168–176. doi: 10.1038/nature05453
- Liang, G., Ward, C., Peng, J., Zhao, Y., Huang, B., and Wei, H. (2010). Isoflurane causes greater neurodegeneration than an equivalent exposure of sevoflurane in the developing brain of neonatal mice. *Anesthesiology* 112, 1325–1334. doi: 10.1097/ALN.0b013e3181d94da5
- Limperopoulos, C., and Clouchoux, C. (2009). Advancing fetal brain MRI: targets for the future. *Semin. Perinatol.* 33, 289–298. doi: 10.1053/j.semper.2009.04.002
- Moldrich, R. X., Pannek, K., Hoch, R., Rubenstein, J. L., Kurniawan, N. D., and Richards, L. J. (2010). Comparative mouse brain tractography of diffusion magnetic resonance imaging. *Neuroimage* 51, 1027–1036. doi: 10.1016/j.neuroimage.2010.03.035
- Mori, S., Itoh, R., Zhang, J., Kaufmann, W. E., van Zijl, P. C., Solaiyappan, M., et al. (2001). Diffusion tensor imaging of the developing mouse brain. *Magn. Reson. Med.* 46, 18–23. doi: 10.1002/mrm.1155
- Mori, S., and Zhang, J. (2006). Principles of diffusion tensor imaging and its applications to basic neuroscience research. *Neuron* 51, 527–539. doi: 10.1016/j.neuron.2006.08.012
- Nieman, B. J., Szulc, K. U., and Turnbull, D. H. (2009). Three-dimensional, *in vivo* MRI with self-gating and image coregistration in the mouse. *Magn. Reson. Med.* 61, 1148–1157. doi: 10.1002/mrm.21945
- Nieman, B. J., Wong, M. D., and Henkelman, R. M. (2011). Genes into geometry: imaging for mouse development in 3D. *Curr. Opin. Genet. Dev.* 21, 638–646. doi: 10.1016/j.gde.2011.08.009
- Norris, F. C., Betts-Henderson, J., Wells, J. A., Cleary, J. O., Siow, B. M., Walker-Samuel, S., et al. (2013a). Enhanced tissue differentiation in the developing mouse brain using magnetic resonance micro-histology. *Magn. Reson. Med.* 70, 1380–1388. doi: 10.1002/mrm.24573
- Norris, F. C., Siow, B. M., Cleary, J. O., Wells, J. A., De Castro, S. C., Ordidge, R. J., et al. (2015). Diffusion microscopic MRI of the mouse embryo: Protocol and practical implementation in the splotch mouse model. *Magn. Reson. Med.* 73, 731–739. doi: 10.1002/mrm.25145
- Norris, F. C., Wong, M. D., Greene, N. D., Scambler, P. J., Weaver, T., Weninger, W. J., et al. (2013b). A coming of age: advanced imaging technologies for characterising the developing mouse. *Trends Genet.* 29, 700–711. doi: 10.1016/j.tig.2013.08.004
- Parasoglou, P., Berrios-Otero, C. A., Nieman, B. J., and Turnbull, D. H. (2013). High-resolution MRI of early-stage mouse embryos. *NMR Biomed.* 26, 224–231. doi: 10.1002/nbm.2843
- Pauly, J., Nishimura, D., and Macovski, A. (1989). A linear class of large-tip-angle selective excitation pulses. *J. Magn. Reson.* 82, 571–587. doi: 10.1016/0022-2364(89)90219-9
- Petiet, A., Hedlund, L., and Johnson, G. A. (2007). Staining methods for magnetic resonance microscopy of the rat fetus. *J. Magn. Reson. Imaging* 25, 1192–1198. doi: 10.1002/jmri.20932
- Petiet, A., and Johnson, G. A. (2010). Active staining of mouse embryos for magnetic resonance microscopy. *Methods Mol. Biol.* 611, 141–149. doi: 10.1007/978-1-60327-345-9_11
- Petiet, A. E., Kaufman, M. H., Goddeeris, M. M., Brandenburg, J., Elmore, S. A., and Johnson, G. A. (2008). High-resolution magnetic resonance histology of the embryonic and neonatal mouse: a 4D atlas and morphologic database. *Proc. Natl. Acad. Sci. U.S.A.* 105, 12331–12336. doi: 10.1073/pnas.0805747105
- Rutherford, M. A. (2002). *MRI of the Neonatal Brain*. New York, NY: Saunders Ltd.
- Saito, T., and Nakatsuji, N. (2001). Efficient gene transfer into the embryonic mouse brain using *in vivo* electroporation. *Dev. Biol.* 240, 237–246. doi: 10.1006/dbio.2001.0439
- Sánchez, D. J., Domingo, J. L., Llobet, J. M., and Keen, C. L. (1993). Maternal and developmental toxicity of manganese in the mouse. *Toxicol. Lett.* 69, 45–52. doi: 10.1016/0378-4274(93)90144-M
- Schneider, J. T., Kalayciyan, R., Haas, M., Herrmann, S. R., Ruhm, W., Hennig, J., et al. (2013). Inner-volume imaging *in vivo* using three-dimensional parallel spatially selective excitation. *Magn. Reson. Med.* 69, 1367–1378. doi: 10.1002/mrm.24381
- Sevely, A., and Manelfe, C. (2001). “Magnetic resonance imaging of the fetal brain,” in *MRI of the Neonatal Brain* ed M. Rutherford (New York, NY: Saunders Ltd.). Available online at: <http://www.mrineonatalbrain.com/ch04-15.php>
- Sharief, A. A., and Johnson, G. A. (2006). Enhanced T2 contrast for MR histology of the mouse brain. *Magn. Reson. Med.* 56, 717–725. doi: 10.1002/mrm.21026
- Smith, B. R., Johnson, G. A., Groman, E. V., and Linney, E. (1994). Magnetic resonance microscopy of mouse embryos. *Proc. Natl. Acad. Sci. U.S.A.* 91, 3530–3533. doi: 10.1073/pnas.91.9.3530

- Szulc, K. U., Lerch, J. P., Nieman, B. J., Bartelle, B. B., Friedel, M., Suero-Abreu, G. A., et al. (2015). 4D MEMRI atlas of neonatal FVB/N mouse brain development. *Neuroimage* 118, 49–62. doi: 10.1016/j.neuroimage.2015.05.029
- Takemura, S. Y., Bharioke, A., Lu, Z., Nern, A., Vitaladevuni, S., Rivlin, P. K., et al. (2013). A visual motion detection circuit suggested by *Drosophila* connectomics. *Nature* 500, 175–181. doi: 10.1038/nature12450
- Toga, A. W., Clark, K. A., Thompson, P. M., Shattuck, D. W., and Van Horn, J. D. (2012). Mapping the human connectome. *Neurosurgery* 71, 1–5. doi: 10.1227/NEU.0b013e318258e9ff
- Tournier, J. D., Calamante, F., and Connelly, A. (2007). Robust determination of the fibre orientation distribution in diffusion MRI: non-negativity constrained super-resolved spherical deconvolution. *Neuroimage* 35, 1459–1472. doi: 10.1016/j.neuroimage.2007.02.016
- Tuch, D. S., Reese, T. G., Wiegell, M. R., and Wedeen, V. J. (2003). Diffusion MRI of complex neural architecture. *Neuron* 40, 885–895. doi: 10.1016/S0896-6273(03)00758-X
- Turnbull, D. H., and Mori, S. (2007). MRI in mouse developmental biology. *NMR Biomed.* 20, 265–274. doi: 10.1002/nbm.1146
- Van Essen, D. C., Smith, S. M., Barch, D. M., Behrens, T. E., Yacoub, E., and Ugurbil, K. (2013). The WU-minn human connectome project: an overview. *Neuroimage* 80, 62–79. doi: 10.1016/j.neuroimage.2013.05.041
- Vannucci, R. C., and Vannucci, S. J. (2005). Perinatal hypoxic-ischemic brain damage: evolution of an animal model. *Dev. Neurosci.* 27, 81–86. doi: 10.1159/000085978
- Verma, R., Mori, S., Shen, D., Yarowsky, P., Zhang, J., and Davatzikos, C. (2005). Spatiotemporal maturation patterns of murine brain quantified by diffusion tensor MRI and deformation-based morphometry. *Proc. Natl. Acad. Sci. U.S.A.* 102, 6978–6983. doi: 10.1073/pnas.0407828102
- Wang, Y., Zhang, J., Mori, S., and Nathans, J. (2006). Axonal growth and guidance defects in *Frizzled3* knock-out mice: a comparison of diffusion tensor magnetic resonance imaging, neurofilament staining, and genetically directed cell labeling. *J. Neurosci.* 26, 355–364. doi: 10.1523/JNEUROSCI.3221-05.2006
- Wedeen, V. J., Hagmann, P., Tseng, W. Y., Reese, T. G., and Weisskoff, R. M. (2005). Mapping complex tissue architecture with diffusion spectrum magnetic resonance imaging. *Magn. Reson. Med.* 54, 1377–1386. doi: 10.1002/mrm.20642
- Wu, D., Gobius, I., Richards, L. J., Mori, S., and Zhang, J. (2014). “High resolution HARDI of early embryonic mouse brain development,” in *International Society for Magnetic Resonance in Medicine* (Red Hook, NY: Curran Associates, Inc.), 0072.
- Wu, D., Lei, J., Rosenzweig, J. M., Burd, I., and Zhang, J. (2015). *In utero* localized diffusion MRI of the embryonic mouse brain microstructure and injury. *J. Magn. Reson. Imaging* 42, 717–728. doi: 10.1002/jmri.24828
- Xu, G., Takahashi, E., Folkerth, R. D., Haynes, R. L., Volpe, J. J., Grant, P. E., et al. (2014). Radial coherence of diffusion tractography in the cerebral white matter of the human fetus: neuroanatomic insights. *Cereb. Cortex* 24, 579–592. doi: 10.1093/cercor/bhs330
- Zhang, J., Aggarwal, M., and Mori, S. (2012). Structural insights into the rodent CNS via diffusion tensor imaging. *Trends Neurosci.* 35, 412–421. doi: 10.1016/j.tins.2012.04.010
- Zhang, J., Miller, M. I., Plachez, C., Richards, L. J., Yarowsky, P., van Zijl, P., et al. (2005). Mapping postnatal mouse brain development with diffusion tensor microimaging. *Neuroimage* 26, 1042–1051. doi: 10.1016/j.neuroimage.2005.03.009
- Zhang, J., Richards, L. J., Yarowsky, P., Huang, H., van Zijl, P. C., and Mori, S. (2003). Three-dimensional anatomical characterization of the developing mouse brain by diffusion tensor microimaging. *Neuroimage* 20, 1639–1648. doi: 10.1016/S1053-8119(03)00410-5

Conflict of Interest Statement: The authors declare that the research was conducted in the absence of any commercial or financial relationships that could be construed as a potential conflict of interest.

Copyright © 2016 Wu and Zhang. This is an open-access article distributed under the terms of the Creative Commons Attribution License (CC BY). The use, distribution or reproduction in other forums is permitted, provided the original author(s) or licensor are credited and that the original publication in this journal is cited, in accordance with accepted academic practice. No use, distribution or reproduction is permitted which does not comply with these terms.



Quantitative and Qualitative Analysis of Transient Fetal Compartments during Prenatal Human Brain Development

Lana Vasung^{1,2*}, Claude Lepage³, Milan Radoš¹, Mihovil Pletikos^{1,4}, Jennifer S. Goldman³, Jonas Richiardi⁵, Marina Raguž¹, Elda Fisci-Gómez², Sherif Karama³, Petra S. Huppi², Alan C. Evans^{3†} and Ivica Kostovic^{1†}

¹ Department of Developmental Neuroscience, Croatian Institute for Brain Research, School of Medicine, University of Zagreb, Zagreb, Croatia, ² Division of Development and Growth, Department of Pediatrics, University of Geneva, Geneva, Switzerland, ³ Ludmer Centre for Neuroinformatics, McGill Centre for Integrative Neuroscience, Department of Biomedical Engineering, Montreal Neurological Institute, Montreal, McGill University, Montreal, QC, Canada, ⁴ Department of Neuroscience and Kavli Institute for Neuroscience, Yale School of Medicine, New Haven, CT, USA, ⁵ Laboratory of Neurology and Imaging of Cognition, Department of Neuroscience, University of Geneva, Geneva, Switzerland

OPEN ACCESS

Edited by:

Hao Huang,
University of Pennsylvania, USA

Reviewed by:

Anthony James Barkovich,
University of California, San Francisco,
USA

Emi Takahashi,
Boston Children's Hospital, USA

*Correspondence:

Lana Vasung
lana.vasung@gmail.com

[†] Last co-authors.

Received: 31 October 2015

Accepted: 01 February 2016

Published: 24 February 2016

Citation:

Vasung L, Lepage C, Radoš M, Pletikos M, Goldman JS, Richiardi J, Raguž M, Fisci-Gómez E, Karama S, Huppi PS, Evans AC and Kostovic I (2016) Quantitative and Qualitative Analysis of Transient Fetal Compartments during Prenatal Human Brain Development. *Front. Neuroanat.* 10:11. doi: 10.3389/fnana.2016.00011

The cerebral wall of the human fetal brain is composed of transient cellular compartments, which show characteristic spatiotemporal relationships with intensity of major neurogenic events (cell proliferation, migration, axonal growth, dendritic differentiation, synaptogenesis, cell death, and myelination). The aim of the present study was to obtain new quantitative data describing volume, surface area, and thickness of transient compartments in the human fetal cerebrum. Forty-four postmortem fetal brains aged 13–40 postconceptional weeks (PCW) were included in this study. High-resolution T1 weighted MR images were acquired on 19 fetal brain hemispheres. MR images were processed using in-house software (MNI-ACE toolbox). Delineation of fetal compartments was performed semi-automatically by co-registration of MRI with histological sections of the same brains, or with the age-matched brains from Zagreb Neuroembryological Collection. Growth trajectories of transient fetal compartments were reconstructed. The composition of telencephalic wall was quantitatively assessed. Between 13 and 25 PCW, when the intensity of neuronal proliferation decreases drastically, the relative volume of proliferative (ventricular and subventricular) compartments showed pronounced decline. In contrast, synapse- and extracellular matrix-rich subplate compartment continued to grow during the first two trimesters, occupying up to 45% of telencephalon and reaching its maximum volume and thickness around 30 PCW. This developmental maximum coincides with a period of intensive growth of long cortico-cortical fibers, which enter and wait in subplate before approaching the cortical plate. Although we did not find significant age related changes in mean thickness of the cortical plate, the volume, gyrification index, and surface area of the cortical plate continued to exponentially grow during the last phases of prenatal development. This cortical expansion coincides developmentally with the transformation of embryonic cortical columns, dendritic differentiation, and ingrowth of axons. These results provide a quantitative description of transient human fetal brain compartments observable with MRI. Moreover, they will improve understanding of structural-functional

relationships during brain development, will enable correlation between *in vitro/in vivo* imaging and fine structural histological studies, and will serve as a reference for study of perinatal brain injuries.

Keywords: cerebral cortex, subplate, cortical plate, human fetal brain

INTRODUCTION

In the developing human brain, the genesis of cerebral cortex takes place in transient fetal compartments (His, 1904; O'Leary and Borngasser, 2006; Rakic, 2006; Kostović and Judaš, 2007, 2015; Bystron et al., 2008). It occurs through precise spatiotemporal gene expression of cell proliferation, cell migration, morphogenesis, dendritic differentiation, synaptogenesis, apoptosis, and myelination (Kang et al., 2011; Pletikos et al., 2014). Although corticogenic events take place in more than one fetal compartment, it was shown that some compartments have a predominant role as sites for particular neurogenetic events. On the boundary of the fetal cerebral ventricles, cells proliferate within the ventricular and subventricular zones, producing neurons and glia through mitotic divisions of cortical progenitors (for review see Bystron et al., 2008). Adjacent to the subventricular zone, the migration of postmitotic cells and the growth of axons occur in the intermediate zone (His, 1904; Rakic, 1972; Kostovic and Rakic, 1990; Bystron et al., 2008). Moving outwards, subplate compartment and marginal zone (at the surface of the developing telencephalon) are critical sites for early synaptic interaction (Molliver et al., 1973; Kostovic and Molliver, 1974; Kostovic and Rakic, 1990). In addition, due to its rich extracellular matrix the subplate compartment is also of great importance for guidance of axons (Molliver et al., 1973; Kostovic and Molliver, 1974; Kostovic and Rakic, 1990). Finally, the cortical plate, situated between subplate compartment and marginal zone, is the main locus of post-migratory cortical neuron differentiation (Mrzljak et al., 1988, 1992; Marín-Padilla, 1992). Compared to other primates, apart from its large size, the human brain during development shows a very prominent subplate compartment (Kostovic and Rakic, 1990; Judaš et al., 2013; Hoerder-Suabedissen and Molnár, 2015) and an enlarged subventricular zone (Kriegstein et al., 2006; Bystron et al., 2008; Rakic, 2009; Rakic et al., 2009). The prominent subplate and subventricular zones have been related to the greater number of neurons and connectivity combinations in humans (Kostovic and Molliver, 1974; Kostovic and Rakic, 1990; Judaš et al., 2013; Hoerder-Suabedissen and Molnár, 2015). However, the growth trajectories of these transient human fetal brain compartments have not been completely characterized.

Modern magnetic resonance imaging (MRI) methods allow excellent opportunities to follow development of transient fetal compartments *in vitro* (Kostović et al., 2002, 2014; Radoš et al., 2006; Widjaja et al., 2010) and even *in vivo* (Maas et al., 2004; Judaš et al., 2005; Prayer et al., 2006; Perkins et al., 2008; Miller and Ferriero, 2009; Rutherford, 2009; Habas et al., 2010a; Kostović et al., 2014). In MRI, T1 (longitudinal) and T2 (transverse) relaxation times rely on water protons,

more specifically, on the mobility of water within the tissues. This changes dramatically during brain development. Thus, the MRI characteristics of telencephalic structures are not easily comparable between fetal and adult brain (Kostović et al., 2002; Radoš et al., 2006). Developmental histogenesis is characterized by transient changes in cellular and extracellular composition of neural tissue and is reflected as changes in MRI T1/T2 signal intensity within the specific developmental phases (Kostović et al., 2002, 2014; Radoš et al., 2006). In the developing brain, the composition and density of cells, un/myelinated axonal fiber amount, and the water percentage within extracellular matrix result in inversion of relative MRI signal intensities between “future cortex” and prospective white matter (Kostović et al., 2002; Radoš et al., 2006; Kostović et al., 2014). Yet, using MRI correlated with histology, it is still possible to define transient compartments and spatiotemporal indicators of fetal cerebral cortical development (Kostović et al., 2002; Radoš et al., 2006; Widjaja et al., 2010; Kostović et al., 2014). As seen on MRI images, from 13 PCW onwards, the cerebral wall displays five laminar compartments (Kostović et al., 2002; Radoš et al., 2006) that vary in MRI T1 signal intensity and can be easily distinguished. These are:

1. Ventricular zone (VZ) and ganglionic eminence (GE), which are composed of tightly packed proliferative cells (as seen, for example, in Nissl stained sections). VZ surrounds the entire surface of the ventricular walls and displays a spatio-temporal pattern in intensity of cell proliferation. It increases in thickness, with a peak thickness approximately around 23 PCW, and afterwards reduces to one cell thick ependymal layer (for review see Bystron et al., 2008). Due to the densely packed cell content, VZ and GE are characterized in T1 MR images with high signal intensity (Kostović et al., 2002; Radoš et al., 2006).
2. Subventricular zone (SVZ) appears 1 week before the cortical plate (for review see Bystron et al., 2008). Similar to the VZ, the SVZ is marked by densely packed dividing cells. Nevertheless, while VZ reduces in thickness during the mid-fetal period, the SVZ continues to increase in thickness (Zecevic et al., 2005). Approximately around 11 PCW, the SVZ is divided into inner and outer layers by tangentially oriented fibers (periventricular fiber rich zone) (Smart et al., 2002). Inner SVZ is characterized by high T1 MRI signal intensity. However, it is difficult to distinguish inner SVZ from VZ by MRI in all the regions of the cerebrum. Contrarily, the periventricular fiber rich zone can be seen as a low signal MRI intensity layer in some regions. The outer SVZ contains dividing neural precursors that are the principal source of cortical neurons after 25 PCW. Due to the less densely packed cells, outer SVZ cannot be discerned from the intermediate zone by

MRI—outer SVZ “blends” with the intermediate zone, both showing the “moderate” T1 MRI signal intensity.

3. Intermediate zone (IZ) is a heterogeneous layer positioned between proliferative compartments and postmigratory compartments. IZ contains migrating cells and topographically organized axonal fibers. Due to the mixed content of fibers and migrating cells, IZ is characterized by moderate T1 signal intensity.
4. Subplate compartment (SP) is a transient cytoarchitectonic compartment enriched with extracellular matrix. SP is composed of subplate neurons, and “waiting” thalamocortical and cortico-cortical fibers (Kostovic and Rakic, 1990). SP is characterized by low MRI signal intensity and can be distinguished clearly on MRI images.
5. Cortical plate (CP) is composed of densely packed postmigratory cells. After the peak of neuronal migration, around 20 PCW, it displays several developmental stages that are characterized by areal, laminar and cytological differentiation. Before 30 PCW, CP is characterized by high T1 MRI signal intensity. After 28 PCW the CP starts to show VI layer divisions with ongoing dendrite differentiation resulting in decrease of T1 MRI intensity. A few months after the birth, CP starts to resemble to the adult cortex in terms of MRI T1 signal intensity (<http://www.bic.mni.mcgill.ca/ServicesAtlases/NIHPD-obj2>).

Despite numerous studies utilizing different imaging modalities (McKinstry et al., 2002; Maas et al., 2004; Perkins et al., 2008; Huang et al., 2009; Trivedi et al., 2009; Habas et al., 2010b; Takahashi et al., 2012; Makropoulos et al., 2014), quantitative data describing the precise growth trajectories of transient embryonic compartments is unfortunately still fragmentary (Kostović et al., 2002, 2014; Radoš et al., 2006; Huang et al., 2009, 2013; Kostovic and Vasung, 2009; Widjaja et al., 2010; Huang and Vasung, 2014). Previous MRI studies of developmental changes in total brain volume (Habas et al., 2010a,b; Kuklisova-Murgasova et al., 2011; Makropoulos et al., 2014) used coarse segmentation of gray and white matter and were not able to relate transient fetal compartments to corticogenic events. One of the reasons is that the fetal transient compartments change dynamically throughout fetal development, as previously mentioned, and show different spatiotemporal relationships with cortical histogenesis (Kostović et al., 2014).

Here we provide quantitative data on the transient fetal compartments using a normative cohort of fetal human brains. The main goal of this study was to generate new volumetric MRI parameters for the analysis of transient fetal compartments, defined on the basis of reliable histological references, as it was shown that some of these parameters are useful for the delineation of cortical growth phases and their correlation with spatiotemporal gene regulation (Kang et al., 2011; Pletikos et al., 2014). Our study had two additional specific goals: (i) to use quantitative analysis of the developmental evolution of transient developmental compartments, especially the subplate compartment, in order to better understand the role of these compartments in later stages of brain development, (ii) to

test the hypothesis that the voluminous transient subplate compartment in late human fetal brain is related to extraordinary richness of growing and “waiting” fronts of cortico-cortical axons (Kostovic and Rakic, 1990). These quantitative data are necessary for studies of structural and functional consequences of intrauterine and perinatal injuries of developing human cortex (Volpe, 2009) and for understanding the selective vulnerability of these fetal neural compartments (Kostovic et al., 2014).

MATERIALS AND METHODS

Materials

Forty-four postmortem brains of human fetuses and prematurely born infants were included in the current study. Human fetuses were obtained in accordance with the Croatian federal law following the medically/legally indicated abortions or spontaneous abortions performed at the School of Medicine, University of Zagreb. Premature infants were obtained after the routine autopsy procedure. The procedure for the human autopsy material was approved and controlled by the Internal Review Board of the Ethical Committee at the School of Medicine, University of Zagreb. Consent for postmortem examination was obtained from each parent.

Only the brains of fetuses (<28 PCW) without any sign of pathology (as reported by routine pathology examination) and without known genetic abnormalities were included in the study. The brains of prematurely born infants (>28 PCW) were included if the cause of death was attributed to the sudden infant death syndrome or a respiratory disease.

The age of the fetuses and prematurely born infants was estimated on the basis of their crown–rump lengths (CRL; O’Rahilly and Müller, 1984), greatest length (caliper length without inclusion of the flexed lower limbs), and pregnancy records. In order to provide accurate age estimation of fetuses and of prematurely born infants, their age was expressed as weeks from conception (PCW), (Olivier and Pineau, 1962). After examination and age estimation the skull was removed in order to prepare the postmortem brains for MRI scanning. We invested major effort, in collaboration with the pathology department, to remove the skull without or with minimal damage to the brain tissue. Nevertheless, we could not avoid small damages of brain tissue (in three cases) or brain shape distortions.

In order to broaden the quantitative and qualitative MRI analysis, and to provide a histology-based atlas, postmortem brains were divided into four groups (**Figure 1**):

- (a) Group I (Quantitative MRI analysis): Nineteen human brain hemispheres from 14 postmortem brains (aged 13–40 PCW) were used for high-resolution quantitative MRI analysis (**Table 1**).
- (b) Group II (Quantitative MRI-histology analysis): From Group I, we have selected five brain hemispheres (aged 13, 16, 24, 26, and 40 PCW) for histological processing. The

TABLE 1 | Characteristics of postmortem human brains included in the quantitative MRI analysis (Group I and Group II).

Age in PCW	Hemisphere	Developmental phase	Cause of death
13	<i>Right</i>	<i>Early fetal phase</i>	<i>Abortus spontaneus</i>
16 [†]	Left	Mid-fetal phase	Abortus spontaneus
16 [†]	<i>Right</i>	<i>Mid-fetal phase</i>	<i>Abortus spontaneus</i>
18 [†]	Right	Mid-fetal phase	Abortus spontaneus
18 [†]	Left	Mid-fetal phase	Abortus spontaneus
19 [†]	Right	Mid-fetal phase	Partus praetemporarius
19 [†]	Left	Mid-fetal phase	Partus praetemporarius
20	Right	Mid-fetal phase	Abortus in tractu completus
21	Left	Mid-fetal phase	Abortus in tractu completus
21	Left	Mid-fetal phase	Abruptio placentae
24 [†]	<i>Right</i>	<i>Late fetal phase</i>	<i>Abruptio placentae</i>
24 [†]	Left	Late fetal phase	Abruptio placentae
25 [†]	Left	Late fetal phase	Partus praetemporarius
25 [†]	Right	Late fetal phase	Partus praetemporarius
26	<i>Right</i>	<i>Late fetal phase</i>	<i>Partus praetemporarius</i>
29	Right	Late fetal phase	Stillborn
30	Left	Late fetal phase	Prematurus
40	Right	Perinatal phase	Asphyxio liquoris amnii
40	<i>Right</i>	<i>Perinatal phase</i>	<i>Abruptio placentae</i>

The hemispheres of the same brains are marked with[†]. The hemispheres that were histologically processed (Group II) are marked in *italic*.

inclusion criteria were; I. time of fixation, II. developmental phase, and III. absence of tissue damage.

(c) Group III (Qualitative MRI analysis):

Ten brains (aged 11, 16, 20, 20, 21, 22, 25, 32, 37, 40 PCW) were selected and scanned with MRI in order to provide additional T1-weighted MRI properties of transient fetal compartments for quality check. T1-weighted MRI images were acquired in order to build neuroanatomical coordinate guidelines for delineation of brain structures and in order to confirm spatio-temporal MRI properties of postmortem brain during different developmental stages.

(d) Group IV (histology analysis):

As an anatomical reference, needed for specimens that were not histologically processed, we have used 20 histologically processed brains [Nissl, PAS, and AChE stained sections of the fetal brains aged 13–40 PCW that are part of the Zagreb Neuro-embryological Collection (Kostovic et al., 1991; Judaš et al., 2011)]. Specimens were selected in order to serve as age-matched controls for delineation of MRI neuroanatomical structures.

Methods

MRI Acquisition

Ex vivo brains or separate hemispheres, with postmortem time ranging from few hours to 10 h maximally, were fixed by immersion in 4% paraformaldehyde in 0.1 M phosphate buffer, pH 7.4, and were used to obtain MR images by using the high-field 3.0T MRI device (Siemens Trio Tim). The fixation period ranged from a few weeks to a few years. As we wanted to have a

uniform set of MRI signal intensity data that could be comparable between brains, one of our major concerns was the alteration of the MRI signal intensity of the brain that occurs due to the tissue fixation *per se*. In addition, formalin fixation is one of the factors that change the microstructure of the tissue, affecting and reducing the difference between the gray and white matter water. As those differences are the key to tissue discriminability using MRI, the standard three-dimensional spoiled gradient-echo (3-D GRE) sequence (magnetization-prepared rapid acquisition gradient echo -MPRAGE) failed to adequately discriminate the transient fetal compartments needed for 3D quantitative and qualitative analyses. In order to acquire the high spatial resolution and high-contrast T1-weighted postmortem fetal brain MR images, suitable for quantitative 3D MRI analysis, we had to modify commercially available VIBE sequence (volumetric interpolated brain examination (Rofsky et al., 1999)). Having in mind the known challenges of postmortem MRI scanning, we have adjusted the MRI acquisition timing parameters taking into account the differences between behavior and microenvironment of water protons in the living and the formalin-fixed developing brains. Thus, we have reduced the FOV, increased the resolution and number of excitations, and finally modified the TE and TR as well as the flip angle. Finally, the parameters used for MRI acquisition were following: repetition time (TR) 14.5 ms, echo time (TE) 5.4 ms, number of excitations (NEX) 5, flip angle of 12°, acquisition time ~1.5 h per brain and section thickness ranging from 0.3 to 0.5 mm depending on the age. All brains were scanned using the wrist small-flexi eight-channel surface coil. The matrix size and the field of view were adjusted in order to obtain an isotropic spatial resolution of at least $0.3 \times 0.3 \times 0.3 \text{ mm}^3$ for 13 PCW old fetal brains, and $0.5 \times 0.5 \times 0.5 \text{ mm}^3$ for the fetal brains older than 15 PCW.

Variability in fixation time can result in differences in MRI signal intensities between brains, however, signal intensity differences within brains were sufficient to distinguish and delineate telecephalic structural changes resulting from microstructural events (Kostović et al., 2002; Widjaja et al., 2010). In addition, according to Tovi and Ericsson, changes in T1 due to fixation occur rapidly but stabilize after 3–4 weeks (Tovi and Ericsson, 1992), which was the minimum fixation period used in our study to ensure tissue stability and comparability between samples.

Histology

Five histologically processed brains, aged 13, 16, 24, 26, and 40 PCW (Table 1) were selected as major representatives for specific phases of prenatal brain development (Kostovic and Vasung, 2009). After the MRI acquisition these brains were embedded in paraffin and serially sectioned with coronal slice thickness of 15–20 μm . Cresyl violet and Periodic Acid Schiff–Alcian Blue (PAS-AB) were used for tissue staining. The PAS histochemical staining was conducted for the visualization of acid-sulphated glycoconjugates (Vacca et al., 1978) which provided us a “gold” standard for visualization of subplate compartment, known to have an abundant extracellular matrix (ECM). In addition, neighboring Nissl-stained celloidin sections were used as guidance for delineation of the cytoarchitectonic boundaries and

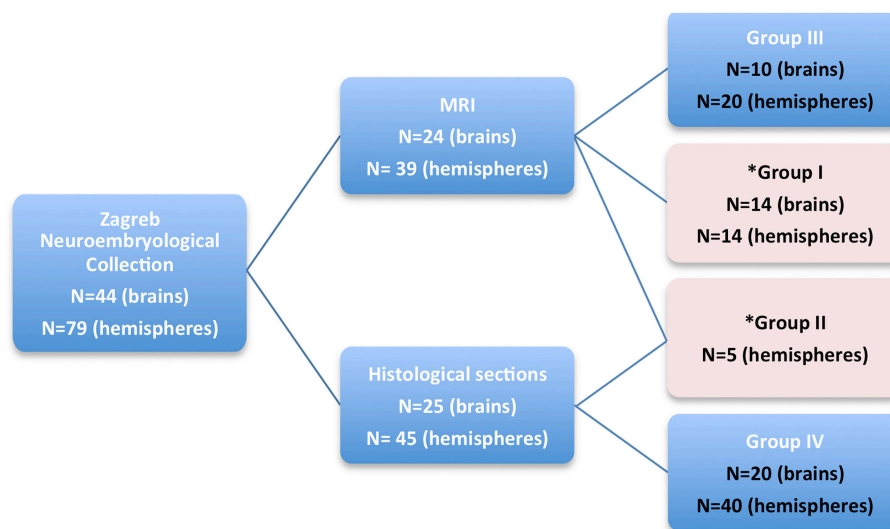


FIGURE 1 | A diagram showing four groups of subjects, taken from Zagreb Neuroembryological Collection, that were included in our study. Quantitative MRI measurements were obtained on fetal brains marked with pink rectangle (Group I and II).

cellular compartments of the human fetal telencephalon. AChE stained sections (acetyl-cholinesterase histochemistry) were used in the brains that arrived to our Institute within 24 h after death. This was done with a goal to show growing thalamocortical afferents and external capsule (Kostovic and Goldman-Rakic, 1983), which have been recognized as a relatively constant border between subplate and intermediate zone (Kostović et al., 2002). Images of histological sections were captured using a charge-coupled device (CCD) camera or Nikon scanner (**Figures 2, 3**) and were processed using Adobe Photoshop®.

Image Pre-Processing

We have adapted and calibrated MR imaging tools, initially developed at the MNI (Montreal Neurological Institute) for processing of adult brains, and we have developed a semi-automated pipeline for processing postmortem fetal brain MR images. First, the images were manually cropped to minimize the field of view. The images were afterwards resampled at isotropic voxel sizes of 0.15 mm (age ≤ 13 PCW) or 0.25 mm (age ≥ 15 PCW). MRI signal intensity nonuniformity, resulting from field non-homogeneities, were corrected using the N3 method (Sled et al., 1998) with a small spline distance of 5 mm. A tissue mask was obtained by thresholding above background.

Tissue classification based on qualitative MRI and histology

Due to the specific anatomical organization of the human fetal brain, modifications to available processing tools designed for adult and postnatal brains are required to extend existing MRI analysis to prenatal brain. One of the major reasons for modifications, as mentioned above, are the age-dependent changes in T1 MRI signal intensity of transient fetal laminar compartments and inversion of relative signal intensities between “cortex” (high T1 signal intensity) and prospective white matter

(moderate T1 signal intensity). In order to process the fetal and premature infant postmortem brains, we have developed a pipeline combining existing automatic MNI tools with several steps requiring semi-automatic and/or manual editing.

An initial tissue classification is performed using the artificial neural network (ANN) algorithm with manually selected tag points for each of the tissue classes (I = background, II = formalin, III = “cortical plate,” IV = “prospective white matter with basal ganglia”). At least 100 points per tissue class are taken for a reliable estimation of its mean intensity and variance (Zijdenbos et al., 1998; Tohka et al., 2004). In comparison to an adult brain, in the fetal brains the partial volumes of CP-Formalin in deep sulci, of white matter-like intermediate intensities, were often mis-classified as white matter. This was caused by the narrowness of the sulci and the inversion of T1 intensities (CP- high T1 signal intensity, formalin and SP- low T1 signal intensity). Consequently, the segmented images needed to be manually corrected to account for partial volume effects for formalin in narrow sulci, for correction of artifacts (tissue damage), and for masking out unwanted tissues that were attributed to the background (brain stem, pons, mesencephalon, and cerebellum). Using the Display module (MNI toolkit), semi-automatically classified tissues were manually corrected and the narrow sulci were painted in order to extract the cortical plate surface.

After semi-automatic classification, tissues labeled as class IV (prospective white matter with basal ganglia) were extracted and manually painted introducing the five new tissue classes, namely: IV = subplate, V = intermedial zone, VI = proliferative compartments, VII = subcortical gray matter, and VIII = diencephalon. The example of tissue classification on coronal slices can be seen in **Figures S1–S3**. Although visible, SVZ does not show a continuous 3D appearance on MRI. Therefore, the SVZ was partially classified as VZ (inner subventricular zone),

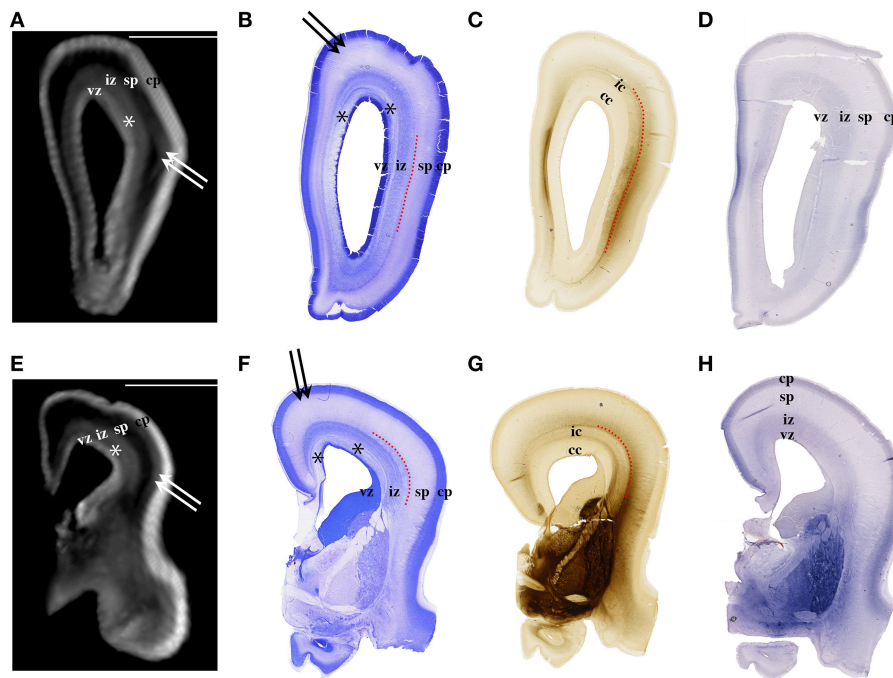


FIGURE 2 | Nissl (B,F), AChE (C,G), and CS-56 immunocytochemistry (D,H) stained coronal brain sections of the 16 PCW human fetus. Corresponding T1-weighted MRI coronal sections of the same brain are shown in (A,E). vz, ventricular zone; *, periventricular fiber rich layer of subventricular zone; iz, intermediate zone; sp, subplate compartment; cp, cortical plate. External capsule and its radiations are marked by a red dotted curved line (B,F,C,G). Double arrows in (A,B,E,F) indicate the upper subplate compartment. Curved dashed red line in (B,C,F,G) illustrates where the border between subplate and intermediate zone was placed during manual segmentation. Scale bar = 10 mm (A,E).

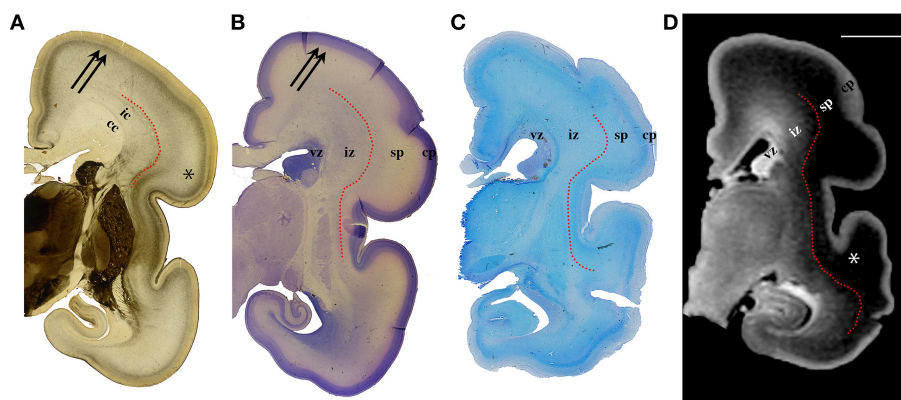


FIGURE 3 | AChE (A), Nissl (B), PAS (C) stained coronal brain sections with a corresponding T1-weighted MRI slice (D), of the human 24 PCW old fetuses. ic, internal capsule; cc, corpus callosum; vz, ventricular zone; *, subplate compartment; iz, intermediate zone; sp, subplate compartment; cp, cortical plate. External capsule and its radiations are marked by a red dotted curved line (A). Double arrows in (A,B) indicate the upper subplate compartment. Curved red line in (A-D) illustrates where the border between subplate and intermediate zone was placed during manual segmentation. Scale bar = 10 mm (D).

and as an IZ (outer subventricular zone that could be easily traced after the appearance of T1 hypointense periventricular fiber rich zone). After 35 PCW, we could not continuously distinguish the SP from IZ, although we have observed regional differences in MRI signal intensity. Thus, after 35 PCW, SP and IZ were measured together and were classified as one compartment (IV + V) called “fetal white matter.”

Volumes of the semi-automatically segmented fetal compartments were calculated by multiplying the number of voxels with the voxel unitary volume. In order to account for the effect of minimal tissue shrinkage caused by formalin fixation [(shrinkage of 2.7–3.5% as reported by Boonstra et al., 1983; Schned et al., 1996)], we have calculated absolute but also relative volume ratios for tissue classes III–VIII. Relative

volumes were expressed as a percentage of the total telencephalic volume of the hemisphere (not including the diencephalon) or as a percentage of the cerebral volume of the hemisphere (including the diencephalon).

Surface extraction and registration

Manual pre-alignment of fetal hemispheres in MRI scans to stereotaxic space was a prerequisite for registration of surfaces and outer surface extraction. Each brain hemisphere was first manually registered to a stereotaxic space defined on an adult human template (ICBM152). Registration of the brain hemisphere to ICBM152 stereotaxic space was performed in Register, a GUI module developed at the MNI. For registration of fetal scans with adult templates, we manually defined 10 anatomical tag points on fetal brain scans with their corresponding counterparts on the ICBM152 model. Each brain hemisphere was then co-registered to the adult model using three translations, three rotations, and one scaling option.

The extraction of inner surfaces from CP and SP, and the CP-pial boundary was fully automated (MacDonald et al., 2000; Kim et al., 2005) and was based on the previously described segmented images. Surfaces were extracted by hemisphere, with 81920 triangles and 40962 vertices. The gyrification index (GI, the ratio of total to exposed area of the pial surface) was evaluated at the pial surface of the cortical plate.

Given the rapid growth and change in fetal brain morphology between 13 and 40 weeks of gestation, it was not possible to define a global static surface model to use for surface registration, as can be done with adult brain. Fetal surfaces were instead longitudinally registered by age with reference one to another. The oldest subjects, near 40 PCW, were registered to the reference adult template (ICBM152), thus defining the latest standard stereotaxic space (Robbins, 2004; Lyttelton et al., 2007; Boucher et al., 2009). On the younger brains, the longitudinal surface registration was driven by matching borders of lobes (or regions) as manually delineated on the extracted “inner” surfaces.

Regional and lobar segmentation was performed manually on the inner surfaces of the CP. The surfaces were first divided into 6 lobes [frontal lobe, parietal lobe, occipital lobe, temporal lobe, outer ring of the limbic lobe (gyrus fornicatus), and insular lobe]. The outer ring of the limbic lobe was further split into parahippocampal gyrus and cingulate gyrus resulting with 7 segmented regions in total (**Figure 4**). After longitudinal alignment of the surfaces, pathlines can be traced in time along the registered vertices of the individual surfaces to observe growth patterns of CP and SP both globally and regionally. For the segmentation of SP and CP, we have used anatomical borders on the inner cortical plate surfaces, i.e. gyri and sulci, which have been used for adult cortical surface segmentation, as described by von Economo and Brodmann (Brodmann, 1909; von Economo and Koskinas, 1925). The CP and SP were segmented only after identifying the primary sulci in fetal brain (Kostovic and Vasung, 2009). The anatomical borders used for surface segmentation were as follows (**Figure 4**).

Frontal lobe

The Sylvian fissure (SF) forms early in fetal development (9–13 PCW). The circular sulcus of insulae (CSI) forms during

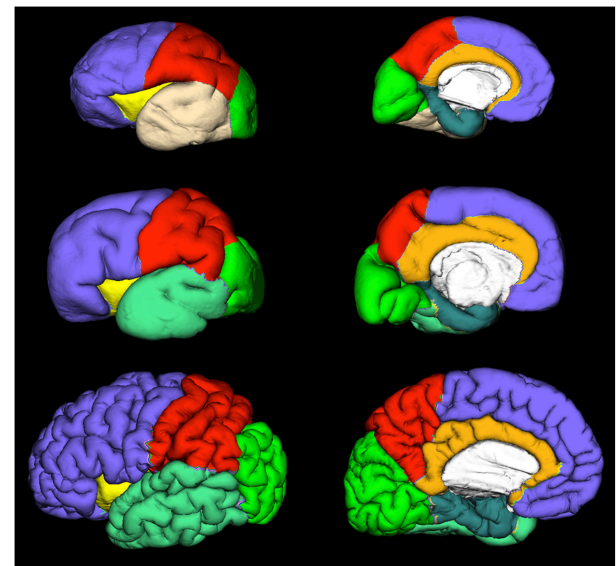


FIGURE 4 | Extracted lateral and medial cortical plate surfaces in 25 (upper row), 30 (middle row), and 40 (bottom row) PCW old fetal brains. Regional and lobar segmentation was performed manually and the surfaces were divided into 6 lobes: frontal lobe (violet), parietal lobe (red), occipital lobe (green), temporal lobe (beige or jungle green), outer ring of the limbic lobe [gyrus fornicatus encompassing: parahippocampal gyrus (celadon green) and cingulate gyrus with subcallosal area (orange)], and insular lobe (yellow).

early fetal and mid-fetal development. During late mid-fetal development, the central sulcus (CS) begins to appear and can be identified continuously in the rostro-caudal direction (Kostovic and Vasung, 2009). Thus, CS, SF, and CSI provide anatomical borders of frontal lobe at lateral aspect. On the medial aspect, the frontal lobe extends to the cingulate sulcus that is continuous in appearance already in the mid fetal phase. The parolfactory sulcus does not appear before the early preterm phase, so from the rostral end of the cingulate sulcus we have extrapolated the line that most resembles the adult parolfactory sulcus (connecting rostral end of the cingulate sulcus with substantia perforata anterior) dividing the subcallosal area from frontal lobe.

Temporal lobe

As there is no sulcus delimiting the temporal from occipital lobe in fetal brain, we have extrapolated line connecting the Sylvian fissure with occipitotemporal incisures on the lateral aspect. On the medial aspect, the temporal lobe was delimited by collateral sulcus.

Occipital lobe

The borders of the occipital lobe were defined as follows: on the lateral aspect the extrapolated lines connecting the occipitotemporal incisures and parieto-occipital fissure with the Sylvian fissure, on the medial aspect occipitotemporal incisures and parieto-occipital fissure.

Parietal lobe

On the lateral aspect, the parietal lobe is delimited by the central sulcus and extrapolated line connecting the parieto-occipital

fissure with the Sylvian fissure. On the medial aspect, the parietal lobe is delimited by the parieto-occipital fissure and cingulate sulcus.

Insular lobe

The circular sulcus of the insula provided a clear border between the insula and the frontal, parietal, and temporal lobes.

Outer ring of the limbic lobe (*gyrus fornicatus*) encompassing

- (i) Gyrus cinguli and area subcallosa

Delimited by cingulate sulcus dorsally and callosal sulcus ventrally.

- (ii) Parahippocampal gyrus, uncus, and substantia perforata anterior

The collateral sulcus and rhinal sulcus were defined as borders between gyrus parahippocampalis and the remaining temporal lobe. The border between isthmus of gyrus cinguli and gyrus parahippocampalis was an extrapolated line connecting the most inferior part of splenium of the corpus callosum with the parieto-occipital fissure.

Telencephalic measurements

The thickness of each CP and SP was defined at the vertices of each surface.

Thickness was measured by taking the absolute distance between corresponding vertices on each surface. It was blurred, on the surface in its native space, with a 5 mm kernel for brains <20 PCW and 10 mm kernel for brains >20 PCW (fwhm) (Boucher et al., 2009). This was done in order to increase signal-to-noise ratio. We have used smaller values for blurring than those applied in adults (20–30 mm) because of the size of the fetal brains.

Measurements of the surface area, volume, and average thickness of the CP (13–40 PCW) and SP (21–30 PCW) were taken for each segmented lobe and region. The surface areas (mm^2) and volumes (mm^3) of the CP and SP in different regions and lobes were calculated by first evaluating elemental areas and volumes at the vertices, then summing these measures over the vertices defining each lobe or region. For an elemental area, the area of a surface triangle is distributed equally (weight 1/3) to each of its three vertices. Similarly, an elemental volume is calculated from the volume of the prism formed by the linked vertices of each triangle pair between the two surfaces. As for volumetric measures, the lobar volumes are expressed as an absolute value or as a percentage they occupy in the specific fetal compartment (CP or SP).

Statistical analysis was performed using the software SPSS® and Matlab®. Detailed description of each analysis is provided in the results.

RESULTS

Relationship between Postconceptional Weeks and Total Volume of Transient Fetal Compartments

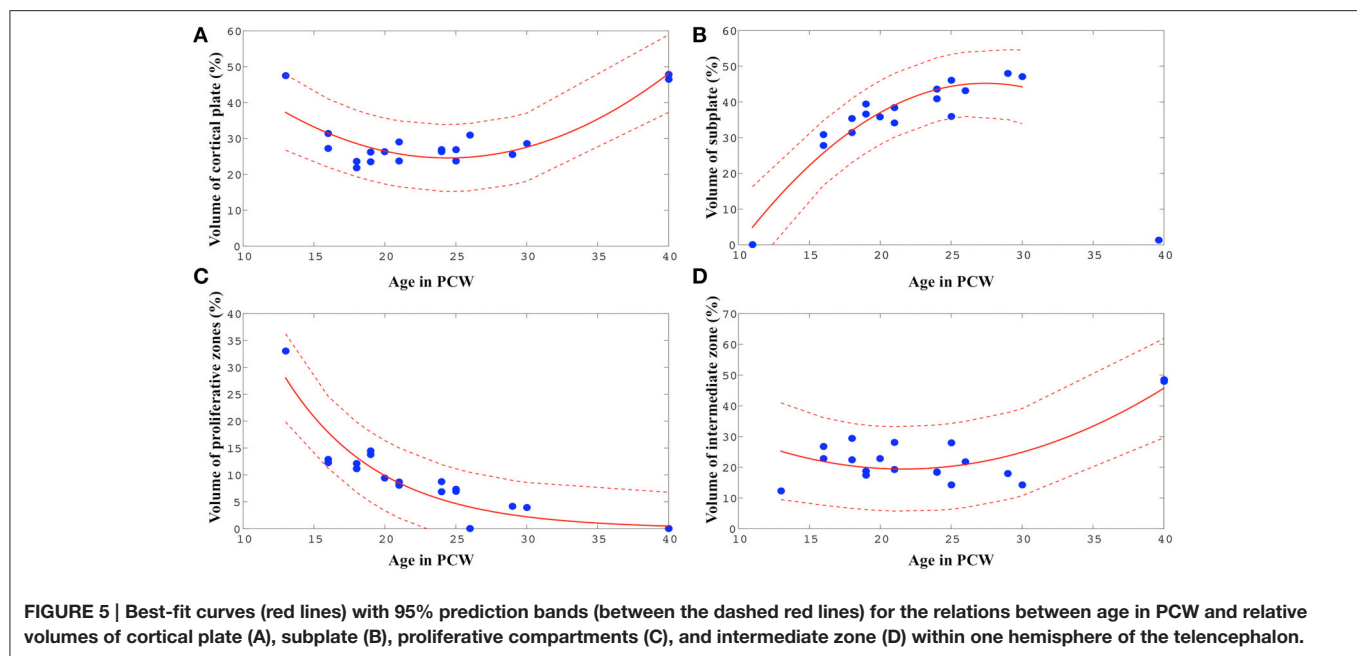
We have used the Spearman correlation in order to test the correlation between age and volume of transient fetal compartments. As expected we found significant positive

correlations between age (in PCW) and absolute volume of the hemisphere ($r_s = 0.953$, $N = 19$, $p < 0.01$), cortical plate ($r_s = 0.937$, $N = 19$, $p < 0.01$), subplate compartment for the period from 13 to 30 PCW ($r_s = 0.935$, $N = 17$, $p < 0.01$), intermediate zone ($r_s = 0.897$, $N = 19$, $p < 0.01$), volume of subcortical gray matter ($r_s = 0.963$, $N = 19$, $p < 0.01$), and diencephalon ($r_s = 0.955$, $N = 19$, $p < 0.01$). The absolute volume of proliferative compartments showed significant positive correlation with developmental age from 13 to 25 PCW ($r_s = 0.917$, $N = 12$, $p < 0.01$). After 25 PCW, when the peak of volume is reached, the volume of proliferative compartments showed negative correlation with developmental age, that is, a rapid decline ($r_s = -0.774$, $N = 7$, $p = 0.04$).

Although it is known that these compartments increase in their volume with age, until now there were no reports on what hemispheric percentage these compartments occupy at the given postconceptional age. For that purpose we took into account the entire volume of the telencephalic hemisphere and we have expressed the volume of each compartment as a percentage of the total volume of the telencephalic hemisphere. We have used the Spearman correlation in order to test the correlation between age and relative volume of transient fetal compartments. The only significant correlations were found between age and relative volume of proliferative compartments (a negative correlation with $r_s = -0.931$, $N = 19$, $p < 0.01$) and relative volume of subplate compartment between 13 and 30 PCW (a positive correlation with $r_s = 0.877$, $N = 17$, $p < 0.01$). This suggests that the relationship between age and percentage of the hemisphere occupied by certain transient fetal compartment may not be linear.

Therefore, in order to reveal the nature of a relationship between age and relative volumes of transient fetal compartments, we fit non-linear models (second-order polynomial, exponential, and Gaussian), using Matlab. For every fit, we chose between the three functional forms based on the adjusted r^2 value. In all cases, these models provided better fits than a simple linear model. The best-fit parameter values are shown in (Figure 5).

The relative volume of the cortical plate was best predicted from age by using a best-fit 2nd degree polynomial curve (Figure 5A, $V_{\text{Cortical_plate}} = 0.10 * \text{PCW}^2 \pm 4.75 * \text{PCW} + 82.59$: adjusted $r^2 = 0.74$). For the prediction of the relationship between the relative volume of the subplate compartment and age (only between 13 and 30 PCW), a 2nd degree polynomial curve was found to be the most adequate fit (Figure 5B, $V_{\text{subplate}} = 0.15 * \text{PCW}^2 + 8.21 * \text{PCW} \pm 67.32$: adjusted $r^2 = 0.87$). The relative volume of intermediate zone was also best predicted from age by using a best-fit 2nd degree polynomial curve (Figure 5D, $V_{\text{Intermediate_zone}} = 0.08 * \text{PCW}^2 \pm 3.37 * \text{PCW} + 55.84$: adjusted $r^2 = 0.60$). An exponential model showed to be the most appropriate for the prediction of the relationship between relative volume of proliferative fetal compartments and age (Figure 5C, $V_{\text{proliferative}} = 194.78^{(-0.15 * \text{PCW})}$, adjusted $r^2 = 0.84$). Finally, in order to assess the relationship between relative volume of diencephalon (percentage of total volume of telencephalon and diencephalon of one hemisphere) and age, we have used best-fit



2nd degree polynomial curve ($V_{\text{Diencephalon}} = 0.01 \cdot \text{PCW}^2 \pm 0.87 \cdot \text{PCW} + 16.01$, adjusted $r^2 = 0.60$).

Changes in Thickness of Cortical Plate and Subplate during Prenatal Brain Development

Mean thickness of CP and SP in segmented lobes and regions was measured in 10 brains (21–40 PCW, **Figure 6**) since we have detected the appearance of the primary sulci at this time [described also by Chi et al. (1977)].

We did not find significant correlation between PCW and mean cortical plate thickness of seven segmented cortical plate areas (**Figure 6**). Moreover, curve fitting did not reveal any satisfactory model (low r^2) describing age dependent changes in the mean cortical plate thickness of segmented regions. This might be due to the small sample size, below resolution sub-millimeter changes in cortical thickness during prenatal brain development, or due to the changes in cortical thickness that do not have lobar predominance (**Figures 6, 7**). Spatio-temporal changes of cortical plate thickness across all vertices throughout the hemisphere have been calculated in all subjects and can be seen in **Figure 7** (upper row).

Since we could not detect the subplate compartment continuously at 40 PCW it was approximated to 0 mm. We have found significant positive correlation between PCW (in the period between 13 and 30 PCW) and mean subplate thickness of five segmented subplate areas (**Figure 6**; $r = 0.884$, $N = 8$, $p = 0.004$ for the parietal lobe thickness, $r = 0.828$, $N = 8$, $p = 0.011$ for the occipital lobe thickness, $r = 0.73$, $N = 8$, $p = 0.04$ for the frontal lobe thickness, $r = 0.774$, $N = 8$, $p = 0.024$ for the cingulate gyrus thickness, and $r = 0.821$, $N = 8$, $p = 0.012$ for the temporal lobe thickness). The average thickness of insula and parahippocampal gyrus did not show significant correlation with PCW. Mean subplate

thickness reached maximal value at 30 PCW in all segmented areas. Spatio-temporal changes of subplate thickness across all vertices throughout the hemisphere can be seen in the **Figure 7** (bottom row).

Regional Surface Growth of Cortical Plate during Prenatal Development

The total surface area of cortex, from 13 to 40 PCW, showed significant and strong positive correlation with age ($r_s = 0.98$, $N = 19$, $p < 0.01$). In addition, the level of gyrification (**Figure 7**), calculated as gyrification index, was also significantly correlated with PCW ($r_s = 0.5$, $N = 19$, $p = 0.03$).

Surface areas across seven cortical plate regions during development were not normally distributed, as revealed by Shapiro-Wilk test. Spearman's rank-order correlation revealed significant positive correlation between age and surface area of parietal lobe ($r_s = 0.82$, $N = 10$, $p = 0.004$), occipital lobe ($r_s = 0.87$, $N = 10$, $p = 0.001$), frontal lobe ($r_s = 0.77$, $N = 10$, $p = 0.009$), temporal lobe ($r_s = 0.67$, $N = 10$, $p = 0.03$), insula ($r_s = 0.91$, $N = 10$, $p < 0.01$), cingulate gyrus ($r_s = 0.924$, $N = 10$, $p < 0.01$), and parahippocampal gyrus ($r_s = 0.77$, $N = 10$, $p < 0.01$; **Figure 8**). Nevertheless, the relative surface of six segmented areas (percentage of the total hemispheric surface of CP) did not show significant correlation with age [except the weak positive correlation between the relative surface of cingulate gyrus and age ($r_s = 0.65$, $N = 10$, $p = 0.04$)]. The largest portion of cortical plate surface was occupied by frontal lobe (~34%), followed by parietal and temporal lobes (~20%). The relative surface areas of six segmented regions remained unchanged during development.

Coordinated Changes of Cortical Plate and Subplate Volumes during Prenatal Human Brain Development

Spearman correlation coefficients were computed between all regional and lobar volumes of cortical plate and all regional

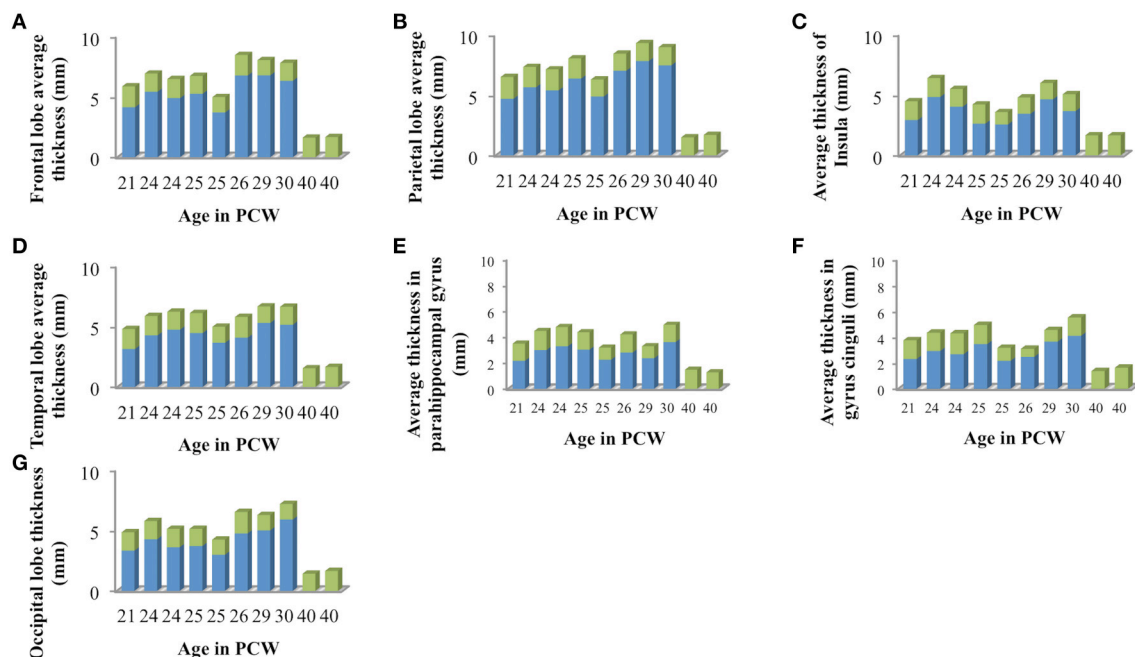


FIGURE 6 | Mean cortical thickness of cortical plate (green) and subplate compartment (blue) in frontal lobe (A), parietal lobe (B), insular lobe (C), temporal lobe (D), in the outer ring of the limbic lobe [gyrus fornicatus encompassing: parahippocampal gyrus (E) and cingulate gyrus with subcallosal area (F)], and occipital lobe (G) measured in millimeters.

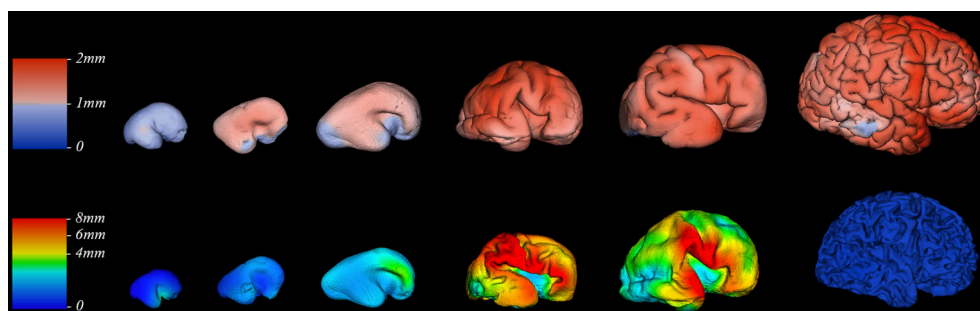


FIGURE 7 | Thickness of cortical plate (upper row) and subplate compartment (bottom row) measured in millimeters (color coded bars) at 13, 16, 18, 24, 30, and 40 PCW (left to right).

and lobar volumes of subplate across eight subjects, each at a different age (from 21 to 30 PCW), yielding a 14×14 correlation matrix and corresponding p -values (Figure 9). The significance level was set at 0.05, and the p -values were adjusted for multiple comparisons using False Discovery Rate. This resulted in 22 significant correlations (Figure 9C). Positive correlations between cortical plate of frontal lobe and parietal lobe, between frontal lobe and occipital lobe, between frontal lobe and temporal lobe, and between temporal lobe and parietal lobe are significant across ages (Figure 9A, asterisks, Figure 9C). Furthermore, we have also found significant positive correlations across ages between the volume of subplate of frontal lobe and parietal lobe, frontal lobe and occipital lobe, frontal lobe and parahippocampal gyrus, parietal lobe and temporal lobe, and between subplate of parietal lobe and parahippocampal gyrus (Figure 9A, asterisk, Figure 9C).

As expected the volume of the subplate of frontal, occipital and parietal lobe showed significant positive correlation with the volume of the cortical plate of the same lobes (Figure 9A, asterisk, Figure 9C). Moreover, the volume of the subplate of frontal lobe showed significant positive correlation also with the cortical plate volume of parietal and occipital lobe, while the volume of the subplate of parietal lobe showed significant correlation with cortical plate of frontal and temporal lobes (Figure 9C).

DISCUSSION

In this study we provide quantitative data on individual transient fetal compartments, such as thickness, as well as total volume, surface area, and gyrification of human brain during development. Using MRI aligned to histological sections, we

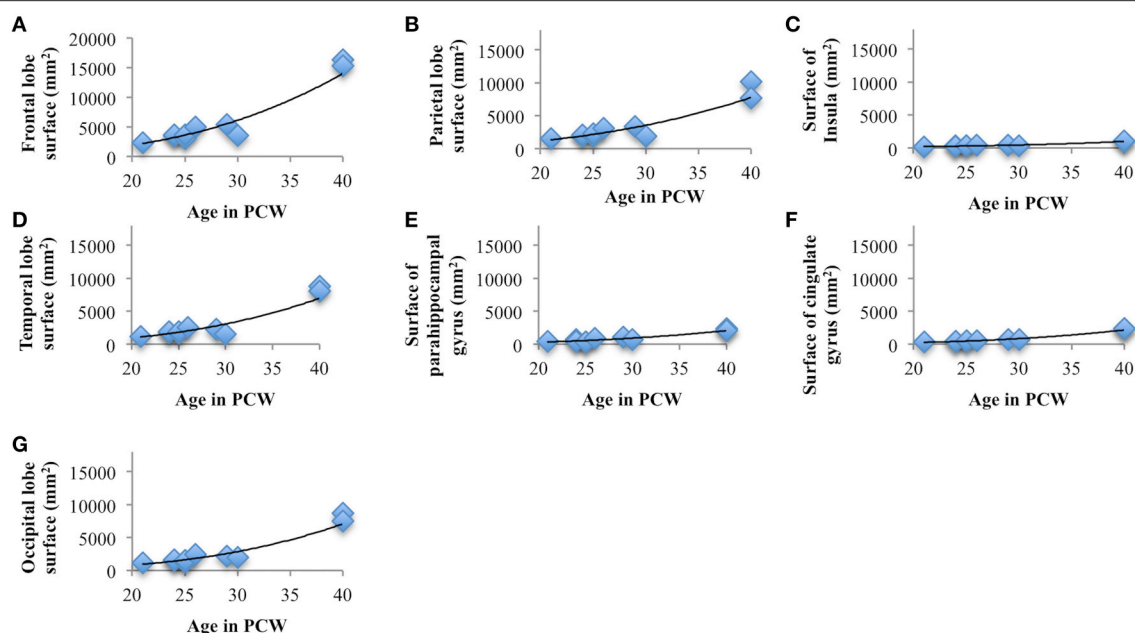


FIGURE 8 | Line charts showing the increase of cortical plate surface area of frontal lobe (A), parietal lobe (B), insular lobe (C), temporal lobe (D), outer ring of the limbic lobe [gyrus fornicatus encompassing: parahippocampal gyrus (E) and cingulate gyrus with subcallosal area (F)], and occipital lobe (G) during prenatal brain development.

show growth trajectories of corticogenic regions during human mid-fetal and late fetal periods of cerebral development. These findings are consistent with general embryological data and previous knowledge on timing of intrauterine corticogenic events in humans (Kostovic and Rakic, 1990; Bystron et al., 2008; Kostovic and Vasung, 2009; Kostović and Judaš, 2015). We have observed significant positive correlation between developmental age and absolute volume of cortical plate, intermediate zone, subcortical gray matter, and diencephalon but also between developmental age and subplate from 13 to 30 PCW, and developmental age and proliferative compartments from 13 to 25 PCW. However, the percentage of hemispheric volume occupied by transient fetal compartments did not show correlation with age, except for relative volumes of proliferative compartments, which showed a negative relationship with age, and relative volumes of subplate compartment, which showed a positive relationship with age from 13 to 30 PCW. These results indicate the importance of these transient compartments during the reorganization of the prenatal human brain. Thus, we have obtained quantitative indicators of transient corticogenic compartments, which are useful for better neurobiological interpretation of existing and future developmental MRI data.

Volume of Transient Fetal Compartments as an Indicator of Intensity of Histogenetic Events

The results of this study demonstrate that precise histological delineation of transient fetal compartments based on different histological, histochemical, and cytological methods (Kostovic

and Rakic, 1990; Kostović et al., 2002; Widjaja et al., 2010; Huang et al., 2013) discloses reliable anatomical landmarks for corresponding MR images (Figures 2, 3) and allows volumetric measurements of individual transient compartments. The proliferative (ventricular and subventricular) compartments decrease in size and hemispheric percentage occupied after 25 PCW (Figure 5) indicating the cessation of neurogenesis and switch to gliogenesis (Bystron et al., 2008). However, the developmental neurological interpretation of growth curves for the relative volumes of other transient compartments is not as straightforward.

Growth curves and changes in thickness of cortical plate reported here are likely difficult to interpret due to the dynamic addition of neurons to increasingly superficial positions of cortex (Rakic, 1982, 1988), regional differences in lamination of isocortical and allocortical (limbic) regions, changes in columnar (vertical) organization, and prominent dendritic growth. MRI studies of fractional anisotropy (FA) indicate microstructural changes of cortical plate (CP) during development (McKinstry et al., 2002; Takahashi et al., 2012). All these changes may contribute to the growth of CP volume during the first half of gestation when CP is recognizable as a cell dense band showing homogenous MRI signal intensity. Nevertheless, during the late mid-fetal and preterm period, when Brodmann (Brodmann, 1909) identified basic six layer lamination so called ground typus, CP shows lamination on histological sections and even on T1w MRI images and (Kostovic et al., 2008). However, the final cytoarchitectonic features are not achieved until 3 years of age (Judaš and Ceganec, 2007). Parallel with the lamination of the CP, changes occur in the organization of vertically aligned

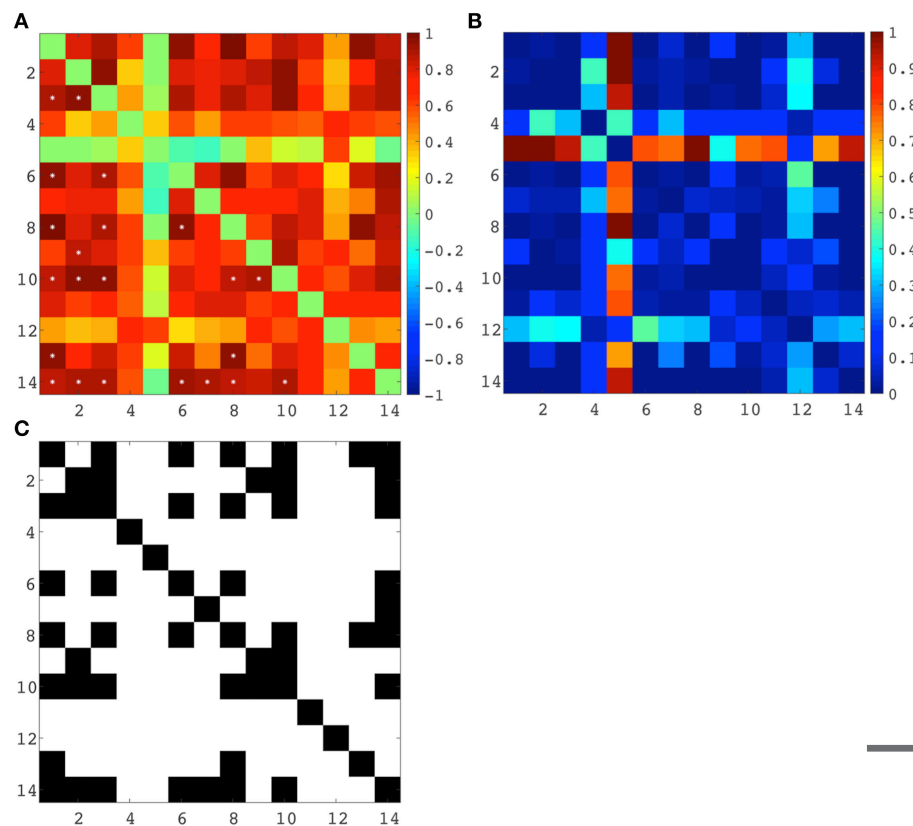


FIGURE 9 | (A) Correlation matrix (Spearman's correlation coefficient - color code on the right) between all seven regional volumes of cortical plate and subplate across eight subjects, each at a different age (21–30 PCW). Significant correlations are marked with *. **(B)** Uncorrected p -values for the correlation coefficients. **(C)** Significant correlations (FDR-adjusted p -value < 0.05), where a black matrix entry indicates significance. Regional volumes of the cortical plate are marked with numbers 1–7 [parietal lobe (1), occipital lobe (2), frontal lobe (3), insula (4), cingulate gyrus (5), temporal lobe (6), and parahippocampal gyrus (7)]. Regional volumes of the subplate compartment are marked with numbers 8–14 [parietal lobe (8), occipital lobe (9), frontal lobe (10), insula (11), cingulate gyrus (12), temporal lobe (13), and parahippocampal gyrus (14)].

embryonic columns, which are composed of young migratory neurons (Rakic, 1988, 1995; McKinstry et al., 2002). Although our results show significant correlation between volume of the cortical plate and age, the relationship between age and the relative volume of telencephalon occupied by cortical plate is not straightforward. The cortical plate occupies the highest percentage of telencephalon in the early development (up to 20 PCW) and during the last trimester (after 30 PCW). This might be explained by the fact that from 20 to 30 PCW the subplate compartment displays a growth spurt. Furthermore, although the growth of CP until 20 PCW can be attributed to addition of neurons, it is very likely that the increase in volume of CP after 25 PCW is not caused by significant addition of new neurons (Bystron et al., 2008; Rakic, 2009; Rakic et al., 2009), although some late migratory neurons (Sanai et al., 2011) may contribute to the late developmental volume of the CP (Kostović and Judaš, 2015). Similarly, the addition of glial cells (Dobbing and Sands, 1973) is also not a massive event in the CP (Mrzljak et al., 1988, 1992). While the growth of dendrites of principal cortical neurons is accelerated after ingrowth of thalamocortical afferents (Mrzljak et al., 1988, 1992), around 24–26 PCW (Molliver et al.,

1973; Kostovic and Rakic, 1990; Kostović and Judaš, 2010), the relocation of thalamocortical fibers from subplate to the CP most likely influences the shape of SP and CP volume growth curves and its thickness during late gestation.

Finally, all these factors may partly explain why we did not find significant difference in mean cortical thickness between segmented regions of cortical plate (Figure 6). This could be also due to the undetectable sub-millimeter discrete differences of immature cortex, but also due to the changes in cortical thickness that are not detectable with our segmentation. Detailed vertex-based analysis revealed that between 16 and 21 PCW the first regions of cortical plate to become thickest are regions around central sulcus (Figure 7, upper row). Afterwards, cortical plate thickening displays central to frontal and central to occipital gradients (Figure 7, upper row). Moreover, a recent study from Huang et al. (2013) revealed that the time courses of FA drop are distinct in different brain regions during the first two trimesters of prenatal development (Huang et al., 2013). According to the authors, the FA drop during first 20 PCW is the most pronounced in the frontal cortical areas (Huang et al., 2013), which coincides with cell differentiation,

cessation of neuronal migration, dendritic and axonal growth, synapse formation, and cell adhesion (Bystron et al., 2008). Thus, our results are in line with those reported previously in the literature.

Subplate Compartment

Delineation of SP from intermediate zone during mid gestation was not problematic due to the presence of the external capsule situated at the deep border of SP (Kostović and Judaš, 2002; Kostović et al., 2014), (Figures 2, 3; red dotted lines). SP is recognizable in MRI due to the hydrophilic extracellular matrix (Kostović et al., 2002; Judaš et al., 2005; Radoš et al., 2006; Widjaja et al., 2010). The delineation of the deep boundary of SP can be challenging during late gestation due to the formation of gyral white matter (Kostović et al., 2014). As well, the superficial border of SP at the interface between SP and CP is difficult to delineate during early stages due to the formation of a second CP (Kostovic and Rakic, 1990). Thus, the changing histological and histochemical properties at the interface between SP and CP, and SP and white matter (Kostovic and Rakic, 1990) certainly influence our measurements.

Despite these factors, it is evident that the volume of SP increases with age between 13 and 30 PCW, reaching the maximum around 30 PCW in most areas, occupying up to 45% of entire telencephalic volume (Figures 5, 6), and being almost 4 times thicker than CP (Figure 6). The maximal size of SP during this period may reflect an increased amount of “waiting” cortical afferents within SP, which form transient synapses before continuing into cortex (Rakic, 1977; Kostovic and Rakic, 1990; Kostović et al., 2002; Kostović and Judaš, 2007). After penetration of thalamocortical fibers into the CP, between 24–28 PCW (Kostović and Judaš, 2010), an additional convergence of associative and commissural fibers also wait in SP before entering the CP (Kostović and Judaš, 2002, 2010; Kostović and Jovanov-Milošević, 2006). Supporting evidence for this possibility is that cortical areas with absence of callosal input, such as primary visual cortex (area 17), contain thin SP while prestriate cortex shows thick SP (Kostovic and Rakic, 1984). The SP is more prominent in associative cortical areas (Figure 7, bottom row), which are strategically arranged in perisylvian cerebral territories. This supports an original hypothesis that evolutionarily, SP is related to the increased number of corticocortical connections (Kostovic and Molliver, 1974; Kostovic and Rakic, 1990; Judaš et al., 2013). Moreover, sequential ingrowth of fibers into the subplate, followed by the waiting period within the subplate, and the final relocation to the cortical plate suggests that during the peak period of fiber ingrowth the volumes of the subplate and cortical plate within same areas should be related. We therefore, expected to find a positive correlation between subplate volume and cortical plate in different anatomical regions during this developmental period (21–30 PCW) (Figure 9). The volume of the cortical plate of the frontal, occipital and parietal lobe showed positive correlation with the volume of the subplate of the same regions (Figure 9, asterisks) indicating related growth of these transient fetal compartments.

Macroscopic Development and Microscopic Histogenetic Changes

The cerebral cortex is expanded in humans largely due to an increase number of cortical columns rather than increased cortical thickness (Rakic, 1995). However, growth of human cerebral cortex is not homogeneous in space or time. During the last trimester of human gestation, telencephalic volume, and surface area expands immensely, especially in frontal, parietal, and temporal areas (Figure 8). The vast expansion of CP occurs after the majority of neurons are born and situated in their final laminar positions, and embryonic columns are formed. This raises the question about the substrates underlying the intensive CP growth during last third of gestation we and others have observed (Retzius, 1900; His, 1904; Dobbing and Sands, 1973; O’Rahilly and Müller, 1984; Garel, 2004; Grossman et al., 2006; Trivedi et al., 2009; Habas et al., 2010a; Clouchoux et al., 2012; Lefèvre et al., 2015). During this phase, the dendrites of pyramidal neurons mature (Mrzljak et al., 1988, 1992; Marín-Padilla, 1992), cortico-cortical afferents arrive (Kostovic and Rakic, 1984; Kostović and Judaš, 2002; Kostović and Jovanov-Milošević, 2006; Kostović et al., 2014) and glia are generated (Bystron et al., 2008). The dendrites of pyramidal neurons develop rapidly after 26 PCW (Mrzljak et al., 1988, 1992) and significantly contribute to cortical volume (Petanjek et al., 2008, 2011). Development of gyral white matter (Kostović et al., 2014), which is related to the diminishment of SP (Figure 7, bottom row) and the formation of gyral convolutions (Figure 7), is also a crucial factor in the morphogenesis of late fetal cortex (Kostovic and Rakic, 1990; Kostović et al., 2014). Patterns of cortical convolutions are unique to each individual human brain (Lohmann et al., 1999). These individual patterns and the majority of gyri and sulci emerge during prenatal and early postnatal development (Connolly, 1950; Chi et al., 1977) reflecting cortical maturation as well as ingrowth of cortical afferents (Goldman and Galkin, 1978; Goldman-Rakic and Rakic, 1984). The appearance of gyri and sulci that we have observed, with the first appearance of deep fissures (sylvian, parieto-occipital, and calcarine) followed by the emergence of central sulcus (around 21 PCW), primary sulci (around 25 PCW), secondary (around 33 PCW), and tertiary sulci (around 40 PCW), is in accordance with previous descriptions from (Retzius, 1900; Connolly, 1950; Chi et al., 1977). The rapid increase of gyrification during late fetal period (Figure 7) coincides with the explosive development of corticocortical fiber connections, suggesting their possible role in gyrification (Kostovic and Rakic, 1990; Van Essen, 1997; Kostović and Jovanov-Milošević, 2006; Huang et al., 2009; Takahashi et al., 2012; Mitter et al., 2015).

CONCLUSION

This study demonstrates that quantitative volumetric, surface area, and thickness data obtained by MRI-histological analysis on transient cellular compartments in the human fetal cerebrum can serve as indicators of spatio-temporal intensity of major developmental prenatal neurogenic events. The volume of proliferative compartments decrease dramatically after 25 PCW,

while extracellular matrix rich synapse containing subplate compartment reached its maximum volume and thickness around 30 PCW before decreasing again. We relate this phenomenon to the pattern of growth of thalamocortical and corticocortical pathways. Moreover, during mid-gestation, the subplate zone occupied nearly half of the total hemispheric volume, indicating the relevance of the subplate compartment during human brain development. Quantitative data on cortical plate show no significant age related mean cortical thickness change, whereas surface area, volume, and level of gyrification show exponential growth during last trimester of gestation. However, as we did observe spatio-temporal areal differences in cortical thickness (vertex-wise analysis), we interpret this pattern of cortical plate differentiation as consistent with coincident differentiation of neurons, growth of dendrites, transformation of embryogenic columns, ingrowth of axons, and synaptogenesis with subsequent development of cortical convolutions. This data will improve our ability to identify transient fetal compartments in neuroimaging data of prenatal human brain.

LIMITATIONS

There are several limitations to our study:

Firstly, the major encountered limitation is our small sample size. Secondly, as fetal brains were extracted from the skull we could not always prevent shape distortions or tissue damage that could affect some of our measurements (gyrification index and cortical plate thickness).

Thirdly, as some of the brains were available as a result of sudden infant death syndrome or especially, respiratory disease, it is possible that some damage may have occurred in these brains, potentially altering their structure.

In order to account for the known tissue shrinkage of 2.7–3.5% that is attributed to the formalin fixation (Boonstra et al., 1983; Schned et al., 1996), we reported relative volumes of transient fetal compartments. Nevertheless, we cannot rule out the minor effects of fixation on obtained absolute measures (such as the changes in cortical thickness).

We have resampled the MR images to isotropic voxel sizes of 0.15 mm (age ≤ 13 PCW) or 0.25 mm (age ≥ 15 PCW) because we needed to scale down from adult-size to fetal-size brains while retaining its structures (gyri and sulci). Although we corrected non-homogeneities with a small spline distance of 5 mm using the N3 method (Sled et al., 1998), we could not fully correct

the non-uniformities in the images and consequently, the initial tissue classification (relying on the discrete classification using ANN (artificial neural network) and partial volume estimations) was not optimal. This led to partial volume effects that, to an extent, influenced our measures.

AUTHOR CONTRIBUTIONS

LV Designed the study, conducted analysis, wrote the paper, and interpreted the results. CL Developed algorithm for fetal MRI image processing. MR and MP contributed to the fetal brain collection and acquisition. JG and SK contributed to data analysis and interpretation. JR and EF contributed to data analysis. MR contributed to data analysis and interpretation. PH contributed to interpretation of results. AE contributed to image processing design and interpretation of results. IK Designed the study, wrote the paper, and interpreted the results.

FUNDING

The project was supported by Croatian Science Foundation (HUMANSUBPLATE) to IK and Fonds national suisse (FNS), project SPUM titled From Cortex to Classroom: Enhancing Brain Development for Premature Infants, No. 140334, to PS.

SUPPLEMENTARY MATERIAL

The Supplementary Material for this article can be found online at: <http://journal.frontiersin.org/article/10.3389/fnana.2016.00011>

Figure S1 | Semiautomatic segmentation (bottom row) of the T1 MRI images (upper row) of the 13 PCW human fetus. Bottom row: Cortical plate in light green, intermediate zone in turquoise, proliferative compartments in pink, and subcortical gray matter with diencephalon in purple.

Figure S2 | Semiautomatic segmentation (bottom row) of the T1 MRI images (upper row) of the 20 PCW human fetus. Bottom row: Cortical plate in light green, subplate compartment in blue, intermediate zone in turquoise, proliferative compartments in pink, and subcortical gray matter with diencephalon in purple.

Figure S3 | Semiautomatic segmentation (bottom row) of the T1 MRI images (upper row) of the 25 PCW human fetus. Bottom row: Cortical plate in light green, subplate compartment in blue, intermediate zone in turquoise, proliferative compartments in pink, and subcortical gray matter with diencephalon in purple.

REFERENCES

- Boonstra, H., Oosterhuis, J., Oosterhuis, A., and Fleuren, G. (1983). Cervical tissue shrinkage by formaldehyde fixation, paraffin wax embedding, section cutting and mounting. *Virchows Archiv A Pathol. Anat. Histopathol.* 402, 195–201. doi: 10.1007/BF00695061
- Boucher, M., Whitesides, S., and Evans, A. (2009). Depth potential function for folding pattern representation, registration and analysis. *Med. Image Anal.* 13, 203–214. doi: 10.1016/j.media.2008.09.001
- Brodman, K. (1909). *Vergleichende Lokalisationslehre der Grosshirnrinde*. Leipzig: Barth.
- Bystron, I., Blakemore, C., and Rakic, P. (2008). Development of the human cerebral cortex: Boulder Committee revisited. *Nat. Rev. Neurosci.* 9, 110–122. doi: 10.1038/nrn2252
- Chi, J. G., Dooling, E. C., and Gilles, F. H. (1977). Gyral development of the human brain. *Ann. Neurol.* 1, 86–93. doi: 10.1002/ana.410010109
- Clouchoux, C., Kudelski, D., Gholipour, A., Warfield, S. K., Viseur, S., Bouyssi-Kobar, M., et al. (2012). Quantitative *in vivo* MRI measurement of cortical development in the fetus. *Brain Struct. Funct.* 217, 127–139. doi: 10.1007/s00429-011-0325-x
- Connolly, C. J. (1950). *External Morphology of the Primate Brain*. Springfield, IL: CC Thomas.

- Dobbing, J., and Sands, J. (1973). Quantitative growth and development of human brain. *Arch. Dis. Child.* 48, 757–767. doi: 10.1136/adc.48.10.757
- Garel, C. (2004). The role of MRI in the evaluation of the fetal brain with an emphasis on biometry, gyration and parenchyma. *Pediatr. Radiol.* 34, 694–699. doi: 10.1007/s00247-004-1249-x
- Goldman, P. S., and Galkin, T. W. (1978). Prenatal removal of frontal association cortex in the fetal rhesus monkey: anatomical and functional consequences in postnatal life. *Brain Res.* 152, 451–485. doi: 10.1016/0006-8993(78)91103-4
- Goldman-Rakic, P. S. and Rakic, P. (1984). “Experimental modification of gyral patterns,” in *Cerebral Dominance: The Biological Foundations*, eds N. Geschwind and A. M. Galaburda (Cambridge, MA: Harvard University Press), 179–192.
- Grossman, R., Hoffman, C., Mardor, Y., and Biegon, A. (2006). Quantitative MRI measurements of human fetal brain development in utero. *Neuroimage* 33, 463–470. doi: 10.1016/j.neuroimage.2006.07.005
- Habas, P. A., Kim, K., Corbett-Detig, J. M., Rousseau, F., Glenn, O. A., Barkovich, A. J., et al. (2010a). A spatiotemporal atlas of MR intensity, tissue probability and shape of the fetal brain with application to segmentation. *Neuroimage* 53, 460–470. doi: 10.1016/j.neuroimage.2010.06.054
- Habas, P. A., Kim, K., Rousseau, F., Glenn, O. A., Barkovich, A. J., and Studholme, C. (2010b). Atlas-based segmentation of developing tissues in the human brain with quantitative validation in young fetuses. *Hum. Brain Mapp.* 31, 1348–1358. doi: 10.1002/hbm.20935
- His, W. (1904). *Die Entwicklung des Menschlichen Gehirns Während der Ersten Monate: Untersuchungsergebnisse*. Leipzig: Hirzel.
- Hoerder-Suabedissen, A., and Molnár, Z. (2015). Development, evolution and pathology of neocortical subplate neurons. *Nat. Rev. Neurosci.* 16, 133–146. doi: 10.1038/nrn3915
- Huang, H., Jeon, T., Sedmak, G., Pletikos, M., Vasung, L., Xu, X., et al. (2013). Coupling diffusion imaging with histological and gene expression analysis to examine the dynamics of cortical areas across the fetal period of human brain development. *Cereb. Cortex* 23, 2620–2631. doi: 10.1093/cercor/bhs241
- Huang, H., and Vasung, L. (2014). Gaining insight of fetal brain development with diffusion MRI and histology. *Int. J. Dev. Neurosci.* 32, 11–22. doi: 10.1016/j.ijdevneu.2013.06.005
- Huang, H., Xue, R., Zhang, J., Ren, T., Richards, L. J., Yarowsky, P., et al. (2009). Anatomical characterization of human fetal brain development with diffusion tensor magnetic resonance imaging. *J. Neurosci.* 29, 4263–4273. doi: 10.1523/JNEUROSCI.2769-08.2009
- Judaš, M., and Cepanec, M. (2007). Adult structure and development of the human fronto-opercular cerebral cortex (Broca’s region). *Clin. Linguist. Phon.* 21, 975–989. doi: 10.1080/02699200701617175
- Judaš, M., Radoš, M., Jovanov-Milošević, N., Hrabac, P., and Kostović, I. (2005). Structural, immunocytochemical, and MR imaging properties of periventricular crossroads of growing cortical pathways in preterm infants. *Am. J. Neuroradiol.* 26, 2671–2684.
- Judaš, M., Sedmak, G., and Kostović, I. (2013). The significance of the subplate for evolution and developmental plasticity of the human brain. *Front. Hum. Neurosci.* 7:423. doi: 10.3389/fnhum.2013.00423
- Judaš, M., Šimić, G., Petanjek, Z., Jovanov-Milošević, N., Pletikos, M., Vasung, L., et al. (2011). The zagreb collection of human brains: a unique, versatile, but underexploited resource for the neuroscience community. *Ann. N.Y. Acad. Sci.* 1225, E105–E130. doi: 10.1111/j.1749-6632.2011.05993.x
- Kang, H. J., Kawasawa, Y. I., Cheng, F., Zhu, Y., Xu, X., Li, M., et al. (2011). Spatio-temporal transcriptome of the human brain. *Nature* 478, 483–489. doi: 10.1038/nature10523
- Kim, J. S., Singh, V., Lee, J. K., Lerch, J., Ad-Dab’bagh, Y., MacDonald, D., et al. (2005). Automated 3-D extraction and evaluation of the inner and outer cortical surfaces using a Laplacian map and partial volume effect classification. *Neuroimage* 27, 210–221. doi: 10.1016/j.neuroimage.2005.03.036
- Kostovic, I., and Goldman-Rakic, P. S. (1983). Transient cholinesterase staining in the mediodorsal nucleus of the thalamus and its connections in the developing human and monkey brain. *J. Comp. Neurol.* 219, 431–447. doi: 10.1002/cne.902190405
- Kostović, I., and Jovanov-Milošević, N. (2006). “The development of cerebral connections during the first 20–45 weeks’ gestation,” in *Seminars in Fetal and Neonatal Medicine*, eds V. Fellman, L. Hellström-Westas, and I. Rosén (Elsevier), 415–422.
- Kostović, I., Jovanov-Milošević, N., Radoš, M., Sedmak, G., Benjak, V., Kostović-Srzić, M., et al. (2014). Perinatal and early postnatal reorganization of the subplate and related cellular compartments in the human cerebral wall as revealed by histological and MRI approaches. *Brain Struct. Funct.* 219, 231–253. doi: 10.1007/s00429-012-0496-0
- Kostović, I., and Judaš, M. (2002). Correlation between the sequential ingrowth of afferents and transient patterns of cortical lamination in preterm infants. *Anat. Rec.* 267, 1–6. doi: 10.1002/ar.10069
- Kostović, I., and Judaš, M. (2007). Transient patterns of cortical lamination during prenatal life: do they have implications for treatment? *Neurosci. Biobehav. Rev.* 31, 1157–1168. doi: 10.1016/j.neubiorev.2007.04.018
- Kostović, I., and Judaš, M. (2010). The development of the subplate and thalamocortical connections in the human foetal brain. *Acta Paediatr.* 99, 1119–1127. doi: 10.1111/j.1651-2227.2010.01811.x
- Kostović, I., and Judaš, M. (2015). Embryonic and fetal development of the human cerebral cortex. *Brain Mapp.* 2, 167–175. doi: 10.1016/B978-0-12-397025-1.00193-7
- Kostovic, I., Judas, M., Kostovic-Knezevic, L., Simic, G., Delalle, I., Chudy, D., et al. (1991). Zagreb research collection of human brains for developmental neurobiologists and clinical neuroscientists. *Int. J. Dev. Biol.* 35, 215–230.
- Kostović, I., Judaš, M., Radoš, M., and Hrabac, P. (2002). Laminar organization of the human fetal cerebrum revealed by histochemical markers and magnetic resonance imaging. *Cereb. Cortex* 12, 536–544. doi: 10.1093/cercor/12.5.536
- Kostovic, I., Kostovic-Srzić, M., Benjak, V., Jovanov-Milošević, N., and Rados, M. (2014). Developmental dynamics of radial vulnerability in the cerebral compartments in preterm infants and neonates. *Front. Neurol.* 5:139. doi: 10.3389/fneur.2014.00139
- Kostovic, I., and Molliver, M. (1974). “New interpretation of laminar development of cerebral-cortex-synaptogenesis in different layers of neopallium in human fetus,” in *Anatomical Record* (New York, NY: Wiley-Liss Div John Wiley & Sons Inc.), 395–395.
- Kostovic, I., and Rakic, P. (1984). Development of prestriate visual projections in the monkey and human fetal cerebrum revealed by transient cholinesterase staining. *J. Neurosci.* 4, 25–42.
- Kostovic, I., and Rakic, P. (1990). Developmental history of the transient subplate zone in the visual and somatosensory cortex of the macaque monkey and human brain. *J. Comp. Neurol.* 297, 441–470. doi: 10.1002/cne.902970309
- Kostovic, I., and Vasung, L. (2009). “Insights from *in vitro* fetal magnetic resonance imaging of cerebral development,” in *Seminars in Perinatology*, ed C. Limperopoulos (Elsevier), 220–233.
- Kostovic, I., Vasung, L., Rados, M., Culjat, M., Ozretic, D., Judaš, M., et al. (2008). *Early Lamination of the Cortical Plate in the Prefrontal Cortex of the Human Fetus: in vitro 3T MR Imaging and Histological Analysis Program No. 820.6/B33 Neuroscience Meeting Planner*. Washington, DC: Society for Neuroscience.
- Kriegstein, A., Noctor, S., and Martínez-Cerdeño, V. (2006). Patterns of neural stem and progenitor cell division may underlie evolutionary cortical expansion. *Nat. Rev. Neurosci.* 7, 883–890. doi: 10.1038/nrn2008
- Kuklisova-Murgasova, M., Aljabar, P., Srinivasan, L., Counsell, S. J., Doria, V., Serag, A., et al. (2011). A dynamic 4D probabilistic atlas of the developing brain. *Neuroimage* 54, 2750–2763. doi: 10.1016/j.neuroimage.2010.10.019
- Lefèvre, J., Germanaud, D., Dubois, J., Rousseau, F., De Macedo Santos, I., Angleys, H., et al. (2015). Are developmental trajectories of cortical folding comparable between cross-sectional datasets of fetuses and preterm newborns? *Cereb. Cortex*. doi: 10.1093/cercor/bhv123. [Epub ahead of print].
- Lohmann, G., von Cramon, D. Y., and Steinmetz, H. (1999). Sulcal variability of twins. *Cereb. Cortex* 9, 754–763. doi: 10.1093/cercor/9.7.754
- Lytelton, O., Boucher, M., Robbins, S., and Evans, A. (2007). An unbiased iterative group registration template for cortical surface analysis. *Neuroimage* 34, 1535–1544. doi: 10.1016/j.neuroimage.2006.10.041
- Maas, L. C., Mukherjee, P., Carballido-Gamio, J., Veeraraghavan, S., Miller, S. P., Partridge, S. C., et al. (2004). Early laminar organization of the human cerebrum demonstrated with diffusion tensor imaging in extremely premature infants. *Neuroimage* 22, 1134–1140. doi: 10.1016/j.neuroimage.2004.02.035
- MacDonald, D., Kabani, N., Avis, D., and Evans, A. C. (2000). Automated 3-D extraction of inner and outer surfaces of cerebral cortex from MRI. *Neuroimage* 12, 340–356. doi: 10.1006/nimg.1999.0534

- Makropoulos, A., Gousias, I. S., Ledig, C., Aljabar, P., Serag, A., Hajnal, J. V., et al. (2014). Automatic whole brain MRI segmentation of the developing neonatal brain. *IEEE Trans. Med. Imaging* 33, 1818–1831. doi: 10.1109/TMI.2014.2322280
- Marin-Padilla, M. (1992). Ontogenesis of the pyramidal cell of the mammalian neocortex and developmental cytoarchitectonics: a unifying theory. *J. Comp. Neurol.* 321, 223–240. doi: 10.1002/cne.903210205
- McKinstry, R. C., Mathur, A., Miller, J. H., Ozcan, A., Snyder, A. Z., Schefft, G. L., et al. (2002). Radial organization of developing preterm human cerebral cortex revealed by non-invasive water diffusion anisotropy MRI. *Cereb. Cortex* 12, 1237–1243. doi: 10.1093/cercor/12.12.1237
- Miller, S. P., and Ferriero, D. M. (2009). From selective vulnerability to connectivity: insights from newborn brain imaging. *Trends Neurosci.* 32, 496–505. doi: 10.1016/j.tins.2009.05.010
- Mitter, C., Prayer, D., Brugger, P. C., Weber, M., and Kasprian, G. (2015). *In vivo* Tractography of fetal association fibers. *PLoS ONE* 10:e0119536. doi: 10.1371/journal.pone.0119536
- Molliver, M. E., Kostovic, I., and van Der Loos, H. (1973). The development of synapses in cerebral cortex of the human fetus. *Brain Res.* 50, 403–407. doi: 10.1016/0006-8993(73)90741-5
- Mrzljak, L., Uylings, H., Kostovic, I., and Van Eden, C. G. (1988). Prenatal development of neurons in the human prefrontal cortex: I. A qualitative golgi study. *J. Comp. Neurol.* 271, 355–386. doi: 10.1002/cne.902710306
- Mrzljak, L., Uylings, H., Kostovic, I., and Van Eden, C. G. (1992). Prenatal development of neurons in the human prefrontal cortex. II. A quantitative Golgi study. *J. Comp. Neurol.* 316, 485–496. doi: 10.1002/cne.903160408
- O'Leary, D. D. M., and Borngasser, D. (2006). Cortical ventricular zone progenitors and their progeny maintain spatial relationships and radial patterning during preplate development indicating an early protomap. *Cereb. Cortex* 16(Suppl. 1), i46–i56. doi: 10.1093/cercor/bhk019
- Olivier, G., and Pineau, H. (1962). Horizons de Streeter et age embryonnaire. *Bull. Assoc. Anat.* 113, 573–576.
- O'Rahilly, R., and Müller, F. (1984). Embryonic length and cerebral landmarks in staged human embryos. *Anat. Rec.* 209, 265–271. doi: 10.1002/ar.1092090212
- Perkins, L., Hughes, E., Srinivasan, L., Allsop, J., Glover, A., Kumar, S., et al. (2008). Exploring cortical subplate evolution using magnetic resonance imaging of the fetal brain. *Dev. Neurosci.* 30, 211–220. doi: 10.1159/000109864
- Petanjek, Z., Judaš, M., Kostović, I., and Uylings, H. B. (2008). Lifespan alterations of basal dendritic trees of pyramidal neurons in the human prefrontal cortex: a layer-specific pattern. *Cereb. Cortex* 18, 915–929. doi: 10.1093/cercor/bhm124
- Petanjek, Z., Judaš, M., Šimić, G., Rašin, M. R., Uylings, H. B., Rakic, P., et al. (2011). Extraordinary neoteny of synaptic spines in the human prefrontal cortex. *Proc. Natl. Acad. Sci. U.S.A.* 108, 13281–13286. doi: 10.1073/pnas.1105108108
- Pletikos, M., Sousa, A. M., Sedmak, G., Meyer, K. A., Zhu, Y., Cheng, F., et al. (2014). Temporal specification and bilaterality of human neocortical topographic gene expression. *Neuron* 81, 321–332. doi: 10.1016/j.neuron.2013.11.018
- Prayer, D., Kasprian, G., Krampl, E., Ulm, B., Witzani, L., Prayer, L., et al. (2006). MRI of normal fetal brain development. *Eur. J. Radiol.* 57, 199–216. doi: 10.1016/j.ejrad.2005.11.020
- Radoš, M., Judaš, M., and Kostović, I. (2006). *In vitro* MRI of brain development. *Eur. J. Radiol.* 57, 187–198. doi: 10.1016/j.ejrad.2005.11.019
- Rakic, P. (1972). Mode of cell migration to the superficial layers of fetal monkey neocortex. *J. Comp. Neurol.* 145, 61–83. doi: 10.1002/cne.901450105
- Rakic, P. (1977). Genesis of the dorsal lateral geniculate nucleus in the rhesus monkey: site and time of origin, kinetics of proliferation, routes of migration and pattern of distribution of neurons. *J. Comp. Neurol.* 176, 23–52. doi: 10.1002/cne.901760103
- Rakic, P. (1982). Early developmental events: cell lineages, acquisition of neuronal positions, and areal and laminar development. *Neurosci. Res. Program Bull.* 20, 439.
- Rakic, P. (1988). Specification of cerebral cortical areas. *Science* 241, 170–176. doi: 10.1126/science.3291116
- Rakic, P. (1995). A small step for the cell, a giant leap for mankind: a hypothesis of neocortical expansion during evolution. *Trends Neurosci.* 18, 383–388. doi: 10.1016/0166-2236(95)93934-P
- Rakic, P. (2006). A century of progress in corticogenesis: from silver impregnation to genetic engineering. *Cereb. Cortex* 16(Suppl. 1), i3–i17. doi: 10.1093/cercor/bhk036
- Rakic, P. (2009). Evolution of the neocortex: a perspective from developmental biology. *Nat. Rev. Neurosci.* 10, 724–735. doi: 10.1038/nrn2719
- Rakic, P., Ayoub, A. E., Breunig, J. J., and Dominguez, M. H. (2009). Decision by division: making cortical maps. *Trends Neurosci.* 32, 291–301. doi: 10.1016/j.tins.2009.01.007
- Retzius, G. (1900). *Biologische Untersuchungen*. Stockholm: Samson & Wallin.
- Robbins, S. M. (2004). *Anatomical Standardization of the Human Brain in Euclidean 3-Space and on the Cortical 2-Manifold*. Ph.D. thesis, McGill University, Montreal, QC.
- Rofsky, N. M., Lee, V. S., Laub, G., Pollack, M. A., Krinsky, G. A., Thomasson, D., et al. (1999). Abdominal MR imaging with a volumetric interpolated breath-hold examination 1. *Radiology* 212, 876–884. doi: 10.1148/radiology.212.3.r99se34876
- Rutherford, M. A. (2009). Magnetic resonance imaging of the fetal brain. *Curr. Opin. Obstet. Gynecol.* 21, 180–186. doi: 10.1097/GCO.0b013e32832947ab
- Sanai, N., Nguyen, T., Ihrie, R. A., Mirzadeh, Z., Tsai, H.-H., Wong, M., et al. (2011). Corridors of migrating neurons in the human brain and their decline during infancy. *Nature* 478, 382–386. doi: 10.1038/nature10487
- Schned, A. R., Wheeler, K. J., Hodorowski, C. A., Heaney, J. A., Ernstoff, M. S., Amdur, R. J., et al. (1996). Tissue-shrinkage correction factor in the calculation of prostate cancer volume. *Am. J. Surg. Pathol.* 20, 1501–1506. doi: 10.1097/00000478-199612000-00009
- Sled, J. G., Zijdenbos, A. P., and Evans, A. C. (1998). A nonparametric method for automatic correction of intensity nonuniformity in MRI data. *IEEE Trans. Med. Imaging* 17, 87–97. doi: 10.1109/42.668698
- Smart, I. H., Dehay, C., Giroud, P., Berland, M., and Kennedy, H. (2002). Unique morphological features of the proliferative zones and postmitotic compartments of the neural epithelium giving rise to striate and extrastriate cortex in the monkey. *Cereb. Cortex* 12, 37–53. doi: 10.1093/cercor/12.1.37
- Takahashi, E., Folkerth, R. D., Galaburda, A. M., and Grant, P. E. (2012). Emerging cerebral connectivity in the human fetal brain: an MR tractography study. *Cereb. Cortex* 22, 455–464. doi: 10.1093/cercor/bhr126
- Tohka, J., Zijdenbos, A., and Evans, A. (2004). Fast and robust parameter estimation for statistical partial volume models in brain MRI. *Neuroimage* 23, 84–97. doi: 10.1016/j.neuroimage.2004.05.007
- Tovi, M., and Ericsson, A. (1992). Measurements of T1 and T2 over time in formalin-fixed human whole-brain specimens. *Acta Radiol.* 33, 400–404. doi: 10.3109/02841859209172021
- Trivedi, R., Gupta, R. K., Husain, N., Rathore, R. K., Saksena, S., Srivastava, S., et al. (2009). Region-specific maturation of cerebral cortex in human fetal brain: diffusion tensor imaging and histology. *Neuroradiology* 51, 567–576. doi: 10.1007/s00234-009-0533-8
- Vacca, L. L., Hobbs, J., and Hogan, M. (1978). Effects of hydrogen ion dissociation and concentration on the reactivity of dichromate-fixed tissue components to the PAS procedure: recommendations for reducing undesirable background staining. *Biotech. Histochem.* 53, 107–112. doi: 10.3109/10520297809111451
- Van Essen, D. C. (1997). A tension-based theory of morphogenesis and compact wiring in the central nervous system. *Nature* 385, 313–318. doi: 10.1038/385313a0
- Volpe, J. J. (2009). Brain injury in premature infants: a complex amalgam of destructive and developmental disturbances. *Lancet Neurol.* 8, 110–124. doi: 10.1016/S1474-4422(08)70294-1
- von Economo, C. F., and Koskinas, G. N. (1925). *Die Cytoarchitektonik der Hirnrinde des Erwachsenen Menschen*. Vienna: Springer.
- Widjaja, E., Geibprasert, S., Mahmoodabadi, S., Blaser, S., Brown, N., and Shannon, P. (2010). Alteration of human fetal subplate layer and intermediate zone during normal development on MR and diffusion tensor imaging. *Am. J. Neuroradiol.* 31, 1091–1099. doi: 10.3174/ajnr.A1985
- Zecevic, N., Chen, Y., and Filipovic, R. (2005). Contributions of cortical subventricular zone to the development of the human cerebral cortex. *J. Comp. Neurol.* 491, 109–122. doi: 10.1002/cne.20714

Zijdenbos, A., Forghani, R., and Evans, A. (1998). "Automatic quantification of MS lesions in 3D MRI brain data sets: validation of INSECT," in *Medical Image Computing and Computer-Assisted Intervention—MICCAI'98*, eds W. M. Wells, A. Colchester, and S. Delp (Springer), 439–448.

Conflict of Interest Statement: The authors declare that the research was conducted in the absence of any commercial or financial relationships that could be construed as a potential conflict of interest.

Copyright © 2016 Vasung, Lepage, Radoš, Pletikos, Goldman, Richiardi, Raguz, Fisch-Gómez, Karama, Huppi, Evans and Kostovic. This is an open-access article distributed under the terms of the Creative Commons Attribution License (CC BY). The use, distribution or reproduction in other forums is permitted, provided the original author(s) or licensor are credited and that the original publication in this journal is cited, in accordance with accepted academic practice. No use, distribution or reproduction is permitted which does not comply with these terms.



Maturation Along White Matter Tracts in Human Brain Using a Diffusion Tensor Surface Model Tract-Specific Analysis

Zhang Chen¹, Hui Zhang², Paul A. Yushkevich³, Min Liu¹ and Christian Beaulieu^{1*}

¹ Department of Biomedical Engineering, Faculty of Medicine and Dentistry, University of Alberta, Edmonton, AB, Canada,

² Department of Computer Science and Centre for Medical Image Computing, University College London, London, UK,

³ Penn Image Computing and Science Laboratory, Department of Radiology, University of Pennsylvania, Philadelphia, PA, USA

OPEN ACCESS

Edited by:

Pratik Mukherjee,
University of California,
San Francisco, USA

Reviewed by:

Lauren Jean O'Donnell,
Harvard Medical School, USA
John B. Colby,
University of California,
San Francisco, USA

*Correspondence:

Christian Beaulieu
christian.beaulieu@ualberta.ca

Received: 29 October 2015

Accepted: 26 January 2016

Published: 16 February 2016

Citation:

Chen Z, Zhang H, Yushkevich PA,
Liu M and Beaulieu C (2016)
Maturation Along White Matter Tracts
in Human Brain Using a Diffusion
Tensor Surface Model Tract-Specific
Analysis. *Front. Neuroanat.* 10:9.
doi: 10.3389/fnana.2016.00009

Previous diffusion tensor imaging tractography studies have demonstrated exponential patterns of developmental changes for diffusion parameters such as fractional anisotropy (FA) and mean diffusivity (MD) averaged over all voxels in major white matter (WM) tracts of the human brain. However, this assumes that the entire tract is changing in unison, which may not be the case. In this study, a surface model based tract-specific analysis was applied to a cross-sectional cohort of 178 healthy subjects (83 males/95 females) aged from 6 to 30 years to spatially characterize the age-related changes of FA and MD along the trajectory of seven major WM tracts – corpus callosum (CC) and six bilateral tracts. There were unique patterns of regions that showed different exponential and linear rates of increasing FA or decreasing MD and age at which FA or MD levels off along each tract. Faster change rate of FA was observed in genu of CC and frontal-parietal part of superior longitudinal fasciculus (SLF). Inferior corticospinal tract (CST), posterior regions of association tracts such as inferior longitudinal fasciculus, inferior frontal occipital fasciculus and uncinate fasciculus also displayed earlier changing patterns for FA. MD decreases with age also exhibited this posterior-to-anterior WM maturation pattern for most tracts in females. Both males and females displayed similar FA/MD patterns of change with age along most large tracts; however, males had overall reached the FA maxima or MD minima later compared with females in most tracts with the greater differences occurring in the CST and frontal-parietal part of SLF for MD. Therefore, brain WM development has spatially varying trajectories along tracts that depend on sex and the tract.

Keywords: neurodevelopment, diffusion tensor imaging, fractional anisotropy, mean diffusivity, tractography

INTRODUCTION

Quantitative magnetic resonance imaging (MRI) has demonstrated significant brain changes during development from infancy to adulthood *in vivo*. Structural MRI studies have reported age-related changes in brain volumes (Giedd et al., 1999; Good et al., 2001), areas (Thompson et al., 2000), cortical thickness (Sowell et al., 2004; Shaw et al., 2008), and regional gray matter (GM)

and white matter (WM) density (Paus et al., 1999; Gogtay et al., 2004). It has been suggested that those developmental changes in GM and WM observed at the macroscopic MRI level may reflect synaptic pruning and myelination at the microscopic neuronal level (Gogtay et al., 2004).

Diffusion tensor imaging (DTI) techniques have enabled the virtual dissection of WM tracts *in vivo* and permit the investigation of tissue microstructure, including indirect measures of myelination and axonal density, that may be more sensitive than conventional imaging to changes with age (Basser et al., 1994; Beaulieu, 2002; Le Bihan, 2003). Using region-of-interest (ROI) by manual placement/tractography or voxel based analysis, brain development studies of children and adolescents using DTI have consistently demonstrated age-related increases of fractional anisotropy (FA) and decreases of overall diffusion mean diffusivity (MD; Klingberg et al., 1999; Morriss et al., 1999; Schmithorst et al., 2002; Schneider et al., 2004; Barnea-Goraly et al., 2005; Snook et al., 2005; Ashtari et al., 2007; Bonekamp et al., 2007; Eluvathingal et al., 2007; Lebel et al., 2008; Tamnes et al., 2010) that differ between tracts with some data suggesting a posterior-to-anterior developmental trend (Colby et al., 2011). The appropriate fit of FA or MD with age depends somewhat on the age span covered. The general course of FA and MD across the lifespan in WM shows average FA values rising throughout childhood, adolescence, peaking between 20 and 42 years of age and then declining, due to aging processes (Han et al., 2007; Lebel et al., 2012). This FA trajectory is mirrored by a similarly decreasing then increasing trajectory with age for MD. However, in neurodevelopmental studies with a limited age range from childhood to adulthood (typically up to 30 years), FA or MD versus age curves have been fit with either an exponential trajectory to account for FA/MD changing faster at younger ages and then leveling off at a plateau (Lebel et al., 2008; Colby et al., 2011; Taki et al., 2013b) or linear model that assumes the same rate of diffusion parameter changes across the given age span (Schmithorst et al., 2002; Barnea-Goraly et al., 2005; Bonekamp et al., 2007).

However, the ROI-based approach requires averaging the scalar values such as FA or MD from all vertices within the ROI, either manually placed on a 2D slice(s) or using tractography in 3D, into a single value for each tract. On the other hand, voxel-based approaches that can assess various portions of tracts simultaneously face issues of inter-subject alignment quality (Jones et al., 2005a; Van Hecke et al., 2009), although methods have been proposed to mitigate these issues, e.g., tract-based spatial statistics, TBSS (Smith et al., 2006), but not without their own limitations (Bach et al., 2014).

The main issue with a global estimate of diffusion parameters over an entire tract is it assumes that the entire length of a tract behaves the same with age and it cannot detect focal changes or regional variations within the tract. The 'whole brain' voxel-based approaches that do attempt to pull out regional differences do not address specific tracts *a priori*. This has led to a growing interest in the development of tract specific methods that can spatially characterize quantitative

imaging parameters along the trajectory of tracts. The main obstacle in any along-tract analysis is the non-uniform spatial sampling of the vertices within each streamline. To overcome the issue, several approaches have been proposed, such as a scale-invariant parameterization by arc-angle (Gong et al., 2005), fiber clustering and measurement (Maddah et al., 2008; Prasad et al., 2014) and fiber tract parameterization by arc length (Jones et al., 2005b; Corouge et al., 2006; Goodlett et al., 2009; O'Donnell et al., 2009; Zhu et al., 2011; Yeatman et al., 2012). Using those along-tract methods, studies have found WM abnormalities (FA, MD) along several major tracts in brain disorders such as epilepsy (Concha et al., 2012), Alzheimer's disease (Nir et al., 2015) and fetal alcohol spectrum disorder (Colby et al., 2012). Brain development cross-sectional studies in infants (1–2 years), toddlers (2–4 years), and children/adolescence (9–16 years) using along-tract analysis showed unique changes with age of DTI parameters such as FA along several tracts (Goodlett et al., 2009; Zhu et al., 2011; Yeatman et al., 2012; Johnson et al., 2013). A recent study also found various diffusion parameters that were variable along multiple WM tracts related to sex, hemisphere, and age within a sample of 26–46 months-old typically developing young children (Johnson et al., 2013). The variations in diffusion at different tract locations likely reflect unique rates of axonal myelination and packing (Beaulieu, 2002; Song et al., 2002, 2005) that might be due to local differences in vasculature, supporting glial structure, and biochemistry throughout the brain (Ito et al., 2005; Yeh et al., 2009; Vasung et al., 2010).

However, those methods are best suited for tracts with tubular geometry such as the cingulum as DTI measurements are averaged across the cross-section along the fibers; larger sheet-like structures such as corpus callosum (CC) have to be divided into several tubular bundles. To overcome these limitations, a recent study has suggested a tract-specific analysis (TSA) using a continuous medial representation (cm-rep) to model individual WM tracts (Yushkevich et al., 2006, 2008; Zhang et al., 2010). The advantage of using cm-rep is that the skeleton of the tract is represented by a parametric surface that allows manifold-based statistical analyses similar to those used in cortical surface mapping (Lerch et al., 2006). As it is an atlas-based approach, it can reduce user bias and improve efficiency of analysis for large data sets examining numerous tracts, albeit with the primary limitation of requiring adequate spatial normalization between individuals. This tract surface methodology has not yet been applied to the study of neurodevelopment.

The purpose of this study is to spatially characterize DTI parameter changes using linear and exponential fits along several major tracts using TSA in both males and females in a large cross-sectional cohort of 178 participants from young childhood to adulthood (6–30 years). We hypothesize that each tract will show a unique pattern of diffusion changes that reflects a more localized developmental pattern, rather than having uniform changes along the entire tract, and will have similar patterns between males and females but with different maturation rates and timing.

MATERIALS AND METHODS

Subjects

This study includes 178 healthy right-handed participants (male/female: 83/95) aged from 6 to 30 years from our previous DTI development study that averaged all the FA or MD values across the entire tract (Lebel et al., 2008), although excluding participants who were left-handed or had images that failed the new pre-processing steps (detailed below). Participants were asked a series of questions to ensure there was no history of neurological or psychiatric disease or brain injury. All participants gave informed consent; child assent and parent/guardian consent was obtained for volunteers under 18 years. The age range was similar for males (6–30 years) and females (6–30 years) with similar mean and standard deviations of 15.6 ± 6.1 and 16.0 ± 6.4 years, respectively. This study was approved by the University of Alberta Human Research Ethics Board.

Image Acquisition

All data was acquired on a single 1.5T Siemens Sonata MRI scanner. Using a protocol set up over a decade ago to enable studies in young children, standard DTI was acquired using a dual spin-echo, single shot echo-planar imaging sequence with the following parameters: 40 3-mm-thick slices with no interslice gap, TR = 6400 ms, TE = 88 ms, six non-collinear diffusion sensitizing gradient directions with $b = 1000$ s/mm², eight averages, field-of-view 220 mm × 220 mm, matrix of 96 × 128 zero-filled to 256 × 256, and scan time of 6:06 min.

Tract-Specific Diffusion Measurements

Image preprocessing steps included motion and eddy current distortion corrections and diffusion tensor fitting (linear), which were performed using FSL 5.0¹. DTI-TK² was then applied to obtain a population-specific tensor template and the medial surface of major tracts from the template. **Figure 1** demonstrates a flowchart of the procedures. The achievement of the optimal spatial normalization requires a tensor template derived from subjects with equal sex distribution and similar age range. We first bootstrapped a population specific template (Zhang et al., 2007) from 12 evenly age/sex distributed subjects across the whole age range (6F/6M, 10–29 years; **Figure 1A**). In short, an initial average template was constructed as a Log-Euclidean mean of the selected DTI images to preserve WM orientation with minimal blurring (Arsigny et al., 2006). Then the template was iteratively refined by affine and non-linear registration in which image similarity is computed based on full tensor images of the subject to the template (Zhang et al., 2006, 2007). This atlas construction approach has been shown to provide a more accurate study specific template compared to the more common scalar parameter methods (Keihaninejad et al., 2013).

Using DtiStudio (Jiang et al., 2006), 13 tracts were manually segmented from the template (**Figures 1B,C**) via the fiber

assignment by continuous tracking (FACT) algorithm with FA threshold 0.15 and angular threshold of 70° (Mori et al., 1999) and the skeleton of each tract was approximated by a parametric surface using the continuous medial representation framework (cm-rep, **Figure 1D**; Yushkevich et al., 2008). Boundaries and medial surfaces of 13 tracts were generated in the template including the CC (15230 vertices, 16690 mm²), as well as the following tracts in the left and right hemispheres: corticospinal tract (CST, left/right: 5683/8167 vertices, 4528/4131 mm²), cingulum (CG, left/right: 4835/5027 vertices, 600/634 mm²), inferior fronto-occipital fasciculus (IFO, left/right: 6615/7591 vertices, 3547/3268 mm²), inferior longitudinal fasciculus (ILF, left/right: 7591/8327 vertices, 2118/2270 mm²), superior longitudinal fasciculus (SLF, left/right: 4931/5959 vertices, 1884/961 mm²), and uncinate fasciculus (UNC, left/right: 6903/4931 vertices, 1270/1417 mm²). Note that depending on the tract characteristic, the number of vertices does not necessarily match directly with surface area (e.g., tracts with higher curvature have more vertices).

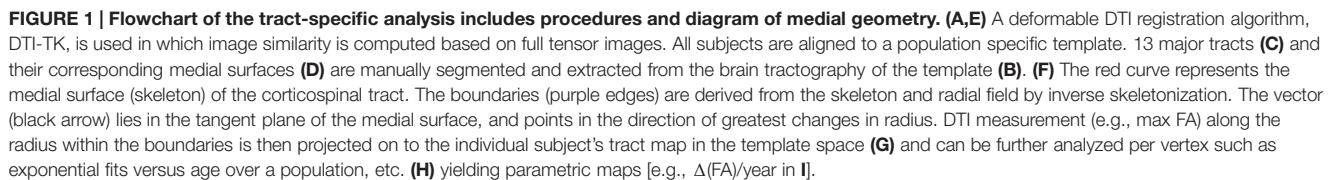
Next, all subjects were aligned to the population-specific template using DTI-TK (**Figure 1E**). Spatially normalized tensor fields were sampled for each subject along directions of radius originating from the tract skeleton to the tract boundary and the largest FA (with a minimum threshold of 0.2) of all the tensors and their corresponding MD values between the boundaries were selected for each point on the parametric skeleton for each subject (**Figure 1F**). FA and MD measurements along the surfaces were then smoothed using a surface-based diffusion smoothing kernel of approximately 8 mm FWHM (**Figure 1G**) that preserves topology of the tracts (Chung et al., 2005). FA and MD values of each vertex on each tract were mapped against age for all subjects (**Figure 1H**).

Vertex-Based Curve Fitting of FA and MD Changes with Age

From our previous paper on a large cohort, we demonstrated that diffusion changes from childhood to adulthood followed an exponential pattern of maturation (Lebel et al., 2008). In this study, all fitting procedures described here were implemented in Matlab2014a and applied to FA and MD values of each vertex on the tract in male and female groups (recall: tractography is not performed in each individual). As some vertices may not have a significant exponential fit, linear fits were also performed at each vertex of the tracts. For linear fit, the linear equation of the form FA (or MD) = $b + a \cdot \text{age}$ yielded b and a as the estimated y-intercept and the slope of the fitting. For exponential fitting, equations of the form FA (or MD) = $C + A e^{-\text{age}/t}$ yielded C as the estimate asymptote value, A as the y-intercept of the function and time constants t indicating the rate of development. The significance of the both linear and exponential fits were measured using F -test ($p < 0.05$) and corrected using random field theory at $p = 0.01$ (Worsley et al., 1999). A significant F -test indicates that the observed R-squared is reliable, and is not a spurious result of oddities in the data set. Thus, the F -test determines whether the proposed relationship between the response variable and the set of predictors is statistically reliable.

¹<http://fsl.fmrib.ox.ac.uk/fsl/fslwiki>

²<http://dti-tk.sourceforge.net/>



Rate and Maximum Development Age of FA and MD Changes

comparisons corrections. In addition the rate of change of FA or MD was given by the slope for the linear fits. These analyses were performed in all 13 tracts (CC and six bilateral) for males and females separately. The maximum development ages were compared between sexes per vertex to see if they overlapped, given the standard error from the exponential fits. For both FA and MD, if the development age plus/minus the standard errors per vertex overlapped between males and females, they were not considered to be significantly different. This method was used in our earlier whole tract development paper (Lebel et al., 2008).

Although the primary interest in this paper is on variable changes along the tract, mean DTI values of each tract averaged over all vertices with significant fits at the individual vertex level were determined to provide overall tract summary parameters for the male and female groups. Exponential and linear fit vertices were combined separately. To simplify this mean over the tract analysis, the FA/MD values of all the significant vertices for each tract were averaged over left and right sides (e.g., SLF.L+SLF.R).

RESULTS

Mean FA and MD Changes with Age

Using the normalized, medial surface model of the tracts resulted in significant exponential/linear fitting of mean FA and MD in many regions of seven major tracts (CC, bilateral CST, SLF, UNC, ILF, IFO, CG) for both male and female groups (Tables 1 and 2). Overall, the percentage of vertices with significant exponential FA increases with age was $27 \pm 10\%$ (range: 15–50%) over the various tracts and was greater for exponential MD decreases over age with $51 \pm 18\%$ (range: 18–84%). Another $14 \pm 8\%$ (range: 4–36%) of the vertices for FA and $13 \pm 10\%$ (range: 1–32%) for MD showed linear changes with age per tract. Combining vertices with either significant exponential or linear fits with age, only $41 \pm 9\%$ (range: 29–56%) and $63 \pm 18\%$ (range: 26–85%) of the vertices showed changes with age for FA or MD, respectively. In general, MD showed more expansive regions that changed with age per tract. The proportion of vertices with exponential fits was greater in the females than the males for all tracts by an absolute $\sim 13 \pm 8\%$ for FA (range: 5–22%) and $\sim 12 \pm 13\%$ for MD (range: 1–40%).

Figure 2 shows the average of the FA or MD over all the vertices with significant exponential changes in the combined left/right tracts, leading to several observations. The CST reaches FA maximum earliest and UNC latest; while for MD the ILF reaches MD minimum earliest and CST the latest. With the exception of these two tracts, the other five tracts each showed similar timings for their FA and MD changes with age. The FA appeared to be higher in males in most of the tracts over the full age span, whereas MD overlapped considerably between sexes

with the exception of the CC. Overall, mean FA and MD of the tracts reach their plateau (T) earlier in females (12–20 years, mean of 15 years) than in males (17–30 years, mean of 21 years), as seen in Table 1 for FA and Table 2 for MD. Females demonstrated a significant earlier plateau of FA in CST and SLF by 6–7 years and MD in CST, SLF, IFO, and ILF by 5–15 years. The degree of absolute change per year for either FA or MD in the time up to the plateau is also typically larger in the females relative to the males. It should be noted that the vertices with significant exponential fits are not necessarily at the same locations for both males and females (shown in Figures 3 and 4 for FA and Figures 6 and 7 for MD).

Developmental Rate and Timing of Tract-Specific FA Changes

Specific areas along each tract showed either significant exponential (Figure 3) or linear (Figure 5) patterns of increases of FA with differing rates (+FA/year). Also, the age to reach 90% of maximum FA from 6 to 30 years varied for the regions with exponential fits (Figure 4). Overall, similar regions of the tracts showed exponential FA increases between the male and female groups, albeit with apparent differences in rates and timing in many cases. Faster exponential FA changes were observed in genu of CC ($>0.006/\text{year}$ for both males and females), inferior CST ($0.004\text{--}0.008/\text{year}$ for males and >0.01 for females) and fronto-parietal part of SLF ($0.004\text{--}0.006/\text{year}$ for males and $>0.01/\text{year}$ for females) relative to the other areas of these three tracts. Smaller frontal tracts such as bilateral CG ($>0.008/\text{year}$), left ILF ($>0.01/\text{year}$), and left IFO ($>0.01/\text{year}$) in females displayed faster exponential changes in the posterior part of the tracts

TABLE 1 | Percentage of vertices with significant exponential (P_{exp}) and linear (P_{lin}) fits and correlation (R_{exp} and R_{lin}), exponential time constant (t), absolute change of FA per year from age 6 to 30 (linear) and age (T) where FA reaches 90% of the plateau maximum (exponential) over those vertices with exponential fits for each tract (left + right combined) of males (M) and females (F) separately.

Tracts	Fractional Anisotropy versus Age					
	Sex	P_{exp} (P_{lin}) %	R_{exp} (R_{lin})	t_{exp} (SE)	Absolute increase per year Exp (Lin)	T_{exp} (SE) year
CST	M	22 (10)	0.59 (0.59)	5.5 (1.4)	0.005 (0.004)	18.8 (3.3)*
	F	27 (4)	0.53 (0.31)	2.8 (0.6)	0.01 (0.003)	12.4 (1.4)*
CG	M	28 (19)	0.56 (0.62)	5.3 (1.5)	0.008 (0.004)	18.3 (3.3)
	F	50 (10)	0.63 (0.52)	4.3 (0.9)	0.01 (0.004)	15.9 (2.1)
CC	M	19 (16)	0.61 (0.65)	5.3 (1.3)	0.006 (0.003)	18.2 (3.1)
	F	24 (8)	0.6 (0.48)	4.4 (1.0)	0.007 (0.003)	16.2 (2.2)
IFO	M	23 (16)	0.52 (0.6)	6.2 (2.0)	0.005 (0.003)	20.3 (4.7)
	F	34 (10)	0.57 (0.42)	4.1 (0.9)	0.008 (0.003)	15.4 (2.1)
SLF	M	18 (22)	0.54 (0.63)	6.8 (2.3)	0.005 (0.003)	21.6 (5.2)*
	F	38 (10)	0.54 (0.47)	3.6 (0.8)	0.009 (0.003)	14.2 (1.8)*
ILF	M	15 (15)	0.5 (0.56)	6.4 (2.3)	0.004 (0.003)	20.8 (5.2)
	F	21 (13)	0.45 (0.52)	5.8 (2.0)	0.004 (0.003)	19.3 (4.5)
UNC	M	20 (35)	0.5 (0.59)	7.6 (2.9)	0.003 (0.003)	23.4 (6.6)
	F	38 (9)	0.51 (0.29)	5.0 (1.4)	0.006 (0.003)	17.4 (3.2)

CST, Corticospinal tract; CC, corpus callosum; CG, cingulum; IFO, inferior fronto-occipital fasciculus; SLF, superior longitudinal fasciculus; UNC, uncinate fasciculus; ILF, inferior longitudinal fasciculus. Tracts are listed in the order of increasing mean T averaged over both sexes for FA exponential fits. SE, standard error. *Significant sex differences.

TABLE 2 | Percentage of vertices with significant exponential (P_{exp}) and linear (P_{lin}) fits and correlation (R_{exp} and R_{lin}), exponential time constant (t), absolute change of MD per year from age 6 to 30 (linear) and age (T) where MD reaches 90% of the plateau minimum (exponential) over those vertices with exponential fits for each tract (left + right combined) of males (M) and females (F) separately.

Tracts	Mean Diffusivity versus Age					
	Sex	P_{exp} (P_{lin}) %	R_{exp} (R_{lin})	t_{exp} (SE)	Absolute decrease per year Exp (Lin) 10^{-3} mm ² /s	T_{exp} (SE) year
ILF	M	61 (19)	0.52 (0.47)	5.9 (1.9)	0.006 (0.004)	19.6 (4.3)*
	F	72 (3)	0.39 (0.27)	2.7 (0.7)	0.014 (0.004)	12.2 (1.6)*
IFO	M	53 (21)	0.57 (0.57)	7.1 (2.4)	0.005 (0.004)	22.4 (5.5)*
	F	64 (4)	0.48 (0.26)	3.2 (0.8)	0.012 (0.004)	13.3 (1.8)*
CC	M	35 (18)	0.55 (0.63)	6.0 (1.9)	0.007 (0.005)	19.8 (4.4)
	F	36 (5)	0.44 (0.37)	4.4 (1.3)	0.008 (0.004)	16.0 (3.1)
SLF	M	44 (41)	0.51 (0.48)	7.6 (3.0)	0.004 (0.004)	23.5 (6.8)*
	F	84 (2)	0.38 (0.20)	3.3 (1.0)	0.009 (0.003)	13.7 (2.4)*
UNC	M	60 (23)	0.58 (0.56)	6.9 (2.2)	0.005 (0.005)	22.1 (5.0)
	F	61 (15)	0.42 (0.28)	4.3 (1.3)	0.008 (0.005)	15.8 (3.0)
CG	M	18 (19)	0.52 (0.48)	6.7 (2.5)	0.006 (0.006)	21.4 (5.6)
	F	25 (1)	0.45 (0.33)	4.7 (1.5)	0.008 (0.004)	16.7 (3.4)
CST	M	42 (22)	0.67 (0.62)	10.3 (3.6)	0.004 (0.004)	29.6 (8.3)*
	F	55 (2)	0.43 (0.31)	4.2 (1.3)	0.007 (0.003)	15.7 (2.9)*

Tracts are listed in the order of increasing mean T averaged over both sexes for MD exponential fits. *Significant sex differences.

relative to the anterior areas. Bilateral tracts exhibited similar distribution patterns with the exception of SLF and ILF where the left side demonstrated either a more widespread pattern or faster rate. Areas of tracts with faster FA rate tended to reach their maximum value at an earlier age relative to other regions (**Figure 4**). Genu of CC and inferior CST in both sexes (before age 20 years for males and 15 years for females) and fronto-parietal part of bilateral SLF, posterior sections of left ILF and IFO in females (before age 15 years) all reach their maximum values earlier compared with other tract regions. Small regions of the right ILF in both sexes and middle sections of bilateral UNC, left SFL, right CG in males show more regions with slower development beyond 20 years to reach the maximum FA.

Most areas with linear increases of FA with age are located in the body of CC, CST, fronto-parietal SLF and UNC (0.002–0.006/year) and are mostly notable in males (**Figure 5**). The distribution of linear increases of FA in smaller tracts, IFO and ILF (0.001–0.004/year), are more focused on middle to frontal areas.

Developmental Rate and Timing of Tract-Specific MD Changes

Numerous tract vertices showed a significant exponential (**Figure 6**) or linear (**Figure 8**) pattern of decrease in MD with differences in the rate (–MD/year). As for FA, the age to reach 90% of the minimum MD from age 6 to 30 years varied across the tracts for the vertices with exponential fits (**Figure 7**). Tract-specific regions with exponential decrease of MD are much more widespread than increased FA regions in most tracts and along tract differences are much more noticeable in females, although many of the same regions as males show exponential reductions of MD. The genu and splenium of CC have a faster decreasing rate of MD (0.004 – 0.008×10^{-3} mm² s^{–1}/year

for male and $>0.008 \times 10^{-3}$ mm² s^{–1}/year for females) relative to the other CC regions. Similar to the FA increasing pattern, inferior CST ($>0.008 \times 10^{-3}$ mm² s^{–1}/year), fronto-parietal section of SLF ($>0.01 \times 10^{-3}$ mm² s^{–1}/year) and posterior sections of ILF ($\sim 0.01 \times 10^{-3}$ mm² s^{–1}/year) and IFO ($\sim 0.01 \times 10^{-3}$ mm² s^{–1}/year) in females also exhibited faster MD decreasing rate relative to other tract areas. In **Figure 7**, most tracts in females reach their minimum MD before age 15 years while many areas of tracts in males displayed a prolonged maturation process after age 20 years and some well into the young adult period such as CST.

Linear decreases of MD are observed mostly in males and the spatial distribution is similar to that observed for linear FA increases in the body of CC, CST, and UNC (**Figure 8**). In addition, linear decreases of MD are greater in the posterior of SLF, right ILF and right IFO relative to other parts of those tracts in males.

Sex Differences for FA and MD Maturation Age

The surface representative tract maps of the age where FA or MD reach their plateau values (only for exponential fits of course) indicate sex differences on a per vertex basis for both FA (**Figure 4**) and MD (**Figure 7**). Sex differences were assessed by a direct vertex comparison of the ages where development is presumed to level off by comparing the overlap of age and standard error of the exponential fits for vertices that had significant exponential fits for both sexes. There were some regions (shown in red) with overlap in age \pm standard error between males and females, mostly for MD (**Figure 9**). Compared with males, females reached their FA plateaus at an earlier age in inferior bilateral CST and superior bilateral SLF. Females reached the MD plateaus earlier in 8 of 13 tracts including splenium

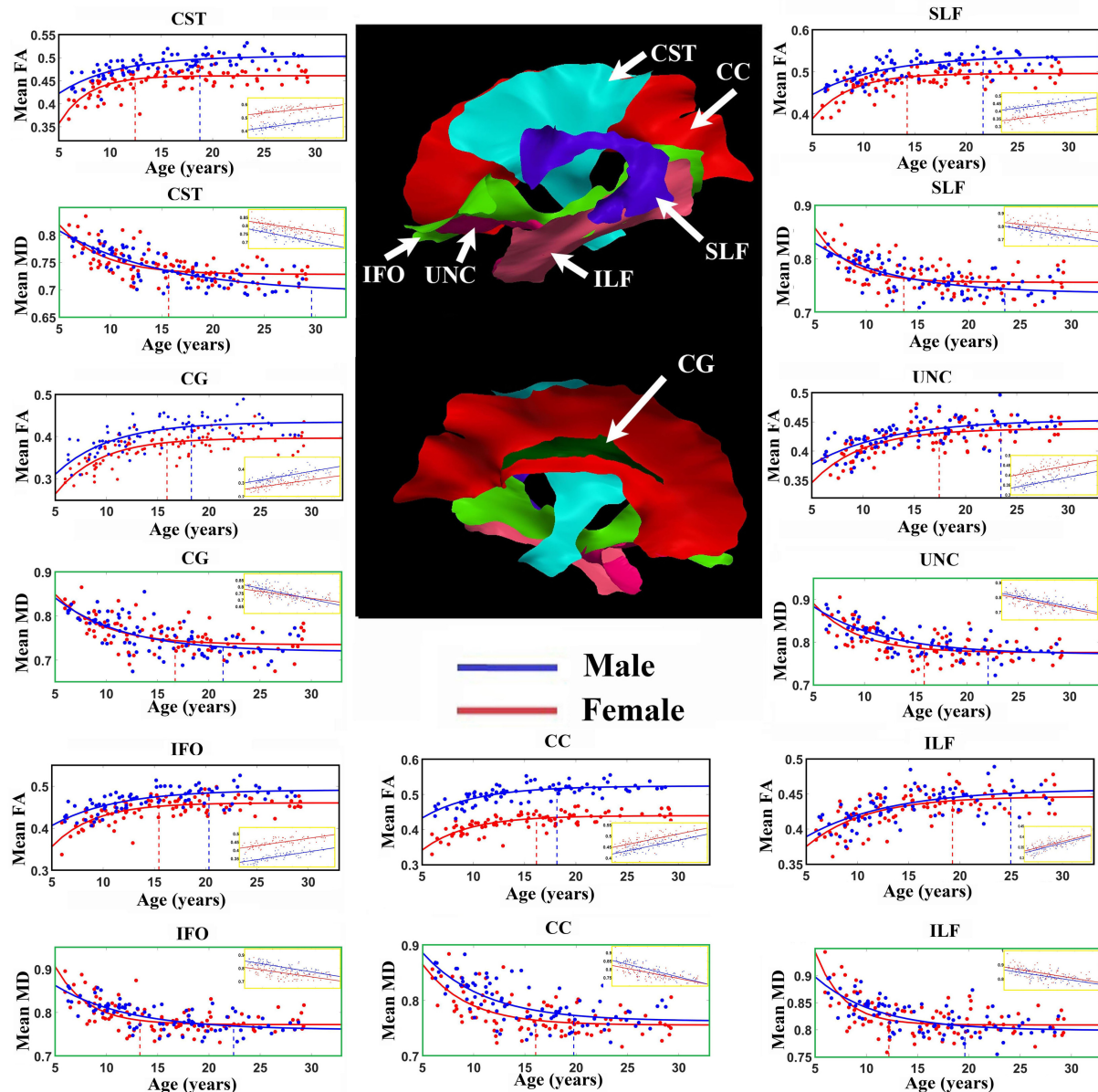


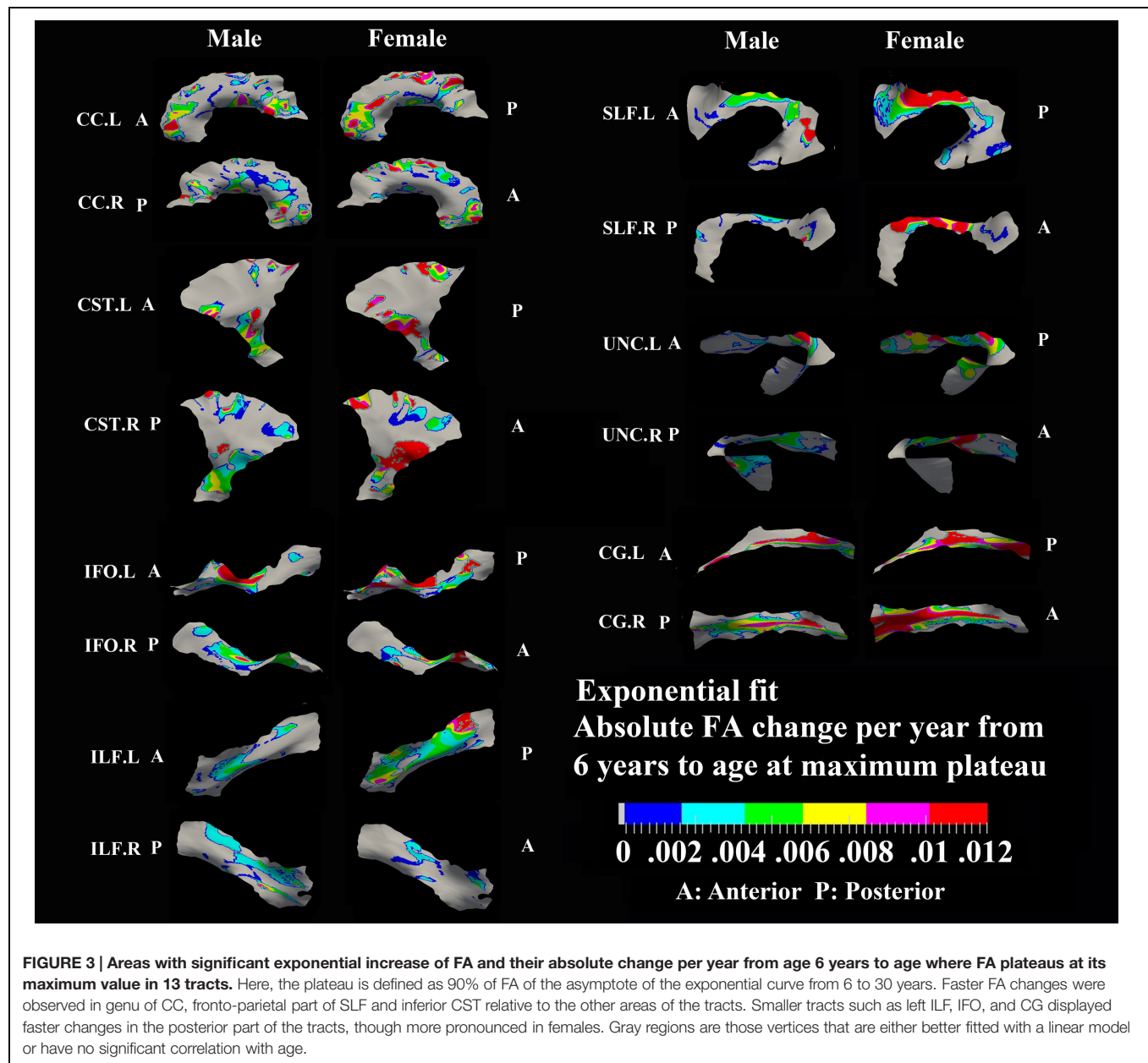
FIGURE 2 | Age-related FA increases and MD (units of $10^{-3} \text{ mm}^2/\text{s}$) decreases averaged over all vertices with either exponential or linear fits (insets) of each tract in males (blue lines) and females (red lines). Middle: Tract surfaces derived from the template are shown, but recall that only a proportion of these vertices contribute to these exponential curves and linear fit (as in **Tables 1** and **2**). Maximum FA and minimum MD plateau of each tract for both female (red) and male (blue) are marked by the vertical dotted lines. Projection and inter-hemispheric tracts such as CST and CC tend to reach the FA plateau earlier than temporal lobe association tracts such as SLF, UNC, and ILF. Generally, males have higher FA over the full age span for the exponential whereas it is quite similar for MD. There are differences in the fit parameters presented in **Tables 1** and **2**. CST, Corticospinal tract; CC, corpus callosum; CG, cingulum; IFO, inferior fronto-occipital fasciculus; ILF, inferior longitudinal fasciculus; SLF, superior longitudinal fasciculus; UNC, uncinate fasciculus.

of CC, inferior bilateral CST, anterior bilateral IFO, superior bilateral SLF, and posterior right ILF.

DISCUSSION

Although several previous studies have used “along the tract” methodologies to investigate changes of regional diffusion

parameters with development in infants (Zhu et al., 2011), young children (Johnson et al., 2013) or children/adolescents (Yeatman et al., 2012), no study has used these methods to study the maturation patterns of diffusion parameters along the major fasciculi from childhood (6 years) to adulthood (30 years). This study was an extension of our previous tractography based approach in mapping the tract maturation pattern in development where in our earlier study each tract yielded one



overall mean FA or MD per subject (Lebel et al., 2008). Although informative, the whole tract averaging approaches appear to oversimplify the WM development by assuming that the diffusion parameters of the entire tract change in unison. Surface-model based TSA identified DTI variability as a function of age along the tracts. Given that diffusion parameters change in WM at unique rates with age and typically reach a developmental peak or plateau within our age window (Lebel et al., 2008, 2012), the focus here is on the vertices with exponential changes with age. The main results included: (1) confirmation of general age-related exponential FA increases and MD decreases with development from childhood to young adulthood, (2) identification of unique patterns of changes of FA or MD along major tracts in both sexes suggesting that the entire tract, as far as water diffusion

is concerned, does not behave identically as a function of age, (3) demonstration of a posterior-to-anterior temporal pattern of WM maturation, and (4) demonstration of earlier maturation of FA and MD to a plateau in females relative to males in specific tract regions.

Many of the tract vertices, but not all, revealed exponential increases of anisotropy and decreases of MD with age from young childhood to adulthood in both male and female groups. These results on a subset of vertices on the surface-defined tracts (15–50% for FA and 18–84% for MD) are consistent with many studies that showed a similar pattern in typically developing children (Schneider et al., 2004; Ben Bashat et al., 2005; Zhang et al., 2005; Lebel et al., 2008; Tamnes et al., 2010; Cancelliere et al., 2013; Taki et al., 2013a), including our own with overlapping samples

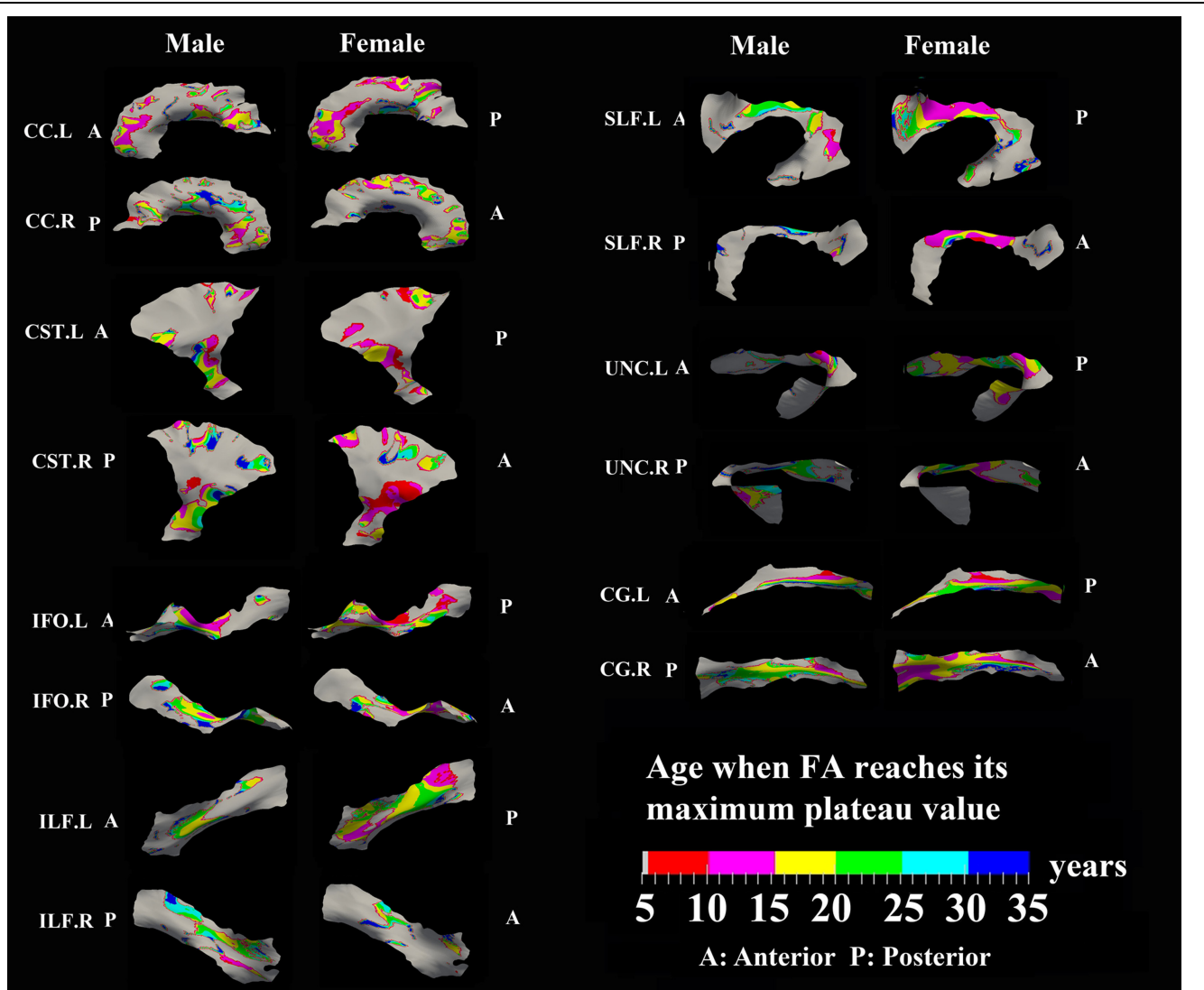
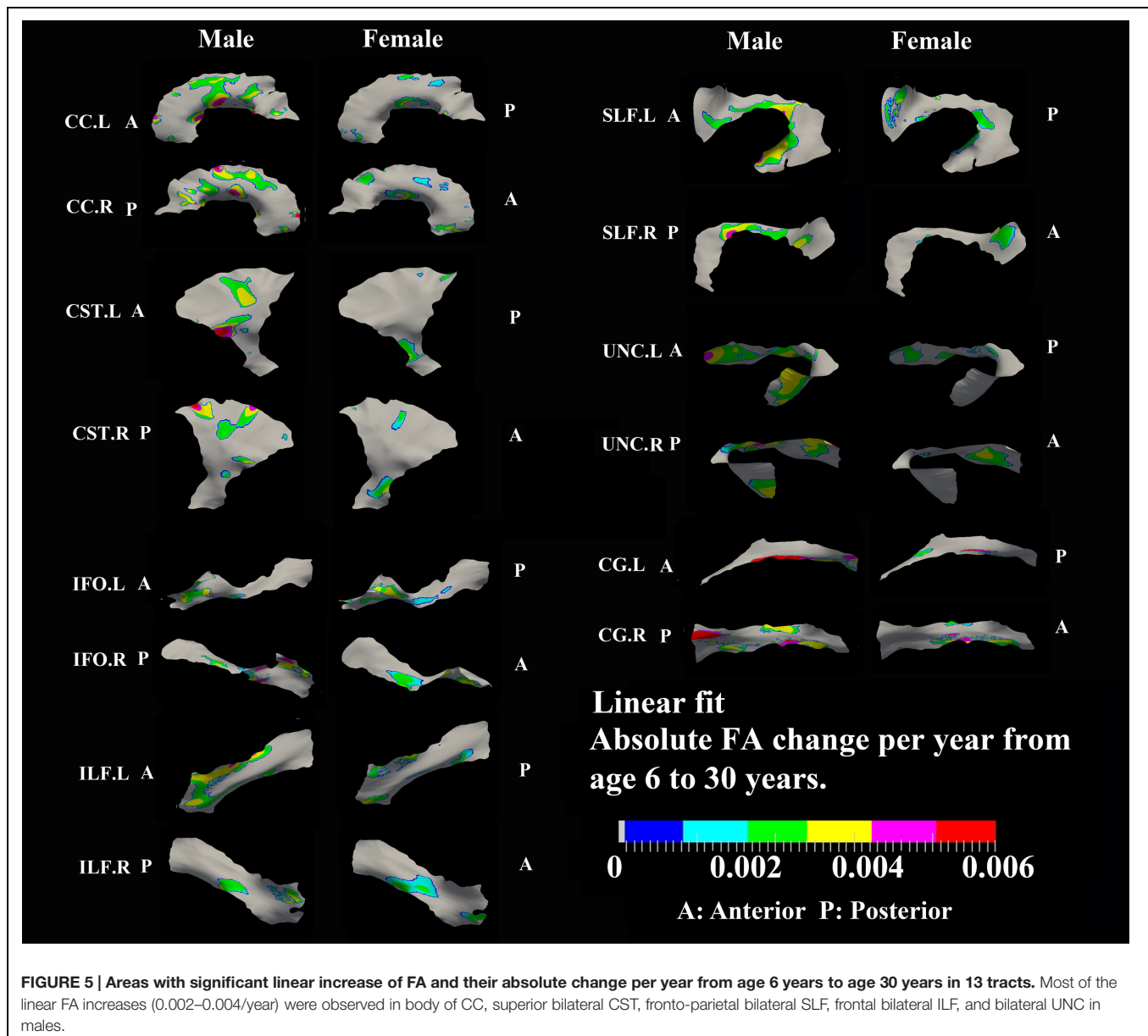


FIGURE 4 | Areas with significant exponential increase of FA and the age needed to reach the maximum plateau value (defined as 90% of maximum) in 13 tracts. Genu of CC, inferior CST, superior portion of SLF, and posterior sections of left ILF and left IFO in females all reach their maximum level before age 15 years. Males have several regions where the maximum level is reached after 20 years, particularly in right CG, right UNC, and left SLF. Gray regions are those vertices that are either better fitted with a linear model or have no significant correlation with age.

analyzed by individual tractography averaged over the entire tract (Lebel et al., 2008). Regions with significant exponential decreasing of MD are much broader in most tracts than those of FA increases with more pronounced differences in females. This observation is also in agreement with several previous studies indicating that decreases in MD appear to be more global in scope (Schmithorst et al., 2002; Bonekamp et al., 2007; Tamnes et al., 2010; Taki et al., 2013a). The within-tract differences of water diffusion parameters along a tract during maturation could reflect unique rates of axonal myelination and packing (Beaulieu, 2002; Song et al., 2002, 2005) that might be due to local differences in vasculature, supporting glial structure, and biochemistry throughout the brain (Ito et al., 2005; Yeh et al., 2009; Vasung et al., 2010). Light microscopic examinations of

the fiber composition in the human CC also revealed complex, heterogeneous structure containing axons of different diameters and densities that vary by region (Aboitiz et al., 1992). This confirms that major WM tracts display intensive maturational changes at earlier ages that slow down and then level off at various ages depending on the tract.

When taking vertices with linear fits with age into account, the proportion of vertices showing changes with age were ~41% on average over all tracts for FA and ~63% for MD, supporting the notion that FA and MD are complementary measures. While some additional vertices showed linear changes of FA or MD with age, there was still a sizeable proportion of vertices in each tract that did not show any change (44–71% for FA and 15–74% for MD). One explanation would be that those regions are



nearly or fully developed by the age of 6 years, thus a clear developmental trend cannot be mapped in this study. Another possible interpretation would be the methodological limitations in analyzing those surface vertices including the confounding fact of regional crossing fibers from tractography, insufficient data smoothing, inadequate spatial correspondence across subjects, strict fitting models and WM structural variability.

Relative to other portions of the same tracts, there were faster increases of FA in genu/splenium of CC, which provide inter-hemispheric connections between homologous neocortical regions, and inferior CST that serve crucial roles in sensorimotor integration. The findings of CC are consistent with previous studies that demonstrated the genu/splenium of the CC was amongst the earlier regions for FA and MD to level off with age during development (Lebel et al., 2008; Cancelliere et al., 2013).

Similarly, inferior (internal capsule) and frontal (corona radiata) part of CST were also shown to display faster developing rate in a whole-brain DTI study of healthy individuals between ages 8 and 28 years (Asato et al., 2010). Furthermore, the fronto-parietal part of SLF also showed a faster developmental rate, suggesting an intensive maturation process of that section of tract from childhood to adolescence. A recent study demonstrated an early development (increased FA) of arcuate fasciculus, from 5 to 8 years that was positively correlated to the receptive/expressive language scores (Broce et al., 2015). The fronto-parietal portion of SLF is also known to be involved in early development of working memory (Nagy et al., 2004; Vestergaard et al., 2011). Association tracts such as CG, ILF, IFO, and UNC either displayed faster exponential changes in the posterior part of the tracts or did not show any age effects (gray areas) that indicate early maturity

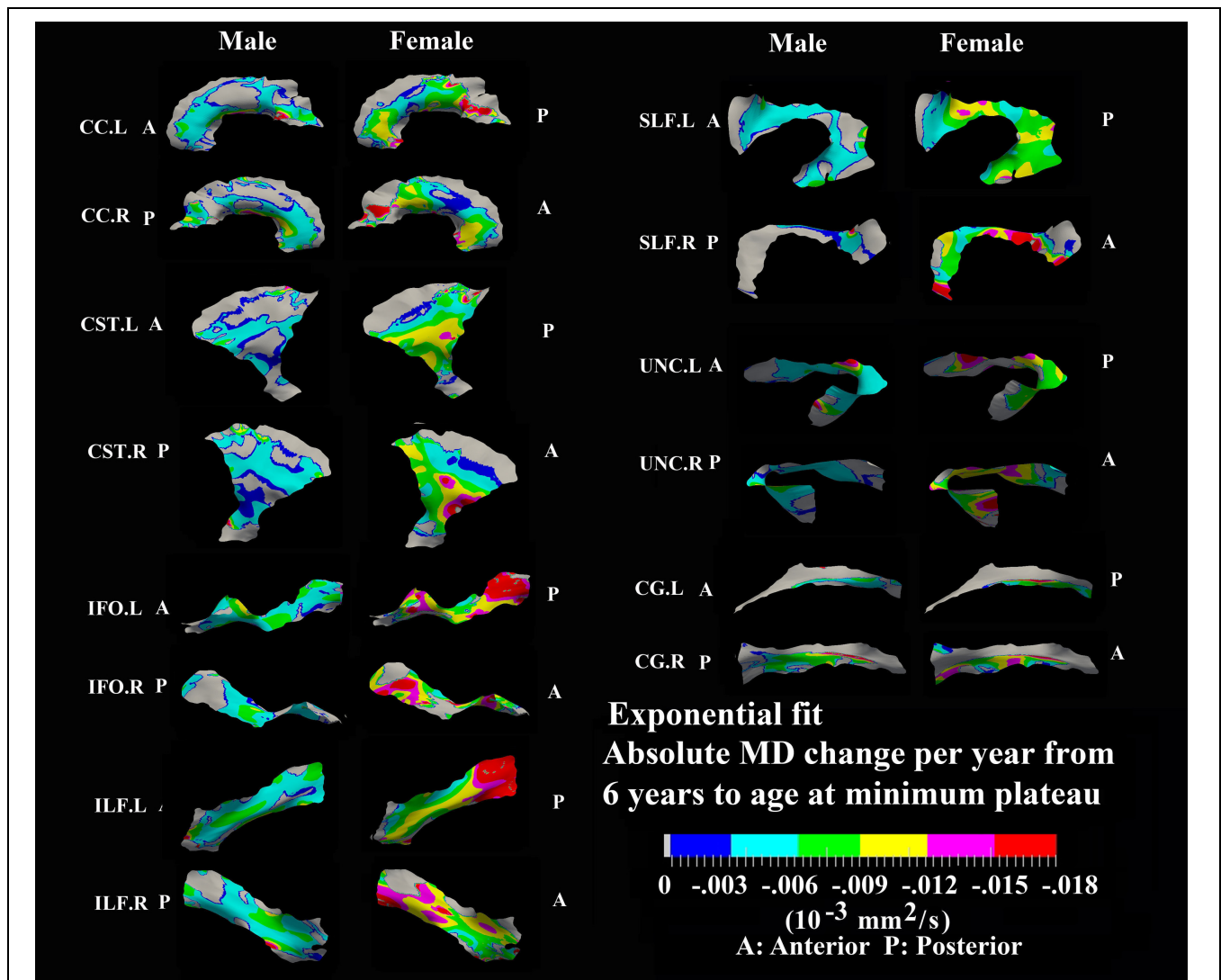


FIGURE 6 | Areas with significant exponential decrease of MD and absolute change per year from age 6 years to age where MD plateaus at its minimum value in 13 tracts. Here, the plateau is defined as 90% of MD of the asymptote of the exponential curve from 6 to 30 years. The genu and splenium of CC have a faster decreasing rate relative to the other CC regions in both sexes. The inferior CST, fronto-parietal section of SLF, superior portion of UNC, and posterior sections of ILF and IFO in females also exhibited faster MD decreasing rate relative to other tract areas. Gray regions are those vertices that are either better fitted with a linear model or have no significant correlation with age.

or a prolonged increase in the anterior part of the tracts. These results are in agreement with previous DTI reports of changes in diffusion parameters that are generally concentrated in more posterior regions during early stages of development (Asato et al., 2010; Colby et al., 2011).

Areas of tracts with faster FA rate tended to reach their maximum value at an earlier age relative to other regions. Genu/splenium of CC, inferior CST and fronto-parietal part of bilateral SLF all reach their peak before age 20 years (males < 20 years/females < 15 years). More importantly, posterior areas of ILF, IFO, CG, and UNC in both sexes reach their maximum values earlier (<15 years) or did not show any peak ages (<5 years) while anterior regions demonstrated longer maximum developmental timing for FA. These results

are consistent with a prolonged frontal maturation pattern in the development of WM suggested in many previous neurodevelopmental studies (Flechsigs, 1901; Yakovlev and Lecours, 1967; Giedd et al., 1996; Paus et al., 2001; Deoni et al., 2012; Dean et al., 2015). Recent post-mortem studies of human brain have shown that the time course of synaptogenesis is earlier in the visual and auditory cortex than in the prefrontal cortex (Huttenlocher, 1979; Huttenlocher et al., 1982; Huttenlocher and Dabholkar, 1997). Additionally, synapse elimination starts earlier in the visual cortex than in the auditory cortex, followed by the prefrontal cortex (Huttenlocher and Dabholkar, 1997). These results suggest that brain maturation starts in the occipital lobe followed by the temporal lobe and then the frontal lobe. Recent DTI development studies in both primate and human also

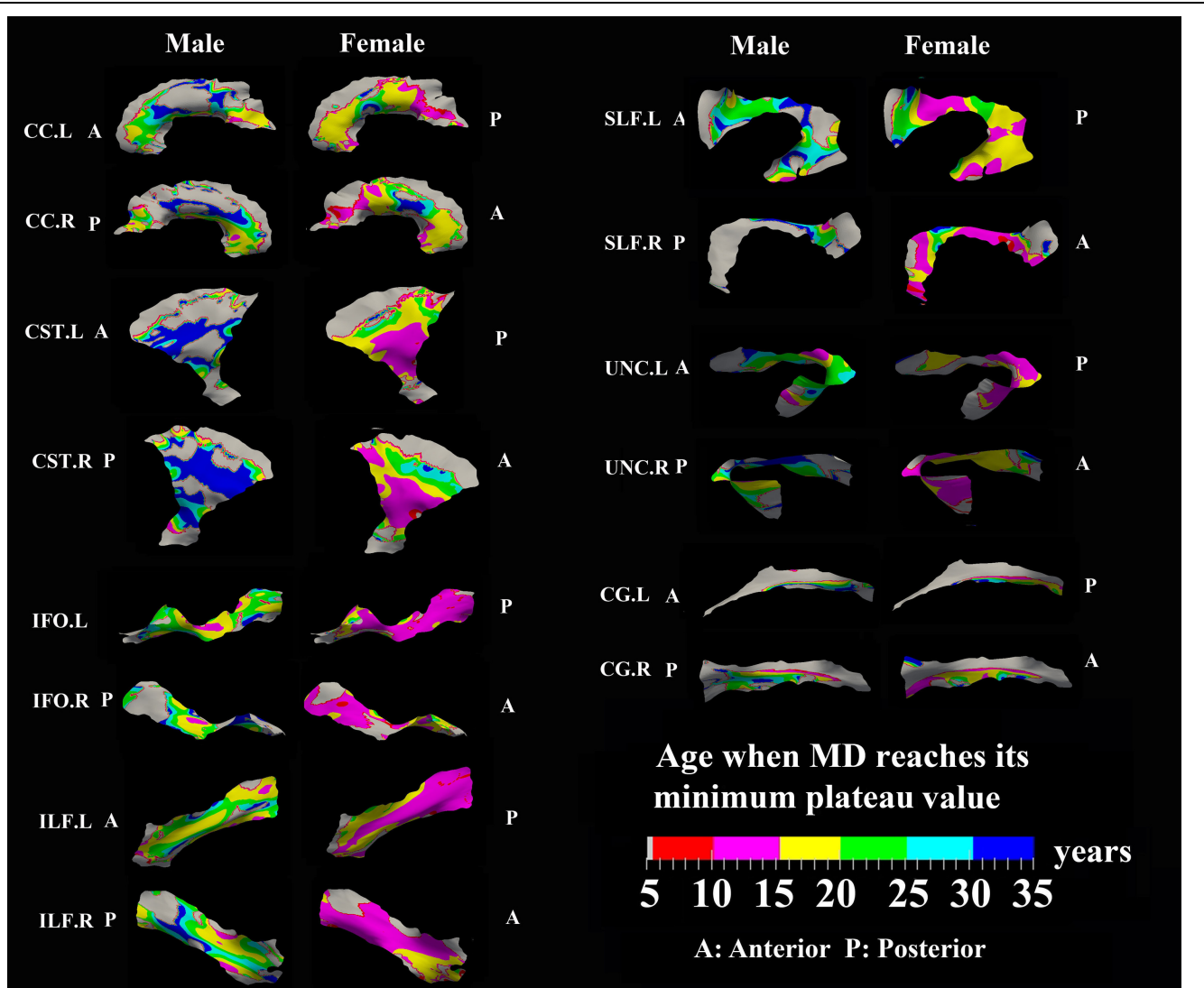
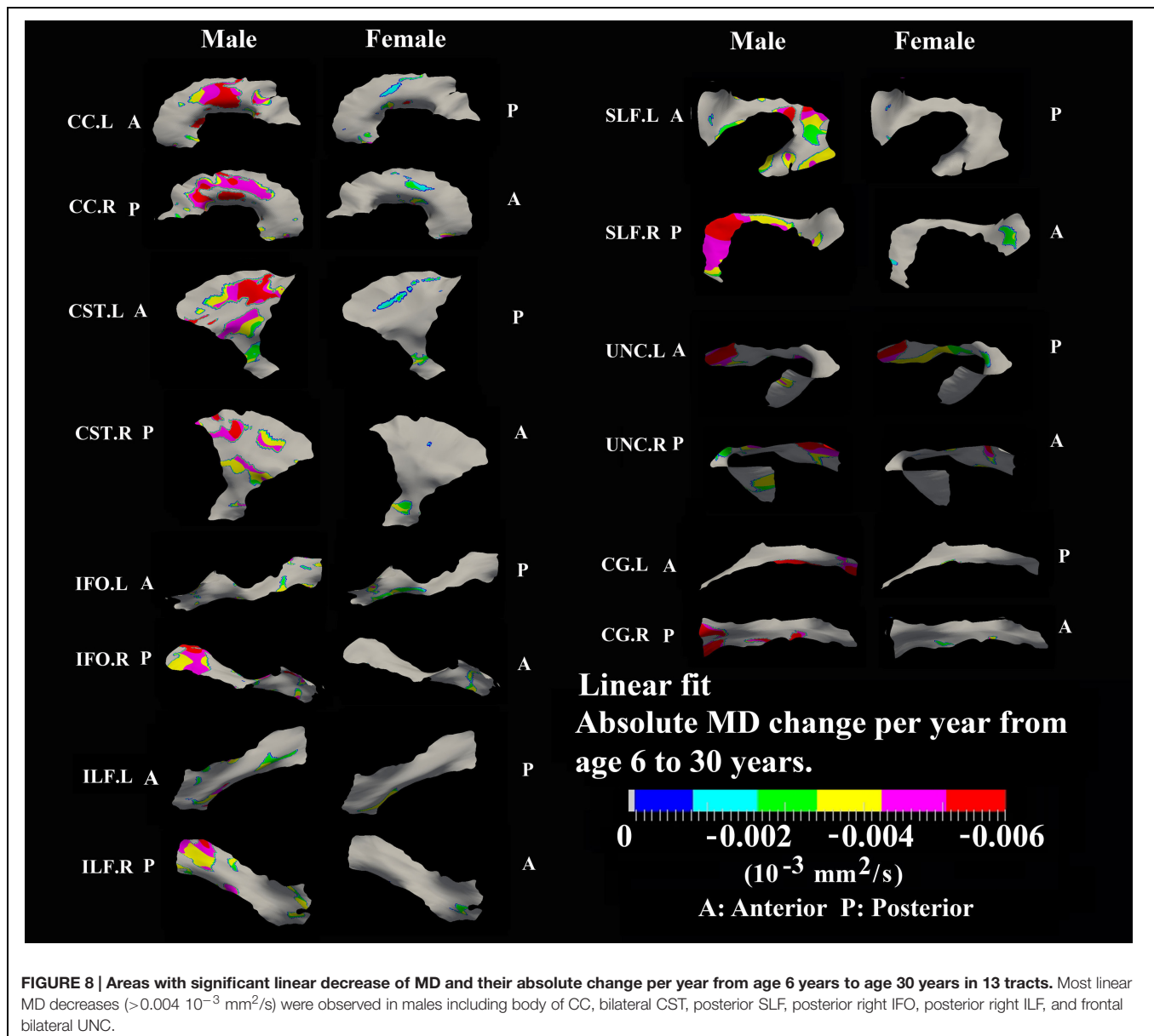


FIGURE 7 | Areas with significant exponential decrease of MD and the age needed to reach the minimum plateau value in 13 tracts. Most tracts in females reach their minimum MD before age 15 years while males reach their minimum values after this age. Gray regions are those vertices that are either better fitted with a linear model or have no significant correlation with age.

demonstrated a similar posterior to anterior pattern suggesting prolonged myelination in frontal regions (Colby et al., 2011; Shi et al., 2013) that is consistent with the protracted trajectory of cognitive development in executive functioning domains, which similarly continues through adolescence and is known to involve processing in the frontal lobe (Luna et al., 2004, 2010). Thus, our results further demonstrate this pattern of late maturation of tracts in the frontal and temporal lobes with a tract-specific approach.

Tract-specific regions with exponential decrease of MD have delayed maturation compared with increased FA regions for most tracts (compare **Figures 3** and **4** for FA versus **Figures 6** and **7** for MD). Differences in timing of WM development has also been observed even when averaging over entire tracts in this same cohort previously (Lebel et al., 2008), and this MD

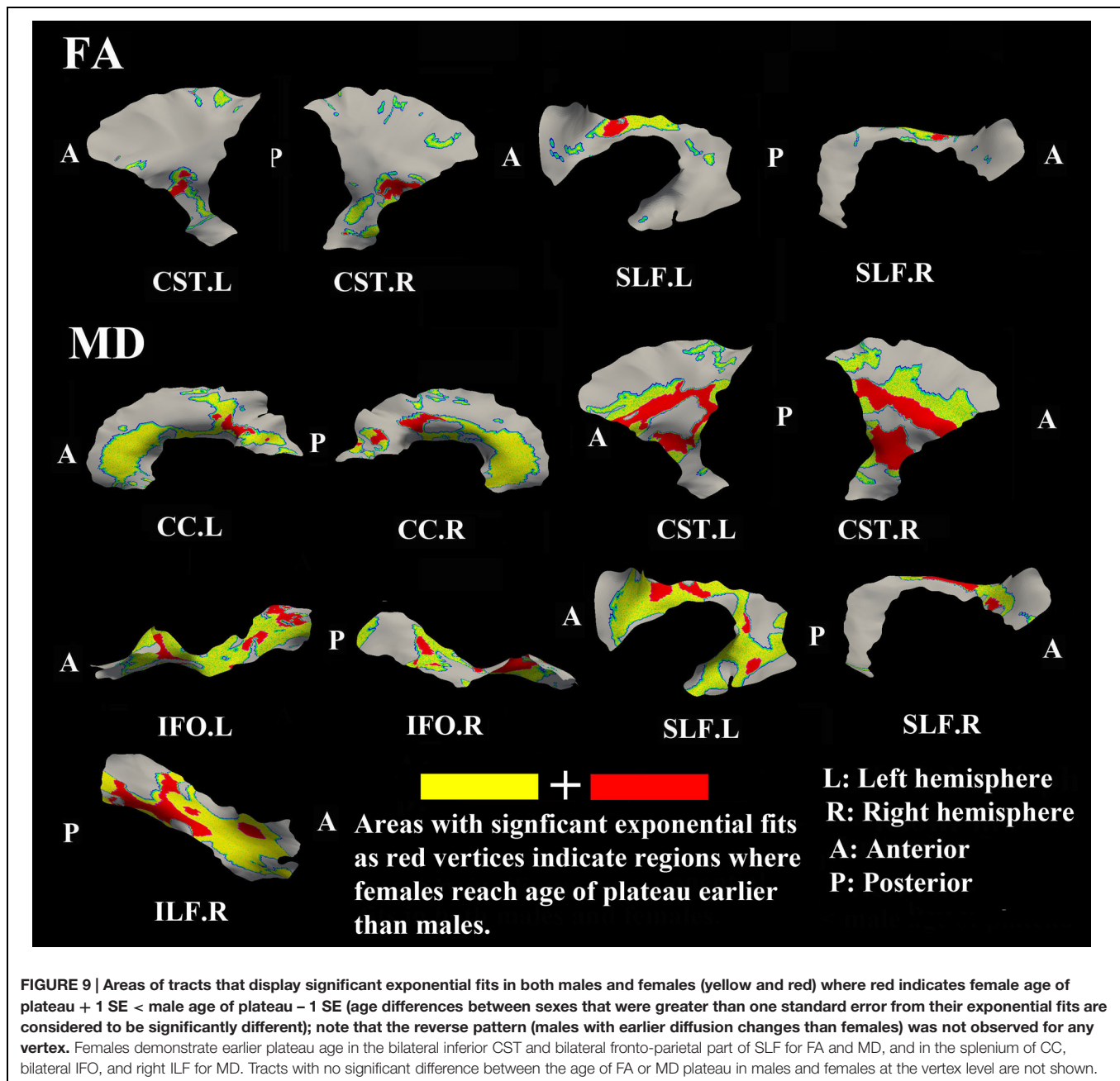
delay persists into aging mostly for association tracts (Lebel et al., 2012). Another aging study using TBSS also demonstrated the timing difference of maximum development among several global diffusion measurements (FA, MD, RD) where MD also displayed a delayed maturation compared to other parameters (Westlye et al., 2010). The discrepancies between FA and MD change trajectories may reflect different FA and MD sensitivities to underlying physiologic processes or possibly less variability in the measure of MD with conventional DTI. The prevalent notion is that increases in FA are associated with organization of the tracts and their myelination and denser axon packing, whereas MD may be more sensitive to decreases of total brain water content and volume of extracellular space (Morris et al., 1999; Beaulieu, 2002; Mukherjee et al., 2002; Hermoye et al., 2006; Dubois et al., 2008; Saksena et al., 2008; Giorgio et al.,



2010). A review of many genetic dysmyelination studies in animal models has also suggested that reductions of MD may be sensitive (more so than FA) to changes in myelination [see Table 8.2 in Beaulieu (2014)], which would fit nicely with our observations of MD reductions along large portions of the tracts. However, the lack of specificity of DTI metrics to microstructure is well known and the exact interpretation of our data on diffusion changes at specific tract regions remains elusive.

Perhaps to be expected, it was shown that males have delayed maturation timing of MD decreases, and less so for FA increases, compared with females in some areas along surfaces of several large tracts. In females, the FA and MD mostly plateau before the age of 15 years, but MD has more regions than FA with protracted leveling off in the 15–25 years range. In males, MD shows later leveling off relative to FA in far more regions, mostly

beyond 20 years. The findings are largely in agreement with previous voxel-based studies demonstrated that by adolescence, females have reached a developmental plateau in most diffusion parameters of the majority of tracts (e.g., CST, SLF, ILF) whereas males had a more protracted course with tracts continuing to develop into adulthood (Asato et al., 2010; Bava et al., 2011; Wang et al., 2012; Taki et al., 2013b; Simmonds et al., 2014). Sexual dimorphism in the development of WM might be attributed to different mechanisms of WM growth in males and females, specifically, an increase in axonal caliber in males and a growth in myelin content in females (Perrin et al., 2009). Increasing testosterone levels may also influence axonal caliber in males, suggesting a role for sex hormones in WM maturation (Perrin et al., 2008). It is important to point out that in our previous paper in the same cohort using mean FA and MD values over



the entire tracts, significant sex differences in exponential fits were not observed (Lebel et al., 2008) suggesting an advantage for examining focal regions of tracts such as the surface-based model approach described here.

One limitation of the study is the relatively small subject number of 178 subjects. Although, there are much larger public DTI datasets available online, most of them involve multi-site scanning which raises other issues related to systematic differences of diffusion parameters. Nonetheless, a similar analysis of such data sets would be helpful for replicating our single-site findings. This study can also be compared directly to our previous tractography-based whole tract analysis in the

same cohort (Lebel et al., 2008). Another caveat of the study is that we only focused on FA and MD analysis to be consistent with our previous study. However, future investigation of axial (AD) and radial diffusivity (RD) could provide more insightful information regarding brain WM development. Compared to the common spline-based along-tract strategies that assume cross-sectional symmetry along the tracts, our automated surface-model approach captures variability along more dimensions within a tract (Yushkevich et al., 2008; Zhang et al., 2010). However, a few methodological issues and limitations with this approach need to be addressed. First, DTI images with six gradient directions and deterministic tractography were

used for atlas tractography that may limit the accuracy and extent of our WM tract surface construction. Although, one study found minimum differences while comparing diffusion parameters measured using six or more diffusion-encoding gradient directions with deterministic tractography (Lebel et al., 2012), in future studies, higher angular resolution diffusion images and more sophisticated tractography approaches could help overcome these limitations. However, while this would enable more accurate tracking of fuller tracts through fiber crossing regions, the effects on the diffusion tensor parameters of FA and MD would not be corrected using more directions. Second, the framework is best suited for sheet-like tracts (e.g., CC), while tube-based tracts (e.g., CG) might result in inaccurate tract surfaces due to difficulty in defining the medial surface of a tube. However, the framework can be extended to include tube-based geometrical models as developed by others (Jones et al., 2005b; Colby et al., 2012) in the future. Third, our statistical method requires the vertex-based DTI values on tract surfaces to be smoothed by a surface-based diffusion smoothing kernel (8 mm). However, surface areas/vertex densities vary among all tracts, thus, making it difficult to choose an optimal kernel size for each surface. Fourth, the number of the vertices for each tract varies depends on the size and shape of the tract surface, and is quite large that might cause oversampling of the surface with respect to the true spatial biological variation in these metrics. In future study, a vertices reduction/optimization step can be applied to overcome this issue. Fifth, we applied an atlas based fiber tract surface analysis for analyzing DTI images of participants with very different ages. The vertex-based results will depend on the accuracy of the registration of each participant with the created DTI atlas, although the use of a deformable DTI registration algorithm (DTI-TK) helps minimize errors relative to other approaches. Also by selecting the tensor with maximal FA along the spokes similar to the TBSS approach, it can lead to increased sensitivity, albeit at the cost of potentially missing significant differences in areas of adjoining fasciculi (Yushkevich et al., 2008). Lastly, although informative,

cross-sectional studies are limited because they cannot provide information about change within individuals. However, future longitudinal tract specific study of brain development using this surface-model approach can be performed to demonstrate within-subject maturation along major tracts from childhood to adulthood.

CONCLUSION

In this study, diffusion anisotropy increased and MD decreased with age in distinct regions of WM tracts with greater changes in childhood that level off into adolescence and even early adulthood depending on the tract. TSA along the major tract surfaces uncovered unique patterns of localized rate and plateau timing of FA and MD changes with age, suggesting differences in developmental maturation. Notably, many tract regions showed an earlier leveling off for FA and MD in females than in males, highlighting sex differences in WM development not appreciated by prior “whole-tract” analyses. The proposed methodology that focuses on specific tracts can provide regional diffusion measures along tracts that will provide insight on brain development and disorders.

AUTHOR CONTRIBUTIONS

ZC and CB designed/analyzed the data and wrote the manuscript; HZ and PY helped designing data processing procedures; ML helped analyzing the data.

ACKNOWLEDGMENTS

This work was supported by Canadian Institutes of Health Research, Alberta Innovates Health Solutions (salary award to co-author CB), and National Institutes of Health grants (R01 EB014346 and R01 EB017255; PY).

REFERENCES

- Aboitiz, F., Scheibel, A. B., Fisher, R. S., and Zaidel, E. (1992). Fiber composition of the human corpus callosum. *Brain Res.* 598, 143–153. doi: 10.1016/0006-8993(92)90179-D
- Akaike, H. (1974). New Look at Statistical-Model Identification. *IEEE Trans. Autom. Control* 19, 716–723. doi: 10.1109/TAC.1974.1100705
- Arsigny, V., Commowick, O., Pennec, X., and Ayache, N. (2006). A log-euclidean framework for statistics on diffeomorphisms. *Med. Image Comput. Comput. Assist. Interv.* 9, 924–931.
- Asato, M. R., Terwilliger, R., Woo, J., and Luna, B. (2010). White matter development in adolescence: a DTI study. *Cereb. Cortex* 20, 2122–2131. doi: 10.1093/cercor/bhp282
- Ashtari, M., Cervellione, K. L., Hasan, K. M., Wu, J., McIlree, C., Kester, H., et al. (2007). White matter development during late adolescence in healthy males: a cross-sectional diffusion tensor imaging study. *Neuroimage* 35, 501–510. doi: 10.1016/j.neuroimage.2006.10.047
- Bach, M., Laun, F. B., Leemans, A., Tax, C. M., Biessels, G. J., Stieltjes, B., et al. (2014). Methodological considerations on tract-based spatial statistics (TBSS). *Neuroimage* 100, 358–369. doi: 10.1016/j.neuroimage.2014.06.021
- Barnea-Goraly, N., Menon, V., Eckert, M., Tamm, L., Bammner, R., Karchemskiy, A., et al. (2005). White matter development during childhood and adolescence: a cross-sectional diffusion tensor imaging study. *Cereb. Cortex* 15, 1848–1854. doi: 10.1093/cercor/bhi062
- Basser, P. J., Mattiello, J., and LeBihan, D. (1994). MR diffusion tensor spectroscopy and imaging. *Biophys. J.* 66, 259–267. doi: 10.1016/S0006-3495(94)80775-1
- Bava, S., Boucquey, V., Goldenberg, D., Thayer, R. E., Ward, M., Jacobus, J., et al. (2011). Sex differences in adolescent white matter architecture. *Brain Res.* 1375, 41–48. doi: 10.1016/j.brainres.2010.12.051
- Beaulieu, C. (2002). The basis of anisotropic water diffusion in the nervous system - a technical review. *NMR Biomed.* 15, 435–455. doi: 10.1002/nbm.782
- Beaulieu, C. (2014). “The biological basis of diffusion anisotropy,” in *Diffusion MRI: From Quantitative Measurement to In-Vivo Neuroanatomy*, eds H. Johansen-Berg and T. E. J. Behrens (London: Academic Press), 166.
- Ben Bashat, D., Ben Sira, L., Graif, M., Pianka, P., Hendler, T., Cohen, Y., et al. (2005). Normal white matter development from infancy to adulthood: comparing diffusion tensor and high b value diffusion weighted MR images. *J. Magn. Reson. Imaging* 21, 503–511. doi: 10.1002/jmri.20281

- Bonekamp, D., Nagae, L. M., Degaonkar, M., Matson, M., Abdalla, W. M., Barker, P. B., et al. (2007). Diffusion tensor imaging in children and adolescents: reproducibility, hemispheric, and age-related differences. *Neuroimage* 34, 733–742. doi: 10.1016/j.neuroimage.2006.09.020
- Broce, I., Bernal, B., Altman, N., Tremblay, P., and Dick, A. S. (2015). Fiber tracking of the frontal aslant tract and subcomponents of the arcuate fasciculus in 5-8-year-olds: relation to speech and language function. *Brain Lang.* 149, 66–76. doi: 10.1016/j.bandl.2015.06.006
- Cancelliere, A., Mangano, F. T., Air, E. L., Jones, B. V., Altaye, M., Rajagopal, A., et al. (2013). DTI values in key white matter tracts from infancy through adolescence. *AJNR Am. J. Neuroradiol.* 34, 1443–1449. doi: 10.3174/ajnr.A3350
- Chung, M. K., Robbins, S. M., Dalton, K. M., Davidson, R. J., Alexander, A. L., and Evans, A. C. (2005). Cortical thickness analysis in autism with heat kernel smoothing. *Neuroimage* 25, 1256–1265. doi: 10.1016/j.neuroimage.2004.12.052
- Colby, J. B., Soderberg, L., Lebel, C., Dinov, I. D., Thompson, P. M., and Sowell, E. R. (2012). Along-tract statistics allow for enhanced tractography analysis. *Neuroimage* 59, 3227–3242. doi: 10.1016/j.neuroimage.2011.11.004
- Colby, J. B., Van Horn, J. D., and Sowell, E. R. (2011). Quantitative in vivo evidence for broad regional gradients in the timing of white matter maturation during adolescence. *Neuroimage* 54, 25–31. doi: 10.1016/j.neuroimage.2010.08.014
- Concha, L., Kim, H., Bernasconi, A., Bernhardt, B. C., and Bernasconi, N. (2012). Spatial patterns of water diffusion along white matter tracts in temporal lobe epilepsy. *Neurology* 79, 455–462. doi: 10.1212/WNL.0b013e31826170b6
- Corouge, I., Fletcher, P. T., Joshi, S., Gouttard, S., and Gerig, G. (2006). Fiber tract-oriented statistics for quantitative diffusion tensor MRI analysis. *Med. Image Anal.* 10, 786–798. doi: 10.1016/j.media.2006.07.003
- Dean, D. C. III, O'Muircheartaigh, J., Dirks, H., Waskiewicz, N., Walker, L., Doernberg, E., et al. (2015). Characterizing longitudinal white matter development during early childhood. *Brain Struct. Funct.* 220, 1921–1933. doi: 10.1007/s00429-014-0763-3
- Deoni, S. C., Dean, D. C. III, O'Muircheartaigh, J., Dirks, H., and Jerskey, B. A. (2012). Investigating white matter development in infancy and early childhood using myelin water fraction and relaxation time mapping. *Neuroimage* 63, 1038–1053. doi: 10.1016/j.neuroimage.2012.07.037
- Dubois, J., Dehaene-Lambertz, G., Perrin, M., Mangin, J. F., Cointepas, Y., Duchesnay, E., et al. (2008). Asynchrony of the early maturation of white matter bundles in healthy infants: quantitative landmarks revealed noninvasively by diffusion tensor imaging. *Hum. Brain Mapp.* 29, 14–27. doi: 10.1002/hbm.20363
- Eluvathingal, T. J., Hasan, K. M., Kramer, L., Fletcher, J. M., and Ewing-Cobbs, L. (2007). Quantitative diffusion tensor tractography of association and projection fibers in normally developing children and adolescents. *Cereb. Cortex* 17, 2760–2768. doi: 10.1093/cercor/bhm003
- Flechsig, P. (1901). Developmental (myelogenetic) localisation of the cerebral cortex in the human subject. *Lancet* 158, 1027–1030. doi: 10.1016/S0140-6736(01)01429-5
- Giedd, J. N., Blumenthal, J., Jeffries, N. O., Castellanos, F. X., Liu, H., Zijdenbos, A., et al. (1999). Brain development during childhood and adolescence: a longitudinal MRI study. *Nat. Neurosci.* 2, 861–863. doi: 10.1038/13158
- Giedd, J. N., Snell, J. W., Lange, N., Rajapakse, J. C., Casey, B. J., Kozuch, P. L., et al. (1996). Quantitative magnetic resonance imaging of human brain development: ages 4–18. *Cereb. Cortex* 6, 551–560. doi: 10.1093/cercor/6.4.551
- Giorgio, A., Watkins, K. E., Chadwick, M., James, S., Winmill, L., Douaud, G., et al. (2010). Longitudinal changes in grey and white matter during adolescence. *Neuroimage* 49, 94–103. doi: 10.1016/j.neuroimage.2009.08.003
- Gogtay, N., Giedd, J. N., Lusk, L., Hayashi, K. M., Greenstein, D., Vaituzis, A. C., et al. (2004). Dynamic mapping of human cortical development during childhood through early adulthood. *Proc. Natl. Acad. Sci. U.S.A.* 101, 8174–8179. doi: 10.1073/pnas.0402680101
- Gong, G., Jiang, T., Zhu, C., Zang, Y., Wang, F., Xie, S., et al. (2005). Asymmetry analysis of cingulum based on scale-invariant parameterization by diffusion tensor imaging. *Hum. Brain Mapp.* 24, 92–98. doi: 10.1002/hbm.20072
- Good, C. D., Johnsrude, I. S., Ashburner, J., Henson, R. N., Friston, K. J., and Frackowiak, R. S. (2001). A voxel-based morphometric study of ageing in 465 normal adult human brains. *Neuroimage* 14, 21–36. doi: 10.1006/nimg.2001.0786
- Goodlett, C. B., Fletcher, P. T., Gilmore, J. H., and Gerig, G. (2009). Group analysis of DTI fiber tract statistics with application to neurodevelopment. *Neuroimage* 45, S133–S142. doi: 10.1016/j.neuroimage.2008.10.060
- Han, B. S., Kim, S. H., Kim, O. L., Cho, S. H., Kim, Y. H., and Jang, S. H. (2007). Recovery of corticospinal tract with diffuse axonal injury: a diffusion tensor image study. *NeuroRehabilitation* 22, 151–155.
- Hermoye, L., Saint-Martin, C., Cosnard, G., Lee, S. K., Kim, J., Nassogne, M. C., et al. (2006). Pediatric diffusion tensor imaging: normal database and observation of the white matter maturation in early childhood. *Neuroimage* 29, 493–504. doi: 10.1016/j.neuroimage.2005.08.017
- Huttenlocher, P. R. (1979). Synaptic density in human frontal cortex - developmental changes and effects of aging. *Brain Res.* 163, 195–205. doi: 10.1016/0006-8993(79)90349-4
- Huttenlocher, P. R., and Dabholkar, A. S. (1997). Regional differences in synaptogenesis in human cerebral cortex. *J. Comp. Neurol.* 387, 167–178. doi: 10.1002/(SICI)1096-9861(19971020)387:2<167::AID-CNE1>3.0.CO;2-Z
- Huttenlocher, P. R., de Courten, C., Garey, L. J., and Van der Loos, H. (1982). Synaptogenesis in human visual cortex—evidence for synapse elimination during normal development. *Neurosci. Lett.* 33, 247–252. doi: 10.1016/0304-3940(82)90379-2
- Ito, H., Kanno, I., and Fukuda, H. (2005). Human cerebral circulation: positron emission tomography studies. *Ann. Nucl. Med.* 19, 65–74. doi: 10.1007/BF03027383
- Jiang, H., van Zijl, P. C., Kim, J., Pearlson, G. D., and Mori, S. (2006). DtiStudio: resource program for diffusion tensor computation and fiber bundle tracking. *Comput. Methods Programs* 81, 106–116. doi: 10.1016/j.cmpb.2005.08.004
- Johnson, R. T., Yeatman, J. D., Wandell, B. A., Buonocore, M. H., Amaral, D. G., and Nordahl, C. W. (2013). Diffusion properties of major white matter tracts in young, typically developing children. *Neuroimage* 88C, 143–154. doi: 10.1016/j.neuroimage.2013.11.025
- Jones, D. K., Symms, M. R., Cercignani, M., and Howard, R. J. (2005a). The effect of filter size on VBM analyses of DT-MRI data. *Neuroimage* 26, 546–554. doi: 10.1016/j.neuroimage.2005.02.013
- Jones, D. K., Travis, A. R., Eden, G., Pierpaoli, C., and Basser, P. J. (2005b). PASTA: pointwise assessment of streamline tractography attributes. *Magn. Reson. Med.* 53, 1462–1467. doi: 10.1002/mrm.20484
- Keihaninejad, S., Zhang, H., Ryan, N. S., Malone, I. B., Modat, M., Cardoso, M. J., et al. (2013). An unbiased longitudinal analysis framework for tracking white matter changes using diffusion tensor imaging with application to Alzheimer's disease. *Neuroimage* 72C, 153–163. doi: 10.1016/j.neuroimage.2013.01.044
- Klingberg, T., Vaidya, C. J., Gabrieli, J. D., Moseley, M. E., and Hedeus, M. (1999). Myelination and organization of the frontal white matter in children: a diffusion tensor MRI study. *Neuroreport* 10, 2817–2821. doi: 10.1097/00001756-199909090-00022
- Le Bihan, D. (2003). Looking into the functional architecture of the brain with diffusion MRI. *Nat. Rev. Neurosci.* 4, 469–480. doi: 10.1038/nrn1119
- Lebel, C., Gee, M., Camicioli, R., Wieler, M., Martin, W., and Beaulieu, C. (2012). Diffusion tensor imaging of white matter tract evolution over the lifespan. *Neuroimage* 60, 340–352. doi: 10.1016/j.neuroimage.2011.11.094
- Lebel, C., Walker, L., Leemans, A., Phillips, L., and Beaulieu, C. (2008). Microstructural maturation of the human brain from childhood to adulthood. *Neuroimage* 40, 1044–1055. doi: 10.1016/j.neuroimage.2007.12.053
- Lerch, J. P., Worsley, K., Shaw, W. P., Greenstein, D. K., Lenroot, R. K., Giedd, J., et al. (2006). Mapping anatomical correlations across cerebral cortex (MACACC) using cortical thickness from MRI. *Neuroimage* 31, 993–1003. doi: 10.1016/j.neuroimage.2006.01.042
- Luna, B., Garver, K. E., Urban, T. A., Lazar, N. A., and Sweeney, J. A. (2004). Maturation of cognitive processes from late childhood to adulthood. *Child Dev.* 75, 1357–1372. doi: 10.1111/j.1467-8624.2004.00745.x
- Luna, B., Padmanabhan, A., and O'Hearn, K. (2010). What has fMRI told us about the development of cognitive control through adolescence? *Brain Cogn.* 72, 101–113. doi: 10.1016/j.bandc.2009.08.005
- Maddah, M., Grimson, W. E., Warfield, S. K., and Wells, W. M. (2008). A unified framework for clustering and quantitative analysis of white matter fiber tracts. *Med. Image Anal.* 12, 191–202. doi: 10.1016/j.media.2007.10.003

- Mori, Y., Shiota, T., Jones, M., Wanitkun, S., Irvine, T., Li, X., et al. (1999). Three-dimensional reconstruction of the color Doppler-imaged vena contracta for quantifying aortic regurgitation: studies in a chronic animal model. *Circulation* 99, 1611–1617. doi: 10.1161/01.CIR.99.12.1611
- Morris, M. C., Zimmerman, R. A., Bilaniuk, L. T., Hunter, J. V., and Haselgrove, J. C. (1999). Changes in brain water diffusion during childhood. *Neuroradiology* 41, 929–934. doi: 10.1007/s002340050869
- Mukherjee, P., Miller, J. H., Shimony, J. S., Philip, J. V., Nehra, D., Snyder, A. Z., et al. (2002). Diffusion-tensor MR imaging of gray and white matter development during normal human brain maturation. *AJNR Am. J. Neuroradiol.* 23, 1445–1456.
- Nagy, Z., Westerberg, H., and Klingberg, T. (2004). Maturation of white matter is associated with the development of cognitive functions during childhood. *J. Cogn. Neurosci.* 16, 1227–1233. doi: 10.1162/0898929041920441
- Nir, T. M., Villalon-Reina, J. E., Prasad, G., Jahanshad, N., Joshi, S. H., Toga, A. W., et al. (2015). Diffusion weighted imaging-based maximum density path analysis and classification of Alzheimer's disease. *Neurobiol. Aging* 36(Suppl. 1), S132–S140. doi: 10.1016/j.neurobiolaging.2014.05.037
- O'Donnell, L. J., Westin, C. F., and Golby, A. J. (2009). Tract-based morphometry for white matter group analysis. *Neuroimage* 45, 832–844. doi: 10.1016/j.neuroimage.2008.12.023
- Paus, T., Collins, D. L., Evans, A. C., Leonard, G., Pike, B., and Zijdenbos, A. (2001). Maturation of white matter in the human brain: a review of magnetic resonance studies. *Brain Res. Bull.* 54, 255–266. doi: 10.1016/S0361-9230(00)00434-2
- Paus, T., Zijdenbos, A., Worsley, K., Collins, D. L., Blumenthal, J., Giedd, J. N., et al. (1999). Structural maturation of neural pathways in children and adolescents: in vivo study. *Science* 283, 1908–1911. doi: 10.1126/science.283.5409.1908
- Perrin, J. S., Herve, P. Y., Leonard, G., Perron, M., Pike, G. B., Pitiot, A., et al. (2008). Growth of white matter in the adolescent brain: role of testosterone and androgen receptor. *J. Neurosci.* 28, 9519–9524. doi: 10.1523/JNEUROSCI.1212-08.2008
- Perrin, J. S., Leonard, G., Perron, M., Pike, G. B., Pitiot, A., Richer, L., et al. (2009). Sex differences in the growth of white matter during adolescence. *Neuroimage* 45, 1055–1066. doi: 10.1016/j.neuroimage.2009.01.023
- Prasad, G., Joshi, S. H., Jahanshad, N., Villalon-Reina, J., Aganj, I., Lenglet, C., et al. (2014). Automatic clustering and population analysis of white matter tracts using maximum density paths. *Neuroimage* 97, 284–295. doi: 10.1016/j.neuroimage.2014.04.033
- Saksena, S., Husain, N., Malik, G. K., Trivedi, R., Sarma, M., Rathore, R. S., et al. (2008). Comparative evaluation of the cerebral and cerebellar white matter development in pediatric age group using quantitative diffusion tensor imaging. *Cerebellum* 7, 392–400. doi: 10.1007/s12311-008-0041-0
- Schmithorst, V. J., Wilke, M., Dardzinski, B. J., and Holland, S. K. (2002). Correlation of white matter diffusivity and anisotropy with age during childhood and adolescence: a cross-sectional diffusion-tensor MR imaging study. *Radiology* 222, 212–218. doi: 10.1148/radiol.2221010626
- Schneider, J. F., Il'yasov, K. A., Hennig, J., and Martin, E. (2004). Fast quantitative diffusion-tensor imaging of cerebral white matter from the neonatal period to adolescence. *Neuroradiology* 46, 258–266. doi: 10.1007/s00234-003-1154-2
- Shaw, P., Kabani, N. J., Lerch, J. P., Eckstrand, K., Lenroot, R., Gogtay, N., et al. (2008). Neurodevelopmental trajectories of the human cerebral cortex. *J. Neurosci.* 28, 3586–3594. doi: 10.1523/JNEUROSCI.5309-07.2008
- Shi, Y., Short, S. J., Knickmeyer, R. C., Wang, J., Coe, C. L., Niethammer, M., et al. (2013). Diffusion tensor imaging-based characterization of brain neurodevelopment in primates. *Cereb. Cortex* 23, 36–48. doi: 10.1093/cercor/bhr372
- Simmonds, D. J., Hallquist, M. N., Asato, M., and Luna, B. (2014). Developmental stages and sex differences of white matter and behavioral development through adolescence: a longitudinal diffusion tensor imaging (DTI) study. *Neuroimage* 92, 356–368. doi: 10.1016/j.neuroimage.2013.12.044
- Smith, S. M., Jenkinson, M., Johansen-Berg, H., Rueckert, D., Nichols, T. E., Mackay, C. E., et al. (2006). Tract-based spatial statistics: voxelwise analysis of multi-subject diffusion data. *Neuroimage* 31, 1487–1505. doi: 10.1016/j.neuroimage.2006.02.024
- Snook, L., Paulson, L. A., Roy, D., Phillips, L., and Beaulieu, C. (2005). Diffusion tensor imaging of neurodevelopment in children and young adults. *Neuroimage* 26, 1164–1173. doi: 10.1016/j.neuroimage.2005.03.016
- Song, S. K., Sun, S. W., Ramsbottom, M. J., Chang, C., Russell, J., and Cross, A. H. (2002). Dysmyelination revealed through MRI as increased radial (but unchanged axial) diffusion of water. *Neuroimage* 17, 1429–1436. doi: 10.1006/nimg.2002.1267
- Song, S. K., Yoshino, J., Le, T. Q., Lin, S. J., Sun, S. W., Cross, A. H., et al. (2005). Demyelination increases radial diffusivity in corpus callosum of mouse brain. *Neuroimage* 26, 132–140. doi: 10.1016/j.neuroimage.2005.01.028
- Sowell, E. R., Thompson, P. M., Leonard, C. M., Welcome, S. E., Kan, E., and Toga, A. W. (2004). Longitudinal mapping of cortical thickness and brain growth in normal children. *J. Neurosci.* 24, 8223–8231. doi: 10.1523/JNEUROSCI.1798-04.2004
- Taki, Y., Hashizume, H., Thyreau, B., Sassa, Y., Takeuchi, H., Wu, K., et al. (2013a). Linear and curvilinear correlations of brain gray matter volume and density with age using voxel-based morphometry with the Akaike information criterion in 291 healthy children. *Hum. Brain Mapp.* 34, 1857–1871. doi: 10.1002/hbm.22033
- Taki, Y., Thyreau, B., Hashizume, H., Sassa, Y., Takeuchi, H., Wu, K., et al. (2013b). Linear and curvilinear correlations of brain white matter volume, fractional anisotropy, and mean diffusivity with age using voxel-based and region-of-interest analyses in 246 healthy children. *Hum. Brain Mapp.* 34, 1842–1856. doi: 10.1002/hbm.22027
- Tamnes, C. K., Ostby, Y., Fjell, A. M., Westlye, L. T., Due-Tønnessen, P., and Walhovd, K. B. (2010). Brain maturation in adolescence and young adulthood: regional age-related changes in cortical thickness and white matter volume and microstructure. *Cereb. Cortex* 20, 534–548. doi: 10.1093/cercor/bhp118
- Thompson, P. M., Giedd, J. N., Woods, R. P., MacDonald, D., Evans, A. C., and Toga, A. W. (2000). Growth patterns in the developing brain detected by using continuum mechanical tensor maps. *Nature* 404, 190–193. doi: 10.1038/35004593
- Van Hecke, W., Sijbers, J., De Backer, S., Poot, D., Parizel, P. M., and Leemans, A. (2009). On the construction of a ground truth framework for evaluating voxel-based diffusion tensor MRI analysis methods. *Neuroimage* 46, 692–707. doi: 10.1016/j.neuroimage.2009.02.032
- Vasung, L., Huang, H., Jovanov-Milosevic, N., Pletikos, M., Mori, S., and Kostovic, I. (2010). Development of axonal pathways in the human fetal fronto-limbic brain: histochemical characterization and diffusion tensor imaging. *J. Anat.* 217, 400–417. doi: 10.1111/j.1469-7580.2010.01260.x
- Vestergaard, M., Madsen, K. S., Baare, W. F., Skimminge, A., Ejersbo, L. R., Ramsoy, T. Z., et al. (2011). White matter microstructure in superior longitudinal fasciculus associated with spatial working memory performance in children. *J. Cogn. Neurosci.* 23, 2135–2146. doi: 10.1162/jocn.2010.21592
- Wang, Y., Adamson, C., Yuan, W., Altaye, M., Rajagopal, A., Byars, A. W., et al. (2012). Sex differences in white matter development during adolescence: a DTI study. *Brain Res.* 1478, 1–15. doi: 10.1016/j.brainres.2012.08.038
- Westlye, L. T., Walhovd, K. B., Dale, A. M., Bjørnerud, A., Due-Tønnessen, P., Engvig, A., et al. (2010). Life-span changes of the human brain white matter: diffusion tensor imaging (DTI) and volumetry. *Cereb. Cortex* 20, 2055–2068. doi: 10.1093/cercor/bhp280
- Worsley, K. J., Andermann, M., Koulis, T., MacDonald, D., and Evans, A. C. (1999). Detecting changes in nonisotropic images. *Hum. Brain Mapp.* 8, 98–101. doi: 10.1002/(SICI)1097-0193(1999)8:2/3<98::AID-HBM5>3.3.CO;2-6
- Yakovlev, P. I., and Lecours, A. R. (1967). "The myelogenetic cycles of regional maturation of the brain," in *Regional Development of the Brain in Early Life*, ed. A. Minkowski (Oxford: Blackwell), 3–69.
- Yeatman, J. D., Dougherty, R. F., Myall, N. J., Wandell, B. A., and Feldman, H. M. (2012). Tract profiles of white matter properties: automating fiber-tract quantification. *PLoS ONE* 7:e49790. doi: 10.1371/journal.pone.0049790
- Yeh, T. H., Lee da, Y., Gianino, S. M., and Gutmann, D. H. (2009). Microarray analyses reveal regional astrocyte heterogeneity with implications for neurofibromatosis type 1 (NF1)-regulated glial proliferation. *Glia* 57, 1239–1249. doi: 10.1002/glia.20845
- Yushkevich, P. A., Zhang, H., and Gee, J. C. (2006). Continuous medial representation for anatomical structures. *IEEE Trans. Med. Imaging* 25, 1547–1564. doi: 10.1109/TMI.2006.884634

- Yushkevich, P. A., Zhang, H., Simon, T. J., and Gee, J. C. (2008). Structure-specific statistical mapping of white matter tracts. *Neuroimage* 41, 448–461. doi: 10.1016/j.neuroimage.2008.01.013
- Zhang, H., Avants, B. B., Yushkevich, P. A., Woo, J. H., Wang, S., McCluskey, L. F., et al. (2007). High-dimensional spatial normalization of diffusion tensor images improves the detection of white matter differences: an example study using amyotrophic lateral sclerosis. *IEEE Trans. Med. Imaging* 26, 1585–1597. doi: 10.1109/TMI.2007.906784
- Zhang, H., Awate, S. P., Das, S. R., Woo, J. H., Melhem, E. R., Gee, J. C., et al. (2010). A tract-specific framework for white matter morphometry combining macroscopic and microscopic tract features. *Med. Image Anal.* 14, 666–673. doi: 10.1016/j.media.2010.05.002
- Zhang, H., Yushkevich, P. A., Alexander, D. C., and Gee, J. C. (2006). Deformable registration of diffusion tensor MR images with explicit orientation optimization. *Med. Image Anal.* 10, 764–785. doi: 10.1016/j.media.2006.06.004
- Zhang, L., Thomas, K. M., Davidson, M. C., Casey, B. J., Heier, L. A., and Ulug, A. M. (2005). MR quantitation of volume and diffusion changes in the developing brain. *AJNR Am. J. Neuroradiol.* 26, 45–49.
- Zhu, H., Kong, L., Li, R., Styner, M., Gerig, G., Lin, W., et al. (2011). FADTTS: functional analysis of diffusion tensor tract statistics. *Neuroimage* 56, 1412–1425. doi: 10.1016/j.neuroimage.2011.01.075

Conflict of Interest Statement: The authors declare that the research was conducted in the absence of any commercial or financial relationships that could be construed as a potential conflict of interest.

Copyright © 2016 Chen, Zhang, Yushkevich, Liu and Beaulieu. This is an open-access article distributed under the terms of the Creative Commons Attribution License (CC BY). The use, distribution or reproduction in other forums is permitted, provided the original author(s) or licensor are credited and that the original publication in this journal is cited, in accordance with accepted academic practice. No use, distribution or reproduction is permitted which does not comply with these terms.



White Matter Microstructure is Associated with Auditory and Tactile Processing in Children with and without Sensory Processing Disorder

Yi-Shin Chang¹, Mathilde Gratiot², Julia P. Owen¹, Anne Brandes-Aitken³, Shivani S. Desai³, Susanna S. Hill³, Anne B. Arnett³, Julia Harris³, Elysa J. Marco^{3,4,5*} and Pratik Mukherjee¹

¹ Department of Radiology and Biomedical Imaging, University of California, San Francisco, San Francisco, CA, USA,

² Department of Cognitive Neuroscience, Université Pierre et Marie Curie, Paris, France, ³ Department of Neurology, School of Medicine, University of California, San Francisco, San Francisco, CA, USA, ⁴ Department of Psychiatry, University of California, San Francisco, San Francisco, CA, USA, ⁵ Department of Pediatrics, University of California, San Francisco, San Francisco, CA, USA

OPEN ACCESS

Edited by:

Yun-Qing Li,
The Fourth Military Medical University,
China

Reviewed by:

Richard S. Nowakowski,
Florida State University, USA
Margaret Lang Bauman,
Boston University School of Medicine,
USA

*Correspondence:

Elysa J. Marco
elysa.marco@ucsf.edu

Received: 25 September 2015

Accepted: 31 December 2015

Published: 26 January 2016

Citation:

Chang Y-S, Gratiot M, Owen JP, Brandes-Aitken A, Desai SS, Hill SS, Arnett AB, Harris J, Marco EJ and Mukherjee P (2016) White Matter Microstructure is Associated with Auditory and Tactile Processing in Children with and without Sensory Processing Disorder. *Front. Neuroanat.* 9:169. doi: 10.3389/fnana.2015.00169

Sensory processing disorders (SPDs) affect up to 16% of school-aged children, and contribute to cognitive and behavioral deficits impacting affected individuals and their families. While sensory processing differences are now widely recognized in children with autism, children with sensory-based dysfunction who do not meet autism criteria based on social communication deficits remain virtually unstudied. In a previous pilot diffusion tensor imaging (DTI) study, we demonstrated that boys with SPD have altered white matter microstructure primarily affecting the posterior cerebral tracts, which subserve sensory processing and integration. This disrupted microstructural integrity, measured as reduced white matter fractional anisotropy (FA), correlated with parent report measures of atypical sensory behavior. In this present study, we investigate white matter microstructure as it relates to tactile and auditory function in depth with a larger, mixed-gender cohort of children 8–12 years of age. We continue to find robust alterations of posterior white matter microstructure in children with SPD relative to typically developing children (TDC), along with more spatially distributed alterations. We find strong correlations of FA with both parent report and direct measures of tactile and auditory processing across children, with the direct assessment measures of tactile and auditory processing showing a stronger and more continuous mapping to the underlying white matter integrity than the corresponding parent report measures. Based on these findings of microstructure as a neural correlate of sensory processing ability, diffusion MRI merits further investigation as a tool to find biomarkers for diagnosis, prognosis and treatment response in children with SPD. To our knowledge, this work is the first to demonstrate associations of directly measured tactile and non-linguistic auditory function with white matter microstructural integrity – not just in children with SPD, but also in TDC.

Keywords: diffusion tensor imaging, sensory processing disorders, auditory processing, tactile processing, white matter

INTRODUCTION

Hypo-and/or hyper responsiveness to sensory stimulation is estimated to occur in 5–16% of children within the general population, and 40–80% of children with neurodevelopmental disorders (Ahn et al., 2004). Such sensory dysfunction can hinder a child's ability to accomplish practical, daily activities and age-appropriate learning tasks, thus resulting in long-term impairment of intellectual and social abilities. Sensory processing disorder (SPD) is reported to be highly co-incident with attention deficit hyperactivity disorder (ADHD) and autism spectrum disorders (ASDs). However, it is also clear that children can have sensory processing dysfunction without the degree of attention, language, or social challenges that would meet criteria for ADHD or ASD. This has been referred to in the literature as isolated SPD. The Diagnostic Classification of Mental Health and Developmental Disorders in Infancy and Early Childhood includes a diagnostic label for Regulation Disorders of Sensory Processing (Zero to Three, 2005), but the Diagnostic and Statistical Manual 5 (DSM-V) does not include SPDs as a standalone category. They do now, however, include hyper- or hyporeactivity to sensory input or unusual interest in sensory aspects of the environment in their revised ASD criteria. These sensory processing differences are being increasingly investigated in the field of autism research and recognized as a core and critical clinical feature—however, children with SPD who do not also have social communication deficits that meet ASD criteria can provide insight into the neural underpinnings of sensory processing in particular.

The present literature on SPD primarily utilizes parent/caregiver report measures that describe sensory-related behaviors and physiological measures that provide information about arousal and sensory reactivity. Recently, our group has published two studies using diffusion tensor imaging (DTI) to better define the neural correlates of these sensory processing deficits. Our first study took a whole-brain, data-driven approach to demonstrate decreased fractional anisotropy (FA) and increased mean diffusivity (MD) and radial diffusivity (RD), reflecting reduced microstructural integrity, in the posterior white matter tracts of 16 boys with SPD compared to 24 neurotypically developing boys (Owen et al., 2013). In addition, we found that FA in affected brain regions correlated with atypical auditory, multisensory, and attention-related behaviors as reported by parents on the Sensory Profile. In a subsequent report, we established that children with SPD and those with ASD both demonstrate decreased FA in parietal-occipital tracts whereas only children with ASD show differences in temporal tracts subserving social-emotional processing (Chang et al., 2014). We recently investigated whether direct assessment measures of tactile and auditory processing might also inform our understanding and evaluation of children with atypical sensory related behaviors both with and without an ASD diagnosis. We found that children with both ASD and SPD show impairment in tactile processing (right hand graphesthesia) whereas only the ASD group showed significant impairment in a measure of cortical auditory processing (Demopoulos et al., 2015). However, correlations including all children (controls,

SPD, and ASD) showed a significant association between a direct measure of auditory processing impairment and a parent report measure of real-world communication ability.

As our previous imaging findings were limited to a small cohort of affected boys, we seek to investigate these results in a larger mixed-gender cohort sample. We hypothesize that boys and girls with SPD will show impaired white matter microstructural integrity, with a posterior predominance, relative to typically developing children (TDC). We further hypothesize that this microstructural integrity will correlate with parent report as well as with direct measurements of sensory processing, but that the direct measurements will show stronger correlation with the underlying microstructure.

MATERIALS AND METHODS

Demographic, Sensory, Cognitive and Behavioral Data

Children ages 8–12 years were enrolled under an institutional review board approved protocol. SPD subjects were recruited from the UCSF Sensory Neurodevelopment and Autism Program (SNAP) and from local online parent board listings. TDC were recruited from online parent group listings as well as referrals from affiliated sensory neurodevelopment and autism research groups. Informed consent was obtained from the parents or legal guardians, with the assent of all participants. Exclusion criteria were brain malformation or injury, movement disorder, bipolar disorder, psychotic disorder, hearing impairment, full-scale IQ (FSIQ) score <70 on the Wechsler Intelligence Scale for Children-Fourth Edition (WISC-IV; Wechsler, 2003), or meeting criteria for ASD. Subjects were also excluded for any anomalies or artifacts on MR imaging or DTI using criteria explained below in Section “DTI Analysis.” A total of 40 right-handed children with SPD (32 male, 8 female) and 41 right-handed TDC (28 male, 13 female) met all inclusion and exclusion criteria for the study.

Autism spectrum disorders was initially screened for using the Social Communication Questionnaire (SCQ; Rutter et al., 2003), a parent report screening measure for autism symptoms, with a score of 15 or above being suggestive of ASD. There were four boys in the SPD cohort who exceeded the SCQ screening cut off score of 15, which prompted a standardized structured play session following the Autism Diagnostic Observation Schedule (ADOS; Lord et al., 2000) and clinical review. All four boys scored less than 3 for the social and communication total score with a score greater than 7 meeting concern for ASD and a score greater than 10 meeting concern for a full autism disorder diagnosis based on DSM IV-TR criteria. Clinical interview and review by Dr. Marco, a pediatric cognitive and behavioral child neurologist was also non-consistent with a clinical ASD diagnosis. None of the TDC cohort and none of the SPD girls met screening criteria for ASD based on the SCQ.

All TDC and SPD subjects were assessed with the Sensory Profile (Dunn and Westman, 1997), a parent report questionnaire which measures atypical sensory related behaviors. A definite difference in each sensory domain is defined as a score that

is greater than two standard deviations from the mean: ≤ 25 out of 40 for auditory processing, ≤ 64 out of 90 for tactile processing, ≤ 26 out of 45 for visual processing, and ≤ 23 out of 35 for multisensory integration. There was one child without an auditory processing score, one without tactile, one without multisensory, two without visual scores, and five without sensory profile total scores given incomplete data from the parent survey. A child was included in the SPD cohort if they carried an outside diagnosis of SPD from a community occupational therapist and they had a score in the definite difference range on at least one of the Sensory Profile subscores listed above. Six of the TDC group scored in the probable difference range for one of the subscales, while the remainder scored in the normative range on all subscales. Finally, two SPD kids and one control were born early (gestational ages 36, 35, 33 weeks, respectively).

The Acoustic Index of the Differential Screening Test for Processing (DSTP) was used to assess auditory processing (Richard and Ferre, 2006) for all subjects. This test was administered by the lead study coordinator in accordance with manualized instructions and with training and supervision by a cognitive and behavioral neurologist. The acoustic index is calculated from totaling correct items in: (1) dichotic listening, an index of interhemispheric auditory processing, in which the participant hears and repeats different numbers simultaneously presented through headphones to each ear; (2) temporal patterning, in which the participant reports the order of high and low tones presented in a sequence; and (3) auditory discrimination, in which a participant repeats nonsense syllables presented in background noise. Thirty four out of the 41 controls and 35 out of the 40 SPD subjects received the DSTP. The graphesthesia subtest of The Sensory Integration Praxis Tests (Ayres, 1989) was used to assess tactile proprioception by asking participants to recreate seven designs (neither numbers nor letters) drawn on the dorsum of each hand with closed eyes. Each drawing is then scored for accuracy. This test was administered by the lead study coordinator in accordance with manualized instructions and with training and supervision by a cognitive and behavioral neurologist. 33 out of the 41 controls and 34 out of the 40 SPD subjects received the graphesthesia assessment.

Summary demographic information is included in **Table 1**. No significant differences were found in any of the demographic or sensory variables between boys and girls, for either TDC or SPD kids.

Image Acquisition

MR imaging was performed on a 3T Tim Trio scanner (Siemens, Erlangen, Germany) using a 12 channel head coil. Structural MR imaging of the brain was performed with an axial 3D magnetization prepared rapid acquisition gradient-echo T1-weighted sequence (TE = 2.98 ms, TR = 2300 ms, TI = 900 ms, flip angle of 90°) with in-plane resolution of 1×1 mm on a 256×256 matrix and 160 1.0 mm contiguous partitions. Whole-brain diffusion imaging was performed with a multislice 2D single-shot twice-refocused spin echo echo-planar sequence with 64 diffusion-encoding directions, diffusion-weighting strength of $b = 2000$ s/mm², iPAT reduction factor of 2, TE/TR = 109/8000 ms, NEX = 1, interleaved 2.2 mm-thick axial

slices with no gap, and in-plane resolution of $2.2 \text{ mm} \times 2.2 \text{ mm}$ on a 100×100 matrix. An additional image volume was acquired with no diffusion weighting ($b = 0$ s/mm²). The total diffusion acquisition time was 8.7 min. Structural MRI for all children was reviewed by Dr. Pratik Mukherjee, a pediatric neuroradiologist, who was blind to cohort assignment. No structural anomalies or other clinically significant findings were reported.

DTI Analysis

Pre-processing

The diffusion-weighted images were corrected for motion and eddy currents using FMRIB's Linear Image Registration Tool (FLIRT¹) with 12-parameter linear image registration (Jenkinson et al., 2002). All diffusion-weighted volumes were registered to the reference $b = 0$ s/mm² volume. To evaluate subject movement, we calculated a scalar parameter quantifying the transformation of each diffusion volume to the reference. Sixteen children (6 TDC, 10 SPD) were excluded for DTI artifacts and/or median relative displacement between volumes greater than 2 mm, where a volume represents a single diffusion directional measurement of the entire brain. This left a total of 81 children (40 SPD, 41 TDC) with DTI datasets meeting quality control criteria. A heteroscedastic two-sample Student's *t*-test verified that there were no significant differences between these SPD and TDC groups in movement during the DTI scan ($p > 0.05$). The non-brain tissue was removed using the Brain Extraction Tool (BET²). FA, mean diffusivity (MD), and radial diffusivity (RD) were calculated using FSL's DTIFIT at every voxel, yielding FA, MD, and RD maps for each subject.

Group Differences

Tract-Based Spatial Statistics (TBSS) in FSL (Smith et al., 2006) was used to skeletonize and register the diffusion maps for each subject in order to perform voxel-wise comparisons along the white matter skeleton. First, each subject's FA map was non-linearly registered to each other subject's FA map to identify the most representative FA map as a registration target. The registered maps were then averaged and skeletonized to the center of the white matter. Next, each subject's FA data was projected onto this mean skeleton to obtain skeletonized FA maps per subject. MD and RD maps were then registered and projected onto the white matter skeleton. Finally, voxelwise statistics were performed on the skeletonized maps to assess for group differences with non-parametric permutation testing using the *randomize* function from FSL. Based on our prior work (Owen et al., 2013), we tested the contrasts of: TDC > SPD for FA, SPD > TDC for MD, and SPD > TDC for RD. The resulting group difference maps for each comparison were corrected for multiple comparisons over the 3D image volume with threshold-free cluster enhancement (TFCE) (Smith and Nichols, 2009) using a significance threshold of $p < 0.05$. It is important to note that, in TFCE, the cluster, and not the individual voxel, is the ultimate object of statistical inference and therefore every voxel in the cluster has exactly the same level of statistical significance

¹www.fmrib.ox.ac.uk/fsl/flirt

²<http://www.fmrib.ox.ac.uk/analysis/research/bet>

TABLE 1 | Demographic information and sensory scores.

	#TDC/#SPD	TDC (mean ± standard deviation)	SPD (mean ± standard deviation)	p
Age (years)	41/40	10.1 ± 1.1	9.6 ± 1.2	0.066
FSIQ	41/40	116 ± 10	112 ± 13	0.077
SP – Auditory	41/39	33.8 ± 3.5	23.2 ± 5.00	1.2E-16
SP – Tactile	41/39	83.5 ± 5.8	62.4 ± 12.2	1.5E-13
DSTP	34/35	36.1 ± 3.53	32.2 ± 5.6	0.0017
Graphesthesia	33/34	21.5 ± 3.91	19.1 ± 4.8	0.0025

Bolded p values indicate statistically significant group differences using an unpaired student t-test ($p < 0.05$).

in the final results. The Johns Hopkins University (JHU) ICBM-DTI-81 White-Matter Labeled Atlas (Wakana et al., 2004) was used to determine the anatomic locations of white matter regions.

Effects of Age and Gender

For each subject, mean FA values were obtained within the significant voxels of each of the four white matter regions implicated in the group difference analyses – the left and right posterior thalamic radiations (PTR), splenium of the corpus

callosum (SCC), and retrolenticular limb of the right internal capsule (RLIC), as defined by the JHU white matter atlas. Then, general linear models (GLMs) of FA as a function of group (TDC or SPD), age, and gender were created for the each of these ROIs:

$$FA_{roi} = \beta_0 + \beta_1*group + \beta_2*age + \beta_3*gender$$

where group is 1 for TDC and 0 for SPD, and gender is 1 for females and 0 for males. The coefficient values ($\beta_1-\beta_3$) and their significance levels were assessed for each ROI.

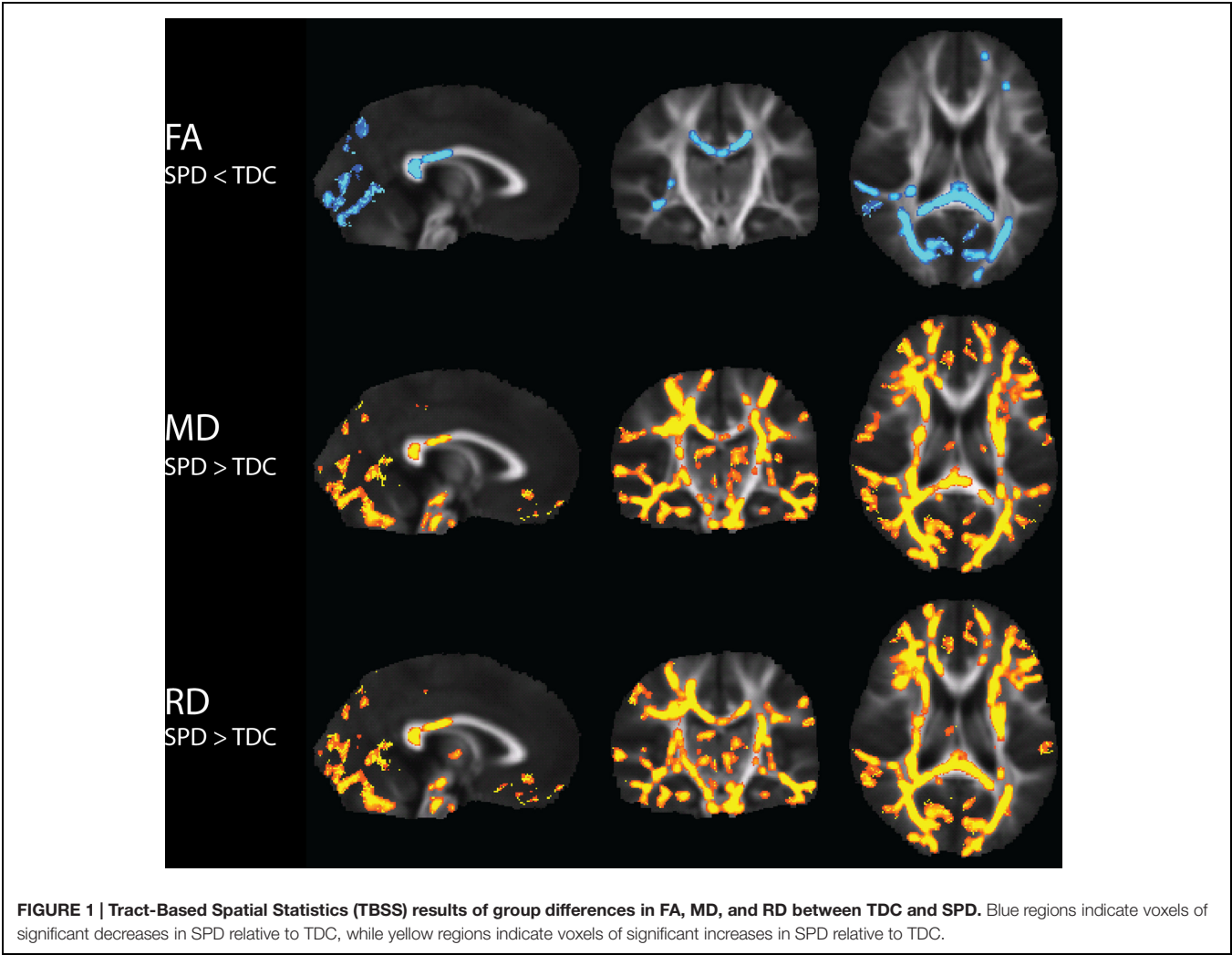
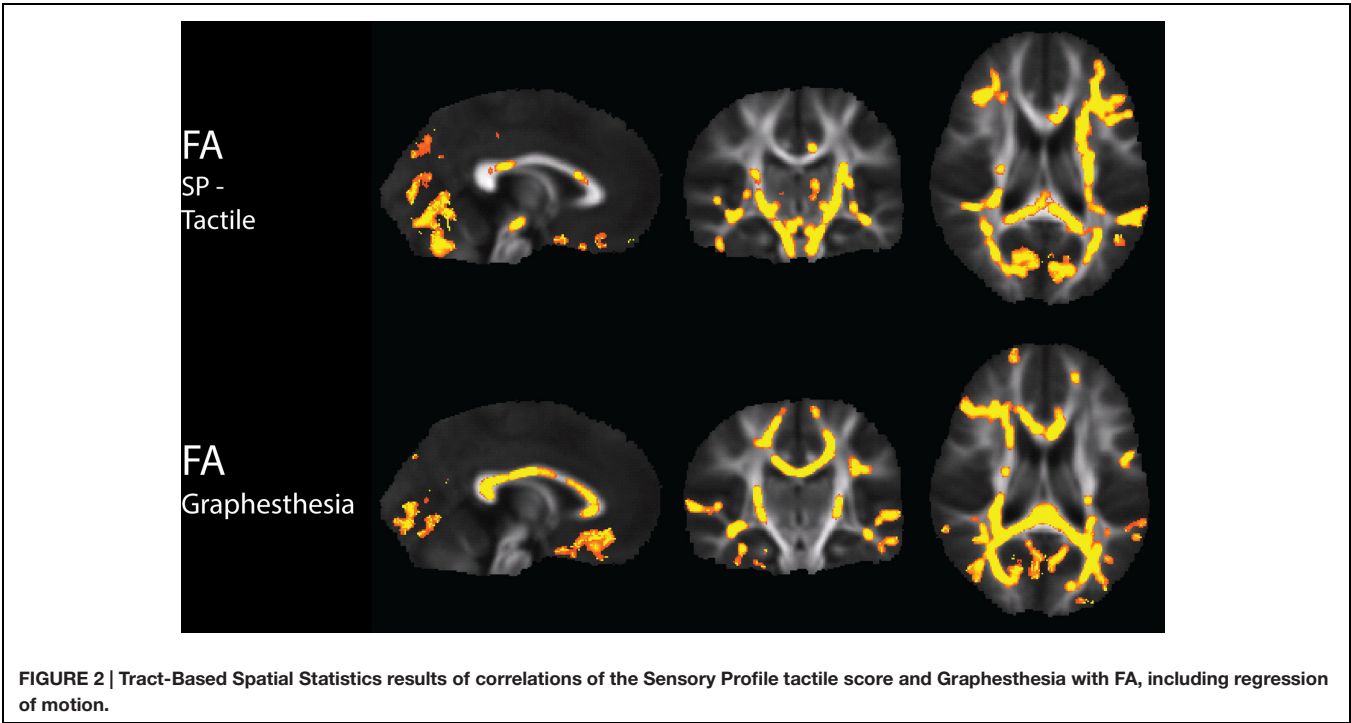


TABLE 2 | Coefficient estimates and *p*-values for the general linear model of FA in a few significant regions as a function of group, age, and gender.

	Group (TDC = 1, SPD = 0)		Age		Gender (F = 1, M = 0)	
	b1	<i>p</i>	b2	<i>p</i>	b3	<i>p</i>
PTR-L	0.028	0.00034	0.0066	0.038	0.012	0.14
PTR-R	0.028	0.00053	0.0080	0.017	0.016	0.063
RLIC-R	0.014	0.011	0.0033	0.16	0.010	0.12
SCC	0.019	0.00033	0.0049	0.022	0.0039	0.49

PTR, posterior thalamic radiation; *RLIC*, retrolenticular limb of the internal capsule; *SCC*, splenium of the corpus callosum. Bolded *p* values indicate statistically significant coefficient estimates (*p* < 0.05).



Sensory Correlations with DTI

In order to limit the number of statistical comparisons, FA alone was examined for correlations with our sensory variables. FA was tested for correlations with the Sensory Profile auditory score and DSTP separately to assess the relationship between white matter microstructure and auditory processing. FA was tested for correlations with the Sensory Profile tactile score and Graphesthesia separately to assess the relationship between white matter microstructure and tactile processing. The correlation analyses were performed on a voxel-wise basis along the white matter skeleton. *Randomize* was used to assess for significant positive correlations of FA with each parent report or direct assessment, with regression of the motion parameters, and the resultant statistical maps were corrected for multiple comparisons using TFCE with *p* < 0.05.

As a *post hoc* analysis to determine contributions of group, age, and gender to the correlational results, for each sensory metric, FA was averaged across the voxels of significant clusters separately for each subject, and separately for several JHU white matter regions. Then, GLMs were constructed with the cognitive metric

as the response variable, and FA, group (TDC vs. SPD), age, and gender as predictor variables. The significance of each predictor variable for each model was determined.

To further investigate the contributions of different types of auditory processing to the correlational results found with DSTP, an additional *post hoc* analysis of correlations between the three subscores of the DSTP acoustic subtest and FA was conducted using the same approach described above.

RESULTS

Group Differences

Significantly lower FA, and higher MD and RD values, were found in the SPD cohort relative to TDC (**Figure 1**). Visual reference with the JHU white matter atlas reveals that the differences in FA are primarily localized to the bilateral PTRs, the SCC, and the right RLIC. MD and RD showed extensive elevations throughout the white matter. Consistent with the FA results, MD and RD are elevated only in the posterior corpus callosum. Also consistent

TABLE 3 | Number of significantly correlated voxels in several ROIs, along with results of the GLMs of Sensory Profile tactile score and Graphesthesia as functions of group, FA, age, and gender.

	SP Tactile			Graphesthesia		
	# sig vox	p_FA	p_TDCvSPD	# sig vox	p_FA	p_TDCvSPD
ACR-L	659	0.074	4.1E-13	361	0.11	0.024
ACR-R	372	0.14	2.0E-12	938	0.039	0.020
SCR-L	179	0.0037	5.6E-15	181	0.034	0.012
SCR-R	24	0.85	9.0E-14	170	0.0072	0.0080
PCR-L	221	0.031	8.4E-14	232	0.023	0.012
PCR-R	229	0.11	1.8E-13	398	0.056	0.031
ALIC-L	267	0.29	9.0E-13	–	–	–
ALIC-R	308	0.10	2.3E-12	234	0.014	0.034
PLIC-L	590	0.014	5.9E-14	49	0.20	0.0077
PLIC-R	506	0.012	2.1E-13	322	0.010	0.016
RLIC-L	393	0.033	3.9E-13	375	0.721	0.011
RLIC-R	333	0.091	3.4E-13	386	0.301	0.021
PTR-L	720	0.0041	3.4E-12	910	0.026	0.056
PTR-R	644	0.032	1.5E-12	425	0.057	0.062
GCC	19	0.069	1.8E-14	1039	0.031	0.022
BCC	398	0.21	1.6E-13	1803	0.046	0.012
SCC	1010	0.027	4.8E-12	1654	0.0012	0.055
CGC-L	172	0.052	2.4E-13	73	0.011	0.038
CGC-R	2	0.41	9.0E-14	–	–	–
EC-L	602	0.0058	2.5E-14	60	0.021	0.014
EC-R	278	0.033	5.3E-14	370	0.033	0.019
SLF-L	98	0.0019	5.9E-15	549	0.0059	0.012
SLF-R	102	0.44	4.9E-13	161	0.0077	0.010
SS-L	156	0.043	1.6E-13	186	0.099	0.013
SS-R	187	0.17	5.3E-13	169	0.021	0.043

The significance of group and FA to the GLMs are displayed. The significance of age and gender are described in the main text. ACR, anterior corona radiata; SCR, superior corona radiata; PCR, posterior corona radiata; ALIC, anterior limb of the internal capsule; PLIC, posterior limb of the internal capsule; RLIC, retrolenticular limb of the internal capsule; PTR, posterior thalamic radiation; GCC, genu of the corpus callosum; BCC, body of the corpus callosum; SCC, splenium of the corpus callosum; CGC, cingulate gyrus part of the cingulum; EC, external capsule; SLF, superior longitudinal fasciculus; SS, sagittal stratum. Bolded *p* values indicate statistically significant effects ($p < 0.05$).

with the FA results, the most significant elevations of both MD and RD occur in the bilateral PTR and right RLIC.

Effects of Age and Gender

The coefficient estimates and *p*-values for the GLM of FA as a function of group, age, and gender, are displayed in **Table 2**. The effect of group remained strongly significant when accounting for age and gender. As expected, increasing age contributed to higher FA in the bilateral PTR and SCC. There were no significant gender effects.

Sensory Correlations with DTI

Tactile Correlations with DTI

There were widespread, significant positive associations of FA across groups with the Sensory Profile tactile score and with graphesthesia, after regression of motion parameters (**Figure 2**). The number of significantly correlated voxels in several ROIs is included in **Table 3**.

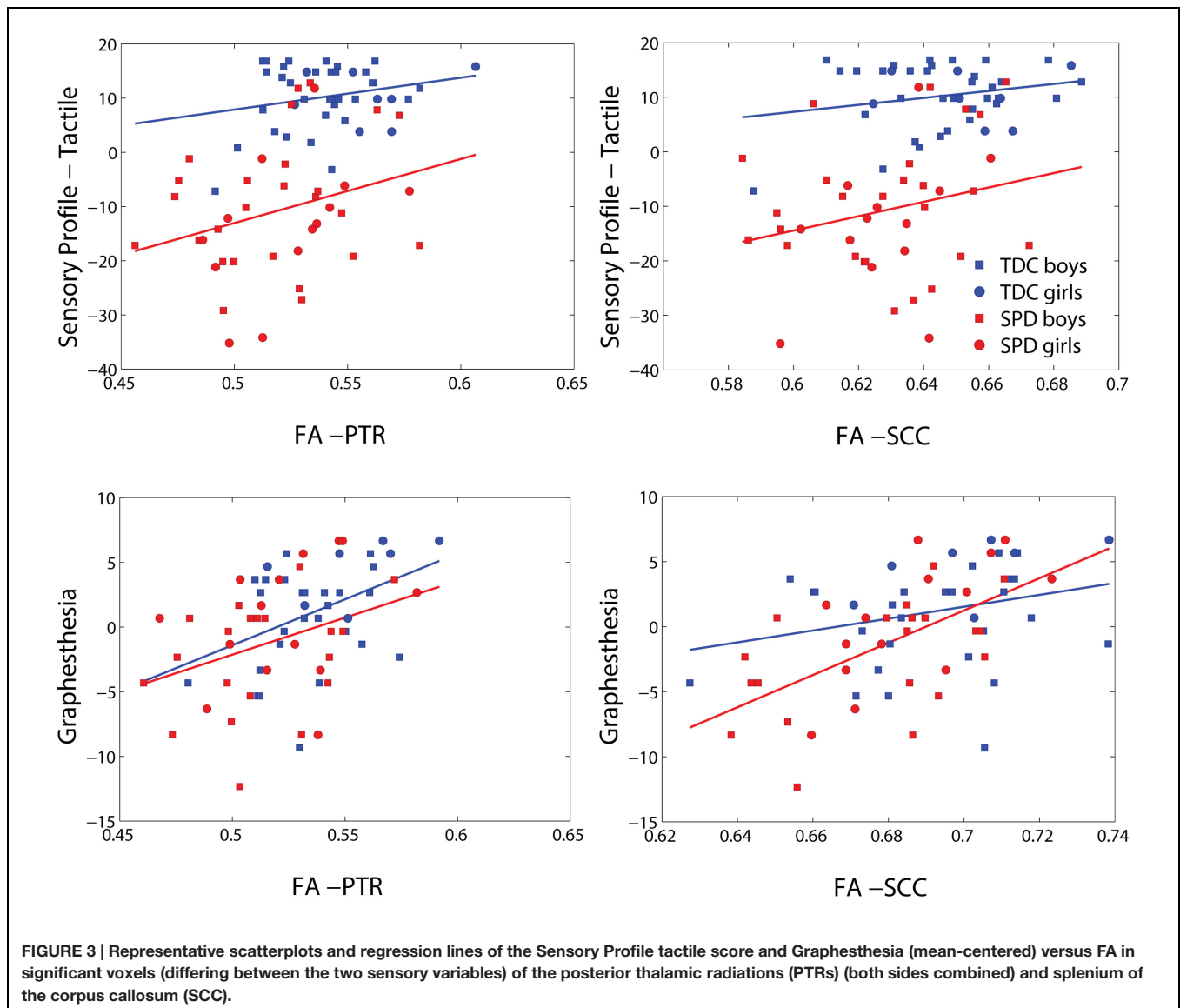
The significance of the group and FA predictor variables in the GLMs for prediction of the Sensory Profile tactile score and Graphesthesia are included in **Table 3**. The effects of group

(TDC vs. SPD) for the Sensory Profile tactile score model were much more strongly significant than the group effects in the Graphesthesia model. The FA effect was significant for many ROIs for both the Sensory Profile tactile score and for Graphesthesia, though the effect was significant for more ROIs with Graphesthesia than with the Sensory Profile tactile score (12 ROIs for Sensory Profile tactile score, 16 ROIs for Graphesthesia). For the Sensory Profile tactile response variable, neither age nor gender was significant for any of the models. For graphesthesia, gender was significant for every model, with females achieving higher scores than males.

Representative plots of the Sensory Profile tactile score model and Graphesthesia vs. FA in significant voxels of the bilateral PTR and SCC are displayed in **Figure 3**. The regression lines for TDC and SPD (of sensory score vs. FA) are more concordant with one another for Graphesthesia than for the Sensory Profile tactile score.

Auditory Correlations with DTI

There were widespread, significant positive associations of FA across groups with the Sensory Profile auditory score and with



DSTP, after regression of motion parameters (Figure 4). The number of significantly correlated voxels in several ROIs is included in Table 4.

The significance of the group and FA predictor variables in the GLMs for prediction of the Sensory Profile auditory score and DSTP are included in Table 4. Similarly to the tactile model, the group effects (TDC vs. SPD) in the Sensory Profile auditory score model were much more strongly significant than group effects in the DSTP model, with the DSTP group effects only reaching weak significance in a few ROIs. The FA effect was significant for many ROIs for DSTP, but only in a few ROIs for the Sensory Profile auditory score. For the Sensory Profile auditory response variable, neither age nor gender was significant for any of the models. For DSTP, age was significant for every model, with increasing age giving rise to higher scores.

Representative plots of the Sensory Profile tactile score model and Graphesthesia versus FA in significant voxels of the bilateral

PTR and SCC are displayed in Figure 5. The regression lines for TDC and SPD (of sensory score vs. FA) are more concordant with one another for Graphesthesia than for the Sensory Profile tactile score.

DSTP Subscore Correlations with DTI

Given the extensive and robust correlations of FA with the DSTP acoustic subscore, additional post-hoc tests for correlations were performed between FA and the three subscores of the DSTP acoustic test – dichotic digits, temporal patterning, and auditory discrimination. The number of significantly correlated voxels in several ROIs is included in Table 5. Overall, the dichotic digits task was significantly associated with the largest number of voxels, as compared with temporal patterning and auditory discrimination.

The significance of the group and FA predictor variables in the GLMs for prediction of each DSTP subscore are included in

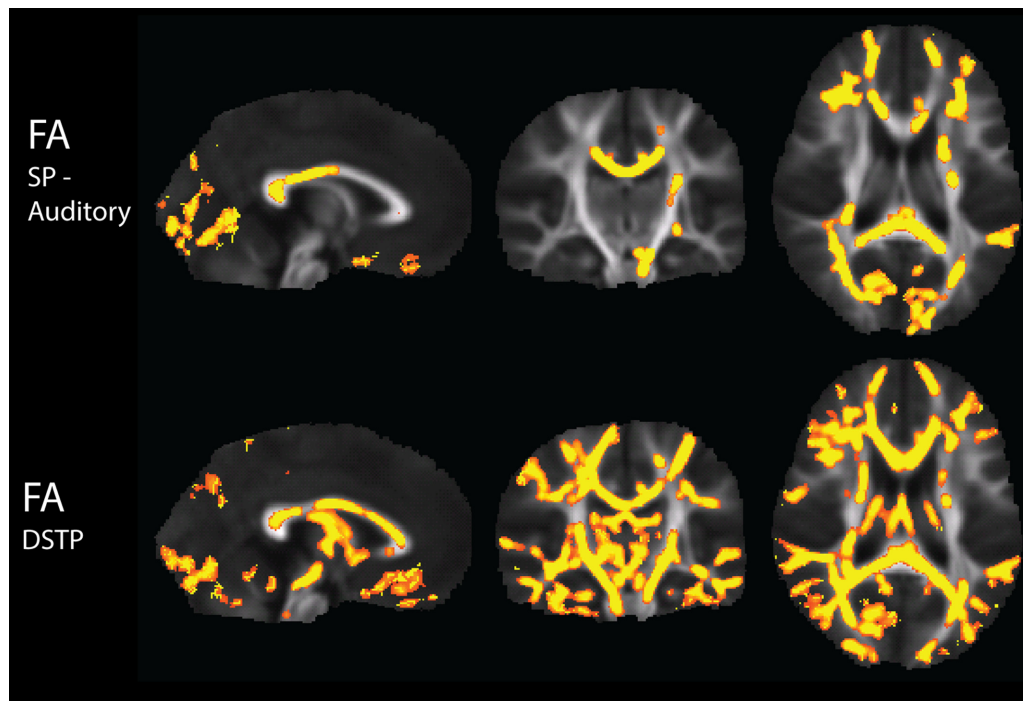


FIGURE 4 | Tract-Based Spatial Statistics results of correlations of the Sensory Profile auditory score and DSTP with FA, including regression of motion.

Table 5. The group effect (TDC vs. SPD) was only significant for the temporal patterning task, while the FA effect was significant for all tasks, but most strongly for dichotic digits. For the dichotic digits test and temporal patterning test, age was a significant contributor for most models, with increasing age giving rise to higher scores, but gender did not contribute significantly to the model. For auditory discrimination, neither age nor gender was significant.

Representative plots of each DSTP subscore versus FA in significant voxels of the bilateral PTR and SCC are displayed in **Figure 6**. The regression lines for TDC and SPD (of sensory score vs. FA) are concordant with one another for dichotic digits and auditory discrimination, but not temporal patterning. A ceiling effect of the dichotic digits and temporal patterning tasks can be observed from these plots, limiting the range of sensory function that can be differentiated between subjects, particularly in the TDC cohort.

DISCUSSION

These findings corroborate and generalize our previous work demonstrating the role of disrupted posterior white matter microstructure in SPD. Furthermore, the larger, mixed-gender cohort unmasks a more extensive distribution of white matter differences which includes anterior white matter. More importantly, to our knowledge, this work is the first to demonstrate a relationship between direct measurements of tactile function and non-linguistic auditory function with white

matter microstructural integrity not just in SPD, but also in TDC.

Group Differences

As in our prior work (Owen et al., 2013), our results show strong decreases of white matter microstructural integrity in the posterior projection and commissural tracts of the bilateral PTR and the SCC, which respectively contain all primary sensory projection pathways excluding olfaction, and connect homologous sensory cortical regions (Huang et al., 2005; Hofer and Frahm, 2006). Our findings additionally reveal marked reductions of microstructural integrity in the RLIC, which contains visual and auditory projection fibers. Overall, microstructural integrity is disrupted extensively, but with a posterior bias, throughout the white matter.

Sensory Correlations with DTI

We find that correlations of white matter microstructure with direct measurements of tactile and auditory processing are stronger than the correlations of microstructure with parent report measures, likely due to the more objective nature of the direct measurements. Furthermore, the stronger concordance between the TDC and SPD regression lines of FA with the direct sensory measurements of Graphesthesia and DSTP, as compared with the sensory profile tactile and auditory scores, suggest that these direct measurements map more closely to the underlying biology. The offset between the TDC and SPD regression lines of the sensory profile metrics with FA may reflect biased parent reporting as a function of the presence or absence of an SPD

TABLE 4 | Number of significantly correlated voxels in several ROIs, along with results of the GLMs of Sensory Profile auditory score and DSTP as functions of group, FA, age, and gender.

	SP – Auditory			DSTP		
	Num vox	p_FA	p_TDCvSPD	Num vox	p_FA	p_TDCvSPD
ACR-L	562	0.13	9.9E-15	1155	0.014	0.077
ACR-R	573	0.26	9.7E-15	1371	0.00036	0.12
SCR-L	79	0.17	1.7E-15	148	0.067	0.038
SCR-R	61	0.77	2.5E-15	464	0.029	0.043
PCR-L	48	0.26	2.5E-15	236	0.081	0.050
PCR-R	298	0.11	4.8E-15	518	0.016	0.068
ALIC-L	276	0.06	1.1E-14	398	0.0074	0.18
ALIC-R	374	0.20	1.8E-14	576	0.010	0.19
PLIC-L	339	0.28	7.8E-16	491	0.016	0.058
PLIC-R	173	0.64	2.8E-15	553	0.011	0.082
RLIC-L	–	–	–	539	0.016	0.075
RLIC-R	5	0.69	6.4E-16	475	0.039	0.11
PTR-L	396	0.026	6.8E-14	647	0.029	0.23
PTR-R	429	0.029	6.5E-14	768	0.013	0.29
GCC	551	0.25	8.1E-15	1234	0.020	0.086
BCC	1718	0.055	9.2E-16	2173	0.048	0.046
SCC	1293	0.096	5.3E-14	1032	0.027	0.18
CGC-L	102	0.038	1.7E-15	255	0.022	0.067
CGC-R	7	0.021	3.9E-15	10	0.26	0.041
EC-L	399	0.00038	2.7E-17	383	0.091	0.048
EC-R	289	0.010	1.7E-16	1104	0.002	0.063
SLF-L	–	–	–	560	0.018	0.068
SLF-R	141	0.062	5.1E-15	852	0.00040	0.060
SS-L	–	–	–	246	0.0055	0.047
SS-R	–	–	–	308	0.00016	0.36

The significance of group and FA to the GLMs are displayed. The significance of age and gender are described in the main text. ACR, anterior corona radiata; SCR, superior corona radiata; PCR, posterior corona radiata; ALIC, anterior limb of the internal capsule; PLIC, posterior limb of the internal capsule; RLIC, retrolenticular limb of the internal capsule; PTR, posterior thalamic radiation; GCC, genu of the corpus callosum; BCC, body of the corpus callosum; SCC, splenium of the corpus callosum; CGC, cingulate gyrus part of the cingulum; EC, external capsule; SLF, superior longitudinal fasciculus; SS, sagittal stratum. Bolded *p* values indicate statistically significant effects ($p < 0.05$).

diagnosis. More explicitly, if a child without an SPD label and a child with an SPD label exhibit the same level of function for a given sensory processing domain, parents of the child who has not been attributed an SPD label may be less likely to report abnormalities than the parents of the child who has been clinically assigned an SPD label.

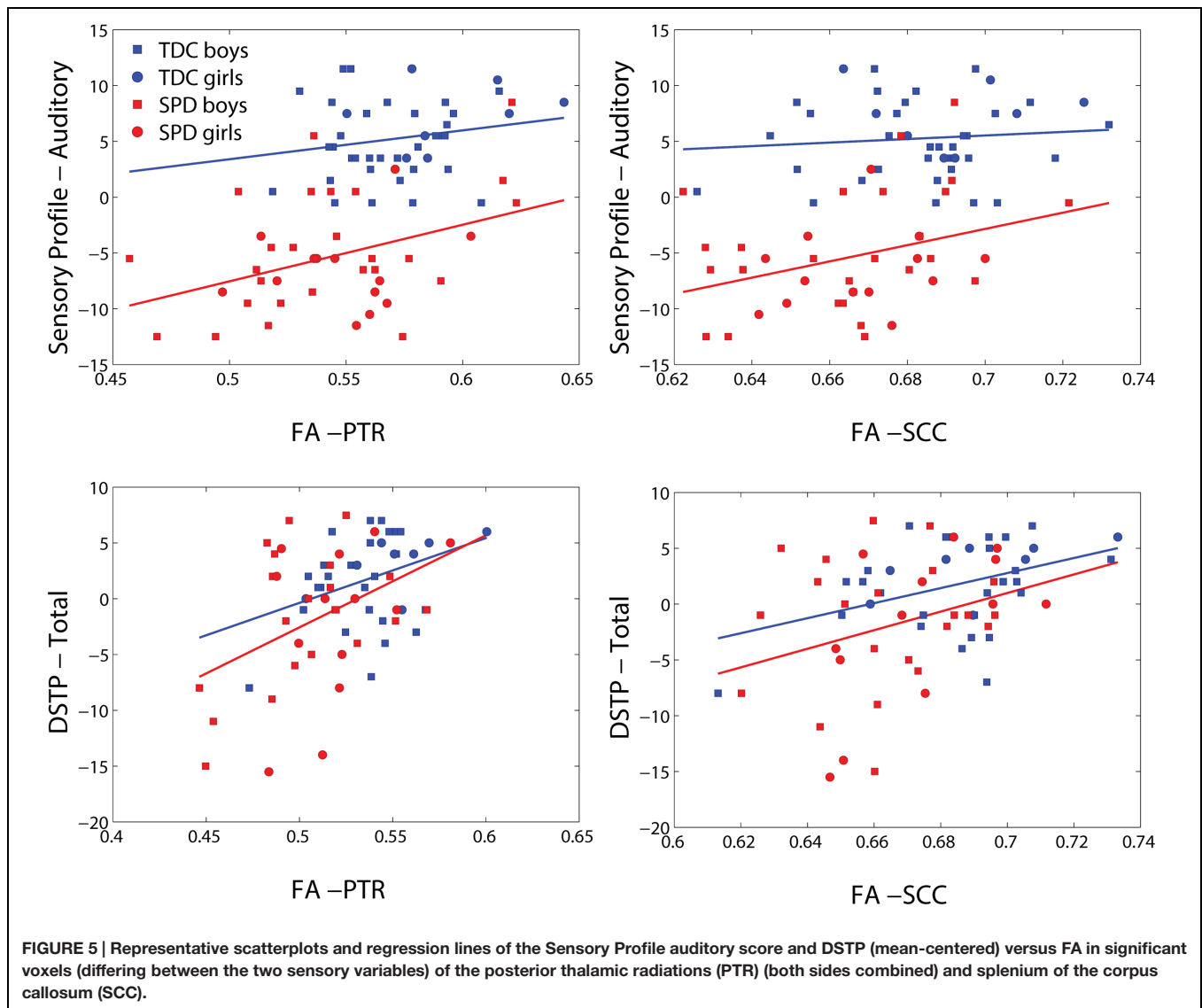
The relative lack of anatomic specificity of these correlations of DTI with sensory processing measures may be due, in part, to the high degree of microstructural covariance between different white matter tracts (Wahl et al., 2010), with a spatially global factor accounting for almost half of the variance in FA (Penke et al., 2010). It is also likely reflective of the multiple functional brain networks required for each of these tests, as reviewed below.

Tactile Processing

Diffusion tensor imaging has previously been used to link degree of periventricular white matter injury in the PTR, as assessed by size reduction of white matter tracts on visual inspection, with contralateral touch threshold, proprioception, and motor severity in children with cerebral palsy (Hoon et al., 2009). However, this prior work used a subjective rater system of white matter

injury. One study has reported a correlation between tactile defensiveness and FA in the inferior longitudinal fasciculus of children with ASD (Pryweller et al., 2014). However, the metric of tactile defensiveness is an assessment of sensory-related behavior, rather than early-stage sensory function. While we are not aware of other studies reporting a relationship between white matter microstructure and primary or secondary tactile processing, there are a multitude of functional imaging studies have demonstrated primarily fronto-parietal network activations in tasks involving either active or passive touch discrimination of macrogeometric object features such as shape or length (Bodegård et al., 2001; Van de Winckel et al., 2005). These circuits include the ventral and dorsal premotor cortex, secondary somatosensory area, superior parietal lobe, anterior part of the intraparietal sulcus (AIP), and supramarginal gyrus (Kawashima et al., 1994; O'Sullivan et al., 1994; Hadjikhani and Roland, 1998; Roland and Zilles, 1998; Binkofski et al., 1999; Bodegård et al., 2000, 2001; Servos et al., 2001; Stoessel et al., 2003, 2004; Stoesz et al., 2003).

Our results are the first to demonstrate associations of white matter microstructure with tactile processing, both among children with SPD as well as among TDC. Both the Sensory



Profile tactile score and Graphesthesia are associated with FA in regions subserving primary sensory processing, including the posterior projection tracts of the superior and posterior corona radiata, the posterior limbs of the internal capsule, and the PTR. Both are also associated with the SCC, which connects homologous sensory areas. However, they are also associated with microstructure in associational tracts such as the external capsules, superior longitudinal fasciculus, sagittal stratum. Unlike the Sensory Profile tactile score, Graphesthesia demonstrates associations with the frontal regions of the right anterior corona radiata, anterior limb of the RLIC, and the genu of the corpus callosum. The widespread nature of these correlations may in part reflect the non-specificity of the assessments used, in addition to the previously mentioned contribution of high microstructural covariance of white matter (from the beginning of the Discussion). For example, in addition to primary tactile processing, Graphesthesia engages secondary modalities requiring synthesis and interpretation of the primary

tactile inputs, including the spatio-temporal analysis of these inputs to form a visual representation of what was drawn on the back of the hand, and the motor planning and coordination to re-create this image.

The tactile sense develops the earliest among all sensory systems, with somatosensory responses detected *in utero* as early as 8 weeks of gestation (Montagu, 1986). Tactile feedback from mechanoreceptors in the skin and joints critically guide the development of motor skills during childhood, both in gross motor (Metcalf et al., 2005) and fine motor (Soechting and Flanders, 2008) functions. Tactile processing has been further suggested to play a central role in the development of social and communicative behaviors, with tactile-centered therapies shown to effectively modulate arousal, attention, and sensory defensiveness (Cascio, 2010). It is thus critical to understand the neural correlates of tactile processing in order to better understand the downstream effects of its abnormalities as well as to better design and evaluate tactile-centered therapies.

Auditory Processing

One prior study reported associations between FA and performance on auditory processing tasks in TDC (Schmithorst et al., 2011). This prior study reports positive correlations of FA around the prefrontal regions with performance in a speech-in-noise task. However, all measures of auditory processing in this previous study involved manipulations of language stimuli, unlike the acoustic test of the DSTP which involves manipulations of non-linguistic stimuli, therefore being more likely to probe basic auditory processing function instead of the integrity of language networks.

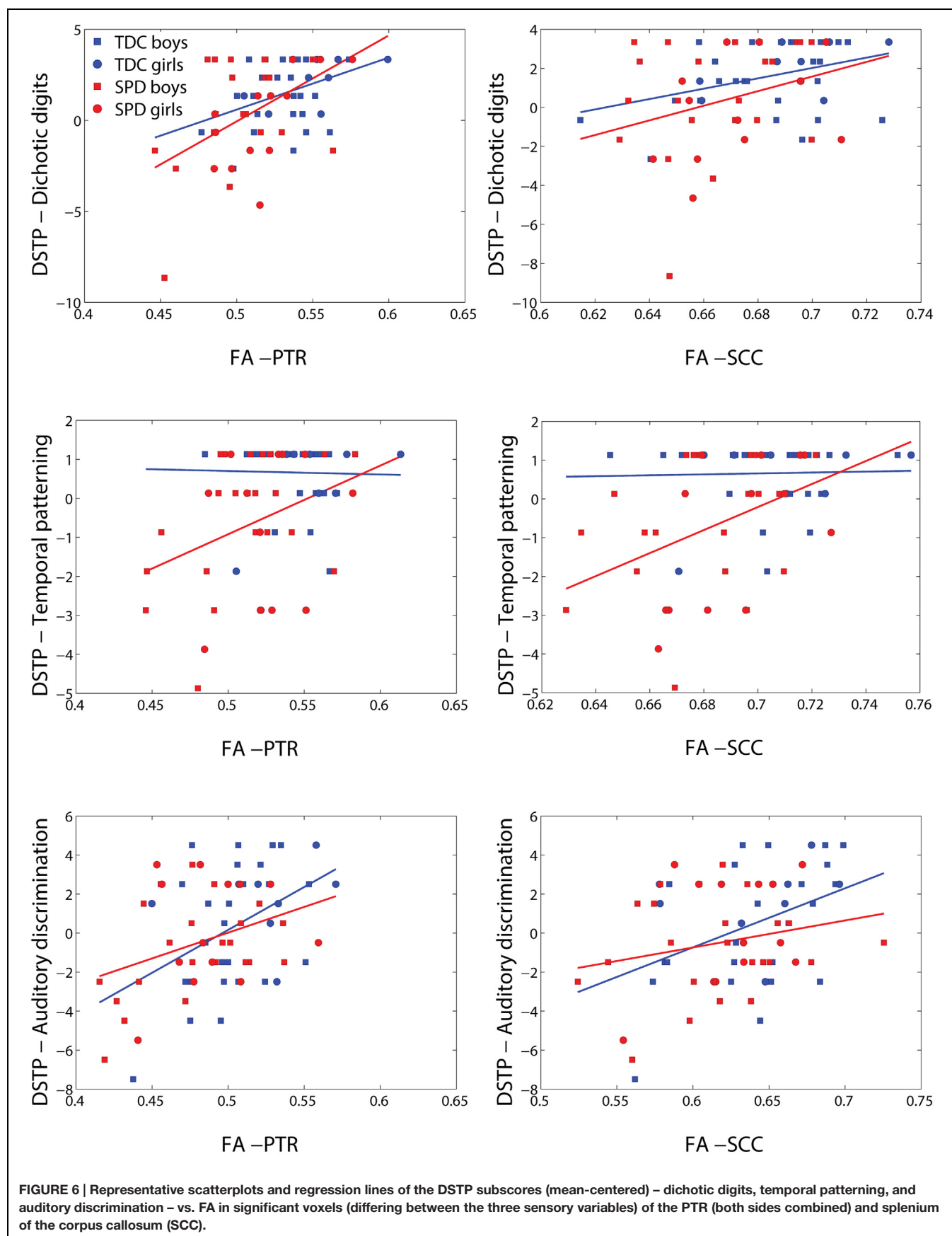
To our knowledge, our study is the first to demonstrate associations of white matter microstructure with non-linguistic auditory processing, both among children with SPD as well as among TDC. Both the Sensory Profile auditory score and DSTP are associated with FA in the PTR, which contains the primary auditory projection pathway. However, they are also associated with microstructure in associational tracts such as the external capsules and the cingulate portion of the cingulum bundles. Unlike the Sensory Profile auditory score,

DSTP demonstrates widespread associations with both frontal and posterior projection and commissural pathways, along with the associational tracts of the superior longitudinal fasciculus and sagittal stratum. Similar to tactile processing, one contributor to the extensive regions of significant correlations with the DSTP task may lie in the test's additional recruitment of attentional processes. For example, dichotic listening tasks have long been used to test different neural models of attention (Broadbent, 1954; Treisman, 1964), and have been used to demonstrate enhanced right ear advantage in individuals with mild Alzheimer's disease (Duchek and Balota, 2005), decreased right ear advantage in children with dyslexia (Helland and Asbjornsen, 2001), and challenges with attention shifting in sleep deprivation (Johnson et al., 2002). The dichotic listening portion of the DSTP demonstrates the most robust correlations with FA of the three DSTP subtests, showing strong FA effects across projection, commissural, and association tracts (Table 5). Temporal patterning shows strong effects in certain projection and association tracts. It has previously been suggested that children with specific language impairment perform worse on

TABLE 5 | Number of significantly correlated voxels in several ROIs, along with results of the three DSTP subscores as functions of group, FA, age, and gender.

	DSTPdd			DSTPtp			DSTPad		
	# sig vox	p_FA	p_TDCvSPD	# sig vox	p_FA	p_TDCvSPD	# sig vox	p_FA	p_TDCvSPD
ACR-L	734	0.016	0.32	582	0.10	0.010	—	—	—
ACR-R	1190	0.0025	0.34	918	0.028	0.011	1176	0.00057	0.52
SCR-L	334	0.037	0.15	7	0.23	0.0022	—	—	—
SCR-R	460	0.022	0.18	326	0.037	0.0033	83	0.029	0.19
PCR-L	255	0.013	0.21	52	0.27	0.0061	—	—	—
PCR-R	499	0.0034	0.27	341	0.046	0.0086	40	0.012	0.25
ALIC-L	268	0.038	0.36	316	0.0074	0.021	—	—	—
ALIC-R	521	0.013	0.50	475	0.037	0.028	326	0.0054	0.64
PLIC-L	584	0.0050	0.21	306	0.077	0.0048	—	—	—
PLIC-R	602	0.0025	0.30	338	0.29	0.0070	18	0.0063	0.55
RLIC-L	455	0.0091	0.28	440	0.043	0.0087	—	—	—
RLIC-R	453	0.0083	0.43	363	0.14	0.012	111	0.026	0.62
PTR-L	596	0.0075	0.67	463	0.32	0.019	—	—	—
PTR-R	894	0.00043	0.99	583	0.12	0.031	305	0.0072	0.81
GCC	1116	0.014	0.33	928	0.095	0.0088	426	0.043	0.44
BCC	2048	0.030	0.18	1788	0.085	0.0044	529	0.041	0.23
SCC	939	0.028	0.43	871	0.074	0.021	129	0.025	0.45
CGC-L	268	0.0064	0.28	153	0.025	0.0091	—	—	—
CGC-R	8	0.11	0.20	69	0.080	0.0080	—	—	—
EC-L	223	0.13	0.18	439	0.049	0.0041	—	—	—
EC-R	911	0.0054	0.23	598	0.013	0.0045	752	0.00054	0.44
SLF-L	702	0.0014	0.24	9	0.14	0.0024	—	—	—
SLF-R	981	0.00046	0.18	715	0.014	0.0067	206	0.0013	0.45
SS-L	177	0.023	0.20	235	0.0068	0.0051	5	0.0026	0.18
SS-R	259	0.0054	0.56	284	0.016	0.032	212	0.00044	0.98

The significance of group and FA to the GLMs are displayed. The significance of age and gender are described in the main text. DSTPdd, dichotic digits; DSTPtp, temporal patterning; DSTPad, auditory discrimination. ACR, anterior corona radiata; SCR, superior corona radiata; PCR, posterior corona radiata; ALIC, anterior limb of the internal capsule; PLIC, posterior limb of the internal capsule; RLIC, retrolenticular limb of the internal capsule; PTR, posterior thalamic radiation; GCC, genu of the corpus callosum; BCC, body of the corpus callosum; SCC, splenium of the corpus callosum; CGC, cingulate gyrus part of the cingulum; EC, external capsule; SLF, superior longitudinal fasciculus; SS, sagittal stratum. Bolded *p* values indicate statistically significant effects ($p < 0.05$).



temporal patterning tasks, but only when the interstimulus interval between tones is short (Tallal and Piercy, 1973). Interestingly, the left RLIC, with which temporal patterning demonstrates an FA effect in our present study (but not with the right RLIC), has been previously associated with reading scores in individuals with dyslexia by a DTI study (Klingberg et al., 2000). Auditory discrimination, which involves a strong element of attentional control, demonstrates the strongest FA effects with the right anterior corona radiata, which is concordant with Schmithorst et al.'s (2011) finding of correlations of language discrimination in noise with FA in white matter of prefrontal regions.

Auditory processing is of primary importance for language acquisition, with speech perception requiring the ability to determine spectral shape, to discriminate modulation of amplitude and spectral frequencies, and to do this at varying temporal resolutions (Bailey and Snowling, 2002). These auditory capabilities are likely sufficient by early infancy to support the discrimination of phonetic elements in language, though attentional capabilities may take longer to develop (Bailey and Snowling, 2002). Given the wealth of evidence that developmental language-based learning disorders can often be traced to non-verbal auditory processing deficits (Tallal et al., 1997), it is highly relevant to characterize the biological underpinnings of these deficits.

Study Limitations and Future Directions

Despite the larger number of subjects in this study, we are still limited by sample size in our ability to harness DTI as a clinically utilizable tool for the diagnosis, prognosis, and treatment of SPD. Going forward, larger sample sizes and multimodal imaging biomarkers from DTI, fMRI, and MEG may aid in better definition and diagnosis of SPD. This could be of particular use if these biomarkers can identify individuals at risk for SPD

at early ages before clinical symptoms are apparent, allowing for early intervention and recruitment of support services. In addition to diagnosis, larger scale longitudinal studies will allow us to evaluate the utility of quantitative imaging biomarkers, as compared with clinical metrics, neuropsychological testing, or direct sensory testing, for the prognostication of behavioral and cognitive development of individuals with SPD. Finally, interventional studies will allow us to evaluate the utility of quantitative imaging biomarkers for the monitoring of behavioral and psychopharmacological interventions, as well as for the prediction of interventional outcome. These biomarkers may further aid in the design of interventions if they can be used to stratify the SPD population into subgroups that will better respond to particular interventions. Overall, future studies will aim to shift SPD from a clinical diagnosis to a "biomarker diagnosis," with imaging, and in particular DTI, metrics among the most promising of these biomarkers.

AUTHOR CONTRIBUTIONS

Conception and design: JO, EM, PM. Acquisition: AB-A, SD, SH, ABA, JH. Analysis: Y-SC, MG, JO, EM, PM. Interpretation: YSC, MG, JPO, EJM, PM.

ACKNOWLEDGMENTS

This work was funded by grants from the Wallace Research Foundation to EJM and to PM and a gift from Toby Mickelson and Donald Brody to EJM. EJM has also received neuroimaging support that contributed to this work from NIH K23 MH083890. We also received generous support from the SPD community of family and friends through gifts large and small to our UCSF Sensory Neurodevelopment and Autism Program (SNAP).

REFERENCES

- Ahn, R. R., Miller, L. J., Milberger, S., and McIntosh, D. N. (2004). Prevalence of parents' perceptions of sensory processing disorders among kindergarten children. *Am. J. Occup. Ther.* 58, 287–293. doi: 10.5014/ajot.58.3.287
- Ayres, A. J. (1989). *Sensory Integration and Praxis Tests: SIPT Manual*. Los Angeles, CA: Western Psychological Services.
- Bailey, P. J., and Snowling, M. J. (2002). Auditory processing and the development of language and literacy. *Br. Med. Bull.* 63, 135–146. doi: 10.1093/bmb/63.1.135
- Binkofski, F., Buccino, G., Posse, S., Seitz, R. J., Rizzolatti, G., and Freund, H. (1999). A fronto-parietal circuit for object manipulation in man: evidence from an fMRI-study. *Eur. J. Neurosci.* 11, 3276–3286. doi: 10.1046/j.1460-9568.1999.00753.x
- Bodgård, A., Geyer, S., Grefkes, C., Zilles, K., and Roland, P. E. (2001). Hierarchical processing of tactile shape in the human brain. *Neuron* 31, 317–328. doi: 10.1016/S0896-6273(01)00362-2
- Bodgård, A., Ledberg, A., Geyer, S., Naito, E., Zilles, K., and Roland, P. E. (2000). Object shape differences reflected by somatosensory cortical activation. *J. Neurosci.* 20, RC51.
- Broadbent, D. E. (1954). The role of auditory localization in attention and memory span. *J. Exp. Psychol.* 44, 51–55. doi: 10.1037/h0056491
- Cascio, C. J. (2010). Somatosensory processing in neurodevelopmental disorders. *J. Neurodev. Disord.* 2, 62–69. doi: 10.1007/s11689-010-9046-3
- Chang, Y. S., Owen, J. P., Desai, S. S., Hill, S. S., Arnett, A. B., Harris, J., et al. (2014). Autism and sensory processing disorders: shared white matter disruption in sensory pathways but divergent connectivity in social-emotional pathways. *PLoS ONE* 9:e103038. doi: 10.1371/journal.pone.0103038
- Demopoulos, C., Brandes-Aitken, A. N., Desai, S. S., Hill, S. S., Antovich, A. D., Harris, J., et al. (2015). Shared and Divergent Auditory and Tactile Processing in Children with Autism and Children with Sensory Processing Dysfunction Relative to Typically Developing Peers. *J. Int. Neuropsychol. Soc.* 6, 1–11. doi: 10.1017/s1355617715000387
- Duchek, J. M., and Balota, D. A. (2005). Failure to control prepotent pathways in early stage dementia of the Alzheimer's type: Evidence from dichotic listening. *Neuropsychology* 19, 687–695. doi: 10.1037/0894-4105.19.5.687
- Dunn, W., and Westman, K. (1997). The sensory profile: the performance of a national sample of children without disabilities. *Am. J. Occup. Ther.* 51, 25–34. doi: 10.5014/ajot.51.1.25
- Hadjikhani, N., and Roland, P. E. (1998). Cross-modal transfer of information between the tactile and the visual representations in the human brain: a positron emission tomographic study. *J. Neurosci.* 18, 1072–1084.
- Helland, T., and Asbjørnsen, A. (2001). Brain asymmetry for language in dyslexic children. *Laterality* 6, 289–301. doi: 10.1080/713754422
- Hofer, S., and Frahm, J. (2006). Topography of the human corpus callosum revisited – Comprehensive fiber tractography using diffusion tensor magnetic resonance imaging. *Neuroimage* 32, 989–994. doi: 10.1016/j.neuroimage.2006.05.044

- Hoon, A. H. Jr., Stashinko, E. E., Nagae, L. M., Lin, D. D., Keller, J., Bastian, A., et al. (2009). Sensory and motor deficits in children with cerebral palsy born preterm correlate with diffusion tensor imaging abnormalities in thalamocortical pathways. *Dev. Med. Child Neurol.* 51, 697–704. doi: 10.1111/j.1469-8749.2009.03306.x
- Huang, H., Zhang, J., Jiang, H., Wakana, S., Poetscher, L., Miller, M. I., et al. (2005). DTI tractography based parcellation of white matter: application to the mid-sagittal morphology of corpus callosum. *Neuroimage* 26, 195–205. doi: 10.1016/j.neuroimage.2005.01.019
- Jenkinson, M., Beckmann, C. F., Behrens, T. E. J., Woolrich, M. W., and Smith, S. M. (2002). Fsl. *Neuroimage* 62, 782–790. doi: 10.1016/j.neuroimage.2011.09.015
- Johnson, B. H., Laberg, J. C., Eid, J., and Hugdahl, K. (2002). Dichotic listening and sleep deprivation. *Scand. J. Psychol.* 43, 413–417. doi: 10.1111/1467-9450.00309
- Kawashima, R., Roland, P. E., and O'Sullivan, B. T. (1994). Activity in the human primary motor cortex related to ipsilateral hand movements. *Brain Res.* 663, 251–256. doi: 10.1016/0006-8993(94)91270-X
- Klingberg, T., Hedehus, M., Temple, E., Salz, T., Gabrieli, J. D., Moseley, M. E., et al. (2000). Microstructure of temporo-parietal white matter as a basis for reading ability: evidence from diffusion tensor magnetic resonance imaging. *Neuron* 25, 493–500. doi: 10.1016/S0896-6273(00)80911-3
- Lord, C., Risi, S., Lambrecht, L., Cook, E. H. Jr., Leventhal, B. L., DiLavore, P. C., et al. (2000). The autism diagnostic observation schedule-generic: a standard measure of social and communication deficits associated with the spectrum of autism. *J. Autism. Dev. Disord.* 30, 205–223. doi: 10.1023/A:1005592401947
- Metcalfe, J. S., McDowell, K., Chang, T. Y., Chen, L. C., Jeka, J. J., and Clark, J. E. (2005). Development of somatosensory-motor integration: and event-related analysis of infant posture in the first year of independent walking. *Dev. Psychobiol.* 46, 19–35. doi: 10.1002/dev.20037
- Montagu, A. (1986). *Touching: the Human Significance of the Skin*. (New York: Perennial Library).
- O'Sullivan, B. T., Roland, P. E., and Kawashima, R. (1994). A PET study of somatosensory discrimination in Man. Microgeometry versus macrogeometry. *Eur. J. Neurosci.* 6, 137–148. doi: 10.1111/j.1460-9568.1994.tb00255.x
- Owen, J. P., Marco, E. J., Desai, S., Fourie, E., Harris, J., Hill, S. S., et al. (2013). Abnormal white matter microstructure in children with sensory processing disorders. *Neuroimage Clin.* 2, 844–853. doi: 10.1016/j.nicl.2013.06.009
- Penke, L., Muñoz Maniega, S., Murray, C., Gow, A. J., Hernández, M. C., Clayden, J. D., et al. (2010). A general factor of brain white matter integrity predicts information processing speed in healthy older people. *J. Neurosci.* 30, 7569–7574. doi: 10.1523/JNEUROSCI.1553-10.2010
- Pryweller, J. R., Schauder, K. B., Anderson, A. W., Heacock, J. L., Foss-Feig, J. H., Newsom, C. R., et al. (2014). White matter correlates of sensory processing in autism spectrum disorders. *Neuroimage Clin.* 6, 379–387. doi: 10.1016/j.nicl.2014.09.018
- Richard, G., and Ferre, J. (2006). *Differential Screening Test for Processing*. East Moline, IL: LinguiSystems, Inc.
- Roland, P. E., and Zilles, K. (1998). Structural divisions and functional fields in the human cerebral cortex. *Brain Res. Rev.* 26, 87–105. doi: 10.1016/S0165-0173(97)00058-1
- Rutter, M., Bailey, A., and Lord, C. (2003). *Social Communication Questionnaire (SCQ)*. Los Angeles, CA: Western Psychological Services.
- Schmithorst, V. J., Holland, S. K., and Plante, E. (2011). Diffusion tensor imaging reveals white matter microstructure correlations with auditory processing ability. *Ear Hear.* 32, 156–167. doi: 10.1097/AUD.0b013e3181f7a481
- Servos, P., Lederman, S., Wilson, D., and Gati, J. (2001). fMRI-derived cortical maps for haptic shape, texture, and hardness. *Cogn. Brain Res.* 12, 307–313. doi: 10.1016/S0926-6410(01)00041-6
- Smith, S. M., Jenkinson, M., Johansen-Berg, H., Rueckert, D., Nichols, T. E., Mackay, C. E., et al. (2006). Tract-based spatial statistics: voxelwise analysis of multi-subject diffusion data. *Neuroimage* 31, 1487–1505. doi: 10.1016/j.neuroimage.2006.02.024
- Smith, S. M., and Nichols, T. E. (2009). Threshold-free cluster enhancement: addressing problems of smoothing, threshold dependence and localisation in cluster inference. *Neuroimage* 44, 83–98. doi: 10.1016/j.neuroimage.2008.03.061
- Soechting, J. F., and Flanders, M. (2008). Sensorimotor control of contact force. *Curr. Opin. Neurobiol.* 18, 565–572. doi: 10.1016/j.conb.2008.11.006
- Stoeckel, M. C., Weder, B., Binkofski, F., Buccino, G., Jon Shah, N., and Seitz, R. J. (2003). A fronto-parietal circuit for tactile object discrimination: an event-related fMRI study. *Neuroimage* 19, 1103–1114. doi: 10.1016/S1053-8119(03)00182-4
- Stoeckel, M. C., Weder, B., Binkofski, F., Choi, H. J., Amunts, K., Pieperhoff, P., et al. (2004). Left and right superior parietal lobule in tactile object discrimination. *Eur. J. Neurosci.* 19, 1067–1072. doi: 10.1111/j.0953-816X.2004.03185.x
- Stoesz, M. R., Zhang, M., Weisser, V. D., Prather, S. C., Mao, H., and Sathian, K. (2003). Neural networks active during tactile form perception: common and differential activity during macrospace and microspace tasks. *Int. J. Psychophysiol.* 50, 41–49. doi: 10.1016/S0167-8760(03)00123-5
- Tallal, P., Miller, S. L., Jenkins, W. M., and Merzenich, M. M. (1997). “The role of temporal processing in developmental language-based learning disorders: research and clinical implications,” in *Foundations of Reading Acquisition and Dyslexia: Implications for Early Intervention*, ed. B. A. Blachman (Mahwah, NJ: Lawrence Erlbaum), 49–66.
- Tallal, P., and Piercy, M. (1973). Developmental aphasia: impaired rate of non-verbal processing as a function of sensory modality. *Neuropsychologia* 11, 389–398. doi: 10.1016/0028-3932(73)90025-0
- Treisman, A. (1964). Verbal cues, language, and meaning in selective attention. *Am. J. Psychol.* 77, 206–209. doi: 10.2307/1420127
- Van de Winckel, A., Sunaert, S., Wenderoth, N., Peeters, R., Van Hecke, P., Feys, H., et al. (2005). Passive somatosensory discrimination tasks in healthy volunteers: differential networks involved in familiar versus unfamiliar shape and length discrimination. *Neuroimage* 26, 441–453. doi: 10.1016/j.neuroimage.2005.01.058
- Wahl, M., Li, Y. O., Ng, J., Lahue, S. C., Cooper, S. R., Sherr, E. H., et al. (2010). Microstructural correlations of white matter tracts in the human brain. *Neuroimage* 51, 531–541. doi: 10.1016/j.neuroimage.2010.02.072
- Wakana, S., Jiang, H., Nagae-Poetscher, L. M., Van Zijl, P. C. M., and Mori, S. (2004). Fiber Tract-based Atlas of Human White Matter Anatomy. *Radiology* 230, 77–87. doi: 10.1148/radiol.2301021640
- Wechsler, D. (2003). *Wechsler Intelligence Scale for Children*, 4th Edn. San Antonio, TX: Harcourt Assessment.
- Zero to Three (2005). *Diagnostic Classification of Mental Health and Developmental Disorders of Infancy and Early Childhood: Revised Edition*. Washington, DC: ZERO TO THREE Press.

Conflict of Interest Statement: The authors declare that the research was conducted in the absence of any commercial or financial relationships that could be construed as a potential conflict of interest.

Copyright © 2016 Chang, Gratiot, Owen, Brandes-Aitken, Desai, Hill, Arnett, Harris, Marco and Mukherjee. This is an open-access article distributed under the terms of the Creative Commons Attribution License (CC BY). The use, distribution or reproduction in other forums is permitted, provided the original author(s) or licensor are credited and that the original publication in this journal is cited, in accordance with accepted academic practice. No use, distribution or reproduction is permitted which does not comply with these terms.



Asymmetry of Radial and Symmetry of Tangential Neuronal Migration Pathways in Developing Human Fetal Brains

Yuta Miyazaki¹, Jae W. Song² and Emi Takahashi^{3,4,5*}

¹ Department of Medicine, Chiba University School of Medicine, Chiba, Japan, ² Department of Radiology and Biomedical Imaging, Yale University School of Medicine, New Haven, CT, USA, ³ Division of Newborn Medicine, Department of Medicine, Boston Children's Hospital, Harvard Medical School, Boston, MA, USA, ⁴ Athinoula A. Martinos Center for Biomedical Imaging, Massachusetts General Hospital, Harvard Medical School, Charlestown, MA, USA, ⁵ Fetal-Neonatal Neuroimaging and Developmental Science Center, Boston Children's Hospital, Harvard Medical School, Boston, MA, USA

OPEN ACCESS

Edited by:

Hao Huang,
University of Pennsylvania, USA

Reviewed by:

Marina Bentivoglio,
University of Verona, Italy
Gavin John Clowry,
Newcastle University, UK

*Correspondence:

Emi Takahashi
emi@nmr.mgh.harvard.edu

Received: 14 September 2015

Accepted: 02 January 2016

Published: 25 January 2016

Citation:

Miyazaki Y, Song JW and Takahashi E (2016) Asymmetry of Radial and Symmetry of Tangential Neuronal Migration Pathways in Developing Human Fetal Brains. *Front. Neuroanat.* 10:2. doi: 10.3389/fnana.2016.00002

The radial and tangential neural migration pathways are two major neuronal migration streams in humans that are critical during corticogenesis. Corticogenesis is a complex process of neuronal proliferation that is followed by neuronal migration and the formation of axonal connections. Existing histological assessments of these two neuronal migration pathways have limitations inherent to microscopic studies and are confined to small anatomic regions of interest (ROIs). Thus, little evidence is available about their three-dimensional (3-D) fiber pathways and development throughout the entire brain. In this study, we imaged and analyzed radial and tangential migration pathways in the whole human brain using high-angular resolution diffusion MR imaging (HARDI) tractography. We imaged ten fixed, postmortem fetal (17 gestational weeks (GW), 18 GW, 19 GW, three 20 GW, three 21 GW and 22 GW) and eight *in vivo* newborn (two 30 GW, 34 GW, 35 GW and four 40 GW) brains with no neurological/pathological conditions. We statistically compared the volume of the left and right radial and tangential migration pathways, and the volume of the radial migration pathways of the anterior and posterior regions of the brain. In specimens 22 GW or younger, the volume of radial migration pathways of the left hemisphere was significantly larger than that of the right hemisphere. The volume of posterior radial migration pathways was also larger when compared to the anterior pathways in specimens 22 GW or younger. In contrast, no significant differences were observed in the radial migration pathways of brains older than 22 GW. Moreover, our study did not identify any significant differences in volumetric laterality in the tangential migration pathways. These results suggest that these two neuronal migration pathways develop and regress differently, and radial neuronal migration varies regionally based on hemispheric and anterior-posterior laterality, potentially explaining regional differences in the amount of excitatory neurons that migrate along the radial scaffold.

Keywords: development, radial migration, ganglionic eminence, human, diffusion imaging, tractography

INTRODUCTION

Corticogenesis is a complex process that occurs during a critical period of brain development. This process begins with subcortical neuroproliferation, followed by neuronal migration and the formation and refinement of axonal connections (Caviness et al., 1996). Neuronal subtypes of different origins migrate differentially along transient pathways to ultimately establish connections that result in a highly conserved, six-layered neocortical structure. In developing human brains, the radial and tangential migration pathways are two primary sources of neural progenitor cells.

Radial glia are recognized as a primary source of progenitor cells and also serve as a scaffold for migrating neurons in the developing brain. During corticogenesis, a complex process of both symmetric and asymmetric divisions of radial glial cells from the ventricular zone (VZ) has been described, with symmetric divisions attributed to increasing the progenitor pool and asymmetric divisions resulting in neuronal generation (Cai et al., 2002). Neuron subtypes that originate from the radial migration pathway include excitatory glutamatergic projection neurons and GABAergic neurons (Haubensak et al., 2004), which migrate along radial glial fascicles toward the cortical plate (CP; Rakic, 1972, 1988; Bystron et al., 2008; Petanjek et al., 2009a,b). One histologic study showed vimentin immunoreactive radial glia in the developing visual cortex in the occipital lobe of the human brain at specific pre- (14 gestational weeks (GW), 19 GW, 36 GW) and post-term (79 GW) ages, describing the fate and destination of radial glia towards this region during development (Honig et al., 1996). Other studies investigated radial pathways with immunohistochemistry at 10–19 GW (Bayatti et al., 2008) and with lipophilic tracing methods at 14–15 GW (Hansen et al., 2010). However, detailed information regarding radial glial pathways remains unknown as these studies lacked specimens from a critical period of brain development (19–36 GW).

Another major neuronal migratory pathway is the tangential migration pathway, which runs tangential to the CP and from which inhibitory GABAergic interneuron progenitors arise (Wonders and Anderson, 2006). The tangential migration pathway originates from the ganglionic eminence (GE), and although the VZ/subventricular zone (SVZ) are also suggested to be important sources of GABAergic interneurons (Radonjić et al., 2014; Al-Jaberi et al., 2015; Arshad et al., 2015), the GE has been suggested to be a major pool of GABAergic interneurons (Hansen et al., 2013; Ma et al., 2013; Keverne, 2014). Both pathways have been extensively studied in rodents (e.g., Price and Thurlow, 1988; Walsh and Cepko, 1988; Anderson et al., 1997), primates (Rakic, 1972; Radonjić et al., 2014) and to a lesser degree, humans (e.g., Rakić and Sidman, 1969; Letinic and Rakic, 2001; Al-Jaberi et al., 2015). Taken together with the literature on rodents and primates, recent studies on human fetal brains showed that certain aspects of neuronal migration are unique to human corticogenesis, emphasizing the need to examine trajectories of neuronal migration pathways directly in the developing human brain (Letinic and Rakic, 2001; Al-Jaberi et al., 2015).

However, due to limitations inherent to microscopic studies, only small regions of neuronal migratory streams have been histologically investigated, and a systematic understanding of the neuronal migratory streams during the human fetal stage is still elusive.

Initial efforts to assess migratory streams include whole brain analysis by magnetic resonance imaging (MRI; Zhang et al., 2013), and analyses of hemispheric asymmetries (Snyder et al., 1995; Kovalev et al., 2003). Several groups have imaged diffusion coherence of migration pathways by conventional diffusion tensor imaging (DTI) tractography (McKinstry et al., 2002; Huang et al., 2009), but many questions still remain regarding the time-course of the development and regression of the migratory streams as well as the need for comprehensive analyses utilizing whole brain specimens and wider age ranges. Moreover, conventional DTI methods are challenged by the reconstruction of crossing neural fibers in the brain (Tuch et al., 2003).

High-angular resolution diffusion imaging (HARDI) tractography is a technique that enables reconstruction of complicated crossing neural fibers in the brain (Tuch et al., 2003), even in immature brains (Takahashi et al., 2011, 2012, 2013, 2014; Song et al., 2014). Given the technical advantage of HARDI tractography, the present study aims to analyze radial and tangential migration pathways in developing human brains using this technique to understand patterns of neuronal migration during a critical period of brain development.

Disorganized neuronal migration from the radial and tangential pathways has been implicated in many neurological and psychiatric disorders (Marin and Rubenstein, 2001; Gressens, 2006; Volpe, 2009) such as intractable epilepsy (Cusmai et al., 2014), developmental dyslexia (Adler et al., 2013; Platt et al., 2013), autism (Wegiel et al., 2010), and schizophrenia (Benes and Berretta, 2001; McIntosh et al., 2008; Hori et al., 2014; Muraki and Tanigaki, 2015). Thus, a better understanding of this complex developmental process is critical to gain further insight into such disease processes.

MATERIALS AND METHODS

Fetal Brain Specimens

Ten fetal brain specimens were imaged for this study. IRB committees at Partners and Boston Children's Hospital (BCH) approved the use of postmortem specimens for MRI studies. The brains were acquired after obtaining informed consent by the parents. **Table 1** reports the details of GW, the sources of specimens, and whether the brain was imaged *ex- or in vivo*. Seven *postmortem* brain specimens were provided by the Department of Pathology, Brigham and Women's Hospital (BWH; Boston, MA, USA), and three *postmortem* brain specimens were obtained from the Allen Institute Brain Bank (AIBB; Seattle, WA, USA). These brains were grossly normal, and standard autopsy examination of all brains undergoing *postmortem* HARDI revealed minimal or no pathologic abnormalities at the macroscopic level. Any cases with suspected abnormality, malformations and disruption were excluded

TABLE 1 | Characteristics of brain specimens.

Subject	Source	Age	Brain image	Age group
1	BWH	17 GW	<i>Ex vivo</i>	Early
2	BWH	18 GW	<i>Ex vivo</i>	Early
3	AIBB	19 GW	<i>Ex vivo</i>	Early
4	BWH	20 GW	<i>Ex vivo</i>	Early
5	BWH	20 GW	<i>Ex vivo</i>	Early
6	BWH	20 GW	<i>Ex vivo</i>	Early
7	BWH	21 GW	<i>Ex vivo</i>	Early
8	AIBB	21 GW	<i>Ex vivo</i>	Early
9	BWH	21 GW	<i>Ex vivo</i>	Early
10	AIBB	22 GW	<i>Ex vivo</i>	Early
11	BCH	30 GW	<i>In vivo</i>	Late
12	BCH	30 GW	<i>In vivo</i>	Late
13	BCH	34 GW	<i>In vivo</i>	Late
14	BCH	35 GW	<i>In vivo</i>	Late
15	BCH	40 GW	<i>In vivo</i>	Late
16	BCH	40 GW	<i>In vivo</i>	Late
17	BCH	40 GW	<i>In vivo</i>	Late
18	BCH	40 GW	<i>In vivo</i>	Late

BWH, Brigham and Women's Hospital; AIBB, Allen Institute Brain Bank; BCH, Boston Children's Hospital; GW, Gestational week.

from this study. *Ex vivo* fetal and postnatal brains and living postnatal infant brains were included in the study, which allowed us to reveal brain structure in unforeseen detail. Although *ex vivo* imaging is superior, we have previously shown that *ex-* and *in vivo* imaging produces comparable tracking results in brains at the fetal, neonatal, and toddler ages (Xu et al., 2014).

In Vivo Subjects

Eight living participants underwent clinically-indicated brain MRI studies that were interpreted to show no abnormalities. The IRB at BCH approved the retrospective use of *in vivo* imaging data. Indications for imaging included concern for hypoxic ischemic injury, apnea and transient choreiform movements after an upper respiratory tract infection. None had clinical concerns for a congenital malformation or genetic disorder. All MR image acquisitions were performed under protocols approved by each hospital's institutional review board for human research.

Tissue Preparation for HARDI

At the time of autopsy, all brains were immersion fixed. The brains from BWH were stored in 4% paraformaldehyde, and the brains from AIBB were stored in 4% periodate-lysine-paraformaldehyde (PLP). During MR image acquisition, BWH brains were placed in Fomblin solution (Ausimont, Thorofare, NJ, USA; Takahashi et al., 2012), and AIBB brains were placed in 4% PLP. While these different solutions tend to change the background contrast (i.e., a dark background outside of the brain is often visualized using Fomblin, and a bright background using PLP), these solutions do not specifically change diffusion properties (e.g., FA and ADC) within the brain parenchyma (Kolasinski et al., 2013; Song et al., 2014).

Diffusion MRI Procedures

Six postmortem brain specimens from BWH were imaged with a 4.7T Bruker Biospec MR system, and three specimens from the AIBB were imaged with a 3T Siemens MR system at the A. A. Martinos Center, Massachusetts General Hospital, Boston, MA, USA. The 3T system was used to accommodate the AIBB brains that were *in cranio* and did not fit in the 4.7T bore. To improve the imaging quality and obtain the best signal-to-noise and high spatial resolution, we used custom-made radio-frequency (RF) coils with one channel on the 4.7T and 3T systems (Takahashi et al., 2012; Xu et al., 2014). We used multiple scanner systems to utilize the best-fit RF coils to ensure optimal imaging with good signal to noise.

For the BWH brains, a three-dimensional (3-D) diffusion-weighted spin-echo echo-planar imaging (SE-EPI) sequence was used with a repetition time/echo time (TR/TE) of 1000/40 ms, with an imaging matrix of $112 \times 112 \times 112$ pixels. Sixty diffusion-weighted measurements (with the strength of the diffusion weighting, $b = 8000 \text{ s/mm}^2$) and one non-diffusion-weighted measurement (no diffusion weighting or $b = 0 \text{ s/mm}^2$) were acquired with $\delta = 12.0 \text{ ms}$ and $\Delta = 24.2 \text{ ms}$. The spatial resolution was $440 \times 500 \times 500 \mu\text{m}$. For the brains from the AIBB, diffusion-weighted data were acquired over two averages using a steady-state free-precession sequence with TR/TE = 24.82/18.76 ms, $\alpha = 60^\circ$, and the spatial resolution was $400 \times 400 \times 400 \mu\text{m}$. Diffusion weighting was isotropically distributed along 44 directions ($b = 730 \text{ s/mm}^2$) with 4 $b = 0$ images. We determined the highest spatial resolution for each brain specimen with an acceptable signal-to-noise ratio of more than 130 for tractography.

The brains of living participants were imaged on a 3T Siemens MR system, BCH, Boston, MA, USA. The diffusion pulse sequence used was a diffusion-weighted SE-EPI sequence, TR/TE 8320/88 ms, with an imaging matrix of $128 \times 128 \times 64$ pixels. The spatial resolution was $2 \times 2 \times 2 \text{ mm}$. Thirty diffusion-weighted measurements ($b = 1000 \text{ s/mm}^2$) and five non-diffusion-weighted measurements ($b = 0 \text{ s/mm}^2$) were acquired with $\delta = 40 \text{ ms}$ and $\Delta = 68 \text{ ms}$.

Reconstruction and Identification of Tractography Pathways

We used Diffusion Toolkit and TrackVis¹ to reconstruct and visualize neural migration pathways. A streamline algorithm for diffusion tractography was used (Mori et al., 1999), described in previous publications (Schmahmann et al., 2007; D'Arceuil et al., 2008; Takahashi et al., 2010, 2011, 2012). The term "streamline" refers to connecting tractography pathways using a local maximum or maxima. This method is true for both DTI and HARDI. The streamline technique is limited in its ability to resolve crossing pathways when used with the traditional DTI technique because one simply connects the direction of the principal eigenvector on a tensor to produce the DTI tractography pathways. This feature is a recognized limitation of DTI (Mori et al., 1999). Hence, in the current

¹<http://trackvis.org>

study, we used HARDI, which can theoretically detect multiple local maxima on an orientation distribution function (ODF). Using each local maxima on an ODF, we applied the streamline algorithm to initiate and continue tractography (Tuch et al., 2003), thus enabling us to identify crossing pathways within a voxel.

Trajectories were propagated by consistently pursuing the orientation vector of least curvature. Tracking was terminated when the angle between two consecutive orientation vectors was greater than the given threshold (40°) or when the fibers extended outside of the brain surface using a brain mask. The brain mask volumes were used to terminate tractography structures instead of the FA threshold (Schmahmann et al., 2007; Wedeen et al., 2008; Takahashi et al., 2010, 2012; Vishwas et al., 2010), because progressive myelination and crossing fibers in the developing brain can result in low FA values and the use of an FA threshold may potentially incorrectly terminate tractography tracking in regions with low FA values.

Regions of Interest (ROIs)

Using previously reported methodology (Takahashi et al., 2012; Kolasinski et al., 2013), a regions of interest (ROIs) approach was used to identify radial and tangential tractography pathways. ROIs for the CP, VZ/SVZ, and GE were identified (Figures 1A,B). We used ROIs of the region of VZ/SVZ and CP for identification of the radial migration pathway (Figure 1A). Tangential pathways were identified using ROIs of the GE (Figure 1B). Previous studies also have shown the GE structure by manually identifying its location (Huang et al., 2009; Kostovic and Vasung, 2009; Takahashi et al., 2012; Song et al., 2014).

Statistical Analyses

Volume measurements are automatically derived by TrackVis for each migration pathway. The volume of pathways was calculated

by counting the number of voxels that touched or passed through the detected pathways, and was compared at different developmental time points.

We defined left and right radial pathways separately between the VZ/SVZ and CP in each hemisphere. We also defined the anterior and posterior radial pathways as the front or posterior half of the radial pathway. Due to challenges in defining the “middle” coronal plane in early fetal stages from only anatomic information without gyral or other mature subcortical structures, we instead measured the length between the anterior and posterior edges of the brain and defined a middle coronal plane to separate the anterior and posterior radial pathways. Left/right hemispheric asymmetry was tested for both the radial and tangential migration pathways, and anterior-posterior differences were tested for the radial pathway.

We statistically analyzed asymmetry with a laterality index (LI), calculated by the following formula:

$$LI_{LR} = (L - R) / \{0.5 \times (L + R)\} \text{ for comparison of Left and Right hemispheres}$$

$$LI_{AP} = (A - P) / \{0.5 \times (A + P)\} \text{ for comparison of Anterior and Posterior regions}$$

LIs range from -2 to 2 , with positive and negative LI values corresponding to left- and rightward, and anterior and posterior asymmetries, respectively (Caviness et al., 1996). The asymmetries of the radial and tangential migration pathways using LIs were statistically analyzed with SPSS version 19.0.0 (IBM SPSS, Chicago, IL, USA). Statistical significance was set at $P < 0.01$.

RESULTS

Qualitative Description of the Development and Regression Time-Lines of Radial and Tangential Migration Pathways

Development and regression of the radial and tangential migration pathways are shown in Figures 2, 3. Radial and tangential migration pathways were both identified in the early age group (17–22 GW), while only radial pathways were identified in the late age group (30–40 GW). The tangential migration pathways in the late age group (30 and 34 GW) became sparse, and after 34 GW they were not identified by tractography.

Radial Migration Pathways

Figure 2 shows reconstructed radial tractography pathways (perpendicular to the cortical mantle) running through the cerebral wall in the sagittal views (Figure 2). Radial pathways gradually decreased density by 21 GW (Figure 2, white arrowheads). Residual fiber pathways were still observed at 40 GW in a few brains suggestive of individual variability. Gradual disappearance of the radial pathways was not evenly observed in the whole brain. The disappearance of radial

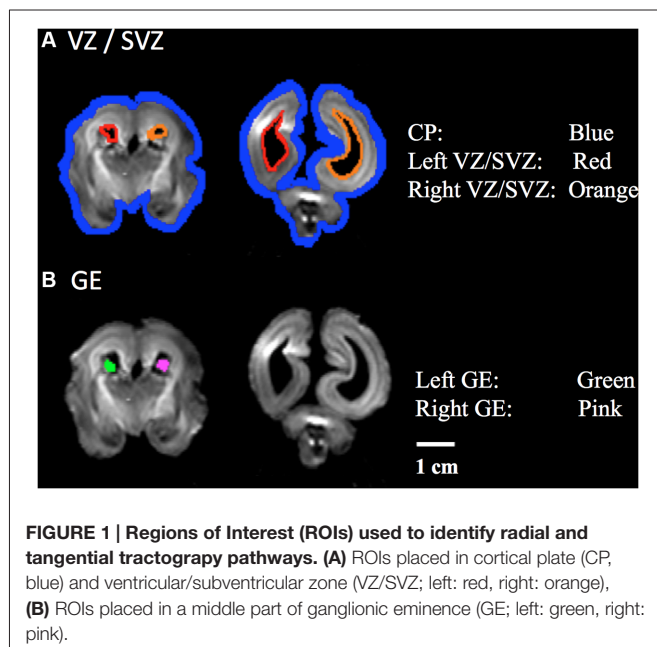


FIGURE 1 | Regions of Interest (ROIs) used to identify radial and tangential tractography pathways. (A) ROIs placed in cortical plate (CP, blue) and ventricular/subventricular zone (VZ/SVZ; left: red, right: orange), **(B)** ROIs placed in a middle part of ganglionic eminence (GE; left: green, right: pink).

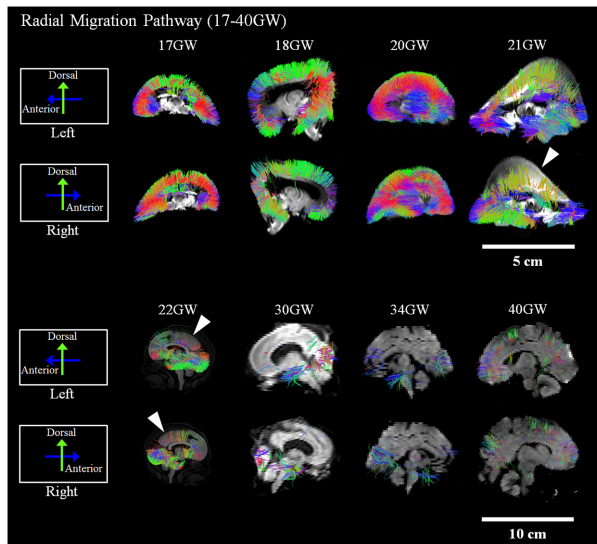


FIGURE 2 | Radial pathways. Tractography at representative ages of the radial pathways are shown in sagittal views. White arrowheads show brain regions where the radial pathways became progressively sparse. Scale bar = 5 cm for 17–21 GW, and 10 cm for 22–40 GW.

pathways by tractography started in the dorsal parietal and superior frontal regions at 21 GW and progressed in an anterior, inferior direction towards the inferior frontal lobe after 21 GW (**Figure 2**, white arrowheads). At 30 GW, a large segment of the radial pathways persisted in the occipital lobe. However, by 40 GW, the density of the radial pathways appeared substantially decreased, globally.

Tangential Migration Pathways

Reconstructed GE tractography pathways are shown in **Figure 3**. Pathways likely corresponding to the GE migration stream were very thick at 17 GW and revealed some radial pathways emanating from the stream at the most distal anterior and posterior regions as it penetrated the cortical mantle (**Figure 3**, white arrowheads). These radial pathways were contiguous with tangentially oriented pathways, as previously described by Kolasinski et al. (2013). Until 22 GW, tangential migration pathways appeared tightly packed with gradual thinning in the sagittal planes (**Figure 3**). After 30 GW, the tangential migration pathways became sparser, and after 34 GW, the tangential migration pathways were not identifiable by tractography (**Figure 3**, white arrowheads).

Quantitative Results

Hemispheric Asymmetry

Next, we studied the volumetric laterality indices (LIs) for the radial and tangential migration pathways in both the early and late ages (**Figures 4A,B**). Significant leftward asymmetry in the radial pathways in the early age group was observed ($p = 0.0045$). In contrast, asymmetry in the late age group was not observed ($p > 0.01$). When combining all ages, significant

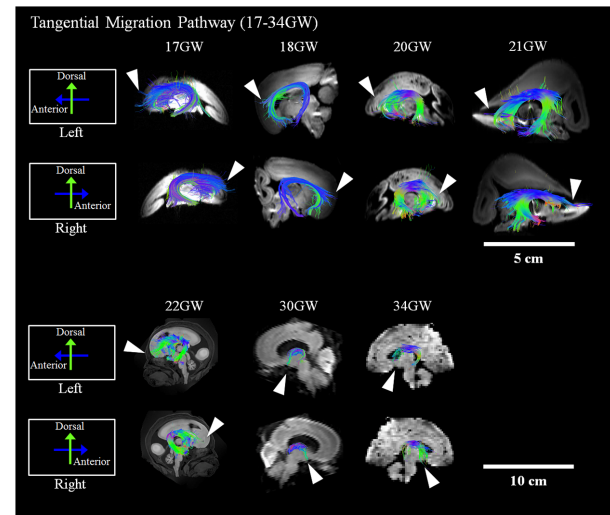


FIGURE 3 | Tangential migration pathways. Tractography at representative ages of the tangential migration pathways are shown in sagittal views. White arrowheads show examples of the tangential migration tract branching into the cerebral walls. Scale bar = 5 cm for 17–21 GW, and 10 cm for 22–40 GW.

leftward asymmetry of the radial pathways emerged ($p = 0.0019$). By contrast, statistically significant hemispheric asymmetry was not observed in any age groups for the GE pathway ($p > 0.01$).

Anterior-Posterior Differences

Results of comparisons between the volume of the anterior and posterior regions of the identified radial pathways are shown in **Figure 4C**. In the early age group, the posterior region was significantly larger than the anterior region ($p < 0.01$). In contrast, no significant difference was observed in the late age group of the radial pathway ($p > 0.01$). Combining all ages, no significant volumetric difference was observed between the anterior and posterior regions of the radial pathways ($p = 0.55$).

DISCUSSION

We investigated two major neural migration pathways, the radial and tangential migration pathways, in human fetal and newborn brains (17–40 GW) using HARDI tractography. Due to limitations of microscopy, previous studies have performed only limited regional analyses of these migration pathways in developing human brains. Our new findings are: (1) significant left-right hemispheric asymmetry and anterior-posterior asymmetry of radial migration pathways between 17 GW and 22 GW by analyzing whole human fetal brain with MR imaging; (2) there were no significant asymmetry of tangential migration pathways between 17 GW and 22 GW, and no significant asymmetry of radial migration pathways between 30 GW and 40 GW. Our previous study (Kolasinski et al., 2013) reported on the radial and tangential migration pathways, but the study just used three specimens between 19 GW and 21 GW and qualitatively described trajectories of pathways without

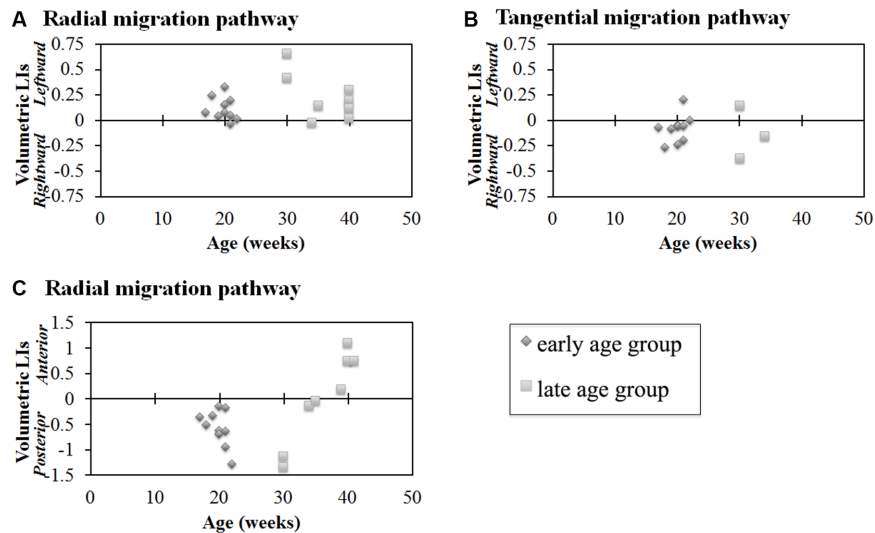


FIGURE 4 | Lateral indices (LIs) for hemispheric asymmetry (A,B) and anterior-posterior asymmetry (C) of radial pathways (A,C) and tangential pathways (B). Radial pathways in the early age group revealed significant hemispheric asymmetry ($p = 0.0045$) (A). In contrast, significant hemispheric asymmetry was not observed in the tangential pathways ($p > 0.01$) (B). In the early age group, the posterior region was significantly larger than the anterior region ($p < 0.0001$, [1.75×10^{-5}]) (C). In contrast, no significant difference was observed in the late age group (C). Diamond shape: early age group (17–22 GW); square: late age group (30–40 GW).

investigating asymmetry. These results suggest that these two neuronal migration pathways develop and regress differently. This study showed, for the first time, hemispheric and anterior-posterior asymmetry of neuronal migration pathways in human fetal brains.

Radial Migration Pathway—Development and Regression Time Line

Many lines of evidence suggest that the majority of radial pathways contribute excitatory glutamatergic projection neurons (Rakic, 1972, 1988; Bystron et al., 2008; Petanjek et al., 2009a,b). Therefore, the volume of the radial pathway may, in part, reflect the relative degree of density of this subtype of glutamatergic neurons originating from this pathway. Our study revealed that the disappearance of radial pathways began at 21 GW. This thinning of radial tractography pathways was most conspicuous in the dorsal parietal and frontal regions and progressed to the inferior frontal lobe around 22 GW. This observation suggests a determined spatiotemporal direction of migration of excitatory neurons that arise from the radial pathway.

Radial Migration Pathway—Hemispheric Asymmetry

While the radial tractography pathways showed structural asymmetries, the tangential migration pathways revealed no significant hemispheric asymmetry in volume in this study. These results suggest that, at least in the pathways that supply inhibitory interneurons to

the cortex, there is no demonstrable laterality by tractography.

The volume of the radial pathway in the left hemisphere was significantly larger than that of the right hemisphere in the early age group (17–22 GW) in our study. In contrast, no significant difference between the left- and right hemispheres was observed in the late age group (30–40 GW). Previous studies reported that the left hemisphere is volumetrically larger than the right hemisphere in right-handed adults (Büchel et al., 2004), and it has been suggested that the leftward asymmetry in Broca's area contributes to human language acquisition (Schenker et al., 2010). Such normal hemispheric asymmetry in adults is often not observed in neurological and psychiatric disorders (e.g., Mackay et al., 2003). However, to date, very few studies have explored the developmental origins of this asymmetry. Although handedness was not confirmed, a larger left temporal area was already observed in the fetal stage by 30 GW (Chi et al., 1977). Even earlier, leftward asymmetry of gyral folding in specific temporal areas started to be observed from 23 GW (Habas et al., 2012). By term (or term-equivalent ages), leftward asymmetries were also detected in some tractography pathways likely corresponding to the superior longitudinal fasciculus, thalamocortical pathways, and the corticospinal tract (Liu et al., 2010). Given the link between neuronal migration and gyral formation in cobblestone lissencephaly (Dobyns et al., 1996), classical lissencephaly (Glesson, 2000; Lammens, 2000; Leventer et al., 2000), and polymicrogyria (Chang et al., 2004; Guerrini and Filippi, 2005; Jansen and Andermann, 2005), one can speculate that the leftward volumetric asymmetry of radial neuronal migration pathways may contribute to hemispheric asymmetry of the number of neurons in the cortex, followed by

hemispheric asymmetry of axonal pathways from the neurons. In fact, the earliest gestational age where Habas et al. (2012) found hemispheric asymmetry of gyral structures (23 GW) coincides with the early age group of the current study (17–22 GW) when we observed leftward asymmetry. Future studies are necessary to directly link the transient leftward asymmetry of the radial pathway to the hemispheric asymmetry in mature brains.

Radial Migration Pathway—Anterior-Posterior Asymmetry

In the current study, the volume of the radial pathway in the posterior region was significantly larger compared to the anterior region when examining ages up to 22 GW in our study. This quantitative analysis was in agreement with the visual tractography of the radial pathways, which revealed a gradual thinning of this pathway in the parieto-occipital regions at 21 GW. This thinning of pathways appeared to progress towards the frontal region by 22 GW. Previous studies reported a higher neural density in the posterior than in the anterior brain regions in primates (Cahalane et al., 2012; Charvet et al., 2015), presumably in adult mature brains, although the studies did not specify the ages of the brains. Our result suggests that a higher density of the radial tractography pathways in the posterior region contributes to the anterior-posterior gradient in neuron density.

While the regression of the radial pathways in the dorsal parietal and frontal regions continued through 21 GW, the regression of the radial pathways in the inferior frontal regions seemed to begin after 22 GW. Although radial pathways in the occipitoparietal regions also decreased in these ages, the late-onset regression in the inferior frontal regions seemed greater than in the occipitoparietal regions, which likely contributed to the relative increase in volume of the posterior radial pathways compared to those in the anterior region. At 30 GW, almost no anterior radial pathways were visible, while there were some residual radial pathways in the posterior regions. By 34 GW and 40 GW, radial pathways almost all disappeared throughout the brain. One reason why no significant difference between the anterior and posterior regions was observed in the late age group may be due to the uneven number of specimens in each age group within the late age group. For instance, in the late age group, only 30 GW ($n = 2$ of 8) brains revealed radial pathways remaining in the posterior regions, yet 40 GW brains ($n = 4$ of 8), which revealed sparse to no pathways in the posterior regions, comprised half of the specimens in this late age group. For future studies, increasing the number of brains and evening out the distribution of ages, specifically of specimens in the 23–29 GW, would be important to gain a more comprehensive understanding of the regression of radial migration pathways.

Tangential Migration Pathway

The tangential migration pathways were observed in the early age group (17–22 GW) and at the beginning of the late age group (30–34 GW), but were not visible at 40 GW. This

observation is consistent with the literature describing the gradual disappearance of the GE by 34 GW (Rakić and Sidman, 1969). Many lines of evidence in primate and human studies report that a substantial percentage of cortical GABAergic neurons arise from the GE (Letinic et al., 2002; Rakic and Zecevic, 2003; Yu and Zecevic, 2011) with the peak of GABAergic neurogenesis occurring at the end of the second trimester of gestation (Petanjek et al., 2008; 15–24 GW). Similarly, in our study, the tangential migration pathways were not distinctly identifiable by tractography in brains developed past the second trimester. This finding is consistent with the literature reporting this pathway as a transient anatomic structure. However, during the early ages of development when the GE was identifiable by tractography, no significant asymmetry was observed.

While Arshad et al. (2015) claimed that interneuron generation in the GE extends beyond 35 GW (not PCW, however), we only showed tangential tractography pathways until 34 GW in the current study. A limitation of our study is a sampling gap between 34–40 GW. Thus it is possible that tractography may have been detectable past 34 GW, if samples were available. Another potential reason for these controversial results is the age grouping in the study by Arshad et al. (2015). They grouped 29–35 GW and 35–40 GW together. The only figure that they showed for the results from the 35–40 GW group (Figure 6, Arshad et al., 2015) is not really convincing regarding the existence of interneuron generation at this age range. Other figures showing results only until 35 GW showed some evidence for interneuron generation, but because 35 GW was grouped with 29–34 GW, it is possible that a younger population primarily contributed to their results.

The coherent diffusivity within the GE visualized by tractography during the early fetal ages is likely attributable to the tangential migratory routes on scaffolds of corticofugal fibers. This directionality of migration has been shown in investigational studies using tracer-labeling (Denaxa et al., 2001) and fate mapping studies (Wichterle et al., 2001). These studies have shown that during the period of corticogenesis, migrating neurons follow multiple tangential routes to their destination in the developing cortex. More specifically, cells from the lateral GE migrate ventrally and anteriorly to give rise to neurons in the striatum. Cells from the medial GE have been shown to migrate dorsally and posteriorly (Wichterle et al., 2001). The temporospatial migratory pattern likely contributes to the diffusivity seen within the GE in this study. Although many studies confirming this tangential migratory pattern have been performed in mice, similar findings have also been described in humans (Hansen et al., 2013; Ma et al., 2013) and further support our tractography findings in human fetal brains.

CONCLUSION

In this study, we examined whether volumetric asymmetries by tractography were present in two critical neuronal migratory

pathways, the radial and tangential migration pathways, from which progenitor neurons have been reported to migrate in the process of corticogenesis in developing human fetal brains. Several conclusions may be drawn from this study. First, our results confirm a postero-dorsal to antero-ventral direction of migration of the radial pathway based on the gradual disappearance of tractography pathways. By tractography, the volume of radial pathways was greater in the posterior region than in the anterior brain region at early stages of development (22 GW and younger). Second, volumetric asymmetry for only the radial pathways was statistically significant in the early age group (22 GW and younger). Third, no volumetric hemispheric asymmetry of the tangential pathway emerged, contrasting with the radial pathway. Taken together, these findings suggest hemispheric volumetric asymmetry related to neural progenitors from the radial glial pathway is established early in development, which contrasts with the GE. Describing the anatomic development and regression of these neuronal migratory pathways is critical as many neurologic and psychological disorders are described to have underlying disorganized corticogenesis. Future investigations aim to include a more comprehensive range of developmental stages to enable a more thorough description of the developmental changes, as well as comparisons of normal and diseased brains to understand what may contribute to the underlying problems in the formation of brain connectivity.

REFERENCES

- Adler, W. T., Platt, M. P., Mehlhorn, A. J., Haight, J. L., Currier, T. A., Etchegaray, M. A., et al. (2013). Position of neocortical neurons transfected at different gestational ages with shRNA targeted against candidate dyslexia susceptibility genes. *PLoS One* 8:e65179. doi: 10.1371/journal.pone.0065179
- Al-Jaberi, N., Lindsay, S., Sarma, S., Bayatti, N., and Clowry, G. J. (2015). The early fetal development of human neocortical GABAergic interneurons. *Cereb. Cortex* 25, 631–645. doi: 10.1093/cercor/bht254
- Anderson, S. A., Eisenstat, D. D., Shi, L., and Rubenstein, J. L. R. (1997). Interneuron migration from basal forebrain to neocortex: dependence on *dlx* genes. *Science* 278, 474–476. doi: 10.1126/science.278.5337.474
- Arshad, A., Vose, L. R., Vinukonda, G., Hu, F., Yoshikawa, K., Csiszar, A., et al. (2015). Extended production of cortical interneurons into the third trimester of human gestation. *Cereb. Cortex* doi: 10.1093/cercor/bhv074 [Epub ahead of print].
- Bayatti, N., Moss, J. A., Sun, L., Ambrose, P., Ward, J. F. H., Lindsay, S., et al. (2008). A molecular neuroanatomical study of the developing human neocortex from 8 to 17 postconceptional weeks revealing the early differentiation of the subplate and subventricular zone. *Cereb. Cortex* 18, 1536–1548. doi: 10.1093/cercor/bhm184
- Benes, F. M., and Berretta, S. (2001). GABAergic interneurons: implications for understanding schizophrenia and bipolar disorder. *Neuropsychopharmacology* 25, 1–27. doi: 10.1016/s0893-133x(01)00225-1
- Büchel, C., Raedler, T., Sommer, M., Sach, M., Weiller, C., and Koch, M. A. (2004). White matter asymmetry in the human brain: a diffusion tensor MRI study. *Cereb. Cortex* 14, 945–951. doi: 10.1093/cercor/bhh055
- Bystron, I., Blakemore, C., and Rakic, P. (2008). Development of the human cerebral cortex: Boulder Committee revisited. *Nat. Rev. Neurosci.* 9, 110–122. doi: 10.1038/nrn2252
- Cahalane, D. J., Charvet, C. J., and Finlay, B. L. (2012). Systematic, balancing gradients in neuron density and number across the primate isocortex. *Front. Neuroanat.* 6:28. doi: 10.3389/fnana.2012.00028
- Cai, L., Hayes, N. L., Takahashi, T., Caviness, V. S. Jr., and Nowakowski, R. S. (2002). Size distribution of retrovirally marked lineages matches prediction from population measurements of cell cycle behavior. *J. Neurosci. Res.* 69, 731–744. doi: 10.1002/jnr.10398
- Caviness, V. S., Meyer, J., Makris, N., and Kennedy, D. N. (1996). MRI-based topographic parcellation of human neocortex: an anatomically specified method with estimate of reliability. *J. Cogn. Neurosci.* 8, 566–587. doi: 10.1162/jocn.1996.8.6.566
- Chang, B. S., Piao, X., Giannini, C., Cascino, G. D., Scheffer, I., Woods, C. G., et al. (2004). Bilateral generalized polymicrogyria (BGP): a distinct syndrome of cortical malformation. *Neurology* 62, 1722–1728. doi: 10.1212/01.wnl.0000125187.52952.e9
- Charvet, C. J., Cahalane, D. J., and Finlay, B. L. (2015). Systematic, cross-cortex variation in neuron numbers in rodents and primates. *Cereb. Cortex* 25, 147–160. doi: 10.1093/cercor/bht214
- Chi, J. G., Doelling, E. C., and Gilles, F. H. (1977). Left-right asymmetries of the temporal speech areas of the human fetus. *Arch. Neurol.* 34, 346–348. doi: 10.1001/archneur.1977.00500180040008
- Cusmai, R., Verrotti, A., Moavero, R., Curatolo, P., Battaglia, D., Matricardi, S., et al. (2014). Rufinamide for the treatment of refractory epilepsy secondary to neuronal migration disorders. *Epilepsy Res.* 108, 542–546. doi: 10.1016/j.epilepsyres.2014.01.013
- D'Arceuil, H., Liu, C., Levitt, P., Thompson, B., Kosofsky, B., and de Crespigny, A. (2008). Three-dimensional high-resolution diffusion tensor imaging and tractography of the developing rabbit brain. *Dev. Neurosci.* 30, 262–275. doi: 10.1159/000110503
- Denaxa, M., Chan, C. H., Schachner, M., Pamavelas, J. G., and Karagogeos, D. (2001). The adhesion molecule TAG-1 mediates the migration of cortical

AUTHOR CONTRIBUTIONS

ET performed the experiments. YM, JWS, and ET analyzed the data and wrote the paper.

ACKNOWLEDGMENTS

This work was supported by Boston Children's Hospital (BCH), NICHD (R01HD078561, R21HD069001, R03NS091587; ET). This research was carried out in part at the Athinoula A. Martinos Center for Biomedical Imaging at the Massachusetts General Hospital, using resources provided by the Center for Functional Neuroimaging Technologies, NIH P41RR14075, a P41 Regional Resource supported by the Biomedical Technology Program of the National Center for Research Resources (NCRR), National Institutes of Health. This work also involved the use of instrumentation supported by the NCRR Shared Instrumentation Grant Program (NIH S10RR023401, S10RR019307, and S10RR023043) and High-End Instrumentation Grant Program (NIH S10RR016811). This study was conducted partly using postmortem human brain specimens from the tissue collection at the Department of Neurobiology at Yale University School of Medicine (supported by grant NIH MH081896), which form a part of the BrainSpan Consortium collection (<http://www.brainspan.org>). The other brain specimens were kindly provided by Dr. Rebecca D. Folkerth, Brigham and Women's Hospital, Boston Children's Hospital and Harvard Medical School.

- interneurons from the ganglionic eminence along the corticofugal fiber system. *Development* 128, 4635–4644.
- Dobyns, W. B., Andermann, E., Andermann, F., Czapansky-Beilman, D., Dubeau, F., Dulac, O., et al. (1996). X-linked malformations of neuronal migration. *Neurology* 47, 331–339. doi: 10.1212/wnl.47.2.331
- Glesson, J. C. (2000). Classical lissencephaly and double cortex (subcortical band heterotopia): LIS1 and doublecortin. *Curr. Opin. Neurol.* 13, 121–125. doi: 10.1097/00019052-200004000-00002
- Gressens, P. (2006). Pathogenesis of migration disorders. *Curr. Opin. Neurol.* 19, 135–140. doi: 10.1097/01.wco.0000218228.73678.e1
- Guerrini, R., and Filippi, T. (2005). Neuronal migration disorders, genetics and epileptogenesis. *J. Child Neurol.* 20, 287–299. doi: 10.1177/08830738050200040401
- Habas, P. A., Scott, J. A., Roosta, A., Rajagopalan, V., Kim, K., Rousseau, F., et al. (2012). Early folding patterns and asymmetries of the normal human brain detected from *in utero* MRI. *Cereb. Cortex* 22, 13–25. doi: 10.1093/cercor/bhr053
- Hansen, D. V., Lui, J. H., Flandin, P., Yoshikawa, K., Rubenstein, J. L., Alvarez-Buylla, A., et al. (2013). Non-epithelial stem cells and cortical interneuron production in the human ganglionic eminences. *Nat. Neurosci.* 16, 1576–1587. doi: 10.1038/nn.3541
- Hansen, D. V., Lui, J. H., Parker, P. R. L., and Kriegstein, A. R. (2010). Neurogenic radial glia in the outer subventricular zone of human neocortex. *Nature* 464, 554–561. doi: 10.1038/nature08845
- Haubensak, W., Attardo, A., Denk, W., and Huttner, W. B. (2004). Neurons arise in the basal neuroepithelium of the early mammalian telencephalon: a major site of neurogenesis. *Proc. Natl. Acad. Sci. U S A* 101, 3196–3201. doi: 10.1073/pnas.0308600100
- Honig, L. S., Herrmann, K., and Shatz, C. J. (1996). Developmental changes revealed by immunohistochemical markers in human cerebral cortex. *Cereb. Cortex* 6, 794–806. doi: 10.1093/cercor/6.6.794
- Hori, K., Nagai, T., Shan, W., Sakamoto, A., Taya, S., Hashimoto, R., et al. (2014). Cytoskeletal regulation by AUTS2 in neuronal migration and neurogenesis. *Cell Rep.* 9, 2166–2179. doi: 10.1016/j.celrep.2014.11.045
- Huang, H., Xue, R., Zhang, J., Ren, T., Richards, L. J., Yarowsky, P., et al. (2009). Anatomical characterization of human fetal brain development with diffusion tensor magnetic resonance imaging. *J. Neurosci.* 29, 4263–4273. doi: 10.1523/jneurosci.2769-08.2009
- Jansen, A., and Andermann, E. (2005). Genetics of the polymicrogyria syndrome. *J. Med. Genet.* 42, 369–378. doi: 10.1136/jmg.2004.023952
- Keverne, E. B. (2014). Significance of epigenetics for understanding brain development, brain evolution and behaviour. *Neuroscience* 264, 207–217. doi: 10.1016/j.neuroscience.2012.11.030
- Kolasinski, J., Takahashi, E., Stevens, A. A., Benner, T., Fisch, B., Zöllei, L., et al. (2013). Randal and tangential neuronal migration pathways in the human fetal brain: anatomically distinct patterns of diffusion MRI coherence. *Neuroimage* 79, 412–422. doi: 10.1016/j.neuroimage.2013.04.125
- Kostovic, I., and Vasung, L. (2009). Insights from *in vitro* fetal magnetic resonance imaging of cerebral development. *Semin. Perinatol.* 33, 220–233. doi: 10.1053/j.semper.2009.04.003
- Kovalev, V. A., Kruggel, F., and von Cramon, D. Y. (2003). Gender and age effects in structural brain asymmetry as measured by MRI texture analysis. *Neuroimage* 19, 895–905. doi: 10.1016/s1053-8119(03)00140-x
- Lammens, M. (2000). Neuronal migration disorders in man. *Eur. J. Morphol.* 38, 327–333. doi: 10.1076/ejom.38.5.0327
- Letinic, K., and Rakic, P. (2001). Telencephalic origin of human thalamic GABAergic neurons. *Nat. Neurosci.* 4, 931–936. doi: 10.1038/nn0901-931
- Letinic, K., Zoncu, R., and Rakic, P. (2002). Origin of GABAergic neurons in the human neocortex. *Nature* 417, 645–649. doi: 10.1038/nature00779
- Leventer, R. J., Mills, P. L., and Dobyns, W. B. (2000). X-linked malformations of cortical development. *Am. J. Med. Genet.* 97, 213–220. doi: 10.1002/1096-8628(200023)97:3<213::aid-ajmg1039>3.0.co;2-w
- Liu, Y., Balériaux, D., Kavec, M., Metens, T., Absil, J., Denolin, V., et al. (2010). Structural asymmetries in motor and language networks in a population of healthy preterm neonates at term equivalent age: a diffusion tensor imaging and probabilistic tractography study. *Neuroimage* 51, 783–788. doi: 10.1016/j.neuroimage.2010.02.066
- Ma, T., Wang, C., Wang, L., Zhou, X., Tian, M., Zhang, Q., et al. (2013). Subcortical origins of human and monkey neocortical interneurons. *Nat. Neurosci.* 16, 1588–1597. doi: 10.1038/nn.3536
- Mackay, C. E., Barrick, T. R., Roberts, N., DeLisi, L. E., Maes, F., Vandermeylen, D., et al. (2003). Application of a new image analysis technique to study brain asymmetry in schizophrenia. *Psychiatry Res.* 124, 25–35. doi: 10.1016/s0925-4927(03)00088-x
- Marín, O., and Rubenstein, J. L. (2001). A long, remarkable journey: tangential migration in the telencephalon. *Nat. Rev. Neurosci.* 2, 780–790. doi: 10.1038/35097509
- McIntosh, A. M., Muñoz Maniega, S., Lymer, G. K. S., McKirdy, J., Hall, J., Sussmann, J. E. D., et al. (2008). White matter tractography in bipolar disorder and schizophrenia. *Biol. Psychiatry* 64, 1088–1092. doi: 10.1016/j.biopsych.2008.07.026
- McKinsty, R. C., Mathur, A., Miller, J. H., Ozcan, A., Snyder, A. Z., Scheff, G. L., et al. (2002). Radial organization of developing preterm human cerebral cortex revealed by non-invasive water diffusion anisotropy MRI. *Cereb. Cortex* 12, 1237–1243. doi: 10.1093/cercor/12.12.1237
- Mori, S., Crain, B. J., Chacko, V. P., and van Zijl, P. C. (1999). Three-dimensional tracking of axonal projections in the brain by magnetic resonance imaging. *Ann. Neurol.* 45, 265–269. doi: 10.1002/1531-8249(199902)45:2<265::aid-ana21>3.0.co;2-3
- Muraki, K., and Tanigaki, K. (2015). Neuronal migration abnormalities and its possible implications for schizophrenia. *Front. Neurosci.* 9:74. doi: 10.3389/fnins.2015.00074
- Petanjek, Z., Berger, B., and Esclapez, M. (2009a). Origins of cortical GABAergic neurons in the cynomolgus monkey. *Cereb. Cortex* 19, 249–262. doi: 10.1093/cercor/bhn078
- Petanjek, Z., Kostović, I., and Esclapez, M. (2009b). Primate-specific origins and migration of cortical GABAergic neurons. *Front. Neuroanat.* 3:26. doi: 10.3389/neuro.05.026.2009
- Petanjek, Z., Dujmović, A., Kostović, I., and Esclapez, M. (2008). Distinct origin of GABA-ergic neurons in forebrain of man, nonhuman primates and lower mammals. *Coll. Antropol.* 32, 9–17.
- Platt, M. P., Adler, W. T., Mehlhorn, A. J., Johnson, G. C., Wright, K. A., Choi, R. T., et al. (2013). Embryonic disruption of the candidate dyslexia susceptibility gene homolog Kiaa0319-like results in neuronal migration disorders. *Neuroscience* 248, 585–593. doi: 10.1016/j.neuroscience.2013.06.056
- Price, J., and Thurlow, L. (1988). Cell lineage in the rat cerebral cortex: a study using retroviral-mediated gene transfer. *Development* 104, 473–482.
- Radonjić, N. V., Ayoub, A. E., Memi, F., Yu, X., Maroof, A., Jakovcević, I., et al. (2014). Diversity of cortical interneurons in primates: the role of the dorsal proliferative niche. *Cell Rep.* 9, 2139–2151. doi: 10.1016/j.celrep.2014.11.026
- Rakic, P. (1972). Mode of cell migration to the superficial layers of fetal monkey neocortex. *J. Comp. Neurol.* 145, 61–83. doi: 10.1002/cne.901450105
- Rakic, P. (1988). Specification of cerebral cortical areas. *Science* 241, 170–176. doi: 10.1126/science.3291116
- Rakić, P., and Sidman, R. L. (1969). Telencephalic origin of pulvinar neurons in the fetal human brain. *Z. Anat. Entwicklungsgesch.* 129, 53–82. doi: 10.1007/bf00521955
- Rakic, S., and Zecevic, N. (2003). Emerging complexity of layer I in human cerebral cortex. *Cereb. Cortex* 13, 1072–1083. doi: 10.1093/cercor/13.10.1072
- Schenker, N. M., Hopkins, W. D., Spocter, M. A., Garrison, A. R., Stimpson, C. D., Erwin, J. M., et al. (2010). Broca's area homologue in chimpanzees (Pan troglodytes): probabilistic mapping, asymmetry and comparison to humans. *Cereb. Cortex* 20, 730–742. doi: 10.1093/cercor/bhp138
- Schmahmann, J. D., Pandya, D. N., Wang, R., Dai, G., D'Arceuil, H. E., de Crespigny, A. J., et al. (2007). Association fibre pathways of the brain: parallel observations from diffusion spectrum imaging and autoradiography. *Brain* 130, 630–653. doi: 10.1093/brain/awl359
- Snyder, P. J., Bilder, R. M., Wu, H., Bogerts, B., and Lieberman, J. A. (1995). Cerebellar volume asymmetries are related to handedness: a quantitative MRI study. *Neuropsychologia* 33, 407–419. doi: 10.1016/0028-3932(94)00125-9
- Song, J. W., Mitchell, P. D., Kolasinski, J., Ellen Grant, P., Galaburda, A. M., and Takahashi, E. (2014). Asymmetry of white matter pathways in developing human brains. *Cereb. Cortex* 25, 2883–2893. doi: 10.1093/cercor/bhu084

- Takahashi, E., Dai, G., Rosen, G. D., Wang, R., Ohki, K., Folkerth, R. D., et al. (2011). Developing neocortex organization and connectivity in cats revealed by direct correlation of diffusion tractography and histology. *Cereb. Cortex* 21, 200–211. doi: 10.1093/cercor/bhq084
- Takahashi, E., Dai, G., Wang, R., Ohki, K., Rosen, G. D., Galaburda, A. M., et al. (2010). Development of cerebral fiber pathways in cats revealed by diffusion spectrum imaging. *Neuroimage* 49, 1231–1240. doi: 10.1016/j.neuroimage.2009.09.002
- Takahashi, E., Folkerth, R. D., Galaburda, A. M., and Grant, P. E. (2012). Emerging cerebral connectivity in the human fetal brain: an MR tractography study. *Cereb. Cortex* 22, 455–464. doi: 10.1093/cercor/bhr126
- Takahashi, E., Hayashi, E., Schmahmann, J. D., and Grant, P. E. (2014). Development of cerebellar connectivity in human fetal brains revealed by high angular resolution diffusion tractography. *Neuroimage* 96, 326–333. doi: 10.1016/j.neuroimage.2014.03.022
- Takahashi, E., Song, J. W., Folkerth, R. D., Grant, P. E., and Schmahmann, J. D. (2013). Detection of postmortem human cerebellar cortex and white matter pathways using high angular resolution diffusion tractography: a feasibility study. *Neuroimage* 68, 105–111. doi: 10.1016/j.neuroimage.2012.11.042
- Tuch, D. S., Reese, T. G., Wiegell, M. R., and Wedeen, V. J. (2003). Diffusion MRI of complex neural architecture. *Neuron* 40, 885–895. doi: 10.1016/s0896-6273(03)00758-x
- Vishwas, M. S., Chitnis, T., Pienaar, R., Healy, B. C., and Grant, P. E. (2010). Tract-based analysis of callosal, projection and association pathways in pediatric patients with multiple sclerosis: a preliminary study. *AJNR Am. J. Neuroradiol.* 31, 121–128. doi: 10.3174/ajnr.A1776
- Volpe, J. J. (2009). Brain injury in premature infants: a complex amalgam of destructive and developmental disturbances. *Lancet Neurol.* 8, 110–124. doi: 10.1016/s1474-4422(08)70294-1
- Walsh, C., and Cepko, C. L. (1988). Clonally related cortical cells show several migration patterns. *Science* 241, 1342–1345. doi: 10.1126/science.3137660
- Wedeen, V. J., Wang, R. P., Schmahmann, J. D., Benner, T., Tseng, W. Y. I., Dai, G., et al. (2008). Diffusion spectrum magnetic resonance imaging (DSI) tractography of crossing fibers. *Neuroimage* 41, 1267–1277. doi: 10.1016/j.neuroimage.2008.03.036
- Wegiel, J., Kuchna, I., Nowicki, K., Imaki, H., Wegiel, J., Marchi, E., et al. (2010). The neuropathology of autism: defects of neurogenesis and neuronal migration and dysplastic changes. *Acta Neuropathol.* 119, 755–770. doi: 10.1007/s00401-010-0655-4
- Wichterle, H., Turnbull, D. H., Nery, S., Fishell, G., and Alvarez-Buylla, A. (2001). *In utero* fate mapping reveals distinct migratory pathways and fates of neurons born in the mammalian basal forebrain. *Development* 128, 3759–3771.
- Wonders, C. P., and Anderson, S. A. (2006). The origin and specification of cortical interneurons. *Nat. Rev. Neurosci.* 7, 687–696. doi: 10.1038/nnr1954
- Xu, G., Takahashi, E., Folkerth, R. D., Haynes, R. L., Volpe, J. J., Grant, P. E., et al. (2014). Radial coherence of diffusion tractography in the cerebral white matter of the human fetus: neuroanatomic insights. *Cereb. Cortex* 24, 579–592. doi: 10.1093/cercor/bhs330
- Yu, X., and Zecevic, N. (2011). Dorsal radial glial cells have the potential to generate cortical interneurons in human but not in mouse brain. *J. Neurosci.* 31, 2413–2420. doi: 10.1523/JNEUROSCI.5249-10.2011
- Zhang, Z., Hou, Z., Lin, X., Teng, G., Meng, H., Zang, F., et al. (2013). Development of the fetal cerebral cortex in the second trimester: assessment with 7T postmortem MR imaging. *AJNR Am. J. Neuroradiol.* 34, 1462–1467. doi: 10.3174/ajnr.A3406

Conflict of Interest Statement: The authors declare that the research was conducted in the absence of any commercial or financial relationships that could be construed as a potential conflict of interest.

Copyright © 2016 Miyazaki, Song and Takahashi. This is an open-access article distributed under the terms of the Creative Commons Attribution License (CC BY). The use, distribution and reproduction in other forums is permitted, provided the original author(s) or licensor are credited and that the original publication in this journal is cited, in accordance with accepted academic practice. No use, distribution or reproduction is permitted which does not comply with these terms.



Multivariate Analyses Applied to Healthy Neurodevelopment in Fetal, Neonatal, and Pediatric MRI

Jacob Levman^{1,2*} and Emi Takahashi^{1,2}

¹ Division of Newborn Medicine, Department of Medicine, Boston Children's Hospital, Harvard Medical School, Boston, MA, USA, ² Athinoula A. Martinos Center for Biomedical Imaging, Massachusetts General Hospital, Charlestown, MA, USA

Multivariate analysis (MVA) is a class of statistical and pattern recognition techniques that involve the processing of data that contains multiple measurements per sample. MVA can be used to address a wide variety of neurological medical imaging related challenges including the evaluation of healthy brain development, the automated analysis of brain tissues and structures through image segmentation, evaluating the effects of genetic and environmental factors on brain development, evaluating sensory stimulation's relationship with functional brain activity and much more. Compared to adult imaging, pediatric, neonatal and fetal imaging have attracted less attention from MVA researchers, however, recent years have seen remarkable MVA research growth in pre-adult populations. This paper presents the results of a systematic review of the literature focusing on MVA applied to healthy subjects in fetal, neonatal and pediatric magnetic resonance imaging (MRI) of the brain. While the results of this review demonstrate considerable interest from the scientific community in applications of MVA technologies in brain MRI, the field is still young and significant research growth will continue into the future.

Keywords: multivariate analysis, machine learning, fetal, neonatal, pediatric, brain MRI

OPEN ACCESS

Edited by:

Julia P. Owen,
University of California San Francisco,
USA

Reviewed by:

Budhachandra Singh Khundrakpam,
McGill University, Canada
Ernestina Menasalvas,
Universidad Politécnica de Madrid,
Spain

*Correspondence:

Jacob Levman
jacob.levman@childrens.harvard.edu

Received: 24 July 2015

Accepted: 04 December 2015

Published: 21 January 2016

Citation:

Levman J and Takahashi E (2016)
Multivariate Analyses Applied to
Healthy Neurodevelopment in Fetal,
Neonatal, and Pediatric MRI.
Front. Neuroanat. 9:163.
doi: 10.3389/fnana.2015.00163

INTRODUCTION

The developing brain undergoes rapid structural and functional changes via a variety of processes including neuronal migration, axonal elongation, pruning, maturation of circuits and the emergence of convolution which support efficient signal processing regionally and among distant brain regions. Basic and higher-cognitive functions both require the coordination and cooperation of neurons located in multiple brain regions all of which are in a state of rapid development with a variety of different growth rates. Differences in brain activity between children and adults (Casey et al., 1997; Thomas et al., 2001; Bunge et al., 2002), the structural changes in many developing regions (Reiss et al., 1996; Gogtay et al., 2004; Fair et al., 2009; Supekar et al., 2009) which is linked to gradual changes in tissue contrast (Ketonen et al., 2004) and the recruitment of large cohorts of age matched subjects are major challenges facing researchers in fetal, neonatal, and pediatric imaging. Higher-order brain functions are supported by distributed patterns of brain activity and structure (Mesulam, 1981; Vaadia et al., 1995; McIntosh et al., 1996; Fox et al., 2005) and assessing and identifying these distributed patterns is particularly challenging in a pediatric/neonatal/fetal population due to small brain sizes, a rapidly changing physiology, a high degree of brain plasticity, patient motion, increased metabolism and an incomplete understanding of brain development.

Multivariate analysis (MVA) techniques (i.e., multivariate regression, multivariate analysis of variance, machine learning etc.) are advanced statistical, computational and pattern recognition technologies that evaluate multiple variables/measurements simultaneously. MVA technologies provide a theoretical improvement over univariate techniques which examine each acquired measurement individually. MVA has particularly large potential in studies of magnetic resonance imaging (MRI)-based brain development as many physiological and structural parameters can be measured, new measurements are constantly under development and distributed measurements across the entire brain are acquired. The ideal way to combine a distributed set of a variety of different physiological measurements for any particular application/investigation is not known *a priori*, making MVA research applied to the developing brain a challenging field of ongoing investigation. MVA techniques can be employed to discover what brain regions and what physiological biomarkers are most correlated with a variety of subject measurements such as sleep cycles in newborns, cognitive/psychological measures including the intelligence quotient (IQ) and language functions and lifestyle habits in older children. It is also possible to retrospectively correlate cognitive abilities (e.g., academic activities), lifestyle choices (e.g., smoking habits), or even pathogenesis of brain diseases exhibited later in life to developmental imaging examinations acquired during early brain development.

MRI provides a wide variety of different physiological measurements distributed across the brain, thus providing a wealth of information that may assist in an array of research problems in both clinical applications and basic research. The most common MRI modality produces basic structural information related to the concentration of hydrogen protons. Water is the most abundant molecule in the human body with two hydrogen protons found in each molecule. Since the body regulates many tissues and organs by controlling the concentration of water molecules across membranes, structural MRI provides excellent tissue contrast. Perfusion MRI measures blood perfusion by tagging fast moving hydrogen protons in the blood stream and monitoring the tissues to which they travel. Functional MRI (fMRI) measures a blood oxygen level-dependent signal which is associated with brain activity, an important method for monitoring brain function during an assigned task. fMRI can also be used to monitor normal blood oxygen levels in the brain while the subject is at rest. Diffusion weighted imaging (DWI) is focused on acquiring measurements of water diffusion which can be a useful physiological measurement in many applications. Diffusion tensor imaging (DTI) is a directional extension of DWI, measuring water diffusion in six or more different spatial directions while assuming a principal direction of water diffusivity at each pixel/voxel location in the brain. DTI allows the tracking of coherent tissue structures that are often associated with axonal and even glial fiber pathways (Takahashi et al., 2012; Xu et al., 2014) which has enormous potential for monitoring brain maturation in early developmental stages. MRI can acquire considerably more types of images as well that have not had a major impact in studies focused on

imaging-based MVA of pediatric, neonatal, and fetal populations such as chemical exchange saturation transfer imaging (which includes pH sensitive amide proton transfer imaging) and MR spectroscopy (which is often not spatially resolved but a single measurement that is acquired across the entire brain or at a localized region-of-interest—ROI).

Recent years have exhibited remarkable growth in the use of MVA techniques in pediatric, neonatal and fetal imaging. An excellent review article on the use of MVA classification technologies in developmental brain imaging was previously published in 2009 (Bray et al., 2009), however, at the time of publication the number of research studies using MVA in a pediatric, neonatal and fetal population was limited. In the years since 2009, pre-adult brain MRI studies employing MVA technologies have exhibited remarkable growth, warranting a thorough systematic review. This article reviews MVA techniques applied to brain MRI of pediatric, neonatal and fetal populations and focuses on the imaging of healthy subjects.

MATERIALS AND METHODS

Multivariate Analysis Techniques

MVA techniques can be divided into several classes. Multivariate statistical techniques are quite varied in their potential applications, with a prominent example being techniques focused on the identification of measurements correlated with an important patient characteristic. With a large set of measurements available, MVA techniques such as multivariable linear regression (Rencher and Christensen, 2012) can be used to identify a subset of variables associated with a patient characteristic of interest. MVA techniques such as multivariate analysis of variance (MANOVA) (Warne, 2014) can help assess the effect of changes in one variable on dependent variables and can generally help elucidate the existing relationships between dependent and independent variables. Multivariate analysis of covariance (MANCOVA) (Smith, 1958) is a technique similar to MANOVA but can factor out noise or error introduced by a covariant variable. This review will discuss many applications of multivariate statistics in pediatric, neonatal and fetal populations without neurological/psychiatric disorders which will help illustrate the wide variety of potential uses of these techniques in a medical research context. Multivariate regression based techniques can also create new measurements that are a combination of existing measures creating customized factors/components associated with underlying physiological conditions. Principal Components Analysis (PCA) (Dunteman, 1989) is a representative example that computes orthogonal components that maximize the variance captured from the underlying measurements provided. Manifold learning performs dimensionality reduction non-linearly (Goldberg et al., 2008). Independent Components Analysis (ICA) (Hyvarinen et al., 2004) is a powerful technique based on discovering non-Gaussian distributions in datasets exhibiting mixed signals. These data reduction methods bridge the gap between statistical analysis techniques and related computational technologies that are used automatically and semi-automatically.

Machine learning (Carbonell et al., 1983) is a related class of analysis technique that exhibits considerable overlap with multivariate statistical approaches in that many also involve the selection of measurements and employ data reduction. However, machine learning is often considered a technology rather than a statistical analysis technique. Machine learning is divided into two main approaches: supervised and unsupervised learning. Supervised learning is a class of technologies that use training data which is a collection of measurements associated with multiple groups such as two different types of tissues of interest. The training data is used to inform future predictions, allowing the computer algorithm to assign new unknown samples to one of the groups for which it was provided example measurements. Some supervised learning algorithms include feature selection as part of the overall technology (the process of selecting measurements to rely upon for prediction), however, many do not and feature selection is often addressed as a separate topic in the scientific literature. Bayesian classification bases prediction on posterior probabilities computed from the distribution of training data provided (Devroye et al., 1996). The support vector machine (Vapnik, 1995) is a popular and high performing statistical machine learning technique that attempts to minimize the error on unseen samples and maximizes the margin that separates a decision function from the neighboring training samples provided. The relevance vector machine (Tipping, 2001) is an adaptation of the support vector machine that incorporates probabilistic Bayesian learning. The artificial neural network (Yegnanarayana, 2009) models the behavior of many neurons connected together in a wide variety of topologies to simulate the natural learning process exhibited in the brain. Linear discriminant analysis (McLachlan, 2004) computes a linear combination of measurements in order to characterize or separate two or more groups of samples. The decision tree is a simple methodology for embedding a series of decisions in a hierarchical structure and boosting trees (Friedman et al., 1998) is an adaptation that involves generating weights for imbalanced prediction or voting. The random forest (Breiman, 2001) is an additional extension of the decision tree in which a large collection of decision trees (dubbed a forest) are created with different predictive behavior allowing the algorithm classify a sample based on the most common predictions among those decision trees in the forest. The k nearest neighbor algorithm classifies a new sample based on the local data density of the provided training samples (Altman, 1992). Finally, the generalized linear model (Nelder and Wedderburn, 1972) is a flexible generalization of linear regression that allows for response variables with error distribution models other than the standard normal distribution. The generalized linear model is sometimes referred to as a multivariate statistical analysis technique, highlighting the considerable overlap between machine learning technologies and traditional statistical MVA techniques.

Unsupervised learning differs from supervised learning in that these MVA technologies are not provided with a set of example training data on which to base predictions. Instead, unsupervised learning technologies are tasked with performing a basic level of pattern recognition on a medical imaging examination based on

the data in the examination itself. This typically involves dividing a medical examination into multiple regions-of-interest which can facilitate a variety of in depth analyses (this is also known as image segmentation). These technologies can be applied to isolating a particular tissue or structure in the brain and can be used to monitor changes due to healthy brain development. Unsupervised learning technology can support the extraction of regional physiological statistics and in turn can play a critical role in computer-aided diagnosis systems, supporting high-level patient-wide diagnoses. Example unsupervised learning technologies include the ISODATA algorithm (Ball and Hall, 1965) and cluster analysis (Manton et al., 2014). Cluster analysis is a family of techniques that includes hierarchical clustering in which data is structured across a hierarchical tree and also includes the k-means algorithm which finds k groups in a high dimensional dataset after random initialization. Graph cuts are formalized as an energy minimization problem (Greig et al., 1989). The Watershed method is inspired from geography and the image is modeled as a topographic map. The image is segmented based on ridge lines separating watershed catchment basins which represent regions-of-interest on the image (Beucher and Meyer, 1993). Also of interest is fuzzy set theory, which is used in situations where available information is incomplete or imprecise and functions by modeling uncertainty (Zadeh, 1965). Finally, the expectation maximization algorithm is a parametric approach that involves iterative refinement of parameter estimates (Dempster et al., 1977).

Several of the research papers included in this review made use of unsupervised learning algorithms and reported evaluative metrics for assessing the quality of the regions-of-interest produced by the learning technique. These metrics are reported in the results section of this paper and each of the relied upon evaluative metrics are introduced here. The Dice coefficient measures the amount of overlap between the computed region-of-interest (ROI) and ground truth data, defining that overlap as 2 times the magnitude of the intersect of the two ROIs divided by the sum of the magnitude of each individual ROI (Dice, 1945). The Jaccard index is closely related to the Dice coefficient though it assesses overlap as the magnitude of the intersection of the two ROIs divided by the magnitude of the union of the two ROIs (Jaccard, 1901). The Kappa statistic measures the agreement between raters by adjusting the relative observed agreement with the hypothetical probability of chance agreement (Cohen, 1960). For all three parameters, higher values indicate greater agreement between the gold standard ROI and the ROI computed by the learning procedure. Finally, Pearson's correlation coefficient (PCC) assesses the linear correlation between two variables. Highly correlated variables approach a PCC of 1, uncorrelated variables yield a PCC of 0 and highly negatively correlated variables approach a PCC of -1.

Review Parameters

The search engine MEDLINE/PubMed was used for this review on May 4th, 2015. The search terms employed were <Multivariate pediatric brain MRI> or <machine learning pediatric brain MRI> or <Multivariate neonatal brain MRI> or <machine learning neonatal brain MRI> or <Multivariate

fetal brain MRI> or <machine learning fetal brain MRI>. This yielded 166 articles whose titles and abstracts were reviewed for their appropriateness for inclusion in this paper. Articles were excluded if brain MRI was not performed in a fetal, neonatal or pediatric population. Articles were excluded if they did not involve an MVA that included brain MRI data acquired as an important component of the analysis. Articles were excluded if not authored in English. Articles were excluded if they were not focused on healthy brains or normal neurological development. Articles from this search process that were not excluded were analyzed for this systematic review and noteworthy citations within these articles were considered for inclusion (subject to the same exclusion criteria).

RESULTS

At present we have an incomplete understanding of healthy human brain development and the results of this review demonstrate that MVA techniques combined with MR imaging can play a substantive role in helping elucidate our knowledge pertaining to developmental brain imaging. In addition to enhancing our fundamental knowledge, theoretically, a more complete understanding of healthy human brain development may lead to the accurate identification of deviations from expected neurodevelopment. This in turn may assist in the detection, characterization, diagnosis and progression monitoring of a wide variety of medical disorders as aberrations

from healthy brain development. MVA technologies can be used to assist in understanding, characterizing, and monitoring healthy brain development. MVA technologies based on MRI can be used to create tools to assist in the analysis of the images we acquire such as assessing gray and white matter volumes, detecting structural changes during development, identifying anatomical substructures associated with a phase of brain development and predicting a subject's age or gender. MVA provides considerable potential over traditional univariate analyses with a wide variety of flexible applications of MVA available. MVA can be used to generate a custom index that combines multiple measurements (as in **Figures 1, 2**). Additionally, MVA can be used to visualize the extent of tissue connectivity (as in **Figure 3**). MVA can also be used to create images that allow for visual comparison of regional differences in group-wise analyses (see **Figures 1, 4**).

Patterns of Brain Development

MVA technologies can be applied to brain MR imaging data to help identify patterns associated with a wide variety of aspects of healthy brain development. Studying human brain development is first possible with fetal imaging, which allows the assessment of a subject's neurodevelopment *in utero*. Schopf et al. (2012) investigated a fetal population with resting state fMRI of the brain using ICA and demonstrated that resting state functional networks in the fetal brain are detectable *in utero*. Their study looked at a population observed across gestational weeks

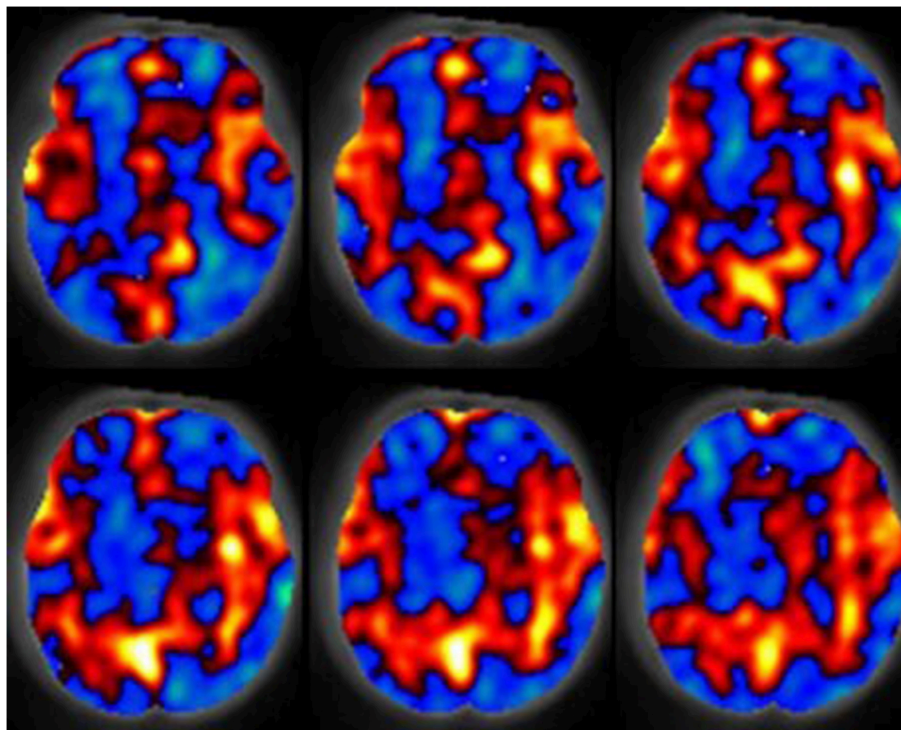
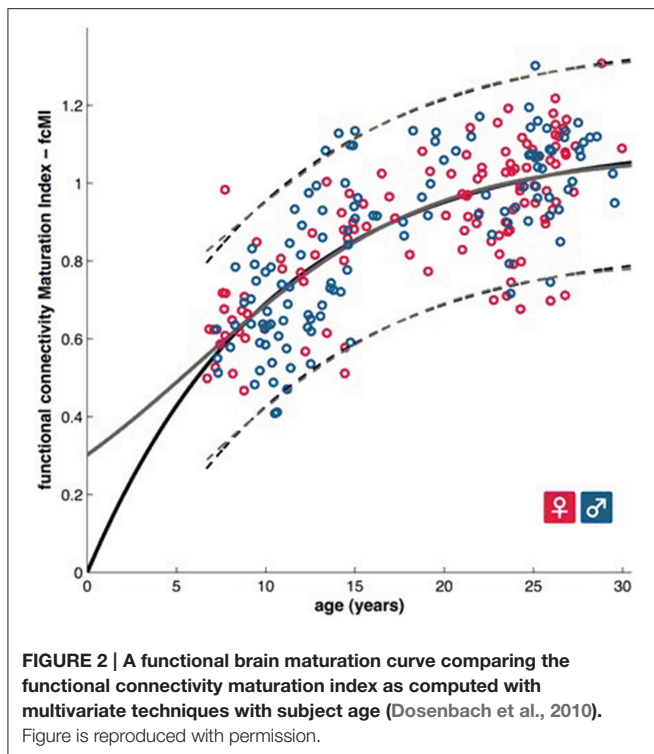


FIGURE 1 | The spatial relative cerebral blood flow discrepancy map comparing groups of subjects 7 and 13 months old. Red values indicate greater blood flow in the 13 month group, blue values indicate greater blood flow in the 7 month group. Results were computed with a support vector machine. Figure is reproduced with permission (Wang et al., 2008).



(GW) 20–36 and found three important network components associated with this developmental stage: a bilateral frontal, a bilateral occipital and a unilateral temporal component located in the left hemisphere. Thomason et al. (2013) studied a healthy fetal population with resting state fMRI also making use of ICA for analysing functional networks of activation in the brain. ICA identified eight bilateral networks. ICA was also able to isolate five components associated with noise, emphasizing the technique's ability to not only identify regions of the brain with similar activation patterns, but also to separate noise from imaging datasets which can assist in improving the signal-to-noise ratio (SNR) of the MR examinations. Jakab et al. (2014) investigated the use of fMRI for *in utero* imaging of the fetal brain. Their work used PCA-based feature measurement reduction as a means of removing noise from the imaging data to support more reliable analyses. Results demonstrated that the overall connectivity network in the brain as well as short range and interhemispheric connections exhibited a sigmoid expansion curve which peaked at 26–29 GW. By contrast, long range connections exhibited a linear increase with no periods of peaking development. Their results demonstrate heterogeneous development of functional networks in the fetal brain. Ferrazzi et al. (2014) presented a framework for improving fetal MRI studies that make use of ICA by correcting for imaging artifacts induced by motion, bias field and spin history. Their results were found to be consistent with identified resting state functional networks reported in previous fetal imaging studies.

Children born healthy but prematurely or with very low birth weight represent an interesting research group which does not necessarily have neurodevelopmental disorders. This

group provides unique opportunities for study as they represent an intermediary between fetal and standard neonatal imaging. Tich et al. (2011) applied multivariable regression to data from very preterm infants and demonstrated that larger birth weight, shorter duration of assisted ventilation and older postmenstrual age (gestational age at birth + postnatal period) at MRI were predictive of larger brain metrics. Furthermore, biparietal diameter was found to be the variable most associated with the Mental Development Index and the Psychomotor Development Index. Nosarti et al. (2004) investigated the size of the corpus callosum among very preterm birth children and its relationship to neuropsychological outcome. Their analysis included MRI and MANCOVA. Their results indicated that in preterm boys only, verbal IQ and verbal fluency scores were positively associated with total mid-sagittal corpus callosum size and mid-posterior surface area. Adams et al. (2010) investigated the use of diffusion tractography in premature newborns and applied multivariate regression which indicated that gestational age at birth was not significantly associated with DTI measures of corticospinal tract development. Fearon et al. (2004) investigated the long-term effect on the brains of very low birth weight newborns by imaging them with MRI during adulthood and analysing the results with the general linear model (GLM). The GLM demonstrated that ventricular volume was larger and posterior corpus callosum volume was smaller in very preterm individuals compared with controls. Delpolyi et al. (2005) investigated the microstructural and macrostructural development of the cerebral cortex in premature newborns using DTI and traditional statistical multivariate techniques. Cortical gyration was measured as the ratio of gyrus height to width on volumetric MRI bilaterally in the superior frontal, superior occipital, precentral, and postcentral gyri. Although, cortical gyration scores, fractional anisotropy and radial diffusivity were all significantly correlated with the estimated gestational age, MVA found no statistically significant relationship between DTI parameters and cortical gyration beyond their common association with estimated gestational age.

Imaging of neonatal brain development is a challenging task as the brain is relatively immature and exhibits a reduction in organized neuronal activity as compared to adults. The newborn brain is also maturing rapidly both structurally and metabolically. Aljabar et al. (2010, 2011) demonstrated that MVA based manifold learning technology can be applied to the developing neonatal brain and has potential toward identifying patterns in the trajectories of brain development. Their results demonstrated a strong correlation between clinical data such as gestational age, weight and head circumference with multivariate MRI-based measurements. Furthermore, their approach was shown to produce improved correlations with subject age over measurements extracted from MR examinations. Wang et al. (2008) demonstrated that blood perfusion MRI can be used in combination with the multivariate technique known as the support vector machine to analyse cerebral blood flow increases in the hippocampi, anterior cingulate, amygdalae, occipital lobes, and auditory cortex demonstrating increased cerebral blood flow in 13 month old infants relative to a 7 month old group. Their results also demonstrated decreased blood perfusion in the right

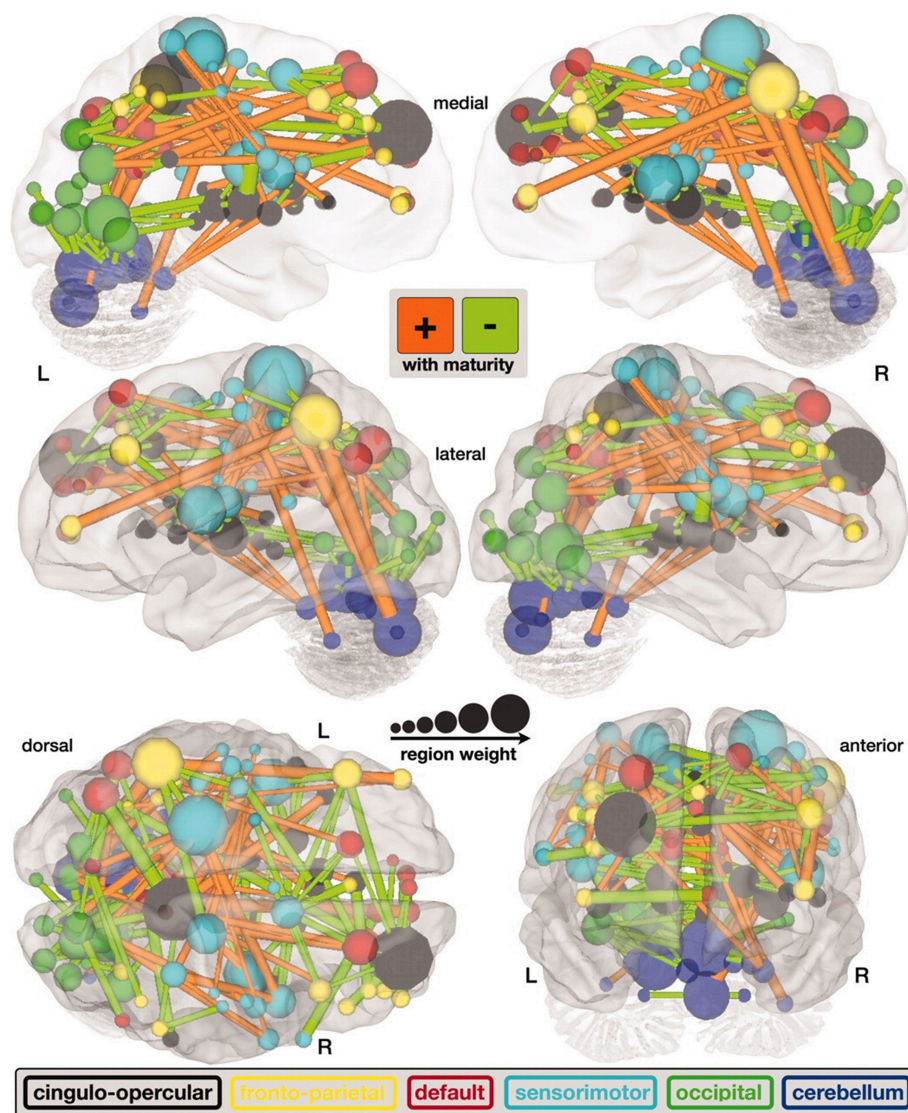


FIGURE 3 | A map of functional connectivity in the brain computed with the support vector machine. Connections positively correlated with age are shown in orange. Negative correlations with age are shown in light green (Dosenbach et al., 2010). Figure is reproduced with permission.

temporal lobe, right prefrontal region and the left putamen. **Figure 1** is provided to demonstrate relative cerebral blood flow discrepancies between the 13 and 7 month old groups as computed by a support vector machine. Matsuzawa et al. (2001) studied age-related volumetric changes in both gray and white matter in healthy infants and children. Their analysis included the use of a Bayesian algorithm to assist in characterizing gray matter, white matter and cerebrospinal fluid from MRI examinations. Their study also included a MANOVA statistical analysis. Their results helped quantify natural growth spurts occurring during the first 2 years after birth, a period during which the frontal lobes grew more rapidly than the temporal lobes. Right-left hemispheric asymmetry was more noticeable in the temporal lobes than in the frontal lobes. White matter volume was shown to increase at a higher rate than gray matter volume

throughout childhood. Koshiba et al. used principal component analysis to examine factors associated with the neurological and behavioral development of “Head Control” and “Roll Over” in a neonatal population (Koshiba et al., 2015). They determined that hematological and brain anatomical factors were correlated with these basic neonatal movement patterns.

Imaging of children that have grown beyond the neonatal phase is another important aspect of neurodevelopmental brain imaging. These pediatric populations are less challenging to image than fetal and neonatal populations due to a variety of factors including a larger nervous system and some degree of cooperation from the subjects regarding remaining still during imaging (movement can corrupt the examination with motion artifacts). Giedd et al. (1999) presented a landmark longitudinal study which helps to introduce this topic. Their analysis included

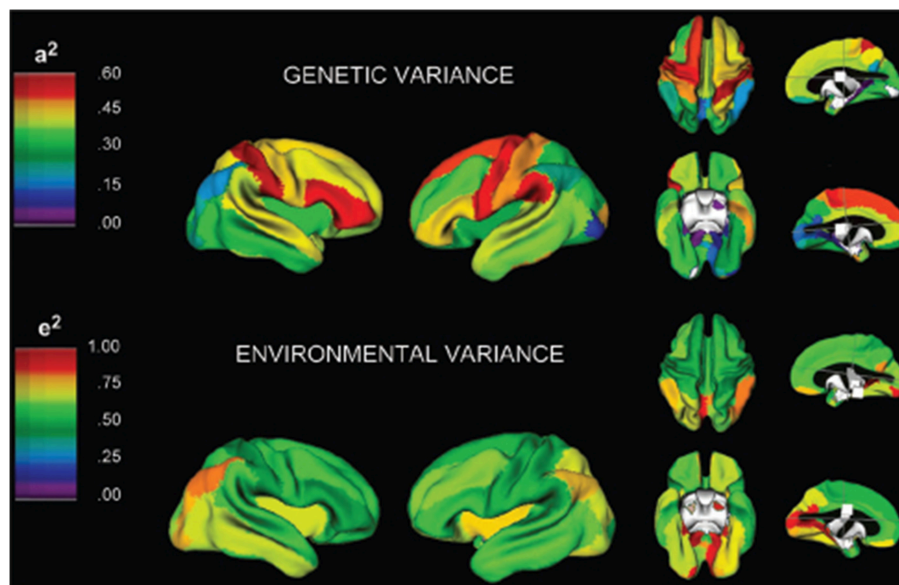


FIGURE 4 | A three-dimensional rendering of the brain with overlaid color maps illustrating the relative contribution to variability of different neurological locations based on genetic and environmental factors (Schmitt et al., 2007). Figure is reproduced with permission.

145 healthy subjects between 4 and 20 years old. Their study incorporated an artificial neural network for tissue classification. Their results demonstrated linear increases in white matter and nonlinear changes in cortical gray matter that varied by brain region. Shaw et al. (2008) presented a large-scale cortical thickness study investigating 764 MRI examinations acquired longitudinally from 375 typically developing children and young adults. They used regression analysis to determine if each cortical measurement was best modeled by a cubic, quadratic, or linear function as they vary with age. They determined that most of the lateral frontal, lateral temporal, parietal, and occipital isocortex developed with a cubic trajectory exhibiting a period of initial childhood increase followed by adolescent decline and then stabilization. The quadratic model exhibiting a period of initial childhood increase followed by a decrease of cortical thickness without a period of stabilization was identified in the insula and the anterior cingulate cortex. A linear growth trajectory was observed in the posterior orbitofrontal and frontal operculum, portions of the piriform cortex, the medial temporal cortex, subgenual cingulate areas, and medial occipitotemporal cortex. Chen et al. (2014) investigated a combination of neonates and children up to 4 years old helping to bridge the gap between neonatal and pediatric imaging analysis of brain development. Their study used multivariate adaptive regression splines to derive data-driven growth trajectories for the three eigenvalues (measures along three principal directions of water diffusivity) associated with DTI and demonstrated that insights into brain maturation can be gained through analysing eigenvalues. Specifically, their work revealed limitations in relying upon the average of the secondary and tertiary eigenvalues for radial diffusivity because they exhibited significantly different growth velocities compared to that of the first eigenvalue. Based on the

three primary eigenvalues, their results also demonstrate growth trajectory differences between the central and peripheral white matter, between the anterior and posterior limbs of the internal capsule and between the inferior and superior longitudinal fasciculus. Schmithorst et al. (2007) investigated the development of effective connectivity pertaining to narrative comprehension in children aged 5–18 using fMRI, independent components analysis and the general linear model. Feedback networks were identified during a narrative processing task involving effective connectivity from Broca's area and the medial aspect of the superior frontal gyrus to the posterior aspects of the superior temporal gyrus bilaterally. They also demonstrated that the effective connectivity from Broca's area to the superior temporal gyrus in the left hemisphere increases with age. The results demonstrate that it is feasible to investigate effective connectivity using MVA applied to multiple subjects in the absence of an *a priori* model. In their analysis functional activation maps in the brain were computed with the general linear model.

Predicting Brain Age/Maturity

Predicting brain age/maturity from MRI examinations has the potential to play an important role in both improving our understanding of healthy brain development and studying the nature by which developmental disorders deviate from expectation. Brown et al. (2012) studied healthy brain development with structural MRI and multivariate regression and demonstrated that their model of human brain maturation accounted for over 92% of the individual variability in brain development as defined by subject age. Mwangi et al. (2013) used the relevance vector machine combined with diffusion tensor imaging demonstrating that they could produce an index closely related to subject age (with Pearson correlation coefficients

ranging from 0.870 to 0.899 depending on the DTI measurement relied upon). Brain maturity assessment was demonstrated to be feasible based on combining resting state fMRI with support vector machine technology in subjects aged 7–30 years old (Dosenbach et al., 2010). The greatest contribution to predicting brain maturity was based on the weakening of short-range functional connectivity between the brain's major functional networks, consistent with the work by Jakab et al. (2014). However, it should be noted that the work by Power et al. (2012) calls into question fMRI findings of a shift from short to long range connectivity in the presence of patient motion artifacts which can bias fMRI based short and long range connectivity analyses. **Figure 2** provides a functional maturation index computed with the aid of multivariate techniques relative to age demonstrating how MVA can be used to help better understand and characterize brain development (Dosenbach et al., 2010). The resultant functional maturation curve accounted for 55% of the sample variance following a nonlinear asymptotic growth curve shape. **Figure 3** provides a connectivity map demonstrating functional connections as computed with the support vector machine (Dosenbach et al., 2010). Greene et al. (2014) utilized the support vector machine to reliably classify individuals as children or adults based on basal ganglia cortical system functional connectivity yielding an accuracy of 83.3%. Smyser and Neil (2015) demonstrated that they could use the MVA technique known as the support vector machine to demonstrate differences between term and very preterm infants based on resting state functional MRI examinations. Franke et al. (2012) demonstrated that the relevance vector machine combined with MRI could accurately predict the age of the brain being analyzed. Furthermore, they demonstrated that preterm-born adolescents exhibited a significantly lower estimated brain age than their chronological age. Correlations between subject age and that estimated by their approach ranged from 0.9 to 0.95 and represents a statistically significant finding. Serag et al. (2012) employed unsupervised learning technologies and reported that their approach can produce a good biomarker of brain development. Toews et al. (2012) presented a model that can be used to identify age-related anatomical structure using Bayesian techniques to predict the age of subjects with an average error of only 72 days. Khundrakpam et al. (2015) presented an approach to assessing brain maturity based on cortical gray matter thickness and a linear regression model and found that the leading predictors were highly localized sensorimotor and association areas. An approach to estimating brain age based on DTI was presented by Han et al. (2014) at conference. Dittrich et al. (2014) used a random forest classifier to construct an atlas of fetal brain development which was used to estimate a brain structure's age morphologically. Erus et al. (2015) demonstrated that multivariate regression can be used to model healthy structural brain maturation and showed that deviations from expectation are correlated with cognitive performance for both developmentally delayed individuals as well as those with cognitive precocity. Results demonstrated that the brain development index that they present is correlated with subject age with a correlation coefficient of 0.89.

Identifying Brain and Tissue Structures

MVA technologies can be used to perform pattern recognition on a pediatric patient's brain MRI examination in order to divide the image into regions-of-interest (ROIs) separating tissues and structures for further analysis, a process referred to in the literature as image segmentation. Such techniques establish a set of ROIs in the examination which can facilitate studies investigating changes in white and gray matter volumes, structural changes, and tissue outcome prediction studies. These techniques can be used as an important component in a computer-aided detection system which can assist in the characterization and identification of a variety of complex regional variations of brain development. This subsection of the results first presents MVA studies applied to a fetal population followed by neonatal and then pediatric populations.

The germinal matrix is a transient deep brain region of developing cells adjacent to ventricles that is present in the fetal brain between 8 and 28 weeks gestational age. Habas et al. (2008) presented an approach to the segmentation of the germinal matrix from *in utero* clinical MRI examinations of the fetal brain at conference. Their approach was based on a constructed tissue atlas formed by a combination of subject MR examinations which yielded average shape and intensity images. Keraudren et al. (2013) developed a technique using MRI to detect the location of the fetal brain from the mother's abdomen and applied it to a database of 59 fetal examinations and also applied their segmentation approach to motion correction (Keraudren et al., 2014). Their work was based on fetal T2 weighted structural MRI.

Altaye et al. (2008) developed infant brain probability templates for MRI segmentation and normalization. Their approach was based on creating tissue probability maps from 76 infants ranging in age from 9 to 15 months. They demonstrate the utility of their approach by segmenting imaging examinations into gray matter, white matter and cerebrospinal fluid. Commowick and Warfield (2010) used an expectation maximization approach to support the segmentation of neonatal brain MRI examinations using T1 and T2 structural imaging. Shi et al. (2010) created an approach to neonatal brain image segmentation based on probabilistic atlases. The authors reported Dice coefficients (range 0.85–0.87) that demonstrated that their approach has similar agreement to the results of two experts. He and Parikh (2013) developed a brain segmentation technique based on T2 relaxometry and demonstrated their work on very preterm infants yielding a Dice coefficient of 0.95.

Weisenfeld and Warfield (2009) presented an approach to the probabilistic segmentation of each pixel/voxel from spatially aligned T1 and T2-weighted neonatal MRI examinations of the brain into cortical and subcortical gray matter, unmyelinated white matter, myelin, cerebrospinal fluid, and background (non-brain). Their approach shares similarities with Bayesian techniques and was reported to have achieved an accuracy comparable to that obtained by semi-automatic methods that require manual interaction from the user (with average Dice coefficients ranging from 0.72 to 0.92 depending on tissue type).

Song et al. (2006) developed an approach to the segmentation of T2 MRI examinations of neonates based on graph cuts

technology incorporating a new method for information integration. Tissue priors and local boundary information are integrated with standard image intensity values into the edge weight metrics used by graph cuts. Their approach also incorporated inhomogeneity correction. They demonstrated that their method outperformed a commonly used optimization method applied to segmentation.

Xue et al. (2007a) developed an automatic approach to cortical segmentation in the developing brain that uses *a priori* knowledge of the inverted contrast exhibited between gray and white matter when myelination is incomplete. Their approach was tested on T2 imaging examinations from 25 neonates and compared with the results of manual segmentations. In an additional study, Xue et al. (2007b) focused on the segmentation and reconstruction of the neonatal cortex from T2 MRI examinations using an expectation maximization Markov Random Field approach. Their results indicated that cortical surface area and curvature increase with age. They determined that whole brain surface area scales to cerebral volume according to a power law while cortical gray matter thickness is not related to age or brain growth. They report Dice coefficients of 0.76 for gray matter and 0.79 for white matter. Isgum et al. (2015) presented the results of the NeoBrainS12 challenge which involved eight participating research teams attempting to segment preterm neonatal T1 and T2 MRI brain examinations into cortical gray matter, non-myelinated white matter, brainstem, basal ganglia and thalami, cerebellum, and cerebrospinal fluid in the ventricles and in the extracerebral space. Teams involved in the competition took a variety of multivariate approaches including one based on watershed segmentation, three techniques based on the *k* nearest neighbor algorithm and four techniques based on expectation maximization. An implementation of *k* nearest neighbor yielded the highest Dice coefficients (0.56–0.95 depending on tissue type) on axial images. Analysis of the results of the competition indicated that the automatic segmentation of brain tissues from neonatal MRI examinations is feasible, however, the automatic segmentation of myelinated white matter in these images is not feasible (with a Dice coefficient of 0.56 corresponding to the segmentation of myelinated white matter).

Zhang et al. (2015) developed a neonatal brain segmentation system using artificial neural networks based on multiple MRI modalities achieving Dice coefficients of 0.83–0.86 depending on tissue type. Wang et al. (2015) presented an approach to neonatal brain segmentation based on the random forest supervised learning algorithm yielding Dice coefficients ranging from 0.83 to 0.92 depending on tissue type. Song et al. (2007) presented an approach to neonatal brain segmentation based on Bayesian analysis and the support vector machine and published their work at conference. A level-set based brain extraction technique was developed by Shi et al. (2012) and applied to both neonatal and pediatric examinations yielding Jaccard indices of 0.95–0.96 depending on subject age. Devi et al. (2014) presented an approach to automatic brain segmentation of neonates employing atlas based probabilities and Gousias et al. (2012) also employed probability based atlases but their approach was applied to a pediatric population yielding Dice coefficients

ranging from 0.9 to 0.92 depending on the brain's substructure being evaluated.

The segmentation of the pediatric brain has been the subject of numerous studies. Glass et al. (2003) developed an approach to the prediction of total cerebral tissue volumes based on multimodal MRI examinations (T1, T2, proton density, FLAIR). Their approach employed a hybrid artificial neural network segmentation and classification algorithm used to identify normal parenchyma. They reported an average error of estimation of total cerebral tissue volumes of 6% in 27 min of computational processing time or alternatively an average error of less than 2% based on 2 h and 4 min of processing time. Shan et al. (2006) developed a brain atlas based on the structural T1 volumetric MRI examination of a 9-year-old girl, involving the construction of a three-dimensional triangular mesh model and indicated that their results could be used to plan treatment, conduct model-driven segmentation and to analyze the shapes of brain structures in pediatric patients. They reported kappa statistics of 0.97 for cortical regions and 0.91 for subcortical regions indicating substantial similarities between their mesh model and the original volumes.

The segmentation of the caudate nucleus from pediatric (aged 2–4 years) MRI examinations was the subject of a component of a grand challenge as part of a workshop associated with the *Medical Image Computing and Computer Assisted Intervention* Conference (van Ginneken et al., 2007). The competition entrants included Arzhaeva et al. (2007) who presented a method based on the *k*-nearest neighbor classifier. Wels et al. presented a method (Wels et al., 2007) based on probabilistic boosting trees. A multiple atlas based approach was presented by van Rikxoort et al. (2007) and a probabilistic atlas approach was presented by Gouttard et al. (2007). Levy et al. (2007) presented an approach based on Bayesian optimization. Babalola et al. (2007) presented an approach based on active appearance models. Tu et al. (2007) presented an approach based on hybrid generative/discriminative models. Schonmeyer and Schmidt (2007) presented an approach combining pixel-based and object-based measurements derived from cognition network technology. Finally, Liu et al. (2007) presented an approach based on active contour models. There were reporting differences between the studies that entered the competition, making direct comparisons of their performance on the pediatric population challenging. However, of those studies that reported a Pearson correlation coefficient specific to the pediatric population included in the competition, Babalola et al.'s results (Babalola et al., 2007) were the most accurate (Pearson coefficient: 0.8320).

Shape Analysis

Shape analysis typically involves a statistical approach to taking measurements from images indicative of a brain structure's morphological properties such as how spherical, irregular or elliptical a region presents on MRI. Shape measurements are typically extracted from ROIs established through image segmentation (see previous subsection). Shape information can be useful for assessing healthy growth patterns and theoretically can assist in creating measurements that may be able to identify aberrations from healthy growth trajectories. In terms

of healthy brain development, Batchelor et al. (2002) proposed an MVA approach to studying the shape of the cerebral cortex using a set of measurements useful to assist in quantifying folding in the brain from fetal MRI examinations. Their study focused on the imaging of *ex vivo* brain specimens which included a wide variety of pathological findings. Their subjects included a sample that was the result of spontaneous miscarriage without pathological findings. Rodriguez-Carranza et al. (2006) developed a system for measuring regional surface folding in neonatal brain MRI examinations, allowing evaluation of surface curvature within subregions of the cortex. Their method was applied to seven premature infants born at 28–37 gestational weeks and gray matter and gray-white matter interface surfaces were extracted. Their research can theoretically support the study of structural development in the neonatal brain within specific subregions. Serag et al. (2012) created a system capable of performing unsupervised learning of shape complexity and reported that their approach can produce a good biomarker of brain development.

Studying Gender in the Brain

Comparing gender differences based on MRI examinations is a common technique used to help elucidate developmental variability between the sexes. There have been a few studies focused on the analysis of gender differences in healthy subjects using MVA techniques. Casanova et al. (2012) used the random forest algorithm to investigate gender differences based on resting state functional imaging yielding a classification accuracy of 65%. They concluded that gender differences may be related to regional connectivity differences between critical nodes. Awate et al. (2010) developed a multivariate modeling approach to the analysis of cerebral cortical folding and demonstrated its utility in studying cerebral cortical folding differences between genders. Skiold et al. (2014) studied boys and girls born extremely preterm with MRI using the generalized linear model and determined that cognitive and language outcomes at 30 months were poorer in boys.

Relating Genetics to Brain MRI

Genetics provides a wealth of information about subjects studied. Given that there is still limited knowledge on the functional role and organization of the human genome, it is expected that genetic analyses will continue to grow in importance. There have been several studies to date focused on combining genetic data with MR brain imaging and also making use of MVA techniques. Giedd et al. (2007) investigated the relative impact of genetic and environmental factors on human brain anatomy during childhood and adolescent development by applying multivariate analysis techniques used in genetic analyses to a large sample of monozygotic and dizygotic pediatric twin's MRI examinations. Their results indicated that cross twin correlations were substantially higher in the monozygotic group relative to the dizygotic group, indicative of a strong genetic impact on brain volume variations. Although, their results indicated that environmental factors provided a much smaller contribution to brain volume variations (both whole brain and in specific

subregions), environmental factors did influence a substantial portion of the variance in the dataset.

Schmitt et al. (2010) demonstrated that in a large pediatric population most of the variance in the brain's substructures is associated with highly correlated lobar latent factors with differences in genetic covariance and heritability driven by a common genetic factor that influences white and gray matter differently. In another study Schmitt et al. (2009) developed a novel method that combines classical quantitative genetic methodologies for variance decomposition with semi-multivariate algorithms for high resolution measurement of phenotypic covariance assessed with structural T1 MRI examinations. Their results indicated that mean cortical gray matter thickness was most strongly correlated with genetic factors in association cortices. Their study suggests that genetics plays a large role in global brain patterning of cortical gray matter thickness. In an additional contribution, Schmitt et al. (2008) employed principal components analysis of the genetic correlation matrix and structural MRI examinations of pediatric twins and siblings. Their results identified genetically mediated fronto-parietal and occipital networks. **Figure 4** provides a three-dimensional rendering of the brain with overlaid color maps which illustrate the relative contribution to the variability seen in different neurological locations based on genetic and environmental factors as computed with the aid of multivariate techniques. In yet another contribution, Schmitt et al. (2007) analyzed MRI examinations and genetic factors with multivariate techniques from genetic analyses to investigate whether different anatomical subdivisions share common genetic factors. Based on the analysis of a large pediatric population, their work suggests that the great majority of variability in cerebrum, thalamus, cerebellum and basal ganglia is determined by a single genetic factor. Most of the variability in the corpus callosum was explained by additive genetic effects that were largely independent of other structures. Their work also observed small but significant environmental effects common to the thalamus, basal ganglia and lateral ventricles.

Optimizing MRI Brain Imaging and Analysis

MVA techniques can play a role in assessing imaging performance and optimizing image acquisition and its analysis. White et al. (2014) employed fuzzy set theory in a pediatric resting state fMRI study and determined that 5.5 min of resting state acquisition time was required to produce a stabilized set of brain network measurements. Zhou et al. (2011) demonstrated that deriving a Granger causality model from multivariate autoregressive models can yield greater accuracy in detecting network connectivity in fMRI examinations. Shehzad et al. (2014) developed a multivariate distance-based regression to assist in connectome-wide association studies and demonstrated it on healthy development data. Pontabry et al. (2013) developed a probabilistic approach to Q-ball imaging (an extension of DTI) tractography and demonstrated the technique on *in utero* fetal brain imaging examinations. They also demonstrated that their technique can outperform existing fiber tracking algorithms based on the Fiber Cup phantom challenge data (Pontabry et al., 2013). Goodlett et al. (2008) presented a

framework for hypothesis testing of differences between DTI tractography pathways identified as bilateral cortico-spinal tracts and tracts running through the genu and splenium of the corpus callosum. Their approach incorporates PCA for signal smoothing. Multivariate discriminant analysis is performed on the PCA smoothed data and normalization is performed across a population with DTI atlas building procedures. Their methodology was evaluated on a pediatric study of 22 one-year-old and 30 two-year-old children.

The Effect of the Senses on the Brain

Sense organs (eyes, ears, etc.) contain concentrations of sensory neurons which can be stimulated by external physical effects (light, sound, etc.). These sensory neurons then stimulate additional neural activity in the brain. Considerable research has looked at the relationship between functional MR brain imaging and controlled sensory stimulation and a few of these studies have also incorporated MVA. Schopf et al. (2014) used fMRI technology to study fetal eye movements *in utero*. Their approach included the use of the random forest machine learning algorithm (Breiman, 2001) to classify whether individual pixels were part of the fetal eye. Their results indicate that the relationship between eye movement and vision develops before birth. Their work also incorporated ICA to identify networks showing the highest correlation with fetal eye movement. This included association related areas such as the angular gyrus, inferior parietal gyrus, the superior frontal gyrus and the medial occipital gyrus.

Jardri et al. (2008) investigated fetal cortical activation due to sound stimulus at 33 GW using fMRI examinations. Their approach included the use of ICA for processing fMRI data to assist in the identification of brain regions exhibiting similar activation patterns. This study involved a direct auditory stimulus applied to six pregnant women's abdomens. Standard univariate voxel-wise analysis demonstrated that two of the six subjects exhibited significant activation in the left temporal lobe. MVA using ICA demonstrated that three out of six subjects exhibited significant activation in the left temporal lobe, implying that MVA techniques have the potential to identify patterns of brain activation missed by traditional univariate analyses. In an additional study, Jardri et al. (2012) studied fetal response to auditory stimulation induced by maternal speech using fMRI and ICA. This analysis was performed *in utero* on subjects at 33 and 34 GW. Their results demonstrated left temporal lobe activation in each of three fetuses imaged without motion artifacts. The authors reported their results as representing the first *in vivo* evidence for the development of maternal voice recognition *in utero*.

DISCUSSION

The results of this systematic review demonstrate a wide variety of applications of multivariate analysis (MVA) techniques applied to brain MRI examinations of healthy pediatric, neonatal and fetal populations. Since the ideal combination of MVA technique and medical imaging derived clinical information is unknown *a priori*, an enormous amount of research is required to fully

optimize MVA's potential in this domain. Recent years have exhibited ample growth in the application of MVA techniques with ongoing growth expected. However, substantial challenges will accompany future research in this domain.

There are substantial strengths and weaknesses of the wide variety of multivariate analysis techniques available. Feature reduction techniques (such as PCA and ICA) can be useful in finding latent factors that can represent underlying physiological conditions that can only be assessed by acquiring a multitude of measurements. These techniques have considerable overlap with the functionality of machine learning algorithms. In supervised learning, the support vector machine (SVM) has shown itself to be a high performing robust learning algorithm which is particularly resilient to situations where it is provided with small numbers of training samples. The related relevance vector machine has been shown to produce learning solutions that rely on fewer training samples than the SVM allowing prediction to be computed more efficiently. Linear discriminant analysis is a classical learning technique which can reliably perform pattern recognition but often underperforms techniques like the SVM. The artificial neural network's strength lies in modeling the learning abilities of the human brain which is unmatched by current machine learning technology. However, artificial neural networks typically attempt to model a learning problem with far fewer neurons than the task would likely need in order to be accomplished in the human brain. The random forest is a high performing algorithm that explores a wide variety of possible decisions that could lead to accurate predictions and is particularly capable of exploiting feature measurements with limited separation information embedded therein. Finally, it should be noted that machine learning technology is too often treated as a black box whose internal behavior is unknown to the researcher. The technologies available provide the ability to analyse their behavior, a task that all pattern recognition researchers should engage in, not only to understand the nature of the technology they've developed, but also to understand the physiological significance of the patterns that the technology exploits in order to make its predictions.

One major obstacle in this application domain is caused by patient motion which is particularly challenging in pediatrics because children tend to have a harder time remaining still during imaging. Children asked to remain still in the scanner may forget over the course of the examination. Image registration is a class of technology used to compensate for patient motion but this is a challenging problem for which there is no accepted gold standard solution. Registration to standard templates (or brain atlases) is typically based on adult brains (Talairach and Tournoux, 1988) and it has been shown that normalization procedures used can cause distortions in the brain examinations of children 6 years old and under (Muzik et al., 2000). Distortional effects may adversely affect MVA results and so care should be taken to avoid providing data exhibiting distortional artifacts to MVA technology.

While feature selection can be addressed as a class of technology independent of supervised learning, some supervised learning techniques incorporate feature selection while others do not. Feature selection is particularly important in the characterization of neurodevelopment in a fetal, neonatal

and pediatric population because we acquire a multitude of measurements distributed across the brain and we don't know *a priori* all the brain regions that should be included in a given analysis. The same is also true for identifying brain regions whose structure or function at a particular time point is critical in a future phase of healthy brain development, thus feature selection technologies have considerable potential in improving our understanding of healthy brain development. Feature selection research could lead to new technologies to assist in the characterization, detection and diagnosis of a variety of medical conditions as aberrations from expected healthy growth patterns.

DTI and tractography are critical tools to assess maturation of brain development, especially emerging or regressing tissue coherency. However, limited MVA research has been conducted incorporating diffusion imaging examinations as compared with T1- or T2-weighted MRI. This may be because of a variety of factors including the complexity of interpretation and analysis of DTI data with multiple directions of tissue coherency, higher sensitivity to motion, higher dependencies on SNR, reliability of tractography reconstruction and DTI's much more limited routine clinical use. However, considerable MVA research incorporating DTI is under development and exciting advances in this field are expected in the next few years that combine advanced MVA technologies with the enormous amounts of data acquired in DTI examinations.

The scientific literature has seen enormous growth in studies focused on developmental imaging of pre-adult populations that make use of MVA technologies. However, much of this work has been focused in pediatric imaging with considerably less focus on neonatal and fetal populations. Neonatal imaging is more challenging as brain size is considerably smaller than in pediatrics and it is more challenging for imaging technicians to get a neonate to remain motionless during their imaging examination. Patient movement induces multiple types of imaging artifacts which can negatively affect MVA. Fetal imaging is the largest challenge of the three as the brain sizes are the smallest and movement remains a major issue. Furthermore, MRI technology is reliant on the spatial proximity of a coil/antenna to the

tissue/organ being imaged. Normal brain imaging benefits from a specialized head coil that is mounted immediately adjacent to the subject's cranium, however, in fetal imaging this is not possible and so coils are located outside the mother's abdomen, inherently reducing image quality. Additional challenges exist in fetal imaging due to *in utero* variations in tissue contrast relative to that observed at later developmental stages. Regardless of the many challenges inherent in the use of MVA in the imaging of fetal, neonatal and pediatric populations, there is considerably large potential for ongoing growth in this research field.

CONCLUSION

Multivariate analysis (MVA) technologies can play a useful role in helping to answer questions about structural and functional organization in the developing brain. Furthermore, MVA techniques have the potential to better characterize subject anatomy and physiology than a univariate technique could produce alone. MVA technologies have tremendous potential in the creation of the next generation of clinical diagnostic tests informed by the large amount of information acquired by MRI. MVA technologies have exhibited enormous growth in developmental brain MRI in pre-adult populations with an emphasis on pediatric imaging. The technologies are very flexible and a wide range of potential applications have already been investigated, however, so many variations on MVA technologies are available in the scientific literature that ample research will need to be performed in order to properly evaluate the trade-offs imposed by the selection of a given MVA technique for any particular analysis task. Future work will look at improving MVA techniques and adapting them to better characterize healthy neurological development in pre-adult populations.

ACKNOWLEDGMENTS

This article was supported by the National Institute of Health grants R01HD078561 and R03NS091587 to ET.

REFERENCES

- Adams, E., Chau, V., Poskitt, K. J., Grunau, R. E., Synnes, A., and Miller, S. P. (2010). Tractography-based quantitation of corticospinal tract development in premature newborns. *J. Pediatr.* 156, 882–888. doi: 10.1016/j.jpeds.2009.12.030
- Aljabar, P., Wolz, R., Srinivasan, L., Counsell, S., Boardman, J. P., Murgasova, M., et al. (2010). Combining morphological information in a manifold learning framework: application to neonatal MRI. *Proc. Med. Image Comput. Comput. Assist. Interv.* 13(Pt 3), 1–8. doi: 10.1007/978-3-642-15711-0_1
- Aljabar, P., Wolz, R., Srinivasan, L., Counsell, S. J., Rutherford, M. A., Edwards, A. D., et al. (2011). A Combined manifold learning analysis of shape and appearance to characterize neonatal brain development. *IEEE Trans. Med. Imag.* 30, 2072–2086. doi: 10.1109/TMI.2011.2162529
- Altaye, M., Holland, S. K., Wilke, M., and Gaser, C. (2008). Infant brain probability templates for MRI segmentation and normalization. *Neuroimage* 43, 721–730. doi: 10.1016/j.neuroimage.2008.07.060
- Altman, N. S. (1992). An introduction to kernel and nearest-neighbor nonparametric regression. *Am. Statistic.* 46, 175–185.
- Arzhaeva, Y., van Rikxoort, E., and van Ginneken, B. (2007). "Automated segmentation of caudate nucleus in MR brain images with voxel classification," in *Proceedings Medical Image Computing and Computer Assisted Intervention Workshop on 3D Segmentation in the Clinic: A Grand Challenge*, eds T. Heimann, M. Styner, and B. van Ginneken (Brisbane, QLD: Springer), 65–72.
- Awate, S. P., Yushkevich, P. A., Song, Z., Licht, D. J., and Gee, J. C. (2010). Cerebral cortical folding analysis with multivariate modeling and testing: studies on gender differences and neonatal development. *NeuroImage* 53, 450–459. doi: 10.1016/j.neuroimage.2010.06.072
- Babalola, K. O., Petrovic, V., Coates, T. F., Taylor, C. J., Twining, C. J., Williams, T. G., et al. (2007). "Automatic segmentation of the caudate nuclei using active appearance models," in *Proceedings Medical Image Computing and Computer Assisted Intervention Workshop on 3D Segmentation in the Clinic: A Grand Challenge*, eds T. Heimann, M. Styner, and B. van Ginneken (Brisbane, QLD: Springer), 57–64.
- Ball, G. H., and Hall, D. J. (1965). ISODATA, A novel method of DATA analysis and classification. *Stanford Res. Inst.* 699, 1–61.
- Batchelor, P. G., Castellano Smith, A. D., Hill, D. L. G., Hawkes, D. J., Cox, T. C. S., and Dean, A. F. (2002). Measures of folding applied to the

- development of the human fetal brain. *IEEE Trans. Med. Imag.* 21, 953–965. doi: 10.1109/TMI.2002.803108
- Beucher, S., and Meyer, F. (1993). “The morphological approach to segmentation: the watershed transformation,” in *Mathematical Morphology in Image Processing*, ed E. R. Dougherty (Rochester, NY: CRC Press), 433–481.
- Bray, S., Chang, C., and Hoeft, F. (2009). Applications of multivariate pattern classification analyses in developmental neuroimaging of healthy and clinical populations. *Front. Hum. Neurosci.* 3:32. doi: 10.3389/neuro.09.032.2009
- Breiman, L. (2001). Random forests. *Mach. Learn.* 45, 5–32. doi: 10.1023/A:1010933404324
- Brown, T. T., Kuperman, J. M., Chung, Y., Erhart, M., McCabe, C., Hagler, D. J. Jr., et al. (2012). Neuroanatomical assessment of biological maturity. *Curr. Biol.* 22, 1693–1698. doi: 10.1016/j.cub.2012.07.002
- Bunge, S. A., Dudukovic, N. M., Thomason, M. E., Vaidya, C. J., and Gabrieli, J. D. E. (2002). Immature frontal lobe contributions to cognitive control in children: evidence from fMRI. *Neuron* 33, 301–311. doi: 10.1016/S0896-6273(01)00583-9
- Carbonell, J. G., Michalski, R. S., and Mitchell, T. M. (1983). “An overview of machine learning,” in *Machine Learning, an Artificial Intelligence Approach*, ed R. S. Michalski (Heidelberg: Springer), 3–23.
- Casanova, R., Whitlow, C. T., Wagner, B., Espeland, M. A., and Maldjian, J. A. (2012). Combining graph and machine learning methods to analyze differences in functional connectivity across sex. *Open Neuroimag. J.* 6, 1–9. doi: 10.2174/18744440001206010001
- Casey, B. J., Trainor, R. J., Orendi, J. L., Schubert, A. B., Nystrom, L. E., Giedd, J. N., et al. (1997). A developmental functional MRI study of prefrontal activation during performance of a Go-No-Go task. *J. Cogn. Neurosci.* 9, 835–847. doi: 10.1162/jocn.1997.9.6.835
- Chen, Y., Zhu, H., An, H., Armado, D., Shen, D., Gilmore, J. H., et al. (2014). More insights into early brain development through statistical analyses of eigen-structural elements of diffusion tensor imaging using multivariate adaptive regression splines. *Brain Struct. Funct.* 219, 551–569. doi: 10.1007/s00429-013-0517-7
- Cohen, J. (1960). A coefficient of agreement for nominal scales. *Educ. Psychol. Meas.* 20, 37–46. doi: 10.1177/001316446002000104
- Commowick, O., and Warfield, S. K. (2010). Estimation of inferential uncertainty in assessing segmentation performance from STAPLE. *IEEE Trans. Med. Imaging* 29, 771–780. doi: 10.1109/TMI.2009.2036011
- Delpolyi, A. R., Mukherjee, P., Gill, K., Henry, R. G., Partridge, S. C., Veeraraghavan, S., et al. (2005). Comparing microstructural and macrostructural development of the cerebral cortex in premature newborns: diffusion tensor imaging versus cortical gyration. *Neuroimage* 27, 579–586. doi: 10.1016/j.neuroimage.2005.04.027
- Dempster, A. P., Laird, N. M., and Rubin, D. B. (1977). Maximum likelihood from incomplete data via the EM algorithm. *J. R. Statist. Soc. B* 39, 1–38.
- Devi, C. N., Chandrasekharan, A., Sundararaman, V. K., and Alex, Z. C. (2014). “Automatic segmentation of neonatal brain magnetic resonance images,” in *Proceedings International Conference on Communications and Signal Processing* (Bangkok: IEEE), 640–643.
- Devroye, L., Györfi, L., and Lugosi, G. (1996). *A Probabilistic Theory of Pattern Recognition*. New York, NY: Springer.
- Dice, L. R. (1945). Measures of the amount of ecologic association between species. *Ecology* 26, 297–302. doi: 10.2307/1932409
- Dittrich, E., Riklin Raviv, T., Kasprian, G., Donner, R., Brugger, P. C., Prayer, D., et al. (2014). A spatio-temporal latent atlas for semi-supervised learning of fetal brain segmentations and morphological age estimation. *Med. Image Anal.* 18, 9–21. doi: 10.1016/j.media.2013.08.004
- Dosenbach, N. U. F., Nardos, B., Cohen, A. L., Fair, D. A., Power, J. D., Church, J. A., et al. (2010). Prediction of Individual Brain Maturity Using fMRI. *Science* 329, 1358–1361. doi: 10.1126/science.1194144
- Dunteman, G. H. (1989). *Principal Components Analysis*. Newbury Park: SAGE Publications Inc.
- Erus, G., Battapady, H., Satterthwaite, T. D., Hakonarson, H., Gur, R. E., Davatzikos, C., et al. (2015). Imaging patterns of brain development and their relationship to cognition. *Cereb. Cortex* 25, 1676–1684. doi: 10.1093/cercor/bht425
- Fair, D. A., Cohen, A. L., Power, J. D., Dosenbach, N. U. F., Church, J. A., Miezin, F. M., et al. (2009). Functional brain networks develop from a “local to distributed” organization. *PLoS Comput. Biol.* 5:e1000381. doi: 10.1371/journal.pcbi.1000381
- Fearon, P., O’Connell, P., Frangou, S., Aquino, P., Nosarti, C., Allin, M., et al. (2004). Brain volumes in adult survivors of very low birth weight: a sibling-controlled study. *Pediatrics* 114, 367–371. doi: 10.1542/peds.114.2.367
- Ferrazzi, G., Murgasova, M. K., Arichi, T., Malamateniou, C., Fox, M. J., Makropoulos, A., et al. (2014). Resting state fMRI in the moving fetus: a robust framework for motion, bias field and spin history correction. *Neuroimage* 101, 555–568. doi: 10.1016/j.neuroimage.2014.06.074
- Fox, M. D., Snyder, A. Z., Vincent, J. L., Corbetta, M., Van Essen, D. C., and Raichle, M. E. (2005). The human brain is intrinsically organized into dynamic, anticorrelated functional networks. *Proc. Natl. Acad. Sci. U.S.A.* 102, 9673–9678. doi: 10.1073/pnas.0504136102
- Franke, K., Luders, E., May, A., Wilke, M., and Gaser, C. (2012). Brain maturation: predicting individual BrainAGE in children and adolescents using structural MRI. *Neuroimage* 63, 1305–1312. doi: 10.1016/j.neuroimage.2012.08.001
- Friedman, J., Hastie, T., and Tibshirani, R. (1998). Additive logistic regression: a statistical view of boosting. *Ann. Stat.* 28, 337–407. doi: 10.1214/aos/1016218223
- Giedd, J. N., Blumenthal, J., Jeffries, N. O., Castellanos, F. X., Liu, H., Zijdenbos, A., et al. (1999). Brain development during childhood and adolescence: a longitudinal MRI study. *Nat. Neurosci.* 2, 861–863. doi: 10.1038/13158
- Giedd, J. N., Schmitt, J. E., and Neale, M. C. (2007). Structural brain magnetic resonance imaging of pediatric twins. *Hum. Brain Mapp.* 28, 474–481. doi: 10.1002/hbm.20403
- Glass, J. O., Ji, Q., Glas, L. S., and Reddick, W. E. (2003). Prediction of total cerebral tissue volumes in normal appearing brain from sub-sampled segmentation volumes. *Magn. Reson. Imaging* 21, 977–982. doi: 10.1016/j.mri.2003.05.010
- Gogtay, N., Giedd, J. N., Lusk, L., Hayashi, K. M., Greenstein, D., Vaituzis, A. C., et al. (2004). Dynamic mapping of human cortical development during childhood through early adulthood. *Proc. Natl. Acad. Sci.* 101, 8174–8179. doi: 10.1073/pnas.0402680101
- Goldberg, Y., Zakai, A., Kushnir, D., and Ritov, Y. (2008). Manifold learning: the price of normalization. *J. Machine Learn. Res.* 9, 1909–1939.
- Goodlett, C. B., Fletcher, P. T., Gilmore, J. H., and Gerig, G. (2008). Group statistics of DTI fiber bundles using spatial functions of tensor measures. *Proc. Med. Image Comput. Comput. Assist. Interv.* 11(Pt 1), 1068–1075. doi: 10.1007/978-3-540-85988-8_127
- Gousias, I. S., Hammers, A., Counsell, S. J., Edwards, A. D., and Rueckert, D. (2012). “Automatic segmentation of pediatric brain MRIs using a maximum probability pediatric atlas,” *Proceedings of the International Conference on Imaging Systems and Techniques* (Manchester: IEEE), 95–100. doi: 10.1109/ist.2012.6295511
- Gouttard, S., Styner, M., Joshi, S., Smith, R. G., Hazlett, H. C., and Gerig, G. (2007). “Subcortical structure segmentation using probabilistic atlas priors,” in *Proceedings Medical Image Computing and Computer Assisted Intervention Workshop on 3D Segmentation in the Clinic: A Grand Challenge*, eds T. Heimann, M. Styner, B. van Ginneken (Brisbane, QLD: Springer), 37–46.
- Greene, D. J., Laumann, T. O., Dubis, J. W., Ihnen, S. K., Neta, M., Power, J. D., et al. (2014). Developmental changes in the organization of functional connections between the basal ganglia and cerebral cortex. *J. Neurosci.* 34, 5842–5854. doi: 10.1523/JNEUROSCI.3069-13.2014
- Greig, D. M., Porteous, B. T., and Seheult, A. H. (1989). Exact maximum a posteriori estimation for binary images. *J. R. Statist. Soc. Ser. B* 51, 271–279.
- Habas, P. A., Kim, K., Rousseau, F., Glenn, O. A., Barkovich, A. J., and Studholme, C. (2008). Atlas-based segmentation of the germinal matrix from in utero clinical MRI of the fetal brain. *Proc. Med. Imaging Comput. Comput. Assist. Interv.* 11(Pt 1), 351–358. doi: 10.1007/978-3-540-85988-8_42
- Han, C. E., Peraza, L. R., Taylor, J.-P., and Kaiser, M. (2014). “Predicting age of human subjects based on structural connectivity from diffusion tensor imaging,” in *Proceedings of the IEEE Biomedical Circuits and Systems Conference* (Lausanne: IEEE), 137–140.
- He, L., and Parikh, N. A. (2013). Automated detection of white matter signal abnormality using T2 relaxometry: application to brain segmentation on term MRI in very preterm infants. *Neuroimage* 64, 328–340. doi: 10.1016/j.neuroimage.2012.08.081
- Hyvarinen, A., Karhunen, J., and Oja, E. (2004). *Independent Component Analysis*. New York, NY: John Wiley & Sons Inc.

- Isgum, I., Benders, M. J. N. L., Avants, B., Cardoso, M. J., Counsell, S. J., Gomez, E. F., et al. (2015). Evaluation of automatic neonatal brain segmentation algorithms: the NeoBrainS12 challenge. *Med. Image Analysis* 20, 135–151. doi: 10.1016/j.media.2014.11.001
- Jaccard, P. (1901). Étude comparative de la distribution florale dans une portion des Alpes et des Jura. *Bull. de la Soc. Vaudoise des Sci. Nat.* 37, 547–579.
- Jakab, A., Schwartz, E., Kasprian, G., Gruber, G. M., Prayer, D., Schopf, V., et al. (2014). Fetal functional imaging portrays heterogeneous development of emerging human brain networks. *Front. Hum. Neurosci.* 8:852. doi: 10.3389/fnhum.2014.00852
- Jardri, R., Houfflin-Debarge, V., Delion, P., Pruvo, J. P., Thomas, P., and Pins, D. (2012). Assessing fetal response to maternal speech using a noninvasive functional brain imaging technique. *Int. J. Dev. Neurosci.* 30, 159–161. doi: 10.1016/j.ijdevneu.2011.11.002
- Jardri, R., Pins, D., Houfflin-Debarge, V., Chaffiotte, C., Rocourt, N., Pruvo, J. P., et al. (2008). Fetal cortical activation to sound at 33 weeks of gestation: a functional MRI study. *Neuroimage* 42, 10–18. doi: 10.1016/j.neuroimage.2008.04.247
- Keraudren, K., Kuklisova-Murgasova, M., Kyriakopoulou, V., Malamateniou, C., Rutherford, M. A., Kainz, B., et al. (2014). Automated fetal brain segmentation from 2D MRI slices for motion correction. *Neuroimage* 101, 633–643. doi: 10.1016/j.neuroimage.2014.07.023
- Keraudren, K., Kyriakopoulou, V., Rutherford, M., Hajnal, J. V., and Rueckert, D. (2013). Localisation of the brain in fetal MRI using bundled SIFT features. *Proc. Med. Image Comput. Comput. Assist. Interv.* 16(Pt 1), 582–589. doi: 10.1007/978-3-642-40811-3_73
- Ketonen, L. M., Hiwatashi, A., Sidhu, R., and Westesson, P.-L. (2004). Pediatric Brain and Spine: *An Atlas of MRI and Spectroscopy*. Heidelberg: Springer.
- Khundrakpam, B. S., Tohka, J., Evans, A. C., and the Brain Development Cooperative Group (2015). Prediction of brain maturity based on cortical thickness at different spatial resolutions. *Neuroimage* 111, 350–359. doi: 10.1016/j.neuroimage.2015.02.046
- Koshiba, M., Kakei, H., Honda, M., Karino, G., Niitsu, M., Miyaji, T., et al. (2015). Early-infant diagnostic predictors of the neuro-behavioral development after neonatal care. *Behav. Brain Res.* 276, 143–150. doi: 10.1016/j.bbr.2014.05.054
- Levy, J. H., Gorczowski, K., Liu, X., Pizer, S. M., and Styner, M. (2007). “Caudate segmentation using deformable M-reps,” in *Proceedings Medical Image Computing and Computer Assisted Intervention Workshop on 3D Segmentation in the Clinic: A Grand Challenge*, eds T. Heimann, M. Styner, and B. van Ginneken (Brisbane, QLD: Springer), 47–55.
- Liu, J., Smith, C., and Chebrolu, H. (2007). “Automatic subcortical structure segmentation using local likelihood-based active contour,” in *Proceedings Medical Image Computing and Computer Assisted Intervention Workshop on 3D Segmentation in the Clinic: A Grand Challenge*, eds T. Heimann, M. Styner and B. van Ginneken (Brisbane, QLD: Springer), 91–98.
- Manton, K. G., Lowmore, G., Yashin, A., and Kovtun, M. (2014). *Cluster Analysis: Overview*. Wiley StatsRef: Statistics Reference Online.
- Matsuzawa, J., Matsui, M., Konishi, T., Noguchi, K., Gur, R. C., Bilker, W., et al. (2001). Age-related volumetric changes of brain gray and white matter in healthy infants and children. *Cereb. Cortex* 11, 335–342. doi: 10.1093/cercor/11.4.335
- McIntosh, A. R., Bookstein, F. L., Haxby, J. V., and Grady, C. L. (1996). Spatial pattern analysis of functional brain images using partial least squares. *Neuroimage* 3, 143–157. doi: 10.1006/nimg.1996.0016
- McLachlan, G. J. (2004). *Discriminant Analysis and Statistical Pattern Recognition*. Hoboken, NJ: Wiley Interscience.
- Mesulam, M. M. (1981). A cortical network for directed attention and unilateral neglect. *Ann. Neurol.* 10, 309–325. doi: 10.1002/ana.410100402
- Muzik, O., Chugani, D. C., Juhasz, C., Shen, C., and Chugani, H. T. (2000). Statistical parametric mapping: assessment of application in children. *Neuroimage* 12, 538–549. doi: 10.1006/nimg.2000.0651
- Mwangi, B., Hasan, K. M., and Soares, J. C. (2013). Prediction of individual subject's age across the human lifespan using diffusion tensor imaging: a machine learning approach. *Neuroimage* 75, 58–67. doi: 10.1016/j.neuroimage.2013.02.055
- Nelder, J. R., and Wedderburn, R. (1972). Generalized linear models. *J. R. Statist. Soc. Ser. A* 135, 370–384. doi: 10.2307/2344614
- Nosarti, C., Rushe, T. M., Woodruff, P. W. R., Stewart, A. L., Rifkin, L., and Murray, R. M. (2004). Corpus callosum size and very preterm birth: relationship to neuropsychological outcome. *Brain* 127(Pt 9), 2080–2089. doi: 10.1093/brain/awh230
- Pontabry, J., Rousseau, F., Oubel, E., Studholme, C., Koob, M., and Dietemann, J. L. (2013). Probabilistic tractography using Q-ball imaging and particle filtering: application to adult and in-utero fetal brain studies. *Med. Image Anal.* 17, 297–310. doi: 10.1016/j.media.2012.11.004
- Power, J. D., Barnes, K. A., Snyder, A. Z., Schlaggar, B. L., and Petersen, S. E. (2012). Spurious but systematic correlations in functional connectivity MRI networks arise from subject motion. *Neuroimage* 59, 2142–2154. doi: 10.1016/j.neuroimage.2011.10.018
- Reiss, A. L., Abrams, M. T., Singer, H. S., Ross, J. L., and Denckla, M. B. (1996). Brain development, gender and IQ in children. A volumetric imaging study. *Brain* 119(Pt 5), 1763–1774. doi: 10.1093/brain/119.5.1763
- Rencher, A. C., and Christensen, W. F. (2012). *Methods of Multivariate Analysis*. New York, NY: John Wiley & Sons Inc.
- Rodriguez-Carranza, C., Mukherjee, P., Vigneron, D., Barkovich, J., and Studholme, C. (2006). A system for measuring regional surface folding of the neonatal brain from MRI. *Proc. Med. Image Comput. Comput. Assist. Interv.* 9(Pt 2), 201–208. doi: 10.1007/11866763_25
- Schmithorst, V. J., Holland, S. K., and Plante, E. (2007). Development of effective connectivity for narrative comprehension in children. *Neuroreport* 18, 1411–1415. doi: 10.1097/WNR.0b013e3282e9a4ef
- Schmitt, J. E., Lenroot, R. K., Ordaz, S. E., Wallace, G. L., Lerch, J. P., Evans, A. C., et al. (2009). Variance decomposition of MRI-based covariance maps using genetically informative samples and structural equation modeling. *Neuroimage* 47, 56–64. doi: 10.1016/j.neuroimage.2008.06.039
- Schmitt, J. E., Lenroot, R. K., Wallace, G. L., Ordaz, S., Taylor, K. N., Kabani, N., et al. (2008). Identification of genetically mediated cortical networks: a multivariate study of pediatric twins and siblings. *Cereb. Cortex* 18, 1737–1747. doi: 10.1093/cercor/bhm211
- Schmitt, J. E., Wallace, G. L., Lenroot, R. K., Ordaz, S. E., Greenstein, D., Clasen, L., et al. (2010). A twin study of intercerebral volumetric relationships. *Behav. Genet.* 40, 114–124. doi: 10.1007/s10519-010-9332-6
- Schmitt, J. E., Wallace, G. L., Rosenthal, M. A., Molloy, E. A., Ordaz, S., Lenroot, R., et al. (2007). A multivariate analysis of neuroanatomic relationships in a genetically informative pediatric sample. *Neuroimage* 35, 70–82. doi: 10.1016/j.neuroimage.2006.04.232
- Schonmeyer, R., and Schmidt, G. (2007). Segmentation of caudate nucleus from magnetic resonance imaging using Cognition Network Technology,” in *Proceedings Medical Image Computing and Computer Assisted Intervention Workshop on 3D Segmentation in the Clinic: A Grand Challenge*, eds T. Heimann, M. Styner, and B. van Ginneken (Brisbane, QLD: Springer), 81–89.
- Schopf, V., Kasprian, G., Brugger, P. C., and Prayer, D. (2012). Watching the fetal brain at ‘rest’. *Int. J. Dev. Neurosci.* 30, 11–17. doi: 10.1016/j.ijdevneu.2011.10.006
- Schopf, V., Schlegl, T., Jakab, A., Kasprian, G., Woitek, R., Prayer, D., et al. (2014). The relationship between eye movement and vision develops before birth. *Front. Hum. Neurosci.* 8:775. doi: 10.3389/fnhum.2014.00775
- Serag, A., Gousias, I. S., Makropoulos, A., Aljabar, P., Hajnal, J. V., Boardman, J. P., et al. (2012). Unsupervised learning of shape complexity: application to brain development. *Spatio Temp. Image Anal. Longit. Time Ser. Image Data* 7570, 88–99. doi: 10.1007/978-3-642-33555-6_8
- Shan, Z. Y., Parra, C., Ji, Q., Ogg, R. J., Zhang, Y., Laningham, F. H., et al. (2006). A digital pediatric brain structure atlas from T1-weighted MR images. *Proc. Med. Image Comput. Comput. Assist. Interv.* 9(Pt 2), 332–339. doi: 10.1007/11866763_41
- Shaw, P., Kabani, N. J., Lerch, J. P., Eckstrand, K., Lenroot, R., Gogtay, N., et al. (2008). Neurodevelopmental trajectories of the human cerebral cortex. *J. Neurosci.* 28, 3586–3594. doi: 10.1523/JNEUROSCI.5309-07.2008
- Shehzad, Z., Kelly, C., Reiss, P. T., Cameron Craddock, R., Emerson, J. W., McMahon, K., et al. (2014). A multivariate distance-based analytic framework for connectome-wide association studies. *Neuroimage* 93, 74–94. doi: 10.1016/j.neuroimage.2014.02.024
- Shi, F., Fan, Y., Tang, S., Gilmore, J. H., Lin, W., and Shen, D. (2010). Neonatal brain image segmentation in longitudinal MRI studies. *Neuroimage* 49, 391–400. doi: 10.1016/j.neuroimage.2009.07.066

- Shi, F., Wang, L., Dai, Y., Gilmore, J. H., Lin, W., and Shen, D. (2012). LABEL: pediatric brain extraction using learning-based meta-algorithm. *Neuroimage* 62, 1975–1986. doi: 10.1016/j.neuroimage.2012.05.042
- Skold, B., Alexandrou, G., Padilla, N., Blennow, M., Vollmer, B., and Aden, U. (2014). Sex differences in outcome and associations with neonatal brain morphology in extremely preterm children. *J. Pediatr.* 164, 1012–1018. doi: 10.1016/j.jpeds.2013.12.051
- Smith, H. F. (1958). A multivariate analysis of covariance. *Biometrics* 14, 107–127. doi: 10.2307/2527733
- Smyser, C. D., and Neil, J. J. (2015). Use of resting-state functional MRI to study brain development and injury in neonates. *Semin. Perinatol.* 39, 130–140. doi: 10.1053/j.semperi.2015.01.006
- Song, Z., Awate, S. P., Licht, D. J., and Gee, J. C. (2007). Clinical neonatal brain MRI segmentation using adaptive nonparametric data models and intensity-based markov pairs. *Proc. Med. Image Comput. Comput. Assist. Interv.* 10(Pt 1), 883–890. doi: 10.1371/journal.pbio.1000157
- Song, Z., Tustison, N., Avants, B., and Gee, J. C. (2006). Integrated graph cuts for brain MRI segmentation. *Proc. Med. Image Comput. Comput. Assist. Interv.* 9(Pt 2), 831–838. doi: 10.1007/11866763_102
- Supekar, K., Musen, M., and Menon, V. (2009). Development of large-scale functional brain networks in children. *PLoS Biol.* 7:e1000157. doi: 10.1371/journal.pbio.1000157
- Takahashi, E., Folkerth, R. D., Galaburda, A. M., and Grant, P. E. (2012). Emerging cerebral connectivity in the human fetal brain: an MR tractography study. *Cereb. Cortex* 22, 455–464. doi: 10.1093/cercor/bhr126
- Talairach, J., and Tournoux, P. (1988). *Co-planar Stereotaxic Atlas of the Human Brain: 3-Dimensional Proportional System – An Approach to Cerebral Imaging*. New York, NY: Thieme Medical Publishers.
- Thomas, K. M., Drevets, W. C., Whalen, P. J., Eccard, C. H., Dahl, R. E., Ryan, N. D., et al. (2001). Amygdala response to facial expressions in children and adults. *Biol. Psychiatry* 49, 309–316. doi: 10.1016/S0006-3223(00)01066-0
- Thomason, M. E., Dassanayake, M. T., Shen, S., Katkuri, Y., Alexis, M., Anderson, A. L., et al. (2013). Cross-hemispheric functional connectivity in the human fetal brain. *Sci. Transl. Med.* 5, 173ra24. doi: 10.1126/scitranslmed.3004978
- Tich, S. N. T., Anderson, P. J., Hunt, R. W., Lee, K. J., Doyle, L. W., and Inder, T. E. (2011). Neurodevelopmental and perinatal correlates of simple brain metrics in very preterm infants. *Arch. Pediatr. Adolesc. Med.* 165, 216–222. doi: 10.1001/archpediatrics.2011.9
- Tipping, M. E. (2001). Sparse bayesian learning and the relevance vector machine. *J. Mach. Learn. Res.* 1, 211–244.
- Toews, M., Wells, W. M. III, and Zollei, L. (2012). A feature-based developmental model of the infant brain in structural MRI. *Proc. Med. Image Comput. Comput. Assist. Interv.* 7511, 204–211. doi: 10.1007/978-3-642-33418-4_26
- Tu, Z., Mizra, M., Dinov, I., and Toga, A. W. (2007). “Automatic caudate segmentation by hybrid generative/discriminative models,” in *Proceedings Medical Image Computing and Computer Assisted Intervention Workshop on 3D Segmentation in the Clinic: A Grand Challenge*, eds T. Heimann, M. Styner, and B. van Ginneken (Brisbane, QLD: Springer), 73–80.
- Vaadia, E., Haalman, I., Abeles, M., Bergman, H., Prut, Y., Slovin, H., et al. (1995). Dynamics of neuronal interactions in monkey cortex in relation to behavioural events. *Nature* 373, 515–518. doi: 10.1038/373515a0
- van Ginneken, B., Heimann, T., and Styner, M. (2007). “3D Segmentation in the clinic: a grand challenge,” in *Proceedings Medical Image Computing and Computer Assisted Intervention Workshop on 3D Segmentation in the Clinic: A Grand Challenge*, eds T. Heimann, M. Styner, and B. van Ginneken (Brisbane, QLD: Springer), 7–15.
- van Rikxoort, E., Arzhaeva, Y., and van Ginneken, B. (2007). “A multi-atlas approach to automatic segmentation of the caudate nucleus in MR brain images,” in *Proceedings Medical Image Computing and Computer Assisted Intervention Workshop on 3D Segmentation in the Clinic: A Grand Challenge*, eds T. Heimann, M. Styner, and B. van Ginneken (Brisbane, QLD: Springer), 29–36.
- Vapnik, V. N. (1995). *The Nature of Statistical Learning Theory*. New York, NY: Springer.
- Wang, L., Gao, Y., Shi, F., Li, G., Gilmore, J. H., Lin, W., et al. (2015). LINKS: learning-based multi-source IntegratioN framework for Segmentation of infant brain images. *Neuroimage* 108, 160–172. doi: 10.1016/j.neuroimage.2014.12.042
- Wang, Z., Fernandez-Seara, M., Alsop, D. C., Liu, W.-C., Flax, J. F., Benasich, A. A., et al. (2008). Assessment of functional development in normal infant brain using arterial spin labelled perfusion MRI. *Neuroimage* 39, 973–978. doi: 10.1016/j.neuroimage.2007.09.045
- Warne, R. T. (2014). A primer on multivariate analysis of variance (MANOVA) for behavioral scientists. *Practical Assess. Res. Eval.* 19, 1–10.
- Weisenfeld, N. I., and Warfield, S. K. (2009). Automatic segmentation of newborn brain MRI. *Neuroimage* 47, 564–572. doi: 10.1016/j.neuroimage.2009.04.068
- Wels, M., Huber, M., and Hornegger, J. (2007). “Fully automated knowledge-based segmentation of the caudate nuclei in 3-D MRI,” in *Proceedings Medical Image Computing and Computer Assisted Intervention Workshop on 3D Segmentation in the Clinic: A Grand Challenge*, eds T. Heimann, M. Styner, and B. van Ginneken (Brisbane, QLD: Springer), 19–27.
- White, T., Muetzel, R., Schmidt, M., Langeslag, S. J., Jaddoe, V., Hofman, A., et al. (2014). Time of acquisition and network stability in pediatric resting-state functional magnetic resonance imaging. *Brain Connect.* 4, 417–427. doi: 10.1089/brain.2013.0195
- Xu, G., Takahashi, E., Folkerth, R. D., Haynes, R. L., Volpe, J. J., Grant, P. E., et al. (2014). Radial coherence of diffusion tractography in the cerebral white matter of the human fetus: neuroanatomic insights. *Cereb. Cortex* 24, 579–592. doi: 10.1093/cercor/bhs330
- Xue, H., Srinivasan, L., Jiang, S., Rutherford, M., Edwards, A. D., Rueckert, D., et al. (2007a). Automatic cortical segmentation in the developing brain. *Inf. Process. Med. Imaging* 20, 257–269. doi: 10.1007/978-3-540-73273-0_22
- Xue, H., Srinivasan, L., Jiang, S., Rutherford, M., Edwards, A. D., Rueckert, D., et al. (2007b). Automatic segmentation and reconstruction of the cortex from neonatal MRI. *Neuroimage* 38, 461–477. doi: 10.1016/j.neuroimage.2007.07.030
- Yegnanarayana, B. (2009). *Artificial Neural Networks*. New Delhi: PHI Learning Pvt. Ltd.
- Zadeh, L. A. (1965). Fuzzy sets. *Informat. Control* 8, 338–353. doi: 10.1016/S0019-9958(65)90241-X
- Zhang, W., Li, R., Deng, H., Wang, L., Lin, W., Ji, S., et al. (2015). Deep convolutional neural networks for multi-modality isointense infant brain segmentation. *Neuroimage* 108, 214–224. doi: 10.1016/j.neuroimage.2014.12.061
- Zhou, Z., Wang, X., Klahr, N. J., Liu, W., Arias, D., Liu, H., et al. (2011). A conditional Granger causality model approach for group analysis in functional magnetic resonance imaging. *Magn. Reson. Imaging* 29, 418–433. doi: 10.1016/j.mri.2010.10.008

Conflict of Interest Statement: The authors declare that the research was conducted in the absence of any commercial or financial relationships that could be construed as a potential conflict of interest.

Copyright © 2016 Levman and Takahashi. This is an open-access article distributed under the terms of the Creative Commons Attribution License (CC BY). The use, distribution or reproduction in other forums is permitted, provided the original author(s) or licensor are credited and that the original publication in this journal is cited, in accordance with accepted academic practice. No use, distribution or reproduction is permitted which does not comply with these terms.



Validation of *In utero* Tractography of Human Fetal Commissural and Internal Capsule Fibers with Histological Structure Tensor Analysis

Christian Mitter^{1,2*}, András Jakab³, Peter C. Brugger⁴, Gerda Ricken², Gerlinde M. Gruber⁴, Dieter Bettelheim⁵, Anke Scharrer⁶, Georg Langs³, Johannes A. Hainfellner², Daniela Prayer¹ and Gregor Kasprian¹

¹ Division of Neuroradiology and Musculoskeletal Radiology, Department of Biomedical Imaging and Image-guided Therapy, Medical University of Vienna, Vienna, Austria, ² Institute of Neurology, Medical University of Vienna, Vienna, Austria, ³ Computational Imaging Research Lab, Department of Biomedical Imaging and Image-guided Therapy, Medical University of Vienna, Vienna, Austria, ⁴ Department of Systematic Anatomy, Center for Anatomy and Cell Biology, Medical University of Vienna, Vienna, Austria, ⁵ Division of Obstetrics and Feto-maternal Medicine, Department of Obstetrics and Gynecology, Medical University of Vienna, Vienna, Austria, ⁶ Clinical Institute for Pathology, Medical University of Vienna, Vienna, Austria

OPEN ACCESS

Edited by:

Hao Huang,
University of Pennsylvania, USA

Reviewed by:

Marina Bentivoglio,
University of Verona, Italy
Matthew D. Budde,
Medical College of Wisconsin, USA

*Correspondence:

Christian Mitter
christian.mitter@meduniwien.ac.at

Received: 29 August 2015

Accepted: 07 December 2015

Published: 24 December 2015

Citation:

Mitter C, Jakab A, Brugger PC, Ricken G, Gruber GM, Bettelheim D, Scharrer A, Langs G, Hainfellner JA, Prayer D and Kasprian G (2015) Validation of *In utero* Tractography of Human Fetal Commissural and Internal Capsule Fibers with Histological Structure Tensor Analysis. *Front. Neuroanat.* 9:164. doi: 10.3389/fnana.2015.00164

Diffusion tensor imaging (DTI) and tractography offer the unique possibility to visualize the developing white matter macroanatomy of the human fetal brain *in vivo* and *in utero* and are currently under investigation for their potential use in the diagnosis of developmental pathologies of the human central nervous system. However, in order to establish *in utero* DTI as a clinical imaging tool, an independent comparison between macroscopic imaging and microscopic histology data in the same subject is needed. The present study aimed to cross-validate normal as well as abnormal *in utero* tractography results of commissural and internal capsule fibers in human fetal brains using postmortem histological structure tensor (ST) analysis. *In utero* tractography findings from two structurally unremarkable and five abnormal fetal brains were compared to the results of postmortem ST analysis applied to digitalized whole hemisphere sections of the same subjects. An approach to perform ST-based deterministic tractography in histological sections was implemented to overcome limitations in correlating *in utero* tractography to postmortem histology data. ST analysis and histology-based tractography of fetal brain sections enabled the direct assessment of the anisotropic organization and main fiber orientation of fetal telencephalic layers on a micro- and macroscopic scale, and validated *in utero* tractography results of corpus callosum and internal capsule fiber tracts. Cross-validation of abnormal *in utero* tractography results could be achieved in four subjects with agenesis of the corpus callosum (ACC) and in two cases with malformations of internal capsule fibers. In addition, potential limitations of current DTI-based *in utero* tractography could be demonstrated in several brain regions. Combining the three-dimensional nature of DTI-based *in utero* tractography with the microscopic resolution provided by histological ST analysis may ultimately facilitate a more complete morphologic characterization of axon guidance disorders at prenatal stages of human brain development.

Keywords: human fetal brain, diffusion tensor imaging, tractography, fetal MRI, structure tensor, histology, validation

INTRODUCTION

The development of the human fetal brain involves a precisely orchestrated sequence of events, from proliferation of neuronal and glial precursor cells within the germinal zones, to migration toward their prospective targets in the cortical plate or deep nuclei, and finally the organization and wiring into both local as well as long-range neuronal networks (Sidman and Rakic, 1973; Marin and Rubenstein, 2003; Bystron et al., 2008; Judaš, 2011). As the molecular mechanisms of axon guidance and synaptogenesis are being gradually uncovered in animal models (Fame et al., 2011; Grant et al., 2012; Molnár et al., 2012), new developmental frameworks for human brain malformations will increasingly incorporate knowledge about axon guidance defects and pathological white matter connectivity into their classification schemes (Fallet-Bianco et al., 2008; Edwards et al., 2014).

Fetal MRI has established itself as an important adjunct to ultrasound in the prenatal assessment of both normal brain development as well as central nervous system pathologies (Girard et al., 1995; Prayer et al., 2006; Prayer, 2011). Advanced MRI techniques like diffusion tensor imaging (DTI) and tractography (Basser et al., 1994; Mori et al., 1999) offer the unique possibility to investigate the three-dimensional anatomy of white matter fiber tracts *in vivo*, and have successfully been used to visualize the corpus callosum, the internal capsule, and even association fibers in the developing fetal brain *in utero* during the second and third trimester (Kasprian et al., 2008; Mitter et al., 2011, 2015). The ability to non-invasively assess abnormal connectivity in brain malformations, as has been shown for Probst bundles in cases of agenesis of the corpus callosum (ACC; Kasprian et al., 2013; Jakab et al., 2015a), demonstrates the potential of this novel technique for the prenatal diagnosis of white matter fiber tract pathologies and disorders of axon guidance. However, a more regular inclusion of DTI in clinical fetal MR protocols (Mailath-Pokorny et al., 2012; Jakab et al., 2015b) also underlines the need for an independent cross-validation of *in utero* DTI and tractography results, as well as insights about their limitations.

Until recently, validation of DTI-based tractography results in the adult human brain relied primarily on gross dissection studies using the Klingler fiber dissection technique (Ludwig and Klingler, 1956; Fernández-Miranda et al., 2008a,b; Martino et al., 2011), or direct comparison to myelin-stained histological sections (Bürgel et al., 2006). Newer histological techniques such as 3D-polarized light imaging (Axer et al., 2011a,b,c) or serial optical coherence scanner imaging (Wang et al., 2014a,b) are able to map the three-dimensional course of axons in postmortem human brain tissue based on the birefringence of myelin sheaths. Unfortunately, all of these techniques require the presence of myelin and are therefore not suited for validation of tractography results in the unmyelinated human fetal brain. Three-dimensional microscopy techniques that rely on rendering tissue transparent (Chung et al., 2013) are to date limited to small tissue volumes, and thus might be impractical for the systematic analysis of whole hemispheres in the human fetal brain. In animal models, DTI results can be microscopically validated by direct

autoradiographic axonal tract tracing (Schmahmann and Pandya, 2006; Schmahmann et al., 2007). However, axonal tracing in the human fetal brain, using lipophilic dyes like DiI, is time-consuming, limited to relatively short distances and challenging, since the dye has to be manually placed within a region of interest (Hevner, 2000).

To date, histological correlates of *in utero* (Kasprian et al., 2013) and postmortem DTI results in the human fetal brain have been identified by visual comparisons of imaging results to histological sections (Ren et al., 2006; Saksena et al., 2008; Trivedi et al., 2009a,b; Vasung et al., 2010, 2011; Widjaja et al., 2010; Huang et al., 2013; Xu et al., 2014). Due to its much higher resolution, postmortem DTI (Huang et al., 2006, 2009; Takahashi et al., 2012; Kolasinski et al., 2013) serves as an important anatomical reference for *in utero* DTI studies, but does not in itself solve the problem of validation.

Structure tensor (ST) analysis is an image processing approach that enables the directional analysis of fibers in histological sections on a microscopic scale (Rezakhaniha et al., 2012), and has already been used to study the microstructural white matter anatomy in whole-hemisphere sections of the adult human brain (Budde and Annese, 2013). In ST analysis, a ST is computed from a local neighborhood to derive the local orientation, anisotropy, and intensity for every pixel of an image. The results have been shown to correlate well to analogous quantitative measures of fiber orientation and fractional anisotropy derived from DTI (Budde and Frank, 2012). Importantly, ST analysis does not require the presence of myelin and can be performed on immunohistochemically stained sections, making it feasible for histology-based validation of DTI in the human fetal brain.

Due to multiple sources of artifacts and the limited resolution of *in utero* DTI, the corresponding tissue structures of *in utero* tractography findings, as well as ultimately their clinical relevance, are currently unclear. In order to establish and strengthen DTI as a diagnostic and prognostic prenatal imaging tool, we aimed at investigating the postmortem histological ST correlates of both normal and abnormal *in utero* tractography results for commissural and internal capsule fibers in seven fetal subjects. To further optimize the postmortem validation of DTI-based tractography (Budde et al., 2011), and to allow for a better macroscopic correlation, we implemented an approach to perform deterministic tractography on digitalized histological sections based on data derived from ST analysis. In addition, we utilized ST analysis to demonstrate the anisotropic organization and main fiber orientation of the transient fetal layers that can be identified in the telencephalic wall during the second trimester (Kostovic et al., 2002; Bystron et al., 2008) on a microscopic scale.

MATERIAL AND METHODS

Subjects

Histopathological specimens from seven human fetal brains were included in this study, in which 1.5 or 3 Tesla *in utero* DTI had been performed within a time span of 2 weeks prior to fetal demise (mean = 10 days). Imaging was performed during clinically indicated fetal MR examinations to

confirm sonographically detected fetal or extrafetal pathologies. In each case, parental counseling regarding termination of pregnancy followed a multidisciplinary conference (radiologists, obstetricians, neuropsychiatrists). Postmortem human brain tissue was obtained during routine neuropathological autopsies of the fetal brain after termination of pregnancy for medical reasons. Fetal subjects were 21–28 gestational weeks of age (GW, calculated from the first day of the woman's last menstrual cycle and determined with reference to a previous sonography examination) at the time of fetal MRI and 22–29 GW at the time of death. In two cases (subjects 1 and 6) neuropathological autopsy revealed normal brain development with no signs of cerebral malformations. The remaining five were fetuses with malformations of the developing white matter, including four cases of ACC and one case of Joubert syndrome. For a more detailed description of fetal pathologies see **Table 1**. All imaged mothers gave written, informed consent for the fetal MRI examination and the study was approved by the Ethics Committee of the Medical University of Vienna (EK Nr.:650/2010).

Fetal MR Imaging Protocol and *In utero* Tractography

Fetal imaging was performed in six cases on a 1.5 T MR system (Philips Gyroscan) using a five-channel phased-array cardiac coil, adjusted to the position of the fetal head. There was no sedation used. An echo planar diffusion tensor sequence was acquired in an axial plane perpendicular to the axis of the brainstem using 16

gradient-encoding directions, b -values of 0 and 700 s/mm² and a reconstructed asymmetric voxel size of 0.94/0.94/3 mm. One case (subject 5) underwent diagnostic 3 T MRI and was retrospectively included (reconstructed voxel size 2.01/2.01/4 mm, b -values of 0 and 700 s/mm², six gradient-encoding directions). Axial T2-weighted sequences were acquired as anatomical references for tractography (**Figures 1A–C**).

In utero tractography was performed using Philips Extended MR Workspace 2.6.3.3 according to the protocols described previously (Kasprian et al., 2008, 2013; Mitter et al., 2015). Briefly summarized, a multiple region of interest approach was used with a minimum of two regions of interest placed within the projection path of the fiber tract of interest. Fiber tracts were visualized using a deterministic linear tracking algorithm with an FA threshold of 0.15 and a maximum angle change of 27.0° (**Figure 1D**). The fiber tracts visualized with *in utero* tractography included the internal capsule in all subjects, the corpus callosum in the three subjects with normal commissural anatomy, and the Probst bundles in the four subjects with ACC. See Kasprian et al. (2008) and Kasprian et al. (2013) for details and images of region of interest placement.

Neuropathological Procedures and Immunohistochemistry

Histological specimens used for this study were obtained from the brain bank of the Institute of Neurology, Medical University of Vienna, Austria. In all cases a routine neurofetalopathological autopsy had been performed after termination of pregnancy

TABLE 1 | Neuropathology and extracranial pathologies of investigated fetal subjects.

Subject #	Gestational age at time of fetal MRI (in gestational weeks + days)	Gestational age at time of death	Neuropathology	Extracranial pathologies
Subject 1	20 + 2	21 + 3	No signs of cerebral malformations	Placental hypoplasia, small for gestational age, coarctation of the aorta
Subject 2	20 + 1	22 + 0	Joubert syndrome with hypoplastic vermis and molar-tooth configuration of the mesencephalon, heterotopic projection of the pyramidal tract into the interpeduncular cistern with interpeduncular white matter heterotopia and absence of the pyramidal tract caudal to the mesencephalon, normal anatomy of corpus callosum and internal capsule	Multicystic kidneys
Subject 3	20 + 4	22 + 1	Complete ACC, abnormal gyri and sulci in both frontal lobes, periventricular and subcortical gray matter heterotopia, malrotation of the right hippocampus, disorganized fiber architecture in the left corona radiata	No extracranial malformations
Subject 4	22 + 0	22 + 4	Complete ACC, subependymal heterotopia, hippocampal malrotation, cerebellar hypoplasia	Hypertelorism
Subject 5	22 + 0	23 + 5	Complete ACC, abnormal gyri and sulci in both frontal lobes, malformation of the left frontal lobe with disturbed lamination of the telencephalic wall, abnormal white matter architecture, and enlarged ganglionic eminence, midline cyst	Hypertelorism, epicanthic folds
Subject 6	25 + 1	26 + 3	No signs of cerebral malformations	Congenital muscular dystrophy, pulmonary hypoplasia, cardiac dilatation
Subject 7	27 + 1	29 + 0	Complete ACC, abnormal gyri and sulci in the right frontal lobe, delayed sulcation in the temporal lobes	Parvovirus infection, no extracranial malformations

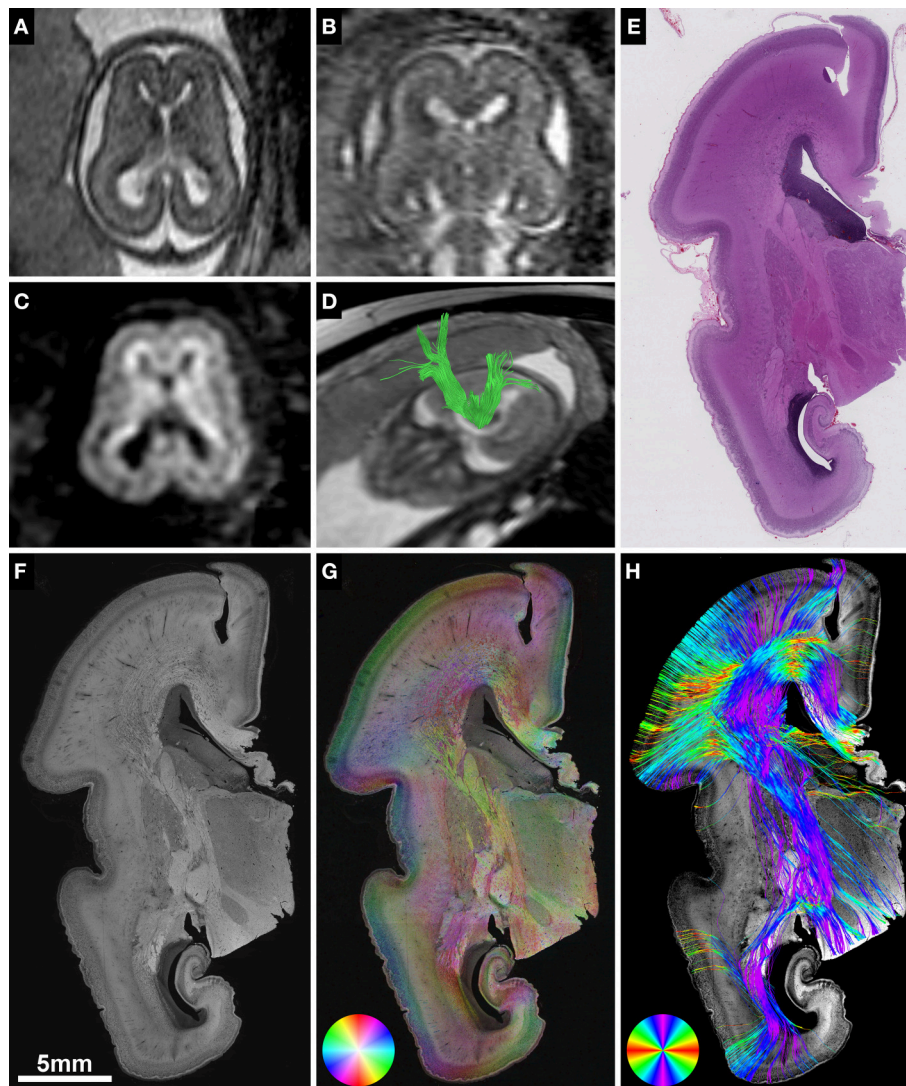


FIGURE 1 | Validation of *in utero* tractography with structure tensor analysis of histological sections. (A–D) Fetal MRI of subject 2 at GW21. **(A)** Axial and **(B)** coronal T2-weighted images. *In utero* DTI **(C)** based tractography **(D)** visualizes the internal capsule (green) in both hemispheres. **(E–H)** Coronal histological sections of the right hemisphere at the level of the posterior limb of the internal capsule in the same subject at GW22. **(E)** H&E staining for anatomical reference. **(F)** Inverted grayscale immunohistochemistry for NCAM to identify axonal tracts. **(G)** Fiber orientation, anisotropy and staining intensity derived from ST analysis are displayed in a color-coded hue-saturation-brightness (HSB) image, respectively. **(H)** Histology-based tractography uses this information to reconstruct streamlines for better macroscopic comparison with the results of *in utero* tractography, with hue representing fiber orientation. Please note the different color-coding schemes for HSB images and histology-based tractography.

for medical reasons. Fetal brains were fixed in 10% buffered formaldehyde solution (0.9% sodium chloride, 0.3% zinc sulfate heptahydrate) for at least 2 weeks, cut in approximately 5 mm thick coronal slices (brainstem and cerebellum were cut in the axial plane) and embedded in paraffin. Tissue blocks at the level of the basal ganglia and thalamus were cut at 3–5 μ m and automated immunohistochemistry was performed on Autostainer 48 Link instruments (Dako, Glostrup, Denmark), using EnVision™ FLEX+ detection system (#K8002 Dako, Glostrup, Denmark) according to manufacturer's recommendations. Briefly, sections were deparaffinized in xylene

and heat-induced epitope retrieval was performed in EnVision™ FLEX Target Retrieval Solution, low pH (#K8005 Dako, Glostrup, Denmark) at 95°C for 20 min. Axonal tracts were identified with antibody against neural cell adhesion molecule (NCAM) (Jakovcsevski et al., 2007). Primary antibody NCAM (#MON9006-1 Monosan, Uden, The Netherlands) was used at a dilution of 1:200 and incubated for 30 min at room temperature. After automated immunohistochemistry, sections were dehydrated through graded alcohols and mounted. Adjacent sections were stained with hematoxylin and eosin (H&E) for anatomical reference (**Figure 1E**).

Digitalization and Structure Tensor Analysis of Histological Sections

NCAM-stained sections were digitalized using an automated slide scanner (Hamamatsu NanoZoomer 2.0-HT) at 40X magnification with a scanning resolution of 0.23 μm . For further image processing, digital images were down-sampled, depending on the size of the region of interest, to magnification levels of 20X, 10X, or 5X, converted into 8-bit grayscale and inverted (**Figure 1F**). ST analysis (Budde and Frank, 2012; Rezakhaniha et al., 2012) was performed with the *OrientationJ* plugin for ImageJ (Sage, 2012) using a cubic spline gradient with a Gaussian window of 5 pix. The results were visualized as hue-saturation-brightness (HSB) images, with hue representing the orientation, saturation the anisotropy/coherency, and brightness the staining intensity (**Figure 1G**).

Histology-Based Tractography in Digitalized Sections

Digitalized histological data with a 10X magnification were transferred to the image-processing workstation in JPEG format. Prior to tractography analysis, pre-processing was carried out using customized software in the Matlab environment (MATLAB and Statistics Toolbox Release R2010a, The MathWorks, Inc., Natick, Massachusetts, United States.). The red channel of the red-green-blue color-coded digital images was converted into 8-bit grayscale values. In order to optimize the image contrast, histogram equalization was performed (Contrast-limited adaptive histogram equalization using the *adapthisteq* command in Matlab R2010a), and values were normalized to a range of 0-256. ST analysis (Budde and Frank, 2012) was estimated using the *Toolbox Diffc* (Peyre, 2008) in Matlab R2010a. The output of the estimated ST was saved as three scalar images in NIFTI image format. The calculation speed was enhanced by using parallelized block-processing program architecture in Matlab, which utilized eight CPU cores.

In addition to the ST, the two-dimensional fractional anisotropy (FA_{2d}) and eigenvalues (λ_1 and λ_2) were also calculated and saved in NIFTI format. The calculation of the FA_{2d} utilized the following formula:

$$FA_{2d} = \frac{\sqrt{(\lambda_1 - \bar{\lambda})^2 + (\lambda_2 - \bar{\lambda})^2}}{\sqrt{(\lambda_1 + \lambda_2)^2}}$$

where λ_1 and λ_2 are the eigenvalues of the structure tensor D , and $\bar{\lambda} = \frac{\lambda_1 + \lambda_2}{2}$.

The eigenvalues and FA_{2d} maps were used to generate a mask of the brain in the cross-sections, and a seed mask for initiating tractography. We separated the background and foreground using an in-house-developed code Matlab R2010a, and the resulting image mask was used to restrict the FA_{2d} image to the areas depicting the brain only. Within the brain mask, the top 95th percentile of FA_{2d} values was calculated and a high-pass thresholding was performed.

The two-dimensional STs were given by three scalar images, which were then generalized to three dimensions by replacing the Z components with zeros:

$$D_{pseudo} = \begin{bmatrix} G_{XX} & G_{XY} \\ G_{XY} & G_{YY} \end{bmatrix} = \begin{bmatrix} G_{XX} & G_{XY} & 0 \\ G_{XY} & G_{YY} & 0 \\ 0 & 0 & 0 \end{bmatrix}$$

where D_{pseudo} is the pseudo-diffusion tensor, derived from the 2D STs, and G_{XX} , G_{XY} , and G_{YY} are components of the 2D ST.

The outputs of the ST, FA_{2d} , and the mask calculation step were down-sampled by a factor of 4 to enable feasible utilization of classical fiber tractography algorithms. The diffusion tensor was saved as a 4D-NIFTI file containing six scalar images, determined from the upper triangle of the matrix form of D_{pseudo} , and these data were directly accessible by image processing toolboxes for the analysis of diffusion tensor images. Histology-based tractography was performed by the Diffusion Toolbox in the CAMINO software environment (Cook et al., 2006).

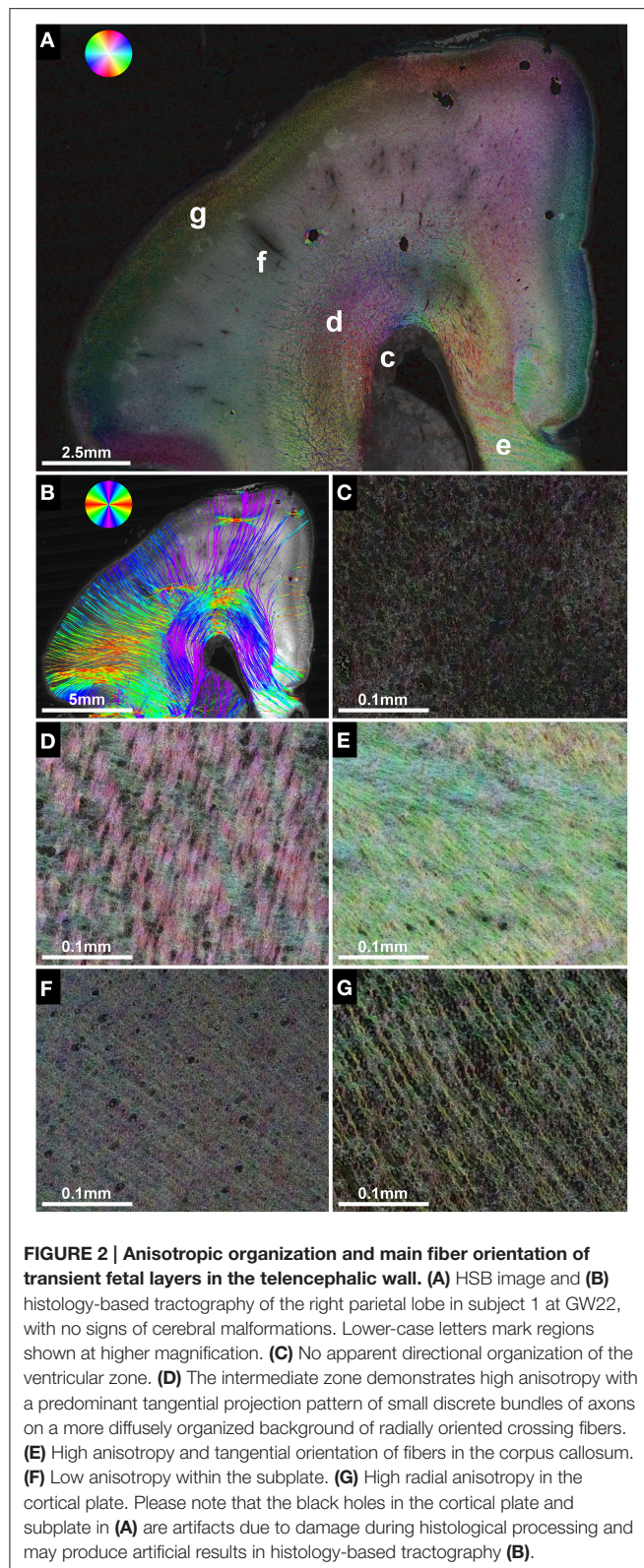
Deterministic histology-based tractography was initiated from the masks covering the top FA_{2d} values of the white matter, and tractography was terminated if streamlines reached out of the estimated 2D brain mask. A fourth-order Runge-Kutta fiber-tracking method (rk4) was utilized with probabilistic nearest neighbor interpolation of streamlines, similar to the interpolation algorithm described in Behrens et al. (2003), while the rk4 tracking approach is detailed in Basser et al. (2000) and further technical documentation is found at: <http://cmic.cs.ucl.ac.uk/camino/>. For each seed voxel, 10 iterations were performed, in steps of 2 pixels, and a curve threshold of 75° while tracking was also constrained to FA_{2d} values higher than 0.1. Streamlines were colored according to the principal eigenvector orientation, and were saved in VTK format for visualization (**Figure 1H**).

RESULTS

ST Analysis of Fetal Telencephalic Layers in Brains with Normal Anatomy of the Internal Capsule and Corpus Callosum

HSB images of the three fetal brains with normal anatomy of the internal capsule and corpus callosum (subjects 1, 2, and 6) demonstrated the anisotropic organization of the transient fetal layers of the telencephalic wall on a histological scale (**Figures 1–3**). Located immediately adjacent to the lateral ventricles, the ventricular zone showed a lower degree of immunoreactivity for NCAM compared to the other layers of the fetal telencephalon, with no apparent directional organization on HSB images (**Figure 2C**).

In contrast, the fetal intermediate zone contained abundant NCAM-positive fibers with a predominant tangential projection pattern of small discrete bundles of axons running parallel to the ventricular wall, and a more diffusely organized fraction of radially oriented crossing fibers (**Figure 2D**). The amount of fiber crossings within the intermediate zone changed gradually from lateral (corona radiata) to medial (corpus callosum), with a progressive decrease of radial fibers and a corresponding increase of tangentially oriented



fibers (Figure 2E). Visualization of the intermediate zone with histology-based tractography displayed a dominant tangential fiber population, showing thick bundles of streamlines

arching in a C-shape from the exit of the internal capsule around the lateral ventricle toward the corpus callosum (Figure 2B).

The subplate zone, located between the intermediate zone and the cortical plate, was characterized by low anisotropy with a diffuse network of crossing fibers and a weak radial organization seen at lower magnifications (Figure 2A). At higher magnifications, however, this was less evident (Figure 2F). Finally, the cortical plate showed a relatively strong anisotropy, with an arrangement of fibers radial to the cortical surface (Figure 2G). The radial organization of the cortical plate and subplate was represented on histology-based tractography images as streamlines projecting in a radial fashion from the intermediate zone toward the surface of the brain (Figure 2B).

***In utero* Identification of the Internal Capsule, Corpus Callosum, and Probst Bundles with DTI-Based Tractography**

In utero tractography of the corpus callosum was successful in three subjects with a mediolateral tangential projection pattern of fibers in the roof of the lateral ventricles. Further lateral, corpus callosum streamlines were traced that diverged radially from the intermediate zone in a U-shape toward the cortical plate (Figure 3A). In the four subjects with ACC, no mediolateral streamlines could be visualized. Instead, massive anterior-posteriorly oriented abnormal fiber tracts, corresponding to the Probst bundles, were found medial to the lateral ventricle in both hemispheres (Figures 4E,J). *In utero* tractography of the internal capsule was successful in all seven subjects in both hemispheres, with fibers showing a predominant inferior-superior projection within the posterior limb of the internal capsule (PLIC) between the basal ganglia and the thalamus. Further superior, internal capsule streamlines projected in a straight inferior-superior direction through the corona radiata toward the superolateral convexity, with a general stop of streamlines above the level of the corpus callosum or Probst bundles (Figure 3A). In subject 3, tractography results were asymmetric, with a discontinuity of left internal capsule streamlines at the exit of the PLIC into the corona radiata (Figure 5C). Results are summarized in Table 2.

Validation of *In utero* Tractography of the Internal Capsule and Corpus Callosum with Histology-Based Tractography

Corresponding to the *in utero* tractography results for the internal capsule, histology-based tractography of NCAM-stained sections successfully visualized tangentially cut fibers of the internal capsule and corona radiata in all subjects (Table 2). Streamlines were located between the basal ganglia and thalamus and projected in an inferior-superior direction through the PLIC and intermediate zone lateral to the lateral ventricle. While some of the fibers diverged radially toward the cortical plate, most of the intermediate zone streamlines followed the lateral ventricular wall in a tangential fashion (Figures 1H, 3B).

Although the corpus callosum was artificially torn during autopsy in subjects 1, 2, and 6, histology-based tractography confirmed the *in utero* tractography finding of normal

TABLE 2 | Detection of internal capsule, corpus callosum and Probst bundles with DTI-based *in utero* tractography and histology-based tractography.

Subject #	DTI-based <i>in utero</i> tractography		Histology-based tractography	
	Internal capsule (IC)	Commissures	Internal capsule (IC)	Commissures
Subject 1	Bilateral IC	Corpus callosum	Bilateral IC	Corpus callosum
Subject 2	Bilateral IC	Corpus callosum	Bilateral IC	Corpus callosum
Subject 3	Bilateral IC*	Bilateral Probst bundles	Bilateral IC	Commissural agenesis***
Subject 4	Bilateral IC	Bilateral Probst bundles	Bilateral IC	Commissural agenesis***
Subject 5	Bilateral IC	Bilateral Probst bundles	Bilateral IC	Commissural agenesis***
Subject 6	Bilateral IC	Corpus callosum	Right IC**	Corpus callosum in right hemisphere**
Subject 7	Bilateral IC	Bilateral Probst bundles	Bilateral IC	Commissural agenesis***

For detailed description see text. *Discontinuity of streamlines in the left hemisphere at the transition of the PLIC into the corona radiata. **In subject 6 histology was only available for the right hemisphere. ***Absence of normal mediolaterally oriented corpus callosum projections, successful tractography of longitudinally cut fibers, and reduced number of streamlines in regions of the Probst bundle with predominantly perpendicularly cut axons.

interhemispheric connections with the visualization of thick bundles of mediolaterally oriented fibers along the roof of the lateral ventricle. Streamlines continued laterally into the tangentially oriented fibers of the intermediate zone, with some fibers diverging radially through the subplate toward the cortical plate (**Figures 1H, 2B, 3B**). In the younger fetal brains (subjects 1 and 2 at GW22) intermediate zone streamlines projected in a C-shape around the lateral ventricle (**Figures 1H, 2B**). In contrast, in subject 6 at GW27 the directional change of intermediate zone streamlines around the lateral ventricle followed a more acute angle (**Figure 3B**).

ST Analysis of Probst Bundles and Validation of *In utero* Tractography Results in Cases of ACC

ST analysis of coronal histological sections successfully identified bilateral perpendicularly cut Probst bundles in all four subjects with ACC, thereby confirming the results of *in utero* tractography (**Table 2**). In addition, ST analysis was able to visualize the internal fiber architecture of Probst bundles, revealing a complex arrangement of both perpendicularly, and longitudinally cut fibers (**Figure 4**). While the center of the Probst bundle consisted of large amounts of perpendicularly cut fibers with high NCAM staining intensity, but low anisotropy within the coronal plane (**Figures 4D,I**), the lateral and dorsal portions contained a large number of longitudinally cut fibers, especially at the border to the intermediate zone, with a relatively high anisotropy (**Figures 4C,H**).

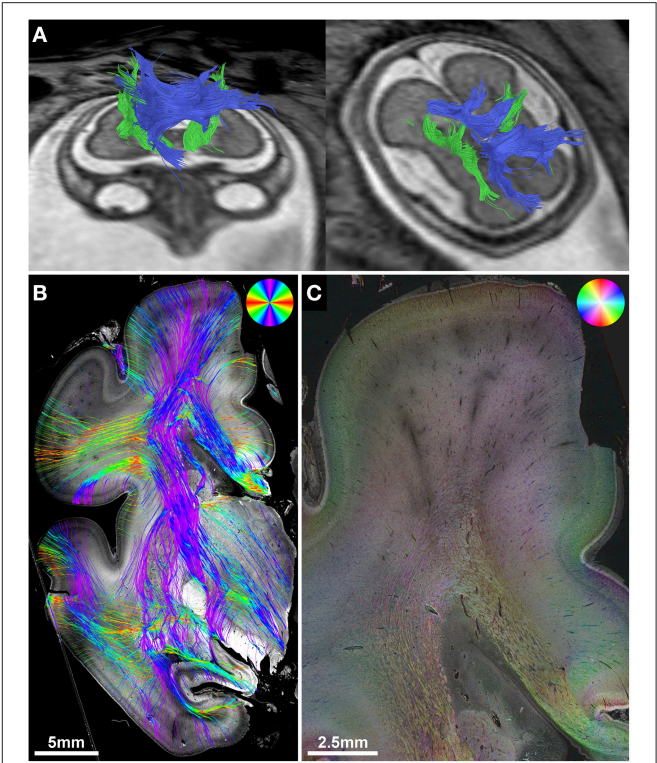


FIGURE 3 | Validation of *in utero* tractography of the internal capsule and corpus callosum. **(A)** *In utero* tractography of the internal capsule (green) and corpus callosum (blue) in subject 6 at GW26. **(B)** Histology-based tractography on coronal sections through the PLIC of the right hemisphere at GW27 demonstrates the main fiber orientation of the corticospinal tract and corpus callosum. **(C)** Corresponding HSB image.

Although histology-based tractography cannot directly visualize off-plane fibers, an indirect correlate of anterior-posteriorly projecting Probst bundle fibers was found as a reduction of streamlines in areas with predominantly perpendicularly cut fibers (**Figure 4F**). In addition, histology-based tractography visualized the longitudinally cut fiber component as streamlines projecting from the intermediate zone into the Probst bundle (**Figures 4A,F**). Histological tractography results of fibers projecting in or out of the Probst bundles corresponded to *in utero* tractography results, which showed bundles of streamlines diverging from an anterior-posterior course within the Probst bundle superiorly into the telencephalic wall (**Figures 4E,J**).

ST Analysis in Malformations of Internal Capsule Fibers

The potential of histological ST analysis for the postmortem validation of malformations of internal capsule fibers, including the corona radiata and corticospinal tract, could be demonstrated in several subjects.

In utero tractography of subject 3 (GW21, ACC with bilateral Probst bundles) revealed a normal-appearing right-hemispheric internal capsule that could be traced through the intermediate

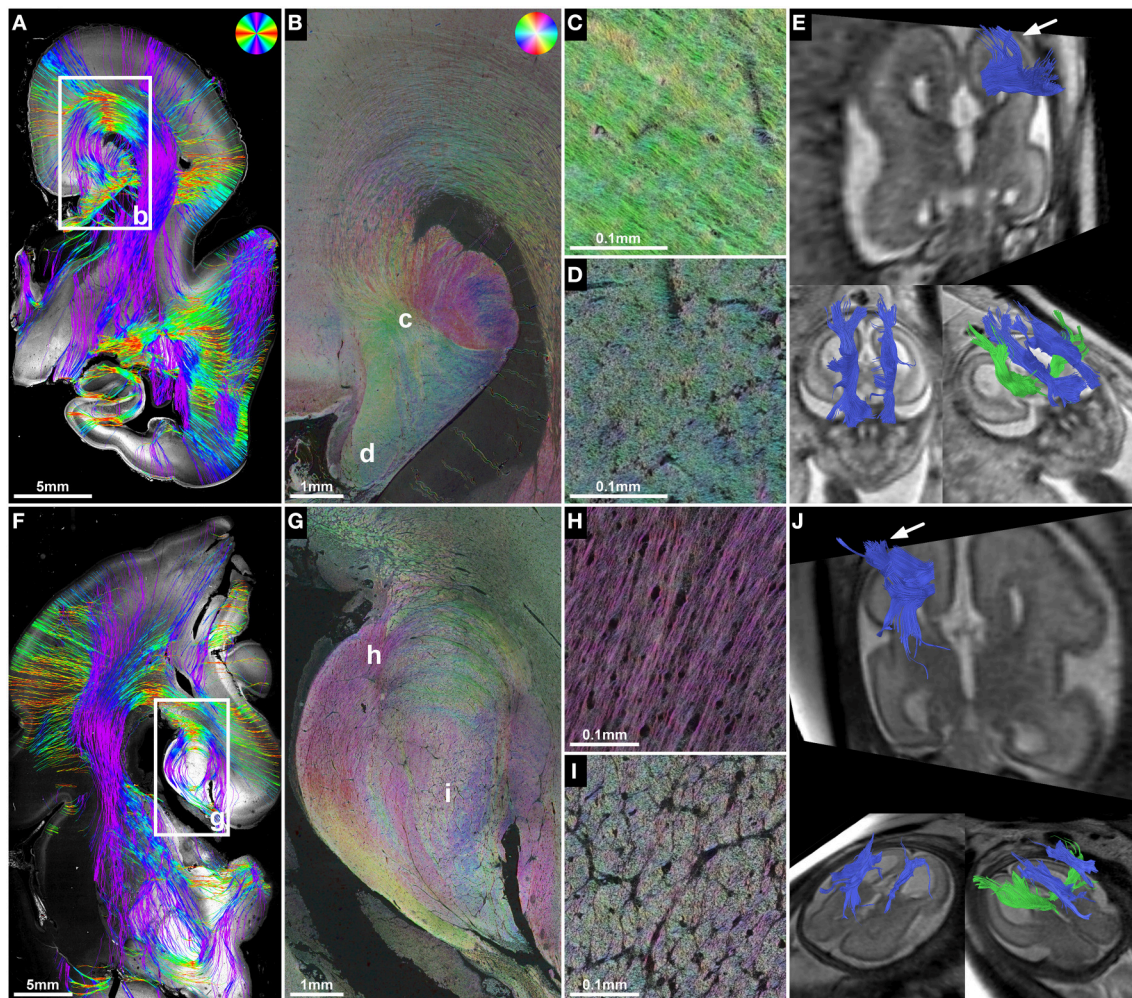


FIGURE 4 | ST analysis reveals the internal fiber architecture of Probst bundles in subjects with ACC. Histology-based tractography of subject 4 at GW23 (**A**) and subject 7 at GW29 (**F**) depicts streamlines projecting from the intermediate zone into the Probst bundle. (**B,G**) ST analysis of Probst bundles reveals their internal structure as a complex arrangement of both longitudinal (**C,H**) and anterior-posteriorly oriented perpendicularly (**D,I**) cut fibers. (**E,J**) Corresponding to the histological ST findings, *in utero* tractography of subject 4 at GW22 and subject 7 at GW28 visualized not only anterior-posteriorly oriented fibers within the Probst bundles (blue), but also bundles of streamlines along its course that diverged superiorly into the telencephalic wall (arrow).

zone into the central region of the developing cortex. In the left hemisphere however, internal capsule streamlines stopped at the transition of the PLIC into the corona radiata (**Figure 5C**). Neuropathological examination at GW23, with histological ST analysis of coronal sections at the level of the PLIC, demonstrated a pronounced malformation of the left corona radiata, with convoluted and abnormally oriented bundles of fibers, and interspersed gray-matter heterotopia within the intermediate zone (**Figures 5B,E**). In contrast, coronal sections of the right hemisphere at the level of the PLIC showed a normal pattern of predominantly tangentially oriented corona radiata fibers lateral to the right lateral ventricle (**Figures 5B,D**). Histology-based tractography was able to validate the *in utero* DTI-based tractography results, with streamlines from the right PLIC extending in a straight inferior-superior direction through the intermediate zone into the cortical plate, while the left corona

radiata showed a chaotic arrangement of inferior-superiorly and mediolaterally oriented streamlines (**Figure 5A**).

Subject 2 demonstrated the potential use of ST analysis in fetal brains with malformations of descending corticospinal tract projection fibers. In this case fetal MRI at GW21 revealed typical features of Joubert syndrome, including molar tooth malformation of the mesencephalon (**Figure 6A**), vermian hypoplasia (**Figures 6C,D**) and multicystic kidneys (not shown). *In utero* tractography showed a normal appearance of the internal capsule within the cerebral hemispheres, but a stop of most streamlines at the level of the cerebral peduncles (**Figure 6E**). Neuropathological examination at GW22 confirmed the unremarkable anatomy of the internal capsule on coronal H&E-sections, HSB images, and histology-based tractography of the cerebral hemispheres (see **Figure 1**), but revealed pronounced abnormalities of fiber tracts within

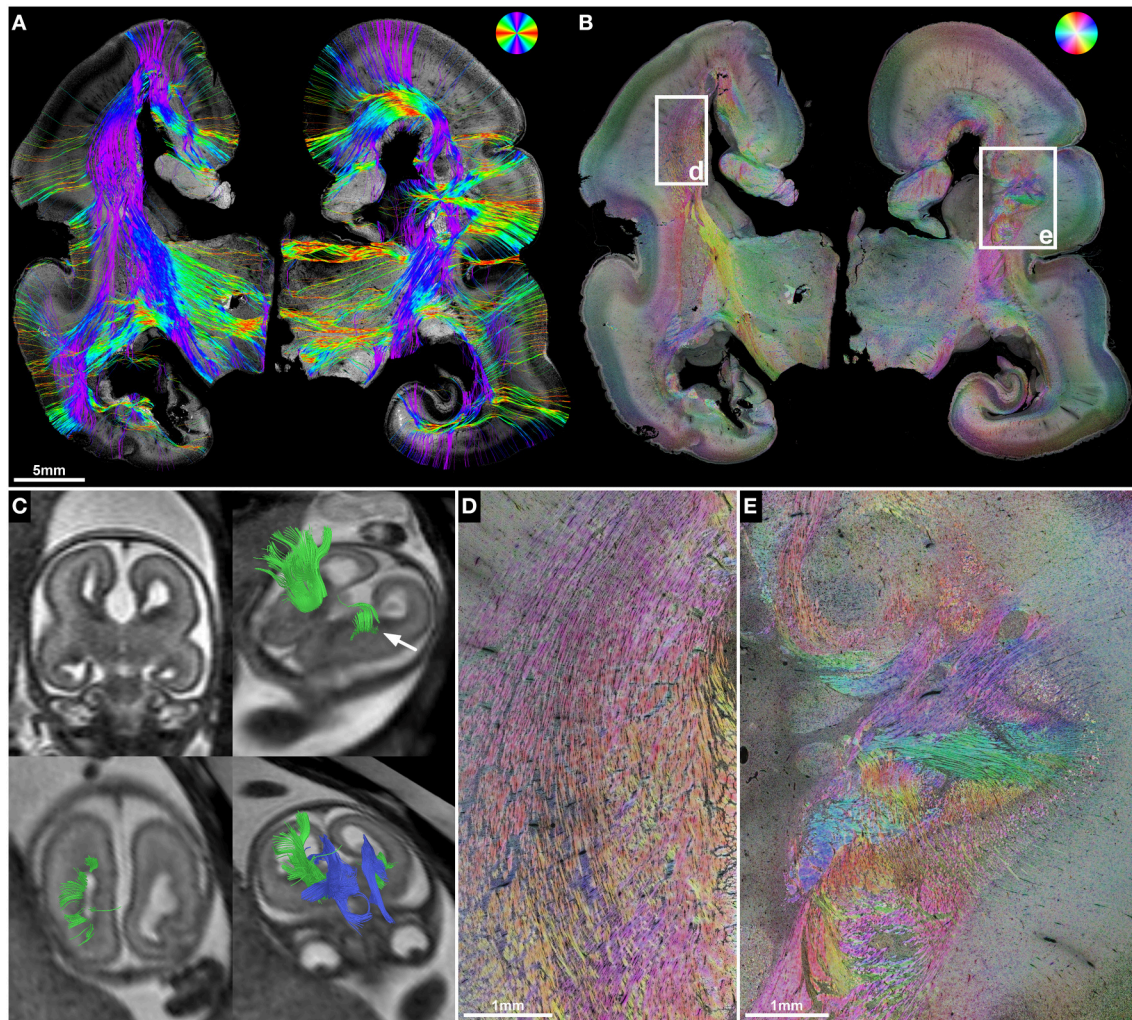


FIGURE 5 | ST validation of abnormal *in utero* tractography results of the internal capsule. (A) Histology-based tractography and (B) HSB image of coronal sections through the PLIC in subject 3 at GW23 demonstrate complete ACC and orientation of main fiber tracts. (C) *In utero* tractography at GW21 visualizes bilateral Probst bundles (blue) and a pronounced asymmetry of internal capsule fibers (green), with normal results for the right hemisphere and a discontinuity of streamlines in the left hemisphere after exiting the PLIC (arrow). HSB images at higher magnification validate the *in utero* findings by visualizing a regular corona radiata anatomy in the right hemisphere (D), and a convolution of abnormally oriented fibers in the left hemisphere, with interspersed gray-matter heterotopia (E).

the brainstem. While the cerebral peduncles could be readily identified at the level of the rostral mesencephalon (Figure 6F), axial sections caudal to the mesencephalon showed an absence of normal descending fiber tracts, with no identifiable corticospinal tract between the pontine nuclei (Figure 6J) and a complete absence of the pyramids at the level of the medulla oblongata (Figure 6G). ST analysis of axial sections at the level of the caudal mesencephalon revealed an abnormal projection of thick bundles of longitudinally cut axons from the cerebral peduncles ventromedially, where fibers broke through the surface of the brain and formed an irregular formation of heterotopic white matter fiber bundles within the interpeduncular cistern (Figure 6H). Histology-based tractography provided similar results, with multiple mediolaterally oriented streamlines projecting from

the cerebral peduncles into the interpeduncular subarachnoid space (Figure 6I). Additional neuropathological abnormalities in this brain included an asymmetric configuration of the basis pontis with a ventral pontine cleft, bilateral fragmented dentate nuclei (not shown) and abnormal heterotopic fiber bundles within the pontine tegmentum and posterior right basis pontis (Figures 6J,K). Finally, retrospective analysis of T2-weighted fetal MR images revealed an interpeduncular mass in the location of the histologically demonstrated white matter heterotopia (Figures 6B,D).

In subject 5, neuropathological autopsy confirmed the fetal MRI findings of complete ACC with bilateral Probst bundles and left frontal lobe malformation with abnormal sulcation (Figure 7A). In addition, HSB images visualized a convolution of abnormally oriented fiber bundles high above

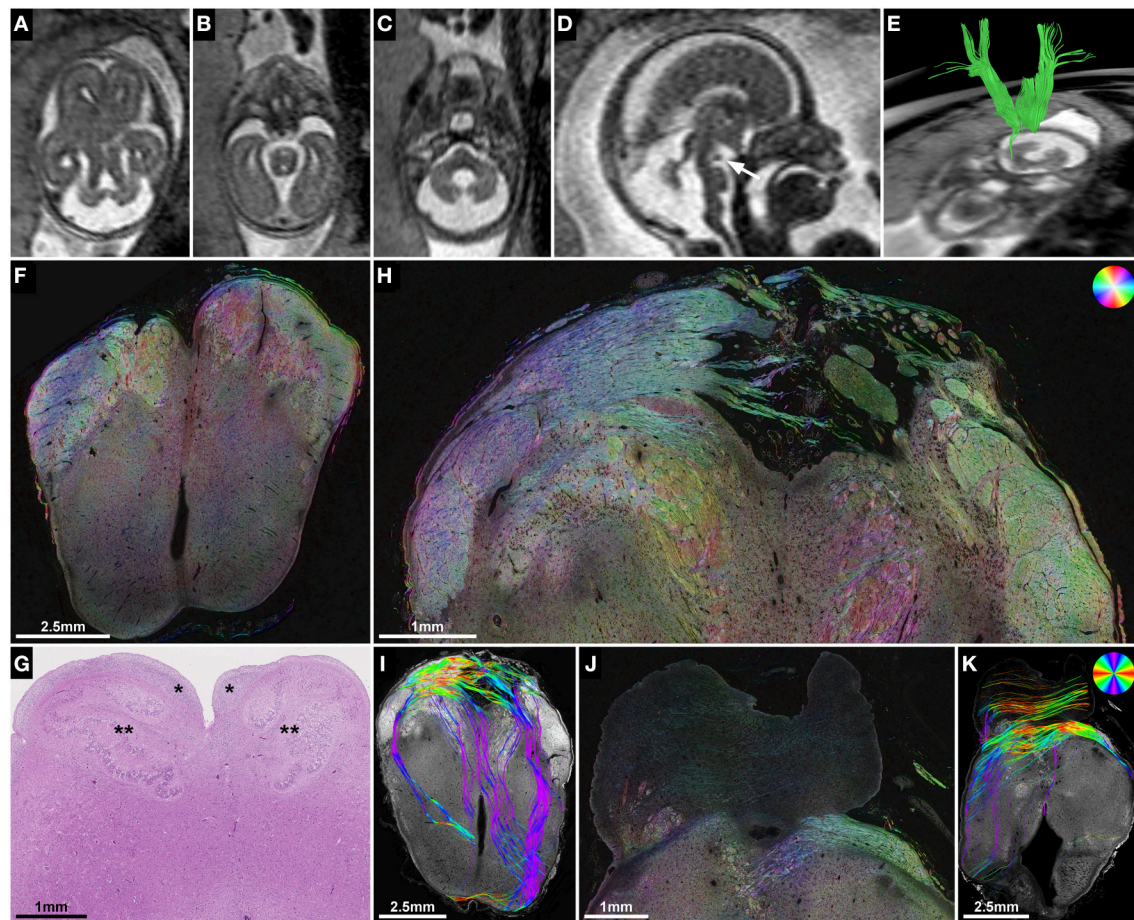


FIGURE 6 | ST analysis of heterotopic corticospinal tract projections in Joubert syndrome. (A–E) Fetal MRI of subject 2 at GW21. Axial T2-weighted images through the brainstem demonstrate molar tooth malformation of the mesencephalon (A) and vermian hypoplasia (C). (D) A midsagittal T2-weighted image shows a nodular hypointense interpeduncular mass (arrow). (E) *In utero* tractography shows a discontinuity of most internal capsule streamlines at the level of the mesencephalon. (F) Neuropathological autopsy at GW22 demonstrated perpendicularly cut fibers in the cerebral peduncles at the level of the rostral mesencephalon, but showed a complete absence of the corticospinal tract in the medulla oblongata (G) between the arcuate nuclei (*) and the inferior olive (**). (H,I) Sections through the caudal mesencephalon show a heterotopic projection of the corticospinal tract from the cerebral peduncles medially into the interpeduncular cistern. (J,K) Sections through the pons visualize some transverse pontine fibers and abnormal fiber tracts in the pontine tegmentum and posterior right basis pontis. Note the absence of normal perpendicularly cut fibers of the corticospinal tract between the pontine nuclei. (F,H,J) HSB images, (I,K) Histology-based tractography, (G) H&E.

the left lateral ventricle frontal horn (Figure 7C), which resembled intermediate-zone fibers at higher magnification, and were visualized by histology-based tractography as a chaotic arrangement of predominantly mediolaterally oriented streamlines (Figure 7B). *In utero* tractography in this case resulted in unremarkable visualization of the internal capsule in both hemispheres with a stop of streamlines at the level of the Probst bundles and no abnormal fiber tracts detected in the left frontal lobe (Figure 7A).

DISCUSSION

This retrospective study demonstrates the validity of *in utero* tractography results of commissural and internal capsule fibers in the developing human fetal brain by correlating DTI findings with the results of postmortem histological ST analysis (Budde

and Frank, 2012; Budde and Annese, 2013) in the same subjects. ST analysis successfully validated abnormal *in utero* tractography findings of commissural fibers in subjects with ACC, and revealed additional information about the internal fiber architecture of Probst bundles. The potential for cross-validation of abnormal *in utero* tractography results of internal capsule fibers was demonstrated in subjects with malformation of the corona radiata and heterotopic projection of the corticospinal tract. Potential limitations of DTI-based *in utero* tractography could be demonstrated in several brain regions. While *in utero* DTI can currently achieve in-plane resolutions down to 1 mm (Kasprian et al., 2008, 2013; Mitter et al., 2015; Jakab et al., 2015a), and postmortem fetal DTI is usually performed with a resolution of several hundred μm (Huang et al., 2009; Vasung et al., 2011; Takahashi et al., 2012, 2014; Kolasinski et al., 2013), the measurement of anisotropic water diffusion within an imaged

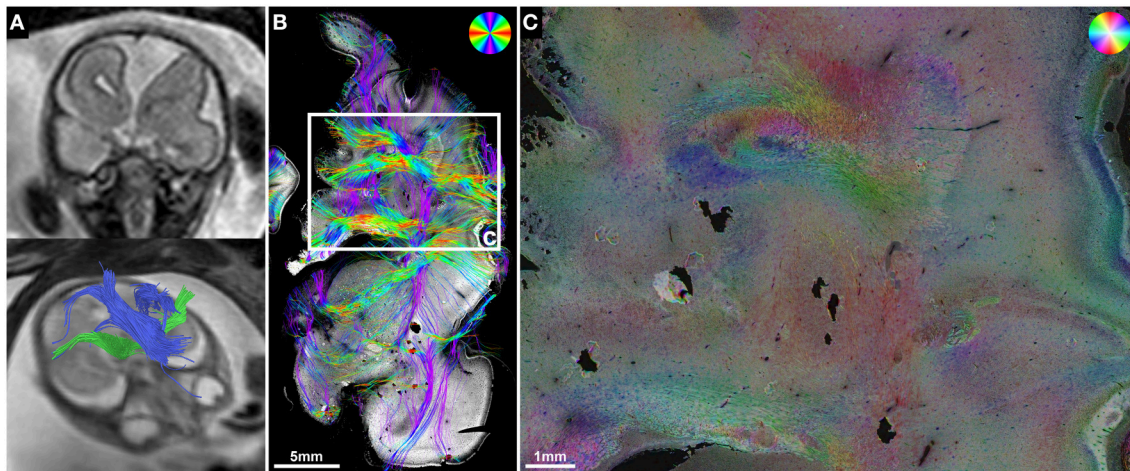


FIGURE 7 | ST analysis reveals limitations of current *in utero* DTI. (A) Fetal MRI of subject 5 at GW22 shows a malformation of the left frontal lobe, complete ACC with Probst bundles and unremarkable internal capsules. **(B)** Histology-based tractography and **(C)** HSB image of the left frontal lobe at GW24 visualized a convolution of abnormally oriented fiber bundles high above the left lateral ventricle frontal horn that was not represented by the *in utero* tractography results.

voxel provides only an indirect estimation of macroscopic fiber orientation. In contrast, ST analysis of histological fetal brain sections enables the direct assessment of the anisotropic organization of the developing fetal brain on a microscopic scale.

Histological ST Analysis Enables the Direct Assessment of the Anisotropic Organization and Fiber Orientation of Fetal Telencephalic Layers on a Micro- and Macroscopic Scale

The main fiber orientation and anisotropy of the transient fetal telencephalic layers (Kostovic et al., 2002; Bystron et al., 2008), as demonstrated by HSB images, corresponds well to the results of DTI in postmortem fetal brains, which depict the cortical plate and subplate as layers of high and low radial anisotropy, respectively, and the intermediate zone as a layer of high tangential anisotropy (Huang et al., 2006). ST analysis results for the corona radiata are particularly interesting, as histological studies have shown that the fetal intermediate zone at the exit of the internal capsule between the caudate nucleus and the putamen contains a high amount of crossing fibers, including thalamocortical, corticofugal, commissural, and external capsule fibers (Judaš et al., 2005; Vasung et al., 2010). HSB images at high magnification clearly visualize these complex “periventricular crossroads” (Kostovic and Judas, 2006; Kostovic et al., 2014) of discrete tangential axon bundles and more diffusely organized radial crossing fibers. Since DTI cannot resolve crossing fibers within a single voxel, and instead depicts the average main diffusion direction, the inferior-superiorly oriented streamlines visualized by *in utero* tractography within the corona radiata represent the dominant tangential projection pattern of thalamocortical and corticofugal axons (Kostovic and Goldman-Rakic, 1983; Kostovic and Rakic, 1984; Ulfig et al., 2000). Likewise, histology-based tractography emphasizes the

dominant tangential fiber components throughout the entire intermediate zone of the central region. Superior to the lateral angle of the lateral ventricle, *in utero* tractography generally failed to visualize tangential fibers and instead emphasized internal capsule and corpus callosum fibers that diverge radially toward the cortical plate, resulting in a straight inferior-superior shape of internal capsule streamlines and a U-shape of the corpus callosum. This resulted most likely from the acute angle change of tangential intermediate zone fibers in this region, especially in older fetal brains.

Histological ST Analysis Allows the Validation of Abnormal *In utero* Tractography Results of Internal Capsule Fibers

The case of interpeduncular heterotopia demonstrates the complementary nature of *in utero* tractography and postmortem histological ST analysis. An interpeduncular mass in patients with Joubert syndrome was first described in a neuroradiological case series (Harting et al., 2011), but due to a lack of neuropathological correlation the exact nature of this heterotopic tissue remained unclear. In subject 2, neuropathological analysis revealed the interpeduncular mass seen on fetal MRI to be composed of the abnormal heterotopic projection of the descending corticospinal tract into the interpeduncular cistern, a finding well visualized by HSB images and histology-based tractography. Of note, the neuropathological phenotype in Joubert syndrome also contains features of axon guidance disorders (Engle, 2010) with a non-decussation of the superior cerebellar peduncles and corticospinal tracts seen in many subjects (Friede and Boltshauser, 1978; Yachnis and Rorke, 1999; Ferland et al., 2004; Juric-Sekhar et al., 2012). Although the results of ST analysis in this case correspond well to the *in utero* tractography findings of a discontinuity of internal capsule

streamlines at the level of the cerebral peduncles, it must be noted that *in utero* tractography of fiber tracts within the fetal brainstem remains a challenge, even in the normal developing brain (Kasprian et al., 2010).

Periventricular nodular and subcortical heterotopia fall into the spectrum of neuronal migration disorders (Barkovich et al., 2012) and are associated with several of the many known ACC syndromes (Edwards et al., 2014). HSB images and histology-based tractography in subject 3 clearly demonstrated the effect of gray matter heterotopia and chaotic intermediate zone fiber orientation on the ability to trace normal inferior-superiorly oriented corona radiata streamlines on histological sections. ST analysis thus validates the *in utero* tractography findings of a discontinuity of streamlines in the left hemisphere and an unremarkable appearance of the internal capsule in the right hemisphere.

Histological ST Analysis can be Used to Visualize the Internal Fiber Architecture of Probst Bundles in Cases of ACC

Although histology-based tractography cannot directly visualize anterior-posteriorly oriented Probst bundle fibers, the absence of normal mediolateral corpus callosum projections in all subjects with ACC provides indirect proof of the *in utero* tractography findings. In addition, high-resolution HSB images revealed the complex internal structure of Probst bundles with centrally arranged perpendicularly cut fibers and longitudinally cut fibers in the lateral and dorsal portions of the bundle. This is in line with the original description of the “Balkenlängsbündel” by Moritz Probst (Probst, 1901). *In utero* tractography streamlines that diverge from their main anterior-posterior projection pattern into a superior direction toward the telencephalic wall may represent the imaging correlate of these hemispheric projections into the Probst bundles. This interpretation is further supported by corresponding results of histology-based tractography.

Insights into Possible Limitations of *In utero* DTI

In addition to valuable insights about the diagnostic possibilities of current fetal DTI sequences, ST analysis may also reveal important clues about their limitations. In subject 5, HSB images and histology-based tractography were able to demonstrate a complex convolution of abnormally oriented fiber bundles within the left frontal lobe that *in utero* tractography failed to visualize. Potential contributing factors that might explain the inability of *in utero* tractography to trace these fibers include resolution limitations as well as marked angle changes within convoluted fiber tracts. The well-known inability of DTI to resolve crossing fibers (Mori and Tournier, 2013) may contribute to the failure of *in utero* tractography to visualize tangential intermediate zone fibers superior to the lateral angle of the lateral ventricle, as mentioned above. Furthermore, it prohibits the direct evaluation of radial crossing fibers within “periventricular crossroad” regions of the corona radiata (Judaš et al., 2005).

Limitations of Histological ST Analysis

Histological ST analysis has important limitations that need to be considered when correlating its findings to the results of DTI-based tractography. First, while DTI acquires a volume dataset and can therefore be used to trace fibers in three dimensions, ST analysis is limited to the two-dimensional images provided by light microscopy. The resulting drawback is an inability to directly characterize perpendicularly cut fibers (Budde and Frank, 2012; Budde and Annese, 2013) and affects in coronal sections predominantly anterior-posteriorly oriented fiber tracts such as the center of the Probst bundles, the fornix, the cingulum, the optic radiation as well as most long association fiber tracts within the lateral hemisphere. However, limitations concerning perpendicularly cut fibers in the coronal plane could be overcome by using either axially or sagittally cut sections. Although it is possible to extend ST analysis to the third dimension by acquiring serial image stacks with confocal microscopy (Khan et al., 2015), such approaches are to date limited to small tissue volumes and thus might be impractical for the systematic analysis of whole-hemisphere human fetal brain sections.

Because of the two-dimensional nature of ST analysis, it is important to emphasize that histology-based tractography is not equivalent to direct axon tracing, since even longitudinally cut fibers usually travel only short distances within a 4 μ m thick histological section. Depicted streamlines therefore represent compound results of multiple similarly oriented fiber bundles and, like the results of DTI-based tractography, should be rather viewed as visualizations of macroscopic white matter anatomy. In our study population fetal MRI was performed within a time span of 2 weeks prior to death, which means that developmental changes during that time must be taken into account when correlating histology to MR images.

Finally it should be noted that postmortem damage to the brain during autopsy or histological processing may produce artificial results in histology-based tractography with either abnormally projecting streamlines or a stop of fibers. Histological sections should therefore be carefully screened for signs of artificial damage prior to interpretation of tractography results.

CONCLUSION

Despite these difficulties, histology-based tractography of commissural and internal capsule fibers in NCAM-stained human fetal brain sections corresponds remarkably well to many of the results of *in utero* tractography. As *in utero* tractography has now been extended from the corpus callosum, the internal capsule (Kasprian et al., 2008) and Probst bundles (Kasprian et al., 2013; Jakab et al., 2015b) to even cortico-cortical association fiber tracts (Mitter et al., 2011, 2015), histological ST analysis may serve as a valuable tool in the postmortem validation and neuropathological examination of a wide range of both normal and pathological axon fiber tracts in the developing human brain. Aside from the retrospective validation of *in utero* tractography in case of fetal demise, a combined approach that complements the three-dimensional nature of DTI with the microscopic resolution provided by histological ST analysis may improve our understanding of abnormal white matter

neuroanatomy in disorders of axon guidance at prenatal stages of human brain development.

AUTHOR CONTRIBUTIONS

CM, AJ, and GK designed the research; CM, PCB, GR, GMG, DB, AS, JAH, DP, and GK collected the data; CM, AJ, and GL analyzed the results; CM, AJ, PCB, GR, and GK wrote the manuscript text. All authors reviewed the manuscript.

REFERENCES

- Axer, H., Beck, S., Axer, M., Schuchardt, F., Heepe, J., Flücken, A., et al. (2011a). Microstructural analysis of human white matter architecture using polarized light imaging: views from neuroanatomy. *Front. Neuroinform.* 5:28. doi: 10.3389/fninf.2011.00028
- Axer, M., Amunts, K., Gräßel, D., Palm, C., Dammers, J., Axer, H., et al. (2011b). A novel approach to the human connectome: Ultra-high resolution mapping of fiber tracts in the brain. *Neuroimage* 54, 1091–1101. doi: 10.1016/j.neuroimage.2010.08.075
- Axer, M., Gräßel, D., Kleiner, M., Dammers, J., Dickscheid, T., Reckfort, J., et al. (2011c). High-resolution fiber tract reconstruction in the human brain by means of three-dimensional polarized light imaging. *Front. Neuroinform.* 5:34. doi: 10.3389/fninf.2011.00034
- Barkovich, A. J., Guerrini, R., Kuzniecky, R. I., Jackson, G. D., and Dobyns, W. B. (2012). A developmental and genetic classification for malformations of cortical development: update 2012. *Brain* 135, 1348–1369. doi: 10.1093/brain/awt019
- Basser, P. J., Mattiello, J., and Lebihan, D. (1994). MR diffusion tensor spectroscopy and imaging. *Biophys. J.* 66, 259–267. doi: 10.1016/S0006-3495(94)80775-1
- Basser, P. J., Pajevic, S., Pierpaoli, C., Duda, J., and Aldroubi, A. (2000). *In vivo* fiber tractography using DT-MRI data. *Magn. Reson. Med.* 44, 625–632. doi: 10.1002/1522-2594(200010)44:4<625::AID-MRM17>3.0.CO;2-O
- Behrens, T. E., Woolrich, M. W., Jenkinson, M., Johansen-Berg, H., Nunes, R. G., Clare, S., et al. (2003). Characterization and propagation of uncertainty in diffusion-weighted MR imaging. *Magn. Reson. Med.* 50, 1077–1088. doi: 10.1002/mrm.10609
- Budde, M. D., and Annese, J. (2013). Quantification of anisotropy and fiber orientation in human brain histological sections. *Front. Integr. Neurosci.* 7:3. doi: 10.3389/fnint.2013.00003
- Budde, M. D., and Frank, J. A. (2012). Examining brain microstructure using structure tensor analysis of histological sections. *Neuroimage* 63, 1–10. doi: 10.1016/j.neuroimage.2012.06.042
- Budde, M. D., Janes, L., Gold, E., Turtzo, L. C., and Frank, J. A. (2011). The contribution of gliosis to diffusion tensor anisotropy and tractography following traumatic brain injury: validation in the rat using Fourier analysis of stained tissue sections. *Brain* 134, 2248–2260. doi: 10.1093/brain/awr161
- Bürgel, U., Amunts, K., Hoemke, L., Mohlberg, H., Gilsbach, J. M., and Zilles, K. (2006). White matter fiber tracts of the human brain: three-dimensional mapping at microscopic resolution, topography and intersubject variability. *Neuroimage* 29, 1092–1105. doi: 10.1016/j.neuroimage.2005.08.040
- Bystron, I., Blakemore, C., and Rakic, P. (2008). Development of the human cerebral cortex: boulder committee revisited. *Nat. Rev. Neurosci.* 9, 110–122. doi: 10.1038/nrn2252
- Chung, K., Wallace, J., Kim, S. Y., Kalyanasundaram, S., Andalman, A. S., Davidson, T. J., et al. (2013). Structural and molecular interrogation of intact biological systems. *Nature* 497, 332–337. doi: 10.1038/nature12107
- Cook, P. A., Bai, Y., Nedjati-Gilani, S., Seunarine, K. K., Hall, M. G., Parker, G. J., et al. (2006). “Camino: open-source diffusion-MRI reconstruction and processing,” in *14th Scientific Meeting of the International Society for Magnetic Resonance in Medicine*, (Seattle, WA), 2759.
- Edwards, T. J., Sherr, E. H., Barkovich, A. J., and Richards, L. J. (2014). Clinical, genetic and imaging findings identify new causes for corpus callosum development syndromes. *Brain* 137, 1579–1613. doi: 10.1093/brain/awt358

ACKNOWLEDGMENTS

This work was supported in part by grants from the Austrian National Bank Anniversary Fund (14812 and 15929) and the European Union FP7 Marie Curie IEF Research grant FABRIC—“Exploring the Formation and Adaptation of the Brain Connectome,” grant no. 2012-PIEF-GA-33003. The authors thank Mary McAllister for help in editing the manuscript.

- Engle, E. C. (2010). Human genetic disorders of axon guidance. *Cold Spring Harb. Perspect. Biol.* 2:a001784. doi: 10.1101/cshperspect.a001784
- Fallet-Bianco, C., Loeuillet, L., Poirier, K., Loget, P., Chapon, F., Pasquier, L., et al. (2008). Neuropathological phenotype of a distinct form of lissencephaly associated with mutations in TUBA1A. *Brain* 131, 2304–2320. doi: 10.1093/brain/awn155
- Fame, R. M., MacDonald, J. L., and Macklis, J. D. (2011). Development, specification, and diversity of callosal projection neurons. *Trends Neurosci.* 34, 41–50. doi: 10.1016/j.tins.2010.10.002
- Ferland, R. J., Eyaid, W., Collura, R. V., Tully, L. D., Hill, R. S., Al-Nouri, D., et al. (2004). Abnormal cerebellar development and axonal decussation due to mutations in AHI1 in Joubert syndrome. *Nat. Genet.* 36, 1008–1013. doi: 10.1038/ng1419
- Fernández-Miranda, J. C., Rhoton, A. L. Jr., Alvarez-Linera, J., Kakizawa, Y., Choi, C., and De Oliveira, E. P. (2008a). Three-dimensional microsurgical and tractographic anatomy of the white matter of the human brain. *Neurosurgery* 62, 989–1026. discussion: 1026–1028. doi: 10.1227/01.neu.0000333767.05328.49
- Fernández-Miranda, J. C., Rhoton, A. L. Jr., Kakizawa, Y., Choi, C., and Alvarez-Linera, J. (2008b). The claustrum and its projection system in the human brain: a microsurgical and tractographic anatomical study. *J. Neurosurg.* 108, 764–774. doi: 10.3171/JNS/2008/108/4/0764
- Friede, R. L., and Boltshauser, E. (1978). Uncommon syndromes of cerebellar vermis aplasia. I: Joubert syndrome. *Dev. Med. Child Neurol.* 20, 758–763. doi: 10.1111/j.1469-8749.1978.tb15307.x
- Girard, N., Raybaud, C., and Poncet, M. (1995). *In vivo* MR study of brain maturation in normal fetuses. *AJNR Am. J. Neuroradiol.* 16, 407–413.
- Grant, E., Hoerder-Suabedissen, A., and Molnár, Z. (2012). Development of the corticothalamic projections. *Front. Neurosci.* 6:53. doi: 10.3389/fnins.2012.00053
- Harting, I., Kotzaeridou, U., Poretti, A., Seitz, A., Pietz, J., Bendszus, M., et al. (2011). Interpeduncular heterotopia in Joubert syndrome: a previously undescribed MR finding. *AJNR Am. J. Neuroradiol.* 32, 1286–1289. doi: 10.3174/ajnr.A2488
- Hevner, R. F. (2000). Development of connections in the human visual system during fetal mid-gestation: a DiI-tracing study. *J. Neuropathol. Exp. Neurol.* 59, 385–392.
- Huang, H., Jeon, T., Sedmak, G., Pletikos, M., Vasung, L., Xu, X., et al. (2013). Coupling diffusion imaging with histological and gene expression analysis to examine the dynamics of cortical areas across the fetal period of human brain development. *Cereb. Cortex* 23, 2620–2631. doi: 10.1093/cercor/bhs241
- Huang, H., Xue, R., Zhang, J., Ren, T., Richards, L. J., Yarowsky, P., et al. (2009). Anatomical characterization of human fetal brain development with diffusion tensor magnetic resonance imaging. *J. Neurosci.* 29, 4263–4273. doi: 10.1523/JNEUROSCI.2769-08.2009
- Huang, H., Zhang, J., Wakana, S., Zhang, W., Ren, T., Richards, L. J., et al. (2006). White and gray matter development in human fetal, newborn and pediatric brains. *Neuroimage* 33, 27–38. doi: 10.1016/j.neuroimage.2006.06.009
- Jakab, A., Kasprian, G., Schwartz, E., Gruber, G. M., Mitter, C., Prayer, D., et al. (2015a). Disrupted developmental organization of the structural connectome in fetuses with corpus callosum agenesis. *Neuroimage* 111, 277–288. doi: 10.1016/j.neuroimage.2015.02.038

- Jakab, A., Pogledic, I., Schwartz, E., Gruber, G., Mitter, C., Brugger, P. C., et al. (2015b). Fetal cerebral magnetic resonance imaging beyond morphology. *Semin. Ultrasound CT MR* 36, 465–475. doi: 10.1053/j.sult.2015.06.003
- Jakovcevski, I., Mo, Z., and Zecevic, N. (2007). Down-regulation of the axonal polysialic acid-neural cell adhesion molecule expression coincides with the onset of myelination in the human fetal forebrain. *Neuroscience* 149, 328–337. doi: 10.1016/j.neuroscience.2007.07.044
- Judaš, M., Rados, M., Jovanov-Milosevic, N., Hrabac, P., Stern-Padovan, R., and Kostovic, I. (2005). Structural, immunocytochemical, and MR imaging properties of periventricular crossroads of growing cortical pathways in preterm infants. *AJNR Am. J. Neuroradiol.* 26, 2671–2684.
- Judaš, M. (2011). “Prenatal development of the human fetal telencephalon,” in *Fetal MRI*, ed D. Prayer (Berlin: Springer), 81–146.
- Juric-Sekhar, G., Adkins, J., Doherty, D., and Hevner, R. F. (2012). Joubert syndrome: brain and spinal cord malformations in genotyped cases and implications for neurodevelopmental functions of primary cilia. *Acta Neuropathol.* 123, 695–709. doi: 10.1007/s00401-012-0951-2
- Kasprian, G., Brugger, P. C., Schöpf, V., Mitter, C., Weber, M., Hainfellner, J. A., et al. (2013). Assessing prenatal white matter connectivity in commissural agenesis. *Brain* 136, 168–179. doi: 10.1093/brain/aww332
- Kasprian, G., Brugger, P. C., Weber, M., Krssák, M., Krampl, E., Herold, C., et al. (2008). *In utero* tractography of fetal white matter development. *Neuroimage* 43, 213–224. doi: 10.1016/j.neuroimage.2008.07.026
- Kasprian, G., Del Rio, M., and Prayer, D. (2010). Fetal diffusion imaging: pearls and solutions. *Top. Magn. Reson. Imaging* 21, 387–394. doi: 10.1097/RMR.0b013e31823e6f80
- Khan, A. R., Cornea, A., Leigland, L. A., Kohama, S. G., Jespersen, S. N., and Kroenke, C. D. (2015). 3D structure tensor analysis of light microscopy data for validating diffusion MRI. *Neuroimage* 111, 192–203. doi: 10.1016/j.neuroimage.2015.01.061
- Kolasinski, J., Takahashi, E., Stevens, A. A., Benner, T., Fischl, B., Zöllei, L., et al. (2013). Radial and tangential neuronal migration pathways in the human fetal brain: anatomically distinct patterns of diffusion MRI coherence. *Neuroimage* 79, 412–422. doi: 10.1016/j.neuroimage.2013.04.125
- Kostovic, I., and Goldman-Rakic, P. S. (1983). Transient cholinesterase staining in the mediodorsal nucleus of the thalamus and its connections in the developing human and monkey brain. *J. Comp. Neurol.* 219, 431–447. doi: 10.1002/cne.902190405
- Kostovic, I., and Judas, M. (2006). Prolonged coexistence of transient and permanent circuitry elements in the developing cerebral cortex of fetuses and preterm infants. *Dev. Med. Child Neurol.* 48, 388–393. doi: 10.1017/S0012162206000831
- Kostovic, I., Judas, M., Rados, M., and Hrabac, P. (2002). Laminar organization of the human fetal cerebrum revealed by histochemical markers and magnetic resonance imaging. *Cereb. Cortex* 12, 536–544. doi: 10.1093/cercor/12.5.536
- Kostovic, I., Kostovic-Szentic, M., Benjak, V., Jovanov-Milosevic, N., and Radoš, M. (2014). Developmental dynamics of radial vulnerability in the cerebral compartments in preterm infants and neonates. *Front. Neurol.* 5:139. doi: 10.3389/fneur.2014.00139
- Kostovic, I., and Rakic, P. (1984). Development of prestriate visual projections in the monkey and human fetal cerebrum revealed by transient cholinesterase staining. *J. Neurosci.* 4, 25–42.
- Ludwig, E., and Klingler, J. (1956). *Atlas Cerebri Humani*. Basel: Karger.
- Mailath-Pokorny, M., Kasprian, G., Mitter, C., Schöpf, V., Nemec, U., and Prayer, D. (2012). Magnetic resonance methods in fetal neurology. *Semin. Fetal Neonatal Med.* 17, 278–284. doi: 10.1016/j.siny.2012.06.002
- Marin, O., and Rubenstein, J. L. (2003). Cell migration in the forebrain. *Annu. Rev. Neurosci.* 26, 441–483. doi: 10.1146/annurev.neuro.26.041002.131058
- Martino, J., De Witt Hamer, P. C., Vergani, F., Brogna, C., De Lucas, E. M., Vázquez-Barquero, A., et al. (2011). Cortex-sparing fiber dissection: an improved method for the study of white matter anatomy in the human brain. *J. Anat.* 219, 531–541. doi: 10.1111/j.1469-7580.2011.01414.x
- Mitter, C., Kasprian, G., Brugger, P. C., and Prayer, D. (2011). Three-dimensional visualization of fetal white-matter pathways *in utero*. *Ultrasound Obstet. Gynecol.* 37, 252–253. doi: 10.1002/uog.8899
- Mitter, C., Prayer, D., Brugger, P. C., Weber, M., and Kasprian, G. (2015). *In vivo* tractography of fetal association fibers. *PLoS ONE* 10:e0119536. doi: 10.1371/journal.pone.0119536
- Molnár, Z., Garel, S., López-Bendito, G., Maness, P., and Price, D. J. (2012). Mechanisms controlling the guidance of thalamocortical axons through the embryonic forebrain. *Eur. J. Neurosci.* 35, 1573–1585. doi: 10.1111/j.1460-9568.2012.08119.x
- Mori, S., Crain, B. J., Chacko, V. P., and Van Zijl, P. C. (1999). Three-dimensional tracking of axonal projections in the brain by magnetic resonance imaging. *Ann. Neurol.* 45, 265–269.
- Mori, S., and Tournier, J. D. (2013). *Introduction to Diffusion Tensor Imaging: And Higher Order Models*. Oxford: Elsevier.
- Peyre, G. (2008). *A Toolbox to Perform Differential Calculus on a Matrix*. Available online at: <http://www.mathworks.com/matlabcentral/fileexchange/5103-toolbox-diffc> (Accessed January 2, 2015).
- Prayer, D. (2011). *Fetal MRI*. Berlin: Springer. doi: 10.1007/978-3-540-73271-6
- Prayer, D., Kasprian, G., Krampl, E., Ulm, B., Witzani, L., Prayer, L., et al. (2006). MRI of normal fetal brain development. *Eur. J. Radiol.* 57, 199–216. doi: 10.1016/j.ejrad.2005.11.020
- Probst, M. (1901). Ueber den Bau des vollständig balkenlosen Grosshirnes sowie über Mikrogryrie und Heterotopie der grauen Substanz. *Arch. Psychiatr. Nervenkr.* 34, 709–786. doi: 10.1007/BF02680175
- Ren, T., Anderson, A., Shen, W. B., Huang, H., Plachez, C., Zhang, J., et al. (2006). Imaging, anatomical, and molecular analysis of callosal formation in the developing human fetal brain. *Anat. Rec. A Discov. Mol. Cell. Evol. Biol.* 288, 191–204. doi: 10.1002/ar.a.20282
- Rezakhaniha, R., Agianniotis, A., Schrauwen, J. T., Griffa, A., Sage, D., Bouten, C. V., et al. (2012). Experimental investigation of collagen waviness and orientation in the arterial adventitia using confocal laser scanning microscopy. *Biomech. Model. Mechanobiol.* 11, 461–473. doi: 10.1007/s10237-011-0325-z
- Sage, D. (2012). *OrientationJ*. Available online at: <http://bigwww.epfl.ch/demo/orientation/> (Accessed July 30, 2015).
- Saksena, S., Husain, N., Das, V., Pradhan, M., Trivedi, R., Srivastava, S., et al. (2008). Diffusion tensor imaging in the developing human cerebellum with histologic correlation. *Int. J. Dev. Neurosci.* 26, 705–711. doi: 10.1016/j.jdeveu.2008.07.007
- Schmahmann, J. D., and Pandya, D. N. (2006). *Fiber Pathways of the Brain*. New York, NY: Oxford University Press. doi: 10.1093/acprof:oso/9780195104233.001.0001
- Schmahmann, J. D., Pandya, D. N., Wang, R., Dai, G., D’arceuil, H. E., De Crespigny, A. J., et al. (2007). Association fibre pathways of the brain: parallel observations from diffusion spectrum imaging and autoradiography. *Brain* 130, 630–653. doi: 10.1093/brain/awl359
- Sidman, R. L., and Rakic, P. (1973). Neuronal migration, with special reference to developing human brain: a review. *Brain Res.* 62, 1–35. doi: 10.1016/0006-8993(73)90617-3
- Takahashi, E., Folkerth, R. D., Galaburda, A. M., and Grant, P. E. (2012). Emerging cerebral connectivity in the human fetal brain: an MR tractography study. *Cereb. Cortex* 22, 455–464. doi: 10.1093/cercor/bhr126
- Takahashi, E., Hayashi, E., Schmahmann, J. D., and Grant, P. E. (2014). Development of cerebellar connectivity in human fetal brains revealed by high angular resolution diffusion tractography. *Neuroimage* 96, 326–333. doi: 10.1016/j.neuroimage.2014.03.022
- Trivedi, R., Gupta, R. K., Husain, N., Rathore, R. K., Saksena, S., Srivastava, S., et al. (2009a). Region-specific maturation of cerebral cortex in human fetal brain: diffusion tensor imaging and histology. *Neuroradiology* 51, 567–576. doi: 10.1007/s00234-009-0533-8
- Trivedi, R., Husain, N., Rathore, R. K., Saksena, S., Srivastava, S., Malik, G. K., et al. (2009b). Correlation of diffusion tensor imaging with histology in the developing human frontal cerebrum. *Dev. Neurosci.* 31, 487–496. doi: 10.1159/000229500
- Ulfing, N., Setzer, M., Neudörfer, F., and Bohl, J. (2000). Distribution of SNAP-25 in transient neuronal circuitries of the developing human forebrain. *Neuroreport* 11, 1259–1263. doi: 10.1097/00001756-200004270-00023
- Vasung, L., Huang, H., Jovanov-Milosevic, N., Pletikos, M., Mori, S., and Kostovic, I. (2010). Development of axonal pathways in the human fetal fronto-limbic brain: histochemical characterization and diffusion tensor imaging. *J. Anat.* 217, 400–417. doi: 10.1111/j.1469-7580.2010.01260.x
- Vasung, L., Jovanov-Milosevic, N., Pletikos, M., Mori, S., Judaš, M., and Kostovic, I. (2011). Prominent periventricular fiber system related to ganglionic eminence

- and striatum in the human fetal cerebrum. *Brain Struct. Funct.* 215, 237–253. doi: 10.1007/s00429-010-0279-4
- Wang, H., Zhu, J., and Akkin, T. (2014a). Serial optical coherence scanner for large-scale brain imaging at microscopic resolution. *Neuroimage* 84, 1007–1017. doi: 10.1016/j.neuroimage.2013.09.063
- Wang, H., Zhu, J., Reuter, M., Vinke, L. N., Yendiki, A., Boas, D. A., et al. (2014b). Cross-validation of serial optical coherence scanning and diffusion tensor imaging: a study on neural fiber maps in human medulla oblongata. *Neuroimage* 100, 395–404. doi: 10.1016/j.neuroimage.2014.06.032
- Widjaja, E., Geibprasert, S., Mahmoodabadi, S. Z., Blaser, S., Brown, N. E., and Shannon, P. (2010). Alteration of human fetal subplate layer and intermediate zone during normal development on MR and diffusion tensor imaging. *AJNR Am. J. Neuroradiol.* 31, 1091–1099. doi: 10.3174/ajnr.A1985
- Xu, G., Takahashi, E., Folkerth, R. D., Haynes, R. L., Volpe, J. J., Grant, P. E., et al. (2014). Radial coherence of diffusion tractography in the cerebral white matter of the human fetus: neuroanatomic insights. *Cereb. Cortex* 24, 579–592. doi: 10.1093/cercor/bhs330
- Yachnis, A. T., and Rorke, L. B. (1999). Neuropathology of Joubert syndrome. *J. Child Neurol.* 14, 655–659. discussion 669–672. doi: 10.1177/088307389901401006
- Conflict of Interest Statement:** The authors declare that the research was conducted in the absence of any commercial or financial relationships that could be construed as a potential conflict of interest.

Copyright © 2015 Mitter, Jakab, Brugger, Ricken, Gruber, Bettelheim, Scharrer, Langs, Hainfellner, Prayer and Kasprian. This is an open-access article distributed under the terms of the Creative Commons Attribution License (CC BY). The use, distribution or reproduction in other forums is permitted, provided the original author(s) or licensor are credited and that the original publication in this journal is cited, in accordance with accepted academic practice. No use, distribution or reproduction is permitted which does not comply with these terms.



Synchronous Changes of Cortical Thickness and Corresponding White Matter Microstructure During Brain Development Accessed by Diffusion MRI Tractography from Parcellated Cortex

Tina Jeon^{1,2*}, Virendra Mishra^{2,3}, Minhui Ouyang^{1,2}, Min Chen⁴ and Hao Huang^{1,5*}

¹ Radiology Research, Children's Hospital of Philadelphia, Philadelphia, PA, USA, ² Advanced Imaging Research Center, University of Texas Southwestern Medical Center at Dallas, Dallas, TX, USA, ³ Lou Ruvo Center for Brain Health, Cleveland Clinic, Las Vegas, NV, USA, ⁴ Department of Mathematical Sciences, University of Texas at Dallas, Richardson, TX, USA, ⁵ Department of Radiology, Perelman School of Medicine, University of Pennsylvania, Philadelphia, PA, USA

OPEN ACCESS

Edited by:

Yun-Qing Li,
The Fourth Military Medical University,
China

Reviewed by:

Guy Elston,
Centre for Cognitive Neuroscience,
Australia
Kenichi Oishi,
Johns Hopkins University, USA

*Correspondence:

Hao Huang
huangh6@email.chop.edu;
Tina Jeon
jeont@email.chop.edu

Received: 29 September 2015

Accepted: 18 November 2015

Published: 02 December 2015

Citation:

Jeon T, Mishra V, Ouyang M, Chen M and Huang H (2015) Synchronous Changes of Cortical Thickness and Corresponding White Matter Microstructure During Brain Development Accessed by Diffusion MRI Tractography from Parcellated Cortex. *Front. Neuroanat.* 9:158. doi: 10.3389/fnana.2015.00158

Cortical thickness (CT) changes during normal brain development is associated with complicated cellular and molecular processes including synaptic pruning and apoptosis. In parallel, the microstructural enhancement of developmental white matter (WM) axons with their neuronal bodies in the cerebral cortex has been widely reported with measurements of metrics derived from diffusion tensor imaging (DTI), especially fractional anisotropy (FA). We hypothesized that the changes of CT and microstructural enhancement of corresponding axons are highly interacted during development. DTI and T1-weighted images of 50 healthy children and adolescents between the ages of 7 and 25 years were acquired. With the parcellated cortical gyri transformed from T1-weighted images to DTI space as the tractography seeds, probabilistic tracking was performed to delineate the WM fibers traced from specific parcellated cortical regions. CT was measured at certain cortical regions and FA was measured from the WM fibers traced from same cortical regions. The CT of all frontal cortical gyri, including Brodmann areas 4, 6, 8, 9, 10, 11, 44, 45, 46, and 47, decreased significantly and heterogeneously; concurrently, significant, and heterogeneous increases of FA of WM traced from corresponding regions were found. We further revealed significant correlation between the slopes of the CT decrease and the slopes of corresponding WM FA increase in all frontal cortical gyri, suggesting coherent cortical pruning and corresponding WM microstructural enhancement. Such correlation was not found in cortical regions other than frontal cortex. The molecular and cellular mechanisms of these synchronous changes may be associated with overlapping signaling pathways of axonal guidance, synaptic pruning, neuronal apoptosis, and more prevalent interstitial neurons in the prefrontal cortex. Revealing the coherence of cortical and WM structural changes during development may open a new window for understanding the underlying mechanisms of developing brain circuits and structural abnormality associated with mental disorders.

Keywords: brain development, white matter microstructure, circuits, tractography, cortical thickness, synchronous

INTRODUCTION

The cerebral cortex contains neuronal bodies, to which afferent and efferent axonal fibers are connected. Perpendicular to the cortical surface, the cerebral cortex contains six layers. Despite substantial overlap, layer III is the major source of corticocortical fibers, layer V of corticostriate fibers, fibers to the brainstem, spinal cord, and layer VI of corticothalamic fibers (Nolte, 2002). Human brain development is remarkably complicated yet organized. During development, arborization takes place in the cerebral cortex and nerve fibers branch out to form brain circuits. Peak cortical thickness (CT) for some areas such as somatic sensory cortex is reached around 7 years (Shaw et al., 2008). Then, the branching stops and the brain starts to prune away some connections of the cerebral cortex (Giedd, 2004). As a result, cerebral CT undergoes an increase at the beginning years and decreases after around 7–10 years. Cortical thinning during brain development is related to complicated cellular and molecular processes including increased proliferation of myelin into the cortical neuropil, synaptic pruning, trophic glial, and vascular changes, cell shrinkage (Gogtay et al., 2004; Shaw et al., 2008) and apoptosis (Cowan, 1973; Morrison and Hof, 1997; Vanderhaeghen and Cheng, 2010). Although why the brain goes through neural pruning is not yet fully understood, one hypothesis is that the brain prunes away unused connections (Giedd, 2004). In addition, pruning of the cerebral cortex occurs in an asynchronous manner. A previous study (Shaw et al., 2008) has shown that cortical maturation rates and CT trajectories from childhood to adulthood vary regionally.

Heterogeneous developmental patterns have also been found for white matter (WM) axons. Most cerebral WM axons are those projected from neurons in the cerebral cortex. WM axons undergo dramatic changes during development, including axonal packing and myelination (Yakovlev and Lecours, 1967; Stiles and Jernigan, 2010). Electrical impulses across axons contribute to myelination, suggesting that training and experience during brain development may enhance myelination (Demerens et al., 1996). Differentiated WM axonal developmental processes were found from the fetal stage to early childhood (Huang et al., 2006, 2009; Dubois et al., 2008) and from childhood to adulthood (e.g., Lebel and Beaulieu, 2011). Taken together, previous findings suggest that the CT reduction and corresponding WM microstructural enhancement during brain development are intrinsically related. However, the relationship of these two processes is poorly understood. These parallel processes are essentially related to the formation of the brain circuits and mental disorders. For example, it has been suggested that excessive pruning and insufficient pruning are related to schizophrenia (Keshavan et al., 1994) and autism (Barnea-Goraly et al., 2004), respectively. It has also been shown that schizophrenia is linked to abnormalities of both WM microstructure and CT (Ehrlich et al., 2014). Therefore, the overarching hypothesis of this study is that changes of CT and WM microstructure are not independent, but highly interacted during brain development for the formation of brain circuits.

Advances in MR imaging techniques have made non-invasive and concurrent measurements of CT and WM axonal microstructure possible with T1-weighted imaging and diffusion

MRI (dMRI) acquired in the same session. T1-weighted MRI offers high contrast of the cerebral cortex and can be used for CT measurements (e.g., Fischl and Dale, 2000). Early CT increases followed by decreases from around 7–10 years of age in development have been well documented with T1-weighted MRI (e.g., Giedd, 2004; Gogtay et al., 2004). Diffusion tensor imaging (DTI; Basser et al., 1994), using a tensor model based on dMRI dataset, is a type of MRI technique that measures the water diffusion properties in brain tissue. DTI-derived metrics are sensitive to microstructural changes of brain WM axons. Fractional anisotropy (FA; Moseley et al., 1990; Pierpaoli et al., 1996; Beaulieu, 2002), derived from the diffusion tensor, characterizes the degree of anisotropy of diffusion and has been widely used to quantify WM axonal microstructure. It has been found that WM FA, which is sensitive to axonal microstructural enhancement, increases dramatically during development (e.g., Beaulieu, 2002; Lebel et al., 2008; Westlye et al., 2010; Lebel and Beaulieu, 2011).

Coherence of changes of CT and FA of WM fibers traced from corresponding cortical regions during brain development may be related to structural connectivity. The structural connectivity can be characterized in two different ways, one with dMRI and the other with structural MRI (i.e., T1 or T2 weighted images). With dMRI tractography (e.g., Mori et al., 1999; Behrens et al., 2007), WM fibers can be traced to infer structural connectivity. With structural MRI, two brain regions are also considered anatomically connected if statistically significant correlations were found for CT at these two regions (He et al., 2007). Based on WM tractography with dMRI, numerous studies have been conducted in the past several years to characterize brain connectivity from a macroscopic perspective by application of graph theory analysis (Bullmore and Sporns, 2009). For example, increased efficiency and connectivity strength (e.g., Hagmann et al., 2010; Huang et al., 2015) based on tractography with dMRI have been found during brain development. Despite these macroscopic findings from graph theory analysis, the relationship of these two parameters (CT and corresponding WM FA) that can be used for constructing brain structural networks remains unknown. Most brain WM consists of axons projected from the neurons in the cerebral cortex. Neurons and associated WM axons behave coherently in development (Budhachandra et al., 2012). The relationship of CT and WM microstructure of developing brains has been investigated recently (Tamnes et al., 2010a; Wu et al., 2014; Smyser et al., 2015) with a different approach from that used in the present study. Specifically, the relationship between cortical regions and the adjacent WM, namely WM confined by certain physical distances from a certain cortical region, were focused on in those studies. To our knowledge, no investigation has been conducted to test the coherence between regional age-dependent CT decreases and age-dependent FA increases of the WM fibers traced from the corresponding cortical region, regardless of physical distance between the cortical region and traced WM fibers. We hypothesize that CT decreases of certain cortical regions and FA increases of WM fibers traced from the same cortical region are coherent. Revealing the link of the age-dependent changes of CT and those of corresponding WM FA could offer a refreshing

perspective to delineate the intrinsic coherence of cortical regions and their connectional pathways. In this study, DTI and T1-weighted images were acquired from 50 normal children and adolescents at 7–25 years of age. WM fibers were directly traced from a certain parcellated cortical gyrus. The age-dependent CT decreases at certain cortical gyri, age-dependent increases of FA of WM fibers traced from corresponding cortical gyri, and the relationship of the changes of CT and those of FA were investigated.

MATERIALS AND METHODS

Participants

A total of 50 healthy children, adolescents and young adults between the ages of 7 and 25 years (31 Male and 19 Female; mean age 16.3 years, standard deviation=6.0 years) were recruited and scanned at the Advanced Imaging Research Center of The University of Texas Southwestern Medical Center (UTSW) at Dallas. **Figure 1** shows the profile of the age and gender of the participated normal subjects. The study was approved by the Institutional Review Board (IRB) at the UTSW. Subjects or their guardians (if subjects are under 18 years old) gave written informed consents for all study procedures. All subjects gave written informed consent. All participants were medically healthy and had no known neurological or psychiatric disorders. They were not under any intervention or medication known to affect the central nervous system. There was no significant correlation between age and gender ($p = 0.42$).

MRI Data Acquisition

All MRI datasets were obtained on a Philips 3T Achieva MR system (Philips Healthcare, Best, The Netherlands). Diffusion weighted images (DWI) were acquired using a single-shot EPI with SENSE parallel imaging scheme (Sensitivity Encoding reduction factor = 2.3). Diffusion parameters were as follows: FOV = 224/224/143 mm, in plane imaging matrix = 112×112 , axial slice thickness = 2.2 mm, $TE = 97$ ms, $TR = 4.41$ s,

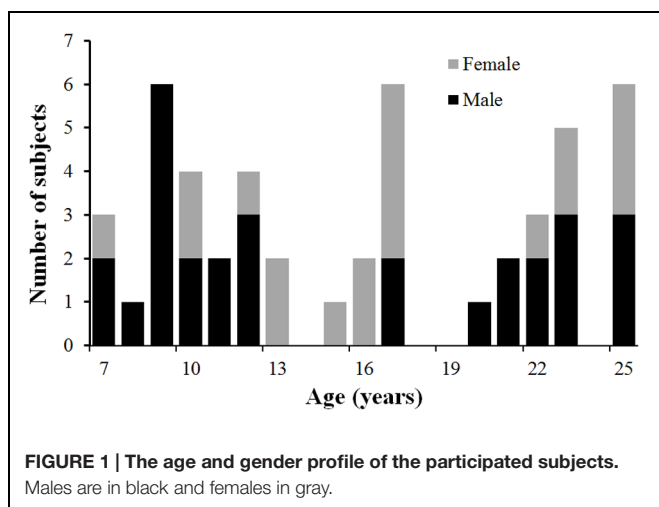
30 independent diffusion-weighted directions (Jones et al., 1999), with b -values of 0 and 1000 sec/mm². To increase signal to noise ratio (SNR), two repetitions were performed, resulting in a total scan time of 11 min for DWI acquisition. T1-weighted magnetization-prepared rapid gradient-echo (MPRAGE) images with FOV = 256/256/160 mm and resolution 1 mm \times 1 mm \times 1 mm were also acquired. The MPRAGE images provide superior gray and WM contrast and were used for CT measurement and parcellation of the cerebral cortex. DTI and T1-weighted images were acquired in the same session.

Cortical Parcellation and Thickness Measurement of the Parcellated Cortical Regions

The pipeline for measuring thickness of a certain cortical gyrus and WM microstructure traced from the same cortical gyrus is demonstrated in **Figure 2**. Based on T1-weighted image of each subject (**Figure 2a**), the brain cortical surface of each hemisphere was rendered and parcellated into 33 gyral labels (Desikan et al., 2006; **Figure 2b**) using *FreeSurfer* (version 5.0.1)¹, a semi-automated software suite. After segmentation of brain into gray matter (**Figure 2c**), WM, and cerebrospinal fluid (CSF) using *FreeSurfer*, the distance between the pial surface and GM-WM boundary at a certain cerebral cortex vertex was measured as the thickness of this vertex. The CT map is shown in **Figure 2d**. The thickness values of all cortical vertices within a particular gyral label were then averaged to obtain the thickness of a certain gyrus.

Quantification of Microstructure of WM Fibers Traced from a Certain Cortical Gyrus

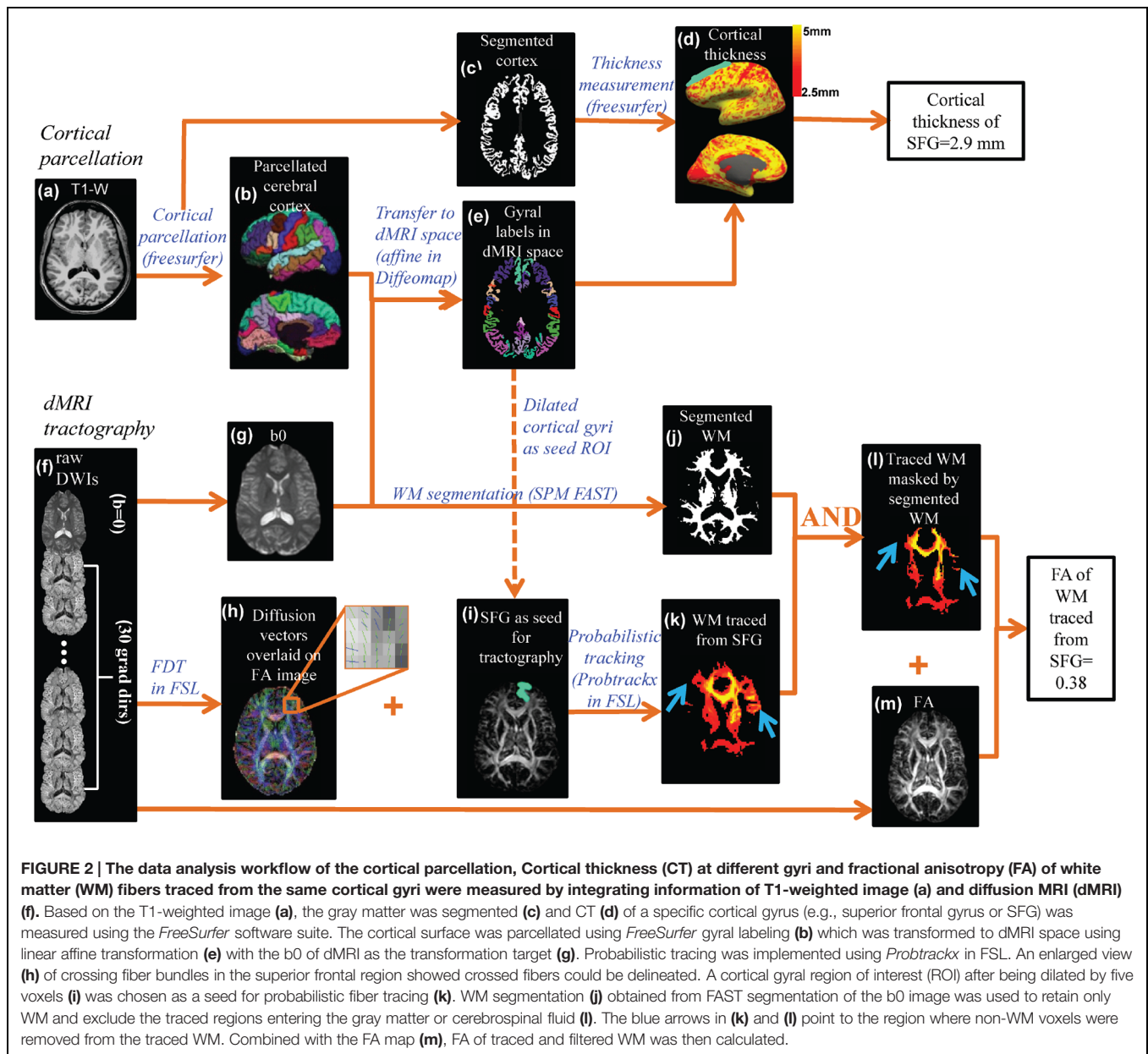
As also shown in **Figure 2**, there are two key components to compute the FA measurement of the WM fibers projected from a cortical gyrus, namely cortical parcellation determining the tractography seed region of interest (ROI) and probabilistic tracking determining the WM traced from a certain cortical gyrus (superior frontal gyrus or SPG was used as an example). For the first component, the parcellated cortical gyrus from the T1-weighted image (**Figure 2b**) was transformed to dMRI space (**Figure 2e**) to serve as the seed ROI for probabilistic tracing (**Figure 2i**). Linear affine transformation was applied to reorient and transform the parcellated cortical labels into dMRI space with the skull-stripped b0 image (**Figure 2g**) and skull-stripped T1-weighted image as the transformation target and subject, respectively, with *Diffeomap*². The same linear transformation re-slices the gyral labeled image using nearest neighbor interpolation. The parcellated cortical ribbon in dMRI space (**Figure 2e**) was then dilated by 5 mm using custom software written in IDL (Interactive Data Language 8.2.3³) to penetrate the superficial WM and reach the deep WM to initiate fiber tracking. For the second component, after eddy current correction with FLIRT, raw dMRI (**Figure 2f**) was processed



¹<http://surfer.nmr.mgh.harvard.edu>

²<http://www.mristudio.org>

³<http://www.exelisvis.com>



with *BedpostX* of FDT of FSL⁴ to generate the diffusion vectors (Figure 2h) and FA (Figure 2m) map. With *Probstackx* in FDT of FSL, probabilistic tracing was conducted with the dilated cortical gyrus as the seed ROI (described above), as shown in Figures 2i,k. A threshold of 100 for *fdt_paths* was applied to retain only WM with high probability of tracing. In addition, a WM mask (Figure 2j) segmented with SPM FAST segmentation tool (Statistical Parametric Mapping 8.0⁵, WM threshold = 0.8) was generated to filter out spurious tracings reaching to non-WM regions. The filtered WM is shown in Figure 2l. Together with the FA map in Figure 2m, the FA value of the WM traced from a certain gyrus was calculated after applying a FA threshold of 0.2.

⁴<http://www.fmrib.ox.ac.uk/fsl>

⁵<http://www.fil.ion.ucl.ac.uk/spm>

Evaluation of Seed ROI for WM Tractography

Due to the dense WM zones just beneath the infragranular layers of the cortex impeding tracking (Reveley et al., 2015), we evaluated (1) how much dilation from the segmented cortical gyrus with *FreeSurfer* would be sufficient to go through the dense WM zones; and (2) if tracing directly from the WM immediately beneath the dense WM zones will yield the same tractography results. dMRI data of three representative subjects of ages 8, 16, and 25 years old were used for the evaluation. For the first evaluation approach, three representative segmented cortical gyri, namely precentral gyrus, lateral orbitofrontal gyrus and superior frontal gyrus, obtained from *FreeSurfer* were dilated by 1, 2, 3, 4, and 5 mm into the WM. These dilated regions

were used as seed ROIs to initiate WM tracing. For the second evaluation approach, similar to the first approach, cortical gyral regions from *FreeSurfer* were first dilated by 2 and 4 mm into the WM, then cortical gyral regions from *FreeSurfer* dilated by 1 mm were subtracted to bypass dense WM zones (Reveley et al., 2015) impeding tracing. Tractography was conducted with the retained WM regions as seed ROIs. To quantify the differences of WM traced from different seed ROIs, we calculated Dice coefficients among traced WM regions. The Dice coefficient (Dice, 1945) or Dice ratio is defined as the positive agreement between two datasets divided by their average size. For quantification of the differences of traced WM regions, the traced WM was binarized and the overlap of two traced WM regions could be calculated as the ratio of number of WM voxels contained in both binary maps divided by average number of WM voxels.

Linear Fitting of CT and Age, Corresponding WM FA and Age and the Relationship between CT Change Rate and Corresponding WM FA Change Rate Among Different Frontal Gyri

Linear model was used to fit the CT and corresponding WM FA of each of the 16 gyri in the left and right frontal lobe against age for all subjects with the equations below:

$$CT_{i,j} = \alpha_{1,i} + \beta_{1,i}t_j + \varepsilon_{1,i,j} \quad (1)$$

$$FA_{i,j} = \alpha_{2,i} + \beta_{2,i}t_j + \varepsilon_{2,i,j} \quad (2)$$

Where t_j is the age of the j th subject; $\alpha_{1,i}$ and $\beta_{1,i}$ (or $\alpha_{2,i}$ and $\beta_{2,i}$) are the unknown intercept and slope for CT (or FA) of the i th frontal gyrus, respectively; $\varepsilon_{1,i,j}$ and $\varepsilon_{2,i,j}$ are the error terms for CT and FA, respectively; j is from 1 to 50; $i \in \{1, 2, \dots, 8\}$ indexes eight left frontal gyri (namely superior frontal, lateral orbitofrontal, caudal middle frontal, rostral middle frontal, pars opercularis, pars orbitalis, pars triangularis, and precentral gyrus) while $i \in \{9, 10, \dots, 16\}$ corresponds to the eight right frontal gyri. The regional analysis was controlled for multiple comparisons using the Benjamini and Hochberg adjustment method (Benjamini and Hochberg, 1995).

Estimates of $\beta_{1,i}$ and $\beta_{2,i}$, the unknown rates of CT and FA changes, can be obtained by fitting the regression models in Equation (1) and (2), and the estimators are denoted by $\hat{\beta}_{1,i}$ and $\hat{\beta}_{2,i}$, respectively. After standardizing the slopes $\hat{\beta}_{1,i}$ and $\hat{\beta}_{2,i}$, a Deming regression (R package 'MethComp') to account for measurement errors in both slopes was used to test if these two rates at all frontal gyri were significantly correlated.

$$\hat{\beta}_{2,i} = c + d\hat{\beta}_{1,i} + \delta_i \quad (3)$$

Note that $\hat{\beta}_{1,i}$ and $\hat{\beta}_{2,i}$ are estimates of the "true" or (expected) values of $\beta_{1,i}$ and $\beta_{2,i}$, respectively, at i th frontal gyrus. All

statistical analysis was computed using R statistical software version 3.0.2⁶.

RESULTS

Significant and Heterogeneous Decreases of CT at Different Frontal Gyri during Development

Significant age-dependent CT decreases in all eight gyral regions in the left frontal cortex (Figure 3A and Table 1) and five gyral regions in the right frontal cortex were found (Table 1). Besides significant CT decreases, regional heterogeneity of the CT temporal courses, specifically dramatically different CT decrease slopes, can also be observed in Figure 3A and Table 1. The heterogeneity of the CT decrease in the frontal lobe was indicated by the colors painted on each frontal lobe gyrus in Figure 4a. Specifically, the green, yellow, and red colors represent slow, median and fast age-dependent CT decrease, respectively (Figure 4a and Table 1). For example, in the left frontal lobe, the CT decreases faster in the left pars triangularis and left rostral middle frontal regions, indicated by red, while the CT decreases slower in the left precentral and lateral orbitofrontal gyri, indicated by green (Figure 4a and Table 1). The CT decrease slopes, correlation coefficients and p -values in all frontal gyri are listed in middle column of Table 1. The categorization of slow, median and fast CT decreases of all frontal gyri can be found in the CT decrease rate histogram (upper panel of Supplementary Figure S1).

Significant and Heterogeneous Increases of FA of WM Traced from Parcellated Cortical Gyri during Development

Significant age-dependent increases of FA were found for WM traced from a majority of parcellated left and right frontal cortical gyri. Figure 3B shows the age-dependent increase in FA for WM traced from all eight left frontal gyri. Similar to heterogeneous age-dependent CT changes, heterogeneity in the FA increase rate among different frontal gyri were observed (Figure 3B and Table 1). FA values of WM traced from certain frontal gyri, such as the left pars orbitalis and right pars triangularis increase faster compared to those traced from other frontal gyri (Table 1). Figure 4b demonstrates the change rates of FA of WM traced from frontal cortical gyri, using the same slow, median, and fast color scheme as those in the CT change rates. As shown in Figures 4a,b, WM FA increase rate and CT decrease rate appear to be coherent, shown by similar color profile all over frontal gyri. For example, the CT of the precentral gyrus decreases slowly, while, coherently, and FA of the WM traced from precentral gyrus increases slowly, with the green color shown on this gyrus in both Figures 4a,b. The FA increase slopes, correlation coefficients and p values in all frontal gyri are listed in the right column of Table 1. The categorization of slow, median and fast FA increases for WM

⁶<http://www.r-project.org>

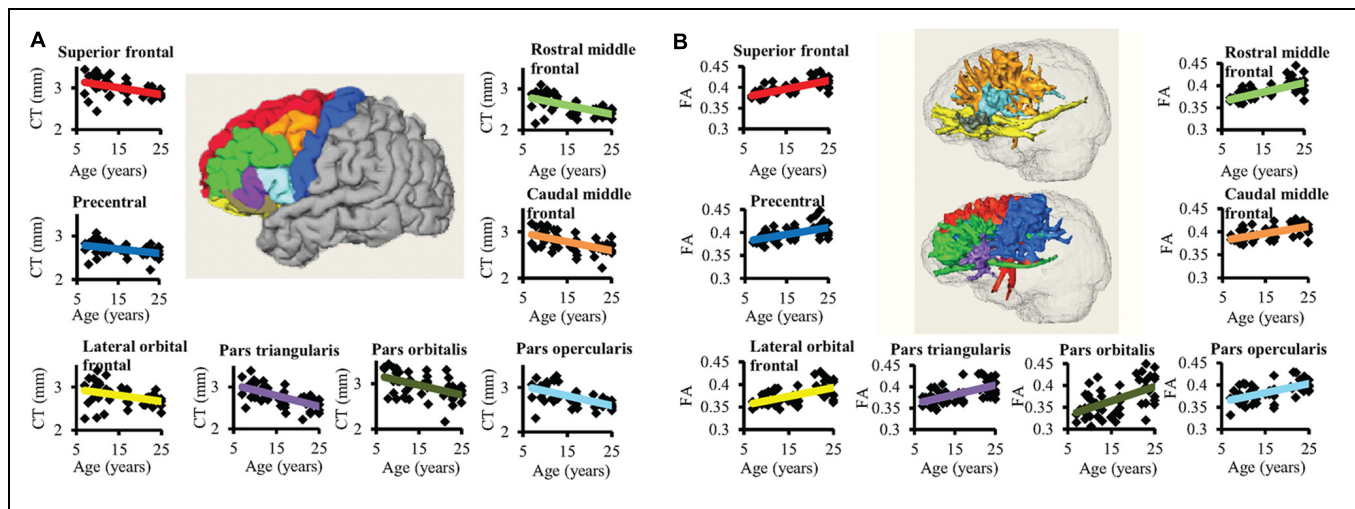


FIGURE 3 | The age-dependent CT decreases and corresponding WM FA increases for eight left frontal regions are shown in (A) and (B), respectively. In the center of (A), parcellated left frontal gyri were encoded with following colors: superior frontal (red), precentral (blue), lateral orbital frontal (yellow), pars triangularis (purple), pars orbitalis (dark green), pars opercularis (light blue), caudal middle frontal (orange), and rostral middle frontal (green). The colors of the fitted CT decrease trend lines in (A) are consistent to those of parcellated gyri in the center. In (B), the three-dimensionally reconstructed WM tracts used for FA measurement in the center were traced from corresponding frontal gyri and encoded with the same colors as those shown in the parcellated left frontal gyri in the center of (A). The same color scheme used in the fitted trend lines in (A) was used for the fitted trend lines in (B).

TABLE 1 | Pearson correlational coefficient (r), correlation significance (p) and slopes of fitted linear trend line are shown for age-dependent cortical thickness (CT) (middle column) and corresponding white matter (WM) fractional anisotropy (FA; right column) for all frontal lobe gyri in the left (lh) and right (rh) hemisphere.

Cortical region	CT vs. age			FA vs. age		
	r	p	Slope (mm/yr)	r	p	Slope (/yr)
lh-superiorfrontal	0.72	<u>2.3E-09</u>	-0.0165	0.90	<u>5.4E-20</u>	0.00201
lh-rostralmiddlefrontal	0.42	<u>2.1E-03</u>	-0.0219	0.38	<u>6.0E-03</u>	0.00213
lh-caudalmiddlefrontal	0.37	<u>7.3E-03</u>	-0.0192	0.55	<u>2.4E-05</u>	0.00153
lh-parsopercularis	0.46	<u>6.9E-04</u>	-0.0166	-0.07	0.604	0.00173
lh-parsorbitalis	0.65	<u>2.5E-07</u>	-0.0217	0.72	<u>2.6E-09</u>	0.00327
lh-parstriangularis	0.70	<u>7.2E-09</u>	-0.0260	0.81	<u>3.8E-13</u>	0.00217
lh-lateralorbitofrontal	0.40	<u>3.3E-03</u>	-0.0119	0.16	0.250	0.00226
lh-precentral	0.45	<u>8.1E-04</u>	-0.0090	0.74	<u>2.6E-10</u>	0.00153
rh-superiorfrontal	0.59	<u>5.2E-06</u>	-0.0104	0.86	<u>4.7E-16</u>	0.00194
rh-rostralmiddlefrontal	0.27	0.056	-0.0165	0.40	<u>3.1E-03</u>	0.00231
rh-caudalmiddlefrontal	0.16	0.250	-0.0132	0.51	<u>1.0E-04</u>	0.00202
rh-parsopercularis	0.41	<u>2.9E-03</u>	-0.0168	0.17	0.241	0.00210
rh-parsorbitalis	0.62	<u>1.1E-06</u>	-0.0197	0.52	<u>8.2E-05</u>	0.00219
rh-parstriangularis	0.61	<u>1.3E-06</u>	-0.0181	0.77	<u>3.5E-11</u>	0.00265
rh-lateralorbitofrontal	0.05	0.707	-0.0103	-0.12	0.449	0.00194
rh-precentral	0.47	<u>4.1E-04</u>	-0.0078	0.78	<u>7.8E-12</u>	0.00151

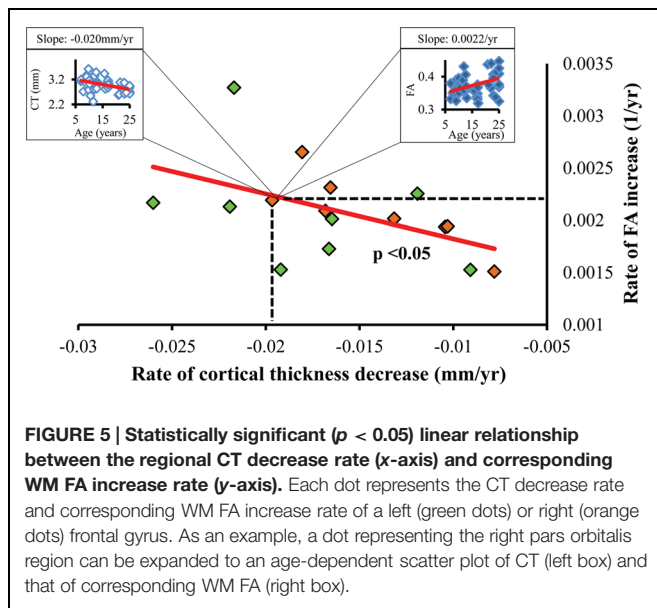
The underlined bold indicates $p < 0.05$ after FDR correction.

traced from all frontal gyri can be found in the FA increase rate histogram (lower panel of Supplementary Figure S1).

Coherent CT Decrease and Corresponding WM FA Increase

Significant correlation between the slopes of CT decrease and those of corresponding WM FA increase were found, as shown in Figure 5. Each point in scatter plot of Figure 5 represents the CT change rate and corresponding WM FA

change rate for one frontal gyrus. Despite long physical distances in the WM axons projected from the cortex, including longitudinal, association, and callosal fibers, the correlation of CT change rate and corresponding WM FA change rate is statistically significant ($p < 0.05$), suggesting coherence of cortical structural changes and corresponding WM microstructural changes during frontal lobe development. In Figure 5, except the points for left caudal middle frontal gyrus, left pars opercularis and right pars triangularis, all other points lie



DISCUSSION

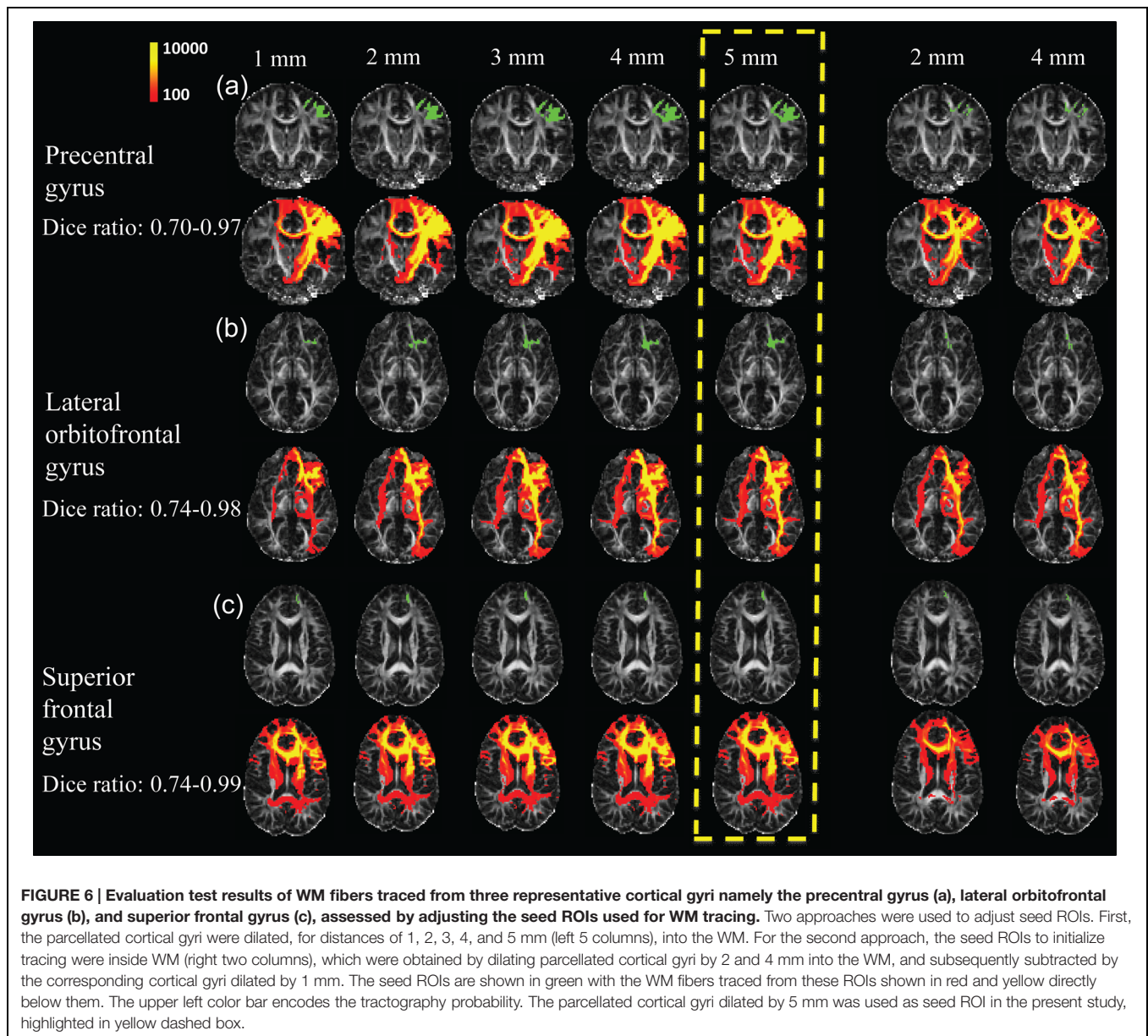
The present study revealed coherence between the CT decrease and corresponding WM FA increase in the frontal lobe during development, which might suggest synchronous cortical pruning and axonal microstructural enhancement. Both cortical thinning and WM microstructural enhancement are essential age-dependent structural processes during normal development from 7 to 25 years of age. Alterations of either of these processes may be related to neuropathological states. Most human brain WM consists of axons projected from neurons in the cerebral cortex, which is likely to underlie our findings of significant correlation between cortical thinning and corresponding WM microstructural enhancement measured by FA increase. To the best of our knowledge, this study marks one of the first attempts to reveal coherence between changes of CT and those of FA of WM connected to a particular cortical gyrus in normal developing brains.

Both age-dependent changes of CT and WM FA, as structural markers of brain maturation, have been related to functional changes during development from childhood to adulthood. It is then likely that the developmental changes of these two structural markers, CT and WM FA, are correlated. For example, executive function in subjects from 8 to 19 years of age has been associated with CT decreases in the frontal lobe (Tamnes et al., 2010b). CT decreases in the left frontal areas coincide with cognitive ability changes affecting intelligence quotient (IQ) in children and adolescents (Burgaleta et al., 2014). On the other hand, the relationship of WM FA increase and enhanced brain function has also been revealed. For example, it has been shown that enhanced WM microstructure (i.e., increased FA) is associated with better performances on inhibitory control and cognitive flexibility tests for children between the ages of 5 to 16 years old (Treit et al., 2014). Increased FA in major WM tracts is correlated with enhanced neurocognitive performance in healthy subjects

between the ages of 8 and 25 years old (Peters et al., 2014). Due to the embryonic link between the cortical interstitial neurons (Von Economo and Koskinas, 2008) and WM axons projected from them, it is intuitive to suggest that age-dependent structural changes of cortex (where the neuronal bodies are located) and those of corresponding WM axons are linked. Primate studies suggest that axon guidance signaling most likely contributes to weak or excessive pruning after the peak has been reached in puberty (Oga et al., 2013; Sasaki et al., 2014). The exact molecular and cellular mechanisms of these coherent changes of CT and WM integrity in development are not known. We speculated that there are some overlapping signaling pathways of axonal guidance and synaptic pruning or neuron apoptosis. A very simplified mechanism is illustrated in the cartoonography in Figure 7.

Besides neuroscientific insight of normal brain development, the present study may shed light on the mechanism of abnormal WM development and its association with the cerebral cortex in different neuropsychiatric disorders such as autism and schizophrenia. In post-mortem studies of schizophrenia, a decrease in frontal cortical volume in adolescence caused by a decrease in the number of synapses and reduction in neuropil was found (Selemon et al., 1995). Decreased FA of the uncinate fasciculus, cingulum bundle and arcuate fasciculus (see e.g., Kubicki et al., 2007 for review) was found to be associated with schizophrenia. Abnormalities in both CT and WM microstructure in schizophrenia suggest a link between the developmental processes of these two structural markers (Paus et al., 2008). Similarly, abnormal WM FA and CT were found for autistic brains. Reduced FA was found for WM adjacent to cortical regions implicated in social cognition as well as WM near the prefrontal cortex (Barnea-Goraly et al., 2004). Significant localized CT reductions within the fronto-striatal network was found for the subjects with autism spectrum disorder (Ecker et al., 2014). Revealing coherence of CT and WM microstructural changes during development could open a new window for understanding underlying mechanism of interacted abnormal CT decrease and WM disruption in mental disorders.

The approach to “trace” WM fibers directly from the cortical gyrus in the present study may be a more connectivity-driven one, which differs from those in previous studies focusing on measuring FA in the superficial WM region “adjacent to” certain cortical gyri (Tamnes et al., 2010a; Wu et al., 2014). In the present study, FA values of WM axons traced from a specific cortical region were measured. These traced WM axons could either project from or get to the neurons in this specified cortical region. The present approach is directly linked to connectivity. Despite that traced WM fibers could have long physical distances away from the seed cortical region, significant correlation between CT changes in the frontal regions and FA changes for WM traced from these regions during development was found (Figures 4 and 5). On the other hand, the anatomical adjacency in the previous studies does not ensure biological association of the WM axons and the cortical regions. As a result, no significant associations between CT and superficial WM FA were identified, while age-dependent changes of CT and superficial WM FA were found to be significant (Tamnes et al., 2010a; Wu et al., 2014).



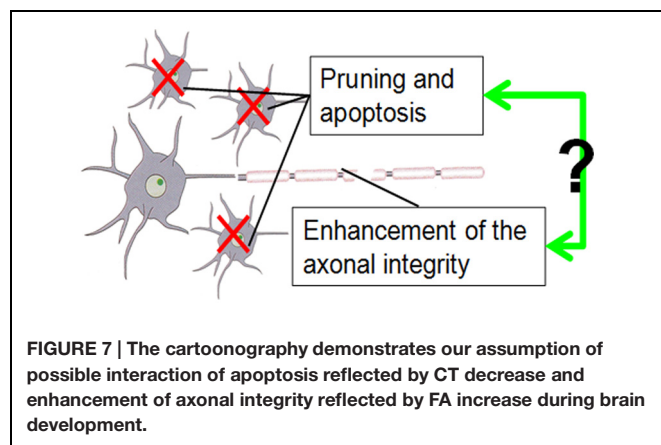
Significant correlation between CT and associated WM microstructural changes was not found for cortical regions other than frontal areas (data not shown). Vast regional differences in cell diversity within the cortex in development have been quantified previously by Conel (1941, 1947, 1955, 1959, 1963, 1967). The densities of the interstitial neurons giving rise to most axonal projections are highest (Meyer et al., 1992; Smiley et al., 1998) in the frontal lobe, which may contribute to the observation that coherence was only found in the frontal lobe. Histological findings in primates and humans suggest asynchronous patterns of synaptogenesis (Bianchi et al., 2013) and different size, dendritic branching patterns, spine density, and complexity of pyramidal cells (Hof and Morrison, 1995; Elston, 2000, 2003; Jacobs et al., 2001; Jacobs and Scheibel, 2002) in the prefrontal cortex. This regional variation of pyramidal

cells are likely to influence underlying circuitry and functional specializations (Elston et al., 2002; Elston, 2003; Elston and Fujita, 2014). Other related factors may include the accelerated growth of the frontal areas during the studied time period (7–25 years; Giedd et al., 1999; Sowell et al., 2001). In addition, different tracing of superficial WM fibers (Oishi et al., 2008), located in the WM region immediately inside the dense WM zone (details in Reveley et al., 2015), among different lobes through dMRI tractography may also play a role. Although the mechanism is not completely known, heterogeneity in superficial WM fiber directions among different lobes affects dMRI tractography. Despite that probabilistic tractography was used, it is a general limitation that dMRI tractography cannot trace through the areas with mixed fibers in many different directions.

TABLE 2 | Mean Dice ratios and standard deviations of the WM fibers traced from the left precentral gyrus (A), left lateral orbitofrontal gyrus (B), and left superior frontal gyrus (C) using two different evaluation tests by adjusting the seed region of interest (ROI) for WM tracing.

(mm)	WM traced from a ROI in the dilated cerebral cortex					WM traced from a ROI inside the WM	
	1	2	3	4	5	2	4
A							
3		0.88 ± 0.10	0.79 ± 0.15	0.78 ± 0.17	0.76 ± 0.15	0.70 ± 0.15	0.73 ± 0.17
5			0.92 ± 0.04	0.90 ± 0.06	0.89 ± 0.04	0.77 ± 0.17	0.84 ± 0.09
7				0.96 ± 0.02	0.94 ± 0.01	0.72 ± 0.20	0.86 ± 0.09
9					0.97 ± 0.02	0.72 ± 0.17	0.85 ± 0.10
11						0.70 ± 0.16	0.84 ± 0.09
2							0.82 ± 0.10
4							
B							
3		0.95 ± 0.01	0.92 ± 0.00	0.91 ± 0.01	0.90 ± 0.00	0.80 ± 0.07	0.85 ± 0.06
5			0.97 ± 0.01	0.96 ± 0.00	0.95 ± 0.02	0.78 ± 0.07	0.78 ± 0.06
7				0.98 ± 0.00	0.98 ± 0.01	0.75 ± 0.07	0.84 ± 0.04
9					0.98 ± 0.02	0.75 ± 0.06	0.83 ± 0.04
11						0.74 ± 0.07	0.80 ± 0.06
2							0.90 ± 0.03
4							
C							
3		0.96 ± 0.01	0.95 ± 0.01	0.95 ± 0.01	0.95 ± 0.02	0.79 ± 0.05	0.84 ± 0.06
5			0.98 ± 0.00	0.98 ± 0.01	0.98 ± 0.01	0.75 ± 0.05	0.81 ± 0.06
7				0.99 ± 0.00	0.98 ± 0.01	0.74 ± 0.06	0.79 ± 0.07
9					0.99 ± 0.01	0.74 ± 0.06	0.79 ± 0.07
11						0.74 ± 0.07	0.79 ± 0.07
2							0.94 ± 0.01
4							

In the left five columns, mean Dice ratios and standard deviations are shown for a ROI from the cortex after being dilated by 1, 2, 3, 4, and 5 mm inward into the WM to initialize tracing. In the right two shaded columns, mean Dice ratios and standard deviations from a ROI at the interior WM are listed. The interior WM seed ROI was obtained by dilating a parcellated cortical gyrus by 2 and 4 mm into the WM, and subsequently subtracted by the corresponding cortical gyri dilated by 1 mm. Dice ratio results from three subjects with the representative ages (8, 16, and 25 years of age) spanning the age range in the present study were averaged.



This study may serve as a bridge between age-dependent CT or WM FA changes and age-dependent changes of network metrics based on graph theory. The application of graph theory to study human brain networks termed the “human connectome” (Bullmore and Sporns, 2009) has immensely advanced our understanding of developmental brain

circuits. For example, studies on the development of structural (Hagmann et al., 2010; Huang et al., 2015) connections have revealed enhanced network properties including efficiency and network strength. Regional CT and WM FA of developing brains offered insight of regional or local age-dependent structural changes. Metrics based on graph theory provided the global view of age-dependent brain configuration changes. Brain development is a highly complicated yet organized process. The coherent CT and WM FA changes found in this study may be the link between the local age-dependent structural changes and global age-dependent network metric changes.

The current approach of tracing WM initialized from a certain cortical gyrus is extended from our previous study mapping the WM axons initialized from a certain cortical lobe to the cortical surface (Huang et al., 2011). Evaluation tests were performed with computation of the Dice ratios by adjusting the seed ROI for WM tracing. As discussed in the literature (Zhang et al., 2010), it is difficult to determine the accuracy of the traced WM fibers, but the selection of seed ROIs can be optimized to capture most of the WM fibers traced from a cortical gyrus. We compared two different types of cortical seed ROIs to initialize WM fiber

tracing. The first type of seed ROIs were directly dilated from relatively “pure” cortex into the WM. For the second type of seed ROI, the cerebral cortex and superficial WM systems directly underlying the boundary between gray and WM were excluded and fiber tracing was initialized from more interior WM. These comprehensive evaluation tests of seed ROIs were conducted due to the dense WM zones directly beneath the infra-granular layer of the cortex that pose a significant barrier to tracing (Reveley et al., 2015). From the test results, only minor differences were found using two different approaches to trace the WM fibers (Figure 6 and Table 2). Depending on different cortical gyri as seed regions, Dice ratios ranged from 70 to 99%. To ensure that traced WM from a cortical ROI accurately represents “true” WM connected to this cortical ROI, the accuracy of tracing WM axons with dMRI may be evaluated by comparison to chemical tracing in the future work.

Methodological limitations are related to the fitting model of age-dependent CT or FA changes, sample size and cross-sectional nature. To reveal the rate of CT or WM FA changes, linear model was used for this selected age-range from mid-childhood to adulthood, where significantly linear changes of CT and FA were observed (Figure 3 and Table 1). Although a quadratic or cubic fitting was used for CT changes over a larger age range, namely 3.5–33 years old (Shaw et al., 2008), linear decrease of CT during the age range of 7–25 years of age in the present study was suggested by the literature (Shaw et al., 2008). Similarly, FA increases followed an exponential or quadratic fit in the age range of 5–32 years (Lebel et al., 2008; Lebel and Beaulieu, 2011). For a narrower age range of 725 years, these same studies suggest linear FA increases. With the age range spanning 18 years, the sample size of 50 in the present study is relatively small. However, it is noteworthy that despite the small sample size, the significant correlation of changes (i.e., slopes) of CT and those of FA for WM traced from corresponding frontal cortical regions could be differentiated from non-significant correlation in cortical regions other than frontal lobe. Cross-sectional data introduced considerable individual variation into the age-dependent CT

or FA changes and correlations of these two changes. Future longitudinal studies are warranted to reduce individual variations in the dataset.

CONCLUSION

The present study revealed the coherence of CT decrease and corresponding WM FA increases during brain development. This finding suggested a possible link of signaling pathways of axonal guidance and synaptic pruning or apoptosis. Revealing synchronous cortical and WM structural changes during development may shed light on understanding underlying mechanisms of normal development and those associated with abnormal CT changes and WM disruption in neuropsychiatric disorders.

AUTHOR CONTRIBUTIONS

TJ conducted data analysis and prepared manuscript; VM conducted data analysis; MO conducted data analysis; MC conducted data analysis; HH designed the project, organized data acquisition and prepared manuscript.

ACKNOWLEDGMENT

This study is sponsored by NIH R01MH092535, R21EB009545, and U54HD086984.

Supplementary Material

The Supplementary Material for this article can be found online at: <http://journal.frontiersin.org/article/10.3389/fnana.2015.00158>

REFERENCES

- Barnea-Goraly, N., Kwon, H., Menon, V., Eliez, S., Lotspeich, L., and Reiss, A. L. (2004). White matter structure in autism: preliminary evidence from diffusion tensor imaging. *Biol. Psychiatry* 55, 323–326. doi: 10.1016/j.biopsych.2003.10.022
- Basser, P. J., Mattiello, J., and LeBihan, D. (1994). MR diffusion tensor spectroscopy and imaging. *Biophys. J.* 66, 259–267. doi: 10.1016/S0006-3495(94)80775-1
- Beaulieu, C. (2002). The basis of anisotropic water diffusion in the nervous system – a technical review. *NMR Biomed.* 15, 435–455. doi: 10.1002/nbm.782
- Behrens, T. E. J., Johansen Berg, H., Jbabdi, S., Rushworth, M. F. S., and Woolrich, M. W. (2007). Probabilistic diffusion tractography with multiple fibre orientations: what can we gain? *Neuroimage* 34, 144–155. doi: 10.1016/j.neuroimage.2006.09.018
- Benjamini, Y., and Hochberg, Y. (1995). Controlling the false discovery rate: a practical and powerful approach to multiple testing. *J. R. Stat. Soc. Series B* 57, 289–300.
- Bianchi, S., Stimpson, C. D., Duka, T., Larsen, M. D., Janssen, W. G., Collins, Z., et al. (2013). Synaptogenesis and development of pyramidal neuron dendritic morphology in the chimpanzee neocortex resembles humans. *Proc. Nat. Acad. Sci. U.S.A.* 110, 10395–10401. doi: 10.1073/pnas.1301224110
- Budhachandra, S. K., Reid, A., Brauer, J., Carbonell, F., Lewis, J., Ameis, S., et al. (2012). Developmental changes in organization of structural brain networks. *Cereb. Cortex* 23, 2072–2085. doi: 10.1093/cercor/bhs187
- Bullmore, E., and Sporns, O. (2009). Complex brain networks: graph and theoretical analysis of structural and functional systems. *Nature* 10, 186–198. doi: 10.1038/nrn2575
- Burgaleta, M., Johnson, W., Waber, D., Colom, R., and Karama, S. (2014). Cognitive ability changes and dynamics of cortical thickness development in healthy children and adolescents. *Neuroimage* 84, 810–819. doi: 10.1016/j.neuroimage.2013.09.038
- Conel, J. L. (1941). *The Postnatal Development of the Human Cerebral Cortex: The Cortex of A One Month Old Infant*. Cambridge, MA: Harvard University Press.
- Conel, J. L. (1947). *The Postnatal Development of the Human Cerebral Cortex: The Cortex of A Three Month Old Infant*. Cambridge, MA: Harvard University Press.
- Conel, J. L. (1955). *The Postnatal Development of the Human Cerebral Cortex: The Cortex of A Fifteen Month Old Infant*. Cambridge, MA: Harvard University Press.
- Conel, J. L. (1959). *The Postnatal Development of the Human Cerebral Cortex: The Cortex of A Twenty-Four Month Old Infant*. Cambridge, MA: Harvard University Press.

- Conel, J. L. (1963). *The Postnatal Development of the Human Cerebral Cortex: The Cortex of A Four Year Old Child*. Cambridge, MA: Harvard University Press.
- Conel, J. L. (1967). *The Postnatal Development of the Human Cerebral Cortex: The Cortex of A Six Year Old Child*. Cambridge, MA: Harvard University Press.
- Cowan, W. M. (1973). "Neuronal death as a regulative mechanism in the control of cell number in the nervous system," in *Development and Aging in the Nervous System*, ed. M. Rockstein (New York, NY: Academic Press), 19–41.
- Demerens, C., Stankoff, B., Logak, M., Anglade, P., Allinquant, B., Couraud, G., et al. (1996). Induction of myelination in the central nervous system by electrical activity. *Proc. Natl. Acad. Sci. U.S.A.* 97, 9887–9892. doi: 10.1073/pnas.93.18.9887
- Desikan, R. S., Segonne, F., Fischl, B., Quinn, B. T., Dickerson, B. C., Blacker, D., et al. (2006). An automated labeling system for subdividing the human cerebral cortex on MRI scans into gyral based regions of interest. *Neuroimage* 31, 968–980. doi: 10.1016/j.neuroimage.2006.01.021
- Dice, L. R. (1945). Measures of the amount of ecologic association between species. *Ecology* 26, 297–302. doi: 10.2307/1932409
- Dubois, J., Dehaene-Lambertz, G., Perrin, M., Mangin, J. F., Cointepas, Y., Duchesnay, E., et al. (2008). Asynchrony of the early maturation of white matter bundles in healthy infants: quantitative landmarks revealed noninvasively by diffusion tensor imaging. *Hum. Brain Mapp.* 29, 14–27. doi: 10.1002/hbm.20363
- Ecker, C., Shahidiani, A., Feng, Y., Daly, E., Murphy, C., D'Almeida, V., et al. (2014). The effect of age, diagnosis, and their interaction on vertex-based measures of cortical thickness and surface area in autism spectrum disorder. *J. Neural Transm.* 121, 1157–1170. doi: 10.1007/s00702-014-1207-1
- Ehrlich, S., Geisler, D., Yendiki, A., Panneck, P., Roessner, V., Calhoun, V. D., et al. (2014). Associations of white matter integrity and cortical thickness in patients with schizophrenia and healthy controls. *Schizophr. Bull.* 40, 665–674. doi: 10.1093/schbul/sbt056
- Elston, G. N. (2000). Pyramidal cells of the frontal lobe: all the more spinous to think with. *J. Neurosci.* 20, RC95.
- Elston, G. N. (2003). Cortex, cognition and the cell: new insights into the pyramidal neuron and prefrontal function. *Cereb. Cortex* 13, 1124–1138. doi: 10.1093/cercor/bhg093
- Elston, G. N., Benavides-Piccone, R., DeFelipe, J., and Rockland, K. (2002). The pyramidal cell in auditory, cingulate and prefrontal cortex of the macaque monkey: areal specialization of cell structure. *Eur. Soc. Neurosci. Abstr.* 10, 222.
- Elston, G. N., and Fujita, I. (2014). Pyramidal cell development: postnatal spinogenesis, dendritic growth, axon growth, and electrophysiology. *Front. Neuroanat.* 8:78. doi: 10.3389/fnana.2014.00078
- Fischl, B., and Dale, A. M. (2000). Measuring the thickness of the human cerebral cortex from magnetic resonance images. *Proc. Natl. Acad. Sci. U.S.A.* 97, 11050–11055. doi: 10.1073/pnas.200033797
- Giedd, J. N. (2004). Structural magnetic resonance imaging of the adolescent brain. *Ann. N. Y. Acad. Sci.* 1021, 77–85. doi: 10.1196/annals.1308.009
- Giedd, J. N., Blumenthal, J., Jeffries, N. O., Castellanos, F. X., Liu, H., Zijdenbos, A., et al. (1999). Brain development during childhood and adolescence: a longitudinal MRI study. *Nat. Neurosci.* 10, 861–863. doi: 10.1038/13158
- Gogtay, N., Giedd, J. N., Lusk, L., Hayashi, K. M., Greenstein, D., Vaituzis, A. C., et al. (2004). Dynamic mapping of human cortical development during childhood through early adulthood. *Proc. Natl. Acad. Sci. U.S.A.* 101, 8174–8179. doi: 10.1073/pnas.0402680101
- Hagmann, P., Sporns, O., Madan, N., Cammoun, L., Pienaar, R., Wedeen, V. J., et al. (2010). White matter maturation reshapes structural connectivity in the late developing human brain. *Proc. Natl. Acad. Sci. U.S.A.* 107, 19067–19072. doi: 10.1073/pnas.1009073107
- He, Y., Chen, Z. J., and Evans, A. C. (2007). Small-world anatomical networks in the human brain revealed by CT from MRI. *Cereb. Cortex* 17, 2407–2419. doi: 10.1093/cercor/bhl149
- Hof, P. R., and Morrison, J. H. (1995). Neurofilament protein defines regional patterns of cortical organization in the macaque monkey visual system: a quantitative immunohistochemical analysis. *J. Comp. Neurol.* 6, 161–186. doi: 10.1002/cne.903520202
- Huang, H., Prince, J. L., Mishra, V., Carass, A., Landman, B., Park, D. C., et al. (2011). A framework on surface-based connectivity quantification for the human brain. *J. Neurosci. Methods* 197, 324–332. doi: 10.1016/j.jneumeth.2011.02.017
- Huang, H., Shu, N., Mishra, V., Jeon, T., Chalak, L., Wang, Z. J., et al. (2015). Development of human brain structural networks through infancy and childhood. *Cereb. Cortex* 25, 1389–1404. doi: 10.1093/cercor/bht335
- Huang, H., Xue, R., Zhang, J., Ren, T., Richards, L. J., Yarowsky, P., et al. (2009). Anatomical characterization of human fetal brain development with diffusion tensor magnetic resonance imaging. *J. Neurosci.* 29, 4263–4273. doi: 10.1523/jneurosci.2769-08.2009
- Huang, H., Zhang, J., Wakana, S., Zhang, W., Ren, T., Richards, L. J., et al. (2006). White and gray matter development in human fetal, newborn, and pediatric brains. *Neuroimage* 33, 27–38. doi: 10.1016/j.neuroimage.2006.06.009
- Jacobs, B., Schall, M., Prather, M., Kapler, E., Driscoll, L., Baca, S., et al. (2001). Regional dendritic and spine variation in human cerebral cortex: a quantitative golgi study. *Cereb. Cortex* 11, 558–571. doi: 10.1093/cercor/11.6.558
- Jacobs, B., and Scheibel, A. B. (2002). "Regional dendritic variation in primate cortical pyramidal cells," in *Cortical Areas: Unity and Diversity*, eds A. Schuz and R. Miller (London: Taylor & Francis), 111–131.
- Jones, D. K., Horsfield, M. A., and Simmons, A. (1999). Optimal strategies for measuring diffusion in anisotropic systems by magnetic resonance imaging. *Magn. Reson. Med.* 42, 515–525. doi: 10.1002/(SICI)1522-2594(199909)42:3<515::AID-MRM14>3.3.CO;2-H
- Keshavan, M. S., Anderson, S., and Pettegrew, J. W. (1994). Is schizophrenia due to excessive synaptic pruning in the prefrontal cortex? The Feinberg hypothesis revisited. *J. Psychiatr. Res.* 28, 239–265. doi: 10.1016/0022-3956(94)90009-4
- Kubicki, M., McCarley, R., Westin, C. F., Park, H. J., Maier, S., Kikinis, R., et al. (2007). A review of diffusion tensor imaging studies in schizophrenia. *J. Psychiatr. Res.* 41, 15–30. doi: 10.1016/j.jpsychires.2005.05.005
- Lebel, C., and Beaulieu, C. (2011). Longitudinal development of human brain wiring continues from childhood into adulthood. *J. Neurosci.* 31, 10937–10947. doi: 10.1523/jneurosci.5302-10.2011
- Lebel, C., Walker, L., Leemans, A., Phillips, L., and Beaulieu, C. (2008). Microstructural maturation of the human brain from childhood to adulthood. *Neuroimage* 40, 1044–1055. doi: 10.1523/jneurosci.5302-10.2011
- Meyer, G., Wahle, P., Castaneya-Pardo, A., and Ferres-Torres, R. (1992). Morphology of neurons in the white matter of adult human neocortex. *Exp. Brain Res.* 88, 204–212. doi: 10.1007/bf02259143
- Mori, S., Crain, B. J., Chacko, V. P., and van Zijl, P. C. M. (1999). Three-dimensional tracking of axonal projections in the brain by magnetic resonance imaging. *Ann. Neurol.* 45, 265–269. doi: 10.1002/1531-8249
- Mori, S., Oishi, K., Jiang, H., Jiang, L., Li, X., Akhter, K., et al. (2008). Stereotaxic white matter atlas based on diffusion tensor imaging in an ICBM template. *Neuroimage* 40, 570–582. doi: 10.1016/j.neuroimage.2007.12.035
- Morrison, J. H., and Hof, P. R. (1997). Life and death of neurons in the aging brain. *Science* 278, 412–419. doi: 10.1126/science.278.5337.412
- Moseley, M. E., Cohen, Y., Kucharczyk, J., Mintorovitch, J., Asgari, H. S., Wendland, M. F., et al. (1990). Diffusion-weighted MR imaging of anisotropic water diffusion in cat central nervous system. *Radiology* 176, 439–445. doi: 10.1002/dev.20055
- Nolte, J. (2002). *The Human Brain: An Introduction to its Functional Anatomy*. St. Louis, MO: Mosby, 736.
- Oga, T., Aoi, H., Sasaki, T., Fujita, I., and Ichinohe, N. (2013). Postnatal development of layer III pyramidal cells in the primary visual, inferior temporal, and prefrontal cortices of the marmoset. *Front. Neural Circuits* 7:31. doi: 10.3389/fncir.2013.00031
- Oishi, K., Zilles, K., Amunts, K., Faria, A., Jiang, H., Li, X., et al. (2008). Human brain white matter atlas: identification and assignment of common anatomical structures in superficial white matter. *Neuroimage* 15, 447–457. doi: 10.1016/j.neuroimage.2008.07.009
- Paus, T., Keshavan, M., and Giedd, J. N. (2008). Why do many psychiatric disorders emerge during adolescence? *Nat. Neurosci.* 9, 947–957. doi: 10.1038/nrn2513
- Peters, B. D., Ikuta, T., DeRosse, P., John, M., Burdick, K. E., Gruner, P., et al. (2014). Age-related differences in white matter tract microstructure are associated with cognitive performance from childhood to adulthood. *Biol. Psychiatry* 75, 248–256. doi: 10.1016/j.biopsych.2013.05.020
- Pierpaoli, C., Jezzard, P., Basser, P. J., Barnett, A., and Di Chiro, G. (1996). Diffusion tensor MR imaging of the human brain. *Radiology* 201, 637–648. doi: 10.1148/radiology.201.3.8939209
- Reveley, C. R., Seth, A. K., Pierpaoli, C., Silva, A. C., Yu, D., Saunders, R. C., et al. (2015). Superficial white matter fiber systems impede detection of long-range

- cortical connections in diffusion MR tractography. *Proc. Natl. Acad. Sci. U.S.A.* 112, 2820–2828. doi: 10.1073/pnas.1418198112
- Sasaki, T., Oga, T., Nakagaki, K., Sakai, K., Sumida, K., Hoshino, K., et al. (2014). Developmental expression profiles of axon guidance signaling and the immune system in the marmoset cortex: potential molecular mechanisms of pruning of dendritic spines during primate synapse formation in late infancy and prepuberty (I). *Biochem. Biophys. Res. Commun.* 474, 302–306. doi: 10.1016/j.bbrc.2014.01.024
- Selemon, L. D., Rajkowska, G., and Goldman-Rakic, P. S. (1995). Abnormally high neuronal density in the schizophrenic cortex. A morphometric analysis of prefrontal area 9 and occipital area 17. *Arch. Gen. Psychiatry* 52, 805–818. doi: 10.1001/archpsyc.1995.03950220015005
- Shaw, P., Kabani, N. J., Lerch, J. P., Eckstrand, K., Lenroot, R., Gogtay, N., et al. (2008). Neurodevelopmental trajectories of the human cerebral cortex. *J. Neurosci.* 28, 3586–3594. doi: 10.1523/jneurosci.5309-07.2008
- Smiley, J. F., Levey, A. I., and Mesulam, M. M. (1998). Infracortical interstitial cells concurrently expressing M2-muscarinic receptors, acetylcholinesterase and nicotinamide adenine dinucleotide phosphate-diaphorase in the human and monkey cerebral cortex. *Neuroscience* 84, 755–769. doi: 10.1016/S0306-4522(97)00524-1
- Smyser, T. A., Smyser, C. D., Rogers, C. E., Gillespie, S. K., Inder, T. E., and Neil, J. J. (2015). Cortical gray and adjacent white matter demonstrate synchronous maturation in very preterm infants. *Cereb. Cortex* doi: 10.1093/cercor/bhv164 [Epub ahead of print].
- Sowell, E. R., Thompson, P. M., Tessner, K. D., and Toga, A. W. (2001). Mapping continued brain growth and gray matter density reduction in dorsal frontal cortex: inverse relationships during postadolescent brain maturation. *J. Neurosci.* 21, 8819–8829.
- Stiles, J., and Jernigan, T. L. (2010). The basics of brain development. *Neuropsychol. Rev.* 20, 327–348. doi: 10.1007/s11065-010-9148-4
- Tamnes, C. K., Ostby, Y., Fjell, A. M., Westlye, L. T., Due-Tønnessen, P., and Walhovd, K. B. (2010a). Brain maturation in adolescence and young adulthood: regional age-related changes in CT and white matter volume and microstructure. *Cereb. Cortex* 20, 534–548. doi: 10.1093/cercor/bhp118
- Tamnes, C. K., Ostby, Y., Walhovd, K. B., Westlye, L. T., Due-Tønnessen, P., and Fjell, A. M. (2010b). Neuroanatomical correlates of executive functions in children and adolescents: a magnetic resonance imaging (MRI) study of cortical thickness. *Neuropsychologia* 48, 2496–2508. doi: 10.1016/j.neuropsychologia.2010.04.024
- Treit, S., Chen, Z., Rasmussen, C., and Beaulieu, C. (2014). White matter correlates of cognitive inhibition during development: a diffusion tensor imaging study. *Neuroscience* 276, 87–97. doi: 10.1016/j.neuroscience.2013.12.019
- Vanderhaeghen, P., and Cheng, H.-J. (2010). Guidance molecules in axon pruning and cell death. *Cold Spring Harb. Perspect. Biol.* 2, a001859. doi: 10.1101/cshperspect.a001859
- Von Economo, C. F., and Koskinas, G. N. (2008). *Atlas of Cytoarchitectonics of the Adult Human Cerebral Cortex*, (trans, rev, ed. Triarhou, L. C.). Basel: Karger Publishers.
- Westlye, L. T., Walhovd, K. B., Dale, A. M., Bjørnerud, A., Due-Tønnessen, P., Engvig, A., et al. (2010). Life-span changes of the human brain white matter: diffusion tensor imaging (DTI) and volumetry. *Cereb. Cortex* 20, 2055–2068. doi: 10.1093/cercor/bhp280
- Wu, M., Lu, L. H., Lowes, A., Yang, S., Passarotti, A. M., Zhou, X. J., et al. (2014). Development of superficial white matter and its structural interplay with cortical gray matter in children and adolescents. *Hum. Brain Mapp.* 35, 2806–2816. doi: 10.1002/hbm.22368
- Yakovlev, P. I., and Lecours, A. R. (1967). “The myelogenetic cycles of regional maturation of the brain,” in *Regional Development of the Brain in Early Life*, ed. A. Minkowski (Oxford: Blackwell Scientific), 3–70.
- Zhang, Y., Zhang, J., Oishi, K., Faria, A. V., Jiang, H., Li, X., et al. (2010). Atlas-guided tract reconstruction for automated and comprehensive examination of the white matter anatomy. *Neuroimage* 52, 1289–1301. doi: 10.1016/j.neuroimage.2010.05.049

Conflict of Interest Statement: The authors declare that the research was conducted in the absence of any commercial or financial relationships that could be construed as a potential conflict of interest.

Copyright © 2015 Jeon, Mishra, Ouyang, Chen and Huang. This is an open-access article distributed under the terms of the Creative Commons Attribution License (CC BY). The use, distribution or reproduction in other forums is permitted, provided the original author(s) or licensor are credited and that the original publication in this journal is cited, in accordance with accepted academic practice. No use, distribution or reproduction is permitted which does not comply with these terms.



High Resolution MRI Reveals Detailed Layer Structures in Early Human Fetal Stages: *In Vitro* Study with Histologic Correlation

Rongpin Wang^{1,2*†}, Guangping Dai^{3†} and Emi Takahashi¹

¹ Division of Newborn Medicine, Department of Medicine, Boston Children's Hospital, Harvard Medical School, Boston, MA, USA, ² Department of Radiology, Guizhou Provincial People's Hospital, Guiyang, China, ³ Department of Radiology, Massachusetts General Hospital, Harvard Medical School, Boston, MA, USA

OPEN ACCESS

Edited by:

Hao Huang,
University of Pennsylvania, USA

Reviewed by:

Christopher D. Kroenke,
Oregon Health & Science University,
USA

Lana Vasung,
University Hospital Geneva,
Switzerland

*Correspondence:

Rongpin Wang
wangrongpin@126.com

†Present address:

Rongpin Wang,
Department of Radiology, Guizhou
Provincial People's Hospital,
Guiyang, China;
Guangping Dai,
Science Center, Wellesley College,
Wellesley, MA, USA

Received: 06 August 2015

Accepted: 09 November 2015

Published: 25 November 2015

Citation:

Wang R, Dai G and Takahashi E
(2015) High Resolution MRI Reveals
Detailed Layer Structures in Early
Human Fetal Stages: *In Vitro* Study
with Histologic Correlation.
Front. Neuroanat. 9:150.
doi: 10.3389/fnana.2015.00150

An understanding of normal fetal brain development is essential in detecting the early onset of brain disorders. It is challenging to obtain high-quality images that show detailed local anatomy in the early fetal stages because the fetal brain is very small with rapidly-changing complex structures related to brain development, including neurogenesis, neuronal migration, and axonal elongation. Previous magnetic resonance imaging (MRI) studies detected three layers throughout the fetal cerebral wall that showed differences in MR contrasts at 10 gestational weeks (GW), which is one of the earliest ages studied using MRI. Contrary to the MRI studies, histological studies found more layers at this fetal age. The purpose of this work is to study the development of brain structures from an early fetal period to an early second trimester stage using *ex vivo* MRI and compare it to histology. Special attention was paid to laminar structures in the cerebral wall. T2-weighted imaging was performed on fetal brain specimens ranging from 10 GW to 18 GW on a 4.7 tesla MR scanner. We obtained standard grayscale as well as color-coded images using weighted red-green-blue scales, and compared them with the histological images. Our study confirmed laminar structure in the cerebral wall in all the fetal specimens studied. We found that MRI detected four layers within the cerebral wall as early as 10 GW during the early fetal period (10–13 GW). Early second trimester (15–18 GW) was characterized by the emergence of subplate structures and five layers within the cerebral wall. The color-coded images were more useful than the standard grayscale images in detecting the laminar structures. Scans with appropriate parameters from a high tesla MR scanner showed detailed laminar structures even through a very small and thin cerebral wall at 10 GW *ex vivo*. A combination of high-resolution structural imaging and color-coding processing with histological analysis may be a potential tool for studying detailed structures of typical developing fetal brains, as well as fetal brains with developmental disorders as references for clinical MRI.

Keywords: human fetal brain, cerebral wall, neurogenesis, structural mri, histology

INTRODUCTION

Fetal brain structure is complex and characterized by rapid growth and dynamic changes from the early stage to term. After embryo stage (which occurs before 10 gestational weeks, GW), early fetal period is considered to be between 10–13 GW, while midfetal period, otherwise known as early second trimester, occurs between 15–18 GW (Vasung et al., 2011). Better understanding of human fetal brain development is critical to assess developmental abnormalities that often cause various neurological and psychiatric disorders later in life (du Plessis and Volpe, 2002; Glenn and Barkovich, 2006a,b; Rakic, 2006; Saleem, 2013). Unlike the internationally accepted Carnegie system staging that is used to describe the human embryonic brain (https://embryology.med.unsw.edu.au/embryology/index.php/Carnegie_Stages), there is no standard staging system in place yet for the fetal period. Regardless of this fact, assessments have still been done by both histological and MRI-related studies on human fetal periods (e.g., Kostović and Vasung, 2009).

Magnetic resonance imaging (MRI) has potential to show fetal brain structures in a three-dimensional manner. In clinical practice, fetal brain MRI *in vivo* can be obtained routinely from 18 GW to term, and relies primarily on T2-weighted and diffusion-weighted sequences (Prayer et al., 2006; Brugger, 2011). However, fetal brain MRI from early fetal period to early second trimester is still dependent on *ex vivo* studies due to small brain-size, poor tissue differentiation, and frequent fetal generic movements. Postmortem MRI or MR-autopsy has proven to be a potential diagnostic alternative to conventional autopsy (Huisman, 2004; Thayyil et al., 2013) because of the advantages in imaging that allows the use of high-field magnets, smaller field of view along with high spatial resolution with increased acquisition time (Zhan et al., 2013). Even with this alternative, anatomical studies of human brain development during the early period are surprisingly scarce.

Previous *ex vivo* MRI studies focused on fetal brain structure using 0.5, 1.5, and 7.0 tesla MRI scanners (Brisse et al., 1997; Bendersky et al., 2006; Huang et al., 2009; Zhan et al., 2013). The earliest gestational weeks in these studies started at 13 GW. To our knowledge, there are only three review articles (Rados et al., 2006; Kostović and Vasung, 2009; Vasung et al., 2010) that refer to using a T1-weighted sequence on early fetal brain structure at 12 GW but without detailed information about the parameters used or the magnetic field intensity. There is only one original *ex vivo* MRI study that looked at 12 GW but it only focused on the periventricular pathway (Vasung et al., 2010). These pioneer MRI studies demonstrated that the cerebral wall has a trilaminar structure at early fetal stage (Rados et al., 2006; Kostović and Vasung, 2009) and a four to five layer structure at midfetal period (Rados et al., 2006; Kostović and Vasung, 2009; Zhan et al., 2013). On the other hand, histological studies revealed more layers in the cerebral wall (Kostović and Rakic, 1990; Kostović and Judas, 2002, 2010; Bayer and Altman, 2006; Rados et al., 2006; Huang et al., 2009, 2013; Kostović and Vasung, 2009).

Due to rapid improvements of MRI techniques, new sequences and post-processing techniques emerged one after

another. Presently, it remains unclear whether a high magnetic field or post-processing techniques can show more detailed structures. That along with a lack of information about T2-weighted sequence in early fetal brain leads to the purpose of this study which focuses on the development of fetal brain structures from early fetal period to early second trimester using *in vitro* T2-weighted sequence studies with histological comparisons. Special attention was paid to the structure of the cerebral wall.

MATERIALS AND METHODS

Specimens

The Institutional Review Board at Boston University (BU) concluded that this research involved de-identified fetal tissues, which is not considered human subjects research, and therefore deemed this an exempt project. The Department of Anatomy and Neurobiology at BU approved the use of the specimens at the Boston Children's Hospital (BCH) and related locations necessary for the current research to be completed.

Six human fetal brain specimens, 10–18 GW, were obtained from a brain specimen collection in the Department of Anatomy and Neurobiology, Boston University School of Medicine. Gestational ages were further confirmed based on foot length (Hern, 1984). Brain specimens came from either miscarriages or abortions. The inclusion criterion was the absence of known and/or suspected malformations. The specimens were fixed in a 4% paraformaldehyde solution, and stored in the same solution. We first imaged specimens without gadolinium (Gd-DTPA) MRI contrast agent to obtain a closer condition to *in vivo* imaging conditions. The specimens between 15 and 18 GW specimens were successfully imaged without Gd-DTPA, while the imaging contrast in the 10 and 12 GW specimens were too weak. Therefore we fixed the 10 and 12 GW specimens in another 4% paraformaldehyde solution that contained 1 mM Gd-DTPA to reduce the T1 relaxation time while ensuring that enough T2-weighted signals remained (Takahashi et al., 2013).

There was no record about the duration of fixation and postmortem times in Boston University. Unlike animal specimens that undergo perfusion processes, human specimens tend to have varied fixation and postmortem durations. It has been reported that fixation and postmortem durations affected tissue properties to some extent (Pfefferbaum et al., 2004; Dawe et al., 2009). However, conventional structural imaging was possibly less affected by fixatives compared to diffusion imaging (e.g., Pfefferbaum et al., 2004). Even though fixation processes reduce the difference of gray/white matter water mobility, the location of the gray/white matter border tends to remain in the same regions over fixation periods. As long as the location of the border remained in the same place, even with a weaker contrast, we believe it possible to detect such a border (in our case, borders of multiple layers) using our method.

MR Imaging

Fetal brain imaging was performed on a 4.7 tesla MRI system (Bruker Biospin GmbH, Germany). Each fetal brain was

immersed in Fomblin oil, and scanned with a custom-made MR coil that had an inner diameter of 60 mm. A spin-echo 2D T2-weighted (T2W) sequence was used for structural imaging. The acquisition parameters were as follows:

TR/TE = 200/8.8 ms, matrix $160 \times 160 \times 128$, NEX = 4, 3D method, for 10 and 12 GW; TR/TE = 6360/42.5 ms, matrix 256×256 , NEX = 16, 2D multi-slice scan, for 15 GW; TR/TE = 6000/42.7 ms, matrix 256×256 , 2D multi-slice scan, for 17 GW. Flip angle was 90° for all specimens. Spatial resolution was set to minimum to secure enough signal-to-noise ratio (over 100): $0.13 \times 0.13 \times 0.13$ mm for 10 GW, $0.16 \times 0.16 \times 0.5$ mm for 15 GW, and $0.20 \times 0.20 \times 0.5$ mm for 17–18 GW. The total acquisition time was approximately 2 h for each imaging session.

When using Gd-DTPA, we used the RARE 3D sequence with shortened TR and TE. The TR had to be much longer to achieve T2-weighted imaging contrast when Gd-DTPA was not used to shorten T1 of the sample. Thus, we used multislice 2D instead of 3D sequence for older samples. Because the T1 of the 10 GW sample was much shorter than TR (200 ms), and T2 was also shortened, we used TR/TE 200/9 ms as T2-weighted, and not T1-weighted.

Paraformaldehyde showed very high signal intensity and the Fomblin oil that was used during the scan showed no perceivable signal.

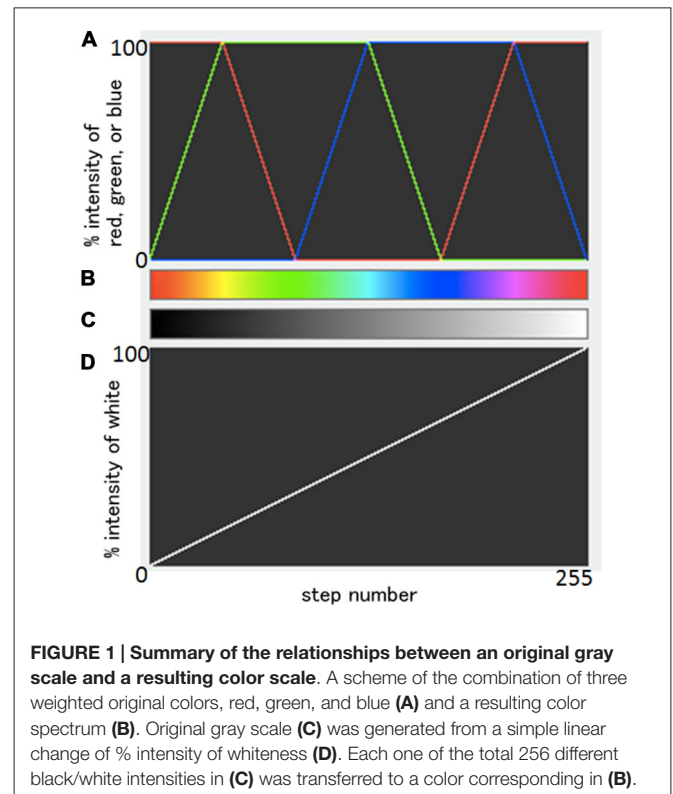
Image Processing

Data processing was performed using ImageJ (<http://rsb.info.nih.gov/ij/download.html>). Standard grayscale images were first generated on a 2D viewer, and were spatially smoothed with a 3×3 mean filter. Next, images were loaded on a 3D volume viewer and subsequently interpolated with a trilinear function for visualization of resliced images. Then, using a transfer function tool, color-coded images were obtained with a so-called “spectrum LUT (look-up-table) style”. The transfer function from grayscale images to color-coded images is summarized in **Figure 1**. Combining three original weighted colors, red, green, and blue, as shown in **Figure 1A**, a color spectrum was generated (**Figure 1B**). The original gray scale (**Figure 1C**) was generated from a simple linear change of % intensity of whiteness (**Figure 1D**). Each one of the total 256 different black/white intensities in **Figure 1C** was transferred to a color corresponding in **Figure 1B**. Note that the same information was projected in both grayscale and color images, and that the chosen colormap aids visualization (i.e., human perception; **Figures 2–8**).

Histology

After completion of MR experiments, the specimens were sectioned into coronal slices at $4 \mu\text{m}$ and stained by hematoxylin-eosin (HE) and Nissl at the Boston Children's Hospital Histology Core, Department of Pathology. Then histological images were obtained under a microscope (Olympus CX41).

It should be noted that there are potential differences between the different brain regions shown in **Figures 3, 5** (10 and



15 weeks) and **Figure 7** (17 weeks). The first two are from posterior brain regions shown in **Figures 2E, 4E** respectively, whereas **Figure 7** is from a middle part of the brain close to the plane shown in **Figure 6C**. We selected the middle part of the brain in **Figure 7** to match it to a good histology slice, since not all the histology slices were presentable. We noticed that the laminar structures between the different brain regions may differ to some extent. However, looking at **Figures 6C,E** the laminar structure of the posterior brain region shown in **Figure 6E** is generally similar to that of the middle brain region in **Figure 6C**, and such similarity was also observed in color images (**Figures 6D,F**).

RESULTS

Cerebral Hemispheres

The most prominent structure seen during early fetal period to early second trimester was the ganglionic eminence (GE; **Figures 2, 4, 8**), which constituted to a part of the inner cerebral wall, protruding into the ventricles. It showed a very low signal intensity on T2-weighted images and a yellow to red color on color-coded images.

During the early fetal period (10–13 GW), many structures were recognizable as early as 10 GW. We were able to recognize different structures of the telencephalon and diencephalon from the coronal view. The anterior part consisted of the front part of the thalamus, basal ganglia (putamen, caudate nucleus), internal capsule, GE, lateral ventricles and cerebral walls (**Figures 2A,B**). The middle part was mainly the thalamus, part of the GE, lateral

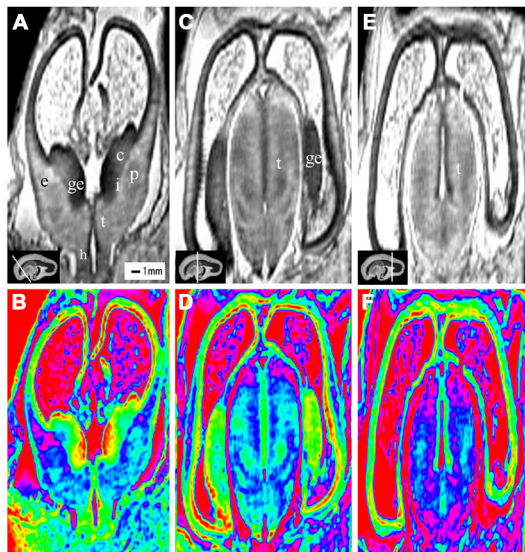


FIGURE 2 | Coronal view images of anterior, middle and posterior brain regions at 10 gestational weeks (GW). The lower row is the color images of corresponding parts of the upper row, which is more visible than the grayscale images in showing the laminar structure and even the nucleus structures. The anterior part consists of the anterior edge of the thalamus, basal ganglia (putamen, caudate nucleus), internal capsule, the ganglionic eminence (GE), lateral ventricles and cerebral walls whose arising part is wedge-shaped (A,B). The middle part of the brain is mainly made up of the thalamus, part of the ganglionic eminence, lateral ventricles and cerebral walls (C,D). The thickness of the cerebral wall in this area is heterogeneous, with the thickest part in the midlateral portion of the outer, and the thinnest in the inferior inner, which is adjacent to the ganglionic eminence (C,D). The posterior part of the fetal brain mainly comprises of the thalamus, lateral ventricles and cerebral walls (E,F). c, caudate nucleus; ge, ganglionic eminence; p, putamen; i, internal capsule; e, external capsule; t, thalamus; h, hypothalamus. The white line in each panel shows the location of the corresponding coronal slice.

ventricles and cerebral walls (Figures 2C,D). The posterior part (behind the GE) consisted primarily of the thalamus, lateral ventricles and cerebral walls (Figures 2E,F).

The youngest specimen, at 10 GW, had four layers in the cerebral wall for both histology and MRI images (Figures 2, 3). We confirmed, using histology, the layers in the following order from the ventricle to the cortex: (1) the ventricular zone, which lay close to the ventricular cavity, accounted for approximately 25% of the cerebral wall (Figure 3H), and presented as a low signal intensity on T2-weighted images and as light blue to green color on color-coded images (Figures 3C–F); (2) the subventricular zone presented as a moderate signal intensity on T2-weighted images and as a yellow band on color-coded images. It was hard to differentiate the subventricular zone from the ventricular zone on the standard grayscale images, while it was clearly delineated from the ventricular zone on the color-coded images (Figure 3); (3) the intermediate zone presented as a high signal intensity on T2-weighted images and as a green band on color-coded images (Figures 3C–F); and (4) the cortical plate, which lay near the surface of the cerebral wall and was composed of densely packed post-migratory neurons, presented as a low signal intensity on T2-weighted images and as a

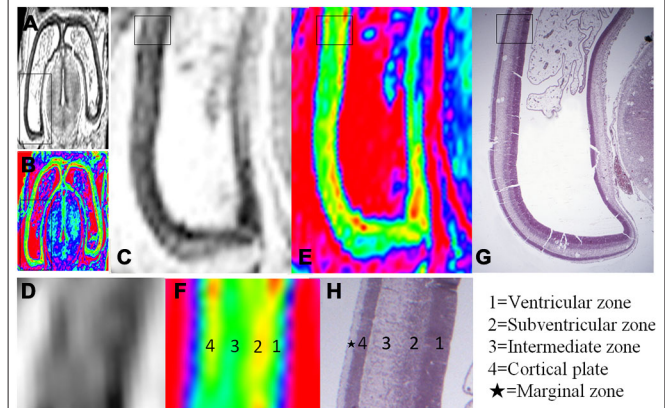


FIGURE 3 | Magnified MR images and corresponding histological images of the posterior region of the brain at 10 GW. (A,B) Whole coronal sections with thick black rectangles magnified in (C,E). Thin rectangles in (C,E) were further magnified in (D,F). Thin rectangle in an hematoxylin-eosin (HE) histology image (G) corresponding to the region of (C,E) was magnified in (H). All images showed four layer organization in the cerebral wall, including the ventricular zone, subventricular zone, intermediate zone and cortical plate in turn from the ventricle. The color images (E,F) more clearly showed the four layer organization than that of grayscale images (C,D), which all correspond to histology (G,H) except for the marginal zone. H, histological image, H&E stained.

yellow band on color-coded images (Figures 3C–F). In addition, the thickness of the cerebral wall was heterogeneous, with the thickest section in the midlateral portion and the thinnest section in the dorsomedial portions (Figures 2, 3).

During early second trimester (15–18 GW), the cerebrum grew rapidly (Figures 4–7; Kostović et al., 2002; Kostović and Vasing, 2009). Seven layers were depicted by histology, including the ventricular zone, periventricular zone, subventricular zone, intermediate zone, subplate, cortical plate and marginal zone (Figure 5E). All layers, not including the marginal layer, were delineated on the magnified T2-weighted images and color images at 15 GW (Figures 4, 5). The proportion of ventricular zone was smaller at 15 GW than at 10 GW, accounting for approximately 10% of the cerebral wall (Figure 5E).

At 17 GW, three distinctive features were found different from those at 15 GW in addition to the thickened cerebral wall. First, at 17 GW, the border of the periventricular zone was much clearer than in 15 GW, which presented relatively high signal intensity on T2-weighted images and as a blue color ribbon on color-coded images (Figures 6, 7). Second, at 17 GW, the subplate zone had thickened remarkably, accounting for approximately 50% thickness of the whole cerebral wall, which presented a high signal intensity on T2-weighted images and as a pink color ribbon on color-coded images (Figures 6, 7). Third, the border between the outer subventricular zone with the inner fiber layer (ingrowing callosal axons) and the ventricular zone could not be separated on MRI images (Figure 7). The increasing thickness of the cerebral wall during the early second trimester resulted in a comparatively reduced ventricular size unlike the typical laminar organization seen in early fetal brain (Figures 4–7).

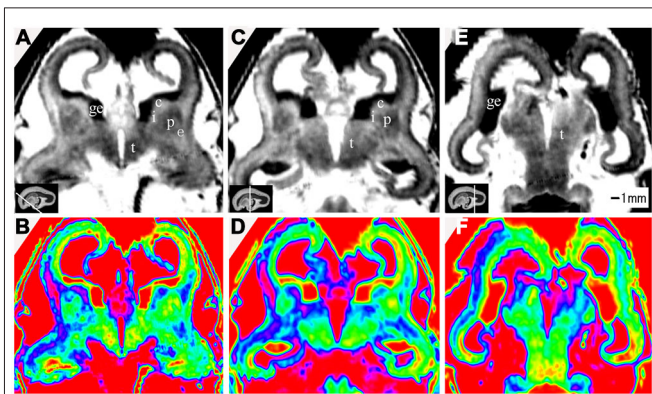


FIGURE 4 | Coronal view images of anterior, middle and posterior brain regions at 15 GW. (A,B) The anterior part is composed of the anterior edge of the thalamus, basal ganglia (putamen, caudate nucleus), internal capsule, ganglionic eminence, lateral ventricles and cerebral walls whose arising part is wedge-shaped. **(C,D)** The middle part of the brain showed the thalamus, part of the ganglionic eminence, lateral ventricles and cerebral walls. The thickness of the cerebral wall is heterogeneous, with the thickest part in the midlateral portion of the outer, and the thinnest in the inferior inner, which is adjacent to ganglionic eminence. **(E,F)** The posterior regions showed the thalamus, lateral ventricles and cerebral walls. The lower row is the color color images of the corresponding parts of the grayscale images in the upper row. c, caudate nucleus; ge, ganglionic eminence; p, putamen; i, internal capsule; e, external capsule; t, thalamus. The white line in each panel shows the location of the corresponding coronal slice.

In addition to the inner cerebral wall thickening faster during early second trimester compared to during early fetal period, the proportion of the ventricular zone became smaller, accounting for approximately 5% of the cerebral wall, and the proportion of cortical plate got thicker at 17 GW compared to 15 GW (Figures 6, 7).

Basal Ganglia

At 10 GW, major structures of the basal ganglia were depicted on T2-weighted MR images and color images (Figures 2, 8A,B). Subcortical nuclear structures such as the thalamus, caudate nucleus and putamen all displayed relatively low signal intensity on T2-weighted images and navy blue color on color-coded images. They were separated by the developing internal and external capsule, which showed a high intensity signal on T2-weighted images and a blue color on color-coded images (Figures 2A,B). At the border of the cerebral wall and basal ganglia, the ventricular zone continued into the GE, which bulged into the ventricle and showed very low MRI signal intensity on T2-weighted images and a yellow to red color on color-coded images (Figures 2,3). On the lateral side, the GE encompassed part of the caudate nucleus which demonstrated relatively low signal intensity on T2-weighted images and a navy blue color on color-coded images (Figures 2, 4, 6). As GW increased, the putamen and caudate got larger and the signal intensity got lower (Figures 2, 4, 6, 8), while the range of high signal intensity of the internal and external capsules became smaller from 10–17 GW on T2-weighted images (Figure 8).

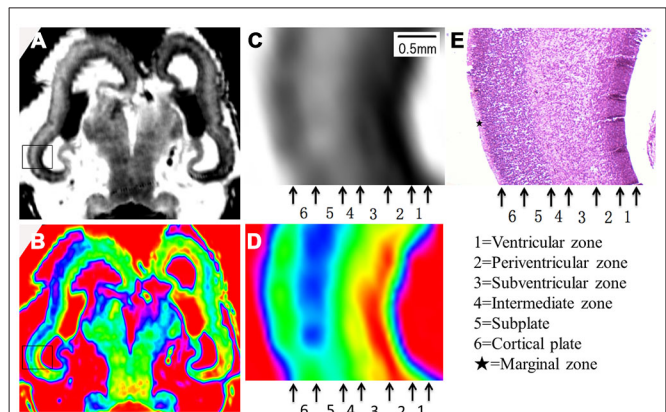


FIGURE 5 | Magnified MR images and corresponding histological images of the posterior part at 15 GW. Rectangles in the grayscale (A) and color-coded (B) images were magnified in (C,D) respectively, and compared to corresponding histology image (E). All images showed a six layer structure within the cerebral wall, including the ventricular zone, periventricular zone, subventricular zone, intermediate zone, subplate zone and cortical plate in turn from the ventricle, and each layer corresponds to its histological image (E). E, histological image, H&E stained.

Thalamus and Hypothalamus

The thalamus was clearly visible at 10 GW, which presented as almost homogeneous low signal intensity on T2-weighted images and as a navy blue color on color images (Figure 2). The two parts of the thalamus symmetrically surrounded the third ventricle, and the medial surface of the thalamus constituted of the upper part of the lateral wall of the third ventricle (Figures 2, 4, 6, 8). With the post-conceptional age increasing from 15–17 GW, the signals of different parts of the thalamus got lower and more heterogeneous (Figures 2, 4, 6, 8). The dorsal thalamus presented as a lower MRI signal intensity on T2-weighted images and as a blue color on color-coded images (Figure 8). The ventral hypothalamus showed relatively higher signal intensity on T2-weighted images and was visible as early as 10 GW (Figure 2).

DISCUSSION

Detailed laminar structures in the human fetal brain were successfully detected in our postmortem T2-weighted imaging. Our study demonstrated rapid growth and dynamic changes of the laminar structure from the early fetal period to the early second trimester. Developmental changes involving the number of layers and the thickness of such layers were depicted by different MR signal intensities with a color-coding scheme, which were consistent with histological sections. We detected four layers in the cerebral wall during the early period (as early as 10 GW), and five to six layers during the early second trimester, characterized by the emergence of the subplate zone. The major structures of the basal ganglia and thalamus could be delineated on T2-weighted MR images and color-coded images. The color images were visually more helpful than standard grayscale images in showing the laminar structures. To our knowledge, this is the first

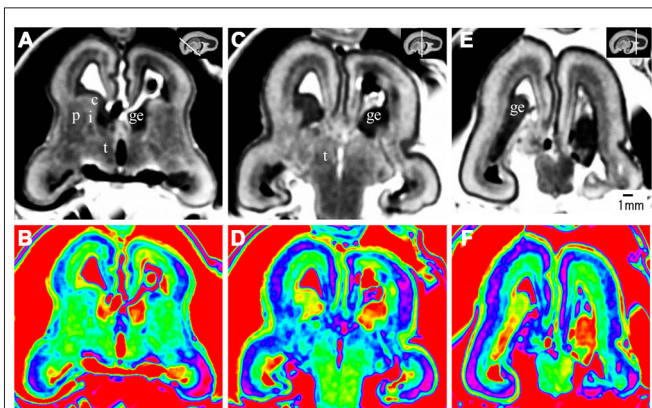


FIGURE 6 | Coronal view images going through the anterior (A,B), middle (C,D), and posterior part (E,F) of the brain at 17 GW. The upper row, the grayscale images, clearly showed the laminar structures of the cerebral wall; the lower row is the corresponding color images of the three parts. c, caudate nucleus; ge, ganglionic eminence; p, putamen; i, internal capsule; e, external capsule; t, thalamus. The white line in each panel shows the location of the corresponding coronal slice.

research study to show fetal brain structure with color-coded images.

The development of the cerebral wall is the most interesting part of the fetal brain structure. Two studies using MRI showed that the cerebral wall at early fetal period was a trilaminar structure and at midfetal period, a five-layer structure (Rados et al., 2006; Kostović and Vasung, 2009). A recent study using 7.0 tesla and T2-weighted sequences showed four layers in the midfetal period (Zhan et al., 2013). Using MRI, our study successfully imaged the cerebral wall of the early fetal period, which is characterized by a four-layer laminar organization, and

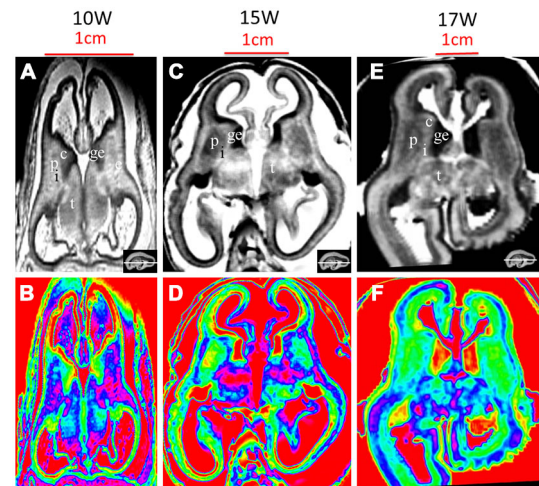


FIGURE 8 | T2-weighted axial MR grayscale images and color images at 10 GW (A,B), 15 GW (C,D) and 17 GW (E,F). During development, the cerebral walls became thicker but with heterogeneous speed; the laminar structure became clearer and the proportion of ventricles got smaller. Nucleus-rich structures such as the thalamus, putamen and caudate nucleus became enlarged and their signals were low and heterogeneous on T2-weighted grayscale images; the signal of the internal capsule and external capsule became lower, and the ganglionic eminence became enlarged. See text for details. c, caudate nucleus; ge, ganglionic eminence; p, putamen; i, internal capsule; e, external capsule; t, thalamus. The white line in each panel shows the location of the corresponding coronal slice.

the early second trimester, which is characterized by five to six layers and specialized with the presence of the periventricular zone and the subplate zone. Six layers were observed at 15 GW on both T2-weighted images and color-coded images, but five layers were found at 17 GW because the subventricular zone merged with the intermediate zone and MRI did not differentiate the border between them, which is similar to studies by Kostović et al. (2002) and Kostović and Vasung (2009). The reason that our study showed more detailed structures in the thin cerebral wall compared to Kostović et al. may be due to the use of high-tesla MRI with scan parameters different from theirs, as well as utilizing the use of a small custom-made MR volume coil to obtain high signal-to-noise. In contrast, a previous study using a 0.5 tesla *ex vivo* MRI found only three layers that were differentiated at 16 GW (Brisse et al., 1997). Our study also found that the development of the cerebral wall from early to midfetal period was not homogenous across brain regions, with the outer regions growing faster in thickness and volume than the inner regions. The marginal zone was not separated in our MRI images potentially because it was very thin or its signal was very close to the cortical plate but it was observed in the histologic images during our studied period.

In the developing brain, many histogenetic events (neurogenesis, gliogenesis, migration, cell differentiation, axonal elongation and synaptogenesis) proceed within laminar compartments or zones (Paus et al., 2001; Jovanov-Milosević et al., 2009). Those dynamic changes can be delineated by varying MRI signal intensities on T2-weighted sequences and

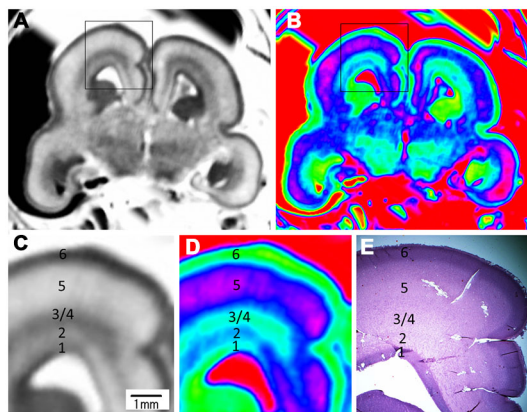


FIGURE 7 | Magnified images and corresponding histological image of the middle brain region at 17 GW. The upper row is grayscale image (A) and color image (B). (C,D) Magnified images of the rectangles in (A,B). All images showed a five layer structure within the cerebral wall, including the ventricular zone, periventricular zone, subventricular zone and intermediate zone, subplate zone and cortical plate; each layer corresponds to its histological image (E); the border of the subventricular zone (3) and intermediate zone (4) was not clearly differentiated even in the histological image. E, histological image, H&E stained.

different colors on color-coded images and confirmed by histology. MR signal changes associated with maturational processes can mainly be ascribed to the changes in tissue composition and organization, which occur at the histological level. MR signal changes include decreases in water content and increasing cell-density, which can be recognized as a shortening of T1- and T2-relaxation times, leading to increased T1-weighted and decreased T2-weighted intensity, respectively (Prayer et al., 2006). The ventricular zone is a germinal matrix with a high density of cells (Kostović et al., 2002; Bayer and Altman, 2006) and is compatible with our results by showing a low signal intensity on T2-weighted images (green color on color-coded images). The periventricular zone is a “waiting” position of fibers with vigorous structural plasticity due to the abundance of extracellular matrixes and guidance molecules (Judas et al., 2005), and it appeared as a relatively high signal intensity on T2-weighted images and a blue color on color-coded images (Figure 7; Judas et al., 2005). The intermediate zone is a migratory and axonal growth zone (Kostović and Vasung, 2009), and presented as a moderate signal intensity on T2-weighted sequence and as a pale green color on color-coded images, which encompasses both the subventricular cellular zone and the fetal white matter (Kostović and Vasung, 2009). Hence it was not differentiated from the subventricular zone at 17 GW. The subplate was characterized by a very large extracellular space and an abundant amount of different glycosaminoglycans and chondroitin sulfate proteoglycans in its extracellular matrix (Ulfig et al., 2000; Kostović et al., 2002; Kostović and Vasung, 2009). It had high proton density and therefore presented with high signal intensity on T2-weighted images and a pink color ribbon on color-coded images. The cortical plate is a cell-dense area with postmigratory neurons (Kostović and Vasung, 2009), thus it presented as a relatively low signal intensity on T2-weighted sequence and as a green color on color-coded images (Ulfig et al., 2000; Kostović and Vasung, 2009). The proportion of the ventricular zone got smaller and the signal intensity got higher on T2-weighted images going from the early fetal period to the early second trimester. Simultaneously, the cortical plate got thicker and the signal intensity got lower on T2-weighted images. These phenomena likely reflect the dynamic changes of neuronal locations as well as their migrating directions. On the other hand, the signal changes of the thalamus from almost homogeneous to heterogeneous reflected the cellular differentiation and aggregation of the nucleus during the course of development.

The dynamic change potentially related to axons was also depicted by varying MRI signal intensity on T2-weighted sequences and different colors on color-coded images. In our study, some fiber-rich tissues such as the internal capsule showed high signal intensity on T2-weighted images during early fetal period. The range of high signals of the internal capsules got narrower from 10–15 GW, and the signal intensity lowered at 17 GW, thus the color on the color-coded images changed from jade-green to navy-blue during this period (Figure 8). Those changes are associated with maturational processes of axons,

which reflect the early dynamic change of axonal density and myelination during its development.

There are some differences between *in vivo* and *ex vivo* studies of fetal brain MRI. First, fetal brain MRI before 18 GW is mainly dependent on *ex vivo* studies due to smaller brain-size, poor tissue differentiations, and frequent fetal movements (Brugger, 2011). However, over 18 GW can be available *in vivo* or *ex vivo* studies. Second, *ex vivo* imaging provides the benefits of high resolution and high signal-to-noise-ratio at the cost of long image acquisition sessions, which, are not practical *in vivo* (Takahashi et al., 2013). High spatial resolution obtained on postmortem brains can be compared at microscopic levels due to the absence of subject movement and unlimited MRI acquisition time (Kostović and Vasung, 2009). Third, the method of specimen preparation, using a size-optimized sample container and an MR coil (Takahashi et al., 2010), and the postmortem specimens can be histologically examined and co-registered with MRI images, allowing detailed three-dimensional quantitative measurement and qualitative assessment (Kostović and Vasung, 2009). In this way, our study was able to obtain high-resolution images, which were consistent with histologic slices.

Color-coded images were transferred from grayscale intensity with a scheme shown in Figure 1, in which a band of grayscale changed into a visible color spectrum by combining the three primary colors red, green and blue. This kind of color spectrum was found to be useful for detecting laminar structures in the thin cerebral walls. For example, the ventricular zone is a cell-rich area that presented as a low intensity signal on T2-weighted images, which corresponds to the first grayscale band (Figure 1), and transferred into a green color on the color-coded images (Figure 3). The subventricular zone presented as a moderate signal intensity on T2-weighted images, which corresponds to the second grayscale band (Figure 1) and transferred into a yellow color on the color-coded images (Figure 3). It is not easy to differentiate the subventricular zone from the ventricular zone on grayscale images, but it is clearly delineated on the color-coded images (Figure 3). This is the same with the periventricular zone, which is line-shaped at 15 GW, and delineated from the ventricular zone on color-coded images (Figure 5). Thus, the color-coded images greatly enhanced our visibility to identify laminar structures. However, even with usage of spectral processing fetal laminae weren't discernible along the entire telencephalic wall. This might be due to the spatio-temporal differences in intensity of histogenetic processes.

There were some limitations in our study. First, the sample size was very small since it had not been easy to get many whole brain specimens in early fetal stages. Second, although the thickness of each layer structure except for the most outer layer (marginal zone) was more than one voxel, it is possible that our results were affected by partial volume effects. For example, at the 10 GW, if the subventricular zone contained a whole voxel along the radial direction to the brain surface, neighboring two voxels towards the ventricular zone and towards the brain surface may have contained a part of the subventricular zone and neighboring layers, which would have caused spatial smoothing of signals from those layers. The subventricular zone could have also been

across two voxels along the radial direction to the brain surface, where the two voxels likely contained both the subventricular zone and neighboring layers, which would have caused spatial smoothing of signals as above but this time both voxels contained the subventricular zone. In any case, the thicknesses of the layers detected by color-processed MR images in the current study were potentially a little thinner or thicker depending on the locations of imaging voxels across the layers. Histologically, the midfetal period brain has seven layers within the cerebral wall (Kostović et al., 2002). However, our MR images could not differentiate the border between the subventricular zone and the intermediate zone at 17 GW because the signals in the two layers were either very close to each other, or the subventricular cellular zone merged with the intermediate zone (fetal white matter) as seen in the previous study (Kostović and Vasung, 2009). It is also possible that the marginal zone was not separated in MRI images because it was very thin and the signal was similar to that of the cortical plate, or because it was affected by partial volume effect.

It should also be noted that the spectral processes used in this study did not differentiate laminar structures along the entire telencephalic wall, for example in a whole coronal plane. With the reserve of limitations already mentioned in this study, the spatio-temporal differences of MRI signal intensity might be partially driven by spatio-temporal regional variations of neuronal migration, cellular differentiation, dendritic arborization, and axonal ingrowth and outgrowth. The fact that during this period of development drastic histogenetical changes occur, it is challenging to delineate borders of transient fetal zones even on the certain histologic sections. Although this study did not explore detailed regional variations of the development of laminar structures, it is an important direction of research on human fetal brains since such variation may be a source of variety of spatially localized, specified human brain functions.

We presented T2-weighted imaging results in this study because the T2-weighted signaled significantly better-dissociated fetal brain structures than the T1-weighted signal, which is consistent with current clinical MRI (Gholipour et al., 2014). The current gold standard sequence for fetal structural imaging is a single-shot Fast Spin Echo (referred to as HASTE on

Siemens scanners). Since it is a single shot sequence, its contrast is not purely T2-weighted, however, it is “T2-weighted-like” images of the fetal brain with fast imaging per slice. HASTE is rarely used in post-natal imaging, due to its sub-optimal contrast. Therefore, there is a potential that our current *ex vivo* MR findings with histology validation could be a reference for clinical fetal MRI. It is also important in future studies to test more detailed correlations between observations from MRI and histology, using multiple staining methods (e.g., see reviews by Kostović and Judas, 2002, 2010) with multiple MR sequences.

CONCLUSION

In this study, we demonstrated that a four-layer-structure could be found within the fetal cerebral wall as early as 10 GW, and five to six layers could be detected during the early second trimester using a high tesla MR scanner and appropriate parameters. The T2-weighted sequence and color-coded images proved to be as reliable as the macroscopic anatomical examination for depicting fetal brain development *ex vivo* from early fetal period to early second trimester, which enriches the appearance of MR imaging for fetal brain structures. Given that our current results might be affected by partial volume effects and was demonstrated only in limited brain regions with limited number of specimens, further studies are needed to collect more cases with different gestational ages to constitute a normal atlas at multiple different gestational weeks.

ACKNOWLEDGMENTS

This work was supported by Boston Children’s Hospital (BCH), Guizhou Provincial People’s Hospital, and NICHD (R01HD078561, R21HD069001, R03NS091587; ET). The authors thank Donald Siwek and Darry R. Ricketts, Boston University School of Medicine for providing the fetal brain specimens from the Departmental collection, Ying Huang in the Center for Molecular Oncologic Pathology of Dana-Farber Cancer Institute for technical assistance, Borjan Gagoski at BCH for discussion, and Molly Wilkinson and Ashley Ruyan Lim at BCH for editorial assistance.

REFERENCES

- Bayer, S. A., and Altman, J. (2006). *The Human Brain During the Late First Trimester*. (Boca Raton, FL: CRC Press), 352.
- Bendersky, M., Musolino, P. L., Rugilo, C., Schuster, G., and Sica, R. E. (2006). Normal anatomy of the developing fetal brain. *Ex vivo* anatomical-magnetic resonance imaging correlation. *J. Neurol. Sci.* 250, 20–26. doi: 10.1016/j.jns.2006.06.020
- Brisse, H., Fallet, C., Sebag, G., Nessmann, C., Blot, P., and Hassan, M. (1997). Supratentorial parenchyma in the developing fetal brain: *in vitro* MR study with histologic comparison. *AJNR Am. J. Neuroradiol.* 18, 1491–1497.
- Brugger, P. C. (2011). “Methods of fetal MRI,” in *Fetal MRI*, ed. D. Prayer (New York, NY: Springer), 65–80.
- Dawe, R. J., Bennett, D. A., Schneider, J. A., Vasireddi, S. K., and Arfanakis, K. (2009). Postmortem MRI of human brain hemispheres: T2 relaxation times during formaldehyde fixation. *Magn. Reson. Med.* 61, 810–818. doi: 10.1002/mrm.21909
- du Plessis, A. J., and Volpe, J. J. (2002). Perinatal brain injury in the preterm and term newborn. *Curr. Opin. Neurol.* 15, 151–157. doi: 10.1097/00019052-200204000-00005
- Glenn, O. A., and Barkovich, A. J. (2006a). Magnetic resonance imaging of the fetal brain and spine: an increasingly important tool in prenatal diagnosis, part 1. *AJNR Am. J. Neuroradiol.* 27, 1604–1611.
- Glenn, O. A., and Barkovich, A. J. (2006b). Magnetic resonance imaging of the fetal brain and spine: an increasingly important tool in prenatal diagnosis: part 2. *AJNR Am. J. Neuroradiol.* 27, 1807–1814.
- Gholipour, A., Estroff, J. A., Barnewolt, C. E., Robertson, R. L., Grant, P. E., Gagoski, B., et al. (2014). Fetal MRI: a technical update with educational aspirations. *Concepts Magn. Reson. Part A Bridg. Educ. Res.* 43, 237–266. doi: 10.1002/cmr.a.21321
- Hern, W. M. (1984). Correlation of fetal age and measurements between 10 and 26 weeks of gestation. *Obstet. Gynecol.* 63, 26–32.
- Huang, H., Jeon, T., Sedmak, G., Pletikos, M., Vasung, L., Xu, X., et al. (2013). Coupling diffusion imaging with histological and gene expression analysis to

- examine the dynamics of cortical areas across the fetal period of human brain development. *Cereb. Cortex* 23, 2620–2631. doi: 10.1093/cercor/bhs241
- Huang, H., Xue, R., Zhang, J., Ren, T., Richards, L. J., Yarowsky, P., et al. (2009). Anatomical characterization of human fetal brain development with diffusion tensor magnetic resonance imaging. *J. Neurosci.* 29, 4263–4273. doi: 10.1523/JNEUROSCI.2769-08.2009
- Huisman, T. A. (2004). Magnetic resonance imaging: an alternative to autopsy in neonatal death? *Semin. Neonatol.* 9, 347–353. doi: 10.1016/j.siny.2003.09.004
- Jovanov-Milosević, N., Culjat, M., and Kostović, I. (2009). Growth of the human corpus callosum: modular and laminar morphogenetic zones. *Front. Neuroanat.* 3:6. doi: 10.3389/neuro.05.006.2009
- Judas, M., Rados, M., Jovanov-Milosevic, N., Hrabac, P., Stern-Padovan, R., and Kostović, I. (2005). Structural, immunocytochemical, and mr imaging properties of periventricular crossroads of growing cortical pathways in preterm infants. *AJNR Am. J. Neuroradiol.* 26, 2671–2684.
- Kostović, I., and Judas, M. (2002). Correlation between the sequential ingrowth of afferents and transient patterns of cortical lamination in preterm infants. *Anat. Rec.* 261, 1–6. doi: 10.1002/ar.10069
- Kostović, I., and Judas, M. (2010). The development of the subplate and thalamocortical connections in the human foetal brain. *Acta Paediatr.* 99, 1119–1127. doi: 10.1111/j.1651-2227.2010.01811.x
- Kostović, I., Judas, M., Rados, M., and Hrabac, P. (2002). Laminar organization of the human fetal cerebrum revealed by histochemical markers and magnetic resonance imaging. *Cereb. Cortex* 12, 536–544. doi: 10.1093/cercor/12.5.536
- Kostović, I., and Rakic, P. (1990). Developmental history of the transient subplate zone in the visual and somatosensory cortex of the macaque monkey and human brain. *J. Comp. Neurol.* 297, 441–470. doi: 10.1002/cne.902970309
- Kostović, I., and Vasung, L. (2009). Insights from *in vitro* fetal magnetic resonance imaging of cerebral development. *Semin. Perinatol.* 33, 220–233. doi: 10.1053/j.semperi.2009.04.003
- Paus, T., Collins, D. L., Evans, A. C., Leonard, G., Pike, B., and Zijdenbos, A. (2001). Maturation of white matter in the human brain: a review of magnetic resonance studies. *Brain Res. Bull.* 54, 255–266. doi: 10.1016/s0361-9230(00)00434-2
- Pfefferbaum, A., Sullivan, E. V., Adalsteinsson, E., Garrick, T., and Harper, C. (2004). Postmortem MR imaging of formalin-fixed human brain. *Neuroimage* 21, 1585–1595. doi: 10.1016/j.neuroimage.2003.11.024
- Prayer, D., Kasprian, G., Krampfl, E., Ulm, B., Witzani, L., Prayers, L., et al. (2006). MRI of normal fetal brain development. *Eur. J. Radiol.* 57, 199–216. doi: 10.1016/j.ejrad.2005.11.020
- Rados, M., Judas, M., and Kostović, I. (2006). *In vitro* MRI of brain development. *Eur. J. Radiol.* 57, 187–198. doi: 10.1016/j.ejrad.2005.11.019
- Rakic, P. (2006). A century of progress in corticogenesis: from silver impregnation to genetic engineering. *Cereb. Cortex* 16, i13–i17. doi: 10.1093/cercor/bhk036
- Saleem, S. N. (2013). Fetal magnetic resonance imaging (MRI): a tool for a better understanding of normal and abnormal brain development. *J. Child Neurol.* 28, 890–908. doi: 10.1177/0883073813486296
- Takahashi, E., Dai, G., Wang, R., Ohki, K., Rosen, G. D., Galaburda, A. M., et al. (2010). Development of cerebral fiber pathways in cats revealed by diffusion spectrum imaging. *Neuroimage* 49, 1231–1240. doi: 10.1016/j.neuroimage.2009.09.002
- Takahashi, E., Song, J. W., Folkerth, R. D., Grant, P. E., and Schmahmann, J. D. (2013). Detection of postmortem human cerebellar cortex and white matter pathways using high angular resolution diffusion tractography: a feasibility study. *Neuroimage* 68, 105–111. doi: 10.1016/j.neuroimage.2012.11.042
- Thayyil, S., Sebire, N. J., Chitty, L. S., Wade, A., Chong, W., Olsen, O., et al. (2013). Post-mortem MRI versus conventional autopsy in fetuses and children: a prospective validation study. *Lancet* 382, 223–233. doi: 10.1016/s0140-6736(13)60134-8
- Ulf, N., Neudörfer, F., and Bohl, J. (2000). Transient structures of the human fetal brain: subplate, thalamic reticular complex, ganglionic eminence. *Histol. Histopathol.* 15, 771–790.
- Vasung, L., Huang, H., Jovanov-Milosević, N., Pletikos, M., Mori, S., and Kostović, I. (2010). Development of axonal pathways in the human fetal fronto-limbic brain: histochemical characterization and diffusion tensor imaging. *J. Anat.* 217, 400–417. doi: 10.1111/j.1469-7580.2010.01260.x
- Vasung, L., Jovanov-Milosević, N., Pletikos, M., Mori, S., Judas, M., and Kostović, I. (2011). Prominent periventricular fiber system related to ganglionic eminence and striatum in the human fetal cerebrum. *Brain Struct. Funct.* 215, 237–253. doi: 10.1007/s00429-010-0279-4
- Zhan, J., Dinov, I. D., Li, J., Zhang, Z., Hobel, S., Shi, Y., et al. (2013). Spatial-temporal atlas of human fetal brain development during the early second trimester. *Neuroimage* 82, 115–126. doi: 10.1016/j.neuroimage.2013.05.063

Conflict of Interest Statement: The authors declare that the research was conducted in the absence of any commercial or financial relationships that could be construed as a potential conflict of interest.

Copyright © 2015 Wang, Dai and Takahashi. This is an open-access article distributed under the terms of the Creative Commons Attribution License (CC BY). The use, distribution and reproduction in other forums is permitted, provided the original author(s) or licensor are credited and that the original publication in this journal is cited, in accordance with accepted academic practice. No use, distribution or reproduction is permitted which does not comply with these terms.



Characterization of Laminar Zones in the Mid-Gestation Primate Brain with Magnetic Resonance Imaging and Histological Methods

Xiaojie Wang¹, David R. Pettersson², Colin Studholme³ and Christopher D. Kroenke^{1,4*}

¹ Division of Neuroscience, Oregon National Primate Research Center, Oregon Health & Science University, Beaverton, OR, USA, ² Department of Radiology, Oregon Health & Science University, Portland, OR, USA, ³ Biomedical Image Computing Group, Departments of Pediatrics, Bioengineering, and Radiology, University of Washington, Seattle, WA, USA, ⁴ Advanced Imaging Research Center and Department of Behavioral Neuroscience, Oregon Health & Science University, Portland, OR, USA

OPEN ACCESS

Edited by:

Hao Huang,
University of Pennsylvania, USA

Reviewed by:

Stephen C. Noctor,
University of California, Davis, USA
Emi Takahashi,
Boston Children's Hospital, USA

*Correspondence:

Christopher D. Kroenke
kroenkec@ohsu.edu

Received: 06 August 2015

Accepted: 05 November 2015

Published: 24 November 2015

Citation:

Wang X, Pettersson DR, Studholme C and Kroenke CD (2015) Characterization of Laminar Zones in the Mid-Gestation Primate Brain with Magnetic Resonance Imaging and Histological Methods. *Front. Neuroanat.* 9:147. doi: 10.3389/fnana.2015.00147

Distinct populations of progenitor and postmitotic neural and glial cells are stratified in the fetal primate brain across developmentally transient tissue zones between the ventricular and pial surfaces. These zones were originally identified by light microscopy. However, it has subsequently been shown that various forms of magnetic resonance image (MRI) contrast can be used to distinguish layers of developing neural tissue in *ex vivo*, as well as *in vivo* (including *in utero*) conditions. Here we compare mid-gestation rhesus macaque tissue zones identified using histological techniques to *ex vivo* as well as *in utero* MRI performed on the same brains. These data are compared to mid-gestation fetal human brain MRI results, obtained *in utero*. We observe strong similarity between MRI contrast *in vivo* and post mortem, which facilitates interpretation of *in utero* images based on the histological characterization performed here. Additionally, we observe differential correspondence between the various forms of *ex vivo* MRI contrast and microscopy data, with maps of the water apparent diffusion coefficient providing the closest match to histologically-identified lamina of the nonhuman primate brain. Examination of histology and post mortem MRI helps to provide a better understanding of cytoarchitectural characteristics that give rise to *in utero* MRI contrast.

Keywords: rhesus macaque, fetal MRI, brain development, subventricular zone, cortical plate, subplate, MRI validation, diffusion MRI

INTRODUCTION

The mid-gestation primate brain is organized into layers, with those proximal to the surface of the lateral ventricles containing progenitor cell populations, and layers proximal to the pial surface containing postmitotic neurons and glial cells (Bayer and Altman, 2005; Bystron et al., 2008; Cunningham et al., 2013). In gyroencephalic species such as humans and old world monkeys, multiple distinct layers that are not apparent in MRI data collected from mammals with smaller brains, can be resolved by MRI at this developmental stage (Kriegstein et al., 2006; Sizonenko et al., 2007; Huang et al., 2008; Barnette et al., 2009). Methods for classifying these bands differ between researchers. However, descriptions of 8–10 layers between the ventricular and pial surface

has been common to most recent studies of primate species (Altman and Bayer, 2002; Kostovic et al., 2002; Smart et al., 2002; Bystron et al., 2008). Increasingly, the importance of progenitor cell populations residing within subventricular zones is being recognized in contributing to the number of cerebral cortical neurons in the mature brain (Hansen et al., 2010) and potentially to the shape of the folded cortex (Reillo et al., 2011). In primate brain at this developmental stage, more superficial layers contain migrating postmitotic cells, as well as axons that will contribute to white matter structures in the mature brain. Experimental strategies that can be used to quantitatively characterize the physical properties (e.g., size and cellular organization) of these tissue zones throughout development are therefore of potential utility for monitoring normal and pathological brain development.

Magnetic resonance imaging (MRI) has long been used as a clinical tool for characterizing human fetal brain development (Glenn and Barkovich, 2006). However, until recently, challenges associated with fetal brain motion have limited the choice of MRI contrast mechanism, and achievable image resolution. Strategies for retrospective motion correction have ameliorated these limitations (Studholme, 2011) and have enabled high resolution 3D reconstructions of T_2 -weighted images throughout the second half of gestation (Kim et al., 2011; Scott et al., 2011), as well as whole-brain diffusion tensor imaging (DTI) measurements on fetal brain (Fogtmann et al., 2014). Three tissue zones, termed the germinal matrix, the subplate (SP), and the cortical plate (CP), are typically resolved in *in utero* MRI studies (Kim et al., 2011). Post mortem MRI, allowing for lengthy scan time, affords the opportunity to obtain higher image resolution than achievable with *in utero* imaging measurements (Gupta et al., 2005; Kroenke et al., 2005; Huang et al., 2006; Xu et al., 2014). Although MRI of post mortem tissue has provided evidence that additional tissue zones can be resolved with increased image resolution and signal to noise ratio (Kostovic et al., 2002; Kroenke et al., 2005, 2006; Huang et al., 2009; Zhang et al., 2011a,b; Kolasinski et al., 2013; Xu et al., 2014), the specific association between tissue zones defined using histological methods and MRI-based contrast patterns have not been established.

The goal for this study was to assign lamina identified by light microscopy in the mid-gestation rhesus macaque brain specifically to zones observable with MRI. Further, in order to determine the degree of correspondence to results observed in humans, comparisons are made between human and nonhuman primate MRI. Previously, Smart et al. (2002) classified the lamina identified in cresyl-violet stained parietal and occipital lobe tissue of the cynomolgus macaque. The banded structure across the cerebral wall differs between rostral and caudal brain regions (Altman and Bayer, 2002; Martínez-Cerdeño et al., 2012), and therefore the current study focuses on the same region characterized by Smart and co-workers. We demonstrate that the previously developed classification scheme can be applied to the parietal and occipital lobes of three rhesus brains at 90 days gestational age (G90, of a 165 day gestational term), which corresponds to ~23 weeks post-conception in humans (<http://www.translatingtime.org>) (Workman et al., 2013). We utilize *in*

utero MRI, post mortem MRI, and light microscopic images of the same brains to establish the correspondence between zones identified by microscopy and those observed by MRI. Immunohistochemical analyses of radial glial cells and neural axons are also used to guide the interpretation of water diffusion anisotropy measurements performed on this tissue. Based on similarities between our findings and post-mortem MRI studies of the developing human brain, comparisons are made with classification systems described for human brains.

METHODS

In utero MRI Acquisition and Image Reconstruction

Human subjects provided written, informed consent to participate in this study, and all procedures involving human subjects were approved by the Oregon Health and Science University Institutional Review Board. A 23-week pregnant woman was imaged using a 1.5T whole body MR scanner (Ingenia; Philips Healthcare, Netherlands). A dStream posterior built-in coil and a dStream anterior torso radiofrequency (RF) coil (Philips Healthcare, Netherlands) were used for signal excitation and reception, respectively. Due to fetal head motion, it is often not possible to acquire a high-resolution 3D volume of the entire brain without implementing procedures such as retrospective motion correction (Rousseau et al., 2006). Therefore, the human imaging performed here follows the current standard clinical practice to acquire a selected series of 2D image slices. A 2D Single-Shot turbo spin-echo (TSE) pulse sequence was used to acquire axial T_2 -weighted images with the following parameters: recycle time (TR) = 1000 ms, echo time (TE) = 110 ms, Sensitivity encoding factor (SENSE, a parallel imaging acceleration parameter) = 3.6, halfscan factor = 0.64, TSE factor = 109, in plane resolution of 1×1 mm, and slice thickness of 3 mm.

All procedures involving nonhuman primate research subjects were approved by the Institutional Animal Care and Use Committee of the Oregon National Primate Research Center (ONPRC). The ONPRC abides by the Animal Welfare Act and regulations enforced by the U.S. Department of Agriculture, the Public Health Service Policy on Humane Care and Use of Laboratory Animals, in accordance with the U.S. National Institutes of Health Guide for the Care and Use of Laboratory Animals. Three pregnant rhesus macaques underwent anatomical examinations at G90 using a Siemens 3T Tim Trio system equipped with a 15-element human knee RF coil (QED, Cleveland, OH). Anesthesia was induced using 10 mg/kg ketamine and maintained using a 1.5% isoflurane-oxygen mixture during the imaging. A tri-plane localizer with half-Fourier acquisition single-shot turbo spin-echo (HASTE)-acquired T_2 -weighted image was used to determine fetal head position. A 2D TSE sequence was used to acquire T_2 -weighted images with the following parameters: TR/TE = 5000/97 ms, generalized autocalibrating partial parallel acquisition (GRAPPA) factor = 2, and TSE factor = 27. As described previously (Fogtmann et al., 2014), multiple

contiguous 2D image stacks, with in-plane resolutions of 0.67×0.67 mm and thicknesses of 1 mm, were acquired along the maternal axial, sagittal, and coronal axes to facilitate the reconstruction of a 3D volume with isotropic resolution. For an additional pregnant rhesus macaque at G85, diffusion MRI data, in addition to T_2 -weighted images, were acquired. A diffusion-weighted, 2D spin-echo based EPI sequence was used to acquire one image volume with $b = 0$ (the "b0" image), and 20 diffusion-weighted volumes with $b = 500$ s/mm². Other acquisition parameters were: TR/TE = 5000/93 ms, GRAPPA factor = 2, EPI factor = 78, and echo spacing = 1.09 ms. As with the T_2 -weighted images, three sets of b0 and diffusion weighted image stacks were acquired along the maternal axial, sagittal, and coronal axes. For the diffusion-weighted data, the in-plane resolution was 1.13×1.13 mm and the slice thickness was 3 mm. In order to compensate for the relatively poor through-plane resolution for the diffusion data, three sets of diffusion-weighted image stacks were acquired along each axis, offset from one another by 1 mm (Fogtmann et al., 2014).

For T_2 -weighted image stacks, 3D slice position and orientation correction with respect to fetal brain anatomy was carried out using the SLIMMER procedure (Kim et al., 2011). This incorporates the Slice Intersection Motion Correction (SIMC) algorithm and iterative bias field inconsistency correction to account for subtle changes in signal that occur when the fetal head moves in relation to the coils, and allows improved delineation of tissue contrast. The final 3D volume was reconstructed using an iterative deconvolution of the slice profiles in the orthogonal slice planes (Fogtmann et al., 2012, 2014) with 0.5 mm isotropic resolution. Reconstruction of DTI data was accomplished using the approach described in Fogtmann et al. (2014). Briefly, four major steps were involved: (1) a slice-to-volume alignment (Rousseau et al., 2006) was performed to generate a high-resolution b0 volume; (2) motion-estimates of the diffusion-weighted images were obtained using previously described procedures (Oubel et al., 2012) to register each slice in the diffusion-weighted data set to a common 3D volume; (3) the b0 volume, motion estimates, and DWI slices were then combined on a 0.75 mm isotropic 3D lattice to compute diffusion tensor parameters at each lattice point following procedures described in Gholipour et al. (2010); (4) The apparent diffusion coefficient [$ADC = (\lambda_1 + \lambda_2 + \lambda_3)/3$] and fractional anisotropy [FA, defined in Bassar and Pierpaoli (1996)] were calculated from the diffusion tensor results obtained in step 3.

Ex vivo MRI Acquisition and DTI Analyses

Following Cesarean section, the three rhesus macaque fetuses imaged at G90 were euthanized with overdose of pentobarbital, and the brains were perfusion fixed with 4% paraformaldehyde (PFA), and then immersed in 4% PFA for 24 h before being transferred to phosphate-buffered saline (PBS). Immediately prior to imaging, the brains were transferred to Fluorinert Electronic Liquid FC-77 (3M, St. Paul, MN) and returned to PBS following MRI procedures. A custom Helmholtz coil (5 cm diameter, 5 cm length) was used for radiofrequency transmission and reception. Experiments were performed on an 11.7 T

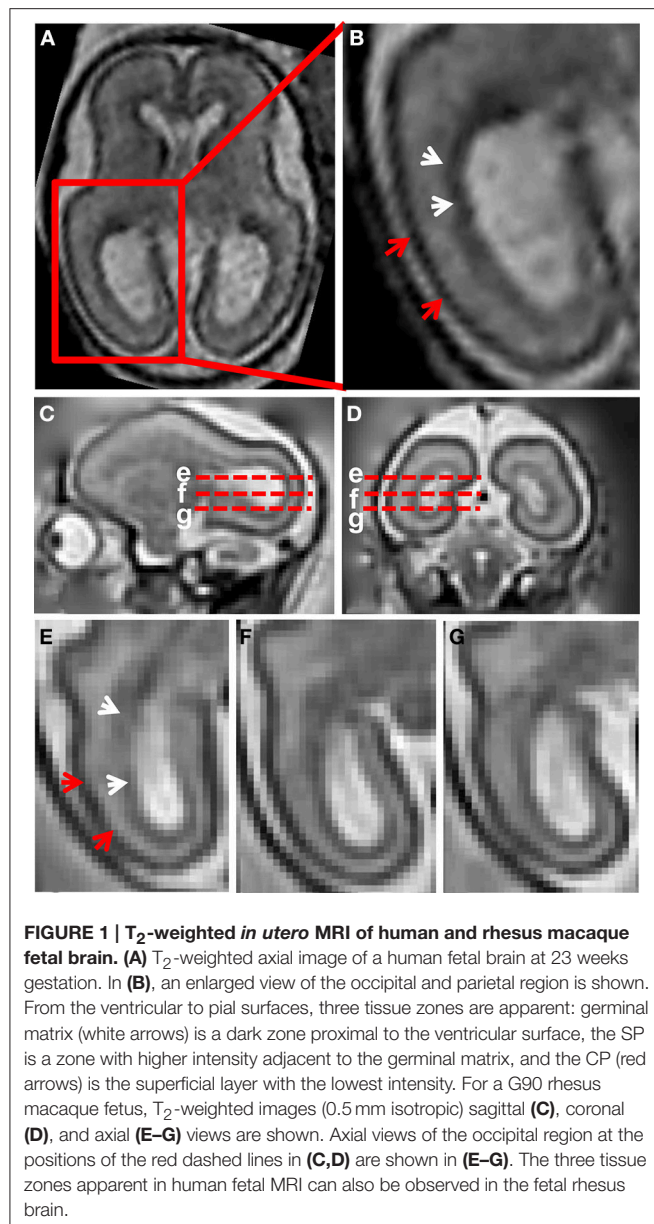
small-animal MRI system interfaced with 9 cm inner diameter magnetic field gradient coil diameter magnetic field gradient coil (Bruker, Rheinstetten, Germany). A multi-slice spin-echo pulse sequence (TR/TE = 15 s/30 ms), incorporating a Stejskal–Tanner diffusion sensitization gradient pair was used to acquire diffusion MRI data at an isotropic resolution of 0.3 mm. A 25-direction, icosahedral sampling scheme (Batchelor et al., 2003) was utilized for all experiments with 3 b0 images, and diffusion weighted images with a b -value of 2500 s/mm². Standard procedures were followed to calculate eigenvalues (λ_1 , λ_2 , and λ_3 , listed from smallest to largest) and eigenvectors (V_1 , V_2 , and V_3). DTI indices such as FA were calculated from the eigenvalues for each voxel. The signal intensity at a b -value of 0 was similarly estimated for each voxel, and the result served as the post mortem T_2 -weighted image.

Histological Analyses

Following *ex vivo* MRI examination, hemispheres from each of the G90 brains were cryo-protected in 15% and then 30% (w/v) sucrose-PBS solution before being frozen-sectioned in the axial plane at 80 μ m thickness using a Zeiss-Microm sliding microtome (Dublin, California). For Nissl staining, sections were mounted onto 2% (w/v) gelatin subbed slides and processed following standard procedures (Paul et al., 2008). For immunohistochemistry, sections were stained in a free-floating fashion in 24-well cell culture plates. Briefly, each section was washed in PBS-Triton X-100 (0.1%, v/v) solution and then blocked with 5% (v/v) goat serum before being incubated with an anti-neurofilament marker SMI312 (1:1000, BioLegend Inc., San Diego, CA, USA) or monoclonal anti-vimentin antibody (1:40, Sigma-Aldrich, Saint Louis, MO, USA) in 4°C for 48 h. After washing in PBS-Triton X-100 solution, the sections were then incubated with secondary antibody conjugated with Alexa Fluor® 488 (1:500, Life Technologies, Grand Island, NY) for 2 h at room temperature. Before being mounted on gelatin subbed slides and sealed with cover slip, the sections were counter-stained with DAPI (Sigma-Aldrich, Saint Louis, MO, USA). A Leica SP5 ABOS confocal laser scan microscope (Leica Microsystems, Wetzlar, Germany) was used to acquire image stacks of SMI312- and vimentin- stained tissue sections. All images were collected using a 40x oil immersion objective at an in-plane resolution of $(0.76 \mu\text{m})^2$ and z step distance of 0.76 μ m. Maximum projections of all image stacks were generated for display of vimentin-positive radial glial cells and SMI312-positive axons within regions of interest. A Zeiss Axioplan system (Carl Zeiss, Jena, Germany) interfaced with Stereo Investigator (MBF Bioscience, Williston, VT, USA) was used to acquire 2D (single z depth) montage photos of Nissl stained sections with an in-plane resolution of $(2.1 \mu\text{m})^2$ using a 5X objective.

RESULTS

Figure 1A shows a T_2 -weighted axial image of a 23 weeks gestation human brain. An enlarged view of the caudal half of the brain, intersecting the occipital and parietal lobes, is shown in **Figure 1B**. At this stage of development, with standard image acquisition procedures, three tissue zones are apparent in the



caudal telencephalon (Barkovich and Raybaud, 2012). The dark zone in T₂-weighted images, proximal to the lateral ventricular surface, has been termed the germinal matrix (white arrows, **Figure 1B**). The zone with high image intensity adjacent to the germinal matrix corresponds to the SP. The CP is the most superficial zone, which is characterized by lower signal intensity than the SP in T₂-weighted images (red arrow heads, **Figure 1B**).

Figures 1C–G shows a T₂-weighted image acquired from a G90 rhesus macaque brain. Parasagittal and coronal views of high-resolution 3D reconstructed images, utilizing retrospective motion correction techniques, are shown in **Figures 1C,D**, respectively. Axial views of the caudal brain at the positions of the red dashed lines in **Figures 1C,D** are shown in **Figures 1E–G**. In spite of the overall smaller brain size, the same three tissue zones apparent in human fetal MRI were observed in high-resolution

fetal images of the rhesus macaque brain. Diffusion MRI data, obtained from a fourth animal at a similar gestational age (G85), are shown in **Figure 2**. Coronal and axial views of a T₂-weighted image, reconstructed at (0.5 mm)³ isotropic resolution, are shown in **Figures 2A,D**, respectively. As a consequence of the lower resolution of the acquired diffusion-weighted, compared to T₂-weighted data, the ADC (**Figures 2B,E**) and FA (**Figures 2C,F**) maps were reconstructed at a lower resolution of (0.75 mm)³. In these images, the CP tissue zone is characterized by relatively lower ADC than the adjacent SP, and markedly high FA. The lateral SP is sufficiently thick to be resolved from the CP and germinal matrix zones, exhibiting relatively high ADC (**Figures 2B,E**, yellow arrow heads) and negligible FA (**Figures 2C,F**, yellow arrow heads). Within the germinal matrix, the water ADC is relatively low (**Figure 2E**, red arrow head), and FA is higher than within the neighboring SP (**Figure 2F**, red arrow head).

Post mortem MRI and histological procedures were performed on the three G90 brains following *in utero* MRI. **Figures 3A–C** shows axial slices of Nissl-stained occipital and parietal lobes for each animal, revealing a more intricate laminar organization than the three tissue zone stratification supported by fetal T₂-weighted MRI. The tissue labeling scheme, and the color-code delineating each zone of Smart et al. (2002) is adopted in **Figures 3D–F**, with the exception that the CP is separated into superficial (dark blue, **Figures 3D–F**) and deep (light blue, **Figures 3D–F**) components, following the intra-cortical Nissl staining intensity variation previously noted by others (e.g., Kostovic and Rakic, 1990). Based on the relative sizes and locations of tissue zones identifiable **Figures 1–3**, the CP observable by MRI corresponds to the marginal zone (MZ) and superficial and deep CP zones observable in Nissl-stained tissue. Thus, the SP and germinal matrix in MRI data overlap the remaining layers defined by Smart and co-workers. If the SP zones are coincident in MRI and histological images (an assumption investigated in more detail below), then the germinal matrix consists of five distinct tissue zones described by Smart and co-workers. These five zones extending from the ventricular surface outward toward the pial surface consist of the ventricular zone (VZ) and inner subventricular zone (ISVZ), the inner fibers layer (IFL), the outer subventricular zone (OSVZ), and the outer fibers layer (OFL; **Figure 3**).

Post mortem MRI data obtained from the three rhesus fetal brains shown in **Figure 3** were examined to determine whether MRI-based contrast could be used to reveal greater detail in the primate brain laminar organization than the three heterogeneous zones identifiable in **Figures 1, 2**. **Figures 4A,B** shows parasagittal and coronal slices of ADC parameter maps from post mortem MRI performed on Monkey 1. Axial views of the occipital and parietal telencephalon at the location indicated in **Figures 4A,B** (red dashed lines) are given for T₂-weighted images, ADC maps, and FA maps of all three monkeys. As shown in **Figures 4C,F,I**, the three tissue zones observed *in utero* were also apparent in T₂-weighted images of post mortem tissue. However, a consistent pattern of additional zones were observed in the high resolution ADC maps of all three post mortem brains, as shown in **Figures 4D,G,J**. Diffusion anisotropy maps in

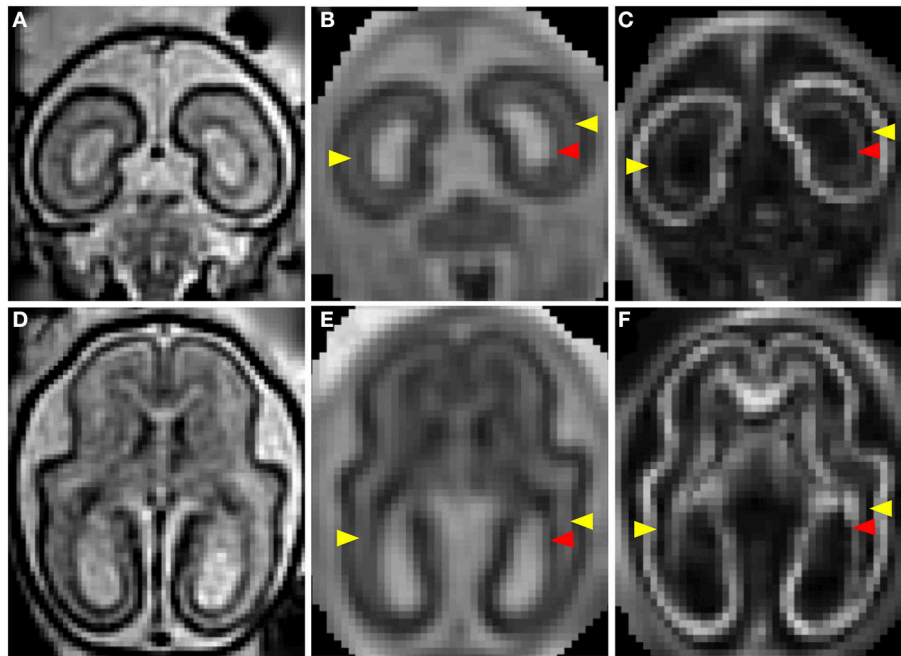


FIGURE 2 | T₂- and diffusion-weighted *in utero* MRI of a G85 rhesus macaque. Coronal and axial views of a T₂-weighted image (A,D), ADC map (B,E), and FA (C,F) map. CP is characterized by relatively lower ADC (B,E) than the adjacent SP, and markedly high FA (C,D). The lateral SP (yellow arrow heads) is sufficiently thick to be resolved from the CP and germinal matrix zones, exhibiting relatively high ADC (B,E) and negligible FA (C,F). Within the germinal matrix (red arrow heads), the water ADC is relatively low (B,E), and FA is higher than within the neighboring SP (C,F).

Figures 4E,H,K also revealed consistent patterns between brains, with high diffusion anisotropy in the CP, which is expected at this developmental stage (McKinstry et al., 2002). Notable diffusion anisotropy is also observed in periventricular zones (Figure 4E, red arrow heads).

In Figure 5, an enlarged region of the axial views of Figure 4 (white box, Figure 4E) is shown. The ADC map was partitioned into five zones, and the boundaries between them were overlaid on the T₂-weighted image (Figure 5A), the ADC map (Figure 5B), and the FA map (Figure 5C). Zone 1 is directly adjacent to the lateral ventricle, and consists of a 0.5–1 mm thick layer characterized by high water diffusivity ($0.3\text{--}0.6\ \mu\text{m}^2/\text{ms}$). Adjacent to this, Zone 2 is characterized by relatively lower water ADC ($0.25\text{--}0.3\ \mu\text{m}^2/\text{ms}$, between green and orange boundaries in Figures 5A–C). This zone exhibits increased FA (Figure 5C) and reduced T₂-weighted image intensity (Figure 5A), relative to neighboring zones. Superficial to this, Zone 3 is characterized by relatively high water diffusivity (between orange and red boundaries in Figures 5A–C). Interestingly, there is a transition to an adjacent zone, Zone 4, of relatively lower water ADC (between red and blue boundaries in Figures 5A–C), that is not accompanied by a corresponding transition in FA or T₂-weighted image intensity, and is not apparent in the lower-resolution ADC maps acquired *in vivo*. The fifth, and most superficial zone is characterized by relatively high water diffusivity, reduced T₂-weighted image intensity, and extremely high water diffusion anisotropy.

A diffusion anisotropy color map is shown in Figure 5D, and a projection of the diffusion tensor primary eigenvector field

onto an axial plane is shown in Figure 5E. Particularly in lateral aspects of the brain, the diffusion tensor primary orientation differed dramatically between the subventricular zones and the CP. However, this arrangement was not found throughout the entire ventricular surface, as the periventricular diffusion tensor principal direction was oriented radially in the occipital pole in Figures 5D,E. In order to determine the radial direction at each voxel center, the distance from the lateral ventricular surface was computed for each voxel in the occipital and parietal lobes (Figure 6A underlay). The gradient of the distance matrix is oriented along the radial direction (Figure 6A, red vectors). For comparison, the principal axis of the diffusion tensor for each voxel in the same brain region is overlaid on an FA parameter map in Figure 6B. An image of the angle θ between the radial direction vector and the primary eigenvector of the diffusion tensor (Figure 6B, green vectors) is shown in Figure 6C. In general, θ is larger near the lateral ventricles, indicating water diffusion is least restricted in tangential directions, and it is smaller in more superficial lamina, indicating radially-oriented diffusion anisotropy. Superimposed on this trend, at many locations throughout the lateral and occipital cerebral wall, a local maximum in θ with respect to laminar position was observed near the ventricular surface (yellow arrow heads, Figure 6C). Comparisons of the radial vectors (Figure 6A) to the diffusion tensor primary eigenvectors (Figure 6B) confirms that voxels with high θ are characterized by non-parallel vectors in Figures 6A,B, in many cases as a result of a significant through-plane diffusion tensor primary eigenvector component. In Figure 5F, a θ map is displayed relative to the five-zone

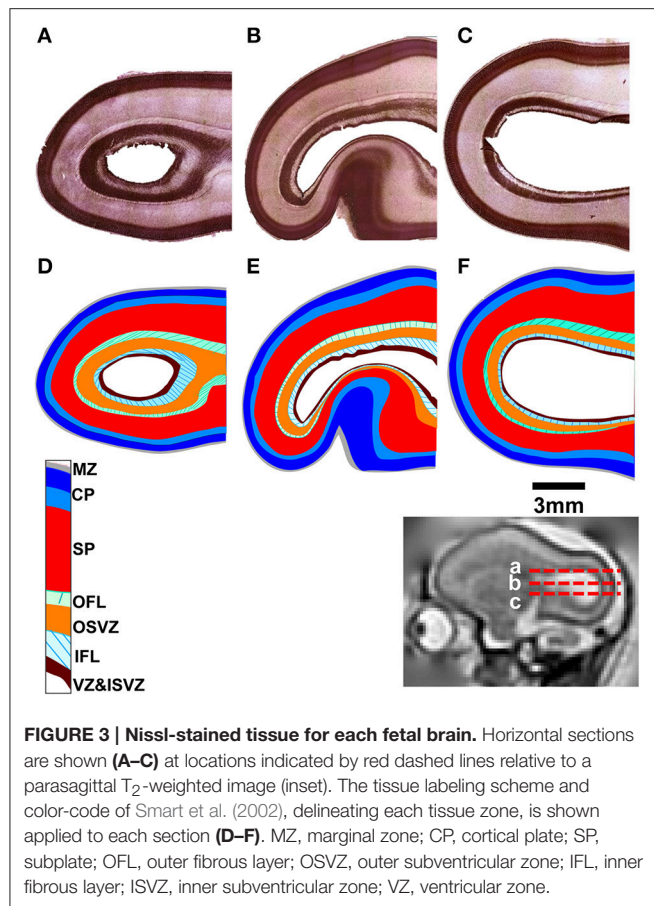


FIGURE 3 | Nissl-stained tissue for each fetal brain. Horizontal sections are shown (A–C) at locations indicated by red dashed lines relative to a parasagittal T₂-weighted image (inset). The tissue labeling scheme and color-code of Smart et al. (2002), delineating each tissue zone, is shown applied to each section (D–F). MZ, marginal zone; CP, cortical plate; SP, subplate; OFL, outer fibrous layer; OSVZ, outer subventricular zone; IFL, inner fibrous layer; ISVZ, inner subventricular zone; VZ, ventricular zone.

partitioning based on other MRI contrast mechanisms. Local maxima were observed in the superficial part of the second tissue zone at several locations within the lateral and occipital cerebral wall in this view as well (yellow arrows, Figure 5F).

In order to quantitatively compare post mortem MRI data from the six hemispheres, each of the parameters presented in Figures 4, 5 were projected onto radial streamlines. As illustrated in Figure 6D, application of the streamline algorithm (using the “stream3” function of Matlab) to the radial vector field, using voxels bordering the lateral and caudal ventricular surface as seed points, yielded radial streamlines spanning the ventricular to pial surfaces. In Figure 6D, streamlines (yellow) are projected onto the FA map axial slice containing a set of seed points located at the ventricular surface. At this axial level, the radial streamlines have a significant component parallel to the dorsal/ventral axis, and therefore the 2D projection creates the appearance that they terminate prior to reaching the pial surface. A parasagittal inset is also shown for a set of streamlines in the occipital lobe, to demonstrate that they actually do extend to the pial surface. For each of the six hemispheres, an average of 600 radial streamlines were constructed, and the T₂-weighted image intensity, ADC, FA, and θ were projected from each voxel intersected by each streamline. In Figure 7, the averaged parameters are plotted for each of the six hemispheres as a function of relative position along the set of streamlines extending from the ventricular to

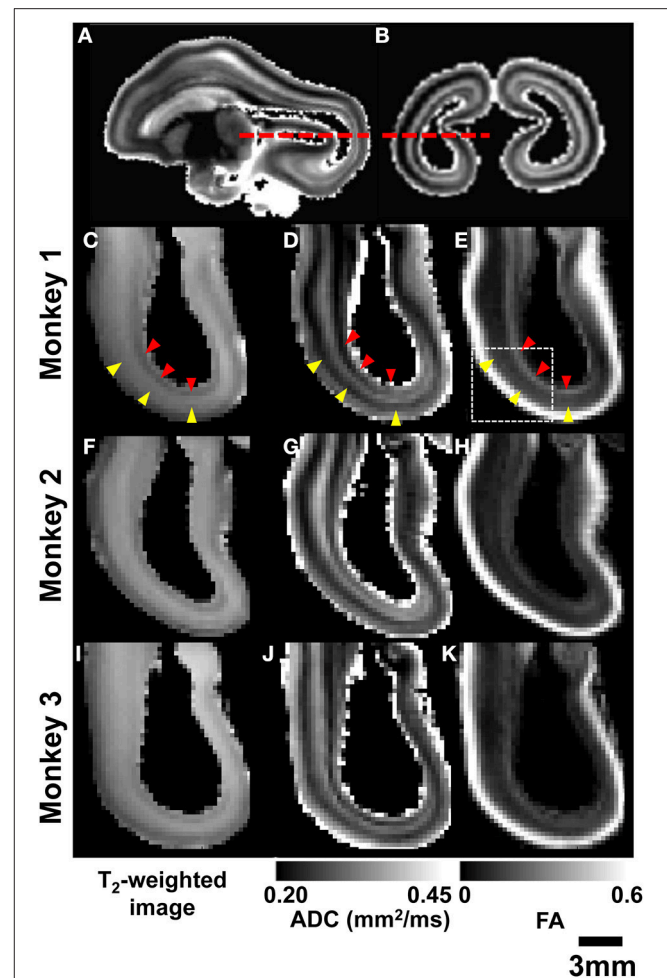


FIGURE 4 | Post-mortem MRI. Parasagittal (A) and coronal (B) ADC maps obtained from monkey 1 are used to indicate the location of axial views of parietal and occipital lobes (red dashed lines). For all three G90 rhesus fetal brains, T₂-weighted images (C,F,I), ADC maps (D,G,J), and FA maps (E,H,K) reveal consistent laminar patterns between the three brains. SP and germinal matrix zones indicated by yellow and red arrow heads, respectively.

the pial surface. For T₂-weighted image intensity, ADC, and FA, highly consistent locations and magnitudes of maxima and minima were observed. More variability between hemispheres was observed for θ . However, for all hemispheres, the rate of reduction in θ with laminar position was highest from 0.05 to 0.15, was very low from 0.15 to 0.35, and was moderate and uniform from 0.35 to 0.9, where it reached a minimal value of $\sim 10^\circ$. The locations of borders between MRI-identified tissue zones are indicated as dashed vertical lines in the Figure 7 plots.

Immunohistochemical analyses were performed to characterize the orientations of dominant cellular constituents across the cerebral wall. Within the CP (Figures 8A,B), SP (Figures 8C,D), and OFL (Figures 8E,F), radial glial processes revealed with vimentin staining appear consistently radially oriented, albeit in an interrupted manner within the OFL due to the presence of palisades of DAPI-negative fibrous tissue.

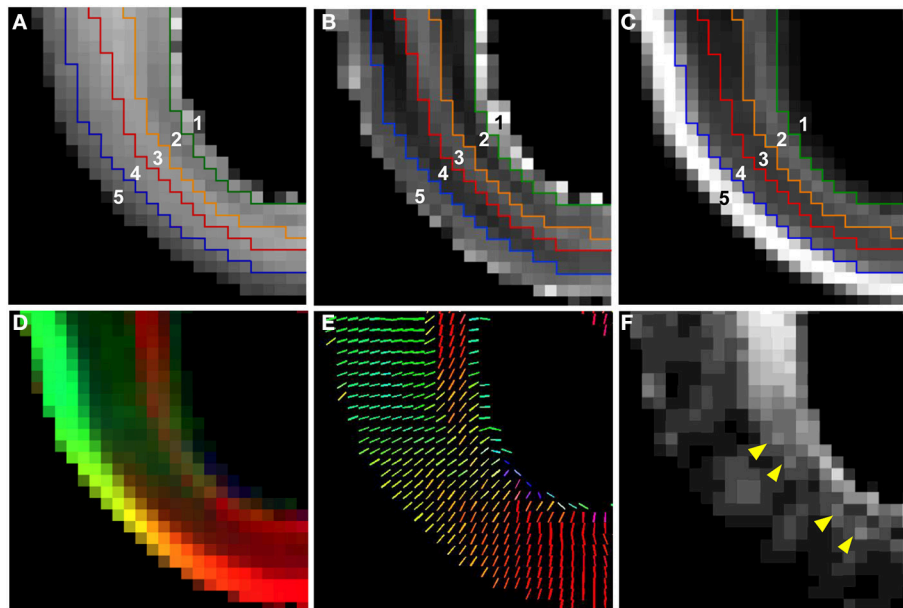


FIGURE 5 | Five tissue zones identified from post mortem MRI. On an enlarged region of the axial views of **Figure 4** (**Figure 4E**, white dashed box), five tissue zones were delineated on ADC maps (**B**) and the boundaries were projected onto T_2 -weighted image (**A**) and FA map (**C**) (see text for details). A diffusion anisotropy color map (**D**), and a projection of the diffusion tensor primary eigenvector (V_1) (**E**) is shown in for the same field of view. For color maps, red, green, and blue channels were scaled by the product of FA and the squared vertical, horizontal, and through-plane component of V_1 , respectively, with the FA map multiplied by a factor of 4. The angle θ between the radial direction vector, and the primary eigenvector of the diffusion tensor is also shown (**F**). Yellow arrows in (**F**) indicate locations of local maxima in θ in the superficial part of Zone 2.

Within the CP (**Figure 8B**), SMI312-positive axons are oriented radially. Within the OFL, in contrast, tangentially oriented axon fascicles are dominant structures (**Figure 8F**). A combination of diminished vimentin-positive, radially-oriented structures, and increased tangentially-oriented axon structures in the OFL, coincides with the laminar position of 0.25 in **Figure 7**. Interestingly, within the OSVZ, where inconsistent orientations of the diffusion tensor primary eigenvector are observed (**Figures 5D,E**), large compliments of radial as well as tangential axons are apparent (**Figure 8G**).

In **Figure 9**, averages for the six hemispheres are plotted as a function of laminar position for the four parameters shown in **Figure 7**. The locations of maxima and minima for each parameter added constructively, indicating that the relative positions and thicknesses of the tissue zones are consistent among the set of hemispheres. This regularity facilitated comparisons to data from Nissl (**Figure 3**) and immunohistochemical (**Figure 8**) staining, as illustrated along the **Figure 9** abscissa.

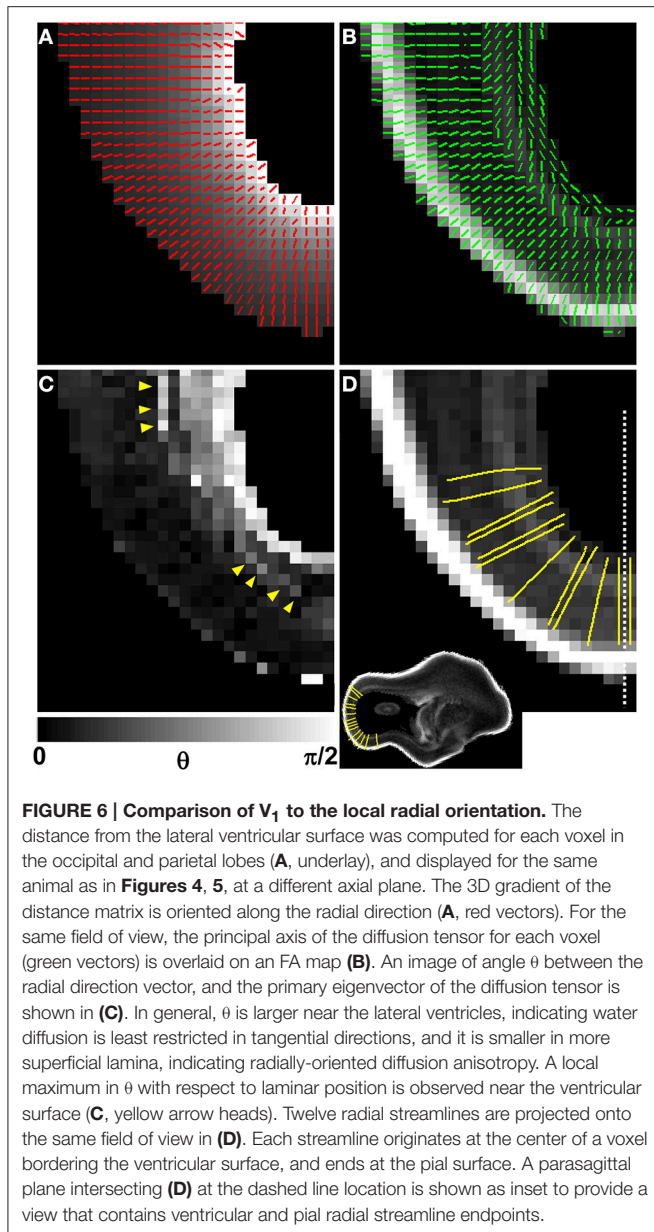
DISCUSSION

Assignment of Zones Identified by Post Mortem MRI to Established Histological Lamina

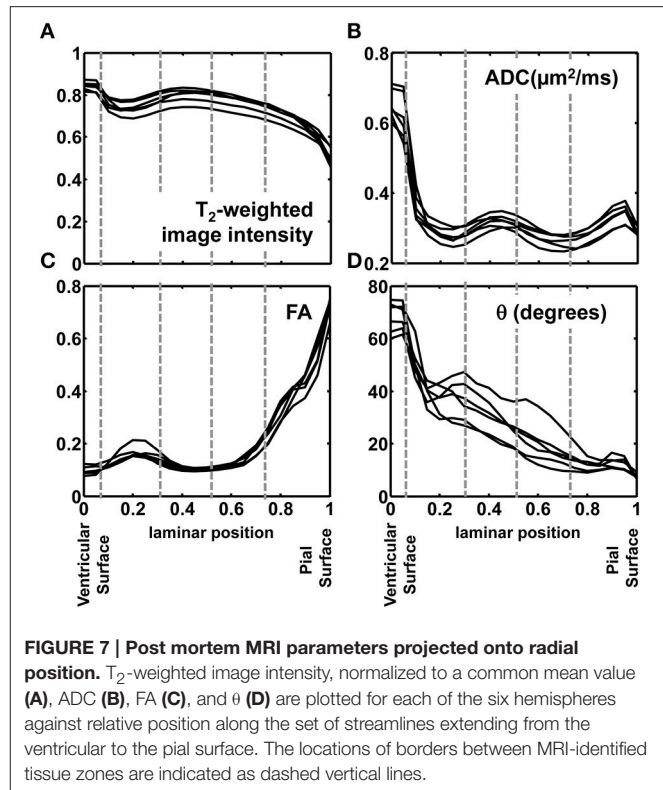
Based on multiple MRI contrast mechanisms, it was possible to identify five distinct laminar zones in the rhesus parietal and

occipital lobes at 90 days gestational age. The correspondence between lamina identified by MRI and histological methods have been previously established for zones near the pia (Kostovic et al., 2002; Kroenke et al., 2006, 2007; Huang et al., 2009; Kolasinski et al., 2013; Xu et al., 2014). However, the associations between MRI and histological studies for zones near the ventricular surface have not been as systematically characterized. As shown in **Figure 9**, diffusion anisotropy in Zone 5 is oriented radially (manifested by low θ values), and diffusion anisotropy increases with proximity to the pial surface. This zone has been assigned to the CP and MZ (Kroenke et al., 2007; Huang et al., 2009). Tangential, rather than radial structures reside in the MZ (**Figure 8B**). However, the MZ is too thin to be resolved by MRI experiments, and therefore diffusion anisotropy throughout the superficial zone is oriented radially. In previous work, the presence of the MZ has been revealed through partial volume averaging to result in reduced diffusion anisotropy relative to neighboring voxels that overlap the CP (Kroenke et al., 2007).

The SP is approximately twice as thick as the combined thickness of the CP and MZ (**Figure 2**). Therefore, the entirety of Zone 4, and at least part of Zone 3 must contribute to the SP, and the SP contains sub-lamina characterized by low water diffusivity (Zone 4) and high water diffusivity (Zone 3). This intra-SP gradient in the water ADC has been noted previously by Huang et al. (2006), and inferred by Kostovic et al. (2002) in post mortem MRI studies of fetal human brains, and is apparent in post mortem ADC measurements of the G90 baboon



(Kroenke et al., 2005). The histological analyses performed here did not reveal differences between superficial and deep SP that could underlie the variation of water diffusivity within this zone. However, Kostovic (Kostovic et al., 2002) has proposed that the region of high diffusivity relates to the hygroscopic properties of SP extracellular matrix components. Although the biochemical mechanism responsible for the gradient in water diffusivity is not completely understood, the intra-SP ADC gradient is a robust phenomenon, as it has been observed by multiple research groups in multiple gyroencephalic species. It is plausibly related to the biological function of this zone by providing a molecular environment appropriate for the diffusion of growth and signaling factors as well as defasciculation of axons to promote innervation of the cerebral cortex (Kostovic et al., 2002).



The border between SP and OFL was assigned to a position in the MRI-identified tissue zones by referencing the direction of anisotropic diffusion relative to the radial direction. As shown in Figure 8F, the OFL contains a high density of tangentially-oriented SMI312 positive fibers compared to the neighboring SP and OSVZ (Figures 8D,G, respectively). This tangentially-oriented structure gives rise to a local maximum in θ in Zone 2 (yellow arrowheads, Figures 5F, 6C) near the border between Zones 2 and 3 (Figure 9). Thus, the OFL forms the outer-most part of Zone 2, and the OFL/SP border coincides with the border between Zones 2 and 3. Tangentially-oriented structures within the OFL (Figure 8F) and IFL give rise to moderately high FA values with tangentially oriented diffusion anisotropy (Figures 5C,F, respectively). Thus, the ISVZ/IFL border is coincident with the border of Zones 1 and 2. Zone 1 is characterized by negligible diffusion anisotropy (Figure 5B), which is appropriate for the “randomly organized cells” of the ISVZ (Smart et al., 2002) and VZ. However, the extremely high values for the water ADC and T_2 -weighted image intensity within this zone, particularly for the inner-most voxels, indicate that significant partial volume averaging with aqueous solution in the adjacent lateral ventricles influences MRI parameter values for at least a subset of voxels. Further, the combined thickness of ISVZ and VZ is expected to be on the order of a single 0.3 mm-sided voxel (Figure 3), which additionally suggests that partial volume averaging confounds interpretations of MRI parameters within this zone. In Figure 9, the MRI-identified tissue zones (dashed gray lines) are aligned to the lamina defined by Smart et al. (2002), relative to the MRI parameters investigated here.

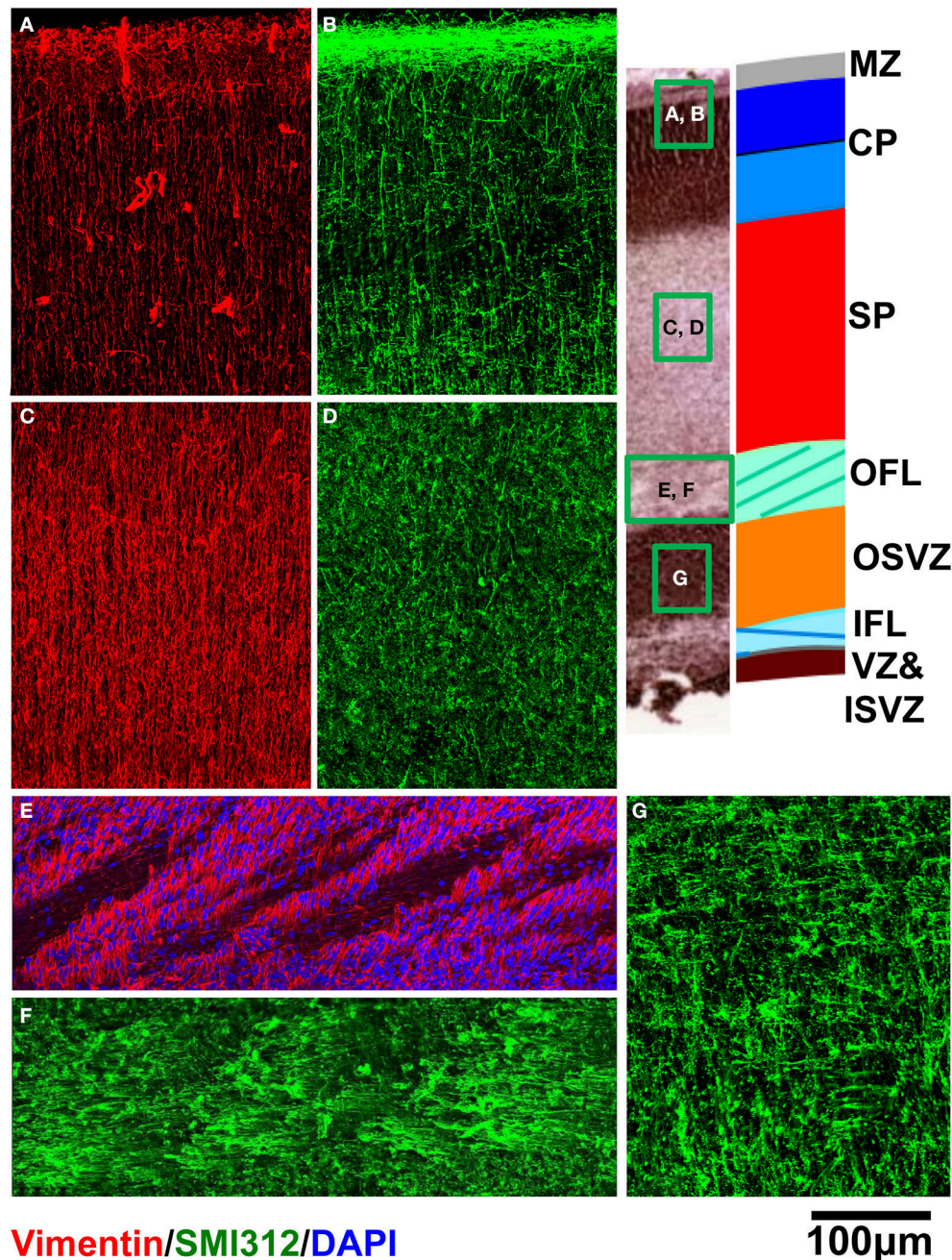


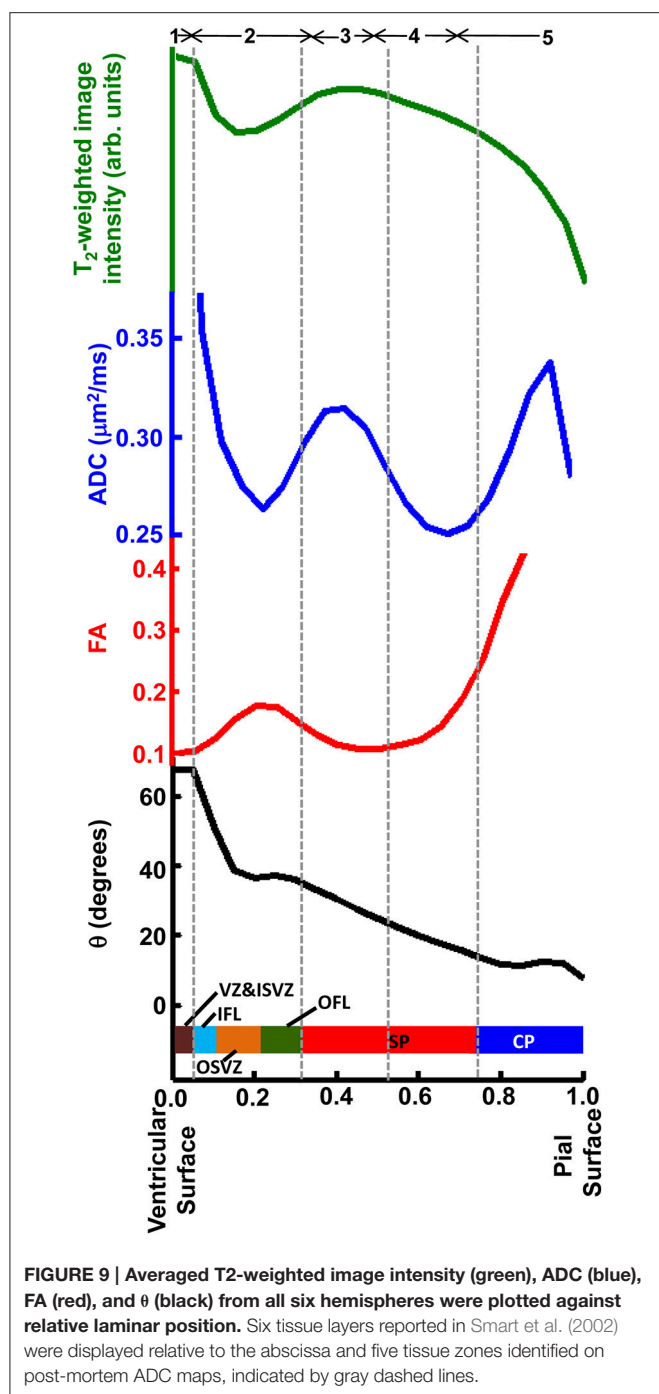
FIGURE 8 | Vimentin (red) and SMI312 (green) stained tissue sections from a representative rhesus macaque fetal brain are shown for regions of CP (A,B), SP (C,D), and OFL (E,F). DAPI (blue) is shown in (E). For OSVZ, SMI312 staining is shown (G).

Relevance to Fetal Brain Measurements Performed *in utero*

Aside from differences in achievable image resolution, the T_2 -weighted image contrast pattern observed in the fetal rhesus brain with post mortem MRI was identical to the pattern observed *in utero*. In turn, similar T_2 -weighted image contrast patterns were observed in rhesus and human fetal brains with *in utero* MRI. Thus, it is anticipated that the associations

described here between histologically-identified tissue zones and post mortem MRI can be extended to the context of human *in utero* fetal brain images.

For diffusion-based MRI contrast, the increased image resolution obtained in post mortem conditions enabled identification and characterization of tissue zones in a manner that was not possible with data collected from fetal brains *in utero*. Specifically, within the SP, two tissue zones were identified



in ADC maps of post mortem tissue. These zones could not be resolved in images collected *in utero* (Figures 2B,E). A likely reason for this difference is that partial volume averaging of the CP and the most superficial SP zone gives rise to a single combined zone with a lower ADC than the remaining component of the SP. A second possibility is that biophysical differences between *in vivo* and *ex vivo* tissue give rise to the low ADC zone within the SP observed in post mortem MRI, but not *in utero*. High resolution *in utero* images will be necessary

to discern between these two possibilities. A second difference between the *ex vivo* and *in vivo* data was the extent to which subventricular zones and associated fibrous layers could be characterized. Within the germinal matrix, voxels with modest FA values are observable in lateral brain regions, but these were too thin to be resolved in occipital regions (Figures 2C,F). With the improved image resolution obtainable with post mortem MRI, this zone could be identified in the occipital pole of FA maps. Further, in post mortem images, regions with varying directions of diffusion anisotropy could be resolved, which facilitated the assignment of the OFL to the germinal matrix zones traditionally identified in fetal brain MRI. These findings imply that future improvements in achievable image resolution in fetal diffusion MRI will be met with qualitative improvements in the ability to characterize SP, germinal zones, and fibrous layers of the fetal brain.


Comparison to Other Labeling Conventions

Several naming systems have been described for the mid-gestation primate parietal and occipital brain (Kostovic and Rakic, 1990; Altman and Bayer, 2002; Kostovic et al., 2002; Smart et al., 2002; Bayer and Altman, 2005; Huang et al., 2006, 2009; Bystron et al., 2008). Herein, tissue zones identifiable by MRI were referenced to the naming system of Smart et al. (2002). Based on the order from the ventricular to the pial surface, and matching tissue zones with similar descriptions, an approximate alignment of multiple other naming systems to the five MRI-identified tissues zones of this study is given in Table 1. It is important to emphasize that the alignment proposed in Table 1 is derived from caudal brain data at mid-gestation. Regional differences in laminar organization (Altman and Bayer, 2002; Martínez-Cerdeño et al., 2012), as well as differences in developmental stage (Smart et al., 2002; Cunningham et al., 2013; Wang et al., 2015), are critical factors that influence the characteristics of the tissue zones listed in Table 1. Notably, in studies of the human brain, Altman and Bayer (Altman and Bayer, 2002; Bayer and Altman, 2005) subdivide the region that corresponds to SP in other studies to a relatively thinner SP, and stratified transition fields (STF) 1 and 2, and potentially in addition, STF3c. Given that variation we observe in the water ADC within the SP (following the naming system of Smart et al.) is also observed by Huang et al. (2006) in human tissue, it is tempting to speculate that STF2 of Altman and Bayer (Altman and Bayer, 2002; Bayer and Altman, 2005) corresponds to Zone 3 of this study, and STF1 and SP of Altman and Bayer (Altman and Bayer, 2002; Bayer and Altman, 2005) corresponds to Zone 4. However, we were unable to identify STF1 and STF2 boundaries in our histological data, and therefore we do not currently have direct evidence to support this association.

Varying Cellular Structures Give Rise to Anisotropy in Water Diffusion

In white matter of the mature brain, myelinated axon fibers are the dominant structures contributing to water diffusion anisotropy. The situation in fetal brain is different, because there are multiple organized cellular constituents, in addition to

TABLE 1 | Terminology for morphological zones in the mid-gestation occipital and parietal lobes from different studies.

Histology				MRI			
Pial surface	Smart et al., 2002	Altman and Bayer, 2002; Bayer and Altman, 2005	Bystron et al., 2008	Kostovic et al., 2002	Huang et al., 2006, 2009	Barkovich and Raybaud, 2012	This study
	MZ	SGL	MZ	MZ	CP	CP	Zone 5
	CP	CP	CP	CP			
	SP	SP, STF1	SP	SP	SP	SP	Zone 4
		STF2					Zone 3
	OFL	STF3	IZ	IZ			
	OSVZ	STF4,5		SVCZ			Zone 2
	IFL	STF6	SVZ	PVfZ			
	ISVZ	SVZ		VZ (GM)	IZ	GM	
Ventricular surface	VZ	NPE ^a	VZ				Zone 1

^aNPE, neuroepithelium; STF, stratified transitional field; SGL, subpial granular layer; IZ, intermediate zone; PVfZ, periventricular fiber rich zone; SVCZ, subventricular cellular zone. See **Figure 1** for remaining abbreviations.

axons, that influence water diffusion. Many cell structures in the developing brain are oriented radially (i.e., perpendicular to the ventricular and pial surfaces), such as radial glial cell processes throughout the cerebral wall (**Figure 8**; Xu et al., 2014), migrating neurons, and radially-oriented neural processes in the CP (Bock et al., 2010; Jespersen et al., 2012). Other cell processes, such as developing axon fibers, are oriented tangentially (parallel to the ventricular and pial surfaces). Developing axon fiber fascicles are most abundant in the IFL and OFL, wherein “palisades” of fascicles are interspersed with radial glial processes and associated migrating neurons (Smart et al., 2002). As a result of the dominant structural orientation changing with radial position, the direction of least restricted water diffusion, relative to the radial direction, varies across tissue zones (Kolasinski et al., 2013; Xu et al., 2014). It is therefore important to consider the effects of these additional cell structures when interpreting the results of diffusion anisotropy measurements in the developing brain. For example, application of diffusion tractography analysis procedures would be likely to generate fiber “tracts” that reflect properties of glial processes and neural dendrites, as well as axons, and as a result it would be erroneous to interpret the results of such analyses strictly in terms of axonal connectivity. Further, interpretations of changes in diffusion anisotropy with development, or differences in anisotropy between experimental groups, should similarly be interpreted with consideration of the various structures that have been shown to influence water diffusion in the fetal brain.

REFERENCES

Altman, J., and Bayer, S. A. (2002). Regional differences in the stratified transitional field and the honeycomb matrix of the developing human cerebral cortex. *J. Neurocytol.* 31, 613–632. doi: 10.1023/A:1025787427576

CONCLUSION

Through the combined use of *in utero* MRI, post mortem MRI, and histological analyses of brains of rhesus macaques, the borders of previously-defined tissue zones have been assigned, with greater precision than previously possible in studies of primate brains, to transitions in various forms of MRI contrast. The *in vivo* and post mortem measurements performed on the same individuals demonstrate the close similarities in image contrast patterns under the two conditions and facilitate interpretations of *in vivo* data in terms of underlying cellular morphological features. Additionally, high resolution images obtained from post mortem tissue demonstrate that improvements in achievable *in utero* image resolution will enable the identification of tissue zone boundaries within individuals. Improved ADC map image resolution may additionally enable more complete characterization of sub-lamina with the SP.

ACKNOWLEDGMENTS

The authors thank Verginia Cuzon Carlson, Jodi McBride, Anda Cornea, and Oleg Varlamov for guidance in histological and microscopy procedures. This work was supported by NIH grants R01AA021981, R01 NS070022, P51 OD011092, and R25 EB016671. Additional support for microscopy facilities was provided through the core support provided through NIH grant P30 NS061800.

Barkovich, A. J., and Raybaud, C. (2012). *Pediatric Neuroimaging*. Philadelphia, PA: Lippincott Williams & Wilkins.
Barnette, A. R., Neil, J. J., Kroenke, C. D., Griffith, J. L., Epstein, A. A., Bayly, P. V., et al. (2009). Characterization of brain development in the ferret via MRI. *Pediatr. Res.* 66, 80–84. doi: 10.1203/PDR.0b013e3181a291d9

- Basser, P. J., and Pierpaoli, C. (1996). Microstructural and physiological features of tissues elucidated by quantitative-diffusion-tensor MRI. *J. Magn. Reson. B* 111, 209–219. doi: 10.1006/jmrb.1996.0086
- Batchelor, P. G., Atkinson, D., Hill, D. L., Calamante, F., and Connelly, A. (2003). Anisotropic noise propagation in diffusion tensor MRI sampling schemes. *Magn. Reson. Med.* 49, 1143–1151. doi: 10.1002/mrm.10491
- Bayer, S. A., and Altman, J. (2005). *The Human Brain During the Second Trimester*. Boca Raton, FL: CRC Press. doi: 10.1201/9780203507483
- Bock, A. S., Olavarria, J. F., Leigland, L. A., Taber, E. N., Jespersen, S. N., and Kroenke, C. D. (2010). Diffusion tensor imaging detects early cerebral cortex abnormalities in neuronal architecture induced by bilateral neonatal enucleation: an experimental model in the ferret. *Front. Syst. Neurosci.* 4:149. doi: 10.3389/fnsys.2010.00149
- Bystron, I., Blakemore, C., and Rakic, P. (2008). Development of the human cerebral cortex: Boulder Committee revisited. *Nat. Rev. Neurosci.* 9, 110–122. doi: 10.1038/nrn2252
- Cunningham, C. L., Martínez-Cerdeño, V., and Nock, S. C. (2013). Diversity of neural precursor cell types in the prenatal macaque cerebral cortex exists largely within the astroglial cell lineage. *PLoS ONE* 8:e63848. doi: 10.1371/journal.pone.0063848
- Fogtmann, M., Chapman, T., Kim, K., Seshamani, S., and Studholme, C. (2012). “A unified approach for motion estimation and super-resolution reconstruction from structural magnetic resonance imaging on moving subjects,” in *MICCAI Workshop on Perinatal and Paediatric Imaging* (Nice: PaPI).
- Fogtmann, M., Seshamani, S., Kroenke, C., Xi, C., Chapman, T., Wilm, J., et al. (2014). A unified approach to diffusion direction sensitive slice registration and 3-D DTI reconstruction from moving fetal brain anatomy. *IEEE Trans. Med. Imaging* 33, 272–289. doi: 10.1109/TMI.2013.2284014
- Gholipour, A., Estroff, J. A., Sahin, M., Prabhu, S. P., and Warfield, S. K. (2010). Maximum a posteriori estimation of isotropic high-resolution volumetric MRI from orthogonal thick-slice scans. *Med. Image Comput. Comput. Assist. Interv.* 13, 109–116. doi: 10.1109/TMI.2013.2284014
- Glenn, O. A., and Barkovich, A. J. (2006). Magnetic resonance imaging of the fetal brain and spine: an increasingly important tool in prenatal diagnosis, part I. *AJNR Am. J. Neuroradiol.* 27, 1604–1611.
- Gupta, R. K., Hasan, K. M., Trivedi, R., Pradhan, M., Das, V., Parikh, N. A., et al. (2005). Diffusion tensor imaging of the developing human cerebrum. *J. Neurosci. Res.* 81, 172–178. doi: 10.1002/jnr.20547
- Hansen, D. V., Lui, J. H., Parker, P. R., and Kriegstein, A. R. (2010). Neurogenic radial glia in the outer subventricular zone of human neocortex. *Nature* 464, 554–561. doi: 10.1038/nature08845
- Huang, H., Xue, R., Zhang, J., Ren, T., Richards, L. J., Yarowsky, P., et al. (2009). Anatomical characterization of human fetal brain development with diffusion tensor magnetic resonance imaging. *J. Neurosci.* 29, 4263–4273. doi: 10.1523/JNEUROSCI.2769-08.2009
- Huang, H., Yamamoto, A., Hossain, M. A., Younes, L., and Mori, S. (2008). Quantitative cortical mapping of fractional anisotropy in developing rat brains. *J. Neurosci.* 28, 1427–1433. doi: 10.1523/JNEUROSCI.3194-07.2008
- Huang, H., Zhang, J., Wakana, S., Zhang, W., Ren, T., Richards, L. J., et al. (2006). White and gray matter development in human fetal, newborn and pediatric brains. *Neuroimage* 33, 27–38. doi: 10.1016/j.neuroimage.2006.06.009
- Jespersen, S. N., Leigland, L. A., Cornea, A., and Kroenke, C. D. (2012). Determination of axonal and dendritic orientation distributions within the developing cerebral cortex by diffusion tensor imaging. *IEEE Trans. Med. Imaging* 31, 16–32. doi: 10.1109/TMI.2011.2162099
- Kim, K., Habas, P. A., Rajagopalan, V., Scott, J. A., Corbett-Detig, J. M., Rousseau, F., et al. (2011). Bias field inconsistency correction of motion-scattered multislice MRI for improved 3D image reconstruction. *IEEE Trans. Med. Imaging* 30, 1704–1712. doi: 10.1109/TMI.2011.2143724
- Kolasinski, J., Takahashi, E., Stevens, A. A., Benner, T., Fischl, B., Zöllei, L., et al. (2013). Radial and tangential neuronal migration pathways in the human fetal brain: anatomically distinct patterns of diffusion MRI coherence. *Neuroimage* 79, 412–422. doi: 10.1016/j.neuroimage.2013.04.125
- Kostovic, I., Judas, M., Rados, M., and Hrabac, P. (2002). Laminar organization of the human fetal cerebrum revealed by histochemical markers and magnetic resonance imaging. *Cereb. Cortex* 12, 536–544. doi: 10.1093/cercor/12.5.536
- Kostovic, I., and Rakic, P. (1990). Developmental history of the transient subplate zone in the visual and somatosensory cortex of the macaque monkey and human brain. *J. Comp. Neurol.* 297, 441–470. doi: 10.1002/cne.902970309
- Kriegstein, A., Nock, S., and Martínez-Cerdeño, V. (2006). Patterns of neural stem and progenitor cell division may underlie evolutionary cortical expansion. *Nat. Rev. Neurosci.* 7, 883–890. doi: 10.1038/nrn2008
- Kroenke, C. D., Bretthorst, G. L., Inder, T. E., and Neil, J. J. (2005). Diffusion MR imaging characteristics of the developing primate brain. *Neuroimage* 25, 1205–1213. doi: 10.1016/j.neuroimage.2004.12.045
- Kroenke, C. D., Bretthorst, G. L., Inder, T. E., and Neil, J. J. (2006). Modeling water diffusion anisotropy within fixed newborn primate brain using Bayesian probability theory. *Magn. Reson. Med.* 55, 187–197. doi: 10.1002/mrm.20728
- Kroenke, C. D., Van Essen, D. C., Inder, T. E., Rees, S., Bretthorst, G. L., and Neil, J. J. (2007). Microstructural changes of the baboon cerebral cortex during gestational development reflected in magnetic resonance imaging diffusion anisotropy. *J. Neurosci.* 27, 12506–12515. doi: 10.1523/JNEUROSCI.3063-07.2007
- Martínez-Cerdeño, V., Cunningham, C. L., Camacho, J., Antczak, J. L., Prakash, A. N., Cziep, M. E., et al. (2012). Comparative analysis of the subventricular zone in rat, ferret and macaque: evidence for an outer subventricular zone in rodents. *PLoS ONE* 7:e30178. doi: 10.1371/journal.pone.0030178
- McKinstry, R. C., Mathur, A., Miller, J. H., Ozcan, A., Snyder, A. Z., Schefft, G. L., et al. (2002). Radial organization of developing preterm human cerebral cortex revealed by non-invasive water diffusion anisotropy MRI. *Cereb. Cortex* 12, 1237–1243. doi: 10.1093/cercor/12.12.1237
- Oubel, E., Koob, M., Studholme, C., Dietemann, J. L., and Rousseau, F. (2012). Reconstruction of scattered data in fetal diffusion MRI. *Med. Image Anal.* 16, 28–37. doi: 10.1016/j.media.2011.04.004
- Paul, C. A., Beltz, B., and Berger-Sweeney, J. (2008). The nissl stain: a stain for cell bodies in brain sections. *CSH Protoc.* 2008:pdb.prot4805. doi: 10.1101/pdb.prot4805
- Reillo, I., de Juan Romero, C., García-Cabezas, M. A., and Borrell, V. (2011). A role for intermediate radial glia in the tangential expansion of the mammalian cerebral cortex. *Cereb. Cortex* 21, 1674–1694. doi: 10.1093/cercor/bhq238
- Rousseau, F., Glenn, O. A., Iordanova, B., Rodriguez-Carranza, C., Vigneron, D. B., Barkovich, J. A., et al. (2006). Registration-based approach for reconstruction of high-resolution *in utero* fetal MR brain images. *Acad. Radiol.* 13, 1072–1081. doi: 10.1016/j.acra.2006.05.003
- Scott, J. A., Habas, P. A., Kim, K., Rajagopalan, V., Hamzelou, K. S., Corbett-Detig, J. M., et al. (2011). Growth trajectories of the human fetal brain tissues estimated from 3D reconstructed *in utero* MRI. *Int. J. Dev. Neurosci.* 29, 529–536. doi: 10.1016/j.ijdevneu.2011.04.001
- Sizonenko, S. V., Camm, E. J., Garbow, J. R., Maier, S. E., Inder, T. E., Williams, C. E., et al. (2007). Developmental changes and injury induced disruption of the radial organization of the cortex in the immature rat brain revealed by *in vivo* diffusion tensor MRI. *Cereb. Cortex* 17, 2609–2617. doi: 10.1093/cercor/bhl168
- Smart, I. H., Dehay, C., Giroud, P., Berland, M., and Kennedy, H. (2002). Unique morphological features of the proliferative zones and postmitotic compartments of the neural epithelium giving rise to striate and extrastriate cortex in the monkey. *Cereb. Cortex* 12, 37–53. doi: 10.1093/cercor/12.1.37
- Studholme, C. (2011). Mapping fetal brain development *in utero* using MRI: the big bang of brain mapping. *Annu. Rev. Biomed. Eng.* 13, 345–368. doi: 10.1146/annurev-bioeng-071910-124654
- Wang, R., Dai, G., and Takahashi, E. (2015). High resolution MRI reveals detailed layer structures in early human fetal stages: *In vitro* study with histologic correlation. *Front. Neuroanat.* 9:150. doi: 10.3389/fnana.2015.00150
- Workman, A. D., Charvet, C. J., Clancy, B., Darlington, R. B., and Finlay, B. L. (2013). Modeling transformations of neurodevelopmental sequences across mammalian species. *J. Neurosci.* 33, 7368–7383. doi: 10.1523/JNEUROSCI.5746-12.2013
- Xu, G., Takahashi, E., Folkert, R. D., Haynes, R. L., Volpe, J. J., Grant, P. E., et al. (2014). Radial coherence of diffusion tractography in the cerebral white matter

- of the human fetus: neuroanatomic insights. *Cereb. Cortex* 24, 579–592. doi: 10.1093/cercor/bhs330
- Zhang, Z., Liu, S., Lin, X., Teng, G., Yu, T., Fang, F., et al. (2011a). Development of laminar organization of the fetal cerebrum at 3.0T and 7.0T: a postmortem MRI study. *Neuroradiology* 53, 177–184. doi: 10.1007/s00234-010-0781-7
- Zhang, Z., Liu, S., Lin, X., Teng, G., Yu, T., Fang, F., et al. (2011b). Development of the fetal brain of 20 weeks gestational age: assessment with post-mortem Magnetic Resonance Imaging. *Eur. J. Radiol.* 80, e432–e439. doi: 10.1016/j.ejrad.2010.11.024

Conflict of Interest Statement: The authors declare that the research was conducted in the absence of any commercial or financial relationships that could be construed as a potential conflict of interest.

Copyright © 2015 Wang, Pettersson, Studholme and Kroenke. This is an open-access article distributed under the terms of the Creative Commons Attribution License (CC BY). The use, distribution or reproduction in other forums is permitted, provided the original author(s) or licensor are credited and that the original publication in this journal is cited, in accordance with accepted academic practice. No use, distribution or reproduction is permitted which does not comply with these terms.



Construction and application of human neonatal DTI atlases

Rajiv Deshpande^{1,2}, Linda Chang³ and Kenichi Oishi^{2*}

¹ Department of Radiology, Johns Hopkins University, Baltimore, MD, USA, ² Biomedical Engineering, Johns Hopkins University, Baltimore, MD, USA, ³ Department of Medicine, School of Medicine, University of Hawaii at Manoa, Honolulu, HI, USA

OPEN ACCESS

Edited by:

Julia P. Owen,
University of California,
San Francisco, USA

Reviewed by:

Antonio Di Ieva,
Macquarie University Hospital,
Australia
Olga Tymofiyeva,
University of California,
San Francisco, USA

*Correspondence:

Kenichi Oishi
koishi@mri.jhu.edu

Received: 13 May 2015

Accepted: 12 October 2015

Published: 26 October 2015

Citation:

Deshpande R, Chang L and Oishi K
(2015) Construction and application
of human neonatal DTI atlases.
Front. Neuroanat. 9:138.
doi: 10.3389/fnana.2015.00138

Atlas-based MRI analysis is one of many analytical methods and is used to investigate typical as well as abnormal neurodevelopment. It has been widely applied to the adult and pediatric populations. Successful applications of atlas-based analysis (ABA) in those cohorts have motivated the creation of a neonatal atlas and parcellation map (PM). The purpose of this review is to discuss the various neonatal diffusion tensor imaging (DTI) atlases that are available for use in ABA, examine how such atlases are constructed, review their applications, and discuss future directions in DTI. Neonatal DTI atlases are created from a template, which can be study-specific or standardized, and merged with the corresponding PM. Study-specific templates can retain higher image registration accuracy, but are usually not applicable across different studies. However, standardized templates can be used to make comparisons among various studies, but may not accurately reflect the anatomies of the study population. Methods such as volume-based template estimation are being developed to overcome these limitations. The applications for ABA, including atlas-based image quantification and atlas-based connectivity analysis, vary from quantifying neurodevelopmental progress to analyzing population differences in groups of neonates. ABA can also be applied to detect pathology related to prematurity at birth or exposure to toxic substances. Future directions for this method include research designed to increase the accuracy of the image parcellation. Methods such as multi-atlas label fusion and multi-modal analysis applied to neonatal DTI currently comprise an active field of research. Moreover, ABA can be used in high-throughput analysis to efficiently process medical images and to assess longitudinal brain changes. The overarching goal of neonatal ABA is application to the clinical setting, to assist with diagnoses, monitor disease progression and, ultimately, outcome prediction.

Keywords: atlas-based analysis, diffusion tensor imaging, neonatal brain atlas, probabilistic, parcellation map, tractography

INTRODUCTION

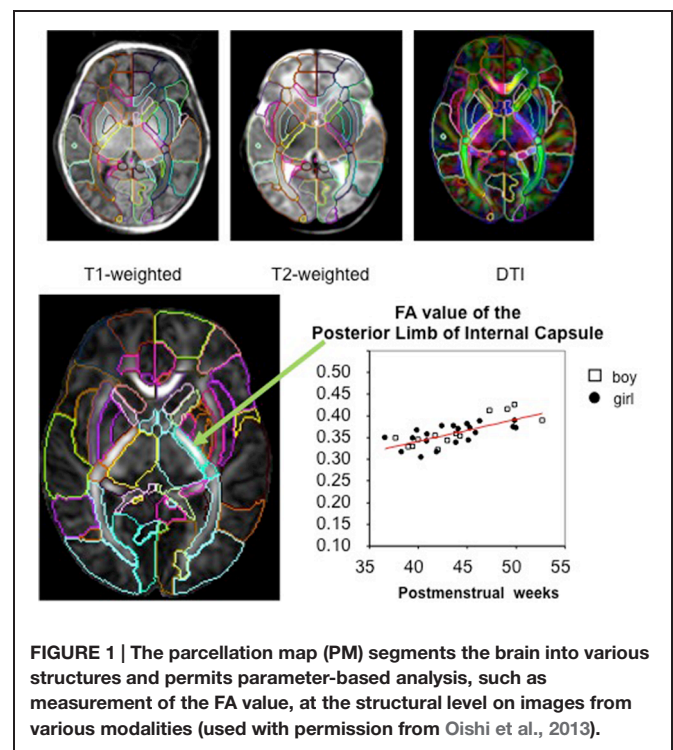
Diffusion tensor imaging (DTI) is a magnetic resonance imaging (MRI) modality that exploits the water diffusion (Brownian motion of water molecules) to compute a tensor, from which various parameters can be calculated. DTI has been developed and used in human brain research since the 1990s, and it still offers many useful features and advantages. DTI is capable of delineating three-dimensional white matter anatomy with high fidelity, and the parameters derived from DTI, such as

fractional anisotropy (FA), mean diffusivity (MD), axial diffusivity (AD), and radial diffusivity (RD), and can potentially indicate the axonal organization, degree of myelination, fiber coherence, and axonal density, which, altogether, can reflect the developmental status of the brain (Beaulieu, 2002; Huppi and Dubois, 2006). Among various MRI modalities based on water diffusion, DTI can be acquired in short scan times with relatively higher signal-to-noise ratio, which is advantageous in clinical studies or studies of babies and the pediatric population, because such short DTI scans minimize the potential motion that often occur during longer scans, which is particularly prevalent in individuals with illnesses or in infants and children.

Quantification of DTI and other modalities in general, is an important process that permits the introduction of statistical analysis. Various methods are used for the quantification of DTI, and the simplest approach is to place regions-of-interest (ROIs) on DTI to measure the parameters of selected anatomical structures. This approach is accordingly useful for hypothesis-testing research, because the ROIs are selected based on an *a priori* hypothesis, and the effect of a disease or condition on the selected ROIs can be investigated. However, this ROI-based approach is not suitable for investigations of anatomical areas where the effects of a disease or condition are initially unknown. For such studies, whole-brain analysis is the method of choice.

In whole-brain analysis, a template is often used as a target image and subject images are mathematically transformed in order to register the brain structures of each individual to those of the template space. The transformation of the image to the template is called “normalization.” Since each brain is different in terms of size, shape, and proportion, a template is necessary to normalize these features to perform a voxel-by-voxel analysis of the DTI parameters. After image normalization, comparison between groups of subjects (e.g., normal vs. diseased groups) or regression to non-image parameters (e.g., age, clinical status, or function) can be performed on a voxel-by-voxel basis, which is known as voxel-based analysis (VBA). In addition to the VBA, the “parcellation map,” (PM), a set of pre-defined anatomical boundaries of the template brain, is used for a parcel-by-parcel statistical analysis (Figure 1). Here, each parcel groups the voxels together to increase the signal-to-noise ratio by averaging signals inside the parcel, and to streamline the neuroscientific or clinical interpretation of the statistical results. Parcel-by-parcel statistical analysis is also applicable to analysis in the individual space. This can be achieved simply by transforming a PM from a template space onto individual images (Figure 2). Currently, there are more sophisticated variations, including a multi-atlas label fusion method (Tang et al., 2014).

This parcel-by-parcel analysis, either in a template space or individual space, is called “atlas-based analysis (ABA),” especially when a standard brain atlas, such as the MNI or ICBM atlas^{1,2}, with the corresponding PM, is used as the template. The use of a standard atlas is advantageous to facilitate communication and comparisons of brain imaging data among different institutions. There are various types of atlases and PMs,



as listed on the websites of the Oxford Center for Functional Magnetic Resonance Imaging of the Brain³, the Laboratory of Neuro Imaging⁴, the University of North Carolina Image Display, Enhancement, and Analysis Group⁵, the Athinoula A. Martinos Center for Biomedical Imaging, Laboratory for Computational Neuroimaging⁶, the Research Center Jülich, Institute of Neuroscience and Medicine⁷, or the Johns Hopkins Laboratory of Brain Anatomical MRI^{8,9}, which are used for different research applications. Various PMs accentuate the unique features of the brain, such as structural units, vascular territory, anatomical connectivity, functional connectivity, and cytoarchitecture. These diverse PMs allow researchers to examine the different ways neurological diseases can affect the brain.

The ABA has been applied to DTI of pediatric and adult populations to investigate normal neurodevelopment as well as the abnormalities caused by various diseases, such as cerebral palsy (Faria et al., 2010; Yoshida et al., 2013), Williams syndrome (Faria et al., 2012b), and Rett syndrome (Oishi et al., 2013). The successes of these researches have engendered the application of ABA to study neurodevelopment in earlier ages, especially in perinatal–neonatal brains. However, application of adult or pediatric brain atlases to neonatal brain research is not straightforward, because there are substantial differences

³<http://fsl.fmrib.ox.ac.uk/fsl/fslwiki/Atlases>

⁴<http://www.loni.usc.edu/atlas/>

⁵<http://www.med.unc.edu/bric/ideagroup/free-software>

⁶<http://martinos.org/lab/lcn/resources>

⁷<http://www.fz-juelich.de/inm/inm-1/EN/Home/>

⁸<http://cmrm.med.jhmi.edu>

⁹<http://www.mristudio.org>

¹<http://www.bic.mni.mcgill.ca/ServicesAtlases/HomePage>

²<http://www.loni.usc.edu/atlas/>

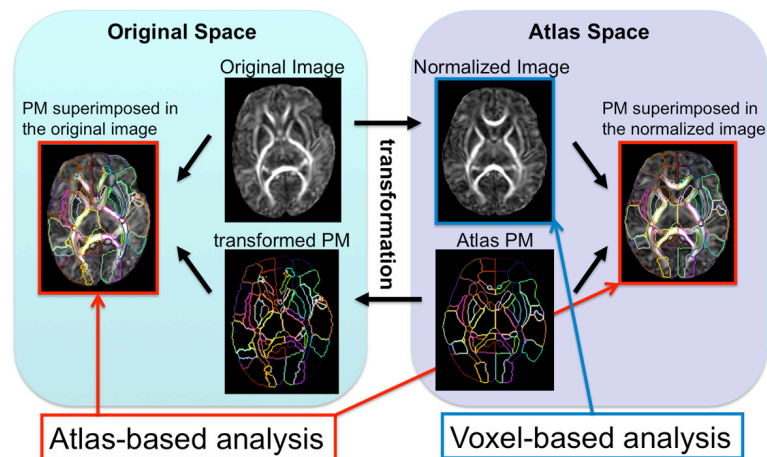


FIGURE 2 | The image transformation pipeline normalizes original subject images to the atlas space and reverse transforms the atlas's PM to apply back onto the subject image.

in cytoarchitecture and myelination between neonatal brains and older brains that can cause differences in DTI-derived contrasts (**Figure 3**). Therefore, DTI atlases with corresponding PMs specifically created for the neonatal brain are often used for ABA of the perinatal–neonatal population. Some of the various types of publicly available atlases and PMs that have been applied to neonatal DTI studies are summarized in **Table 1**.

In this review, currently available neonatal DTI atlases are introduced, along with studies that applied these atlases.

NEONATAL DTI ATLASES

The initial step for the ABA comprises the creation of a template (or a set of templates) and the corresponding PM. There are two types of template images: one in a study-specific space and one in the standardized coordinates. Study-specific templates retain the average features of the study population and are advantageous for accurate image normalization (Hamm et al., 2009; Tang et al., 2009; Klein et al., 2010; Fonov et al., 2011; Jia et al., 2011). However, standardized templates are particularly valuable when the specific brain regions will be compared across different studies.

Two studies are examples of pioneering work in study-specific DTI templates (Marc et al., 2010; Wang et al., 2012); both used an unbiased diffeomorphic atlas-building method based on a non-linear high-dimensional fluid deformation. Namely, they first created an initial FA template, which was intensity-histogram-normalized. Then, non-linear transformations were applied to the initial template to produce a deformation field for each image. All the tensor images were then reoriented into the unbiased space using the finite strain approximation. The atlas was then developed by averaging all the reoriented tensor images in log-Euclidean space. Once template is created and DTIs are normalized to the template space, Tract-Based Spatial Statistics (TBSS) has been widely used for the VBM, to

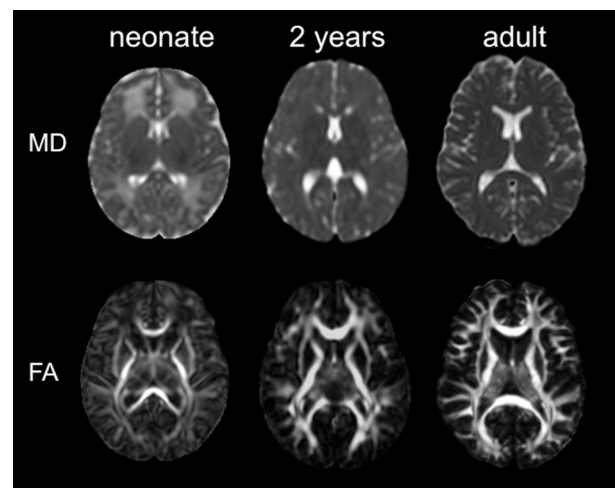


FIGURE 3 | The mean diffusivity (MD) map and the fractional anisotropy (FA) map of a neonate, a 2 years child, and an adult (used with permission from Oishi et al., 2013).

enhance sensitivity by focusing on the improved registration accuracy of the core white matter voxels. One TBSS approach was optimized for neonates by reducing registration errors through the identification of an appropriate single-subject FA map from the study population, followed by the creation of a study-specific FA map template (Ball et al., 2010).

After creating the template, the next step is to construct the corresponding PM. Producing a PM can be accomplished manually (Wang et al., 2012), but unless the PM covers the whole brain, the manually drawn PM is suitable only for the hypothesis-driven studies. One can also warp a whole-brain gray matter PM from a standard non-DTI template to the study-specific template, such as that employed using the University of North Carolina Chapel Hill neonatal atlas (Brown et al., 2014). This approach

TABLE 1 | Atlases applied to neonatal DTI studies.

Name of atlas	Description/parcellation map (PM) availability	Contrasts	Age range	Reference
University of North Carolina-Chapel Hill Brain Atlas	Atlas components include intensity models, tissue probability maps. Uses an anatomical PM	T1w and T2w	Neonates, 1 years, and 2 years	Brown et al., 2014
4D Imperial College London Neonatal Brain Atlas	Dynamic, probabilistic atlas for stages (29–44 weeks gestational age) in neonatal brain development	T1w and T2w	Neonate	Brown et al., 2014
JHU-MNI Single-Subject Brain Atlas (Eve Atlas)	Provides co-registered T1, T2, and DTI images from a single subject. Uses a white and gray matter anatomical PM	T1w, T2w, and DTI	Adult	Djamanakova et al., 2014 Faria et al., 2010 Geng et al., 2012 Melbourne et al., 2014 Tang et al., 2014
ICBM DTI-81 Brain Atlas	Stereotaxic and probabilistic white matter atlas integrating DTI-based data with ICBM 152 template. Uses a white matter anatomical PM	DTI	Adult	Fonov et al., 2011 Klein et al., 2010 Miller et al., 2013 Oishi et al., 2011a Oishi et al., 2009
JHU Neonatal Brain Atlas	Group averaged and single subject brain atlas of the neonatal brain that integrates DTI-data with co-registered anatomical MRI. Uses a white and gray matter anatomical PM	T1w, T2w, and DTI	Neonate	Oishi et al., 2011b Pannek et al., 2013 Ratnarajah et al., 2013 Rose et al., 2014a Rose et al., 2014b Kersbergen et al., 2014 Zhang et al., 2014

was effective for the analysis of anatomical connectivity among cortical structures; however, since the white matter structures were not fully parcellated, structure-by-structure analysis of the white matter was outside the focus of that study. For such studies, whole-brain PM, including white matter structures, is required. Nevertheless, generating a whole-brain PM for a study-specific DTI template is laborious and time-consuming, as it needs to cover the entire brain three-dimensionally, and manual drawing requires professional anatomical knowledge.

Using a standard template and the corresponding PM is beneficial for DTI studies, because the white matter area, which looks homogeneous on conventional T1- and T2-weighted images, can be parcellated into numerous fiber bundles (**Figure 4**). In addition, since defining anatomical boundaries is often ambiguous, using a standard PM can increase reproducibility in defining anatomical regions. Templates from the Montreal Neurological Institute (MNI) and the International Consortium of Brain Mapping¹⁰ (ICBM) have long been used as the standard template for adult brain images. PMs from these templates are well-developed and can be applied as a tool for ABA.

Creating the ICBM atlas and the single-subject atlas follows a protocol that is highlighted by the alignment of the anterior commissure–posterior commissure (AC-PC) line. Using similar steps, a set of neonatal DTI atlases was constructed with co-registered T1- and T2-weighted atlases (Oishi et al.,

2011b). The set included the Johns Hopkins University neonate linear (JHU-neonate-linear), non-linear (JHU-neonate-non-linear), and single-subject (JHU-neonate-SS) atlases¹¹. The JHU-neonate-linear and the JHU-neonate-non-linear atlases are group-averaged images based on co-registered T1- and T2- weighted DTI images acquired from normal term-born neonates. The JHU-neonate-linear was created using only linear transformations, such as rotation, translation, scaling, and shear, among the component images. The large deformation diffeomorphic metric mapping (LDDMM; Ceritoglu et al., 2009) was used to create the JHU-neonate-non-linear atlas. The JHU-neonate-SS atlas was created from a representative single-individual image with the shape and size adjusted to represent population-averaged features. The associated PMs include both gray and white matter structures that cover the entire neonatal brain.

The possible drawback of using standard templates is that they may not necessarily represent the average anatomical features of the study population, although, for DTI without visible abnormalities, the study-specific template and the standardized template resulted in similar normalization accuracy, as demonstrated by (Zhang and Arfanakis, 2013). However, when the template is applied to a population with specific diseases, which typically demonstrates local alterations in volume and shape, the accuracy in image normalization is usually lower than when a study-specific template is applied. An attempt

¹⁰<http://www.loni.usc.edu/atlas/>

¹¹<http://cmrm.med.jhmi.edu>

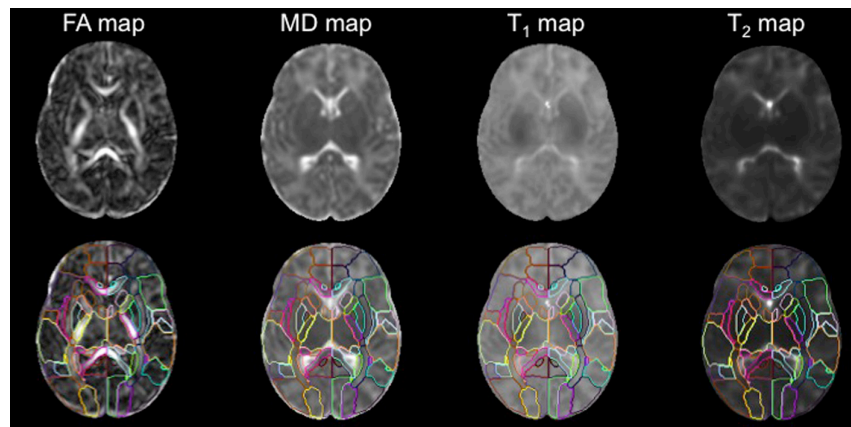


FIGURE 4 | The DTI, T1, and T2 maps were transformed from the subject space to the atlas space via co-registration and normalization. The application of the PM permits analysis of FA, MD, T1, and T2 values at the structural level (used with permission from Oishi et al., 2011b).

to overcome this limitation is the Volume-based Template Estimation (VTE) method (Zhang et al., 2014). VTE enables iterative modifications of the standard atlas toward the average of the study population to create a template and a PM that are customized for the study. This method can increase the accuracy of image normalization, especially in the cortical area of neonatal brains, while the boundary definitions of the PM are maintained at those of the JHU-neonate-SS atlas.

APPLICATION OF NEONATAL ATLASES

The neonatal atlas has been applied to perform ABA on neonatal brains. It has been used to measure parameters derived from DTI and to investigate connectivity among brain regions. Such applications demonstrate the potential utility of quantitative tools in neurodevelopmental assessments.

ANALYSIS OF DTI-DERIVED PARAMETERS

Brain Development

To examine developmental changes of the neonatal brain with age, the JHU-neonate-SS atlas was applied to full-term healthy neonates at 37–53 post-conception weeks (Oishi et al., 2011b, 2013). A multimodality approach that consists of DTI, T1-, and T2-maps was adopted to assess the microstructural development of 122 anatomical structures determined by the PM. Increases in FA and decreases in diffusivity, T1, and T2 with age were generally observed, congruent with the histopathological evidence of ongoing myelination and axonal development during this age-range that occurs in the posterior-to-anterior and central-to-peripheral directions (Kinney et al., 1988). Following this healthy neonatal DTI study, Rose et al. (2014a) examined whether these specific directions of brain maturation could be seen in very-low-birth-weight neonates as well. Sixty-six such neonates with no evidence of congenital brain abnormalities

successfully underwent DTI scans and the JHU-neonate-SS atlas was used for the quantification. The posterior-to-anterior and central-to-peripheral pattern was again observed, especially in the corona radiata, corpus callosum, and internal capsule. Within projection and association fibers, centrally located fibers, such as the cerebellar peduncles and the posterior limb of the internal capsule, were also observed with greater FA values than those in peripheral areas, such as the superior longitudinal fasciculus or the external capsule. These studies demonstrated the possibility of creating a standardized growth percentile chart of brain development based on MRI- and DTI-derived parameters via ABA. However, since the study design was cross-sectional, information about intra-individual changes in MRI- or DTI-derived parameters was not provided.

To overcome the limitation of cross-sectional analysis, longitudinal design was adopted to investigate developmental changes during 30 to 40 post-conceptional weeks (Kersbergen et al., 2014). The JHU-neonate-SS atlas was used for the ABA to quantify FA and diffusivity measures from 40 preterm neonates without brain injury and with normal developmental outcome at 15 months of age. FA was found to have increased in 84 brain regions, most significantly in the posterior limb of the internal capsule, the cerebral peduncles, the sagittal stratum, the corona radiata, and other central structures. Conversely, FA values decreased most in the temporal and occipital cortical regions, while MD, AD, and RD values decreased in most brain regions.

Genetic Effects

To assess how influential genetic and environmental factors could be on WM microstructure in neonates, Geng et al. (2012) analyzed the heritability of WM microstructures evaluated by DTI in healthy full-term neonate twins. The JHU-DTI-MNI (a.k.a. “Eve”) atlas (Oishi et al., 2009) with the PM was adjusted to the study-specific template to perform ABA of 98 anatomical structures in 173 neonates; 63 twin sets, and 47 unpaired twins were included. To assess the genetic and environmental effects

on the DTI-derived parameters of each structure, a univariate twin modeling approach was applied (Neale and Cardon, 1992). Namely, effects of additive genetic factors and environment, shared or unshared by twin pairs, were modeled and fitted to test the significance of each effect on DTI measures. The results indicated that structures with high FA and low RD, which might be associated with high maturation at the time of the DTI scan, tended to show less influence of genetic effects on DTI than that of other structures. For example, the genetic contribution to the FA of right posterior limb of the internal capsule was 0.00, while the contribution of common environmental factors was 0.50. The study suggests that the strength of the genetic effect depends on the regional maturation status of the neonatal brain.

Population Differences

To investigate differences in neuroanatomical features among ethnic groups, Bai et al. (2012), quantified brain size, morphology, and DTI parameters of Malay, Chinese, and Indian neonates. The JHU-neonate-SS was iteratively transformed to construct a study-customized atlas to evaluate 177 neonates. Indian neonates had more elongated brains despite similar brain volume among the three ethnicities. Compared to Indian neonates, the Malay neonates had lower FAs in the left anterior limb of the internal capsule, the left thalamus, the anterior corpus callosum, and the left midbrain, while the Chinese neonates had only lower FA in the anterior part of the corpus callosum. These results suggest that ethnicities should be considered when performing a statistical comparison of the DTI-derived parameters among groups.

Effects of Prematurity and Related Risk Factors

Prematurity is one amongst a host of perinatal stressors that is known to adversely affect neurological development in neonates. Preterm birth is also related to the occurrence of other risk factors that might affect brain development. Therefore, it is important to investigate the respective contributions of prematurity and other risk factors to explain developmental alterations that occur in babies born preterm. The effects of other medical factors, including bronchopulmonary dysplasia, retinopathy of prematurity, necrotizing enterocolitis, sepsis, and serum levels of C-reactive protein, albumin, glucose, and bilirubin, were studied (Rose et al., 2014b). The JHU-neonate-SS atlas was used for the ABA on a cohort of 66 very-low-birth-weight preterm infants who underwent DTI scans at a term-equivalent age. Among anatomical structures, the posterior thalamus MD was associated with lower gestational age at birth and lower levels of albumin and bilirubin. These findings imply that the thalamus may be a structure vulnerable to prematurity and accompanying risk factors. However, interactions among brain abnormality, prematurity, and risk factors still need to be demonstrated.

Effect of *In Utero* Exposure to Stimulants

To investigate the effects of prenatal exposure to stimulants, such as methamphetamine or nicotine, DTI scans were acquired

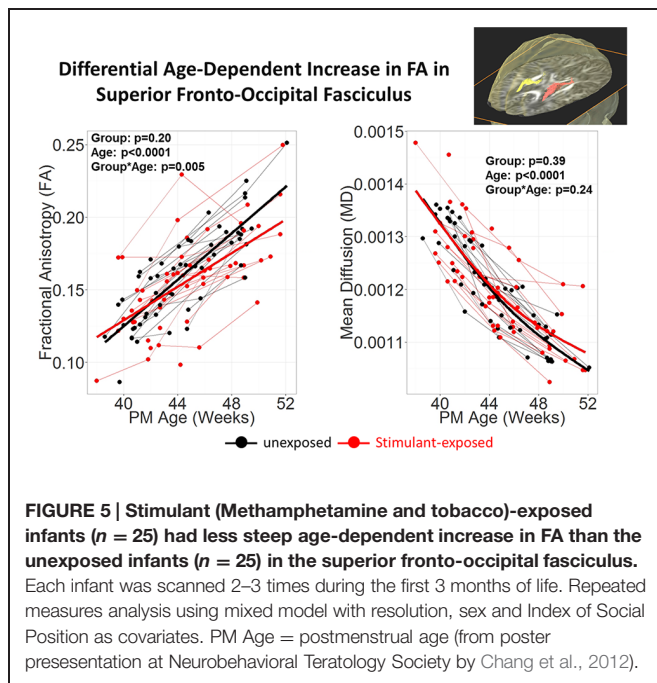
longitudinally from babies who were prenatally exposed to stimulants, and the results were compared to those from babies without any prenatal stimulant exposure (Chang et al., 2012). The JHU-neonate-SS atlas was applied for the ABA to quantify the FA, MD, AD, and RD of each structure. Although conventional T1- and T2- weighted images of these babies were normal appearing, the age-related increase in FA tended to be lower in stimulant-exposed infants, especially in the superior fronto-occipital fasciculus (**Figure 5**), which suggests a slower rate or delayed myelination in stimulant-exposed babies. This indicated the potential for ABA to detect anatomical alterations related to stimulant exposure, although relationships between detected anatomical alterations and later neurological, behavioral, and cognitive functional outcomes need to be elucidated.

ANALYSIS OF BRAIN CONNECTIVITY

Diffusion tensor imaging, analyzed with graph theory, is useful in non-invasively mapping and assessing neural networks (connectome) of the brain in adults (for review, Lo et al., 2011; Griffa et al., 2013). Brain atlases and the PMs are often used to parcellate the brain into local areas that serve as the network nodes (de Reus and van den Heuvel, 2013; O'Donnell et al., 2013). Although the application to investigate developmental changes is still challenging (for review, Tymofiyeva et al., 2014), an increasing number of studies are investigating connectomes of neonatal brains, some of which are introduced below.

Asymmetrical Neural Network Development

The human brain is structurally asymmetrical, a feature that reflects its diverse, specialized functions. However, it has not been well-established whether such asymmetries can be traced back to the perinatal period. This was one of the aims in a study (Ratnarajah et al., 2013) that acquired DTI in 124 healthy, full-term neonates, and the FA maps were transformed to the JHU-neonate-SS atlas for the image parcellation. For whole-brain tractography, the fiber-assignment by continuous tracking (FACT) algorithm (Mori et al., 1999) was used to compute the fiber trajectories that connect between parcels. In order to characterize the brain, the fibers were analyzed for small-worldness, type of efficiency (global or local), and betweenness-centrality. Small-worldness defines a network wherein any two nodes are not necessarily neighbors, but are relatively well-connected (Watts and Strogatz, 1998). Global efficiency describes how efficiently information can pass through the network (Latora and Marchiori, 2001). Local efficiency indicates how well information can be exchanged in a local neighborhood, or subnetwork (Rubinov and Sporns, 2010). Betweenness-centrality is a statistic that identifies the most central nodes of a network (Freeman, 1978). These values were used altogether to calculate a lateralization index (LI), a proxy for brain asymmetry. The analysis on connectivity revealed that, in neonates, both cerebral hemispheres exhibited small-world characteristics, and that the LI was higher in the left hemisphere. This suggested that the left hemisphere of neonates was better equipped to balance



local necessities and wide-range interactions. Furthermore, the study insinuates that the neonatal brain favors a local flow of information and seeks to reduce the number of long-distance connections. This small-world preference of the neonatal brain has also been observed in the brains of adults (Gong et al., 2009), which suggests that the brain provides an efficient network from birth. In addition, LI values indicate a significantly leftward tendency in the precentral gyrus, the precuneus fusiform, the entorhinal cortex, and the insular cortex, and, likewise, a rightward tendency in the gyrus rectus, the cingulate gyrus, the hippocampus, and the putamen. Such LI values indicated that those structures communicated more efficiently in their respective hemispheres, demonstrating a betweenness-centrality asymmetry in the neural network. These results suggest that the brain already exhibits asymmetry at birth.

Effect of Prematurity at Birth

The effect of prematurity was also examined from a network-based perspective (Pannek et al., 2013). To investigate the effect of prematurity, cortico-cortical connections in 18 preterm and nine full-term babies were compared. The JHU-neonate non-linear atlas was used as an initial template to create a study-specific FA map upon which the structural PM could be applied, and to define 24 cortical regions as nodes for connectivity analysis. Network-based statistical analysis was then performed to compare DTI-derived measurements (FA and MD) and T2 values between the cohorts. In all, 433 connections were analyzed. FA was lower in preterm neonates than in full-term controls in a network of nodes whose central nodes were the superior temporal lobe, the left fusiform gyrus, and a network of connections between the frontal and motor nodes. MD was found to be higher for preterm infants in a majority of the connections, leading to a global elevation of diffusivity. T2 was higher in the preterm

group in a network that included the left superior frontal lobe, the left cingulate gyrus, and the right precuneus. Although there were no correlations between gestational age at birth and DTI-derived measurements, a negative correlation between T2 and gestational age at birth was identified in a network that included the bilateral precuneus, the left lateral orbito-frontal gyrus, the left middle temporal gyrus, the left superior temporal gyrus, and left lingual gyrus. This study demonstrated the possible influence of prematurity on brain microstructure, as assessed by DTI and T2, as well as the utility of multimodal analyses to detect different developmental processes in the neonatal brain.

Relationship between White Matter Connections and the Cortical Folding Patterns

The cortex has developed over evolutionary time an exquisitely complex folding pattern, which is unique to the human brain. The role and nature of cortical folding still remains controversial, although the folding of the brain was hypothesized as a natural consequence of connectivity to subcortical areas (Van Essen, 1997). To investigate correlations between white matter connections and the cortical folding pattern, one study quantified the amount of cortical connectivity through tractography and the local cortical folding patterns through ABA of the gyrification index, as well as the sulcation ratio using the JHU-neonate atlas (Melbourne et al., 2014). The white matter connectivity correlated specifically with the sulcation ratio of the overlying cortex, suggesting that the gyrification pattern represents the development of the underlying white matter. As demonstrated, the ABA is especially useful for the integration of information from multiple modalities.

FUTURE OF NEONATAL DTI ATLAS

Multi-atlas-based Structural Parcellation

Conventional ABA methods usually utilize a single atlas. However, the limitation of a single-atlas approach is that the template does not necessarily represent the features of a study population. The possibility of voxel mismatch due to differences in contrast and morphology between the subject image and the template image is a factor that can contribute to inaccuracy in the parcellation. In order to overcome this limitation, a multi-atlas label fusion method has been developed and applied to adult brain images. In this approach, multiple atlases with different anatomical features are transformed to the target image, and the anatomical labels based on the transformed PMs are fused to define a target-specific PM. Studies have been performed to assess the accuracy of parcellations via multiple atlas fusion protocols, and have reported higher accuracy than single-atlas methods in the adult and pediatric populations (Heckemann et al., 2006; Aljabar et al., 2009; Tang et al., 2013, 2014). Such successes encourage the application of such methods to the neonatal population and to create accurate PM for each brain.

Multi-modal Analysis

A multi-modal approach rather than a single-modality approach has been shown to be superior in detecting abnormalities related to neurological diseases (Allder et al., 2003; Brockmann et al., 2003; Rostasy et al., 2003; Kauczor, 2005; Wiest et al., 2005; Oishi et al., 2011a). Typically, the different modalities complement each other, and, together, can permit more detailed interpretation of the brain. However, one of the biggest challenges for multi-modal analysis is to establish a common anatomical framework that can integrate intra-subject as well as cross-subject multi-modal imaging data, which would enable structure-by-structure, location-dependent statistical analysis. ABA is suitable for such a multi-modal approach because it can be applied to serve as the common anatomical framework (Oishi et al., 2011b, 2013; Faria et al., 2012a). The application of a multi-modal approach to the neonatal population is anticipated, as it can enhance the information available to describe the variety of anatomical features seen in neonatal brains.

Multiple PMs and Multiple Granularity Analysis

The application of a predefined single PM has several limitations, the most important of which, perhaps, is that there are multiple criteria that can be used to define structures. For instance, when using a PM to detect pathological changes related to a specific disease, the ideal PM should define the brain structures or areas vulnerable to the disease. In diseases that affect the vasculature of the brain, a PM that is based on vascular territories might be able to quantify changes with higher sensitivity than an ontology-based brain parcellation. Application of multiple PMs with different criteria enables reasonable extraction of anatomical features. Moreover, in order to detect changes related to diseases that cause widespread pathology of the brain, a PM with lower granularity can detect such changes with higher sensitivity than a PM with higher granularity. However, a PM with higher granularity is suitable for the detection of focal changes. To extract anatomical features of various diseases, a multiple granularity approach was developed (Djamanakova et al., 2014) that can flexibly change the granularity level of the PM based on the hierarchical relationships of 254 structures (parcels) defined in the JHU-MNI-SS atlas (Oishi et al., 2009). In this multiple granularity approach, the 254 structures were dynamically combined at five different hierarchical levels, down to 11 structures, to provide a flexible view from which to extract the anatomical features of the brain. This approach is also anticipated for neonatal image analysis since various diseases can cause either widespread changes (e.g., leukodystrophies or metabolic diseases) or focal changes (e.g., focal cortical dysplasia).

High-throughput Analysis

The ABA is an ideal method for use in the emergent big-data analysis because it can quantify and extract relevant information from medical images. The PM could compress raw images (usually more than 100 MB pixels each) into a

manageable size (~200 structural units each) in an interpretable way. High-throughput analysis is advantageous because of its potential to efficiently analyze the large amounts of imaging data using machine-learning and supervised clustering algorithms. There is also the possibility of integrating non-image related parameters. Research in the emerging field of neuroinformatics seeks to incorporate all of these data, such as those constructed in a pipeline to evaluate neuropsychiatric disorders (Miller et al., 2013) or for normal neurodevelopment in typically developing children (Jernigan et al., 2015). Particularly for the neonatal studies, in which early prediction of the later neurological, psychological, and cognitive outcomes is the desired goal, big-data analysis is essential since multiple factors, from genetics to environment, might affect the result and all of these factors need to be incorporated into the analysis.

Clinical Applications

Atlas-based analysis has the potential to enhance the usefulness of DTI as a modality with which to predict neurological and psychiatric outcomes. However, scientific success does not necessarily guarantee clinical success. Contrary to research MRIs, clinical MRIs contain artifactual heterogeneity, which comprises variations in scan protocol and hardware performance (Back and Miller, 2014). Consequently, the image quality is usually not as stable as that of research MRIs. Moreover, there is biological heterogeneity, which comprises variations of demographics and co-morbidities, as opposed to the homogeneous research population selected through strict inclusion and exclusion criteria. In general, heterogeneity in clinical practice is one of the major causes of failure in the clinical application of scientific discovery. Extending the ABA to test its robustness in clinical scenarios, especially with age and sex-appropriate age-related growth curves for the individual brain regions, is required in the future, and is a future direction of DTI research in general.

CONCLUSION

Atlas-based analysis has shown great potential for the study of neurodevelopmental patterns in normal and abnormal cohorts in the pediatric and adult populations. Currently, DTI studies incorporating ABA to study the neonatal population has demonstrated its utility in assessing neurodevelopmental progress. Further studies are needed to overcome the current limitations of ABA and incorporate it into high-throughput analyses, with the ultimate goal of application to the clinical setting.

ACKNOWLEDGMENTS

This study was supported by NIH grant R01-HD065955 (KO) and K24-DA016170 (LC). Its contents are solely the responsibility of the authors and do not necessarily represent the official view of NICHD, NIDA, or NIH.

REFERENCES

- Aljabar, P., Heckemann, R. A., Hammers, A., Hajnal, J. V., and Rueckert, D. (2009). Multi-atlas based segmentation of brain images: atlas selection and its effect on accuracy. *Neuroimage* 46, 726–738. doi: 10.1016/j.neuroimage.2009.02.018
- Allder, S. J., Moody, A. R., Martel, A. L., Morgan, P. S., Delay, G. S., Gladman, J. R., et al. (2003). Differences in the diagnostic accuracy of acute stroke clinical subtypes defined by multimodal magnetic resonance imaging. *J. Neurol. Neurosurg. Psychiatry* 74, 886–888. doi: 10.1136/jnnp.74.7.886
- Back, S. A., and Miller, S. P. (2014). Brain injury in premature neonates: a primary cerebral dysmaturation disorder? *Ann. Neurol.* 75, 469–486. doi: 10.1002/ana.24132
- Bai, J., Abdul-Rahman, M. F., Rifkin-Graboi, A., Chong, Y. S., Kwek, K., Saw, S. M., et al. (2012). Population differences in brain morphology and microstructure among Chinese, Malay, and Indian neonates. *PLoS ONE* 7:e47816. doi: 10.1371/journal.pone.0047816
- Ball, G., Counsell, S. J., Anjari, M., Merchant, N., Arichi, T., Doria, V., et al. (2010). An optimised tract-based spatial statistics protocol for neonates: applications to prematurity and chronic lung disease. *Neuroimage* 53, 94–102. doi: 10.1016/j.neuroimage.2010.05.055
- Beaulieu, C. (2002). The basis of anisotropic water diffusion in the nervous system - a technical review. *NMR Biomed.* 15, 435–455. doi: 10.1002/nbm.782
- Brockmann, K., Dechent, P., Wilken, B., Rusch, O., Frahm, J., and Hanefeld, F. (2003). Proton MRS profile of cerebral metabolic abnormalities in Krabbe disease. *Neurology* 60, 819–825. doi: 10.1212/01.WNL.0000049469.29011.E9
- Brown, C. J., Miller, S. P., Booth, B. G., Andrews, S., Chau, V., Poskitt, K. J., et al. (2014). Structural network analysis of brain development in young preterm neonates. *Neuroimage* 101, 667–680. doi: 10.1016/j.neuroimage.2014.07.030
- Ceritoglu, C., Oishi, K., Li, X., Chou, M. C., Younes, L., Albert, M., et al. (2009). Multi-contrast large deformation diffeomorphic metric mapping for diffusion tensor imaging. *Neuroimage* 47, 618–627. doi: 10.1016/j.neuroimage.2009.04.057
- Chang, L., Cloak, C., Buchthal, S., Wright, T., Jiang, C., Oishi, K., et al. (2012). Brain imaging in children prenatally exposed to methamphetamine. *Neurotoxicol. Teratol.* 34, 376. doi: 10.1016/j.ntt.2012.05.026
- de Reus, M. A., and van den Heuvel, M. P. (2013). The parcellation-based connectome: limitations and extensions. *Neuroimage* 80, 397–404. doi: 10.1016/j.neuroimage.2013.03.053
- Djavanakova, A., Tang, X., Li, X., Faria, A. V., Ceritoglu, C., Oishi, K., et al. (2014). Tools for multiple granularity analysis of brain MRI data for individualized image analysis. *Neuroimage* 101, 168–176. doi: 10.1016/j.neuroimage.2014.06.046
- Faria, A. V., Joel, S. E., Zhang, Y., Oishi, K., Van Zijl, P. C., Miller, M. I., et al. (2012a). Atlas-based analysis of resting-state functional connectivity: evaluation for reproducibility and multi-modal anatomy-function correlation studies. *Neuroimage* 61, 613–621. doi: 10.1016/j.neuroimage.2012.03.078
- Faria, A. V., Landau, B., O'hearn, K. M., Li, X., Jiang, H., Oishi, K., et al. (2012b). Quantitative analysis of gray and white matter in Williams syndrome. *Neuroreport* 23, 283–289. doi: 10.1097/WNR.0b013e3283505b62
- Faria, A. V., Zhang, J., Oishi, K., Li, X., Jiang, H., Akhter, K., et al. (2010). Atlas-based analysis of neurodevelopment from infancy to adulthood using diffusion tensor imaging and applications for automated abnormality detection. *Neuroimage* 52, 415–428. doi: 10.1016/j.neuroimage.2010.04.238
- Fonov, V., Evans, A. C., Botteron, K., Almli, C. R., Mckinstry, R. C., Collins, D. L., et al. (2011). Unbiased average age-appropriate atlases for pediatric studies. *Neuroimage* 54, 313–327. doi: 10.1016/j.neuroimage.2010.07.033
- Freeman, L. C. (1978). Central in social networks: conceptual clarification. *Social Netw.* 1, 215–239. doi: 10.1016/0378-8733(78)90021-7
- Geng, X., Prom-Wormley, E. C., Perez, J., Kubarych, T., Styner, M., Lin, W., et al. (2012). White matter heritability using diffusion tensor imaging in neonatal brains. *Twin Res. Hum. Genet.* 15, 336–350. doi: 10.1017/thg.2012.14
- Gong, G., He, Y., Concha, L., Lebel, C., Gross, D. W., Evans, A. C., et al. (2009). Mapping anatomical connectivity patterns of human cerebral cortex using in vivo diffusion tensor imaging tractography. *Cereb. Cortex* 19, 524–536. doi: 10.1093/cercor/bhn102
- Griffa, A., Baumann, P. S., Thiran, J. P., and Hagmann, P. (2013). Structural connectomics in brain diseases. *Neuroimage* 80, 515–526. doi: 10.1016/j.neuroimage.2013.04.056
- Hamm, J., Davatzikos, C., and Verma, R. (2009). Efficient large deformation registration via geodesics on a learned manifold of images. *Med. Image Comput. Comput. Assist. Interv.* 12, 680–687.
- Heckemann, R. A., Hajnal, J. V., Aljabar, P., Rueckert, D., and Hammers, A. (2006). Automatic anatomical brain MRI segmentation combining label propagation and decision fusion. *Neuroimage* 33, 115–126. doi: 10.1016/j.neuroimage.2006.05.061
- Huppi, P. S., and Dubois, J. (2006). Diffusion tensor imaging of brain development. *Semin. Fetal Neonatal Med.* 11, 489–497. doi: 10.1016/j.siny.2006.07.006
- Jernigan, T. L., Brown, T. T., Hagler, D. J. Jr., Akshoomoff, N., Bartsch, H., Newman, E., et al. (2015). The Pediatric Imaging, Neurocognition, and Genetics (PING) Data Repository. *Neuroimage* doi: 10.1016/j.neuroimage.2015.04.057 [Epub ahead of print].
- Jia, H., Yap, P. T., Wu, G., Wang, Q., and Shen, D. (2011). Intermediate templates guided groupwise registration of diffusion tensor images. *Neuroimage* 54, 928–939. doi: 10.1016/j.neuroimage.2010.09.019
- Kauczor, H. U. (2005). Multimodal imaging and computer assisted diagnosis for functional tumour characterisation. *Cancer Imaging* 5, 46–50. doi: 10.1102/1470-7330.2005.0013
- Kersbergen, K. J., Leemans, A., Groenendaal, F., Van Der Aa, N. E., Viergever, M. A., De Vries, L. S., et al. (2014). Microstructural brain development between 30 and 40 weeks corrected age in a longitudinal cohort of extremely preterm infants. *Neuroimage* 103, 214–224. doi: 10.1016/j.neuroimage.2014.09.039
- Kinney, H. C., Brody, B. A., Kloman, A. S., and Gilles, F. H. (1988). Sequence of central nervous system myelination in human infancy. II. Patterns of myelination in autopsied infants. *J. Neuropathol. Exp. Neurol.* 47, 217–234. doi: 10.1097/00005072-198805000-00003
- Klein, J. C., Rushworth, M. F., Behrens, T. E., Mackay, C. E., De Crespigny, A. J., D'arceuil, H., et al. (2010). Topography of connections between human prefrontal cortex and mediodorsal thalamus studied with diffusion tractography. *Neuroimage* 51, 555–564. doi: 10.1016/j.neuroimage.2010.02.062
- Latora, V., and Marchiori, M. (2001). Efficient behavior of small-world networks. *Phys. Rev. Lett.* 87, 198701. doi: 10.1103/PhysRevLett.87.198701
- Lo, C. Y., He, Y., and Lin, C. P. (2011). Graph theoretical analysis of human brain structural networks. *Rev. Neurosci.* 22, 551–563. doi: 10.1515/RNS.2011.039
- Marc, C., Vachet, C., Gerig, G., Blocher, J., Gilmore, J., and Styner, M. (2010). Changes of MR and DTI appearance in early human brain development. *Proc. SPIE Int. Soc. Opt. Eng.* 7623. doi: 10.1117/12.844912
- Melbourne, A., Kendall, G. S., Cardoso, M. J., Gunny, R., Robertson, N. J., Marlow, N., et al. (2014). Preterm birth affects the developmental synergy between cortical folding and cortical connectivity observed on multimodal MRI. *Neuroimage* 89, 23–34. doi: 10.1016/j.neuroimage.2013.11.048
- Miller, M. I., Faria, A. V., Oishi, K., and Mori, S. (2013). High-throughput neuroimaging informatics. *Front. Neuroinform.* 7:31. doi: 10.3389/fninf.2013.00031
- Mori, S., Crain, B. J., Chacko, V. P., and Van Zijl, P. C. (1999). Three-dimensional tracking of axonal projections in the brain by magnetic resonance imaging. *Ann. Neurol.* 45, 265–269. doi: 10.1002/1531-8249(199902)45:2<265::AID-ANA21>3.0.CO;2-3
- Neale, M. C., and Cardon, L. R. (1992). *Methodology for Genetic Studies of Twins and Families*. Dordrecht: Kluwer Academic Publishers.
- O'Donnell, L. J., Golby, A. J., and Westin, C. F. (2013). Fiber clustering versus the parcellation-based connectome. *Neuroimage* 80, 283–289. doi: 10.1016/j.neuroimage.2013.04.066
- Oishi, K., Akhter, K., Mielke, M., Ceritoglu, C., Zhang, J., Jiang, H., et al. (2011a). Multi-modal MRI analysis with disease-specific spatial filtering: initial testing to predict mild cognitive impairment patients who convert to Alzheimer's disease. *Front. Neurol.* 2:54. doi: 10.3389/fneur.2011.00054
- Oishi, K., Mori, S., Donohue, P. K., Ernst, T., Anderson, L., Buchthal, S., et al. (2011b). Multi-contrast human neonatal brain atlas: application to normal neonate development analysis. *Neuroimage* 56, 8–20. doi: 10.1016/j.neuroimage.2011.01.051
- Oishi, K., Faria, A., Jiang, H., Li, X., Akhter, K., Zhang, J., et al. (2009). Atlas-based whole brain white matter analysis using large deformation diffeomorphic

- metric mapping: application to normal elderly and Alzheimer's disease participants. *Neuroimage* 46, 486–499. doi: 10.1016/j.neuroimage.2009.01.002
- Oishi, K., Faria, A. V., Yoshida, S., Chang, L., and Mori, S. (2013). Quantitative evaluation of brain development using anatomical MRI and diffusion tensor imaging. *Int. J. Dev. Neurosci.* 31, 512–524. doi: 10.1016/j.ijdevneu.2013.06.004
- Pannek, K., Hatzigeorgiou, X., Colditz, P. B., and Rose, S. (2013). Assessment of structural connectivity in the preterm brain at term equivalent age using diffusion MRI and T2 relaxometry: a network-based analysis. *PLoS ONE* 8:e68593. doi: 10.1371/journal.pone.0068593
- Ratnarajah, N., Rifkin-Graboi, A., Fortier, M. V., Chong, Y. S., Kwek, K., Saw, S. M., et al. (2013). Structural connectivity asymmetry in the neonatal brain. *Neuroimage* 75, 187–194. doi: 10.1016/j.neuroimage.2013.02.052
- Rose, J., Vassar, R., Cahill-Rowley, K., Guzman, X. S., Stevenson, D. K., and Barnea-Goraly, N. (2014a). Brain microstructural development at near-term age in very-low-birth-weight preterm infants: an atlas-based diffusion imaging study. *Neuroimage* 86, 244–256. doi: 10.1016/j.neuroimage.2013.09.053
- Rose, J., Vassar, R., Cahill-Rowley, K., Stecher Guzman, X., Hintz, S. R., Stevenson, D. K., et al. (2014b). Neonatal physiological correlates of near-term brain development on MRI and DTI in very-low-birth-weight preterm infants. *Neuroimage Clin.* 5, 169–177. doi: 10.1016/j.nicl.2014.05.013
- Rostasy, K. M., Diepold, K., Buckard, J., Brockmann, K., Wilken, B., and Hanefeld, F. (2003). Progressive muscle weakness after high-dose steroids in two children with CIDP. *Pediatr. Neurol.* 29, 236–238. doi: 10.1016/S0887-8994(03)00222-4
- Rubinov, M., and Sporns, O. (2010). Complex network measures of brain connectivity: uses and interpretations. *Neuroimage* 52, 1059–1069. doi: 10.1016/j.neuroimage.2009.10.003
- Tang, S., Fan, Y., Wu, G., Kim, M., and Shen, D. (2009). RABBIT: rapid alignment of brains by building intermediate templates. *Neuroimage* 47, 1277–1287. doi: 10.1016/j.neuroimage.2009.02.043
- Tang, X., Oishi, K., Faria, A. V., Hillis, A. E., Albert, M. S., Mori, S., et al. (2013). Bayesian parameter estimation and segmentation in the Multi-Atlas Random Orbit Model. *PLoS ONE* 8:e65591. doi: 10.1371/journal.pone.0065591
- Tang, X., Yoshida, S., Hsu, J., Huisman, T. A., Faria, A. V., Oishi, K., et al. (2014). Multi-contrast multi-atlas parcellation of diffusion tensor imaging of the human brain. *PLoS ONE* 9:e96985. doi: 10.1371/journal.pone.0096985
- Tymofiyeva, O., Hess, C. P., Xu, D., and Barkovich, A. J. (2014). Structural MRI connectome in development: challenges of the changing brain. *Br. J. Radiol.* 87, 20140086. doi: 10.1259/bjr.20140086
- Van Essen, D. C. (1997). A tension-based theory of morphogenesis and compact wiring in the central nervous system. *Nature* 385, 313–318. doi: 10.1038/385313a0
- Wang, J. Y., Abdi, H., Bakhadirov, K., Diaz-Arrastia, R., and Devous, M. D. Sr. (2012). A comprehensive reliability assessment of quantitative diffusion tensor tractography. *Neuroimage* 60, 1127–1138. doi: 10.1016/j.neuroimage.2011.12.062
- Watts, D. J., and Strogatz, S. H. (1998). Collective dynamics of 'small world' networks. *Nature* 393, 440–442. doi: 10.1038/30918
- Wiest, R., Kassubek, J., Schindler, K., Loher, T. J., Kiefer, C., Mariani, L., et al. (2005). Comparison of voxel-based 3-D MRI analysis and subtraction ictal SPECT coregistered to MRI in focal epilepsy. *Epilepsy Res.* 65, 125–133. doi: 10.1016/j.eplepsyres.2005.05.002
- Yoshida, S., Faria, A. V., Oishi, K., Kanda, T., Yamori, Y., Yoshida, N., et al. (2013). Anatomical characterization of athetotic and spastic cerebral palsy using an atlas-based analysis. *J. Magn. Reson. Imaging* 38, 288–298. doi: 10.1002/jmri.23931
- Zhang, S., and Arfanakis, K. (2013). Role of standardized and study-specific human brain diffusion tensor templates in inter-subject spatial normalization. *J. Magn. Reson. Imaging* 37, 372–381. doi: 10.1002/jmri.23842
- Zhang, Y., Chang, L., Ceritoglu, C., Skranes, J., Ernst, T., Mori, S., et al. (2014). A Bayesian approach to the creation of a study-customized neonatal brain atlas. *Neuroimage* 101, 256–267. doi: 10.1016/j.neuroimage.2014.07.001

Conflict of Interest Statement: The authors declare that the research was conducted in the absence of any commercial or financial relationships that could be construed as a potential conflict of interest.

Copyright © 2015 Deshpande, Chang and Oishi. This is an open-access article distributed under the terms of the Creative Commons Attribution License (CC BY). The use, distribution or reproduction in other forums is permitted, provided the original author(s) or licensor are credited and that the original publication in this journal is cited, in accordance with accepted academic practice. No use, distribution or reproduction is permitted which does not comply with these terms.



The maturation of auditory responses in infants and young children: a cross-sectional study from 6 to 59 months

J. Christopher Edgar^{1*}, Rebecca Murray¹, Emily S. Kushner¹, Kevin Pratt², Douglas N. Paulson², John Dell¹, Rachel Golemski¹, Peter Lam¹, Luke Bloy¹, William Gaetz¹ and Timothy P. L. Roberts¹

¹ Lurie Family Foundations MEG Imaging Center, Department of Radiology, Children's Hospital of Philadelphia, Philadelphia, PA, USA, ² Tristan Technologies, Inc., San Diego, CA, USA

OPEN ACCESS

Edited by:

Hao Huang,
University of Pennsylvania, USA

Reviewed by:

Guy Elston,
Centre for Cognitive Neuroscience,
Australia
Mitsuru Kikuchi,
Kanazawa University, Japan

*Correspondence:

J. Christopher Edgar
edgarj@email.chop.edu

Received: 03 August 2015

Accepted: 22 September 2015

Published: 16 October 2015

Citation:

Edgar JC, Murray R, Kushner ES, Pratt K, Paulson DN, Dell J, Golemski R, Lam P, Bloy L, Gaetz W and Roberts TPL (2015) The maturation of auditory responses in infants and young children: a cross-sectional study from 6 to 59 months. *Front. Neuroanat.* 9:131. doi: 10.3389/fnana.2015.00131

Background: An understanding of the maturation of auditory cortex responses in typically developing infants and toddlers is needed to later identify auditory processing abnormalities in infants at risk for neurodevelopmental disorders. The availability of infant and young child magnetoencephalography (MEG) systems may now provide near optimal assessment of left and right hemisphere auditory neuromagnetic responses in young populations. To assess the performance of a novel whole-head infant MEG system, a cross-sectional study examined the maturation of left and right auditory cortex responses in children 6- to 59-months of age.

Methods: Blocks of 1000 Hz (1st and 3rd blocks) and 500 Hz tones (2nd block) were presented while MEG data were recorded using an infant/young child biomagnetometer (Artemis 123). Data were obtained from 29 children (11 males; 6- to 59-months). Latency measures were obtained for the first positive-to-negative evoked response waveform complex in each hemisphere. Latency and age associations as well as frequency and hemisphere latency differences were examined. For the 1000 Hz tone, measures of reliability were computed.

Results: For the first response—a response with a “P2m” topography—latencies decreased as a function of age. For the second response—a response with a “N2m” topography—no N2m latency and age relationships were observed. A main effect of tone frequency showed earlier P2m responses for 1st 1000 Hz (150 ms) and 2nd 1000 Hz (148 ms) vs. 500 Hz tones (162 ms). A significant main effect of hemisphere showed earlier N2m responses for 2nd 1000 Hz (226 ms) vs. 1st 1000 Hz (241 ms) vs. 500 Hz tones (265 ms). P2m and N2m interclass correlation coefficient latency findings were as follows: left P2m (0.72, $p < 0.001$), right P2m (0.84, $p < 0.001$), left N2m (0.77, $p < 0.001$), and right N2m (0.77, $p < 0.01$).

Conclusions: Findings of strong age and latency associations, sensitivity to tone frequency, and good test-retest reliability support the viability of longitudinal infant MEG

studies that include younger as well as older participants as well as studies examining auditory processing abnormalities in infants at risk for neurodevelopmental disorders.

Keywords: infant, young child, magnetoencephalography, auditory

INTRODUCTION

Electroencephalography (EEG) studies have identified characteristic patterns of auditory long-latency responses in infants, with full-term neonates demonstrating a midline negativity that soon becomes a positive component (Kurtzberg et al., 1984). This midline positivity is sometimes referred to as the infantile P2 (Graziani et al., 1974; Barnet, 1975; Ohlrich et al., 1978; Rotteveel et al., 1987; Shucard et al., 1987). During development, a response of the opposite polarity is initially observed as a discontinuity in the P2 (Novak et al., 1989). Although there is nomenclature variability in the literature, with some groups referring to this opposite polarity response at about 200 ms as N1 (Barnet, 1975; Ohlrich et al., 1978; Novak et al., 1989) and others as N2 (Rotteveel et al., 1987; Shucard et al., 1987), the auditory event-related potential (ERP) is dominated by this positive-to-negative waveform morphology in infants and young children (Ceponiene et al., 2002; Kushnerenko et al., 2002).

Across infant and young child development there is rapid change in the latency of auditory responses. As an example, Barnet (1975) examined auditory responses (EEG electrode Cz) during sleep in 130 infants and children between the ages of 10 days and 37 months. Cross-sectional findings showed that over a 3-year period the latency decrease for P2 was approximately 75 ms and for N2 215 ms. A few longitudinal studies have studied also the maturation of auditory responses in infants and young children (Novak et al., 1989; Kushnerenko et al., 2002; Choudhury and Benasich, 2011). For example, Ohlrich et al. (1978) examined changes in auditory responses (EEG Cz) in 16 typically developing children tested repeatedly between the ages of 2 weeks and 3 years. Consistent with the cross-sectional studies, significant changes in P2 and N2 latency were observed.

Although the majority of electrophysiological studies examining cortical auditory responses in infants and young children have used EEG, a few more recent studies have used adult magnetoencephalography (MEG) systems (Bosseler et al., 2013; Kuhl et al., 2014) and more recently, infant and young child whole-head MEG systems (Yoshimura et al., 2012; Roberts et al., 2014). For examining cortical auditory activity, MEG is sometimes preferred over EEG as the superior temporal gyrus (STG) auditory generators are favorably positioned to provide distinct measures of left and right STG activity given MEG's selective sensitivity to superficial tangentially-oriented neural currents and thus spatially-separated left and right auditory neuromagnetic fields (Edgar et al., 2003), even in infants and children (Paetau et al., 1995; Huotilainen et al., 2008). MEG is also sometimes preferred in studies examining neural brain activity in infants and young children as MEG is much less sensitive than EEG to distortions of the volume

current caused by the incompletely developed fontanels and sutures in young populations and thus to inaccurate estimates of skull conductivity (Lew et al., 2013). Finally, MEG is also much less sensitive to conductivity differences between the brain to cerebral spinal fluid to skull to scalp, and thus for source localization MEG is sometimes preferred over EEG (Hämäläinen et al., 1993). Despite the difficulties examining auditory responses in infants using EEG, dense-array EEG and advanced source localization procedures (co-registering to age-appropriate MRI templates and using age-specific EEG conductivity measures) have been used to study the neural mechanisms associated with the acquisition of language in infants (Ortiz-Mantilla et al., 2012, 2013; Musacchia et al., 2013).

A limitation of conventional MEG is the fixed adult-sized sensor helmet, resulting in a substantial distance between brain neural generators and MEG detection coils in infants and young children, with this increased distance resulting in less-than-optimal MEG recordings due to a loss of brain signal as a function of (the square of the) distance. To address this limitation, whole-head infant MEG system optimized for children have been developed (see reviews in Gaetz et al., 2015; Kikuchi et al., 2015). A few whole-head infant MEG studies have examined auditory neural responses in infants and young children (Yoshimura et al., 2012, 2013). For example, in a longitudinal infant MEG study, Yoshimura et al. (2014) measured auditory P1 m responses in twenty TD children at 36–75 months and then again 11–25 months later. A primary finding was that left hemisphere P51 m amplitude change was associated with positive change on a language conceptual inference task.

The present study used a recently developed whole-head MEG system—Artemis 123—with a helmet designed for the median 3-year-old head circumference and thus ideal for studying infants and children given a decreased distance between neural brain activity and MEG detectors (Roberts et al., 2014). The present study reports on the sensitivity and reliability of the left and right auditory measures obtained using this novel MEG system, examining children aged 6- to 59-months. Based on prior findings, quality MEG auditory recordings would be demonstrated via the following findings: (1) the latency of the prominent positive-to-negative auditory response would decrease with age (left and right hemisphere auditory measures); (2) left and right auditory responses would be earlier to higher frequency (1000 Hz) vs. lower frequency tones (500 Hz), reflecting tonochronic principles (Roberts and Poeppel, 1996; Roberts et al., 1998, 2000); and (3) the latency of the response to the 1st and 3rd 1000 Hz tone blocks would be similar, indicating that the MEG obtained auditory measures are reliable. Positive findings would indicate that Artemis 123 provides quality primary/secondary auditory cortex recordings in infants and young children.

MATERIALS AND METHODS

Participants

Participants were selected according to the following criteria: (1) between 6 and 60 months old; (2) speak/hear English as their first language; (3) no seizure disorder in the child or any immediate family members; (4) no premature birth; (5) no non-removable metal in the body; (6) no known genetic conditions or neurological disorders; (7) no known hearing loss; and (8) no language or developmental delay concerns. Participants were included or excluded based on parental report via a phone screen. The study was approved by the Children's Hospital of Philadelphia IRB and all participants' families gave written consent.

Thirty-six children meeting study inclusion and exclusion criteria were enrolled. Of the enrolled children, MEG data were not obtained from four children because they were not able to place (or keep) their head in the MEG helmet: one 9-month-old male, one 10-month-old male, one 16-month-old female, and one 48-month-old male. MEG data were obtained but unusable from three children due to muscle artifact or technical problems: one 7-month-old female, one 10-month-old female, and one 12-month-old male. Of the remaining 29 participants, a full dataset (1000 Hz 1st, 500 Hz 1st, 1000 Hz 2nd) was obtained from 26 participants. A partial dataset (1000 Hz 1st, 500 Hz 1st,) was obtained from the remaining three participants. In the final group of 29 participants, ages ranged from 6- to 59-months, with a mean age of 27.2 months ($SD = 17.0$). In the 6–11 month age group there were four males and four females, in the 12 month to 23 month age group no males and five females, in the 24–35 month age group three males and four females, in the 36–47 month age group one male and two females, and in the 48–59 month age group four males and two females.

MEG Data Acquisition

Whole-head MEG data were recorded using Artemis 123 (Tristan Technologies, San Diego, CA, USA) with a sampling rate of 5000 Hz and a 0.1–330 Hz bandpass. Stimuli consisted of 500 and 1000 Hz tones of 300 ms duration and 10 ms rise time. Stimuli were presented via a free field speaker at 80 dB SPL (Panphonics Sound Shower). Exams were blocked, presenting 1000 Hz tones (1000 Hz 1st), then 500 Hz tones (500 Hz 1st), and then a repeated block of 1000 Hz tones (1000 Hz 2nd). All tones were presented with a 2100 ms (± 500 ms) inter-trial interval. As sleep can have an effect on the amplitude and latency of auditory responses (Weitzman et al., 1965; Barnet, 1975; Picton et al., 1981), recording were obtained only during an awake state. A variety of strategies were used to keep infants still and awake, including projecting a preferred video on the ceiling, toys to maintain their attention and focus (e.g., finger puppets, books, visually interesting sensory toys), and using a pacifier.

MEG data were analyzed using BESA 6.0 (BESA GmbH). MEG data were downsampled to 300 Hz. Epochs with large amplitude or gradient artifacts were manually rejected. The number of artifact-free trials per condition was: 1000 Hz 1st mean = 117 (range 53–206); 500 Hz mean = 119 (range 30–194), and 1000 Hz 2nd mean = 119 (range 82–158). Epochs 200 ms

pre- to 400 ms post-stimulus were defined from the continuous recording, artifact-free epochs averaged according to stimulus type, and a 2–55 Hz bandpass filter applied. In almost all participants, an auditory response with a positive topography was observed at approximately 150 ms, followed by a response with an opposite field pattern. Given similar findings from previous studies (see “Introduction” Section), the present study focused on this positive-to-negative evoked complex. Kushnerenko et al. (2002) noted that during early maturation an initial broad positivity in infants is divided into two positive peaks by the emergence of a growing negativity (N250), sometimes referred to as the P150 and the P350. In the present study, the first positivity preceding the N2 was measured. As in Barnet (1975), in the present study, these “positive” and “negative” responses are referred to as P2 and N2, although adding an “m” to obtain P2m and N2m, as the recorded activity is magnetic rather than electric (for a similar approach, see also the language acquisition studies conducted by Rivera-Gaxiola et al. (2005, 2007, 2012) examining the P150–250 and N250–550 in infants).

Given that continuous head position indicator (HPI) information was available only for the last few participants, the following procedure was used to obtain left and right P2m and N2m latency measures. First, after excluding all MEG sensors opposite the hemisphere of interest, P2m and N2m latencies were obtained from the 1st component derived from a principal components analysis (PCA) applied to the sensor data. In all participants, field topography was examined to ensure that the P2m response and the N2m response had the characteristic magnetic field pattern. N2m was first identified, with P2m operationally defined as the first preceding response showing a reversed field pattern. **Figure 1** shows example timecourse waveforms associated with the 1st PCA component for a subject in each age group.

RESULTS

P2m and N2m Latency and Age Associations

Correlations examined associations between P2m and N2m latency with age for each tone and hemisphere. As shown in **Table 1**, age and P2m latency associations were observed for all tones and in both hemispheres except right 500 Hz, with a slope of -0.6 ms/month observed for most conditions. Age and N2m latency associations were not observed for any condition. The **Figure 2** top row scatterplots compare age and latency associations for 500 and 1000 Hz 2nd tones. The **Figure 2** bottom row scatterplots compare age and latency associations for the 1000 Hz 1st and 1000 Hz 2nd tones.

P2m and N2m Latency

Repeated measures ANOVA examined tone (1000 1st, 500 1st, and 1000 2nd) and hemisphere differences in P2m and N2m latency. **Table 2** shows P2m and N2m mean and standard deviation latency values for each condition. For P2m, a main effect of tone, $F_{(2,18)} = 7.18$, $p < 0.01$, showed earlier P2m responses for 1st 1000 Hz (150 ms) and 2nd 1000 Hz (148 ms)

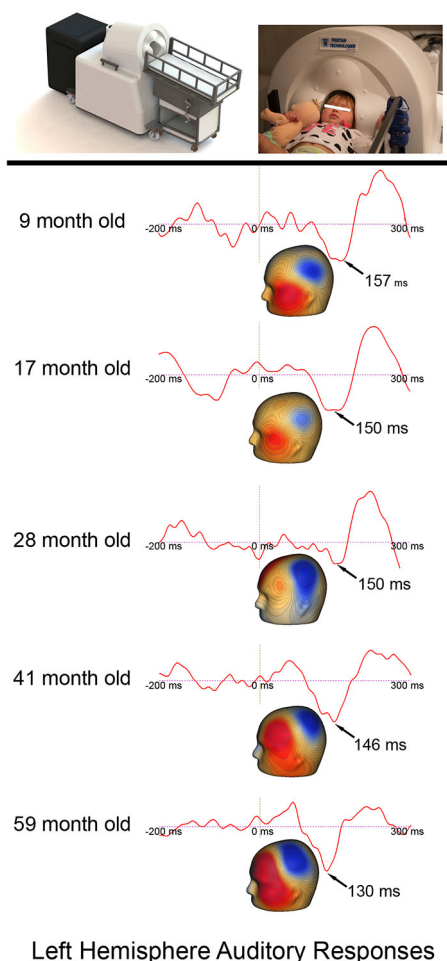


FIGURE 1 | The Artemis 123 system and a child placed in the helmet, along with left hemisphere auditory responses from five participants ranging in age from 6- to 59-months-old. The expected earlier P2m (magnetic field topography shown) auditory latencies in older (~130 ms) vs. younger children (~157 ms) is observed. Permission was granted by the family to publish the participant's photograph in the top panel.

vs. 500 Hz tones (162 ms). For N2m, a main effect of tone, $F_{(2,18)} = 18.35$, $p < 0.001$, showed earlier N2m responses for 2nd 1000 Hz (226 ms) vs. 1st 1000 Hz (241 ms) vs. 500 Hz tones (265 ms). No hemisphere or tone by hemisphere effects were observed for P2m or N2m (p 's > 0.19).

P2m and N2m Reliability

To examine the similarity of the auditory measures, correlation analyses examined associations between P2m and N2m latencies to the 1000 Hz 1st and 1000 Hz 2nd tones. Left P2m latencies ($r = 0.57$, $p < 0.01$) and right P2m latencies were significantly associated ($r = 0.76$, $p < 0.001$). Left N2m latencies ($r = 0.62$, $p < 0.01$) and right N2m latencies were also significantly associated ($r = 0.71$, $p < 0.001$). Intraclass correlation coefficient (ICC) findings were as follows: left P2m (0.72, $p < 0.001$), right P2m (0.84, $p < 0.001$), left N2m (0.77, $p < 0.001$), and right N2m (0.77, $p < 0.01$).

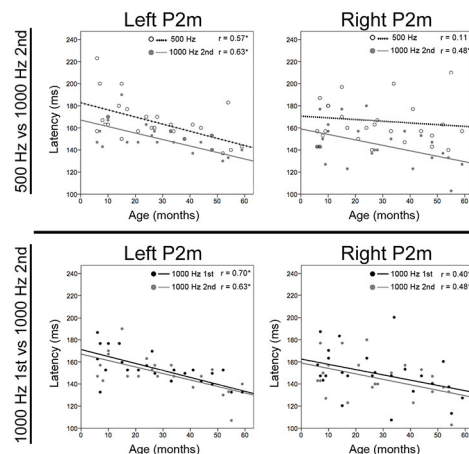


FIGURE 2 | Scatterplots showing associations for each tone between age and left and right P2m latency. The top row shows associations for 500 Hz (open circle and dotted line) and 1000 Hz 2nd tones (gray circle and line), and the bottom row shows associations for 1000 Hz 1st (black circle and line) and 1000 Hz 2nd tones. The x axis shows age and the y axis latency. Significant correlations are marked with an “*”.

DISCUSSION

Strong cross-sectional P2m age and latency associations, robust findings of sensitivity to 500 Hz vs. 1000 Hz tone frequency, and good reliability measures (0.70–0.84), all support the viability of infant and young child Artemis 123 MEG auditory studies. Below, present findings are discussed within the context of previous findings.

Although direct comparisons to previous studies are difficult given that many earlier studies examined infants and children during sleep (Ohlrich et al., 1978), examined auditory responses at a single midline EEG electrode (Barnet, 1975; Ohlrich et al., 1978), or used an inter-stimulus interval shorter than that used in the present study Sharma et al. (2002), present findings were generally consistent with previous studies. For example, Ohlrich et al. (1978) reported a P2 latency of 153 ms in 3-year-old children, and Barnet (1975) a P2 latency between 150 and 170 in children between the ages of 1.5–3 years. Examining 4-year-old children, Ceponiene et al. (2002) observed a P1 latency of 114 ms and a N2 latency of 295 ms (midline EEG electrodes). Examining the auditory Cz response in 3- and 4-year-olds using a 2000 ms ISI, Gilley et al. (2005) reported a P2 latency of 145 ms. Using high-density EEG and assessing source localized left and right STG activity, Ortiz-Mantilla et al. (2013) observed in 6-month-olds a grand average left P1 latency of 176 ms and right P1 latency of 208 ms in response to consonant-vowel syllable stimuli and presenting stimuli at an approximately 700 ms ISI. Latencies in the present study, however, were somewhat longer than the P150 latencies of 139 ms in 9-month-olds and 142 ms in 12-month-olds reported in Kushnerenko et al. (2002), and the P1 latencies of 150 ms in 12-month-olds and 130 ms in 36-month-olds reported in Choudhury and Benasich (2011), with study differences perhaps due to the use of a shorter ISI in these two studies vs. the present study.

TABLE 1 | P2m and N2m latency associations with age.

	P2m			N2m		
	1st 1000 Hz <i>r</i> -value and slope	500 Hz <i>r</i> -value and slope	2nd 1000 Hz <i>r</i> -value and slope	1st 1000 Hz <i>r</i> -value and slope	500 Hz <i>r</i> -value and slope	2nd 1000 Hz <i>r</i> -value and slope
Left	0.70** (−0.6 ms/month)	0.57** (−0.6 ms/month)	0.63** (−0.6 ms/month)	0.11 (0.2 ms/month)	0.11 (−0.2 ms/month)	0.27 (−0.2 ms/month)
Right	0.40* (−0.5 ms/month)	0.11 (−0.2 ms/month)	0.48* (−0.5 ms/month)	0.17 (0.3 ms/month)	0.30 (0.6 ms/month)	0.30 (−0.6 ms/month)

* $p < 0.05$, ** $p < 0.01$.

In the present study, a latency decrease of 0.6 ms/month was observed for P2m (i.e., 7.2 ms/year), with 1000 Hz P2m latencies estimated to be approximately 170 ms at 6 months and 130 ms at 5 years. These rate-of-change estimates are again generally consistent with prior studies (Ohlrich et al., 1978; Novak et al., 1989). For example, in a longitudinal study following children from 6 months to 4 years, Choudhury and Benasich (2011) reported age-related decreases for the positive-going peaks of 20–80 ms over 4 years, and a decrease for the negative peaks of 9–50 ms over 4 years.

Infant and young child auditory responses differ from adult responses, and there is evidence that the P2m response examined in the present study eventually “becomes” the adult P50/M50 (P1) response (Kushnerenko et al., 2002; Ceponiene et al., 2003, 2008). The 1.9 ms/year rate-of change for P1 (EEG Fz) reported in Sharma et al. (1997) is slower than the rate-of-change observed in the present sample, suggesting more rapid changes to P2m earlier in development, and then with slower although continued changes through childhood, and with adult-like STG P50/M50 latencies not observed until late adolescence.

The first negative component identified in infants is often labeled the N1, N250, or N2. The literature suggests that the N2m component does not develop into the adult M100 response. For example, in a longitudinal study (birth to 12 months), using harmonic tones, the infant N1 was identified at birth and showed consolidation by 6 months of age (Kushnerenko et al., 2002). The authors found that the infant N1 component did not change in latency from birth until 12 months of age, and they thus suggested that the infant N1 may be a correlate of the childhood N250. Similar findings have been reported in other studies (Pang and Taylor, 2000; Ponton et al., 2000). In the present study, the finding that N2m latency did not change as a function of age in children 6 months and older is consistent with previous studies (Onishi and Davis, 1969; Tanguay et al., 1973; Kushnerenko et al., 2002; Choudhury

and Benasich, 2011), including observations from other studies showing that the adult N100/M100 is not robustly observed until early adolescence (Ponton et al., 2000, 2002; Edgar et al., 2014).

Previous studies have reported hemisphere differences in the maturation of left and right STG auditory cortex (Gomes et al., 2001). Although in older children and in adults earlier right than left M50 latencies are observed, in the present study, no P2m or N2m hemisphere latency differences were observed. Paetau et al. (1995) observed that in children 3–15 years auditory latencies tended to be earlier over the right than left hemisphere only in the older children. Examining EEG source localized left and right STG activity in 4-month-old infants, Musacchia et al. (2013) observed earlier right than left “P1” responses. The (Musacchia et al., 2013) inter-trial interval was much shorter than in the present study, perhaps suggesting that a right hemisphere auditory encoding advantage may be observed only under more demanding encoding conditions. Longitudinal studies following children from infancy through early adolescence are needed to better understand the development of infant and young child P2m responses and transition to adult M50 responses.

Changes to the auditory response (morphology and latency) as a function of age are hypothesized to be due to maturation of gray and white matter structure, such as age-related changes in synaptic efficiency (Goodin et al., 1978; Eggermont, 1988), cortical layer maturational changes (Steinschneider et al., 1994; Eggermont and Ponton, 2003). Maturation changes to the morphology of primary auditory cortex pyramidal cells are also observed (Elston et al., 2010; Elston and Fujita, 2014), with such changes of interest as MEG recordings primarily reflect pyramidal cell activity (Lewine and Orrison, 1995; Spruston, 2008). Multimodal human *in vivo* imaging studies are beginning to demonstrate how brain structure is related to brain function. For example, multimodal MEG and diffusion MR children and adolescent studies have shown that the latency

TABLE 2 | P2m and N2m latency.

	P2m			N2m		
	1st 1000 Hz Latency (ms) and SD	500 Hz Latency (ms) and SD	2nd 1000 Hz Latency (ms) and SD	1st 1000 Hz Latency (ms) and SD	500 Hz Latency (ms) and SD	2nd 1000 Hz Latency (ms) and SD
Left	154 (15)	163 (20)	149 (16)	230 (25)	263 (28)	222 (22)
Right	149 (21)	163 (19)	146 (22)	242 (40)	268 (38)	229 (41)

of auditory responses decreases as a function of maturation of local white matter myelination (Roberts et al., 2009, 2013). In adults, studies have noted associations between gray matter cortical thickness and the strength of auditory responses (Edgar et al., 2012). Studies examining auditory cortex function and structure associations in infants and young children are now needed.

A few limitations of the present study are of note. First, given that HPI coil information was not available from most of the participants, it was not possible to determine the exact location of the infant or child's head in the helmet and thus not possible to accurately estimate the strength of auditory responses. As such, although age-related auditory component amplitude changes are of interest in infants and young children (Ponton et al., 2002; Gilley et al., 2005; Yoshimura et al., 2014), examination of amplitude and age associations was not possible in the present study. Second, auditory responses in infants and children likely depend on the type of stimuli such as speech or non-speech stimuli (Friedman et al., 1984; Kurtzberg et al., 1984;

Pang and Taylor, 2000), with present findings thus limited in their generality. Finally, a limitation of the present study is that acquisitions, and thus analyses, were cross-sectional rather than longitudinal.

CONCLUSION

Strong cross-sectional P2m age and latency associations, robust findings of sensitivity to tone frequency, and good reliability measures all support the viability of infant and young child Artemis 123 MEG auditory studies.

FUNDING

This research was supported by grants from the Nancy Lurie Marks Family Foundation, a IDDRC grant to CHOP (U54 HD08694), and the Pennsylvania Department of Health. The Pennsylvania Department of Health specifically disclaims responsibility for any analyses, interpretations or conclusions.

REFERENCES

- Barnet, A. B. (1975). Auditory evoked potentials during sleep in normal children from ten days to three years of age. *Electroencephalogr. Clin. Neurophysiol.* 39, 29–41. doi: 10.1016/0013-4694(75)90124-8
- Bosseler, A. N., Taulu, S., Pihko, E., Mäkelä, J. P., Imada, T., Ahonen, A., et al. (2013). Theta brain rhythms index perceptual narrowing in infant speech perception. *Front. Psychol.* 4:690. doi: 10.3389/fpsyg.2013.00690
- Ceponiene, R., Lepistö, T., Alku, P., Aro, H., and Naatanen, R. (2003). Event-related potential indices of auditory vowel processing in 3-year-old children. *Clin. Neurophysiol.* 114, 652–661. doi: 10.1016/s1388-2457(02)00436-4
- Ceponiene, R., Rinne, T., and Näätänen, R. (2002). Maturation of cortical sound processing as indexed by event-related potentials. *Clin. Neurophysiol.* 113, 870–882. doi: 10.1016/s1388-2457(02)00078-0
- Ceponiene, R., Torki, M., Alku, P., Koyama, A., and Townsend, J. (2008). Event-related potentials reflect spectral differences in speech and non-speech stimuli in children and adults. *Clin. Neurophysiol.* 119, 1560–1577. doi: 10.1016/j.clinph.2008.03.005
- Choudhury, N., and Benasich, A. A. (2011). Maturation of auditory evoked potentials from 6 to 48 months: prediction to 3 and 4 year language and cognitive abilities. *Clin. Neurophysiol.* 122, 320–338. doi: 10.1016/j.clinph.2010.05.035
- Edgar, J. C., Huang, M. X., Weisend, M. P., Sherwood, A., Miller, G. A., Adler, L. E., et al. (2003). Interpreting abnormality: an EEG and MEG study of P50 and the auditory paired-stimulus paradigm. *Biol. Psychol.* 65, 1–20. doi: 10.1016/s0301-0511(03)00094-2
- Edgar, J. C., Hunter, M. A., Huang, M., Smith, A. K., Chen, Y., Sadek, J., et al. (2012). Temporal and frontal cortical thickness associations with M100 auditory activity and attention in healthy controls and individuals with schizophrenia. *Schizophr. Res.* 140, 250–257. doi: 10.1016/j.schres.2012.06.009
- Edgar, J. C., Lanza, M. R., Daina, A. B., Monroe, J. F., Khan, S. Y., Blaskey, L., et al. (2014). Missing and delayed auditory responses in young and older children with autism spectrum disorders. *Front. Hum. Neurosci.* 8:417. doi: 10.3389/fnhum.2014.00417
- Eggermont, J. J. (1988). On the rate of maturation of sensory evoked potentials. *Electroencephalogr. Clin. Neurophysiol.* 70, 293–305. doi: 10.1016/0013-4694(88)90048-x
- Eggermont, J. J., and Ponton, C. W. (2003). Auditory-evoked potential studies of cortical maturation in normal hearing and implanted children: correlations with changes in structure and speech perception. *Acta Otolaryngol.* 123, 249–252. doi: 10.1080/0036554021000028098
- Pang and Taylor, (2000), with present findings thus limited in their generality. Finally, a limitation of the present study is that acquisitions, and thus analyses, were cross-sectional rather than longitudinal.
- Elston, G. N., and Fujita, I. (2014). Pyramidal cell development: postnatal spinogenesis, dendritic growth, axon growth and electrophysiology. *Front. Neuroanat.* 8:78. doi: 10.3389/fnana.2014.00078
- Elston, G. N., Okamoto, T., Oga, T., Dornan, D., and Fujita, I. (2010). Spinogenesis and pruning in the primary auditory cortex of the macaque monkey (*Macaca fascicularis*): an intracellular injection study of layer III pyramidal cells. *Brain Res.* 1316, 35–42. doi: 10.1016/j.brainres.2009.12.056
- Friedman, D., Brown, C., Vaughan, H. G. Jr., Cornblatt, B., and Erlenmeyer-Kimling, L. (1984). Cognitive brain potential components in adolescents. *Psychophysiology* 21, 83–96. doi: 10.1111/j.1469-8986.1984.tb02322.x
- Gaetz, W., Gordon, R. S., Papadelis, C., Fujiwara, H., Rose, D. F., Edgar, J. C., et al. (2015). Magnetoencephalography for clinical pediatrics: recent advances in hardware, methods and clinical applications. *J. Pediatr. Epilepsy* 4, (in press). doi: 10.1055/s-0035-1563726
- Gilley, P. M., Sharma, A., Dorman, M., and Martin, K. (2005). Developmental changes in refractoriness of the cortical auditory evoked potential. *Clin. Neurophysiol.* 116, 648–657. doi: 10.1016/j.clinph.2004.09.009
- Gomes, H., Dunn, M., Ritter, W., Kurtzberg, D., Brattson, A., Kreuzer, J. A., et al. (2001). Spatiotemporal maturation of the central and lateral N1 components to tones. *Brain Res. Dev. Brain Res.* 129, 147–155. doi: 10.1016/s0165-3806(01)00196-1
- Goodin, D. S., Squires, K. C., Henderson, B. H., and Starr, A. (1978). Age-related variations in evoked potentials to auditory stimuli in normal human subjects. *Electroencephalogr. Clin. Neurophysiol.* 44, 447–458. doi: 10.1016/0013-4694(78)90029-9
- Graziani, L. J., Katz, L., Cracco, Q., Cracco, J. B., and Weitzman, E. D. (1974). The maturation and interrelationship of EEG patterns and auditory evoked response in premature infants. *Electroencephalogr. Clin. Neurophysiol.* 36, 367–375. doi: 10.1016/0013-4694(74)90186-2
- Hämäläinen, M., Hari, R., Ilmoniemi, R. J., Knuutila, J., and Lounasmaa, O. V. (1993). Magnetoencephalography-theory, instrumentation and applications to noninvasive studies of the working human brain. *Rev. Mod. Phys.* 65, 413–497. doi: 10.1103/revmodphys.65.413
- Huottilainen, M., Shestakova, A., and Hukki, J. (2008). Using magnetoencephalography in assessing auditory skills in infants and children. *Int. J. Psychophysiol.* 68, 123–129. doi: 10.1016/j.ijpsycho.2007.12.007
- Kikuchi, M., Yoshimura, Y., Mutou, K., and Minabe, Y. (2015). Magnetoencephalography in the study of children with autism spectrum disorder. *Psychiatry Clin. Neurosci.* doi: 10.1111/pcn.12338 [Epub ahead of print].

- Kuhl, P. K., Ramírez, R. R., Bosseler, A., Lin, J. F., and Imada, T. (2014). Infants' brain responses to speech suggest analysis by synthesis. *Proc. Natl. Acad. Sci. U S A* 111, 11238–11245. doi: 10.1073/pnas.1410963111
- Kurtzberg, D., Hilpert, P. L., Kreuzer, J. A., Vaughan, H. G. Jr. (1984). Differential maturation of cortical auditory evoked potentials to speech sounds in normal fullterm and very low-birthweight infants. *Dev. Med. Child Neurol.* 26, 466–475. doi: 10.1111/j.1469-8749.1984.tb04473.x
- Kushnerenko, E., Ceponiene, R., Balan, P., Fellman, V., Huotilaine, M., and Näätäne, R. (2002). Maturation of the auditory event-related potentials during the first year of life. *Neuroreport* 13, 47–51. doi: 10.1097/00001756-200201210-00014
- Lew, S., Sliva, D. D., Choe, M. S., Grant, P. E., Okada, Y., Wolters, C. H., et al. (2013). Effects of sutures and fontanels on MEG and EEG source analysis in a realistic infant head model. *Neuroimage* 76, 282–293. doi: 10.1016/j.neuroimage.2013.03.017
- Lewine, J. D., and Orrison, W. W. (1995). "Magnetencephalography and magnetic source imaging," in *Functional Brain Imaging*, eds W. W. L. J. Orrison, J. A. Sanders, and M. F. Hartshorne (St. Louis: Mosby), 369–417.
- Musacchia, G., Choudhury, N. A., Ortiz-Mantilla, S., Realpe-Bonilla, T., Roesler, C. P., and Benasich, A. A. (2013). Oscillatory support for rapid frequency change processing in infants. *Neuropsychologia* 51, 2812–2824. doi: 10.1016/j.neuropsychologia.2013.09.006
- Novak, G. P., Kurtzberg, D., Kreuzer, J. A., and Vaughan, H. G. Jr. (1989). Cortical responses to speech sounds and their formants in normal infants: maturational sequence and spatiotemporal analysis. *Electroencephalogr. Clin. Neurophysiol.* 73, 295–305. doi: 10.1016/0013-4694(89)90108-9
- Ohlrich, E. S., Barnet, A. B., Weiss, I. P., and Shanks, B. L. (1978). Auditory evoked potential development in early childhood: a longitudinal study. *Electroencephalogr. Clin. Neurophysiol.* 44, 411–423. doi: 10.1016/0013-4694(78)90026-3
- Onishi, S., and Davis, H. (1969). Auditory evoked responses in the sleeping infant. *Electroencephalogr. Clin. Neurophysiol.* 26:114.
- Ortiz-Mantilla, S., Hämäläinen, J. A., and Benasich, A. A. (2012). Time course of ERP generators to syllables in infants: a source localization study using age-appropriate brain templates. *Neuroimage* 59, 3275–3287. doi: 10.1016/j.neuroimage.2011.11.048
- Ortiz-Mantilla, S., Hämäläinen, J. A., Musacchia, G., and Benasich, A. A. (2013). Enhancement of gamma oscillations indicates preferential processing of native over foreign phonemic contrasts in infants. *J. Neurosci.* 33, 18746–18754. doi: 10.1523/jneurosci.3260-13.2013
- Paetau, R., Ahonen, A., Salonen, O., and Sams, M. (1995). Auditory evoked magnetic fields to tones and pseudowords in healthy children and adults. *J. Clin. Neurophysiol.* 12, 177–185. doi: 10.1097/00004691-199503000-00008
- Pang, E. W., and Taylor, M. J. (2000). Tracking the development of the N1 from age 3 to adulthood: an examination of speech and non-speech stimuli. *Clin. Neurophysiol.* 111, 388–397. doi: 10.1016/s1388-2457(99)00259-x
- Picton, T. W., Stapells, D. R., and Campbell, K. B. (1981). Auditory evoked potentials from the human cochlea and brainstem. *J. Otolaryngol. Suppl.* 9, 1–41.
- Ponton, C., Eggermont, J. J., Khosla, D., Kwong, B., and Don, M. (2002). Maturation of human central auditory system activity: separating auditory evoked potentials by dipole source modeling. *Clin. Neurophysiol.* 113, 407–420. doi: 10.1016/s1388-2457(01)00733-7
- Ponton, C. W., Eggermont, J. J., Kwong, B., and Don, M. (2000). Maturation of human central auditory system activity: evidence from multi-channel evoked potentials. *Clin. Neurophysiol.* 111, 220–236. doi: 10.1016/s1388-2457(99)00236-9
- Rivera-Gaxiola, M., Garcia-Sierra, A., Lara-Ayala, L., Cadena, C., Jackson-Maldonado, D., and Kuhl, P. (2012). Event-related potentials to an english/spanish syllabic contrast in mexican 10–13-month-old infants. *ISRN Neurol.* 2012:702986. doi: 10.5402/2012/702986
- Rivera-Gaxiola, M., Silva-Pereyra, J., Klarman, L., Garcia-Sierra, A., Lara-Ayala, L., Cadena-Salazar, C., et al. (2007). Principal component analyses and scalp distribution of the auditory P150–250 and N250–550 to speech contrasts in Mexican and American infants. *Dev. Neuropsychol.* 31, 363–378. doi: 10.1080/87565640701229292
- Rivera-Gaxiola, M., Silva-Pereyra, J., and Kuhl, P. K. (2005). Brain potentials to native and non-native speech contrasts in 7- and 11-month-old American infants. *Dev. Sci.* 8, 162–172. doi: 10.1111/j.1467-7687.2005.00403.x
- Roberts, T. P., Ferrari, P., and Poeppel, D. (1998). Latency of evoked neuromagnetic M100 reflects perceptual and acoustic stimulus attributes. *Neuroreport* 9, 3265–3269. doi: 10.1097/00001756-199810050-00024
- Roberts, T. P., Ferrari, P., Stufflebeam, S. M., and Poeppel, D. (2000). Latency of the auditory evoked neuromagnetic field components: stimulus dependence and insights toward perception. *J. Clin. Neurophysiol.* 17, 114–129. doi: 10.1097/00004691-200003000-00002
- Roberts, T. P., Khan, S. Y., Blaskey, L., Dell, J., Levy, S. E., Zarnow, D. M., et al. (2009). Developmental correlation of diffusion anisotropy with auditory-evoked response. *Neuroreport* 20, 1586–1591. doi: 10.1097/wnr.0b013e3283306854
- Roberts, T. P., Lanza, M. R., Dell, J., Smieh, S., Hines, K., Blaskey, L., et al. (2013). Maturation differences in thalamocortical white matter microstructure and auditory evoked response latencies in autism spectrum disorders. *Brain Res.* 1537, 79–85. doi: 10.1016/j.brainres.2013.09.011
- Roberts, T. P., Paulson, D. N., Hirschko, E., Pratt, K., Mascarenas, A., Miller, P., et al. (2014). Artemis 123: development of a whole-head infant and young child MEG system. *Front. Hum. Neurosci.* 8:99. doi: 10.3389/fnhum.2014.00099
- Roberts, T. P., and Poeppel, D. (1996). Latency of auditory evoked M100 as a function of tone frequency. *Neuroreport* 7, 1138–1140. doi: 10.1097/00001756-199604260-00007
- Rottevel, J. J., de Graaf, R., Stegeman, D. F., Colon, E. J., and Visco, Y. M. (1987). The maturation of the central auditory conduction in preterm infants until three months post term. V. The auditory cortical response (ACR). *Hear. Res.* 27, 95–110. doi: 10.1016/0378-5955(87)90029-3
- Sharma, A., Dorman, M. F., and Spahr, A. J. (2002). A sensitive period for the development of the central auditory system in children with cochlear implants: implications for age of implantation. *Ear Hear.* 23, 532–539. doi: 10.1097/00003446-200212000-00004
- Sharma, A., Kraus, N., McGee, T. J., and Nicol, T. G. (1997). Developmental changes in P1 and N1 central auditory responses elicited by consonant-vowel syllables. *Electroencephalogr. Clin. Neurophysiol.* 104, 540–545. doi: 10.1016/s0168-5597(97)00050-6
- Shucard, D. W., Shucard, J. L., and Thomas, D. G. (1987). Auditory event-related potentials in waking infants and adults: a developmental perspective. *Electroencephalogr. Clin. Neurophysiol.* 68, 303–310. doi: 10.1016/0168-5597(87)90051-7
- Spruston, N. (2008). Pyramidal neurons: dendritic structure and synaptic integration. *Nat. Rev. Neurosci.* 9, 206–221. doi: 10.1038/nrn2286
- Steinschneider, M., Schroeder, C. E., Arezzo, J. C., and Vaughan, H. G. Jr. (1994). Speech-evoked activity in primary auditory cortex: effects of voice onset time. *Electroencephalogr. Clin. Neurophysiol.* 92, 30–43. doi: 10.1016/0168-5597(94)90005-1
- Tanguay, P. E., Lee, J. C., and Ornitz, E. M. (1973). A detailed analysis of the auditory evoked response wave form in children during REM and stage 2 sleep. *Electroencephalogr. Clin. Neurophysiol.* 35, 241–248. doi: 10.1016/0013-4694(73)90235-6
- Weitzman, E. D., Fishbein, W., and Graziani, L. (1965). Auditory evoked responses obtained from the scalp electroencephalogram of the full-term human neonate during sleep. *Pediatrics* 35, 458–462.
- Yoshimura, Y., Kikuchi, M., Shitamichi, K., Ueno, S., Munesue, T., Ono, Y., et al. (2013). Atypical brain lateralisation in the auditory cortex and language performance in 3- to 7-year-old children with high-functioning autism spectrum disorder: a child-customised magnetoencephalography (MEG) study. *Mol. Autism* 4:38. doi: 10.1186/2040-2392-4-38
- Yoshimura, Y., Kikuchi, M., Shitamichi, K., Ueno, S., Remijn, G. B., Haruta, Y., et al. (2012). Language performance and auditory evoked fields in 2- to

5-year-old children. *Eur. J. Neurosci.* 35, 644–650. doi: 10.1111/j.1460-9568.2012.07998.x

Yoshimura, Y., Kikuchi, M., Ueno, S., Shitamichi, K., Remijn, G. B., Hiraishi, H., et al. (2014). A longitudinal study of auditory evoked field and language development in young children. *Neuroimage* 101, 440–447. doi: 10.1016/j.neuroimage.2014.07.034

Conflict of Interest Statement: The Associate Editor Dr. Huang declares that, despite being affiliated to the same university as the authors, the review process was handled objectively. The authors declare that the research was conducted in

the absence of any commercial or financial relationships that could be construed as a potential conflict of interest.

Copyright © 2015 Edgar, Murray, Kushner, Pratt, Paulson, Dell, Golembski, Lam, Bloy, Gaetz and Roberts. This is an open-access article distributed under the terms of the Creative Commons Attribution License (CC BY). The use, distribution and reproduction in other forums is permitted, provided the original author(s) or licensor are credited and that the original publication in this journal is cited, in accordance with accepted academic practice. No use, distribution or reproduction is permitted which does not comply with these terms.



Abnormal surface morphology of the central sulcus in children with attention-deficit/hyperactivity disorder

Shuyu Li^{1*}, Shaoyi Wang¹, Xinwei Li¹, Qionglin Li¹ and Xiaobo Li^{2,3*}

¹ School of Biological Science and Medical Engineering, Beihang University, Beijing, China, ² Department of Biomedical Engineering, New Jersey Institute of Technology, Newark, NJ, USA, ³ The Gruss Magnetic Resonance Research Center, Department of Radiology, Albert Einstein College of Medicine, New York, NY, USA

OPEN ACCESS

Edited by:

Hao Huang,
University of Pennsylvania, USA

Reviewed by:

Jean-François Mangin,
Commissariat à l'Energie Atomique
et aux Energies Alternatives, France
Islem Rekik,
University of North Carolina
at Chapel Hill, USA

*Correspondence:

Shuyu Li,
School of Biological Science
and Medical Engineering, Beihang
University, Beijing 100191, China
shuyuli@buaa.edu.cn;
Xiaobo Li,
Department of Biomedical
Engineering, New Jersey Institute
of Technology, Room 600, Fenster
Hall, 333 Martin Luther King
Jr. Boulevard, Newark,
NJ 07102, USA
xli.aecom@gmail.com

Received: 04 May 2015

Accepted: 08 August 2015

Published: 28 August 2015

Citation:

Li S, Wang S, Li X, Li Q and Li X
(2015) Abnormal surface morphology
of the central sulcus in children with
attention-deficit/hyperactivity
disorder. *Front. Neuroanat.* 9:114.
doi: 10.3389/fnana.2015.00114

The central sulcus (CS) divides the primary motor and somatosensory areas, and its three-dimensional (3D) anatomy reveals the structural changes of the sensorimotor regions. Attention-deficit/hyperactivity disorder (ADHD) is a neurodevelopmental disorder that is associated with sensorimotor and executive function deficits. However, it is largely unknown whether the morphology of the CS alters due to inappropriate development in the ADHD brain. Here, we employed the sulcus-based morphometry approach to investigate the 3D morphology of the CS in 42 children whose ages spanned from 8.8 to 13.5 years (21 with ADHD and 21 controls). After automatic labeling of each CS, we computed seven regional shape metrics for each CS, including the global average length, average depth, maximum depth, average span, surface area, average cortical thickness, and local sulcal profile. We found that the average depth and maximum depth of the left CS as well as the average cortical thickness of bilateral CS in the ADHD group were significantly larger than those in the healthy children. Moreover, significant between-group differences in the sulcal profile had been found in middle sections of the CSs bilaterally, and these changes were positively correlated with the hyperactivity-impulsivity scores in the children with ADHD. Altogether, our results provide evidence for the abnormality of the CS anatomical morphology in children with ADHD due to the structural changes in the motor cortex, which significantly contribute to the clinical symptomatology of the disorder.

Keywords: central sulcus, ADHD, surface morphology, MRI

Introduction

The central sulcus (CS) is one of the most prominent and stable sulci of the human brain, which divides the primary motor and somatosensory areas. The three-dimensional (3D) anatomy of the CS includes motor and sensory maps, somatotopically organized according to Penfield's (1937) classical 'homunculus.' Investigation of the 3D sulcal anatomy of the CS could reveal characteristic morphological features and further explore the associations between anatomy and function (Sastre-Janer et al., 1998). Many studies have reported that the morphological characteristics of the CS can be affected by factors such as handedness (Sun et al., 2012), learning (Li et al., 2010), gender (Cykowski et al., 2008), normal aging (Li et al., 2011), and neuropsychiatric disorders (Fujiwara et al., 2007).

Attention-Deficit/Hyperactivity Disorder (ADHD) is one of the most common childhood-onset neuropsychiatric disorders, characterized by hyperactivity, impulsivity, inattention, or a

combination (First, 1994). Deficits of motor functions in children with ADHD have been frequently reported, such as slower speed (Denckla and Rudel, 1978) and greater degree of motor overflow movements (Mostofsky et al., 2003) when performing timed motor tasks, compared with typically developing controls. Previous functional neuroimaging studies have demonstrated dysfunctional neural activity of the motor cortex in ADHD children, such as reduced cortical activity and spatial extent of activation in the primary motor and parietal cortices (Mostofsky et al., 2006). Meanwhile, structural MRI studies in children with ADHD have reported atypical brain morphology in sensorimotor brain regions, such as gray matter (GM) volume decreases in the left precentral and postcentral areas (Carmona et al., 2005), and cortical thickness reductions of the precentral cortex (Shaw et al., 2006; Narr et al., 2009; Hoekzema et al., 2012). However, the morphological characteristics of the CS in children with ADHD and their relationships with the clinical symptoms have not yet been investigated.

Surface-based approaches provide a framework for identifying local changes across the surface anatomy of the sulcus. This is accomplished using 3D surface parameterization following automated sulcal mesh reconstruction, which would enable further shape analysis, such as the encoding of statistical properties in local anatomical variations within individual sulci. Sulcal parameterization is a critical step, and it can create a normalized coordinate system on the CS surfaces that allows to compare the morphological differences at each location of the CS across individuals. The method based on the heat-equation diffusion process along the CS surface (Cykowski et al., 2008) has been applied in sulcal parameterization (Coulon et al., 2011; McKay et al., 2013; Leroy et al., 2015). In addition, Large Diffeomorphic Deformation Mapping Metric (LDDMM; Trounev, 1998), as a powerful surface mapping method, can perform two cortical surfaces mapping by treating the two-dimensional manifolds of the cortical surfaces as one-dimensional features (curves), or two-dimensional structure of the manifold as a whole, or combination of one- and two-dimensional features (curves and surface; Glaunès et al., 2008; Zhong et al., 2010).

Here, we utilized a surface-based computational approach to investigate the 3D morphology of the CSs in children with ADHD. We first extracted the CS from individual, high-resolution structural MR images, followed by 3D surface reconstruction and parameterization. We then computed several surface metrics (sulcal length, depth, surface area, sulcal span, cortical thickness, and sulcal profile) based on the parameterized surface maps. Finally, we statistically analyzed the differences between the children with ADHD and the controls with regard to these metrics.

Materials and Methods

Participants

The sample for this study consisted of 21 children with ADHD and 21 demographically group-matched control children, ages from 9 to 15 years old. All of the subjects were strongly right-handed, evaluated using the Edinburgh Handedness Inventory

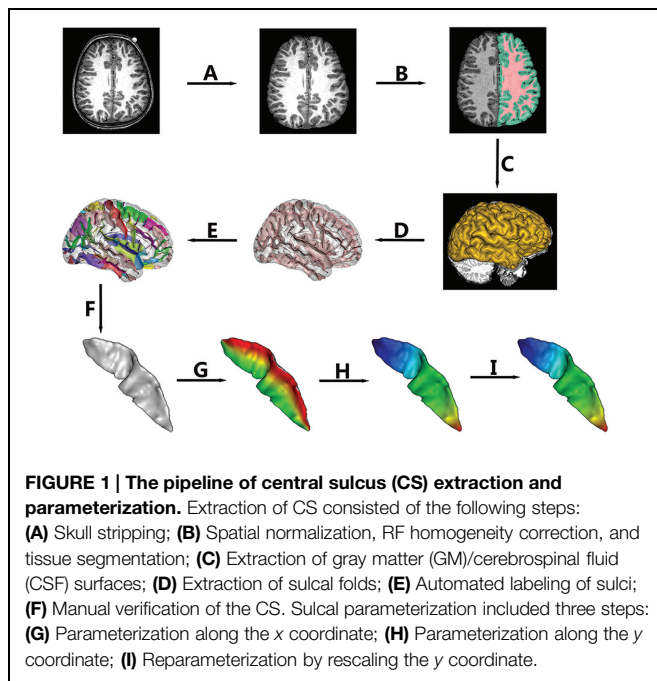
(Oldfield, 1971) and had estimated full-scale IQ ≥ 80 , measured by Wechsler Abbreviated Scale of Intelligence (WASI; Wechsler, 1999), to minimize neurobiological heterogeneity.

The patient group included children who met *DSM-IV* criteria for ADHD combined type, by combining the Conners Rating Scale—Revised-L for both parent and self-reports (Conners, 1997). This was confirmed with a parent interview using the Schedule for Affective Disorders and Schizophrenia for Children—Present and Lifetime Version (K-SADS-PL; Kaufman et al., 1997). The normal control group included children who had *T*-scores <60 (<1 SD) on all Conners parent and self-reports. For both groups, we included the K-SADS-PL screening questions and supplements to rule out pervasive developmental disorders, substance use and abuse, and posttraumatic stress disorder. Similarly, oppositional defiant disorder with physical aggression (using *DSM-IV* diagnostic criteria), and all other current Axis I disorders (except for fear of the dark) were exclusionary. Children with any specific learning disorders were also excluded. The basic reading, mathematical reasoning, reading comprehension, and numerical operations subtests of the Wechsler Individual Achievement Test Second Edition (WIAT-II; Wechsler, 2001) were administered to determine the presence of impairments in reading or math. General exclusion criteria for both groups also included chronic medical/neurological illness or was taking systemic medication; specific or focal neurological disorder including epilepsy; treatment with any non-stimulant psychotropic within the past 3 months; and contraindications to magnetic resonance imaging (MRI) scanning. In addition, we also avoided including siblings, considering that genetic factors might influence the morphological patterns of the CS.

The children with ADHD were recruited from the Children's Evaluation and Rehabilitation Center at the Albert Einstein College of Medicine, and the Max and Celia Parnes Family Psychological and Psycho-educational Services Clinic at the Ferkauf Graduate School of Psychology. The control children were recruited from local schools through newspaper advertisements. This study received Institutional Review Board approval for human subjects' research at the Albert Einstein College of Medicine. Written informed consents were provided by all participants and their parents after the nature of the study and its procedures were carefully explained. All procedures were conducted in keeping with the tenets for the ethical conduct of research as outlined in the Declaration of Helsinki.

MRI Scan Acquisition and Image Preprocessing

High-resolution three-dimensional T1-weighted structural MRI data were acquired from each subject using a 3T Philips Achiva TX MR system with a 32-channel phased array head coil (Invivo, Gainesville, FL, USA). Axial images were acquired using MPRAGE with the following scan parameters: TR = 9.8 ms, TE = 4.6 ms, flip angle = 8° , voxel size = $0.94 \text{ mm} \times 0.94 \text{ mm} \times 1 \text{ mm}$, field of view = $240 \text{ mm} \times 188 \text{ mm} \times 220 \text{ mm}$, SENSE reduction factor = 2.5, 235 contiguous slices. Then, all images were resliced at a $0.94 \text{ mm} \times 0.94 \text{ mm} \times 0.94 \text{ mm}$ isotropic resolution. The non-brain tissue was stripped (See **Figure 1A**) using the Brain



Extraction Tool (Smith, 2002) provided as an add-on for the MRIcro software package¹ (FMRIB Image Analysis Group, Oxford, UK).

Extraction of the CS

In this study, BrainVISA (BV) software² (version 4.3.0) was used to extract the CS for all of the individuals. The whole pipeline is shown in **Figure 1**. The detailed procedures were as follows.

(a) Normalization

To remove gross differences in brain size and orientation, we normalized all images into Talairach space. First, two professional neuroanatomists manually labeled four points in each axial image, i.e., the anterior commissure, the posterior commissure, an inter-hemispheric point, and a point in the left hemisphere. Then, a transformation based on the two points defined by the anterior and posterior commissures to the Talairach AC/PC referential was computed and applied to the whole image.

(b) Brain Tissue Segmentation

The intensities in raw images not only depend on the properties of different tissues but also on the location in the field of view due to the inhomogeneity of magnetic field. Thus, we first corrected the spatial bias (Mangin, 2000) in normalized images. Then, a fuzzy-classifier-based anatomical segmentation method (Mangin et al., 1998) was used to segment brain tissue into GM, white matter (WM), and cerebrospinal fluid (CSF; See **Figure 1B**).

(c) Sulcal Extraction and Identification of the CS

A 3D mesh of the external surface of the cortex for each hemisphere was computed based on the boundary between GM

and CSF, as shown in **Figure 1C**. Sulcal structures were then reconstructed as the medial surfaces of two opposing gyral banks, which spanned from the GM/CSF border at the most internal point of the sulcus to the convex hull of the cortex (See **Figure 1D** and Mangin et al., 2004). Finally, an automated sulcal recognition algorithm was used to assign standard anatomical labels to these sulci, including the CS (See **Figure 1E**).

(d) Manual Verification of the CS

We observed some small, accessory sulci on the surfaces of the extracted CSs. They were usually shorter than 5 mm, originating at a right angle from the stem of the main sulcus, and were considered to be random folds (Ono et al., 1990). In this study, two experienced neuroanatomists checked each extracted CS and removed these small and accessory sulci. An example of the finally extracted CS was shown in **Figure 1F**.

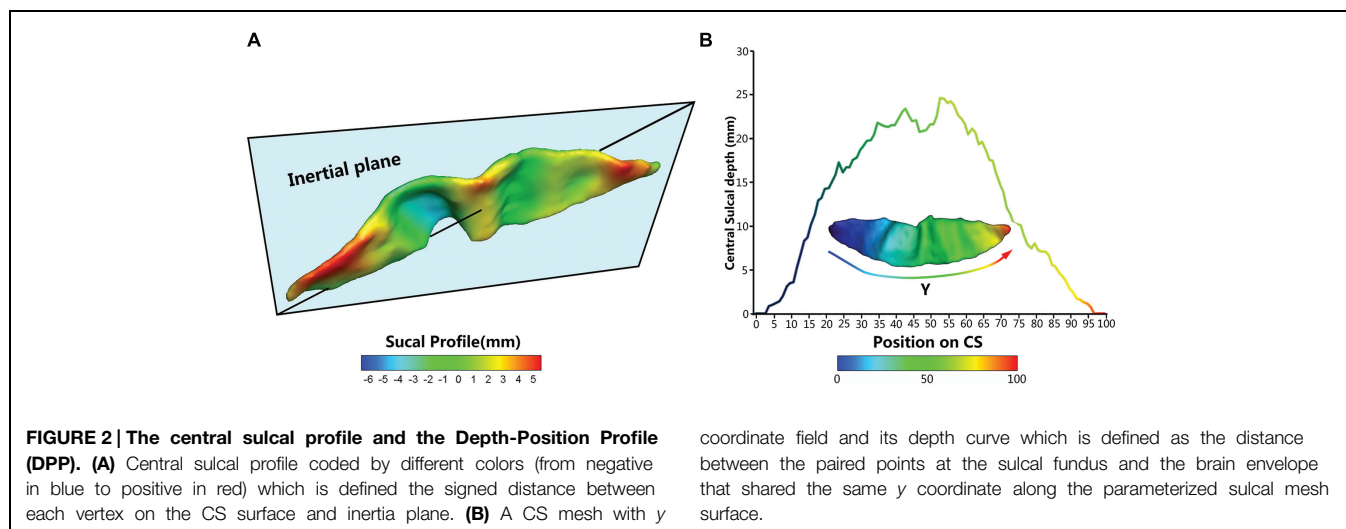
Sulcal Parameterization

To compare the morphological differences at each location of the CS across individuals, we need to parameterize each CS to create a normalized coordinate system on the CS surfaces. Our sulcal parameterization included two steps. The first step was to acquire the x - y coordinate system for each CS using the sulcal parameterization method based on the heat-equation diffusion process along the CS surface (Cykowski et al., 2008). Two coordinate fields (x : from the lateral to the medial edge; and y : from the superior to the inferior end of the sulcus) were extrapolated by solving the heat equation on the surface, and the bottom and top ridges of the sulcal mesh as well as the endpoints of the sulcus where these top and bottom ridges joined behaved as constant heat sources (**Figures 1G,H**). In this way, the normalized coordinate system was constructed for each CS surface.

To provide a better inter-subject matching of the CS anatomy, a reparameterization procedure based on two anatomical landmarks on the sulcal profile was performed as the second step. This method was similar to those used in this literature (Coulon et al., 2011). The sulcal profile was defined as the function of the y position that represented the average value of the signed distance of each node on the mesh at the same position y to the inertial plane of the CS. The inertial plane was defined by the barycenter and was reflected in two orthogonal principal orientations of the CS (See **Figure 2A**). The sulcal profile was a morphological characteristic to measure shape variations along the superior-inferior direction (i.e., the direction along the y -axis) of the CS (Coulon et al., 2011 and See **Figure 2A**). Then, two stable anatomical landmarks, L_1 and L_2 , relating to the functional primary motor area of the hand, were detected on the CS along the sulcal profile curve according to the literature (Coulon et al., 2011). For each group, the average L_1 and L_2 were obtained by averaging the L_1 and L_2 positions across subjects within the same group. The reparameterization was computed by rescaling the y coordinates in a piecewise linear fashion by exactly matching the coordinates of the two anatomical landmarks L_1 and L_2 across subjects within each group. This step ensured the correspondences of the surface

¹<http://www.sph.sc.edu/comd/rorden/micro.html>

²<http://brainvisa.info/>



morphology of the hand area in the CS across subjects, as depicted in **Figure 11**. Finally, all parameterized CS meshes were remeshed to the template mesh to obtain an inter-subject node-to-node correspondence. The template CS mesh was constructed from an unbiased standard MRI template brain data within the 10-to-14-year-old age range (Almli et al., 2007).

Surface-based Measurements

We employed five metrics (i.e., sulcal depth, length, span, surface area, and cortical thickness) to describe the entire morphometry of the CS surface. The *sulcal depth* at each position was defined as the distance between the paired points at the sulcal fundus and the brain envelope that shared the same *y* coordinate along the parameterized sulcal mesh surface (See **Figure 2B**). The average sulcal depth was calculated as the mean value of the sulcal depths at all positions. The maximum depth was also chosen from all sulcal depths for each subject. The *sulcal length* was defined as the average length along the exterior and interior sulcal boundaries of CS. The average *sulcal span* for the CS was defined as an average 3D distance between opposing gyral banks along the normal directions of the medial sulcal mesh (Kochunov et al., 2008). The *sulcal surface area* was evaluated as the sum of the areas of all triangles of the mesh of the CS. The average *cortical thickness* was the mean distance between the CSF/GM interface and the GM/WM interface along the CS.

In addition, we used the signed distance of each node on the mesh to the inertial plane of the CS to characterize the local shape variations on the surface. The signed distance was defined as $d_i = (n_i - \bar{n}) \cdot u_3$ where \bar{n} is the barycenter of the CS mesh and $n_i = (n_{xi}, n_{yi}, n_{zi})^T$ represents the node of the mesh and where a given sulcus mesh could be defined as the vector of nodes $S = (n_i)_{i=1, \dots, N}$. The centered mesh S_c was defined as $(n_i - \bar{n})$. We generated the covariance matrix $A = S_c S_c^T$, and u_1 , u_2 , and u_3 are the three eigenvectors of A ordered by decreasing eigen-value. Thus, u_1 and u_2 represent the main orientation of the CS and construct the inertia plane, and u_3

reflects the normal direction of the inertial plane (Coulon et al., 2011).

Statistical Analysis

For each sulcal metric, we used a multiple linear regression model to explore the between-group differences, with age and gender as covariates, because the 3D morphology of the CS could be affected by age and gender (Amunts et al., 2000; Luders et al., 2003). *P*-values less than 0.05 were considered to be statistically significant.

To determine whether the CS depth and profile in the children with ADHD were different along the superior-inferior direction (i.e., the *y*-axis) of the CS compared with controls, we performed multiple linear regression analyses at each *y* position with age and gender as the covariates. Significant differences were evident in the sulcal depth and profile curves. To further estimate the local shape variations on the surface, we compared the between-group differences in the signed distance on the mesh to the inertial plane in a node-by-node manner. Statistical difference maps for the sulcal profiles between the groups are displayed on the template. The false discovery rate (FDR) was used for multiple-comparison corrections.

Furthermore, we assessed the associations between these sulcal metrics and hyperactivity-impulsivity scores as well as inattention scores in the regions showing significant between-group differences across all subjects, using age, and gender as the covariates.

Results

Group Statistics

The children with ADHD and typically developing controls had no significant differences in demographic measures (all $P > 0.1$). The *t*-scores of inattention, hyperactivity-impulsivity, and DSM-IV total in ADHD children were significantly higher when compared to that in controls. Detailed statistics are shown in **Table 1**.

TABLE 1 | Demographic and clinical data of the healthy children and the children with attention-deficit/hyperactivity disorder (ADHD).

	ADHD (<i>n</i> = 21) Mean (SD)	Healthy (<i>n</i> = 21) Mean (SD)	<i>P</i>
Age (months)	130.14 (23.83)	139.19 (22.71)	0.2152
Gender (boys/girls)	18/3	15/6	0.1571
Inattention score**	64.52 (9.27)	46.95 (5.63)	<<0.001
Hyperactivity-impulsivity scores**	71.67 (14.00)	50.00 (10.93)	<<0.001
DSM-IV total scores**	69.19 (10.68)	48.40 (8.22)	<<0.001
IQ	104.90 (15.61)	107.38 (12.10)	0.5688

*Inattention score, Hyperactivity-impulsivity scores, and DSM-IV total scores reflect DSM-IV criteria for ADHD. The threshold value is 60. A Wilcoxon rank-sum test and a two-sample *t*-test were separately used to examine differences in the gender and age distributions between the ADHD and control groups. ***P* < 0.001.*

Between-Group Differences in Global Measures of the CS

Results of statistic analyses in the global measures (average depth, maximum depth, average length, average span, surface area, and average cortical thickness) of the CS are summarized in **Table 2**. The ADHD group showed a significantly greater sulcal depth (average depth: *P* < 0.01; maximum depth: *P* = 0.018) in the left CS compared to the control group. The average cortical thicknesses along the bilateral CS of the ADHD group were significantly larger than those of the control group (left: *P* < 0.01; right: *P* < 0.01).

Sulcal Depth and Sulcal Profile along the CS

We measured the CS depth along the *y* coordinate at 100 successive points and then produced the depth-position

profile (DPP) after sulcal parameterization. The between-group differences of the local CS depth, along the superior-inferior direction of the bilateral CS, are shown in the **Figures 3A,B**. *Ps* less than 0.05 were shown as red asterisks after FDR correction. Between group comparison of this local measure found that children with ADHD had significantly greater local depth in the middle section (i.e., *y* = 52~57) of left side CS.

A similar analysis was applied to the sulcal profile. Scatter plots are shown in **Figures 3C,D**. The two clinical groups showed significant (*P* < 0.05, FDR corrected) differences of local CS profiles in large areas of the superior and middle sections (*y* = 15~26, 38~49, and 52~54) of the left side CS, and in the middle section (*y* = 46~52) of the right side CS.

Node-based Analysis in the Sulcal Profile of the CS

We also performed a node-based analysis to detect between-group differences in the absolute value of the signed distance of each node to the inertial plane on the CS surface. We found that regional shape variations were located in the middle sections of the bilateral CS (**Figure 4**). The warm color indicated that these regions on the CS surface were much farther from the inertial plane (i.e., exhibited more complex morphology) in the ADHD group compared with the control group. Moreover, the left CS showed more differences than the right CS.

Relationships between the Sulcal Metrics and Clinical Measures

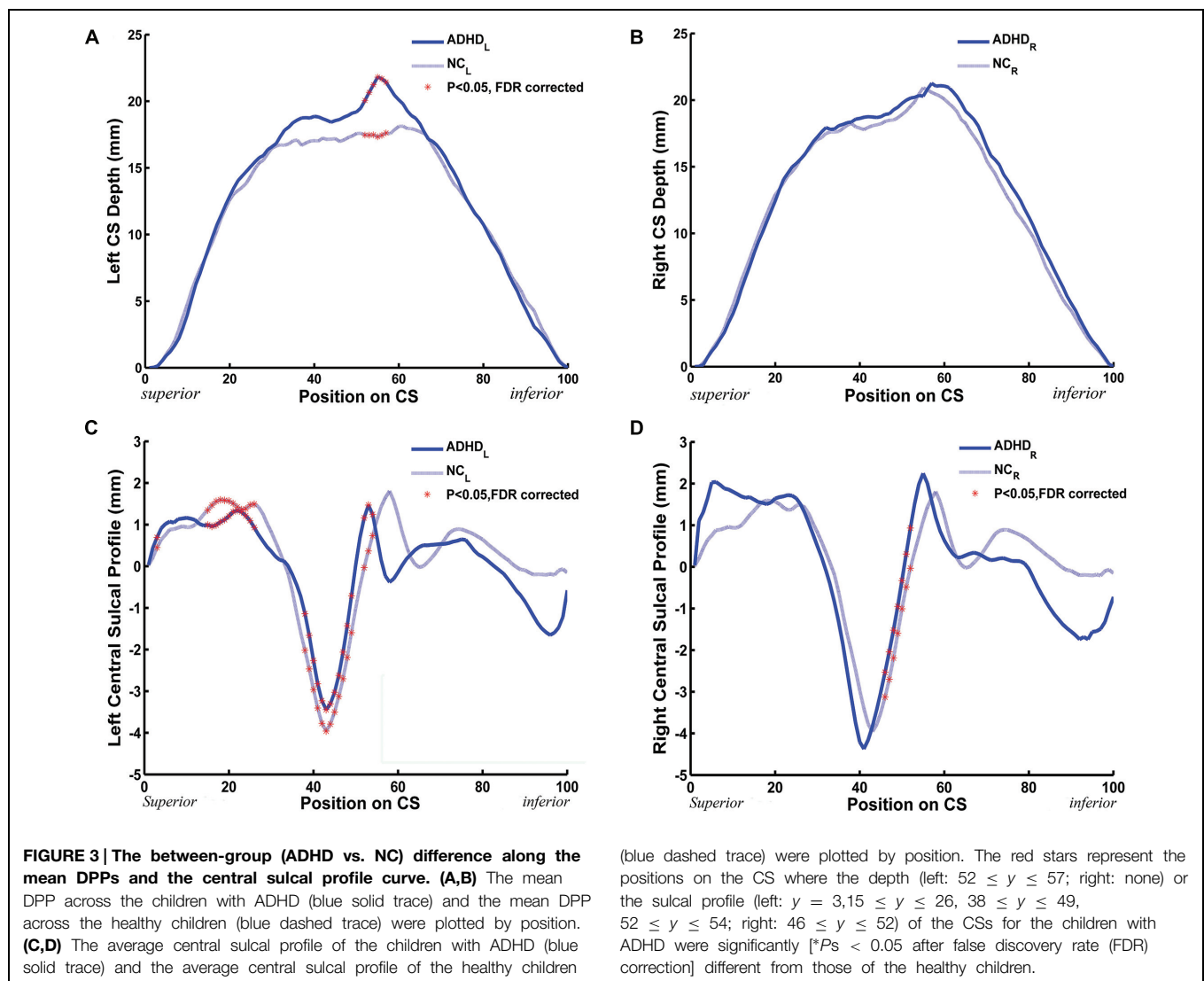
Significant positive associations between the cortical thickness along the bilateral CS and the inattention scores were found in the whole study sample (left: *P* = 0.0181; right: *P* = 0.0082),

TABLE 2 | The global measures of the central sulcus (CS; Means ± SD).

	ADHD	Controls	<i>P</i> -value	<i>t</i> -value
Average length (mm)				
Left	99.31 ± 10.14	97.97 ± 8.41	0.619	0.502
Right	97.29 ± 7.61	94.89 ± 7.17	0.406	0.840
Average depth (mm)				
Left	14.33 ± 1.28	13.00 ± 1.08	0.003**	3.173
Right	14.64 ± 1.65	13.82 ± 0.97	0.074	1.837
Maximum depth (mm)				
Left	19.42 ± 1.49	18.25 ± 1.31	0.018**	2.470
Right	19.66 ± 1.91	18.53 ± 1.59	0.056	1.968
Average span (mm)				
Left	2.35 ± 0.16	2.43 ± 0.19	0.275	-1.106
Right	2.35 ± 0.15	2.29 ± 0.15	0.398	0.855
Surface area (× 10³ mm²)				
Left	3.56 ± 0.45	3.47 ± 0.38	0.460	0.747
Right	3.52 ± 0.49	3.45 ± 0.80	0.843	0.120
Average cortical thickness(mm)				
Left	3.83 ± 0.33	3.23 ± 0.59	0.0005**	3.83
Right	3.78 ± 0.37	3.13 ± 0.59	0.0003**	3.99

t > 0 represents the ADHD were larger than the controls.

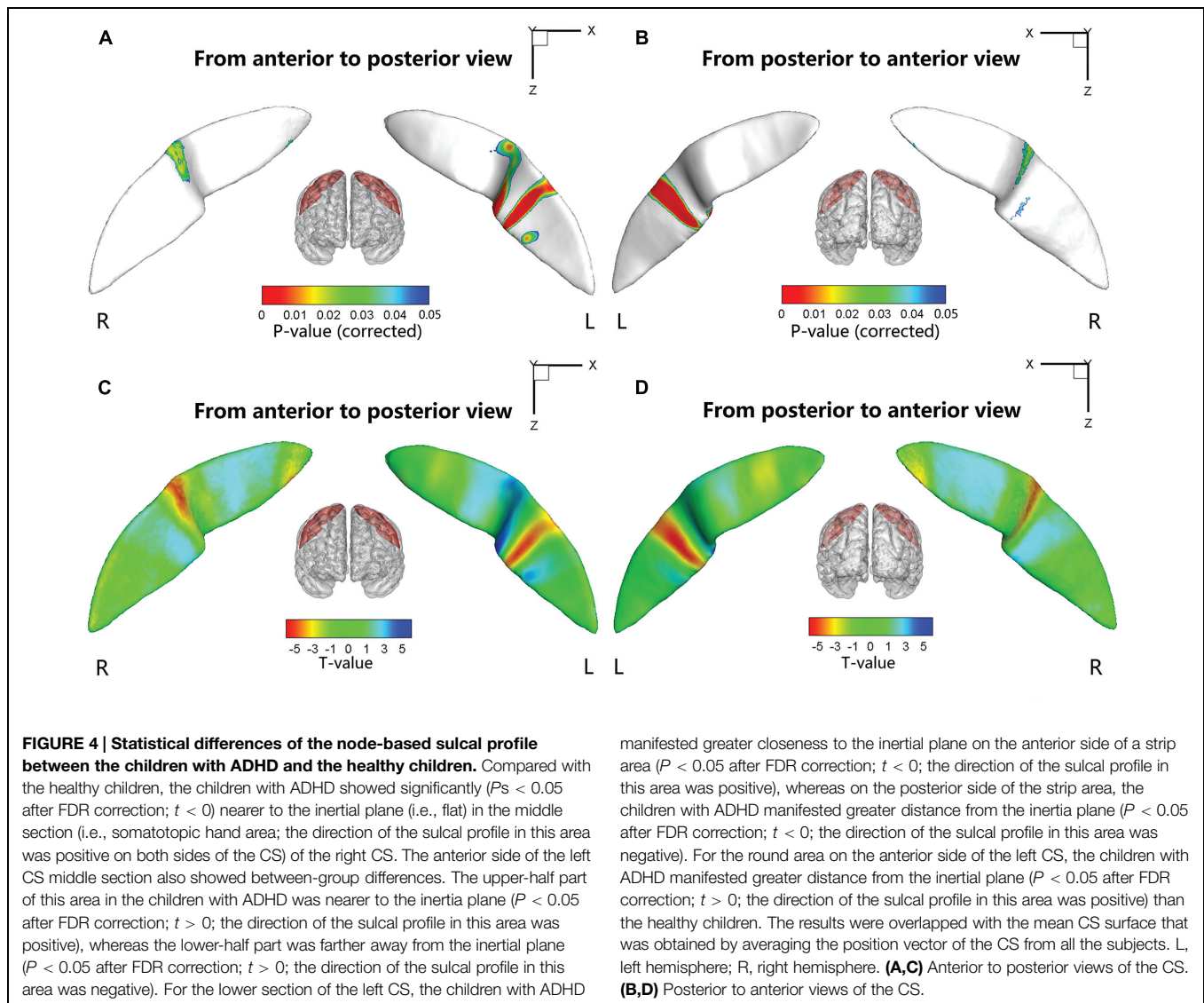
***P* < 0.01.



when using age and gender as the covariates. No significant associations among other global measures and hyperactivity-impulsivity scores as well as inattention scores were found in the whole study sample. For those regions showing significant between-group differences in node-based analysis, we further evaluated the relationships between the sulcal metrics and hyperactivity-impulsivity as well as inattention scores in the whole study sample. Significant ($P < 0.05$) negative correlations between the CS profile and the hyperactivity-impulsivity scores were found in several surface clusters on anterior side of the left CS, which were around the “hand knob” area, whereas the regions showing significant positive correlations located in the posterior side of left CS (anterior: **Figures 5A,C**; posterior: **Figures 5B,D**). Meanwhile, significant ($P < 0.05$) negative correlations between the CS profile and the inattention scores were found in clusters on anterior side of the left CS, while the regions showing positive correlations located in the posterior side of left CS (anterior: **Figures 6A,C**; posterior: **Figures 6B,D**).

Discussion

In this study, we employed a sulcus-based computational approach to investigate the 3D morphology of the CS in children with ADHD. The morphological measures including the global average length, average depth, maximum depth, average span, surface area, and local sulcal profile were computed based on parameterized surface maps. Compared with healthy children, the children with ADHD had no significant differences in average length, average span, or surface area in the CS. However, we found that the children with ADHD showed significantly greater average and maximum depths of the left CS. Meanwhile, the between-group differences had been found in the sulcal profile of bilateral CS, and this change was associated with the hyperactivity-impulsivity scores and inattention scores of the ADHD children. Together, our results provided evidence for the abnormality of structural morphology of the CS in children with ADHD due to structural changes in the motor cortices of the brain.



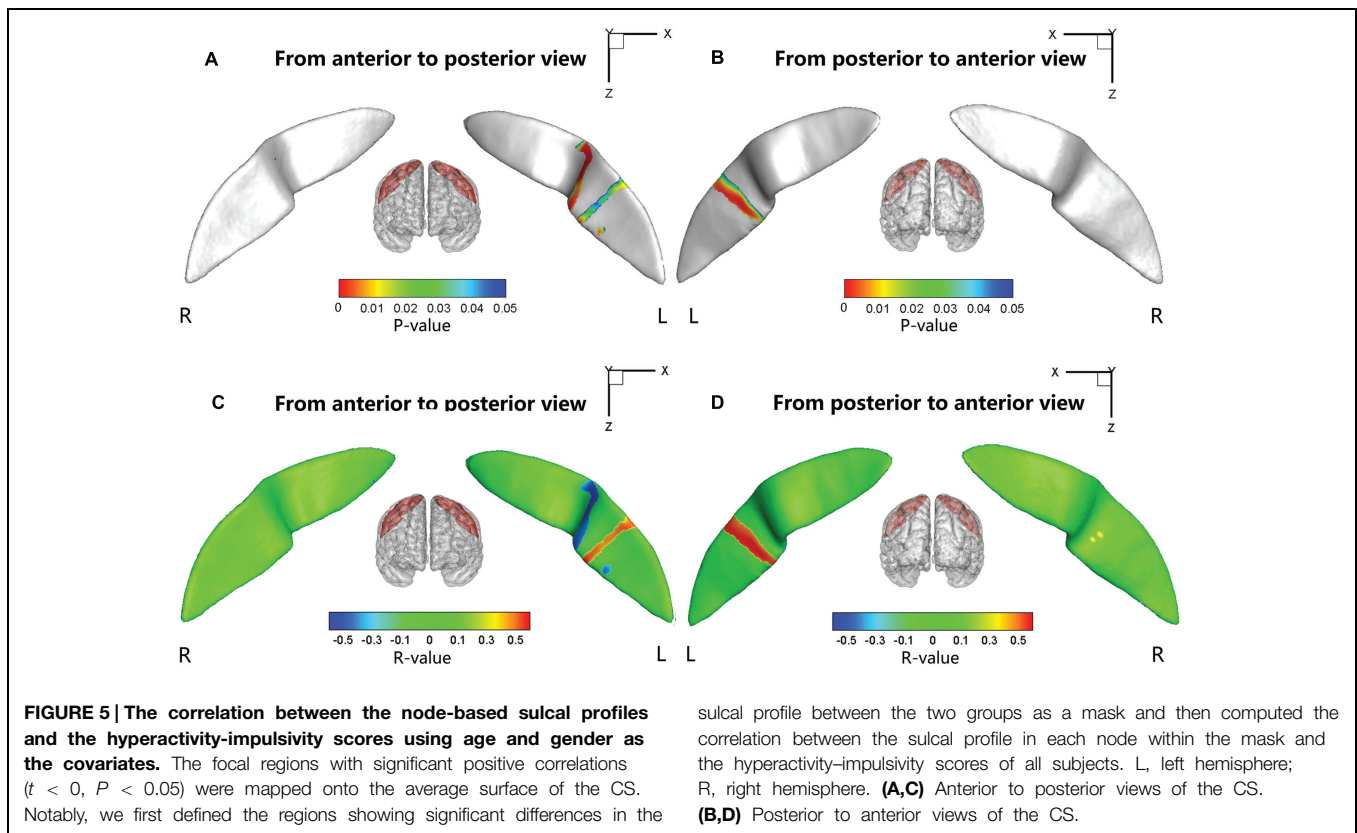
Morphometric Differences in the CS between the Children with ADHD and the Controls

We found that there were no significant differences in average length, average span and surface area of the bilateral CS between the children with ADHD and the healthy controls. However, the average and maximum depths of the left CS reflected a significantly deeper fold associated with ADHD compared with normal controls.

Sulcal depth has been widely used to characterize the morphology of cortical folding. Previous studies have suggested that changes in sulcal depth might result from altered axonal mechanical tension generated by cortico-cortical connections (Davatzikos and Bryan, 2002; Van Essen et al., 2006). Mostofsky et al. (2002) found that the premotor cortex of children with ADHD showed WM reduction on both sides, suggesting a primarily axonal abnormality in children with ADHD (Ranta et al., 2009). The maximum depth corresponds to the deepest part of a sulcus and was thought to be where the folding

of the structure began (Smart and McSherry, 1986; Welker, 1990; Lefèvre et al., 2009); thus, it might be associated with geometrical features influenced by genetic factors. A substantial family (Biederman et al., 1990; Faraone et al., 1992), twin (Levy et al., 1997), and adoption studies (Alberts-Corush et al., 1986) have demonstrated genetic elements existing in ADHD. The heritability of ADHD has been estimated to be 0.50–0.98 (Levy et al., 1997). Meanwhile, the deep sulcal regions are thought to be the first cortical folds to form in the early stages of development (Régis et al., 2005), and their formation might be related to genetic control and cytoarchitectonic areas. Differences in depth might signal abnormal developmental events occurring in the early life stage, which would support the hypothesis of a departure from typical cortical developmental trajectory occurring very early in ADHD (Shaw et al., 2006).

Using DPPs, we further found that the depths at the positions (52–57) of the left CS in the ADHD group were significantly



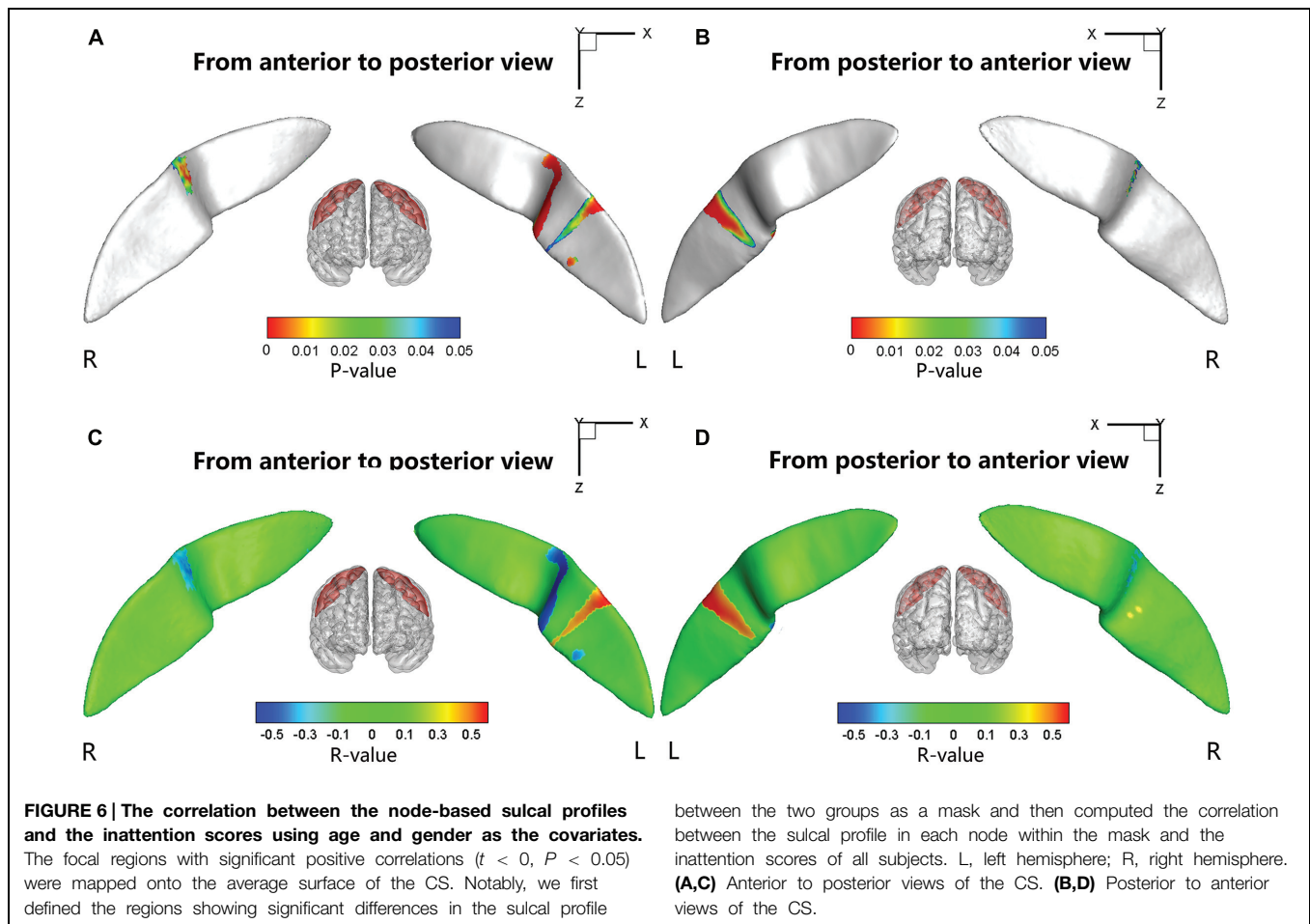
larger than those of the typically developing children. These positions of the CS DPP are near the Sylvian fissure. Many published studies contributed to the mapping of the finger-tapping area (25~47) of the DPP and to the mapping of the oral movement area, involving lip pursing, tongue movement, and smiling (57~85), of the DPP (McKay et al., 2013). The abnormality in CS depth that is partly located on the oral movement area might explain the symptom of talkativeness in children with ADHD.

The sulcal profile curve is defined as the average signed distance of nodes that share the same position y to the inertial plane of the CS, which provides more shape information across subjects than the depth curve. In this study, we found that the between-group differences of the sulcal profile along the left CS were located in the middle section, which involved the function of finger tapping as well as oral movement. Subsequently, we further employed node-based analysis on the sulcal surface and located specific regions in the middle section of the bilateral CS showing significant between-group differences. Many studies have suggested that the middle section of the CS is mainly composed of the somatotopic hand area (White et al., 1997; Sastre-Janer et al., 1998; Boling et al., 1999). Functional neuroimaging studies have suggested that this region shows neuronal activation during hand motor tasks (Rao et al., 1995). Moll et al. (2001) used transcranial magnetic stimulation (TMS) to investigate the hand area of the left motor cortex and found a distinct dysfunctional pattern of deficient inhibitory motor control for ADHD and chronic tic disorder

(TD), which could be a neurobiological correlate of hypermotoric symptoms in children with both disorders. Our findings of abnormalities in the hand area of bilateral CS might account for the related ADHD deficits in executive and motor function. In addition, we also found that the lower section on both sides of the left CS showed significant between-group differences. Using functional MRI, Fesl et al. (2003) demonstrated that the inferolateral segment of the CS was mainly associated with the primary motor/sensory tongue area. These abnormalities of the CS might explain the symptom of talkativeness in children with ADHD.

Relationships between Sulcal Shape and the Gray Matter Volume, White Matter Volume, and Cortical Thickness of the Motor Area

Structural change in the motor area is of interest because motor hyperactivity is a cardinal feature of ADHD. Previous studies have reported the structural abnormality of the motor area in children with ADHD. The reduction of GM volume in the left perirolandic area (Carmona et al., 2005) or bilateral premotor areas (Mostofsky et al., 2002) were observed in children with ADHD, Shaw et al. (2007) observed cortical thickness maturational delays in ADHD and found that the maturational peak of the motor cortex in ADHD was 4 months ahead of the controls. They (Shaw et al., 2007) also found that children with ADHD manifested global thinning of the cortex, including the left precentral regions. We found the maximum and average depths of the left CS as well as average cortical thickness along



bilateral CS in children with ADHD to be larger than those of the healthy children, whereas the other global sulcal metrics showed no between-group differences. A previous multiple regression analysis revealed that dilation of the sulcal space was related to reductions in the cortical GM thickness observed in normal aging (Kochunov et al., 2008). Im et al. (2008) suggest that there may be other effects that change the depth of the cortical sulci in normal subjects, i.e., severely reduced cortical thickness and gyral WM volume may overwhelm other effects and primarily lead to the sulcal depth changes. In our study, the increased sulcal depth and changes in the sulcal profile might be mostly caused by volumetric changes in the WM or GM and in cortical thickness, which can induce different biological and clinical interpretations and remains to be proved experimentally.

Correlations between the CS Metrics and Clinical Measures

Very interestingly, this study found that in the whole study population, the average sulcal depth and node-based geometric properties of the anterior and posterior sides of the left CS (around the “hand knob” area) associated with the attention and inhibition capacities in similar ways. This finding first time placed the left CS into the brain

networks (traditionally thought to involve prefrontal lobe, anterior cingulate cortex, striatum, thalamus, etc. (Castellanos et al., 2006) that may modulate the normality of attention and inhibition functions in a developmental brain, and contribute to the behavioral capacities of attention and inhibition.

Further Considerations

To build upon this study, several issues need to be addressed. Firstly, it is not yet well known about how sulcal features directly relate to brain function and the functional implications of the findings need therefore to be explored in future studies. Secondly, we included both male and female subjects in both groups. We acknowledge possible gender-related differences of the GM and WM maturation patterns in typically developing children (Reiss et al., 1996; Eliez et al., 2001), and possible sex-related heterogeneity in ADHD (Ramtekkar et al., 2010). However, the sample size of our study was not large enough to run the between-gender comparisons in each group. Although we added gender as a fixed effect covariate for group comparisons, a future study should focus specifically on examining the gender effects

upon abnormalities of the shape of the CS. Thirdly, there are some robust and straightforward shape morphometry analysis methods such as LDDMM (Troune, 1998; Joshi and Miller, 2000) that can be used to investigate the CS morphology. In future studies, it would be meaningful to compare different surface analysis methods in characterizing sulcal geometry.

In summary, we presented a sulcal geometry-based statistical analysis approach to investigating the morphology of the CS in ADHD. Our study demonstrated significant morphological abnormalities in bilateral CS in children with ADHD, which were significantly associated with their clinical symptoms. These findings suggest that morphological alterations of the sensorimotor cortex in children with ADHD could significantly contribute to the anatomical substrates underlying clinical symptomatology of the disorder.

References

- Alberts-Corush, J., Firestone, P., and Goodman, J. T. (1986). Attention and impulsivity characteristics of the biological and adoptive parents of hyperactive and normal control children. *Am. J. Orthopsychiatry* 56, 413. doi: 10.1111/j.1939-0025.1986.tb03473.x
- Almli, C. R., Rivkin, M. J., and McKinstry, R. C. (2007). The NIH MRI study of normal brain development (Objective-2): newborns, infants, toddlers, and preschoolers. *Neuroimage* 35, 308–325. doi: 10.1016/j.neuroimage.2006.08.058
- Amunts, K., Jäncke, L., and Mohlberg, H. (2000). Interhemispheric asymmetry of the human motor cortex related to handedness and gender. *Neuropsychologia* 38, 304–312. doi: 10.1016/S0028-3932(99)00075-5
- Biederman, J., Faraone, S. V., Keenan, K., Knee, D., and Tsuang, M. T. (1990). Family-genetic and psychosocial risk factors in DSM-III attention deficit disorder. *J. Am. Acad. Child. Adolesc. Psychiatry* 29, 526–533. doi: 10.1097/00004583-199007000-00004
- Boling, W., Olivier, A., Bittar, R. G., and Reutens, D. (1999). Localization of hand motor activation in Broca's pli de passage moyen. *J. Neurosurg.* 91, 903–910. doi: 10.3171/jns.1999.91.6.0903
- Carmona, S., Vilarroya, O., Bielsa, A., Tremols, V., Soliva, J. C., Rovira, M., et al. (2005). Global and regional gray matter reductions in ADHD: a voxel-based morphometric study. *Neurosci. Lett.* 389, 88–93. doi: 10.1016/j.neulet.2005.07.020
- Castellanos, F. X., Sonuga-Barke, E. J., Milham, M. P., and Tannock, R. (2006). Characterizing cognition in ADHD: beyond executive dysfunction. *Trends Cogn. Sci.* 10, 117–123. doi: 10.1016/j.tics.2006.01.011
- Conners, C. K. (1997). *Conners' Rating Scales-Revised: User's Manual*. North Tonawanda, NY: Multi-Health Systems, Inc.
- Coulon, O., Pizzagalli, F., Operto, G., Auzias, G., Delon-Martin, C., and Dojat, M. (2011). "Two new stable anatomical landmarks on the Central Sulcus: definition, automatic detection, and their relationship with primary motor functions of the hand," in *Proceedings of the Engineering in Medicine and Biology Society, EMBC, 2011 Annual International Conference of the IEEE, 2011* (Boston: IEEE), 7795–7798. doi: 10.1109/iembs.2011.6091921
- Cykowski, M. D., Coulon, O., Kochunov, P. V., Amunts, K., Lancaster, J. L., Laird, A. R., et al. (2008). The central sulcus: an observer-independent characterization of sulcal landmarks and depth asymmetry. *Cereb. Cortex* 18, 1999–2009. doi: 10.1093/cercor/bhm224
- Davatzikos, C., and Bryan, R. N. (2002). Morphometric analysis of cortical sulci using parametric ribbons: a study of the central sulcus. *J. Comput. Assist. Tomogr.* 26, 298–307. doi: 10.1097/00004728-200203000-00024
- Denckla, M. B., and Rudel, R. G. (1978). Anomalies of motor development in hyperactive boys. *Ann. Neurol.* 3, 231–233. doi: 10.1002/ana.410030308
- Eliez, S., Blasey, C. M., Freund, L. S., Hastie, T., and Reiss, A. L. (2001). Brain anatomy, gender and IQ in children and adolescents with fragile X syndrome. *Brain* 124, 1610–1618. doi: 10.1093/brain/124.8.1610
- Faraone, S. V., Biederman, J., Chen, W. J., Krifcher, B., Keenan, K., Moore, C., et al. (1992). Segregation analysis of attention deficit hyperactivity disorder. *Psychiatr. Genet.* 2, 257–276. doi: 10.1097/00041444-199210000-00004
- Fesl, G., Moriggl, B., Schmid, U. D., Naidich, T. P., Herholz, K., and Yousry, T. A. (2003). Inferior central sulcus: variations of anatomy and function on the example of the motor tongue area. *Neuroimage* 20, 601–610. doi: 10.1016/S1053-8119(03)00299-4
- First, M. B. (1994). *Diagnostic and Statistical Manual of Mental Disorders (DSM IV)*, 4th Edn. Arlington: APA, 97–327.
- Fujiwara, H., Hirao, K., Namiki, C., Yamada, M., Shimizu, M., Fukuyama, H., et al. (2007). Anterior cingulate pathology and social cognition in schizophrenia: a study of gray matter, white matter and sulcal morphometry. *Neuroimage* 36, 1236–1245. doi: 10.1016/j.neuroimage.2007.03.068
- Glaunès, J., Qiu, A., Miller, M. I., and Younes, L. (2008). Large deformation diffeomorphic metric curve mapping. *Int. J. Comput. Vis.* 80, 317–336. doi: 10.1007/s11263-008-0141-9
- Hoekzema, E., Carmona, S., Ramos-Quiroga, J. A., Fernández, V. R., Picado, M., Bosch, R., et al. (2012). Laminar thickness alterations in the fronto-parietal cortical mantle of patients with attention-deficit/hyperactivity disorder. *PLoS ONE* 7:e48286. doi: 10.1371/journal.pone.0048286
- Im, K., Lee, J. M., Seo, S. W., Kim, S. H., Kim, S. I., and Na, D. L. (2008). Sulcal morphology changes and their relationship with cortical thickness and gyral white matter volume in mild cognitive impairment and Alzheimer's disease. *Neuroimage* 43, 103–113. doi: 10.1016/j.neuroimage.2008.07.016
- Joshi, S. C., and Miller, M. I. (2000). Landmark matching via large deformation diffeomorphisms. *IEEE Trans. Image Process.* 9, 1357–1370. doi: 10.1109/83.855431
- Kaufman, J., Birmaher, B., Brent, D., Rao, U. M. A., Flynn, C., Moreci, P., et al. (1997). Schedule for affective disorders and schizophrenia for school-age children-present and lifetime version (K-SADS-PL): initial reliability and validity data. *J. Am. Acad. Child. Adolesc. Psychiatry* 36, 980–988. doi: 10.1097/00004583-199707000-00021
- Kochunov, P., Thompson, P. M., Coyle, T. R., Lancaster, J. L., Kochunov, V., Royall, D., et al. (2008). Relationship among neuroimaging indices of cerebral health during normal aging. *Hum. Brain. Mapp.* 29, 36–45. doi: 10.1002/hbm.20369
- Lefèvre, J., Leroy, F., Khan, S., Dubois, J., Huppi, P. S., Baillet, S., et al. (2009). "Identification of growth seeds in the neonate brain through surfacic Helmholtz decomposition," in *Information Processing in Medical Imaging*, eds J. L. Prince, D. L. Pham, and K. J. Myers (Berlin: Springer), 252–263.
- Leroy, F., Cai, Q., Bogart, S. L., Dubois, J., Coulon, O., Monzalvo, K., et al. (2015). New human-specific brain landmark: the depth asymmetry of superior temporal sulcus. *Proc. Natl. Acad. Sci. U.S.A.* 112, 1208–1213. doi: 10.1073/pnas.1412389112
- Levy, F., Hay, D. A., McStephen, M., Wood, C., and Waldman, I. (1997). Attention-deficit hyperactivity disorder: a category or a continuum? Genetic analysis of a

Author Contributions

SL and XBL designed the research; XBL collected the data; SW, XWL, and QL analyzed the results; SL, SW, and XBL wrote the main manuscript text. All authors reviewed the manuscript.

Acknowledgments

This work was partially supported by the Rose F. Kennedy Intellectual and Developmental Disabilities Research Center (RFK-IDDRC) through a program grant (HD071593) from the Eunice Kennedy Shriver National Institute of Child Health and Human Development (NICHD), the National Science Foundation of China (Nos. 81171403, and 81471731).

- large-scale twin study. *J. Am. Acad. Child. Adolesc. Psychiatry* 36, 737–744. doi: 10.1097/00004583-199706000-00009
- Li, S., Han, Y., Wang, D., Yang, H., Fan, Y. B., Lv, Y., et al. (2010). Mapping surface variability of the central sulcus in musicians. *Cereb. Cortex* 20, 25–33. doi: 10.1093/cercor/bhp074
- Li, S., Xia, M., Pu, F., Li, D., Fan, Y., Niu, H., et al. (2011). Age-related changes in the surface morphology of the central sulcus. *Neuroimage* 58, 381–390. doi: 10.1016/j.neuroimage.2011.06.041
- Luders, E., Rex, D. E., Narr, K. L., Woods, R. P., Jancke, L., Thompson, P. M., et al. (2003). Relationships between sulcal asymmetries and corpus callosum size: gender and handedness effects. *Cereb. Cortex* 13, 1084–1093. doi: 10.1093/cercor/13.10.1084
- Mangin, J. F. (2000). “Entropy minimization for automatic correction of intensity nonuniformity,” in *Proceedings of the IEEE Workshop on Mathematical Methods in Biomedical Image Analysis* (Hilton Head Island, SC: IEEE), 162–169. doi: 10.1109/mmmbia.2000.852374
- Mangin, J. F., Coulon, O., and Frouin, V. (1998). “Robust brain segmentation using histogram scale-space analysis and mathematical morphology,” in *Proceedings of the Medical Image Computing and Computer-Assisted Intervention—MICCAI’98*, (Berlin: Springer), 1230–1241. doi: 10.1007/BFb0056313
- Mangin, J. F., Riviere, D., Cachia, A., Duchesnay, E., Cointepas, Y., Papadopoulos-Orfanos, D., et al. (2004). A framework to study the cortical folding patterns. *Neuroimage* 23, 129–138. doi: 10.1016/j.neuroimage.2004.07.019
- McKay, D. R., Kochunov, P., Cykowski, M. D., Kent, J. W., Laird, A. R., Lancaster, J. L., et al. (2013). Sulcal depth-position profile Is a genetically mediated neuroscientific trait: description and characterization in the central sulcus. *J. Neurosci.* 33, 15618–15625. doi: 10.1523/JNEUROSCI.1616-13.2013
- Moll, G. H., Heinrich, H., Trott, G. E., Wirth, S., Bock, N., and Rothenberger, A. (2001). Children with comorbid attention-deficit-hyperactivity disorder and tic disorder: evidence for additive inhibitory deficits within the motor system. *Ann. Neurol.* 49, 393–396.
- Mostofsky, S. H., Cooper, K. L., Kates, W. R., Denckla, M. B., and Kaufmann, W. E. (2002). Smaller prefrontal and premotor volumes in boys with attention-deficit/hyperactivity disorder. *Biol. Psychiatry* 52, 785–794. doi: 10.1016/S0006-3223(02)01412-9
- Mostofsky, S. H., Newschaffer, C. J., and Denckla, M. B. (2003). Overflow movements predict impaired response inhibition in children with ADHD. *Percept. Mot. Skills* 97, 1315–1331. doi: 10.2466/pms.2003.97.3f.1315
- Mostofsky, S. H., Rimrodt, S. L., Schafer, J. G., Boyce, A., Goldberg, M. C., Pekar, J. J., et al. (2006). Atypical motor and sensory cortex activation in attention-deficit/hyperactivity disorder: a functional magnetic resonance imaging study of simple sequential finger tapping. *Biol. Psychiatry* 59, 48–56. doi: 10.1016/j.biopsych.2005.06.011
- Narr, K. L., Woods, R. P., Lin, J., Kim, J., Phillips, O. R., Del’Homme, M., et al. (2009). Widespread cortical thinning is a robust anatomical marker for attention-deficit/hyperactivity disorder. *J. Am. Acad. Child. Adolesc. Psychiatry* 48, 1014–1022. doi: 10.1097/CHI.0b013e3181b395c0
- Oldfield, R. C. (1971). The assessment and analysis of handedness: the Edinburgh inventory. *Neuropsychologia* 9, 97–113. doi: 10.1016/0028-3932(71)90067-4
- Ono, M., Kubik, S., and Abernathy, C. D. (1990). *Atlas of the Cerebral Sulci*. Stuttgart: Thieme.
- Penfield, W. (ed.). (1937). “The cerebral cortex and consciousness,” in *The Harvey Lectures*. Faculty Publications and Presentations.
- Ramtekkar, U. P., Reiersen, A. M., Todorov, A. A., and Todd, R. D. (2010). Sex and age differences in attention-deficit/hyperactivity disorder symptoms and diagnoses: implications for DSM-V and ICD-11. *J. Am. Acad. Child. Adolesc. Psychiatry* 49, 217–228. doi: 10.1097/00004583-201003000-00005
- Ranta, M. E., Crocetti, D., Clauss, J. A., Kraut, M. A., Mostofsky, S. H., and Kaufmann, W. E. (2009). Manual MRI parcellation of the frontal lobe. *Neuroimage* 172, 147–154. doi: 10.1016/j.psychnres.2009.01.006
- Rao, S. M., Binder, J. R., Hammeke, T. A., Bandettini, P. A., Bobholz, J. A., Frost, J. A., et al. (1995). Somatotopic mapping of the human primary motor cortex with functional magnetic resonance imaging. *Neurology* 45, 919–924. doi: 10.1212/WNL.45.5.919
- Régis, J., Mangin, J. F., Ochiai, T., Frouin, V., Rivière, D., Cachia, A., et al. (2005). “Sulcal root” generic model: a hypothesis to overcome the variability of the human cortex folding patterns. *Neurol. Med. Chir.* 45, 1–17. doi: 10.2176/nmc.45.1
- Reiss, A. L., Abrams, M. T., Singer, H. S., Ross, J. L., and Denckla, M. B. (1996). Brain development, gender and IQ in children A volumetric imaging study. *Brain* 119, 1763–1774. doi: 10.1093/brain/119.5.1763
- Sastre-Janer, F. A., Régis, J., Belin, P., Mangin, J. F., Dormont, D., Masure, M. C., et al. (1998). Three-dimensional reconstruction of the human central sulcus reveals a morphological correlate of the hand area. *Cereb. Cortex* 8, 641–647. doi: 10.1093/cercor/8.7.641
- Shaw, P., Eckstrand, K., Sharp, W., Blumenthal, J., Lerch, J. P., Greenstein, D., et al. (2007). Attention-deficit/hyperactivity disorder is characterized by a delay in cortical maturation. *Proc. Natl. Acad. Sci. U.S.A.* 104, 19649–19654. doi: 10.1073/pnas.0707741104
- Shaw, P., Lerch, J., Greenstein, D., Sharp, W., Clasen, L., Evans, A., et al. (2006). Longitudinal mapping of cortical thickness and clinical outcome in children and adolescents with attention-deficit/hyperactivity disorder. *Arch. Gen. Psychiatry* 63, 540–549. doi: 10.1001/archpsyc.63.5.540
- Smart, I. H., and McSherry, G. M. (1986). Gyrus formation in the cerebral cortex in the ferret. I. Description of the external changes. *J. Anat.* 146, 141.
- Smith, S. M. (2002). Fast robust automat ed brain extraction. *Hum. Brain. Mapp.* 17, 143–155. doi: 10.1002/hbm.10062
- Sun, Z. Y., Klöppel, S., Rivière, D., Perrot, M., Frackowiak, R., Siebner, H., et al. (2012). The effect of handedness on the shape of the central sulcus. *Neuroimage* 60, 332–339. doi: 10.1016/j.neuroimage.2011.12.050
- Troune, A. (1998). Diffeomorphic groups and pattern matching in image analysis. *Int. J. Comput. Vision* 28, 213–221. doi: 10.1023/A:1008001603737
- Van Essen, D. C., Dierker, D., Snyder, A. Z., Raichle, M. E., Reiss, A. L., and Korenberg, J. (2006). Symmetry of cortical folding abnormalities in Williams syndrome revealed by surface-based analyses. *J. Neurosci.* 26, 5470–5483. doi: 10.1523/JNEUROSCI.4154-05.2006
- Wechsler, D. (1999). *Manual for the Wechsler Abbreviated Intelligence Scale (WASI)*. San Antonio, TX: The Psychological Corporation.
- Wechsler, D. (2001). *Wechsler Individual Achievement Test—II—Abbreviated Manual*. San Antonio, TX: The Psychological Corporation.
- Welker, W. (1990). Why does cerebral cortex fissure and fold? *Cereb. Cortex* 8B, 3–136. doi: 10.1007/978-1-4615-3824-0_1
- White, L. E., Andrews, T. J., Hulette, C., Richards, A., Groelle, M., Paydarfar, J., et al. (1997). Structure of the human sensorimotor system. II: lateral symmetry. *Cereb. Cortex* 7, 31–47. doi: 10.1093/cercor/7.1.31
- Zhong, J., Phua, D. Y., and Qiu, A. (2010). Quantitative evaluation of lddmm, freesurfer, and caret for cortical surface mapping. *Neuroimage* 52, 131–141. doi: 10.1016/j.neuroimage.2010.03.085

Conflict of Interest Statement: The authors declare that the research was conducted in the absence of any commercial or financial relationships that could be construed as a potential conflict of interest.

Copyright © 2015 Li, Wang, Li, Li and Li. This is an open-access article distributed under the terms of the Creative Commons Attribution License (CC BY). The use, distribution or reproduction in other forums is permitted, provided the original author(s) or licensor are credited and that the original publication in this journal is cited, in accordance with accepted academic practice. No use, distribution or reproduction is permitted which does not comply with these terms.



The autistic brain in the context of normal neurodevelopment

Mark N. Ziats^{1,2*†}, Catherine Edmonson^{1,3†} and Owen M. Rennert¹

¹ National Institute of Child Health and Human Development, NIH, Bethesda, MD, USA, ² Medical Scientist Training Program, Baylor College of Medicine, Houston, TX, USA, ³ College of Medicine, University of Florida, Gainesville, FL, USA

OPEN ACCESS

Edited by:

Julia P. Owen,
University of California
San Francisco, USA

Reviewed by:

Stephen D. Ginsberg,
Nathan Kline Institute, USA
Janice M. Juraska,
University of Illinois, USA

*Correspondence:

Mark N. Ziats,
National Institute of Child Health
and Human Development, NIH,
49 Convent Drive, Building 49,
Room 2c08, Bethesda,
MD 20814, USA
ziats@bcm.edu

[†]These authors have contributed
equally to this work.

Received: 28 March 2015

Accepted: 12 August 2015

Published: 25 August 2015

Citation:

Ziats MN, Edmonson C and Rennert
OM (2015) The autistic brain in the
context of normal neurodevelopment.
Front. Neuroanat. 9:115.
doi: 10.3389/fnana.2015.00115

The etiology of autism spectrum disorders (ASDs) is complex and largely unclear. Among various lines of inquiry, many have suggested convergence onto disruptions in both neural circuitry and immune regulation/glia cell function pathways. However, the interpretation of the relationship between these two putative mechanisms has largely focused on the role of exogenous factors and insults, such as maternal infection, in activating immune pathways that in turn result in neural network abnormalities. Yet, given recent insights into our understanding of human neurodevelopment, and in particular the critical role of glia and the immune system in *normal* brain development, it is important to consider these putative pathological processes in their appropriate normal neurodevelopmental context. In this review, we explore the hypothesis that the autistic brain cellular phenotype likely represents intrinsic abnormalities of glial/immune processes constitutively operant in normal brain development that result in the observed neural network dysfunction. We review recent studies demonstrating the intercalated role of neural circuit development, the immune system, and glial cells in the normal developing brain, and integrate them with studies demonstrating pathological alterations in these processes in autism. By discussing known abnormalities in the autistic brain in the context of normal brain development, we explore the hypothesis that the glial/immune component of ASD may instead be related to intrinsic exaggerated/abnormal constitutive neurodevelopmental processes such as network pruning. Moreover, this hypothesis may be relevant to other neurodevelopmental disorders that share genetic, pathologic, and clinical features with autism.

Keywords: autistic disorder, autism spectrum disorder, neurodevelopment, microglia, mini-columns, neural networks

Introduction

The complex processes that lead to the fully formed human brain encompass a spectrum of mechanisms spanning genetic determinates to environmental and experiential influences. While the specific mechanisms underlying human disorders of neurodevelopment, such as autism spectrum disorder (ASD), remain poorly understood, over the past several decades significant advances have been made to document the cellular and anatomical events that occur as the normal human brain develops and matures. It is therefore important to consider studies of autism in the context of normal cellular/anatomic brain developmental patterns, as it is likely that abnormalities in the autistic brain represent an over-exaggeration and/or under-utilization of normal physiological processes that are constitutively operant in neurodevelopment. This

hypothesis is particularly relevant to studies of cytokines, the immune system, and glia in autistic patients, as abnormalities in these processes are often thought of as reaction to exogenous insults, yet it is entirely plausible instead that these findings represent aberrations of otherwise normal neurodevelopmental mechanisms. In this review, we explore this hypothesis by integrating what is known about normal human neurodevelopment with recent work suggesting immune and glial abnormalities may play a role in the development of autism.

Discussion

Cellular human brain development is a protracted process that begins around the third post-conception week (pcw) and arguably extends nearly into adulthood (Stiles and Jernigan, 2010). Conventionally, human brain development is considered in gross stages within which major cellular and anatomic transitions occur: namely the embryonic, fetal, early and late postnatal, adolescent, and adult periods (Insel, 2010).

Embryonic Period

Beginning early in the embryonic period (defined as conception to eight pcw), the basic structures of the brain, spinal cord, and peripheral nervous system are established. The first major differentiating event of the embryonic period is gastrulation, during which the single-layered blastula forms a trilaminar structure containing the ectoderm, mesoderm, and endoderm. Gastrulation is completed by the third pcw, at which time some cells of the ectodermal layer differentiate into neural progenitors (Ozair et al., 2013). The first well-defined neural structure, the neural tube, begins forming during the third pcw and serves as the basis of the early developing central nervous system (CNS), within which reside populations of neural stem cells. From this basic tubular structure, more specific neural patterning of what will become the major brain structures and compartments occurs through the creation and migration of neural cells from the stem cell proliferative zones. Through graded patterns of molecular signaling, neural progenitors migrate outward from proliferative zones and begin differentiation such that a primitive map of the brain is established by the end of the embryonic period. For instance, through comparative studies of other mammals it has been suggested that the sensomotor regions of the neocortex, the major compartments of the diencephalon and midbrain, and the organization of the hindbrain and spinal column are all well established by the end of the embryonic period in humans (Lumsden and Keynes, 1989; Bishop et al., 2002; Gavalas et al., 2003; Kiecker and Lumsden, 2004; Nakamura et al., 2005).

Fetal Period

Around the ninth pcw, the fetal period of development ensues and extends until birth, during which time there is rapid growth of the structures established during the embryonic period. Grossly, the brain develops its characteristic gyri and sulci during the fetal period, reflecting the underlying dramatic cellular changes occurring during this period (Chi et al., 1977). The majority of neuronal and glial proliferation occurs between the

9th and 16th pcw, with the peak period of migration of these cells to their appropriate region following closely thereafter (Volpe, 2000). In fact, production of new neurons is largely finished by mid-gestation, except for the ongoing production of neurons in a few specialized areas (Bystron et al., 2008).

After their production in the proliferative regions, neurons migrate in an orderly manner to their final position in the developing brain. In the neocortex, the arriving cells establish a 6-layered structure, with the earlier migrating neurons forming the deeper layers and the later migrating neurons forming the more superficial layers (Cooper, 2008). Their migration from the proliferative zone to their final position in the neocortex is helped by the guidance of radial glial cells, a population of stem cells that serve as a scaffold in the developing brain of all vertebrates (Borrell and Götz, 2014). Different layers of the neocortex contain different types of neurons as a result of both cell-intrinsic mechanisms operant in the progenitor cells from which they derive, and through soluble signaling cascades that direct progenitors toward a restricted mature neuronal type (Desai and McConnell, 2000; Leone et al., 2008).

Transient Structures

Of particular note in this migration process are a set of structures that appear only transiently during the fetal period to help guide the migration of progenitors to the developing neocortical layers. The very first neurons to populate the developing neocortex form a primitive and transient structure termed the preplate, which is then split into two separate structures by arriving neurons—the marginal zone and the subplate (Molnár et al., 2006). The region between the marginal zone and subplate serves as a hub for new arriving neurons, and will eventually become layer 6 (the deepest) of the developing neocortex. Subsequently, all newly arriving cells will form progressively more superficial layers of the neocortex from this base structure.

Intriguingly, both the marginal zone and subplate have been shown to highly express some of the genes most significantly linked to neurodevelopmental disorders such as autism and schizophrenia, such as *Reelin* and *TBR1* (Hevner et al., 2001; Bielle et al., 2005; Hoerder-Suabedissen et al., 2013). Specifically, studies have shown that a complete loss of *Reelin* or *TBR1* in post-mortem mouse brains results in severe disruption of subplate and marginal zone formation, leading to significant deficits in early-born cortical neuronal differentiation, migration, and axonal generation, ultimately resulting in a loss of regional identity (Hevner et al., 2001; Rice and Curran, 2001; Bedogni et al., 2010). While complete knockout of these genes may not be present in most ASD cases, it is plausible that smaller changes affecting *Reelin* and *TBR1*, such as copy number variations or single nucleotide variants, may cause changes in their expression resulting in subtle changes in cortical organization, and therefore contribute to the abnormalities in neocortical connectivity thought to underlie much of ASD pathology. While the marginal zone and subplate are clearly instrumental in the proper migration and formation of neurons to form mature neocortical networks, the transient nature of this structure during development makes it impossible to study in human post-mortem brain assessments of ASD patients. Further

work to define the role of this structure in animal models of ASD will be important to explore the contribution these largely understudied structures may have to neurodevelopmental disorders.

Cortical Mini-Columns

Similar to the unique structure and function of the marginal zone and subplate, cortical mini-columns and their formation are likely to be integral to the ASD phenotype. During the process of neuronal migration in the normal brain, developing neurons migrate from the germinal zones to predetermined areas of the neocortex and form mini-columns, the basic organizational unit of neuronal circuitry within the cortex (Rakic, 1988). Each mini-column is composed of 60–100 neurons, all with apical dendrites, myelinated, and double-bouquet axons (Mountcastle, 1997). Groups of mini-columns are organized into radial structures to form macro-columns, which then combine to make large networks that span layers II through VI of the neocortex (Mountcastle, 1978). The precise arrangement of neurons within these mini-columns is essential to cortical development, as it has been shown that even subtle alterations in the spacing of these mini-columns can alter the processing of information and overall circuitry of the neocortex (Seldon, 1981).

Intriguingly, post-mortem autistic brain tissue has been shown to have mini-columns that are narrower and contain more neurons than control brains, and additionally, the neurons within the autistic mini-columns are more dispersed (Casanova et al., 2002). Moreover, the abnormalities in mini-column structure that the authors observed in this study were most apparent in areas where GABA-ergic inhibitory interneurons predominated, suggesting lateral inhibition may be disrupted in autism brains (Marín-Padilla, 1970; DeFelipe and Jones, 1985; Casanova et al., 2002). This is of particular interest as many other separate investigations have provided support for global GABA-ergic dysfunction in ASD (Palmen et al., 2004; Voineagu et al., 2011). Specifically, aberrant GABA-ergic signaling in ASD is thought to create a more hyper-excitable state and result in deficits of filtering capacity and information processing within the cortex (Casanova et al., 2003; Rubenstein and Merzendich, 2003). It has been proposed that this deficit in inhibitory function may explain in part some of the behavioral phenotype of autism and the higher prevalence of seizures in ASD patients (Casanova et al., 2003; Brooks-Kayal, 2010).

As with the pre-plate and subplate, the migration of neurons into the developing mini-columns is impossible to study in human brain tissue, and can only be assessed after the completion of this process in post-mortem tissue from autistic patients. It is therefore impossible to determine whether the migration into mini-columns is aberrant, or if their migration is normal but the patterning and wiring of these newly arrived neurons is aberrant after they arrive in autistic patients. Animal and perhaps cellular models such as induced pluripotent stem cells (iPSCs) again will be important in helping to discern these possibilities, although it is entirely possible that both mechanisms are abnormal. In fact, there is a large body of evidence showing that fully-migrated neurons abnormally join neural networks and these networks are abnormally pruned in autistic brains, as is discussed next.

Microglia and Synaptic Pruning

After the process of neuronal migration, young neurons begin to be incorporated into newly developing neural networks through a dynamic process of synaptogenesis and pruning that continues late into adolescence. Young neurons initially develop processes (dendrites and axons) that allow them to form synapses with other neurons both locally and long-distance. The growth cone of an axon is able to sample the neuron's environment for both chemical and electrical signals that guide its wiring to other neurons to create a new synapse (Brown et al., 2002). Initial patterns of connectivity in the fetal and early postnatal brain are characterized by exuberant synaptic connections that will later be pruned away to leave only the connections indicated through postnatal experience (Stiles and Jernigan, 2010; Kettenmann et al., 2013). This process of network refinement occurs through both synaptic rewiring and neuronal apoptosis, with rates of apoptosis as high as 70% of cells in some regions of the cortex (Rabinowicz et al., 1996). Physiological neuronal apoptosis in development occurs both as the result of intrinsic neuronal cell death mechanisms mainly responding to the absence of local neurotrophic factors, and also through glial-initiated mechanisms which have recently become more widely recognized (Marín-Teva et al., 2004; Takahashi et al., 2005; Bessis et al., 2007).

While most research in the glial contribution to neurodevelopment has focused specifically on astrocytes, microglia—the resident immune cells of the CNS—were recently demonstrated to be involved in many fundamental neurodevelopmental processes including directing the invading vasculature and removing apoptotic cells (Parnaik et al., 2000; Streit, 2001; Stevens et al., 2007; Calderó et al., 2009; Paolicelli et al., 2011). Importantly, Paolicelli et al. (2011) demonstrated that microglial pruning of developing synapses is an absolute requirement for normal brain development. Moreover, others have shown that microglial cells in the developing cerebral cortex of prenatal and postnatal macaques and rats limit the production of cortical neurons by phagocytizing neural precursor cells as neurogenesis nears completion (Cunningham et al., 2013). Furthermore, studies of mice with abnormal numbers of microglia have shown that an alteration in microglial number perturbs neural development by directly affecting embryonic neural precursors and inducing astrogliosis (Antony et al., 2011). There is even evidence that microglia contribute to network remodeling in response to learning and stimulation (Dong and Greenough, 2004).

Despite these recent findings, the number of studies assessing the role of microglia in autistic brain tissue directly is strikingly small. Pardo et al. (2005) initially demonstrated that post-mortem brain tissue from patients with autism exhibits an increased microglial density in gray matter. Moreover, it was shown that microglia from MeCP2-null mice—a model of Rett Syndrome—produced a conditioned media that damaged synaptic connectivity via a glutamate-excitotoxicity mechanism (Stevens et al., 2007). Importantly, this effect was not seen in MeCP2-null astrocytes from the same animals, suggesting aberrant microglial activation during development

may lead to improper brain development independent of other glial populations. Additionally, it was shown that microglia in autistic brain samples display an activated morphology and secrete a cytokine profile consistent with a pro-inflammatory state (Bailey et al., 1995). Furthermore, we recently demonstrated abnormal expression of both microglial- and astrocyte-specific cell markers in two regions of post-mortem autistic brain tissue (Edmonson et al., 2014). These findings are interesting as the immune response in the CNS of patients with ASD has received a considerable amount of attention since autism was first described. However, most theories suggest either an exogenous factor stimulating neuro-inflammation or an autoimmune activation in the CNS. Yet, as the contribution of microglia to proper neuronal network formation—independent of their immune function—becomes increasingly recognized, it is important to consider that the intrinsic developmental component of microglia may be perturbed in ASD, such that their role in construction of neural networks is abnormal independent of inflammatory reaction (Garbett et al., 2008). This is in contrast to the traditional view that an exogenous immune response causes neural network destruction, although again it is possible that both mechanisms may contribute to the ASD phenotype. We suggest, however, that the former has received far less attention in the ASD literature and a more thorough assessment of this hypothesis may help significantly reconcile the disparate findings of neural network dysfunction and immune/glial abnormalities in ASD.

Postnatal Development

By the end of fetal development, all major adult brain structures are present, major connections between them are established, and the brain is poised for the rapid and dynamic growth that occurs in the first few years of life. The brain develops rapidly in the first few years after birth, reaching almost adult volume by age six (Lenroot and Giedd, 2006). While the production and migration of neurons are mainly prenatal events (with the notable exception of subventricular zone), glial progenitors have been shown to proliferate and differentiate throughout childhood, likely helping to sculpt the developing synaptic networks (Cayre et al., 2009).

One main function of proliferating glial cells during the early and late postnatal periods is to accomplish the extensive amount of axon myelination that occurs during this time. Increased myelination of axons allows for increased growth of axon diameter, and ultimately enables faster and long-distance neuronal connections (Zalc et al., 2008). Robust increases in myelination have been reported across the brain from ages 5–12 years, with a varying rate of fiber tract myelination in various brain regions (Lebel et al., 2008; Lebel and Beaulieu, 2009). These findings led to the thought that aberrant myelination may be contributing to ASD pathology, and contributed to the recent trend in the field towards diffusion tensor imaging (DTI) and functional magnetic resonance imaging (fMRI) studies. Kleinhans et al. (2012) reported white matter microstructure changes in multiple tracts of ASD brains across postnatal development as compared to control brains using DTI.

Specifically, they reported decreased fractional anisotropy with increased radial diffusivity in all tracts except the brainstem, hypothesizing that these observed changes may reflect an underlying defect in long distance myelin tracts in ASD (Kleinhans et al., 2012). These findings support a previous report that showed post-mortem autistic brains had a decreased number of long distance axons in the white matter, and additionally, that the axons in autistic brains had increased branching and thinner myelin when compared to controls (Zikopoulos and Barbas, 2010). Integrating these observations with studies supporting increased local synaptic excitation in ASD, many have hypothesized that abnormalities in the autism brain are a consequence of increased local neocortical connectivity and decreased cortical inter-region connectivity (Courchesne and Pierce, 2005; Casanova et al., 2006; Casanova and Tillquist, 2008).

Finally, while much of the organization of the postnatal brain is genetically determined, it has been clearly demonstrated that this intrinsic development remains extremely malleable to experience-dependent processes (Hubel and Wiesel, 1977; Markham and Greenough, 2004; Stiles and Jernigan, 2010). Moreover, epigenetic mechanisms that ultimately converge to influence gene expression have been shown to be one of the main mediators between environmental experiences and developmental synaptic plasticity (Fagioli et al., 2009). For instance, studies in mice have shown that environmental enrichment results in increased chromatin remodeling that modifies gene expression patterns in the hippocampus, resulting in improved spatial memory (Fischer et al., 2007). Alternatively, an increase in methylation of the *BDNF* promoter and consequent decrease in *BDNF* mRNA in the prefrontal cortex was found in association with exposure to periods of abusive maternal care, and these effects are perpetuated to the F1 generation suggesting a role for trans-generational effects (Champagne, 2008). Similarly, environmental insults to the developing brain, such as in fetal alcohol syndrome, have been shown to effect glial cells and their subsequent ability to effectively modulate neuronal development (Guizzetti et al., 2014). Yet, while studies of model organisms are beginning to demonstrate that gene expression represents a critical nexus of experience dependent plasticity, human studies of neurodevelopmental disorders in which this process may go awry are limited, and the general landscape of gene expression in the developing human brain as relates to neurodevelopmental disorders like autism is largely unexplored in relation to their corresponding cellular and network level changes. Integrating these scales of evidence will be an important future endeavor for the field to begin to truly integrate environmental/experiential influences with intrinsic mechanisms that ultimately shape neural network development and their aberration formation in ASD.

Conclusion

In summary, great progress in understanding the anatomical and cellular trends underlying human brain development

have been made over the past few decades. We have come to appreciate though various approaches that human neurodevelopment is a dynamic and protracted process, characterized by an initial period of neurogenesis leading to the formation of the basic CNS framework in early embryonic development. This is followed by substantial cellular proliferation, migration, and differentiation in the fetal period that establishes the main areas and pathways of the brain by birth. The early postnatal period is a time of rapid growth through glial proliferation, myelination, and organization of developing neural networks. Importantly, this process is very malleable particularly with regard to environmental and experiential events. Precise refinement of these developing neural networks occurs throughout adolescence and into early adulthood.

Previous research has led to the notion that ASD represent a complex interplay between the genome, immune signaling, and synaptic wiring; specifically, many of these studies have focused on the consequences of exogenous events on already developed neural networks. However, another potential explanation for these findings is that they represent an exaggeration or abnormality of normal processes that occur during the completion of brain development. Here, we propose that exaggerated and/or underutilized glial processes may be contributing to the construction of aberrant neural networks, apart from their more well-recognized immune functions.

References

- Antony, J. M., Paquin, A., Nutt, S. L., Kaplan, D. R., and Miller, F. D. (2011). Endogenous microglia regulate development of embryonic cortical precursor cells. *J. Neurosci. Res.* 89, 286–298. doi: 10.1002/jnr.22533
- Bailey, A., Le Couteur, A., Gottesman, I., Bolton, P., Simonoff, E., Yuzda, E., et al. (1995). Autism as a strongly genetic disorder: evidence from a British twin study. *Psychol. Med.* 25, 63–77. doi: 10.1017/s0033291700028099
- Bedogni, F., Hodge, R. D., Elsen, G. E., Nelson, B., Daza, R. A., Beyer, R. P., et al. (2010). Tbr1 regulates regional and laminar identity of postmitotic neurons in the developing neocortex. *Proc. Natl. Acad. Sci. U S A* 107, 13129–13134. doi: 10.1073/pnas.1002285107
- Bessis, A., Béchade, C., Bernard, D., and Roumier, A. (2007). Microglial control of neuronal death and synaptic properties. *Glia* 55, 233–238. doi: 10.1002/glia.20459
- Bielle, F., Griveau, A., Narboux-Nême, N., Vigneau, S., Sigrist, M., Arber, S., et al. (2005). Multiple origins of Cajal-Retzius cells at the borders of the developing pallium. *Nat. Neurosci.* 8, 1002–1012. doi: 10.1038/nn1511
- Bishop, K. M., Ruvenstein, J. L., and O'Leary, D. D. (2002). Distinct actions of Emx1, EMX2 and Pax6 in regulating the specification of areas in the developing neocortex. *J. Neurosci.* 22, 7627–7638.
- Borrell, V., and Götz, M. (2014). Role of radial glial cells in cerebral cortex folding. *Curr. Opin. Neurobiol.* 27, 39–46. doi: 10.1016/j.conb.2014.02.007
- Brooks-Kayal, A. (2010). Epilepsy and autism spectrum disorders: are there common developmental mechanisms? *Brain Dev.* 32, 731–738. doi: 10.1016/j.braindev.2010.04.010
- Brown, M., Keynes, R., and Lumsden, A. (2002). *The Developing Brain*. Oxford: Oxford University Press.
- Burbach, J. P., and van der Zwaag, B. (2009). Contact in the genetics of autism and schizophrenia. *Trends Neurosci.* 32, 69–72. doi: 10.1016/j.tins.2008.11.002
- Bystron, I., Blakemore, C., and Rakic, P. (2008). Development of the human cerebral cortex: boulder committee revised. *Nat. Rev. Neurosci.* 9, 110–112. doi: 10.1038/nrn2252
- Moreover, as the genetic, pathologic, and clinical features of other neurobehavioral diseases like schizophrenia overlap considerably with ASD, it is possible that this hypothesis linking known immune and glial cell dysfunction in autism to aberrations in normal processes of neurogenesis may be broadly relevant to other neurodevelopmental disorders (Burbach and van der Zwaag, 2009; Tuchman et al., 2010; Mitchell, 2011). For instance, a large body of evidence has demonstrated glial abnormalities in both post-mortem human brain and animal models of Fragile × Syndrome (the most common single-gene disorder with autism as a component) and in Down Syndrome (Goodison et al., 1993; Greco et al., 2006; Jacobs and Doering, 2010). Future work should concentrate on further understanding precisely how these normal neurodevelopmental mechanisms go awry in autism and in related disorders, and how we can use these findings to develop biomarkers to help diagnose and ultimately treat neurodevelopmental disorders.
- ## Funding
- This work was supported by the Intramural Research Program (IRP) of the National Institute of Child Health and Human Development, NIH. MNZ was also supported by the NIH-Cambridge Biomedical Scholars Program, and the Baylor College of Medicine Medical Scientist Training Program.
- Calderó, J., Brunet, N., Ciutat, D., Hereu, M., and Esquerda, J. E. (2009). Development of microglia in the chick embryo spinal cord: implications in the regulation of motoneuronal survival and death. *J. Neurosci. Res.* 87, 2447–2466. doi: 10.1002/jnr.22084
- Casanova, M. F., Buxhoeveden, D. P., and Gomez, J. (2003). Disruption in the inhibitory architecture of the cell minicolumn: implications for autism. *Neuroscientist* 9, 496–507. doi: 10.1177/1073858403253552
- Casanova, M. F., Buxhoeveden, D. P., Switala, A. E., and Roy, E. (2002). Minicolumnar pathology in autism. *Neurology* 58, 428–432. doi: 10.1212/wnl.58.3.428
- Casanova, M. F., and Tillquist, C. R. (2008). Encephalization, emergent properties and psychiatry: a minicolumnar perspective. *Neuroscientist* 14, 101–118. doi: 10.1177/1073858407309091
- Casanova, M. F., van Kooten, I. A., Switala, A. E., van Engeland, H., Heinsen, H., Steinbusch, H. W., et al. (2006). Minicolumnar abnormalities in autism. *Acta Neuropathol.* 112, 287–303. doi: 10.1007/s00401-006-0085-5
- Cayre, M., Canoll, P., and Goldman, J. E. (2009). Cell migration in the normal and pathological postnatal mammalian brain. *Prog. Neurobiol.* 88, 41–63. doi: 10.1016/j.pneurobio.2009.02.001
- Champagne, F. A. (2008). Epigenetic mechanisms and the transgenerational effects of maternal care. *Front. Neuroendocrinol.* 29, 386–397. doi: 10.1016/j.yfrne.2008.03.003
- Chi, J. G., Dooling, E. C., and Gilles, F. H. (1977). Gyral development of the human brain. *Ann. Neurol.* 1, 86–93. doi: 10.1002/ana.410010109
- Cooper, J. A. (2008). A mechanism for inside-out lamination in the neocortex. *Trends Neurosci.* 31, 113–119. doi: 10.1016/j.tins.2007.12.003
- Courchesne, E., and Pierce, K. (2005). Why the frontal cortex in autism might be talking only to itself: local over-connectivity but long-distance disconnection. *Curr. Opin. Neurobiol.* 15, 225–230. doi: 10.1016/j.conb.2005.03.001
- Cunningham, C. L., Martínez-Cerdeño, V., and Noctor, S. C. (2013). Microglia regulate the number of neural precursor cells in the developing cerebral cortex. *J. Neurosci.* 33, 4216–4233. doi: 10.1523/JNEUROSCI.3441-12.2013

- DeFelipe, J., and Jones, E. G. (1985). Vertical organization of γ -aminobutyric acid-accumulating intrinsic neuronal systems in monkey cerebral cortex. *J. Neurosci.* 5, 3246–3260.
- Desai, A. R., and McConnell, S. K. (2000). Progressive restriction in fate potential by neural progenitors during cerebral cortical development. *Development* 127, 2863–2872.
- Dong, W. K., and Greenough, W. T. (2004). Plasticity of nonneuronal brain tissue: roles in developmental disorders. *Ment. Retard. Dev. Disabil. Res. Rev.* 10, 85–90. doi: 10.1002/mrdd.20016
- Edmonson, C., Ziats, M. N., and Rennett, O. M. (2014). Altered glial marker expression in autistic post-mortem prefrontal cortex and cerebellum. *Mol. Autism* 5:3. doi: 10.1186/2040-2392-5-3
- Fagioli, M., Jensen, C. L., and Champagne, F. A. (2009). Epigenetic influences on brain development and plasticity. *Curr. Opin. Neurobiol.* 19, 207–212. doi: 10.1016/j.conb.2009.05.009
- Fischer, A., Sananbenesi, F., Wang, X., Dobbin, M., and Tsai, L. H. (2007). Recovery of learning and memory is associated with chromatin remodeling. *Nature* 447, 178–182. doi: 10.1038/nature05772
- Garbett, K., Ebert, P. J., Mitchell, A., Lintas, C., Manzi, B., Mirnics, K., et al. (2008). Immune transcriptome alterations in the temporal cortex of subjects with autism. *Neurobiol. Dis.* 30, 303–311. doi: 10.1016/j.nbd.2008.01.012
- Gavalas, A., Ruhrberg, C., Livet, J., Henderson, C. E., and Krumlauf, R. (2003). Neuronal defects in the hindbrain of Hoxa1, Hoxb2 and Hoxb2 mutants reflect regulatory interactions among these hox genes. *Development* 130, 5663–5679. doi: 10.1242/dev.00802
- Goodison, K. L., Parhad, I. M., White, C. L., Sima, A. A., and Clark, A. W. (1993). Neuronal and glial gene expression in neocortex of Down's syndrome and Alzheimer's disease. *J. Neuropathol. Exp. Neurol.* 52, 192–198. doi: 10.1097/00005072-199305000-00002
- Greco, C. M., Berman, R. F., Martin, R. M., Tassone, F., Schwartz, P. H., Chang, A., et al. (2006). Neuropathology of fragile X-associated tremor/ataxia syndrome (FXTAS). *Brain* 129, 243–255. doi: 10.1093/brain/awh683
- Guizzetti, M., Zhang, X., Goeke, C., and Gavin, D. P. (2014). Glia and neurodevelopment: focus on fetal alcohol spectrum disorders. *Front. Pediatr.* 2:123. doi: 10.3389/fped.2014.00123
- Hevner, R., Shi, L., Justice, N., Hsueh, Y., Sheng, M., Smiga, S., et al. (2001). Tbr1 regulates differentiation of the preplate and layer 6. *Neuron* 29, 353–366. doi: 10.1016/s0896-6273(01)00211-2
- Hoerder-Suabedissen, A., Oeschger, F. M., Krishnan, M. L., Belgard, T. G., Wang, W. Z., Lee, S., et al. (2013). Expression profiling of mouse subplate reveals a dynamic gene network and disease association with autism and schizophrenia. *Proc. Natl. Acad. Sci. U S A* 110, 3555–3560. doi: 10.1073/pnas.1218510110
- Hubel, D. H., and Wiesel, T. N. (1977). Ferrier lecture: functional architecture of macaque monkey visual cortex. *Proc. R. Soc. Lond. B Biol. Sci.* 198, 1–59. doi: 10.1098/rspb.1977.0085
- Insel, T. R. (2010). Rethinking schizophrenia. *Nature* 468, 187–193. doi: 10.1038/nature09552
- Jacobs, S., and Doering, L. C. (2010). Astrocytes prevent abnormal neuronal development in the fragile x mouse. *J. Neurosci.* 30, 4508–4514. doi: 10.1523/jneurosci.5027-09.2010
- Kettenmann, H., Kirchhoff, F., and Verkhratsky, A. (2013). Microglia: new roles for the synaptic stripper. *Neuron* 77, 10–18. doi: 10.1016/j.neuron.2012.12.023
- Kiecker, C., and Lumsden, A. (2004). Hedgehog signaling from ZLI regulates diencephalic regional identity. *Nat. Neurosci.* 7, 1242–1249. doi: 10.1038/nn1338
- Kleinmans, N. M., Pauley, G., Richards, T., Neuhaus, E., Martin, N., Corrigan, N. M., et al. (2012). Age-related abnormalities in white matter microstructure in autism spectrum disorders. *Brain Res.* 1479, 1–16. doi: 10.1016/j.brainres.2012.07.056
- Lebel, C., and Beaulieu, C. (2009). Lateralization of the arcuate fasciculus from childhood to adulthood and its relation to cognitive abilities in children. *Hum. Brain Mapp.* 30, 3563–3573. doi: 10.1002/hbm.20779
- Lebel, C., Walker, L., Leemans, A., Phillips, L., and Beaulieu, C. (2008). Microstructural maturation of the human brain from childhood to adulthood. *Neuroimage* 40, 1044–1055. doi: 10.1016/j.neuroimage.2007.12.053
- Lenroot, R. K., and Giedd, J. N. (2006). Brain development in children and adolescents: insights from anatomical magnetic resonance imaging. *Neurosci. Biobehav. Rev.* 30, 718–729. doi: 10.1016/j.neubiorev.2006.06.001
- Leone, D. P., Srinivasan, K., Chen, B., Alcamo, E., and McConnell, S. K. (2008). The determination of projection neuron identity in the developing cerebral cortex. *Curr. Opin. Neurobiol.* 18, 28–35. doi: 10.1016/j.conb.2008.05.006
- Lumsden, A., and Keynes, R. (1989). Segmental patterns of neuronal development in the chick hindbrain. *Nature* 337, 424–428. doi: 10.1038/37424a0
- Marin-Padilla, M. (1970). Prenatal and early postnatal ontogenesis of the human motor cortex: a golgi study. II. The basket-pyramidal system. *Brain Res.* 23, 185–191. doi: 10.1016/0006-8993(70)90038-7
- Marín-Teva, J. L., Dusart, I., Colin, C., Gervais, A., van Rooijen, N., and Mallat, M. (2004). Microglia promote the death of developing Purkinje cells. *Neuron* 41, 535–547. doi: 10.1016/s0896-6273(04)00069-8
- Markham, J. A., and Greenough, W. T. (2004). Experience-driven brain plasticity: beyond the synapse. *Neuron Glia Biol.* 1, 351–363. doi: 10.1017/s1740925x05000219
- Mitchell, K. J. (2011). The genetics of neurodevelopmental disease. *Curr. Opin. Neurobiol.* 21, 197–203. doi: 10.1016/j.conb.2010.08.009
- Molnár, Z., Métin, C., Stoykova, A., Tarabykin, V., Price, D. J., Francis, F., et al. (2006). Comparative aspects of cerebral cortical development. *Eur. J. Neurosci.* 23, 921–934. doi: 10.1111/j.1460-9568.2006.04611.x
- Mountcastle, V. B. (1978). An organizing principle for cerebral function, in *The Mindful Brain*, eds G. M. Edelman and V. B. Mountcastle (Cambridge MA: MIT Press), 7–50.
- Mountcastle, V. B. (1997). The columnar organization of the neocortex. *Brain* 120, 701–722. doi: 10.1093/brain/120.4.701
- Nakamura, H., Katahira, T., Matsunaga, E., and Sato, T. (2005). Isthmus organizer for midbrain and hindbrain development. *Brain Res. Brain Res. Rev.* 49, 120–126. doi: 10.1016/j.brainresrev.2004.10.005
- Ozair, M. Z., Kintner, C., and Brivanlou, A. H. (2013). Neural induction and early patterning in vertebrates. *Wiley Interdiscip. Rev. Dev. Biol.* 2, 479–498. doi: 10.1002/wdev.90
- Palmen, S. J., van Engeland, H., Hof, P. R., and Schmitz, C. (2004). Neuropathological findings in autism. *Brain* 127, 2572–2583. doi: 10.1093/brain/awh287
- Paolicelli, R. C., Bolas, G., Pagani, F., Maggi, L., Scianni, M., Panzanelli, P., et al. (2011). Synaptic pruning by microglia is necessary for normal brain development. *Science* 333, 1456–1458. doi: 10.1126/science.1202529
- Pardo, C. A., Vargas, D. L., and Zimmerman, A. W. (2005). Immunity, neuroglia and neuroinflammation in autism. *Int. Rev. Psychiatry* 17, 485–495. doi: 10.1080/02646830500381930
- Parnaik, R., Raff, M. C., and Scholes, J. (2000). Differences between the clearance of apoptotic cells by professional and non-professional phagocytes. *Curr. Biol.* 10, 857–860. doi: 10.1016/s0960-9822(00)00598-4
- Rabinowicz, T., de Courten-Myers, G., Petetot, J. M. C., Xi, G., and de los Reyes, E. (1996). Human cortex development: estimates of neuronal numbers indicate major loss late during gestation. *J. Neuropathol. Exp. Neurol.* 55, 320–328. doi: 10.1097/00005072-199603000-00007
- Rakic, P. (1988). Specification of cerebral cortical areas. *Science* 241, 170–176. doi: 10.1126/science.3291116
- Rice, D., and Curran, T. (2001). Role of the reelin signaling pathway in central nervous system development. *Annu. Rev. Neurosci.* 24, 1005–1039. doi: 10.1146/annurev.neuro.24.1.1005
- Rubenstein, J. L. R., and Merzandich, M. M. (2003). Model of autism: increased ratio of excitation/inhibition in key neural systems. *Genes Brain Behav.* 2, 255–267. doi: 10.1034/j.1601-183x.2003.00037.x
- Seldon, H. L. (1981). Structure of human auditory cortex I: cytoarchitectonics and dendritic distributions. *Brain Res.* 229, 277–294. doi: 10.1016/0006-8993(81)90994-x
- Stevens, B., Aller, N. J., Vazquez, L. E., Howell, G. R., Christopherson, K. S., Nouri, N., et al. (2007). The classical complement cascade mediates CNS synapse elimination. *Cell* 131, 1164–1178. doi: 10.1016/j.cell.2007.10.036
- Stiles, J., and Jernigan, T. L. (2010). The basics of brain development. *Neuropsychol. Rev.* 20, 327–348. doi: 10.1007/s11065-010-9148-4
- Streit, W. J. (2001). Microglia and macrophages in the developing CNS. *Neurotoxicology* 22, 619–624. doi: 10.1016/s0161-813x(01)00033-x
- Takahashi, K., Rochford, C. D., and Neumann, H. (2005). Clearance of apoptotic neurons without inflammation by microglial triggering receptor

- expressed on myeloid cells-2. *J. Exp. Med.* 201, 647–657. doi: 10.1084/jem.20041611
- Tuchman, R., Cuccaro, M., and Alessandri, M. (2010). Autism and epilepsy: historical perspective. *Brain Dev.* 32, 709–718. doi: 10.1016/j.braindev.2010.04.008
- Voineagu, I., Wang, X., Johnston, P., Lowe, J. K., Tian, Y., Horvath, S., et al. (2011). Transcriptomic analysis of autistic brain reveals convergent molecular pathology. *Nature* 474, 380–384. doi: 10.1038/nature10110
- Volpe, J. J. (2000). Overview: normal and abnormal human brain development. *Ment. Retard. Dev. Disabil. Res. Rev.* 6, 1–5. doi: 10.1002/(sici)1098-2779(2000)6:1<1::aid-mrdd1>3.0.co;2-j
- Zalc, B., Goujet, D., and Colman, D. (2008). The origin of the myelination program in vertebrates. *Curr. Biol.* 18, R511–R512. doi: 10.1016/j.cub.2008.04.010
- Zikopoulos, B., and Barbas, H. (2010). Changes in prefrontal axons may disrupt the network in autism. *J. Neurosci.* 30, 14595–14609. doi: 10.1523/jneurosci.2257-10.2010
- Conflict of Interest Statement:** The authors declare that the research was conducted in the absence of any commercial or financial relationships that could be construed as a potential conflict of interest.

Copyright © 2015 Ziats, Edmonson and Rennert. This is an open-access article distributed under the terms of the Creative Commons Attribution License (CC BY). The use, distribution and reproduction in other forums is permitted, provided the original author(s) or licensor are credited and that the original publication in this journal is cited, in accordance with accepted academic practice. No use, distribution or reproduction is permitted which does not comply with these terms.

One hand clapping: lateralization of motor control

Quentin Welniarz^{1,2}, Isabelle Dusart¹, Cécile Gallea² and Emmanuel Roze^{2,3*}

¹ Neuroscience Paris Seine, CNRS UMR8246, Inserm U1130, Sorbonne Universités, UPMC UM119, Paris, France, ² Inserm U1127, CNRS UMR 7225, Sorbonne Universités, UPMC UMR S1127, Institut du Cerveau et de la Moelle épinière, ICM, Paris, France, ³ Département des Maladies du Système Nerveux, AP-HP, Hôpital Pitié Salpêtrière, Paris, France

Lateralization of motor control refers to the ability to produce pure unilateral or asymmetric movements. It is required for a variety of coordinated activities, including skilled bimanual tasks and locomotion. Here we discuss the neuroanatomical substrates and pathophysiological underpinnings of lateralized motor outputs. Significant breakthroughs have been made in the past few years by studying the two known conditions characterized by the inability to properly produce unilateral or asymmetric movements, namely human patients with congenital “mirror movements” and model rodents with a “hopping gait”. Whereas mirror movements are associated with altered interhemispheric connectivity and abnormal corticospinal projections, abnormal spinal cord interneurons trajectory is responsible for the “hopping gait”. Proper commissural axon guidance is a critical requirement for these mechanisms. Interestingly, the analysis of these two conditions reveals that the production of asymmetric movements involves similar anatomical and functional requirements but in two different structures: (i) lateralized activation of the brain or spinal cord through contralateral silencing by cross-midline inhibition; and (ii) unilateral transmission of this activation, resulting in lateralized motor output.

Keywords: mirror movement, hopping gait, corticospinal tract, corpus callosum, spinal cord, axon guidance

OPEN ACCESS

Edited by:

Yun-Qing Li,
The Fourth Military Medical
University, China

Reviewed by:

José A. Armengol,
University Pablo de Olavide, Spain
Yu-Qiang Ding,
Tongji University, China

*Correspondence:

Emmanuel Roze,
Département des Maladies du
Système Nerveux, AP-HP, Hôpital
Pitié Salpêtrière, 47–83 boulevard de
l'Hôpital, 75013 Paris, France
emmanuel.flamand-roze@psl.aphp.fr

Received: 31 March 2015

Accepted: 17 May 2015

Published: 02 June 2015

Citation:

Welniarz Q, Dusart I, Gallea C and
Roze E (2015) One hand clapping:
lateralization of motor control.
Front. Neuroanat. 9:75.
doi: 10.3389/fnana.2015.00075

Introduction

Lateralization of motor control is required for a variety of coordinated movements, including skilled bimanual tasks and locomotion. To our knowledge, only two conditions are associated with the inability to produce asymmetric movements in mammals: human “mirror movements” and rodent “hopping gait”.

Mirror movements are involuntary symmetrical movements of one side of the body that mirror voluntary movements of the other side. The affected individuals are unable to perform purely unimanual movements and have difficulties to perform tasks requiring independent actions with the two hands such as holding a cup while filling it with water, opening a jar or playing a musical instrument. During these tasks, the effectors produce different motor outputs that are usually bound together by a shared, object-directed goal.

Quadrupedal locomotion is characterized by coordinated, alternating bilateral activation of limb muscles, in which effectors repeatedly produce similar motor outputs in a specific temporal order. A “hopping gait” is a switch from alternate to synchronous activity of the limbs during locomotion that is observed in rodent mutants with impaired axonal guidance.

Here we discuss the neuroanatomical substrates and pathophysiological underpinnings of lateralized motor output through the study “mirror movements” and “hopping gait”. Whereas mirror movements are associated with altered interhemispheric connectivity and abnormal corticospinal projections, abnormal spinal cord interneurons trajectory is responsible for the “hopping gait”. Interestingly, the analysis of these two conditions indicates that the production of asymmetric movements involves similar anatomical and functional requirements but in two different structures, the cerebral cortex and the spinal cord, and it emphasizes the importance of proper commissural axon guidance in this process.

The “Mirror Movement” Paradigm: Inability to Produce Asymmetric Skilled Hand Movements

Humans have a greater ability than other species to produce purposeful handling movements, most of them being asymmetric. With training, we can master highly complex skills ranging from the fluid movements of the virtuoso pianist to the precise life-saving gestures of the heart surgeon. In humans, execution of unimanual movements requires lateralized activation of the primary motor cortex (M1), which then transmits the motor command to the contralateral hand through the crossed corticospinal tract (CST; **Figure 1A**; Chouinard and Paus, 2010; Galléa et al., 2011).

Loss of this lateralization results in mirror movements (MM), which consist of involuntary symmetrical movements of one side of the body that mirror voluntary movements of the other side. Congenital mirror movement disorder (CMM) is a rare genetic disorder transmitted in autosomal dominant manner in which mirror movements are the only clinical abnormality. These mirror movements predominate in the distal upper limbs, leaving affected individuals unable to perform independent actions with the two hands or to perform purely unimanual movements. They usually have hand clumsiness and pain in the upper limbs during sustained manual activities. The two main culprit genes are *Dcc* (deleted in colorectal cancer) and *Rad51* (Srouf et al., 2010; Depienne et al., 2011, 2012; Méneret et al., 2014a). A third gene, *Dnal4*, might also be involved (Ahmed et al., 2014; Méneret et al., 2014b). *Dcc* plays a key role in CST midline crossing (Finger et al., 2002), while *Rad51* is well known for its role in DNA repair and may also have a major role in motor system development (Depienne et al., 2012; Gallea et al., 2013). In addition to isolated congenital mirror movements caused by *Dcc* or *Rad51* mutations, syndromic forms of MM may be accompanied by numerous other symptoms, in disorders such as Dandy walker syndrome, Joubert’s syndrome, X-linked Kallmann syndrome, Klippel Feil syndrome and congenital hemiparesis (Vulliemoz et al., 2005; Galléa et al., 2011; Peng and Charron, 2013).

CMM provides a unique paradigm for studying the lateralization of motor control (Carson, 2005; Galléa et al., 2011; Peng and Charron, 2013). Two main non exclusive mechanisms may account for MM: (i) abnormal

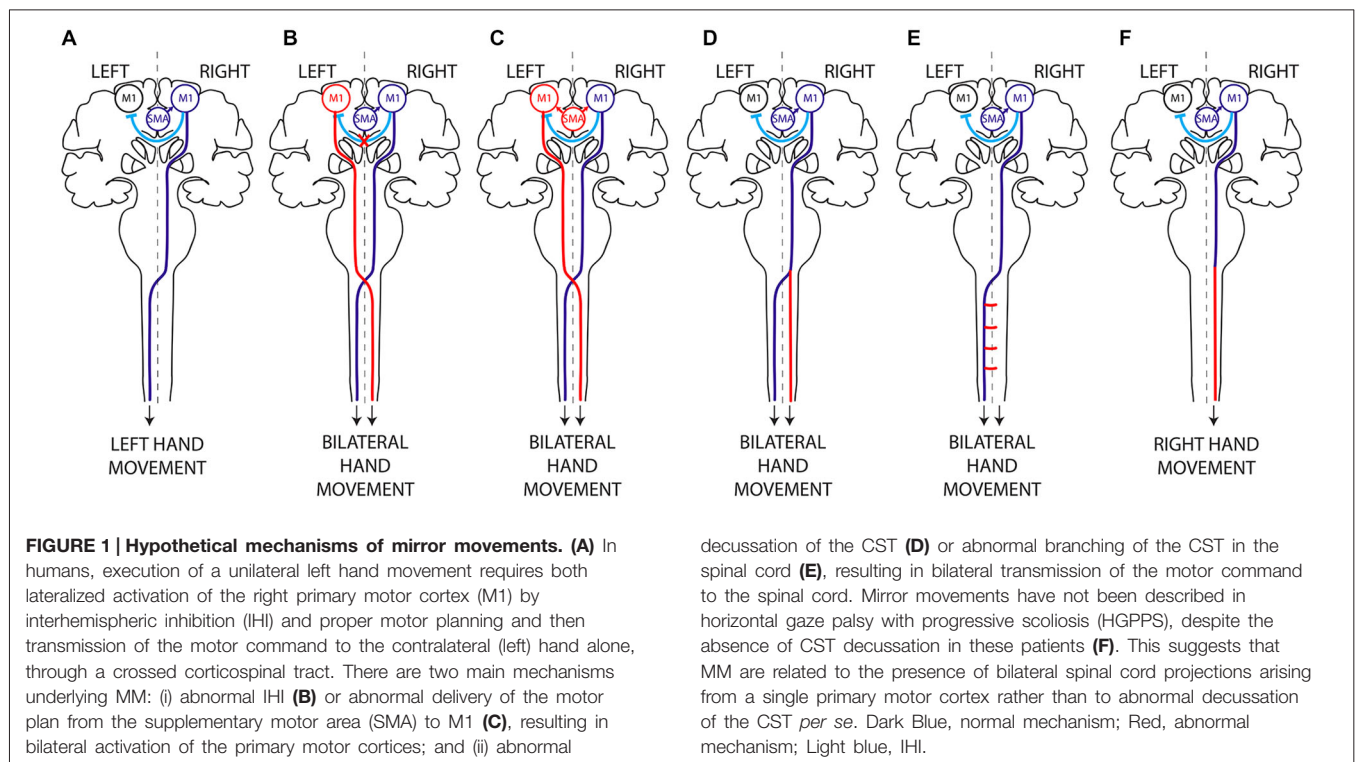
interhemispheric communication resulting in bilateral activation of primary motor areas (**Figures 1B,C**); and (ii) a corticospinal tract abnormality leading to bilateral downstream transmission of the motor command (**Figures 1D,E**; Gallea et al., 2013).

Interhemispheric Connectivity and Motor Lateralization

In humans, the default set-up of motor behavior is probably a mirror program (Chan and Ross, 1988; Meyer et al., 1995; Cincotta and Ziemann, 2008). Unilateral and bilateral voluntary movements are preceded by slow negativity on EEG recordings, known as the *Bereitschaftspotential* (Shibasaki and Hallett, 2006), which starts 2 s before movement onset and is distributed over the two hemispheres. This *Bereitschaftspotential* may reflect bilateral activation of the supplementary motor areas (SMA) and dorsal premotor cortices (dPMC) during motor planning. Just before movement onset, cortical activity is restricted to the primary motor cortex and dPMC contralateral to the intended movement (Shibasaki and Hallett, 2006). An active mechanism is required to restrict motor activation to one hemisphere during execution of a pure unimanual movement.

Our current understanding of this “non mirror transformation” derives mainly from the study of “physiological” mirror movements. Healthy subjects have a default tendency to produce minimal mirror movements when performing highly complex and effortful unimanual tasks (Koerte et al., 2010; Sehm et al., 2010; Beaulé et al., 2012). Activation of the mirror M1 (ipsilateral to the voluntary movement) is the main explanation for this tendency (Mayston et al., 1999; Cincotta et al., 2004; Zijdwind et al., 2006; Hübers et al., 2008). In order to achieve this “non mirror transformation”, the active M1 (contralateral to the intended movement) inhibits the mirror M1 via fibers that pass through the corpus callosum (transcallosal tract, TCT), thereby restricting the motor output to the active M1. This inhibition of one motor cortex by the other is called interhemispheric inhibition (IHI). IHI is thought to rely on transcallosal glutamatergic connections to inhibitory interneurons that in turn innervate pyramidal cells in the receiving hemisphere (Meyer et al., 1995; Reis et al., 2008). Several lines of evidence support the importance of TCT-mediated IHI in the lateralization of motor control. For example, the gradual disappearance of minimal MM frequently observed in young children correlates with the degree of TCT myelination and with the level of IHI (Koerte et al., 2010; Beaulé et al., 2012). Also, experimental modulation of IHI directed from the active M1 to the mirror M1 affects mirror activity: a transient increase in IHI is associated with a decrease in mirror activity, and *vice versa* (Hübers et al., 2008).

IHI between the two primary motor cortices is modulated differently during the different phases of unimanual movements. IHI is balanced between the two motor cortices at the onset of movement preparation, then shifts towards the ipsilateral M1 (ipsilateral to the voluntary movement) at the end of movement preparation and at movement onset (Murase et al.,



2004; Duque et al., 2007). In parallel, IHI of the contralateral M1 decreases during movement preparation and shifts towards facilitation at movement onset (Murase et al., 2004; Perez and Cohen, 2008). These subtle time-dependent bilateral variations of IHI are necessary to avoid premature execution (Duque and Ivry, 2009), and to prevent mirror activity in the ipsilateral M1 (Giovannelli et al., 2009). Impairment of IHI may thus result in bilateral M1 activation and transmission of the motor command to both hands through the two crossed CSTs.

In patients with CMM and X-linked Kallmann syndrome, several studies have revealed abnormal, bilateral M1 activation during voluntary unimanual movements and have confirmed that activation of the mirror M1 is not a sensory consequence of the mirror movement but rather participates actively in the mirroring motor activity (Shibasaki and Nagae, 1984; Cohen et al., 1991; Mayer et al., 1995; Cincotta et al., 1996; Krams et al., 1997; Verstynen et al., 2007). However, studies based on indirect methods have failed to demonstrate consistent impairment of IHI mechanisms in CMM patients (Cincotta et al., 1996, 2002; Papadopoulou et al., 2010). Using dual-site transcranial magnetic stimulation (TMS), a more direct method (Perez and Cohen, 2008), we found that CMM patients with *Rad51* mutations had abnormal IHI between the primary motor cortices at rest, together with morphological abnormalities of the TCT (Figure 1B; Gallea et al., 2013). It has been proposed that this impaired IHI is due to an abnormal input of the transcallosal glutamatergic connections onto the inhibitory interneurons in the receiving hemisphere. It is noteworthy that most individuals lacking a corpus

callosum do not exhibit mirror movements, suggesting that the absence of the corpus callosum and interhemispheric connections alone might not be sufficient to generate MM. Finally, a study of a CMM patient with complete agenesis of the corpus callosum concluded that the absence of TCT played little part in the pathophysiology of MM (Lepage et al., 2012).

Interhemispheric pathways are not limited to direct M1-M1 interactions and IHI but also include circuits linking secondary motor areas (SMA and PMd) to contralateral motor areas. These circuits might be involved in restricting the generation of motor output to the active hemisphere during movement preparation. For these reasons it has been proposed that abnormal motor planning and/or abnormal transmission of the motor plan from the secondary motor areas to the primary motor areas might also be involved in MM generation (Chan and Ross, 1988; Cincotta et al., 2004; Duque et al., 2010; Galléa et al., 2011; Gallea et al., 2013). Evidence of abnormal motor planning associated with MM was first obtained through studies of two CMM patients and a patient with Kallmann's syndrome, who showed an abnormal, bilateral (instead of unilateral) distribution of the *Bereitschaftspotential* during movement preparation (Shibasaki and Nagae, 1984; Cohen et al., 1991). However, two other studies argued against a role of abnormal movement planning in MM: the first showed that movement-related cortical EEG potentials were identical (that is to say, lateralized and not bilateral) in healthy volunteers and in six CMM patients (Mayer et al., 1995), while the second study, a case report, showed normal, unilateral cortical activation during fMRI imaging of imagined movements

closely related to motor planning (Verstynen et al., 2007). More recently, we found that the SMA activation pattern and connectivity are abnormal during both unimanual and bimanual movements in *Rad51*-mutated CMM patients (Figure 1C; Gallea et al., 2013). This suggested that cortical activation and connectivity might be modified in CMM patients during movement preparation, resulting in inappropriate delivery of the motor program from the SMA to both primary motor cortices.

Together, these results suggest that interhemispheric connectivity is critical for lateralized activation of the motor cortex when a unilateral movement is intended.

The Corticospinal Tract and Motor Lateralization

The CST is a crossed tract that transmits the motor command from one motor cortex to the contralateral spinal cord. The CST first appeared in mammals and was likely critical for the development of voluntary skilled movements through evolution (Vulliemoz et al., 2005). Selective lesions of the CST in humans, non human primates and rodents impair skilled digit movements such as reaching (Schieber, 2007). The CST is massively crossed in humans. About 70–95% of all CST axons cross the midline at the junction between the medulla and the spinal cord, forming the so-called “pyramidal decussation”, and establish direct contacts with the motor neurons located in the anterior horn of the spinal cord (Vulliemoz et al., 2005). The approximately 10% of CST axons that do not decussate at the medulla remain ipsilateral, and this ipsilateral tract is mainly located in the ventral part of the spinal cord in both humans and rodents (Brösamle and Schwab, 1997; Vulliemoz et al., 2005). The ipsilateral CST component does not target motor neurons innervating distal limb muscles but rather motor neurons innervating the proximal or axial musculatures (Bawa et al., 2004; Vulliemoz et al., 2005). In humans, cats and rodents, the CST initially establishes strong bilateral projections to the spinal cord. The ipsilateral projections consist of uncrossed CST axons (Joosten et al., 1992; Brösamle and Schwab, 1997; Eyre et al., 2001), and/or of normally crossed CST axons that recross the midline within the spinal cord (Li and Martin, 2000; Rosenzweig et al., 2009). This CST projection pattern is refined during early post-natal development, resulting in the elimination of the majority of the ipsilateral projections (Joosten et al., 1992; Eyre et al., 2000, 2001; Li and Martin, 2000). This refinement of the ipsilateral projections is an activity-dependent process of competition with the crossed CST fibers originating from the contralateral motor cortex (Martin and Lee, 1999; Eyre et al., 2001; Eyre, 2003; Martin et al., 2004; Friel and Martin, 2007; Friel et al., 2014).

Human MM could result from the presence of CST projections to both the ipsilateral and contralateral spinal cord. In patients with CMM, Kallmann syndrome, Klippel-Feil syndrome or congenital hemiparesis, unilateral stimulation of the primary motor cortex hand area at rest by TMS elicits bilateral hand muscle responses with identical latencies, whereas in healthy volunteers the muscle response is strictly contralateral to the stimulated hemisphere (Nass, 1985; Farmer et al., 1990; Benecke et al., 1991; Mayston et al., 1997; Alagona

et al., 2001; Staudt et al., 2002; Cincotta et al., 2003; Bawa et al., 2004; Srouf et al., 2010; Depienne et al., 2011; Gallea et al., 2013). This reveals the presence of fast-conducting corticospinal projections from the hand area of one primary motor cortex to both sides of the spinal cord in CMM patients and suggests an anatomic-functional link between anomalies in the CST trajectory and the inability to produce lateralized movements.

Bilateral corticospinal projections to the spinal cord could be due to: (i) abnormal pyramidal decussation resulting in an aberrant uncrossed ipsilateral CST (Figure 1D); or (ii) aberrant branching of crossed CST axons in the spinal cord (Figure 1E). In both cases, the aberrant CST projection pattern could result from abnormal guidance of the CST axons or from an abnormal persistence of the ipsilateral CST projections that are normally eliminated during development. An elegant TMS study of two CMM patients supports the existence of a separate uncrossed ipsilateral CST (Cincotta et al., 2003). Diffusion tensor imaging (DTI) was used to study the precise anatomy of the pyramidal decussation in *Rad51*-mutated patients, confirming abnormal CST decussation (Gallea et al., 2013), although *Dcc*-mutated CMM patients have yet to be studied. *Rad51* expression pattern in the mouse central nervous system (Depienne et al., 2012), and the known role of *DCC* in commissural axons guidance (Kennedy et al., 1994; Serafini et al., 1994; Keino-Masu et al., 1996; Finger et al., 2002), suggest that abnormal axonal guidance rather than impaired CST maturation is responsible for the bilateral CST projections observed in *Rad51*- and *Dcc*-mutated patients. Electrophysiological studies also support the existence of an aberrant uncrossed CST in X-linked Kallmann patients (Mayston et al., 1997; Farmer et al., 2004). In patients with congenital hemiparesis, MM may be explained by an abnormal maturation of the CST due to the unequal activity between the affected and unaffected motor cortices (Eyre et al., 2001; Eyre, 2003; Friel et al., 2014). This would lead to the maintenance and reinforcement of the ipsilateral CST from the unaffected motor cortex, combined with aberrant branching of corticospinal fibers in the spinal cord (Benecke et al., 1991; Alagona et al., 2001; Staudt et al., 2002; Galléa et al., 2011; Friel et al., 2014). Mirror movements have not been described in patients with horizontal gaze palsy with progressive scoliosis (HGPPS), despite their lack of CST decussation. HGPPS is linked to mutations in the axon guidance receptor *ROBO3* (Jen et al., 2004). The CST is completely uncrossed in HGPPS patients, and each hemisphere thus projects in a strictly ipsilateral manner to the spinal cord (Figure 1F). Together, these findings suggest that MM are related to the presence of bilateral spinal cord projections arising from a single primary motor cortex rather than to abnormal decussation of the CST *per se*.

Study of MM patients enlightened the critical importance of two mechanisms for the generation of asymmetric movements: (i) lateralized activation of the brain through contralateral silencing by IHI and proper motor planning; and (ii) unilateral transmission of the motor command to the contralateral spinal cord via the CST. Both abnormal interhemispheric connectivity

and an altered CST trajectory could be responsible for MM, but the respective importance of each factor is unclear.

Control of Left-Right Alternation During Locomotion: New Insights from Genetically Modified Mice with Developmental Motor System Anomalies

Quadrupedal locomotion requires repeated coordinated activity of each limb in a specific temporal sequence. Alternating left-right activity of the forelimbs and hindlimbs is observed at low locomotor frequencies (walking and trotting), while synchronized activity of the homologous limbs is observed at high locomotor frequencies (galloping) in mice, cats, horses and dogs (Forssberg et al., 1980; Dickinson et al., 2000; Serradj and Jamon, 2009). Lateralized motor output is thus a crucial aspect of locomotion, especially at low motor frequencies. In the past decade, careful analysis of genetically modified mice with a “hopping gait” has shed light on the respective contributions of the corticospinal tract and spinal central pattern generators (CPG) to left-right alternation during mouse locomotion.

The Corticospinal Tract and Left-Right Alternation During Locomotion

The CST forms a crossed (lateralized) motor circuit controlling voluntary movements of the four limbs. In rodents, the CST is composed of neurons originating from cortical layer V, projecting mainly to the contralateral side of the spinal cord and eventually connecting to motor neurons via a multisynaptic pathway (Figure 2; Canty and Murphy, 2008). A role of the CST in the control of alternating left-right activity during mouse locomotion was initially suggested by the “hopping gait” described in mice with genetically induced alterations of CST projections (mice with mutations of the EphA4 signaling pathway and *kanga* mice). EphA4 (a member of the Eph family of tyrosine-kinase receptors) and its ligand ephrinB3 are involved in axonal guidance of the CST during development. Deletion of EphA4, Ephrin-B3 or proteins involved in the EphA4 downstream signaling pathway (α 2-chimaerin, Nck, RhoA) results in a hopping-gait phenotype (Dottori et al., 1998; Kullander et al., 2001a,b; Yokoyama et al., 2001; Beg et al., 2007; Fawcett et al., 2007; Iwasato et al., 2007; Mulherkar et al., 2013). In EphA4 and EphrinB3 knockout mice, the CST trajectory is normal from the cortex to the pyramidal decussation. In the spinal cord, CST axons re-cross the midline, resulting in bilateral innervation of the spinal cord by each of the two hemispheres. In wild-type animals, EphA4-expressing CST axons are repelled by ephrin-B3 secreted at the midline, deterring them from re-crossing the midline at the spinal level (Dottori et al., 1998; Kullander et al., 2001a,b; Yokoyama et al., 2001). These findings suggested that the hopping gait might be explained by transmission of motor commands to both sides of the spinal cord through abnormally re-crossed CST axons. Similarly to mice with genetic alterations of the EphA4 signaling pathway, a mutant mouse line carrying a viable mutation of the DCC receptor have a “kangaroo-like” hopping gait phenotype and

are thus named “*kanga*” (Finger et al., 2002). The DCC ligand Netrin-1 belongs to the netrin family of extracellular guidance molecules. Netrin-1 has an attractive effect on growth cones when it interacts with the DCC receptor (Keino-Masu et al., 1996). This attraction allows commissural axons to approach and cross the midline (Kennedy et al., 1994; Serafini et al., 1994). DCC is expressed within the main forebrain descending tracts during their development (Shu et al., 2000). In *kanga* mice, the CST fails to cross the midline at the pyramidal decussation and projects exclusively to the ipsilateral side of the spinal cord (Finger et al., 2002).

However, other experimental findings do not support a major contribution of the CST to alternating left-right activity during locomotion. Indeed, abnormal CST midline crossing is not systematically associated with synchronized activity of the limbs during locomotion: mutants for L1 (Cohen et al., 1998; Jakeman et al., 2006), NCAM (Rolf et al., 2002), Sema6A and PlexinA3/PlexinA4 (Faulkner et al., 2008; Runker et al., 2008), exhibit normal locomotion despite having an abnormal CST. In rodents, a lateralized lesion of the cortex or CST, occurring during the first week of life, leads to sprouting of the remaining CST across the midline and thus to bilateral spinal cord projections (Leong and Lund, 1973; Kartje-Tillotson et al., 1987). This results in altered skilled forelimb movements without affecting left-right alternation during locomotion (Kunkel-Bagden et al., 1992; Whishaw et al., 1993; Whishaw, 2000; Metz and Whishaw, 2002; Tennant and Jones, 2009). Thus, abnormal CST projections do not necessarily induce a hopping gait.

It is important to recall that the genetic alterations induced in EphA4, ephrin-B3 and DCC *kanga* mutant mice not only impact CST development but also affect commissural cell populations expressing these proteins, such as pre-cerebellar commissural neurons (Hashimoto et al., 2012), and commissural spinal cord interneurons (Kullander et al., 2003; Beg et al., 2007; Iwasato et al., 2007; Rabe Bernhardt et al., 2012). This implies that the hopping gait observed in these mice is not necessarily due to their CST abnormalities. Two recent studies took advantage of the conditional knockout mouse *Emx1::cre;EphA4^{fllox/fllox}* in which genetic deletion of EphA4 is restricted to the forebrain. These mice exhibit normal stereotypical locomotion despite bilateral CST projections to the spinal cord (Borgius et al., 2014; Serradj et al., 2014). Together, these results show that proper CST wiring is not necessary for stereotypic left-right alternation.

Supra-spinal control plays a critical role in voluntary movements and adaptive locomotion when sensory-motor integration is required (for example when stepping over an obstacle). *Emx1::cre;EphA4^{fllox/fllox}* mice with bilateral CST projections to the spinal cord exhibit symmetric voluntary movements under conditions when asymmetric limbs movements are normally produced (Borgius et al., 2014; Friel et al., 2014; Serradj et al., 2014). These results emphasize the role of the CST in voluntary asymmetric movements.

In addition to the CST, supra-spinal structures playing an important role in the control of gait are located in the cerebral cortex, the cerebellum and in the brainstem, and constitute an interconnected network. There is no clear evidence implicating a supra-spinal control for left-right alternation and lateralization

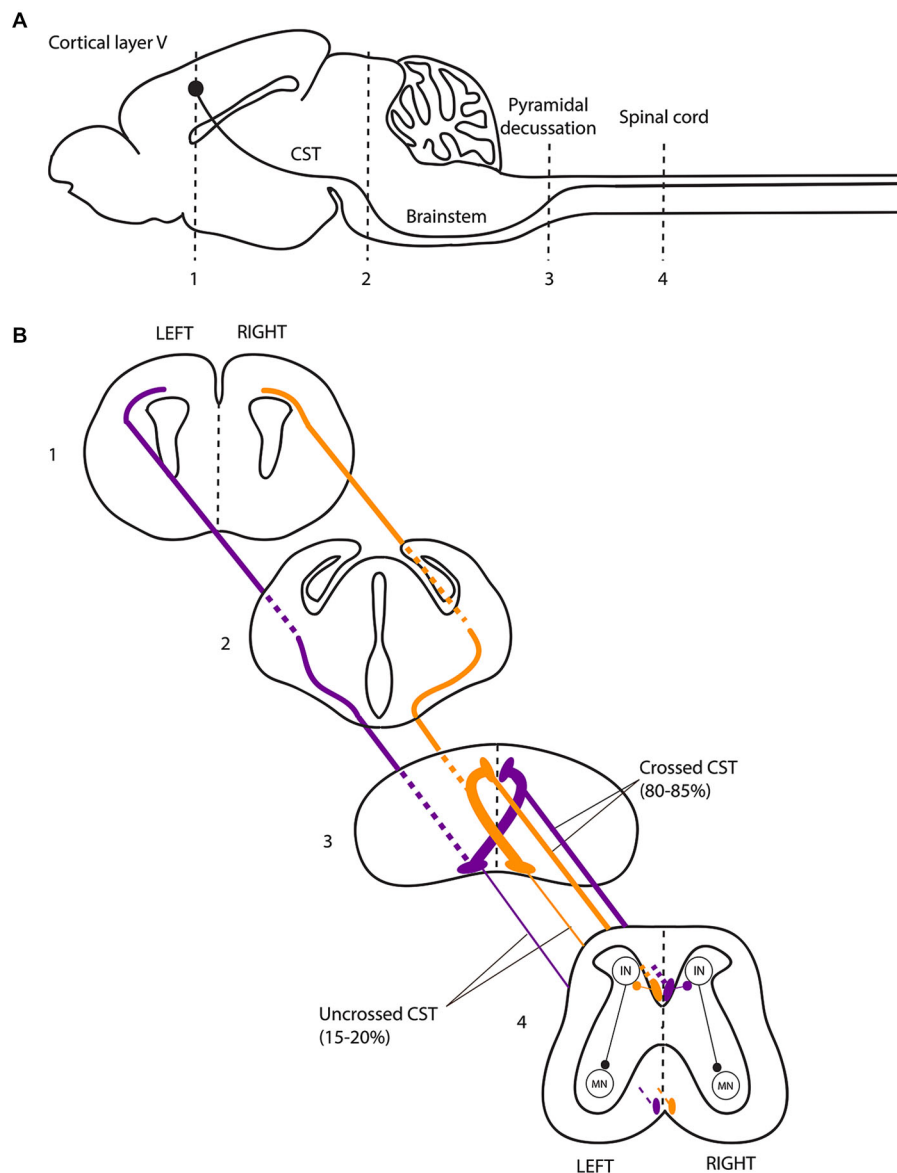


FIGURE 2 | The corticospinal tract forms a crossed motor system in mice. (A) Sagittal view of the mouse central nervous system and corticospinal tract (CST). (B) Coronal views of the CST trajectory. The level of each coronal schematic section is indicated in figure A. At the junction between the hindbrain and the spinal cord (pyramidal decussation, level 3), the vast majority (80–85%) of corticospinal tract (CST) axons cross the midline and continue their trajectory through the

most ventral part of the dorsal funiculus within the half of the spinal cord contralateral to their hemisphere of origin. In the spinal cord, the CST undergoes collateral branching principally at the level of the cervical and lumbar enlargement, eventually transmitting motor commands to the forelimb and hindlimb muscles, respectively, via a multisynaptic pathway involving interneurons mainly located in the dorsal horn of the spinal cord. CST, corticospinal tract; IN, interneurons; MN, motor neurons.

of motor control during gait. Among the locomotor centers with direct spinal projections, the mesencephalic locomotor region (MLR) is of particular interest for our purpose. Electrical stimulation of the brainstem in decerebrate cats placed on a treadmill recapitulates normal alternate locomotion without the need of descending commands from the cortex (Shik et al., 1966, 1967). The MLR, which comprises the pedunculopontine (PPN) and cuneiform (CN) nuclei, sends outputs to the basal ganglia, the cerebellar and the cerebral locomotor areas. The MLR plays

a major role in gait initiation and in internal generation of adaptive lower limb movement during the automated gait cycle (Alam et al., 2011; Grabli et al., 2012). The MLR could be involved in the control of gait cadence (Piallat et al., 2009; Karachi et al., 2010), but this involvement is more likely related to higher-order functions during faster gait rather than basic motor control as suggested by rodent models (Winn, 2008). Dysfunction of the MLR and cerebral locomotor centers is observed in patients with Parkinson disease and freezing of

gait (Fling et al., 2013, 2014), which is the inability to move the feet despite the effort to overcome the motor block and move forward. These patients exhibit alteration of gait rhythm, gait symmetry and bilateral coordination in stepping (Plotnik and Hausdorff, 2008; Plotnik et al., 2008). However, freezing of gait and bilateral coordination problems are triggered by particular circumstances, when adaptive locomotion is needed (Grabli et al., 2012). In addition, freezing also occurs during writing and speech, although the MLR is not involved in such tasks. MPTP monkeys with selective loss of cholinergic neurons in the PPN have gait impairments but no specific problem in the alternation of lower limb movements (Karachi et al., 2010). In cats, electrical stimulation of the PPN suppresses postural muscle tone, whereas CN stimulation elicits locomotor movements (Takakusaki et al., 2003). In humans, activity of the PPN seems to be modulated during rhythmical stepping, but the increased demands of postural control and attention during stepping could not be cancelled out (Fraix et al., 2013). Therefore, the structures constituting the MLR might play different roles in gait control, but none of them is known to be specifically involved in left-right alternation of the lower limbs.

In non mammalian vertebrates the descending motor pathways are mainly composed of reticulospinal tracts originating from the hindbrain (Vulliemoz et al., 2005). In zebrafish, descending motor pathways include Mauthner cells and other reticulospinal neurons (MiD2cm, MiD3cm and MiD3cl). This crossed network plays a critical role in adaptive locomotor activity such as escape behavior: a stimulus delivered to one side of the head results first in tail bending towards the opposite side, followed by a counter-bend that enables efficient propulsion (Kohashi and Oda, 2008; Jain et al., 2014). *DCC* mutations, leading to midline guidance defects of MiD2cm and MiD3cm neurons that project bilaterally instead of contralaterally, cause an abnormal counter-bend in the same direction as the first. Escape behavior of these mutant zebrafish is thereby compromised. This phenotype is rescued by ablation of the aberrantly projecting MiD2cm and MiD3cm neurons, demonstrating that supra-spinal pathways predominate over spinal circuitry during adaptive locomotion (Jain et al., 2014).

Altogether, these results suggest that supra-spinal control plays a critical role in motor lateralization during voluntary movements and adaptive locomotion but is not involved in left-right alternation during stereotypic locomotion.

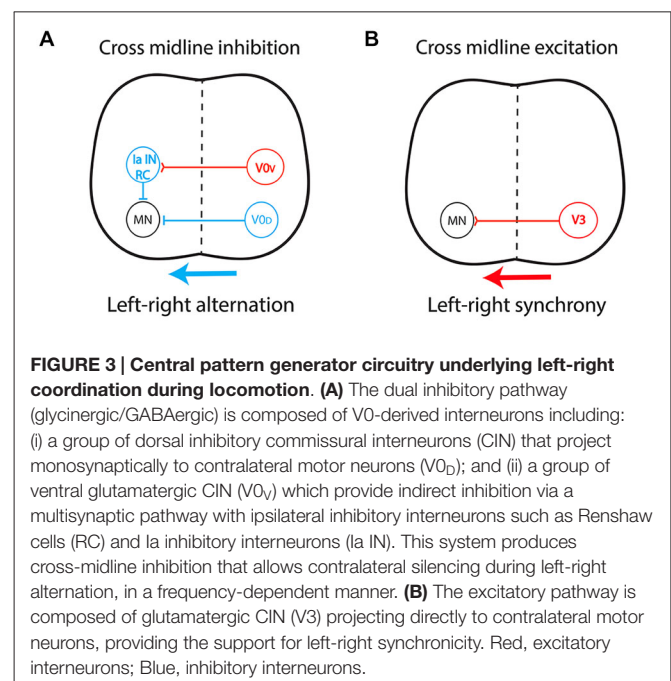
Spinal Control of Left-Right Alternation During Locomotion

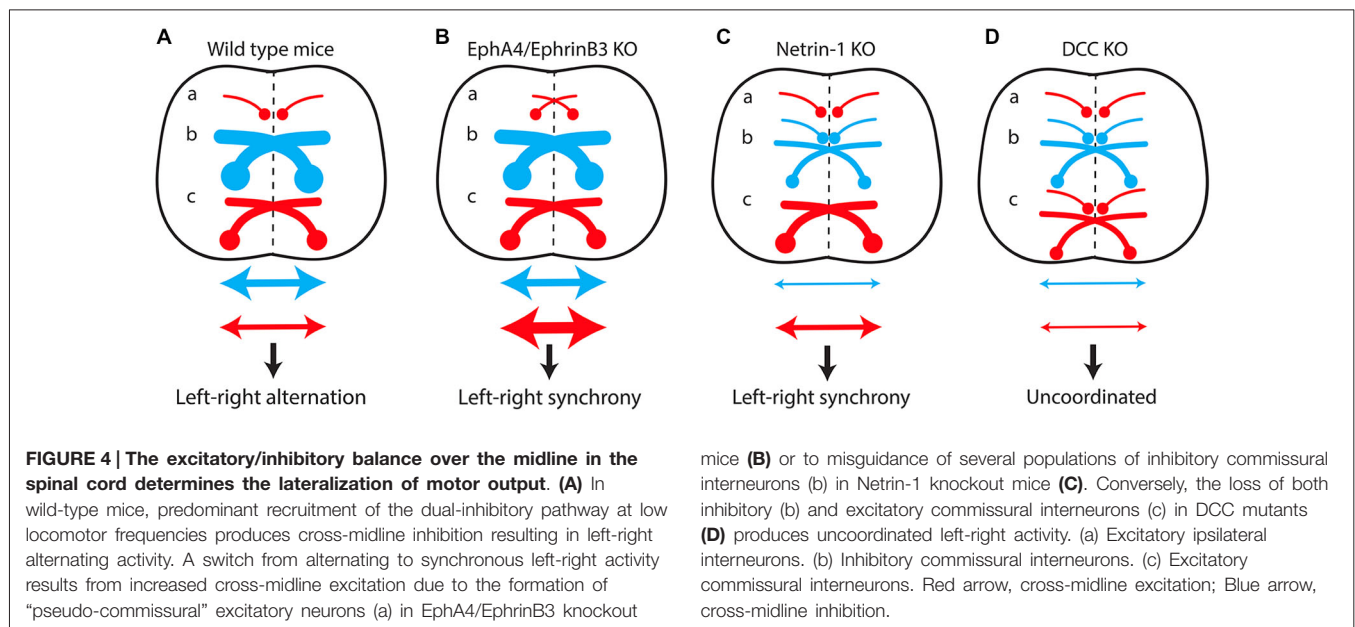
The importance of local spinal circuitry in locomotion is supported by “fictive locomotion” experiments performed *in vitro*. Exposure of isolated rodent spinal cords to neurotransmitter agonists such as serotonin and dopamine produces rhythmic activity at the lumbar level lasting several hours. This activity is characterized by alternating ipsilateral flexor-extensor activity and alternating left-right activity (Smith and Feldman, 1987; Kiehn and Kjaerulff, 1996). Successful replication of left-right alternation in spinal cords isolated from the forebrain strongly suggests that the spinal neuronal network plays a critical role in locomotion. This network is called the

central pattern generator (CPG), and its role in swimming and walking has been extensively studied (Grillner, 2003; Goulding, 2009; Kiehn et al., 2010; Kiehn, 2011). The CPG generates rhythm, ipsilateral flexor-extensor alternation, and left-right alternation. Spinal commissural interneurons (CIN), mostly located in the ventromedial spinal cord (lamina VIII), play a key role in left-right alternation (Stokke et al., 2002). Fictive locomotion experiments *in vitro* have shown that removal of the dorsal part of the spinal cord does not affect left-right alternation, whereas sectioning of the ventral spinal cord commissure completely abolishes it (Kjaerulff and Kiehn, 1996). When inhibitory GABAergic or glycinergic CIN are neutralized by the use of antagonists, spinal left-right alternating activity switches to synchronous activity, demonstrating that this cross-midline inhibition is critical for lateralized motor activity (Cowley and Schmidt, 1995). Conversely, suppression of glutamatergic excitatory transmission in the spinal cord of *Vglut2* mutants does not affect the generation of left-right alternation or locomotor rhythms (Gezelius et al., 2006; Wallén-Mackenzie et al., 2006).

The specific characteristics and fate of spinal cord interneurons are determined by the progenitor subtype from which they originate. During the early phases of CNS development, transcription-factor gradients result in dorsoventral patterning of spinal neurons. There are 11 progenitor domains in the spinal cord, six dorsal (dI1–dI6) and five ventral (V0, V1, V2, motor neurons and V3 interneurons, in dorsal-to-ventral order; Jessell, 2000; Arber, 2012). Delineation of the CPG circuitry through the use of mutant mice improved our understanding of spinal alternating left-right activity.

By connecting the two sides of the spinal cord, CIN determine the excitatory/inhibitory balance over the midline. Most CIN involved in left-right coordination originate from the ventral spinal cord, from V0 and V3 progenitors (Kiehn, 2011; Chédotal,





2014), but the role of dorsally derived interneurons was recently highlighted (Andersson et al., 2012; Vallstedt and Kullander, 2013). Cross-midline inhibition relies on a dual inhibitory pathway (Figure 3A) composed mainly of V0-derived CIN and comprising: (i) a group of dorsal inhibitory CIN (V0_D) that project monosynaptically to contralateral motor neurons; and (ii) a group of ventral glutamatergic CIN (V0_V) which provide indirect inhibition via multisynaptic connections with ipsilateral inhibitory interneurons such as Renshaw cells (RC) and Ia inhibitory interneurons (Moran-Rivard et al., 2001; Pierani et al., 2001; Lanuza et al., 2004; Goulding, 2009; Kiehn et al., 2010). This system allows contralateral silencing during left-right alternation, in a frequency-dependent manner (Talpalar et al., 2013). In contrast, an excitatory pathway (Figure 3B) composed of glutamatergic CIN derived from V3 progenitors and projecting directly to contralateral motor neurons provides support for left-right synchrony (Zhang et al., 2008; Rabe et al., 2009; Borowska et al., 2013). This organization has been described in rodents (Quinlan and Kiehn, 2007; Restrepo et al., 2009) and cats (Jankowska et al., 2009). Additionally, ipsilaterally projecting interneurons are key components of multisynaptic pathways that provide indirect cross-midline inhibition and, as such, also participate in left-right alternation (Crone et al., 2008, 2009).

Mutant mice with commissural axon guidance defects have been critical for studying the spinal locomotor circuitry (Figure 4). Spinal CIN cross the midline at the floor plate, a structure located in the ventral spinal cord that secretes several molecules such as Ephrin-B3 and Netrin-1 involved in commissural axon guidance (Nawabi and Castellani, 2011). EphA4 and Ephrin-B3 knockout mice both have a hopping-gait phenotype (Dottori et al., 1998; Kullander et al., 2001b; Yokoyama et al., 2001). Fictive locomotion was studied with isolated spinal cords from EphA4 and ephrin-B3 null mutants aged between post-natal day 0 (P0) and P5, a period when

the CST has not yet reached the lumbar spinal cord (Gianino et al., 1999). A switch from left-right alternating activity to synchronous activity was observed, together with an increased number of CIN in the ventral spinal cord. Reinforcement of cross-midline inhibition by GABA/glycine uptake blockers completely reversed this effect (Kullander et al., 2003). It was postulated that EphA4 is expressed in a population of excitatory interneurons projecting ipsilaterally, and that loss of EphA4 or ephrin-B3 leads to aberrant midline crossing of this population, resulting in “pseudo-commissural” excitatory connections. This would push the excitatory/inhibitory balance over the midline towards excitation (Figure 4B). In keeping with this hypothesis, specific deletion of EphA4 in the spinal cord or in glutamatergic interneurons is sufficient to induce a hopping gait both *in vivo* and *in vitro* (Borgius et al., 2014).

Netrin-1 knockout mice lack several inhibitory CIN populations, whereas their excitatory CIN are unaffected (Rabe et al., 2009). The inhibitory/excitatory balance over the midline is therefore shifted toward excitation, resulting in synchronous left-right locomotor activity *in vitro* (Figure 4C; Rabe et al., 2009). Surprisingly, suppression of the expression of DCC, the Netrin-1 receptor, leads to a different phenotype. DCC knockout mice exhibit uncoordinated left-right activity *in vitro*, reflecting the preservation of the excitatory/inhibitory balance over the midline, due to the loss of both inhibitory and excitatory CIN populations (Figure 4D; Rabe Bernhardt et al., 2012).

A hopping gait has also been described in Nkx mutant mice (Holz et al., 2010). Nkx transcription factors are involved in the development of the floor plate. The misguidance of V0 and dI6 CIN might be responsible for the phenotype of Nkx mutant mice (Holz et al., 2010).

Lateralization of motor output between the two sides of the spinal cord during stereotypic locomotion mainly relies on the excitatory/inhibitory balance over the midline. Recruitment of inhibitory pathways results in cross-midline inhibition and

left-right alternation, whereas recruitment of the excitatory pathway results in a shift toward excitation and left-right synchrony. Supra-spinal control and descending pathways (CST in mammals, reticulospinal tracts in non mammalian vertebrates) do not participate in stereotypic left-right alternation but rather contribute to motor lateralization during voluntary movements and adaptive locomotion.

Conclusion

The study of human “mirror movements” and rodent “hopping gait” reveals analogous mechanisms underlying the generation of asymmetric movements. Lateralized activation of the brain or spinal cord is first achieved through contralateral silencing by cross-midline inhibition. In the brain, this inhibition relies on excitatory neurons of the transcallosal tract that connect to

inhibitory interneurons in the receiving hemisphere, while in the spinal cord both direct and indirect inhibition is involved during locomotion. Unilateral transmission of these activations results in lateralized motor output. When commissural axon guidance is compromised during development, the formation of projections to both sides of the spinal cord results in bilateral motor output. In mice, the formation of aberrant crossed excitatory connections in the spinal cord induces a hopping gait, while abnormal guidance of the CST in humans results in mirror movements.

Author's Role

QW, ID, CG and ER drafted the manuscript. QW, CG produced the figures. QW, ID, CG and ER critically reviewed the manuscript.

References

- Ahmed, I., Mittal, K., Sheikh, T. I., Vasli, N., Rafiq, M. A., Mikhailov, A., et al. (2014). Identification of a homozygous splice site mutation in the dynein axonemal light chain 4 gene on 22q13.1 in a large consanguineous family from pakistan with congenital mirror movement disorder. *Hum. Genet.* 133, 1419–1429. doi: 10.1007/s00439-014-1475-8
- Alagona, G., Delvaux, V., Gérard, P., De Pasqua, V., Pennisi, G., Delwaide, P. J., et al. (2001). Ipsilateral motor responses to focal transcranial magnetic stimulation in healthy subjects and acute-stroke patients. *Stroke* 32, 1304–1309. doi: 10.1161/01.str.32.6.1304
- Alam, M., Schwabe, K., and Krauss, J. K. (2011). The pedunculopontine nucleus area: critical evaluation of interspecies differences relevant for its use as a target for deep brain stimulation. *Brain* 134, 11–23. doi: 10.1093/brain/awq322
- Andersson, L. S., Larhammar, M., Memic, F., Wootz, H., Schwowchow, D., Rubin, C. J., et al. (2012). Mutations in DMRT3 affect locomotion in horses and spinal circuit function in mice. *Nature* 488, 642–646. doi: 10.1038/nature11399
- Arber, S. (2012). Motor circuits in action: specification, connectivity and function. *Neuron* 74, 975–989. doi: 10.1016/j.neuron.2012.05.011
- Bawa, P., Hamm, J. D., Dhillon, P., and Gross, P. A. (2004). Bilateral responses of upper limb muscles to transcranial magnetic stimulation in human subjects. *Exp. Brain Res.* 158, 385–390. doi: 10.1007/s00221-004-2031-x
- Beaulé, V., Tremblay, S., and Théoret, H. (2012). Interhemispheric control of unilateral movement. *Neural Plast.* 2012:627816. doi: 10.1155/2012/627816
- Beg, A. A., Sommer, J. E., Martin, J. H., and Scheiffele, P. (2007). $\alpha 2$ -Chimaerin is an essential EphA4 effector in the assembly of neuronal locomotor circuits. *Neuron* 55, 768–778. doi: 10.1016/j.neuron.2007.07.036
- Benecke, R., Meyer, B. U., and Freund, H. J. (1991). Reorganisation of descending motor pathways in patients after hemispherectomy and severe hemispheric lesions demonstrated by magnetic brain stimulation. *Exp. Brain Res.* 83, 419–426. doi: 10.1007/bf00231167
- Borgius, L., Nishimaru, H., Caldeira, V., Kunugise, Y., Löw, P., Reig, R., et al. (2014). Spinal glutamatergic neurons defined by EphA4 signaling are essential components of normal locomotor circuits. *J. Neurosci.* 34, 3841–3853. doi: 10.1523/JNEUROSCI.4992-13.2014
- Borowska, J., Jones, C. T., Zhang, H., Blacklaws, J., Goulding, M., and Zhang, Y. (2013). Functional subpopulations of V3 interneurons in the mature mouse spinal cord. *J. Neurosci.* 33, 18553–18565. doi: 10.1523/JNEUROSCI.2005-13.2013
- Brösamle, C., and Schwab, M. E. (1997). Cells of origin, course and termination patterns of the ventral, uncrossed component of the mature rat corticospinal tract. *J. Comp. Neurol.* 386, 293–303. doi: 10.1002/(SICI)1096-9861(19970922)386:2%3C293::AID-CNE9%3E3.0.CO;2-X
- Canty, A. J., and Murphy, M. (2008). Molecular mechanisms of axon guidance in the developing corticospinal tract. *Prog. Neurobiol.* 85, 214–235. doi: 10.1016/j.pneurobio.2008.02.001
- Carson, R. G. (2005). Neural pathways mediating bilateral interactions between the upper limbs. *Brain Res. Brain Res. Rev.* 49, 641–662. doi: 10.1016/j.brainresrev.2005.03.005
- Chan, J. L., and Ross, E. D. (1988). Left-handed mirror writing following right anterior cerebral artery infarction: evidence for nonmirror transformation of motor programs by right supplementary motor area. *Neurology* 38, 59–63. doi: 10.1212/wnl.38.1.59
- Chédotal, A. (2014). Development and plasticity of commissural circuits: from locomotion to brain repair. *Trends Neurosci.* 37, 551–562. doi: 10.1016/j.tins.2014.08.009
- Chouinard, P. A., and Paus, T. (2010). What have we learned from “Perturbing” the human cortical motor system with transcranial magnetic stimulation? *Front. Hum. Neurosci.* 4:173. doi: 10.3389/fnhum.2010.00173
- Cincotta, M., Borgheresi, A., Balestrieri, F., Giovannelli, F., Rossi, S., Ragazzoni, A., et al. (2004). Involvement of the human dorsal premotor cortex in unimanual motor control: an interference approach using transcranial magnetic stimulation. *Neurosci. Lett.* 367, 189–193. doi: 10.1016/j.neulet.2004.06.003
- Cincotta, M., Borgheresi, A., Balzini, L., Vannucchi, L., Zeloni, G., Ragazzoni, A., et al. (2003). Separate ipsilateral and contralateral corticospinal projections in congenital mirror movements: neurophysiological evidence and significance for motor rehabilitation. *Mov. Disord.* 18, 1294–1300. doi: 10.1002/mds.10545
- Cincotta, M., Borgheresi, A., Boffi, P., Vigliano, P., Ragazzoni, A., Zaccara, G., et al. (2002). Bilateral motor cortex output with intended unimanual contraction in congenital mirror movements. *Neurology* 58, 1290–1293. doi: 10.1212/wnl.58.8.1290
- Cincotta, M., Lori, S., Gangemi, P. F., Barontini, F., and Ragazzoni, A. (1996). Hand motor cortex activation in a patient with congenital mirror movements: a study of the silent period following focal transcranial magnetic stimulation. *Electroencephalogr. Clin. Neurophysiol.* 101, 240–246. doi: 10.1016/0924-980x(96)95621-0
- Cincotta, M., and Ziemann, U. (2008). Neurophysiology of unimanual motor control and mirror movements. *Clin. Neurophysiol.* 119, 744–762. doi: 10.1016/j.clinph.2007.11.047
- Cohen, L. G., Meer, J., Tarkka, I., Bierner, S., Leiderman, D. B., Dubinsky, R. M., et al. (1991). Congenital mirror movements. Abnormal organization of motor pathways in two patients. *Brain* 114(Pt. 1B), 381–403. doi: 10.1093/brain/114.1.381
- Cohen, N. R., Taylor, J. S., Scott, L. B., Guillery, R. W., Soriano, P., and Furley, A. J. (1998). Errors in corticospinal axon guidance in mice lacking the neural cell adhesion molecule L1. *Curr. Biol.* 8, 26–33. doi: 10.1016/s0960-9822(98)70017-x
- Cowley, K. C., and Schmidt, B. J. (1995). Effects of inhibitory amino acid antagonists on reciprocal inhibitory interactions during rhythmic motor activity in the *in vitro* neonatal rat spinal cord. *J. Neurophysiol.* 74, 1109–1117.

- Crone, S. A., Quinlan, K. A., Zagoraoui, L., Droho, S., Restrepo, C. E., Lundfald, L., et al. (2008). Genetic ablation of V2a ipsilateral interneurons disrupts left-right locomotor coordination in mammalian spinal cord. *Neuron* 60, 70–83. doi: 10.1016/j.neuron.2008.08.009
- Crone, S. A., Zhong, G., Harris-Warrick, R., and Sharma, K. (2009). In mice lacking V2a interneurons, gait depends on speed of locomotion. *J. Neurosci.* 29, 7098–7109. doi: 10.1523/JNEUROSCI.1206-09.2009
- Depienne, C., Bouteiller, D., Méneret, A., Billot, S., Groppa, S., Klebe, S., et al. (2012). RAD51 haploinsufficiency causes congenital mirror movements in humans. *Am. J. Hum. Genet.* 90, 301–307. doi: 10.1016/j.ajhg.2011.12.002
- Depienne, C., Cincotta, M., Billot, S., Bouteiller, D., Groppa, S., Brochard, V., et al. (2011). A novel DCC mutation and genetic heterogeneity in congenital mirror movements. *Neurology* 76, 260–264. doi: 10.1212/WNL.0b013e318207b1e0
- Dickinson, M. H., Farley, C. T., Full, R. J., Koehl, M. A., Kram, R., and Lehman, S. (2000). How animals move: an integrative view. *Science* 288, 100–106. doi: 10.1126/science.288.5463.100
- Dottori, M., Hartley, L., Galea, M., Paxinos, G., Polizzotto, M., Kilpatrick, T., et al. (1998). EphA4 (Sek1) receptor tyrosine kinase is required for the development of the corticospinal tract. *Proc. Natl. Acad. Sci. U S A* 95, 13248–13253. doi: 10.1073/pnas.95.22.13248
- Duque, J., Davare, M., Delaunay, L., Jacob, B., Saur, R., Hummel, F., et al. (2010). Monitoring coordination during bimanual movements: where is the mastermind? *J. Cogn. Neurosci.* 22, 526–542. doi: 10.1162/jocn.2009.21213
- Duque, J., and Ivry, R. B. (2009). Role of corticospinal suppression during motor preparation. *Cereb. Cortex* 19, 2013–2024. doi: 10.1093/cercor/bhn230
- Duque, J., Murase, N., Celnik, P., Hummel, F., Harris-Love, M., Mazzocchio, R., et al. (2007). Intermanual differences in movement-related interhemispheric inhibition. *J. Cogn. Neurosci.* 19, 204–213. doi: 10.1162/jocn.2007.19.2.204
- Eyre, J. A. (2003). Development and plasticity of the corticospinal system in man. *Neural Plast.* 10, 93–106. doi: 10.1155/np.2003.93
- Eyre, J. A., Miller, S., Clowry, G. J., Conway, E. A., and Watts, C. (2000). Functional corticospinal projections are established prenatally in the human foetus permitting involvement in the development of spinal motor centres. *Brain* 123(Pt. 1), 51–64. doi: 10.1093/brain/123.1.51
- Eyre, J. A., Taylor, J. P., Villagra, F., Smith, M., and Miller, S. (2001). Evidence of activity-dependent withdrawal of corticospinal projections during human development. *Neurology* 57, 1543–1554. doi: 10.1212/wnl.57.9.1543
- Farmer, S. F., Harrison, L. M., Mayston, M. J., Parekh, A., James, L. M., and Stephens, J. A. (2004). Abnormal cortex-muscle interactions in subjects with X-linked Kallmann's syndrome and mirror movements. *Brain* 127, 385–397. doi: 10.1093/brain/awh047
- Farmer, S. F., Ingram, D. A., and Stephens, J. A. (1990). Mirror movements studied in a patient with Klippel-Feil syndrome. *J. Physiol.* 428, 467–484. doi: 10.1113/jphysiol.1990.sp018222
- Faulkner, R. L., Low, L. K., Liu, X. B., Coble, J., Jones, E. G., and Cheng, H. J. (2008). Dorsal turning of motor corticospinal axons at the pyramidal decussation requires plexin signaling. *Neural Dev.* 3:21. doi: 10.1186/1749-8104-3-21
- Fawcett, J. P., Georgiou, J., Ruston, J., Bladt, F., Sherman, A., Warner, N., et al. (2007). Nck adaptor proteins control the organization of neuronal circuits important for walking. *Proc. Natl. Acad. Sci. U S A* 104, 20973–20978. doi: 10.1073/pnas.0710316105
- Finger, J. H., Bronson, R. T., Harris, B., Johnson, K., Przyborski, S. A., and Ackerman, S. L. (2002). The netrin 1 receptors Unc5h3 and Dcc are necessary at multiple choice points for the guidance of corticospinal tract axons. *J. Neurosci.* 22, 10346–10356.
- Fling, B. W., Cohen, R. G., Mancini, M., Carpenter, S. D., Fair, D. A., Nutt, J. G., et al. (2014). Functional reorganization of the locomotor network in Parkinson patients with freezing of gait. *PLoS One* 9:e100291. doi: 10.1371/journal.pone.0100291
- Fling, B. W., Cohen, R. G., Mancini, M., Nutt, J. G., Fair, D. A., and Horak, F. B. (2013). Asymmetric pedunculopontine network connectivity in parkinsonian patients with freezing of gait. *Brain* 136, 2405–2418. doi: 10.1093/brain/awt172
- Forsberg, H., Grillner, S., Halbertsma, J., and Rossignol, S. (1980). The locomotion of the low spinal cat. II. Interlimb coordination. *Acta Physiol. Scand.* 108, 283–295. doi: 10.1111/j.1748-1716.1980.tb06534.x
- Fraix, V., Bastin, J., David, O., Goetz, L., Ferraye, M., Benabid, A. L., et al. (2013). Pedunculopontine nucleus area oscillations during stance, stepping and freezing in Parkinson's disease. *PLoS One* 8:e83919. doi: 10.1371/journal.pone.0083919
- Friel, K. M., and Martin, J. H. (2007). Bilateral activity-dependent interactions in the developing corticospinal system. *J. Neurosci.* 27, 11083–11090. doi: 10.1523/jneurosci.2814-07.2007
- Friel, K. M., Williams, P. T., Serradj, N., Chakrabarty, S., and Martin, J. H. (2014). Activity-based therapies for repair of the corticospinal system injured during development. *Front. Neurol.* 5:229. doi: 10.3389/fneur.2014.00229
- Galléa, C., Popa, T., Billot, S., Méneret, A., Depienne, C., and Roze, E. (2011). Congenital mirror movements: a clue to understanding bimanual motor control. *J. Neurol.* 258, 1911–1919. doi: 10.1007/s00415-011-6107-9
- Gallea, C., Popa, T., Hubsch, C., Valabregue, R., Brochard, V., Kundu, P., et al. (2013). RAD51 deficiency disrupts the corticospinal lateralization of motor control. *Brain* 136, 3333–3346. doi: 10.1093/brain/awt258
- Gezelius, H., Wallén-Mackenzie, A., Enjin, A., Lagerström, M., and Kullander, K. (2006). Role of glutamate in locomotor rhythm generating neuronal circuitry. *J. Physiol. Paris* 100, 297–303. doi: 10.1016/j.jphysparis.2007.05.001
- Gianino, S., Stein, S. A., Li, H., Lu, X., Biesiada, E., Ulas, J., et al. (1999). Postnatal growth of corticospinal axons in the spinal cord of developing mice. *Brain Res. Dev. Brain Res.* 112, 189–204. doi: 10.1016/s0165-3806(98)00168-0
- Giovannelli, F., Borgheresi, A., Balestrieri, F., Zaccara, G., Viggiano, M. P., Cincotta, M., et al. (2009). Modulation of interhemispheric inhibition by volitional motor activity: an ipsilateral silent period study. *J. Physiol.* 587, 5393–5410. doi: 10.1113/jphysiol.2009.175885
- Goulding, M. (2009). Circuits controlling vertebrate locomotion: moving in a new direction. *Nat. Rev. Neurosci.* 10, 507–518. doi: 10.1038/nrn2608
- Grabli, D., Karachi, C., Welter, M. L., Lau, B., Hirsch, E. C., Vidailhet, M., et al. (2012). Normal and pathological gait: what we learn from Parkinson's disease. *J. Neurol. Neurosurg. Psychiatry* 83, 979–985. doi: 10.1136/jnnp-2012-302263
- Grillner, S. (2003). The motor infrastructure: from ion channels to neuronal networks. *Nat. Rev. Neurosci.* 4, 573–586. doi: 10.1038/nrn1137
- Hashimoto, M., Ito, R., Kitamura, N., Namba, K., and Hisano, Y. (2012). EphA4 controls the midline crossing and contralateral axonal projections of inferior olive neurons. *J. Comp. Neurol.* 520, 1702–1720. doi: 10.1002/cne.23008
- Holz, A., Kollmus, H., Ryge, J., Niederkofler, V., Dias, J., Ericson, J., et al. (2010). The transcription factors Nkx2.2 and Nkx2.9 play a novel role in floor plate development and commissural axon guidance. *Development* 137, 4249–4260. doi: 10.1242/dev.053819
- Hübner, A., Orekhov, Y., and Ziemann, U. (2008). Interhemispheric motor inhibition: its role in controlling electromyographic mirror activity. *Eur. J. Neurosci.* 28, 364–371. doi: 10.1111/j.1460-9568.2008.06335.x
- Iwasato, T., Katoh, H., Nishimaru, H., Ishikawa, Y., Inoue, H., Saito, Y. M., et al. (2007). Rac-GAP alpha-chimerin regulates motor-circuit formation as a key mediator of EphrinB3/EphA4 forward signaling. *Cell* 130, 742–753. doi: 10.1016/j.cell.2007.07.022
- Jain, R. A., Bell, H., Lim, A., Chien, C. B., and Granato, M. (2014). Mirror movement-like defects in startle behavior of zebrafish dcc mutants are caused by aberrant midline guidance of identified descending hindbrain neurons. *J. Neurosci.* 34, 2898–2909. doi: 10.1523/JNEUROSCI.2420-13.2014
- Jakeman, L. B., Chen, Y., Lucin, K. M., and McTigue, D. M. (2006). Mice lacking L1 cell adhesion molecule have deficits in locomotion and exhibit enhanced corticospinal tract sprouting following mild contusion injury to the spinal cord. *Eur. J. Neurosci.* 23, 1997–2011. doi: 10.1111/j.1460-9568.2006.04721.x
- Jankowska, E., Bannatyne, B. A., Stecina, K., Hammar, I., Cabaj, A., and Maxwell, D. J. (2009). Commissural interneurons with input from group I and II muscle afferents in feline lumbar segments: neurotransmitters, projections and target cells. *J. Physiol.* 587, 401–418. doi: 10.1113/jphysiol.2008.159236
- Jen, J. C., Chan, W. M., Bosley, T. M., Wan, J., Carr, J. R., Rüb, U., et al. (2004). Mutations in a human ROBO gene disrupt hindbrain axon pathway crossing and morphogenesis. *Science* 304, 1509–1513. doi: 10.1126/science.1096437
- Jessell, T. M. (2000). Neuronal specification in the spinal cord: inductive signals and transcriptional codes. *Nat. Rev. Genet.* 1, 20–29. doi: 10.1038/35049541
- Joosten, E. A., Schuitman, R. L., Vermelis, M. E., and Dederen, P. J. (1992). Postnatal development of the ipsilateral corticospinal component in rat spinal cord: a light and electron microscopic anterograde HRP study. *J. Comp. Neurol.* 326, 133–146. doi: 10.1002/cne.903260112

- Karachi, C., Grabli, D., Bernard, F. A., Tandé, D., Wattiez, N., Belaid, H., et al. (2010). Cholinergic mesencephalic neurons are involved in gait and postural disorders in Parkinson disease. *J. Clin. Invest.* 120, 2745–2754. doi: 10.1172/JCI42642
- Kartje-Tillotson, G., O'Donoghue, D. L., Dauzvardis, M. F., and Castro, A. J. (1987). Pyramidotomy abolishes the abnormal movements evoked by intracortical microstimulation in adult rats that sustained neonatal cortical lesions. *Brain Res.* 415, 172–177. doi: 10.1016/0006-8993(87)90283-6
- Keino-Masu, K., Masu, M., Hinck, L., Leonardo, E. D., Chan, S. S., Culotti, J. G., et al. (1996). Deleted in Colorectal Cancer (DCC) encodes a netrin receptor. *Cell* 87, 175–185. doi: 10.1016/S0092-8674(00)81336-7
- Kennedy, T. E., Serafini, T., de la Torre, J. R., and Tessier-Lavigne, M. (1994). Netrins are diffusible chemotropic factors for commissural axons in the embryonic spinal cord. *Cell* 78, 425–435. doi: 10.1016/0092-8674(94)90421-9
- Kiehn, O. (2011). Development and functional organization of spinal locomotor circuits. *Curr. Opin. Neurobiol.* 21, 100–109. doi: 10.1016/j.conb.2010.09.004
- Kiehn, O., Dougherty, K. J., Hägglund, M., Borgius, L., Talpalar, A., and Restrepo, C. E. (2010). Probing spinal circuits controlling walking in mammals. *Biochem. Biophys. Res. Commun.* 396, 11–18. doi: 10.1016/j.bbrc.2010.02.107
- Kiehn, O., and Kjaerulff, O. (1996). Spatiotemporal characteristics of 5-HT and dopamine-induced rhythmic hindlimb activity in the *in vitro* neonatal rat. *J. Neurophysiol.* 75, 1472–1482.
- Kjaerulff, O., and Kiehn, O. (1996). Distribution of networks generating and coordinating locomotor activity in the neonatal rat spinal cord *in vitro*: a lesion study. *J. Neurosci.* 16, 5777–5794.
- Koerte, I., Eftimov, L., Laubender, R. P., Esslinger, O., Schroeder, A. S., Ertl-Wagner, B., et al. (2010). Mirror movements in healthy humans across the lifespan: effects of development and ageing. *Dev. Med. Child Neurol.* 52, 1106–1112. doi: 10.1111/j.1469-8749.2010.03766.x
- Kohashi, T., and Oda, Y. (2008). Initiation of Mauthner- or non-Mauthner-mediated fast escape evoked by different modes of sensory input. *J. Neurosci.* 28, 10641–10653. doi: 10.1523/jneurosci.1435-08.2008
- Krams, M., Quinton, R., Mayston, M. J., Harrison, L. M., Dolan, R. J., Bouloux, P. M., et al. (1997). Mirror movements in X-linked Kallmann's syndrome II. A PET study. *Brain* 120(Pt. 7), 1217–1228. doi: 10.1093/brain/120.7.1217
- Kullander, K., Butt, S. J., Lebet, J. M., Lundfald, L., Restrepo, C. E., Rydström, A., et al. (2003). Role of EphA4 and EphrinB3 in local neuronal circuits that control walking. *Science* 299, 1889–1892. doi: 10.1126/science.1079641
- Kullander, K., Croll, S. D., Zimmer, M., Pan, L., McClain, J., Hughes, V., et al. (2001a). Ephrin-B3 is the midline barrier that prevents corticospinal tract axons from recrossing, allowing for unilateral motor control. *Genes Dev.* 15, 877–888. doi: 10.1101/gad.868901
- Kullander, K., Mather, N. K., Diella, F., Dottori, M., Boyd, A. W., and Klein, R. (2001b). Kinase-dependent and kinase-independent functions of EphA4 receptors in major axon tract formation *in vivo*. *Neuron* 29, 73–84. doi: 10.1016/S0896-6273(01)00181-7
- Kunkel-Bagden, E., Dai, H. N., and Bregman, B. S. (1992). Recovery of function after spinal cord hemisection in newborn and adult rats: differential effects on reflex and locomotor function. *Exp. Neurol.* 116, 40–51. doi: 10.1016/0014-4886(92)90174-o
- Lanuza, G. M., Gosgnach, S., Pierani, A., Jessell, T. M., and Goulding, M. (2004). Genetic identification of spinal interneurons that coordinate left-right locomotor activity necessary for walking movements. *Neuron* 42, 375–386. doi: 10.3410/f.1019388.218551
- Leong, S. K., and Lund, R. D. (1973). Anomalous bilateral corticofugal pathways in albino rats after neonatal lesions. *Brain Res.* 62, 218–221. doi: 10.1016/0006-8993(73)90630-6
- Lepage, J. F., Beaulé, V., Srouf, M., Rouleau, G., Pascual-Leone, A., Lassonde, M., et al. (2012). Neurophysiological investigation of congenital mirror movements in a patient with agenesis of the corpus callosum. *Brain Stimul.* 5, 137–140. doi: 10.1016/j.brs.2011.02.004
- Li, Q., and Martin, J. H. (2000). Postnatal development of differential projections from the caudal and rostral motor cortex subregions. *Exp. Brain Res.* 134, 187–198. doi: 10.1007/s002210000454
- Martin, J. H., Choy, M., Pullman, S., and Meng, Z. (2004). Corticospinal system development depends on motor experience. *J. Neurosci.* 24, 2122–2132. doi: 10.1523/jneurosci.4616-03.2004
- Martin, J. H., and Lee, S. J. (1999). Activity-dependent competition between developing corticospinal terminations. *Neuroreport* 10, 2277–2282. doi: 10.1097/00001756-199908020-00010
- Mayer, M., Bötzel, K., Paulus, W., Plendl, H., Pröckl, D., and Danek, A. (1995). Movement-related cortical potentials in persistent mirror movements. *Electroencephalogr. Clin. Neurophysiol.* 95, 350–358. doi: 10.1016/0013-4694(95)00100-d
- Mayston, M. J., Harrison, L. M., Quinton, R., Stephens, J. A., Krams, M., and Bouloux, P. M. (1997). Mirror movements in X-linked Kallmann's syndrome. I. A neurophysiological study. *Brain* 120(Pt. 7), 1199–1216. doi: 10.1093/brain/120.7.1199
- Mayston, M. J., Harrison, L. M., and Stephens, J. A. (1999). A neurophysiological study of mirror movements in adults and children. *Ann. Neurol.* 45, 583–594. doi: 10.1002/1531-8249(199905)45:5<583::aid-ana6>3.0.co;2-w
- Méneret, A., Depienne, C., Riant, F., Trouillard, O., Bouteiller, D., Cincotta, M., et al. (2014a). Congenital mirror movements: mutational analysis of RAD51 and DCC in 26 cases. *Neurology* 82, 1999–2002. doi: 10.1212/wnl.0000000000000477
- Méneret, A., Trouillard, O., Vidailhet, M., Depienne, C., and Roze, E. (2014b). Congenital mirror movements: no mutation in DNAL4 in 17 index cases. *J. Neurol.* 261, 2030–2031. doi: 10.1007/s00415-014-7505-6
- Metz, G. A., and Whishaw, I. Q. (2002). Cortical and subcortical lesions impair skilled walking in the ladder rung walking test: a new task to evaluate fore- and hindlimb stepping, placing and co-ordination. *J. Neurosci. Methods* 115, 169–179. doi: 10.1016/S0165-0270(02)00012-2
- Meyer, B. U., Roricht, S., Grafin Von Einsiedel, H., Kruggel, F., and Weindl, A. (1995). Inhibitory and excitatory interhemispheric transfers between motor cortical areas in normal humans and patients with abnormalities of the corpus callosum. *Brain* 118(Pt. 2), 429–440. doi: 10.1093/brain/118.2.429
- Moran-Rivard, L., Kagawa, T., Saueressig, H., Gross, M. K., Burrill, J., and Goulding, M. (2001). Evx1 is a postmitotic determinant of v0 interneuron identity in the spinal cord. *Neuron* 29, 385–399. doi: 10.1016/S0896-6273(01)00213-6
- Mulherkar, S., Liu, F., Chen, Q., Narayanan, A., Couvillon, A. D., Shine, H. D., et al. (2013). The small GTPase RhoA is required for proper locomotor circuit assembly. *PLoS One* 8:e67015. doi: 10.1371/journal.pone.0067015
- Murase, N., Duque, J., Mazzocchio, R., and Cohen, L. G. (2004). Influence of interhemispheric interactions on motor function in chronic stroke. *Ann. Neurol.* 55, 400–409. doi: 10.1002/ana.10848
- Nass, R. (1985). Mirror movement asymmetries in congenital hemiparesis: the inhibition hypothesis revisited. *Neurology* 35, 1059–1062. doi: 10.1212/wnl.35.7.1059
- Nawabi, H., and Castellani, V. (2011). Axonal commissures in the central nervous system: how to cross the midline? *Cell. Mol. Life Sci.* 68, 2539–2553. doi: 10.1007/s00018-011-0691-9
- Papadopoulou, M., Chairopoulos, K., Anagnostou, E., Kokotis, P., Zambelis, T., and Karandreas, N. (2010). Concurrent bilateral projection and activation of motor cortices in a patient with congenital mirror movements: a TMS study. *Clin. Neurol. Neurosurg.* 112, 824–828. doi: 10.1016/j.clineuro.2010.06.016
- Peng, J., and Charron, F. (2013). Lateralization of motor control in the human nervous system: genetics of mirror movements. *Curr. Opin. Neurobiol.* 23, 109–118. doi: 10.1016/j.conb.2012.08.007
- Perez, M. A., and Cohen, L. G. (2008). Mechanisms underlying functional changes in the primary motor cortex ipsilateral to an active hand. *J. Neurosci.* 28, 5631–5640. doi: 10.1523/jneurosci.0093-08.2008
- Piallat, B., Chabardes, S., Torres, N., Fraix, V., Goetz, L., Seigneuret, E., et al. (2009). Gait is associated with an increase in tonic firing of the sub-cuneiform nucleus neurons. *Neuroscience* 158, 1201–1205. doi: 10.1016/j.neuroscience.2008.10.046
- Pierani, A., Moran-Rivard, L., Sunshine, M. J., Littman, D. R., Goulding, M., and Jessell, T. M. (2001). Control of interneuron fate in the developing spinal cord by the progenitor homeodomain protein Dbx1. *Neuron* 29, 367–384. doi: 10.1016/S0896-6273(01)00212-4
- Plotnik, M., Giladi, N., and Hausdorff, J. M. (2008). Bilateral coordination of walking and freezing of gait in Parkinson's disease. *Eur. J. Neurosci.* 27, 1999–2006. doi: 10.1111/j.1460-9568.2008.06167.x
- Plotnik, M., and Hausdorff, J. M. (2008). The role of gait rhythmicity and bilateral coordination of stepping in the pathophysiology of freezing of gait in

- Parkinson's disease. *Mov. Disord.* 23(Suppl. 2), S444–S450. doi: 10.1002/mds.21984
- Quinlan, K. A., and Kiehn, O. (2007). Segmental, synaptic actions of commissural interneurons in the mouse spinal cord. *J. Neurosci.* 27, 6521–6530. doi: 10.1523/jneurosci.1618-07.2007
- Rabe, N., Gezelius, H., Vallstedt, A., Memic, F., and Kullander, K. (2009). Netrin-1-dependent spinal interneuron subtypes are required for the formation of left-right alternating locomotor circuitry. *J. Neurosci.* 29, 15642–15649. doi: 10.1523/jneurosci.5096-09.2009
- Rabe Bernhardt, N., Memic, F., Gezelius, H., Thiebes, A. L., Vallstedt, A., and Kullander, K. (2012). DCC mediated axon guidance of spinal interneurons is essential for normal locomotor central pattern generator function. *Dev. Biol.* 366, 279–289. doi: 10.1016/j.ydbio.2012.03.017
- Reis, J., Swayne, O. B., Vandermeeren, Y., Camus, M., Dimyan, M. A., Harris-Love, M., et al. (2008). Contribution of transcranial magnetic stimulation to the understanding of cortical mechanisms involved in motor control. *J. Physiol.* 586, 325–351. doi: 10.1113/jphysiol.2007.144824
- Restrepo, C. E., Lundfald, L., Szabó, G., Erdelyi, F., Zeilhofer, H. U., Glover, J. C., et al. (2009). Transmitter-phenotypes of commissural interneurons in the lumbar spinal cord of newborn mice. *J. Comp. Neurol.* 517, 177–192. doi: 10.1002/cne.22144
- Rolf, B., Bastmeyer, M., Schachner, M., and Bartsch, U. (2002). Pathfinding errors of corticospinal axons in neural cell adhesion molecule-deficient mice. *J. Neurosci.* 22, 8357–8362.
- Rosenzweig, E. S., Brock, J. H., Culbertson, M. D., Lu, P., Moseanko, R., Edgerton, V. R., et al. (2009). Extensive spinal decussation and bilateral termination of cervical corticospinal projections in rhesus monkeys. *J. Comp. Neurol.* 513, 151–163. doi: 10.1002/cne.21940
- Runker, A. E., Little, G. E., Suto, F., Fujisawa, H., and Mitchell, K. J. (2008). Semaphorin-6A controls guidance of corticospinal tract axons at multiple choice points. *Neural Dev.* 3:34. doi: 10.1186/1749-8104-3-34
- Schieber, M. H. (2007). Chapter 2 comparative anatomy and physiology of the corticospinal system. *Handb. Clin. Neurol.* 82, 15–37. doi: 10.1016/s0072-9752(07)80005-4
- Sehm, B., Perez, M. A., Xu, B., Hidler, J., and Cohen, L. G. (2010). Functional neuroanatomy of mirroring during a unimanual force generation task. *Cereb. Cortex* 20, 34–45. doi: 10.1093/cercor/bhp075
- Serafini, T., Kennedy, T. E., Galko, M. J., Mirzayan, C., Jessell, T. M., and Tessier-Lavigne, M. (1994). The netrins define a family of axon outgrowth-promoting proteins homologous to *C. elegans* UNC-6. *Cell* 78, 409–424. doi: 10.1016/0092-8674(94)90420-0
- Serradj, N., and Jamon, M. (2009). The adaptation of limb kinematics to increasing walking speeds in freely moving mice 129/Sv and C57BL/6. *Behav. Brain Res.* 201, 59–65. doi: 10.1016/j.bbr.2009.01.030
- Serradj, N., Paixao, S., Sobocki, T., Feinberg, M., Klein, R., Kullander, K., et al. (2014). EphA4-mediated ipsilateral corticospinal tract misprojections are necessary for bilateral voluntary movements but not bilateral stereotypic locomotion. *J. Neurosci.* 34, 5211–5221. doi: 10.1523/JNEUROSCI.4848-13.2014
- Shibasaki, H., and Hallett, M. (2006). What is the Bereitschaftspotential? *Clin. Neurophysiol.* 117, 2341–2356. doi: 10.1016/j.clinph.2006.04.025
- Shibasaki, H., and Nagae, K. (1984). Mirror movement: application of movement-related cortical potentials. *Ann. Neurol.* 15, 299–302. doi: 10.1002/ana.410150317
- Shik, M. L., Severin, F. V., and Orlovskii, G. N. (1966). [Control of walking and running by means of electric stimulation of the midbrain]. *Biofizika* 11, 659–666.
- Shik, M. L., Severin, F. V., and Orlovskii, G. N. (1967). [Structures of the brain stem responsible for evoked locomotion]. *Fiziol. Zh. SSSR Im. I M Sechenova* 53, 1125–1132.
- Shu, T., Valentino, K. M., Seaman, C., Cooper, H. M., and Richards, L. J. (2000). Expression of the netrin-1 receptor, deleted in colorectal cancer (DCC), is largely confined to projecting neurons in the developing forebrain. *J. Comp. Neurol.* 416, 201–212. doi: 10.1002/(sici)1096-9861(20000110)416:2<201::aid-cne6>3.0.co;2-z
- Smith, J. C., and Feldman, J. L. (1987). *In vitro* brainstem-spinal cord preparations for study of motor systems for mammalian respiration and locomotion. *J. Neurosci. Methods* 21, 321–333. doi: 10.1016/0165-0270(87)90126-9
- Srour, M., Rivière, J. B., Pham, J. M., Dube, M. P., Girard, S., Morin, S., et al. (2010). Mutations in DCC cause congenital mirror movements. *Science* 328:592. doi: 10.1126/science.1186463
- Staudt, M., Grodd, W., Gerloff, C., Erb, M., Stitz, J., and Krageloh-Mann, I. (2002). Two types of ipsilateral reorganization in congenital hemiparesis: a TMS and fMRI study. *Brain* 125, 2222–2237. doi: 10.1093/brain/awf227
- Stokke, M. F., Nissen, U. V., Glover, J. C., and Kiehn, O. (2002). Projection patterns of commissural interneurons in the lumbar spinal cord of the neonatal rat. *J. Comp. Neurol.* 446, 349–359. doi: 10.1002/cne.10211
- Takakusaki, K., Habaguchi, T., Ohtinata-Sugimoto, J., Saitoh, K., and Sakamoto, T. (2003). Basal ganglia efferents to the brainstem centers controlling postural muscle tone and locomotion: a new concept for understanding motor disorders in basal ganglia dysfunction. *Neuroscience* 119, 293–308. doi: 10.1016/s0306-4522(03)00095-2
- Talpal, A. E., Bouvier, J., Borgius, L., Fortin, G., Pierani, A., and Kiehn, O. (2013). Dual-mode operation of neuronal networks involved in left-right alternation. *Nature* 500, 85–88. doi: 10.1038/nature12286
- Tennant, K. A., and Jones, T. A. (2009). Sensorimotor behavioral effects of endothelin-1 induced small cortical infarcts in C57BL/6 mice. *J. Neurosci. Methods* 181, 18–26. doi: 10.1016/j.jneumeth.2009.04.009
- Vallstedt, A., and Kullander, K. (2013). Dorsally derived spinal interneurons in locomotor circuits. *Ann. N Y Acad. Sci.* 1279, 32–42. doi: 10.1111/j.1749-6632.2012.06801.x
- Verstynen, T., Spencer, R., Stinear, C. M., Konkle, T., Diedrichsen, J., Byblow, W. D., et al. (2007). Ipsilateral corticospinal projections do not predict congenital mirror movements: a case report. *Neuropsychologia* 45, 844–852. doi: 10.1016/j.neuropsychologia.2006.08.019
- Vulliemoz, S., Raineteau, O., and Jabaudon, D. (2005). Reaching beyond the midline: why are human brains cross wired? *Lancet Neurol.* 4, 87–99. doi: 10.1016/s1474-4422(05)00990-7
- Wallén-Mackenzie, A., Gezelius, H., Thoby-Brisson, M., Nygård, A., Enjin, A., Fujiyama, F., et al. (2006). Vesicular glutamate transporter 2 is required for central respiratory rhythm generation but not for locomotor central pattern generation. *J. Neurosci.* 26, 12294–12307. doi: 10.3410/f.1052770.504685
- Whishaw, I. Q. (2000). Loss of the innate cortical engram for action patterns used in skilled reaching and the development of behavioral compensation following motor cortex lesions in the rat. *Neuropharmacology* 39, 788–805. doi: 10.1016/s0028-3908(99)00259-2
- Whishaw, I. Q., Pellis, S. M., Gorny, B., Kolb, B., and Tetzlaff, W. (1993). Proximal and distal impairments in rat forelimb use in reaching follow unilateral pyramidal tract lesions. *Behav. Brain Res.* 56, 59–76. doi: 10.1016/0166-4328(93)90022-i
- Winn, P. (2008). Experimental studies of pedunculo-pontine functions: are they motor, sensory or integrative? *Parkinsonism Relat. Disord.* 14(Suppl. 2), S194–S198. doi: 10.1016/j.parkreldis.2008.04.030
- Yokoyama, N., Romero, M. I., Cowan, C. A., Galvan, P., Helmbacher, F., Charnay, P., et al. (2001). Forward signaling mediated by ephrin-B3 prevents contralateral corticospinal axons from recrossing the spinal cord midline. *Neuron* 29, 85–97. doi: 10.1016/s0896-6273(01)00182-9
- Zhang, Y., Narayan, S., Geiman, E., Lanuza, G. M., Velasquez, T., Shanks, B., et al. (2008). V3 spinal neurons establish a robust and balanced locomotor rhythm during walking. *Neuron* 60, 84–96. doi: 10.3410/f.1125790.582877
- Zijdewind, I., Butler, J. E., Gandevia, S. C., and Taylor, J. L. (2006). The origin of activity in the biceps brachii muscle during voluntary contractions of the contralateral elbow flexor muscles. *Exp. Brain Res.* 175, 526–535. doi: 10.1007/s00221-006-0570-z

Conflict of Interest Statement: The authors declare that the research was conducted in the absence of any commercial or financial relationships that could be construed as a potential conflict of interest.

Copyright © 2015 Welniarz, Dusart, Gallea and Roze. This is an open-access article distributed under the terms of the Creative Commons Attribution License (CC BY). The use, distribution and reproduction in other forums is permitted, provided the original author(s) or licensor are credited and that the original publication in this journal is cited, in accordance with accepted academic practice. No use, distribution or reproduction is permitted which does not comply with these terms.

Advantages of publishing in Frontiers



OPEN ACCESS

Articles are free to read,
for greatest visibility



COLLABORATIVE PEER-REVIEW

Designed to be rigorous
– yet also collaborative,
fair and constructive



FAST PUBLICATION

Average 85 days from
submission to publication
(across all journals)



COPYRIGHT TO AUTHORS

No limit to article
distribution and re-use



TRANSPARENT

Editors and reviewers
acknowledged by name
on published articles



SUPPORT

By our Swiss-based
editorial team



IMPACT METRICS

Advanced metrics
track your article's impact



GLOBAL SPREAD

5'100'000+ monthly
article views
and downloads



LOOP RESEARCH NETWORK

Our network
increases readership
for your article

Frontiers

EPFL Innovation Park, Building I • 1015 Lausanne • Switzerland
Tel +41 21 510 17 00 • Fax +41 21 510 17 01 • info@frontiersin.org
www.frontiersin.org

Find us on

